School of Food and Nutritional Sciences, University College Cork, Co. Cork, Ireland

Teagasc Food Research Centre, Moorepark, Fermoy, Co. Cork, Ireland

Walsh Scholar Programme

Development of *In Vitro* Infant Intestinal Models to Assess Responses to Infant Formulae

Thesis submitted to the National University of Ireland

for Degree of Doctor of Philosophy

by

Francesca Bietto, M.Sc.

ORCID: 0000-0001-5812-4477

Head of School: Prof. Alan Kelly

Supervisors: Dr. Linda Giblin (Teagasc), Dr. Alice Lucey (UCC), Dr. Elena Arranz (CIAL), Dr. Eva Rath (TUM)

Submitted: November 2025

Table of Contents

Declaration ..... **xx**

Acknowledgements ..... **xxii**

Publications and Awards ..... **xxv**

Publications ..... *xxv*

Conference presentations ..... *xxv*

Awards ..... *xxvi*

Abstract ..... **xxvii**

Glossary of Terms ..... **xxx**

1. Chapter 1 Unraveling the Infant Gut Barrier: Key Characteristics, Differences from the Adult and *In Vitro* Models *Literature Review* **1**

Abstract *2*

1.1. Introduction *3*

1.2. Cellular and Molecular Features of the Infant Gut Barrier *11*

1.2.1. Mucus Layer: The First Adaptive Shield of the Neonatal Gut 11

1.2.2. Dynamic Membranes: Fluidity as a Developmental Gatekeeper of Nutrient Uptake 13

1.2.3. Adaptive Permeability: Tight Junction Plasticity as a Developmental Signal 16

1.2.4. Enzymatic Maturation: From Milk Digestion to Omnivore Efficiency 23

1.2.5. Nutrient Gateways: Transporter Reprogramming During Early Life 32

1.3. Feeding for Maturity: Human Milk Supports Intestinal Barrier Development *46*

1.4. Modeling the Immature Barrier: How Close Are We to the Real Infant Gut? 48

1.4.1. Caco-2 and Co-culture Models 50

1.4.2. The IPEC-J2 cell line 55

1.4.3. Human Fetal Intestinal Cell Lines (FHs 74 Int, HIEC-6) 57

1.5. Experimental Strategies for Modelling the Infant Gut Barrier *62*

1.6. Conclusion *66*

1.7. References *67*

Rational and Objectives of the Thesis *108*

2. Chapter 2 Modeling Leaky Gut *In Vitro*: Sodium Butyrate-Induced Barrier Disruption of Caco-2 monolayers 111

Abstract *112*

2.1. Introduction *113*

2.2. Materials and Methods *116*

2.2.1. Materials 116

2.2.2. Cell Culture 116

2.2.3. 2.3 NADH dehydrogenase activity and ATP levels 117

2.2.4. Caspase-3 activity 118

2.2.5. NaB treatment of Caco-2 or Caco-2/HT29-MTX monolayers 119

2.2.6. Monolayer recovery 120

2.2.7. TEER measurements with isosmotic NaB and Man solutions.....120
2.2.8. Treatment with dexamethasone.....121
2.2.9. Lucifer Yellow permeability.....121
2.2.10. NaB and Man quantification in apical and basolateral samples 122
2.2.11. RT-qPCR.....123
2.2.12. Lactate Dehydrogenase (LDH) cytotoxicity assay 124
2.2.13. Statistical analysis.....125
2.3. Results.....125
2.3.1. NaB impairs epithelial barrier integrity monolayers without subsequent recovery.....125
2.3.2. NaB does not reduce TEER under isosmotic conditions 128
2.3.3. NaB is transported across and into Caco-2 monolayers.....131
2.3.4. NaB is not utilized as an energy source in Caco-2 cells 133
2.3.5. NaB induces apoptosis (Caspase-3 activity).....135
2.3.6. NaB induces mRNA expression of butyrate transporters, stress markers and cytokines.....136
2.3.7. Dexamethasone promotes recovery of Caco-2 monolayers treated with 75 mM NaB.....139
2.4. Discussion.....142
2.5. References.....149
2.6. Supplementary Information.....158
3. Chapter 3 Using sodium glycodeoxycholate to develop a temporary infant-like gut barrier model, *in vitro* 163
Abstract.....164

3.1. Introduction *165*

3.2. 2 Materials and Methods *171*

3.2.1. Materials 171

3.2.2. Cell Culture 172

3.2.3. MTS Assay 172

3.2.4. Caspase-3 Assay 173

3.2.5. Intracellular cAMP quantification 174

3.2.6. GDC treatment of Caco-2/HT29-MTX monolayers 175

3.2.7. Monolayer recovery 176

3.2.8. Permeability to Lactulose 177

3.2.9. Lactate Dehydrogenase (LDH) assay 178

3.2.10. Alkaline phosphatase activity 179

3.2.11. Cytokine Quantification 180

3.2.12. OCLN immunofluorescence 180

3.2.13. mRNA Expression by Real Time PCR 182

3.2.14. Mucus Quantification by Alcian Blue 183

3.2.15. Gastrointestinal digestion of Dairy Infant Formula (IF) 183

3.2.16. Caco-2/HT29-MTX monolayers exposure to digested dairy IF 184

3.2.17. Quantification of the total amino acid in the basolateral chamber 185

3.2.18. Statistical analysis 186

3.3. Results *186*

3.3.1. IC_{50} of GDC on Caco-2/HT29-MTX is 2.49 mM 186

3.3.2. GDC decreases TEER with subsequent recovery 186

3.3.3. GDC-treated monolayers have a higher permeability to lactulose 188

3.3.4. GDC treatment does not cause monolayer cytotoxicity 190

3.3.5. GDC increases extracellular, but not intracellular, alkaline phosphatase activity 190
3.3.6. GDC treatment does not cause monolayer inflammation 190
3.3.7. GDC reduces OCLN fluorescence intensity and modulates tight junction proteins mRNA expression 192
3.3.8. GDC increases mucus production but not mucins expression 195
3.3.9. GDC does not activate the apoptotic cascade but decreases cAMP levels 197
3.3.10. GDC (0.8 mM) increases amino acids transport after exposure to digested dairy IF 199
3.4. Discussion 201
3.5. Conclusions 207
3.6. References 208
3.7. Supplementary Materials 222
4. Chapter 4 Comparative effects of human milk and infant formulae on peptide transport and epithelial barrier function in infant- and adult-like *in vitro* gut models 229
Abstract 230
4.1. Introduction 231
4.2. Materials and Methods 234
4.2.1. Materials 234
4.2.2. Simulated static infant gastrointestinal digestion (SGID) 235
4.2.3. SDS-PAGE 236

4.2.4. Total nitrogen content by o-phthaldialdehyde (OPA) assay 237
4.2.5. Size Exclusion Chromatography (SEC) 237
4.2.6. Free and total AAs analysis in the digested samples 238
4.2.7. Cell Culture 239
4.2.8. MTS Assay 239
4.2.9. Caco-2/HT29-MTX monolayers exposure to GDC and digesta 240
4.2.10. Immunofluorescence and confocal microscopy 241
4.2.11. Free AAs transported in the basolateral side 243
4.2.12. Peptide Profiling by UHPLC-HRMS/MS 244
4.2.13. Peptide identification 245
4.2.14. Bioinformatics analysis 246
4.2.15. Statistical analysis 248
4.3. Results 248
4.3.1. IF and human milk exhibit similar protein hydrolysis with differences in molecular size distribution and amino acid profiles 248
4.3.2. Digested IF and human milk maintain infant-like barrier integrity 254
4.3.3. Digested human milk enhances OCLN–actin co-localization in infant-like monolayers 256
4.3.4. AA IF shows the highest basolateral free AA levels 260
4.3.5. Infant-like monolayers exhibit higher peptide transport and higher sequence diversity 263
4.3.6. Apical peptides reflect active brush border enzyme cleavage 267
4.3.7. Infant-like monolayers show enhanced basolateral peptide load in response to human milk 269

4.3.8. Human milk-derived bioactive peptides are more abundant in infant-like monolayers 271

4.4. Discussion 275

4.5. Conclusions 282

4.6. References 284

4.7. Supplementary Materials 296

5. Chapter 5 Culture Optimization of the IPEC-J2 Piglet Jejunum Cell Line for Applications in Infant Nutrition Research 307

Abstract 308

5.1. Introduction 310

5.2. Materials and Methods 315

5.2.1. Materials 315

5.2.2. Cell Culture 316

5.2.3. TEER 317

5.2.4. Alkaline phosphates (ALP) and lactate dehydrogenase (LDH) activity 318

5.2.5. Lactulose: Mannitol Permeability Assay 319

5.2.6. Reverse Transcription Quantitative PCR (RT-qPCR) 321

5.2.7. Immunofluorescence Staining of ZO1 322

5.2.8. Preparation and Characterization of Dairy Infant Formula (IF) Digesta 323

5.2.9. IPEC-J2 Exposure to Digesta 325

5.2.10. Statistical analysis 327

5.3. Results *328*

5.3.1. Media dictates TEER values of IPEC-J2 monolayers 328

5.3.2. ALP and LDH Activity Reflect Media-Dependent IPEC-J Differentiation 331

5.3.3. PS5+EGF+ITS Increases Lactulose and Mannitol Permeability in IPEC-J2 Monolayers 334

5.3.4. Media Modulates mRNA levels of Transport, Barrier and Immune Genes in IPEC-J2 monolayers 337

5.3.5. Media Influences ZO1 Distribution and Cell Density in IPEC-J2 Monolayers 343

5.3.6. IPEC-J2 Viability Is Maintained After Exposure to Inactivated Digesta 346

5.3.7. Heat-inactivated digested dairy IF (HI) increases TEER in IPEC-J2 monolayers cultured in PS10 medium 348

5.3.8. PS10 increases basolateral free AA after exposure to dairy IF digesta 350

5.4. Discussion *353*

5.5. Conclusions *360*

5.6. References *362*

5.7. Supplementary Materials *371*

6. Chapter 6 General discussion 378

6.1. General discussion *379*

6.2. References *390*

Appendix A Publications from this thesis.....401

Appendix B Full Peptide Data from Chapter 4.....453

Appendix C Additional Research Outputs and Activities.....527

List of Figures

Fig. 1.1 Overview of the main epithelial cell types forming the small intestinal barrier. 5

Fig. 1.2 Schematic representation of the intestinal epithelial tight junction complex. 7

Figure 1.3 Key Differences Between Infant and Adult Small Intestinal Barrier Function. 45

Fig. 2.1 Effects of Sodium Butyrate (NaB) and Mannitol (Man) on Caco-2 Monolayer Permeability. 127

Fig. 2.2 Transepithelial electrical resistance (TEER) values for 20 day Caco-2 monolayers treated with NaB or Man at 367.4 ± 4.86 mOsm/kg. 130

Fig. 2.3 Quantification of NaB and Man solutions applied to Caco-2 Monolayers. 132

Fig. 2.4 Metabolic activity of undifferentiated Caco-2 cells after treatment with NaB or Man. 134

Fig. 2.5 Caspase 3 activity in undifferentiated Caco-2 cells treated with NaB or Man. 135

Fig. 2.6 mRNA Expression of MCT-1, SMCT-1, SCAD, AQP-3, HSP-70, IL-6, IL-8, and TNF in Caco-2 Monolayers treated with NaB or Man. 138

Fig. 2.7 Effect of dexamethasone (Dexa) on NaB-treated Caco-2 monolayers. 141

Fig. 3.1 GDC treated day 25 Caco-2/HT29-MTX monolayers Trans-Epithelial Electrical Resistance (TEER) and lactulose permeability. 189

Figure 3.2 Effect of GDC treatment on LDH release, intracellular and extracellular alkaline phosphatase activity in Caco-2/HT29-MTX monolayers. 191

Fig. 3.3 Effect of GDC treatment on occludin (OCLN) localization and tight junction protein expression in Caco-2/HT29-MTX monolayers. 193

Fig. 3.4 (A) Mucus staining (B) and mucins mRNA expression in Caco-2/HT29-MTX monolayers treated with GDC. 196
Fig. 3.5 Caspase-3 activity and intracellular cAMP levels in undifferentiated Caco-2/HT29-MTX cells treated with GDC and proposed mechanism of action. 198
Fig. 3.6 (A) TEER values and (B) total amino acid content in the basolateral side of Caco-2/HT29-MTX monolayers treated with GDC and digested dairy Infant Formula (IF). 200
Fig. 4.1 Infant gastrointestinal digestion of Dairy, Soya and amino acid-based (AA) infant formulae (IF) and human milk. 252
Fig. 4.2 Transepithelial electrical resistance (TEER) of Caco-2/HT29-MTX monolayers treated with digested infant formulae (IF) or Human Milk. 255
Fig. 4.3 Occludin (OCLN) localization in infant and adult-like Caco-2/HT29-MTX monolayers treated with digested Human Milk. 258
Fig. 4.4 Colocalization of occludin (OCLN) and actin in infant- and adult-like Caco-2/HT29-MTX monolayers exposed to digested infant formulae (IF) and Human Milk. 259
Figure 4.5 Free Amino Acid Concentrations in the basolateral compartments of Caco-2/HT29-MTX monolayers treated with digested Infant Formulas (IF) and Human Milk. 262
Fig. 4.6 Venn diagrams of unique peptides detected in infant- and adult-like monolayers treated with digested Dairy IF, Soya IF or Human Milk. 266
Fig. 4.7 Cleavage events attributed to specific brush border enzymes. 268
Fig. 4.8 Peptide transport across infant- and adult-like monolayers after exposure to digested infant formulae (IFs) and Human Milk. 270

Figure 4.9 Volcano plots of peptide abundance differences between infant- and adult-like models after exposure to digested infant formulas (IF) and Human Milk. 274

Fig. 5.1 Transepithelial electrical resistance (TEER) measurements in IPEC-J2 monolayers cultured under different media conditions. 330

Fig. 5.2 Alkaline phosphatase (ALP) and lactase dehydrogenase (LDH) activity in IPEC-J2 monolayers at days 7 and 14. 333

Fig. 5.3 Media-dependent permeability to lactulose and mannitol in IPEC-J2 monolayers. 336

Fig. 5.4 Relative mRNA expression in IPEC-J2 monolayers under different culture media. 340

Fig. 5.5 Effect of media composition on ZO1 localization and epithelial cell density in IPEC-J2 monolayers. 345

Fig. 5.6 Viability of undifferentiated IPEC-J2 cells exposed to dairy infant formula (IF) digesta. 347

Fig. 5.7 TEER values of undifferentiated IPEC-J2 cells before and after exposure to dairy infant formula (IF) digesta. 349

Fig. 5.8 Free amino acid (AA) in basolateral chamber of IPEC-J2 monolayers treated with dairy infant formula (IF) digesta. 352

List of Supplementary Figures

Supplementary Fig 2.1 Transepithelial Electrical Resistance (TEER) of Caco-2 and Caco-2/HT29-MTX (90:10) monolayers from day 7 to day 20.....159

Supplementary Fig 2.2 : Transepithelial electrical resistance (TEER) values of Caco-2/HT29-MTX 90:10 monolayers treated with sodium butyrate (NaB) or mannitol (Man).....160

Supplementary Fig 2.3 % of Cytotoxiciy as LDH release in the apical compartment of 20-day old Caco-2 monolayers. 161

Supplementary Fig 3.1 GDC IC50 on undifferentiated Caco-2/HT29-MTX cells..223

Supplementary Fig 3.2 Trans Epithelial Electrical Resistance (TEER) of the (90:10) Caco-2/HT29-MTX monolayers from day 7 to day 25. 224

Supplementary Fig 3.3 mRNA expression of p21 and p53 as markers to cellular response to stress.....225

Supplementary Fig 3.4 Direct inhibition of Protein Kinase A (PKA) by GDC.....226

Supplementary Fig 3.5 MTS viability assay of undifferentiated Caco-2/HT29-MTX after exposure to digesta.....227

Supplementary Fig 4.1 Protein concentration and profile of digested samples measured by BCA assay and SDS page. 296

Supplementary Fig 4.2 Characterization of the simulated gastrointestinal digestion (SGID) water control (SGID H_2O).....297

Supplementary Fig 4.3 Cell viability of Caco-2/HT29-MTX treated with digested infant formulae (IF) and Human Milk. 298

Supplementary Fig 4.4 Occludin (OCLN) localization in adult-like and infant-like Caco-2/HT29-MTX monolayers following exposure to digested infant formulae (IF). 300

Supplementary Fig 4.5 Monolayer thickness of control adult-like and infant-like intestinal models. 301
Supplementary Fig 4.6 Free amino acids in the basolateral compartment of HBSS-treated monolayers and digesta. 302
Supplementary Fig 5.1 Tracking protein digestion during simulated gastrointestinal digestion of dairy infant formula (IF). 371
Supplementary Fig 5.2 : Free amino acid (AA) levels in IPEC-J2 monolayers exposed to digested dairy infant formula (IF) or HBSS. 373

List of Tables

Table 1.1 Summary of studies asessing age-dependent changes in intestinal paracellular permeability across mammalian species. 18

Table 1.2 Developmental differences in tight junction protein expression and localization between infant/newborn and adult intestinal epithelium. 21

Table 1.3 Summary of studies describing developmental and age-related changes in intestinal brush border enzyme activity and expression between infants/newborns and adults. 30

Table 1.4 Summary of studies describing developmental changes in intestinal peptide transport across mammalian species. 37

Table 1.5 Summary of commonly used *in vitro* intestinal epithelial cell models and their functional characteristics in relation to infant/newborn gut physiology..... 60

Table 2.1 Average osmolality (mOsmol/kg) of DMEM D1145, NaB, and Man solutions. 128

Table 5.1 mRNA expression in porcine jejunal scrapings relative to IPEC-J2 monolayers cultured in FBS10. 341

List of Supplementary Tables

Supplementary Table 2.1 Gene name, GenBank accession number, primers and annealing temperature (Ta) for RT-PCR analysis. 158

Supplementary Table 3.1 Gene name, GenBank accession number and primers sequences for RT-PCR analysis. 222

Supplementary Table 4.1 Concentrations (ρmol/µL) of total amino acids in post-intestinal (I60) digesta of infant formulae and human milk, measured by UPLC. ..303

Supplementary Table 4.2 Concentrations (ρmol/µL) of free amino acids in post-intestinal (I60) digesta of infant formulae and human milk, measured by UPLC. ..304

Supplementary Table 4.3 Concentrations (mg/L) of free amino acids in the basolateral compartment after exposure of Adult-like and Infant-like Caco-2/HT29-MTX monolayers to infant formulae and human milk, measured by UHPLC-HRMS. 305

Supplementary Table 4.4 Concentrations (mg/L) of free amino acids in post-intestinal (I60) digesta of infant formulae and human milk, measured by UHPLC-HRMS. 306

Supplementary Table 5.1 Gene name, GenBank accession number and primers sequences for RT-PCR analysis. 374

Supplementary Table 5.2 Free amino acid concentrations in dairy infant formula (IF) digesta. 376

Supplementary Table 5.3 Free amino acid concentrations in the basolateral chamber of IPEC-J2 monolayers exposed to dairy IF digesta. 377

Appendix Table 1 Summary matrix reporting the unique peptides in each compartment (digesta, apical, basolateral), their overlaps, and unique distributions across infant- and adult-like models for Dairy IF. 453
Appendix Table 2 Summary matrix reporting the unique peptides in each compartment (digesta, apical, basolateral), their overlaps, and unique distributions across infant- and adult-like models for Soya IF. 477
Appendix Table 3 Summary matrix reporting the unique peptides in each compartment (digesta, apical, basolateral), their overlaps, and unique distributions across infant- and adult-like models for Human Milk. 505
Appendix Table 4 Bioactive peptides comparisons in the apical and basoalteral compartments between infant- and adult-like models exposed to digested Dairy IF. 519
Appendix Table 5 Bioactive peptides comparisons in the apical and basoalteral compartments between infant- and adult-like models exposed to digested Soya IF. 524
Appendix Table 6 Bioactive peptides comparisons in the apical and basoalteral compartments between infant- and adult-like models exposed to digested Human Milk. 525

Declaration

This is to certify that the work I am submitting is my own and has not been submitted for another degree, either at University College Cork or elsewhere. All external references and sources are clearly acknowledged and identified within the contents. I have read and understood the regulations of University College Cork concerning plagiarism and intellectual property.

All the work presented in this thesis was designed, executed, and interpreted by the author unless otherwise stated.

Specific analytical or technical contributions by collaborators are acknowledged below:

- **Chapter 2:** Osmolality analyses were performed by Mónica Mechoud (Teagasc).
- **Chapter 3:** Cristina Gómez-Marín (CIAL) provided assistance with amino acid analyses.
- **Chapter 4:** The Technical Services of CIAL (CSIC-UAM) conducted Kjeldahl nitrogen determinations and assisted with confocal microscopy imaging. Cristina Gómez-Marín contributed to the UPLC analyses. Francesco Romaniello (INRiM) and Simona Cirrincione (CNR-ISPA) carried out the UHPLC–HRMS/MS analyses.
- **Chapter 5:** Paula O'Connor (Teagasc) performed the HPLC amino acid analyses. Myriam Grundy and Sandra Wiard-Letort (INRAE) performed Apotome microscopy imaging. Cathal Dold (Teagasc) provided the cDNA samples of pig jejunal scrapings used for gene expression analyses.

The author was responsible for the overall experimental design, sample preparation, data analysis, and interpretation across all chapters.

Digital signature of the candidate: Francesca Bietto

Name: Francesca Bietto

Date: 13/11/2025

Acknowledgements

This research was supported by Teagasc (InfBar MDBY1370). I would also like to acknowledge the support received through the Teagasc Walsh Scholarship (2021007).

First and foremost, I want to thank Dr. Linda Giblin for her supervision. On my very first day, she told me that she was going to train a leader, not a scientist — and I have carried those words with me ever since. They have continuously empowered me throughout this journey.

I am deeply grateful to Dr. Alice Lucey from University College Cork, Dr. Elena Arranz from Institute of Food Science Research (CIAL, Madrid, Spain), and Dr. Eva Rath from the Technical University of Munich for their support and guidance.

My sincere thanks also go to our collaborators at CIAL — Beatriz Miralles, Dr. Isidra Recio, and Cristina Gómez Marín — for welcoming me into their lab and making me feel at home.

I would like to thank National Research Council (CNR-ISPA, Turin, Italy) and National Institute of Metrological Research (INRiM, Turin, Italy) — Dr. Simona Cirrincione, Simona Bavaro, Cristina Lamberti, Francesco Romaniello, and Laura Cavallarin — for hosting me and for the great collaborations we started together.

My gratitude also goes to Dr. Myriam Grundy and Sandra Wiart-Letort from National Research Institute for Agriculture, Food and Environment (INRAE, UMR

Pegase, Rennes, France) for their collaboration and for helping to crack the mystery of the IPEC-J2 cells together.

A heartfelt thanks to my lab, Lab 102, especially Ailynne Sepúlveda Gonzáles, Cathal Dold, Charlotte Oliver and Monica Mechoud, for their continuous collaboration, training, and friendship.

I am also deeply thankful to Ramya Balasubramanian for training me and for the opportunity to collaborate with her on her mice work, as well as for the deep friendship that grew alongside it.

To my wonderful flatmates, Orla Cooney and Somiame Okuofu, thank you for making this place feel like home. A special thanks to Orla Cooney for proofreading the thesis chapters with care and patience.

To my friends at Teagasc — Alanna Slater, Della Della, Giulia Amore Bonapasta, Renata Kostovska, Emmanuel Osei, Gaëtan Drouin, Raffaele Magliulo, and Vincenzo Fiore — and to those who have since moved on — Giulia Bisson, Maria Gloria Mora, Yasmin Sabino, Talita Comunian and Antoni Taraszkiewicz— your presence has made this journey not only possible, but truly beautiful.

I also want to thank my friends in Cork — Ludovica Damato, Chiara Penaglia, Martina Becchio, Matteo Fava, Sonia Damato, and Hairo Cruzado — for always keeping your promise of being there for me, from the very beginning to the end.

Finally, I wish to thank my family and my friends at home — being far apart is hard, but being there for each other despite the distance is even harder.

And to Guglielmo, thank you for your unconditional love and support, and for moving to the rainy town of Fermoy so I could pursue my ambitions— you have been my anchor through it all.

Publications and Awards

Publications

Bietto, F., Arranz, E., Mechoud, M., Rath, E., Lucey, A.J., Giblin, L., 2026a. Modeling a leaky gut In vitro: Sodium butyrate-induced barrier disruption of Caco-2 monolayers. The Journal of Nutritional Physiology 6, 100021. https://doi.org/10.1016/j.jnphys.2026.100021.

Bietto F, Arranz E, Miralles B, Gómez-Marín C, Rath E, Lucey AJ, et al. Using sodium glycodeoxycholate to develop a temporary infant-like gut barrier model, in vitro. Front Nutr 2025;12:1577369. https://doi.org/10.3389/fnut.2025.1577369.

Bietto, F., Cirrincione, S., Gómez-Marín, C., Miralles, B., Romaniello, F., Arranz, E., Lamberti, C., Bavaro, S.L., Cavallarin, L., Rath, E., Lucey, A.J., Giblin, L., 2026. Comparative effects of digested human milk and infant formulas on peptide transport and gut barrier function in infant- and adult-like Caco-2/HT29-MTX models. Food Research International 235, 119071. https://doi.org/10.1016/j.foodres.2026.119071.

Conference presentations

Bietto F, Miralles B, Arranz E, Lucey AJ, Rath E, Giblin L (2024). Pioneering In Vitro Models of the Immature Gut Barrier for Advancing Infant Formula. Oral Presentation. 8th International Conference on Food Digestion (ICFD2024), 9-11 April 2024, Porto, Portugal.

Taraszkiewicz A, Sinkiewicz I, Bietto F, Dold C, Oliver C, Sommer A, Staroszczyk H, Giblin L (2024). Effects Of Enzymatic Hydrolysis, The Maillard Reaction And In

Vitro Gastro-Intestinal Digestion On Antioxidant Properties Of Feather Keratin. Co-author of oral presentation. International Conference on Food Digestion (ICFD2024), 9-11 April 2024, Porto, Portugal.

Bietto F, Arranz E, Lucey AJ, Rath E, Giblin L (2023). Developing An *In Vitro* Model Of The Infant Gut Barrier Via Permeability Enhancers. Poster presentation. The 4th International Conference on Food Bioactives and Health 2023 (FBHC2023). Prague, Czechia. 18 - 21st September 2023

Awards

Walsh Scholars of the Year (2nd place, Food Bioscience Programme, Teagasc, 2025) for research impact and communication.

Postgraduate Travel Bursary, College of Science, Engineering & Food Science, University College Cork. €500 in financial support to present at the Food Bioactive and Health Conference (Prague, Sept 2023).

Research-in-3 competition (1st place, School of Food and Nutritional Sciences, University College Cork, 2 December 2025).

Abstract

Early postnatal nutrition and intestinal barrier maturation are intimately linked, with the neonatal gut characterized by higher permeability than in adults. The aim of this thesis was to develop and validate *in vitro* models that mimic the infant intestinal barrier. Once developed, these models were employed to study epithelial responses to digested human milk and infant formulae (IF). The central hypothesis was that physiologically relevant, infant-like epithelial models would better capture the biological effects of infant food on nutrient absorption and barrier function than the conventional adult-like Caco-2/HT29-MTX co-culture.

In chapter 2, Caco-2/HT29-MTX polarized monolayers were treated with the short-chain fatty acid salt sodium butyrate (NaB), previously reported to increase permeability without harm. High NaB concentrations (50–125 mM) reduced transepithelial electrical resistance (TEER) and increased paracellular permeability of Caco-2 monolayers in a dose-dependent manner under hyperosmotic conditions. NaB uptake occurred via monocarboxylate transporters (MCT-1, SMCT-1). However, NaB caused elevated apoptosis (Caspase-3 activity), stress responses (p21, HSP-70), and cytokine secretion (IL6, IL8, TNF). Therefore, NaB disturbed barrier integrity, and this disruption was not reversible after compound removal. Partial recovery following steroid treatment indicated that NaB-treated Caco-2/HT29-MTX monolayers may be more suitable for modeling gut inflammation than for representing the infant barrier.

In chapter 3, the bile-derived sodium glycodeoxycholate (GDC) was evaluated in Caco-2/HT29-MTX monolayers. Treatment with 0.8 mM GDC decreased TEER and increased lactulose permeability 1.6-fold without inducing cytotoxicity or inflammation. GDC also reduced occludin (OCLN) localization at tight junctions,

increased acidic mucins, and elevated extracellular alkaline phosphatase activity, consistent with neonatal mucosal features. Crucially, the GDC effect was transient: TEER recovered within 4 h of removal, supporting its use as a controllable, reversible infant-like gut barrier model.

In chapter 4, the infant-like GDC model was then employed to compare gastrointestinal digestion and epithelial responses to human milk, dairy-, soya-, and amino acid-based IFs. Using infant-specific digestion conditions, peptide and amino acid transport were quantified in both infant- and adult-like Caco-2/HT29-MTX monolayers. In infant-like monolayers, human milk uniquely enhanced OCLN–actin co-localization ($P < 0.05$) and increased the diversity and basolateral abundance of bioactive peptides identified by UHPLC-HRMS/MS. The amino acid-based IF increased OCLN fluorescence intensity but reduced TEER in adult-like monolayers, indicating formulation-specific differences in epithelial compatibility. Across all digesta, peptide diversity and transport were significantly greater in infant-like than adult-like models ($P < 0.05$), with human milk promoting the richest basolateral peptide profile.

Chapter 5 examined the intestinal porcine enterocyte cell line IPEC-J2 as an alternative to Caco-2/HT29-MTX. This cell line, isolated from the jejunum of an unsuckled neonatal piglet, differentiates into tightly adherent, columnar epithelial monolayers exhibiting apical–basal polarity and dense brush borders. However, standardized culture protocols are lacking. Four media were compared for their effects on TEER, permeability, and differentiation. Porcine serum (PS10) supported the most balanced epithelial phenotype, with intermediate TEER (~2400 $\Omega \times cm^2$), low lactulose:mannitol permeability, strong zonula occludens-1 localization, and low fibroblast marker S100A4 expression. Following exposure to *in vitro*–digested IF,

PS10-cultured IPEC-J2 monolayers exhibited increased TEER and enhanced basolateral amino acid transport, demonstrating suitability for dietary bioavailability studies in infant nutrition.

In conclusion, this thesis establishes two *in vitro* models of the infant gut barrier: GDC-treated Caco-2/HT29-MTX and PS10-cultured IPEC-J2. GDC treatment provides a reproducible and reversible system to model transient infant gut permeability, while the IPEC-J2 line offers a stable, species-relevant platform. Together, these models advance mechanistic understanding of gut maturation and offer novel tools to design next-generation infant formulas that better emulate the functional benefits of human milk.

Keywords: infant gut barrier, sodium glycodeoxycholate, sodium butyrate, Caco-2, HT29-MTX, IPEC-J2, INFOGEST, human milk, infant formula, peptide transport, tight junctions, TEER, gastrointestinal digestion, occludin

Glossary of Terms

A
AA – Amino Acids
ALP – Alkaline Phosphatase
ATP – Adenosine Triphosphate
AQP-3 – Aquaporin-3

B
BCA – Bicinchoninic Acid Assay
BSA – Bovine Serum Albumin (appears in digestion buffers)

C
Caco-2 – Human colorectal adenocarcinoma cell line
cAMP – Cyclic Adenosine Monophosphate

D
Dexa – Dexamethasone
DMEM – Dulbecco's Modified Eagle Medium
DPP-IV, DPP8/9 – Dipeptidyl Peptidase IV, VIII, IX
DNA – Deoxyribonucleic Acid

E
EGF – Epidermal Growth Factor
EGFR – Epidermal Growth Factor Receptor
ERK – Extracellular Signal–Regulated Kinase
ELISA – Enzyme-Linked Immunosorbent Assay (referenced in supplementary methods)

F
FBS – Fetal Bovine Serum
FDR – False Discovery Rate
FHs 74 Int – Human fetal small intestinal epithelial cell line
FXR – Farnesoid X Receptor

G
GDC – Sodium Glycodeoxycholate
GLUT2/5 – Glucose Transporter 2 / 5

H
HBSS – Hank's Balanced Salt Solution
HIEC-6 – Human Intestinal Epithelial Cell line-6
HI – Heat-Inactivated (used for digesta)
HMOs – Human Milk Oligosaccharides
HSP-70 – Heat Shock Protein 70
HRMS/MS – High-Resolution Tandem Mass Spectrometry

I
I60 – 60-minute intestinal digestion point, end of digestion
IC50 – Half-Maximal Inhibitory Concentration
IF – Infant Formula
IL6, IL8 – Interleukin-6 / Interleukin-8
IPEC-J2 – Porcine jejunal epithelial cell line
ITS – Insulin–Transferrin–Selenium supplement

L
LAT – L-Amino Acid Transport System
LDH – Lactate Dehydrogenase
LTBP2 – Latent Transforming Growth Factor Beta-Binding Protein 2
LY – Lucifer Yellow

M
Man – Mannitol
MCT-1 – Monocarboxylate Transporter-1
MFGM – Milk Fat Globule Membrane
MS/MS – Tandem Mass Spectrometry
MTS – MTS Cell Viability Assay

N
NaB – Sodium Butyrate
NADH – Nicotinamide Adenine Dinucleotide (Reduced Form)
NEC – Necrotizing Enterocolitis

O
OCLN – Occludin

P
PCR / RT-qPCR – Polymerase Chain Reaction / Reverse-Transcription Quantitative PCR
PEPT1 – Peptide Transporter-1
PKA – Protein Kinase A
PS5 / PS10 – Porcine Serum 5% / 10%
PSM – Peptide-Spectrum Match

Q
qPCR – Quantitative Polymerase Chain Reaction

R
RT-PCR – Reverse Transcription PCR
RNA – Ribonucleic Acid
RAGE – Receptor for Advanced Glycation End Products

S
SCAD – Short-Chain Acyl-CoA Dehydrogenase
SDS-PAGE – Sodium Dodecyl Sulfate Polyacrylamide Gel Electrophoresis
SEM – Standard Error of the Mean
SGID – Simulated Gastrointestinal Digestion
SGLT1 – Sodium-Glucose Co-Transporter-1
SMCT-1 – Sodium-Coupled Monocarboxylate Transporter-1
SV – Sequence Version (UniProt)

T
T_a – Annealing Temperature
TEER – Transepithelial Electrical Resistance
TGR5 – G-Protein Coupled Bile Acid Receptor 1
TNF – Tumor Necrosis Factor

U
UHPLC – Ultra-High-Performance Liquid Chromatography
UPLC – Ultra-Performance Liquid Chromatography

Z
ZO – Zonula Occludens

1. Chapter 1

Unraveling the Infant Gut Barrier: Key Characteristics, Differences from the Adult and *In Vitro* Models

Literature Review

Abstract

The intestinal barrier of newborns develops through distinct stages that balance nutrient absorption with protection against microbes and harmful molecules. In early life, the gut is naturally more permeable, allowing the passage of milk-derived bioactive molecules that drive epithelial and immune maturation. This temporary "leaky" state reflects a more permeable mucus layer, increased membrane fluidity, and immature tight-junction architecture, resulting in enhanced paracellular transport. At the same time, digestive enzymes and nutrient transporters undergo developmental transitions, shifting from neonatal profiles optimized for milk digestion toward more mature absorptive functions. These processes are controlled by age-dependent physiological changes within the intestine, and are further influenced by external factors such as diet and microbial colonization. Understanding this critical early period—when nutrition shapes long-term intestinal function—is essential for developing *in vitro* models that more accurately reflect the infant gut. These models will be fundamental to the design of infant formulae capable of supporting barrier maturation. Current cell-based systems, including the adult-like Caco-2 cell line, neonatal porcine IPEC-J2 cells, and human fetal intestinal lines, provide valuable platforms for studying how human milk and formulae influence epithelial development. However, no model physiologically represents the high permeability of the neonatal intestine. Transiently increasing permeability in these cellular models offer promising strategies to model the immature intestinal barrier and guide nutritional interventions that promote intestinal development and lifelong health.

Keywords: Infant gut barrier, Permeability, Mucus, Brush border, *In vitro* epithelial barrier, Human Milk

1.1. Introduction

The intestinal barrier is a dynamic, multilayered structure that regulates the selective exchange of nutrients and water while preventing the translocation of pathogens and harmful macromolecules from the gut lumen into systemic circulation (Vancamelbeke and Vermeire, 2017). In newborns, this barrier is functionally immature. During the first days after birth, the epithelium is highly permeable to allow the passage of macromolecules (*i.e.*, maternal immunoglobulin A (IgA) and immunoglobulin M (IgM)) that provide passive immunity. Within 72 h after birth, the epithelial barrier undergoes a reduction in macromolecules (~150 kDa) absorption—the so-called "gut closure" (Weström et al., 2020). However, even after this initial closure, the infant intestinal barrier remains more permeable than that of adults, displaying enhanced paracellular transport up to 15 months (Catassi et al., 1995; Kosek et al., 2017; Weaver et al., 1984).

Human milk supports gut closure (Ballard and Morrow, 2013) by strengthening the epithelial barrier, decreasing intestinal permeability and promoting mucosal development (Catassi et al., 1995). In contrast, infants fed with formula, do not exhibit the same degree of improvement in barrier integrity as those who are breastfed (Catassi et al., 1995). A slower gut maturation poses a risk to infants, as high permeability may facilitate antigen and bacterial translocation, leading to inflammation and gastrointestinal disorder such as necrotizing enterocolitis (NEC) (Anand et al., 2007). Understanding the functional maturation of the infant gut barrier is thus critical for informing strategies to enhance formula composition that supports barrier maturity.

Structurally, the gut barrier is composed of several interdependent layers (Fig. 1.1). The outermost mucus layer, secreted by goblet cells, forms the most intimate barrier between the gut epithelium and the lumen. It serves as a physical and biochemical defense against microorganisms (McGuckin et al., 2011), dietary antigens (Parrish et al., 2022), and digestive secretions (Song et al., 2023). In the small intestine, a single, penetrable mucus layer permits nutrient diffusion and brush border enzymes activities (Herath et al., 2020), while in the colon, a double-layered mucus structure separates the dense microbial population from the epithelium (Johansson et al., 2011b). The mucus is primarily composed of glycoproteins known as mucins, which can be neutral or acidic, either sulfated (sulfomucins) or sialylated (sialomucins), contributing to regional and functional heterogeneity along the intestine (Johansson et al., 2011a).

Beneath the mucus, the epithelial monolayer forms the core of the small intestinal barrier. It consists mainly of enterocytes (~70-80% of epithelial cells (Hickey et al., 2023)), which mediate nutrient, ion, and water absorption and contribute to barrier integrity through tight junctions and antimicrobial peptide secretion (Peterson and Artis, 2014). Goblet cells (~15-20 % of epithelial cells (Hickey et al., 2023)) produce and secrete mucins, mainly MUC2, that form the protective mucus layer and modulate host–microbe interactions (Birchenough et al., 2015). Paneth cells (~2–5 % of epithelial cells (Hickey et al., 2023) are located at the base of crypts and release antimicrobial peptides such as α-defensins and lysozyme (Bevins and Salzman, 2011). Enteroendocrine cells (< 1 % of epithelial cells (Hickey et al., 2023) act as chemo-sensors that detect luminal nutrients and secrete hormones (e.g., GLP-1, CCK) to regulate digestion, motility, and appetite (Gribble and Reimann, 2019). Tuft

cells (~0.4–2 %) function as sentinels that detect parasitic and chemical stimuli and initiate type-2 immune responses via secretion of IL-25 (Silverman et al., 2024). Finally, sparse M (microfold) cells (< 1 %) overlying Peyer's patches facilitate antigen sampling and transport to mucosal immune cells, initiating adaptive responses (Mabbott et al., 2013). Although each epithelial cell type fulfills specialized functions, enterocytes play a central role in integrating absorption with barrier regulation. Their organization and junctional architecture are therefore key to understanding how the intestinal epithelium balances permeability and nutrient uptake.

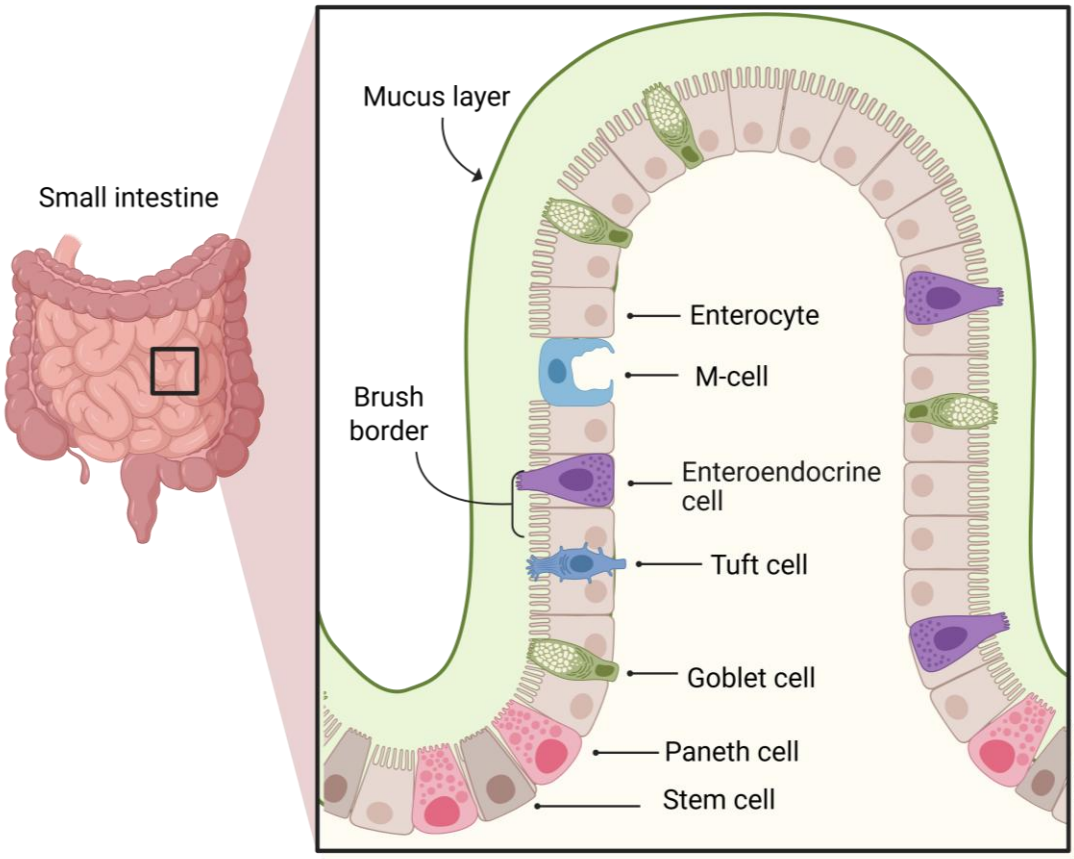


Fig. 1.1 Overview of the main epithelial cell types forming the small intestinal barrier.

In enterocytes, tight junctions regulate paracellular permeability (Otani and Furuse, 2020). Tight junctions are multiprotein complexes that seal the paracellular space between enterocytes and control selective permeability across the intestinal epithelium (Fig. 1.2). They are composed of transmembrane proteins, mainly claudins, occludin (OCLN), and junctional adhesion molecules (JAMs), anchored to cytoplasmic scaffolds such as zonula occludens (ZO1, ZO2, ZO3), which link the junction to the perijunctional actomyosin ring (Citi et al., 2024; Otani and Furuse, 2020). Claudins form charge- and size-selective pores that regulate ionic flux, whereas OCLN and ZO proteins primarily stabilize the junction and modulate the "leak" pathway for larger solutes (Otani and Furuse, 2020). Tight junction integrity is influenced by luminal factors, including foods. Disruption of tight junctions structure and signaling is a key event in the pathogenesis of NEC (Managlia et al., 2022), where loss of CLDN3 and OCLN expression (Bein et al., 2018; Clark et al., 2005) correlates with epithelial sloughing, bacterial translocation, and mucosal inflammation (Clark et al., 2005; Ravisankar et al., 2018). Collectively, tight junctions act as dynamic regulators of intestinal barrier integrity, responsive to nutritional and environmental cues.

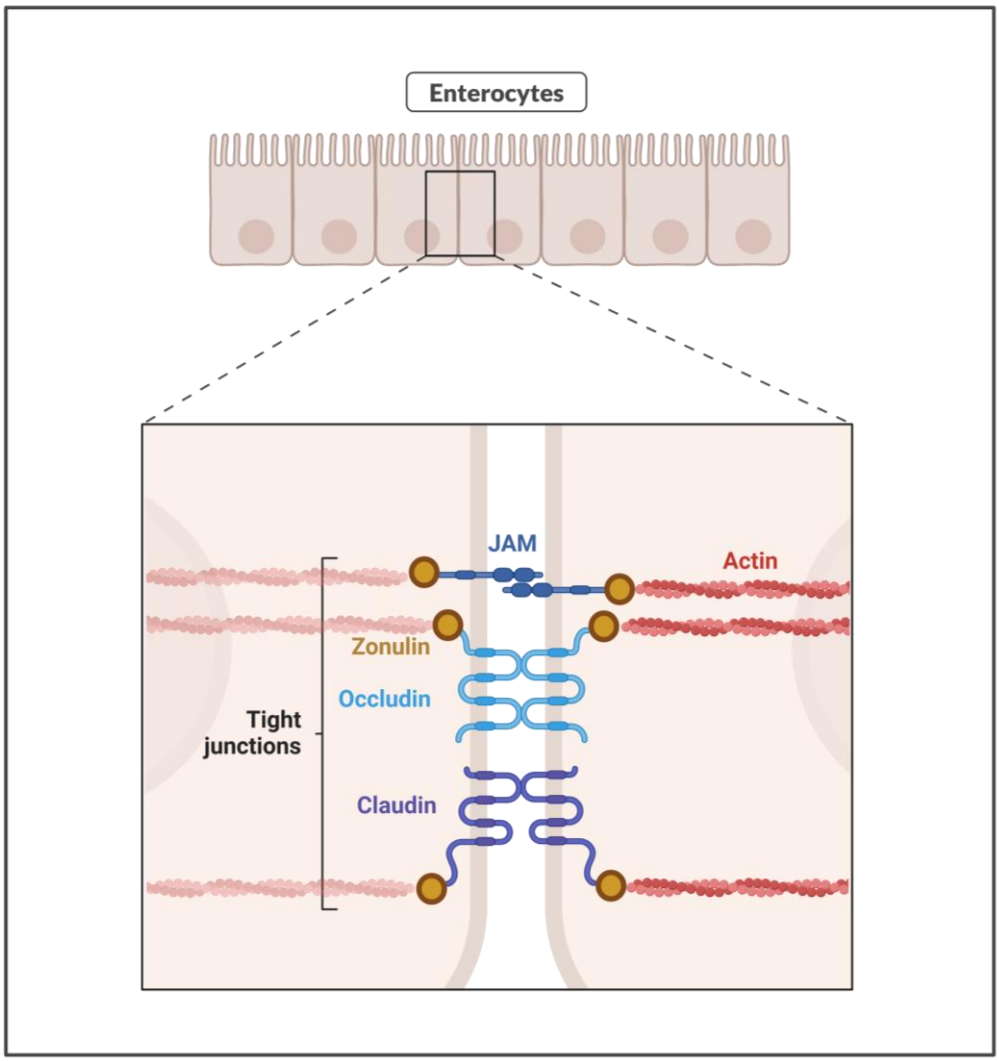


Fig. 1.2 Schematic representation of the intestinal epithelial tight junction complex. Transmembrane proteins such as occludin (OCLN), claudins (CLDNs), and junctional adhesion molecules (JAMs) form selective seals between adjacent enterocytes. These proteins are anchored to cytoplasmic scaffolding proteins including zonula occludens (ZOs), which connect the junctional complex to the perijunctional actomyosin ring composed of filamentous actin.

On the apical surface of enterocytes, dense microvilli form the brush border, which greatly expands the absorptive surface area and houses both digestive enzymes and membrane transport proteins essential for nutrient assimilation. The plasma membrane of these enterocytes forms the structural basis of the brush border, functioning as a dynamic lipid bilayer whose composition determines its physical properties and behavior. Its lipid makeup directly influences membrane fluidity, which in turn governs the diffusion of small molecules, the activity and trafficking of transporters and enzymes, and ultimately the efficiency of nutrient absorption (Harayama and Riezman, 2018). The brush border enzymes are membrane-anchored hydrolases that catalyze the final steps of nutrient digestion immediately before absorption. They are functionally classified into oligosaccharidases, oligopeptidases, and lipases (Hooton et al., 2015). Among the oligosaccharidases, lactase–phlorizin hydrolase (LPH, *LCT*, 2q21, EC 3.2.1.108/3.2.1.62) contains two active sites, one hydrolyzing lactose into glucose and galactose, and the other splitting phlorizin into phloretin and glucose (Hooton et al., 2015). Sucrase–isomaltase (SI, *3q26.1*, EC 3.2.1.10/3.2.1.48) is a dual enzyme complex: sucrase hydrolyzes α-1,4-linked oligosaccharides, while isomaltase acts on α-1,4 and α-1,6 linkages in starch and branched glucans (Hooton et al., 2015). The oligopeptidases include aminopeptidase N (APN, ANPEP, 15q25.1, EC 3.4.11.2), aminopeptidase A (APA, ENPEP, 4q25, EC 3.4.11.7), dipeptidyl peptidase IV (DPP-IV, DPP4, 2q24.2, EC 3.4.14.5), aminopeptidase P (APP, XPNPEP2, Xp22.11, EC 3.4.11.9), carboxypeptidases such as ACE (17q23.3, EC 3.4.15.1) and GCPII (11p11.2, EC 3.4.17.21), and the endopeptidases meprin β (18q12.1, EC 3.4.24.63) and neprilysin (3q25.2, EC 3.4.24.11), which together aim to complete hydrolysis of peptides to free amino acids. The brush border also contains lipases such as alkaline sphingomyelinase

(*ENPP7*, 17q25.3, EC 3.1.4.12) and neutral ceramidase (*ASAH2*, 10q11.23, EC 3.5.1.23), which hydrolyze sphingolipids (Duan et al., 2007). In addition, the brush border enzyme alkaline phosphatase (IAP, *ALPI*, 2q37.1, EC 3.1.3.1), is a multifunctional enzyme involved in lipid absorption, detoxification of bacterial lipopolysaccharide (LPS), and regulation of gut microbiota diversity (Singh et al., 2020).

Following enzymatic digestion, the resulting monosaccharides, amino acids, peptides, and lipids are transported into enterocytes through highly specialized membrane transporters. For carbohydrates, absorption is mediated by a set of sodium-dependent and facilitative transporters that ensure efficient monosaccharide uptake. Glucose and galactose enter the enterocytes across the apical membrane through the Na^+-dependent cotransporter SGLT1 (SLC5A1) and are exported basolaterally by the facilitative transporter GLUT2 (SLC2A2), whereas fructose is transported through GLUT5 (SLC2A5) on the apical side and GLUT2 on the basolateral side (Koepsell, 2020).

Peptide transport is primarily mediated by the H^+-dependent cotransporter PEPT1 (SLC15A1) (Choudhuri and Chanderbhan, 2016). In parallel, amino acid transport across the apical brush border is mediated by several Na^+- or H^+-coupled cotransporters, including B^0AT1 (SLC6A19) for neutral amino acids, EAAT3 (SLC1A1) for acidic amino acids and SIT1 (SLC6A20) and PAT1 (SLC36A1) for amino acids like proline and glycine. At the basolateral membrane, facilitative exchangers such as LAT1 (SLC7A5) and LAT2 (SLC7A8) mediate the efflux of large neutral amino acids, while y^+LAT1 (SLC7A7) and y^+LAT2 (SLC7A6) enable the exchange of cationic and neutral amino acids (Kandasamy et al., 2018).

Lipid absorption involves both passive diffusion and protein-mediated transport mechanisms, notably via FAT/CD36 (CD36, 7q11.2; SR-B2) for long-chain fatty acids (Glatz & Luiken, 2017), and Niemann–Pick C1-like 1 transporter (NPC1L1, 7p13) for cholesterol (Altmann et al., 2004). Inside the enterocyte, lipids are re-esterified and assembled into chylomicrons by microsomal triglyceride transfer protein (MTP, 4q24) with apoB-48 (APOB, 2p24.1) and apoA-IV (APOA4, 11q23.3) before secretion into the lymphatic system (Mansbach and Siddiqi, 2010).

Paracellular pathways provide a size- and charge-selective route for small hydrophilic solutes through two distinct routes: a highly selective pore pathway and a leak pathway that permits intermittent passage of larger molecules (Horowitz et al., 2023). Together, these routes contribute not only to ion and water homeostasis but also to the paracellular absorption of small, water-soluble nutrients (Horowitz et al., 2023). The composition of tight-junction proteins defines the relative contribution of these pathways and thus the overall paracellular transport properties ((Citi et al., 2024).

All of these components, mucus, tight junctions, paracellular pathways, brush border enzymes, and membrane transporters, are developmentally regulated. Their expression, localization, and activity change markedly from the fetal period through infancy and into adulthood. This dynamic maturation process determines how efficiently nutrients are digested and absorbed, while also influencing the barrier's permeability to xenobiotics and microbial products.

At birth, the small intestine of a full-term infant measures approximately ~2–4 m, whereas in adults it extends to about ~5–6 m (Weaver et al., 1991). Yet, the differences go far beyond size.

In this review, the infant intestinal barrier and its *in vitro* models are examined, focusing on how structural and functional immaturity affects permeability, digestion, and nutrient transport.

1.2. Cellular and Molecular Features of the Infant Gut Barrier

1.2.1. Mucus Layer: The First Adaptive Shield of the Neonatal Gut

The postnatal intestinal mucus barrier has been investigated at multiple levels, from direct transport properties to protein composition and transcript-level regulation. Together, these studies reveal age-dependent changes in mucus structure and function, which differ across species and experimental models. In human preterm infants recovering from NEC, Schaart et al. (2009) provided the only direct measurement of mucus biosynthesis to date. By infusing [U-^{13}C]threonine and collecting enterostomy effluent, the study revealed a remarkably high MUC2 fractional synthesis rate (FSR; median 67% per day), corresponding to a turnover time of only 3–12 hours (Schaart et al., 2009). In comparison, adult small intestinal mucosal proteins exhibit much slower synthesis rates, typically ranging from 15–51% per day along the intestine (Nakshabendi et al., 1999; Rittler et al., 2000).
In pigs, neonatal mucus is more permeable and less viscous, with higher particle diffusivity than in adults (Krupa et al., 2020; Macierzanka et al., 2014). Viral transport studies by Saleem et al. (2024) observed that transmissible gastroenteritis virus moved freely in mucus from 3-day piglets but was significantly hindered in mucus from 3-week piglets. This hinderance lowered, infection rates nearly threefold (Saleem et al., 2024). In premature piglets, nanoparticle mobility decreases and goblet cell density increases as piglets are born closer to gestational term (Mortensen et al., 2024).

Rodent models mirror these patterns. In rats, protective mucus first appears around day 4 of age and matures by day 9–11, coinciding with resistance to *E. coli* K1 (Birchenough et al., 2017). In the mouse colon, the inner mucus layer thickens from ~50 μm at birth to ~100 μm by day 15, shifting from penetrable to impenetrable by day 3 (Johansson et al., 2025). Lock et al. (2020) showed that neonatal rat mucus is more permeable than at weaning, but human milk components (lysozyme, DHA) reduce particle diffusion and bacterial motility (Lock et al., 2020). Interestingly, rabbit mucus shows a progressive decline in phospholipids from birth to adulthood, as determined by phospholipid extraction and thin-layer chromatography (Okuyama et al., 1998).

Protein quantification studies provide additional information. In pigs, studies show an age-dependent switch in mucin isoforms, with early MUC13 expression giving way to MUC2 dominance and increased goblet cell output during weaning (Mortensen et al., 2024; Saleem et al., 2024). Pig colonic mucins also undergo chemical maturation, transitioning from sulfate-rich at birth to reduced sulfate by weaning, with adults showing further declines in sulfate and protein levels (Turck et al., 1993). In rats, MUC2 staining demonstrates the stepwise appearance of protective mucus in the small intestine during the first postnatal week (Birchenough et al., 2017). In mice, MUC2 and its processing enzymes, Clca1 and Tgm3, increase during early life, peaking around day 15 before stabilizing at lower adult levels (Johansson et al., 2025). Histochemical and comparative evidence indicate that neonatal goblet cells predominantly secrete sulfated mucins, which reorganize into an adult-like, more sialylated profile during weaning. Notably, this postnatal transition depends on microbial colonization (Deplancke and Gaskins, 2001; Hill et

al., 1990). Finally, Cummins et al. (1988) showed that in rat jejunum, goblet cells increased 19-fold between days 12 and 22, and then declined after weaning (Cummins et al., 1988).

In summary, studies across humans, pigs, and rodents consistently demonstrate that neonatal intestinal mucus is structurally distinct from the adult barrier.

1.2.2. Dynamic Membranes: Fluidity as a Developmental Gatekeeper of Nutrient Uptake

The most direct evidence for developmental changes in intestinal membrane permeability and lipid organization comes from Meddings and Theisen (1989), who combined *in vivo* functional assays with *ex vivo* biophysical measurements in the developing rat small intestine. Using *in situ* perfusion of jejunal and ileal loops with non-polar lipid probes, the study quantified epithelial lipid permeability at different postnatal ages and found that permeability was maximal during the suckling period (9 days) and declined sharply at weaning (25 days) (Meddings and Theisen, 1989). To relate these functional changes to membrane structure, fluorescence anisotropy of isolated microvillus membranes from the same tissues was measured, revealing a developmental reduction in membrane fluidity occurring in parallel with the fall in permeability (Meddings and Theisen, 1989). Moreover, the membrane hydrophobicity decreased from -459 ± 30 to -358 ± 60 cal·mol^{-1}, indicating tighter lipid packing (Meddings and Theisen, 1989).

Similarly, in rats, Brasitus et al. (1984) found that membrane fluidity in the small intestine fell by about twofold between day 1 and day 7, reflecting tighter lipid packing as the tissue matured (Brasitus et al., 1984). Lindner et al. (1987) later showed that this trend continues into adulthood with membrane flexibility

decreasing steadily from newborn to adult rats (Lindner et al., 1987). Hübner et al. (1988) quantified this change and reported a significant increase in membrane rigidity during development, confirming a steady loss of lipid mobility (Hübner et al., 1988). Comparable results were obtained in rabbits. Schwarz et al. (1984) observed that membranes from both the jejunum and ileum became progressively more ordered, from the suckling stage (14–21 days) to adulthood (≥ 42 days) (Schwarz et al., 1992). Specifically, adult membranes displayed a distinct thermal transition at 23–25 °C, a temperature point where lipids reorganize from a fluid to a more tightly packed state, indicating the emergence of ordered lipid domains. Such a transition was absent in younger animals, whose membranes remained uniformly fluid. Supporting these observations, Pang et al. (1983) showed that newborn rabbit membranes lacked this thermal transition and remained uniformly fluid, whereas adult membranes exhibited a clear transition at 39.6 ± 0.3 °C, marking the development of ordered lipid domains characteristic of mature intestinal membranes (Pang et al., 1983). Changes in membrane composition parallel the developmental decline in fluidity. In rats, Lindner et al. (1987) measured a cholesterol-to-phospholipid ratio (C:P) increase from 0.90 ± 0.16 in neonates (1-3 weeks) to 1.45 ± 0.15 in adults (12-weeks), and Hübner et al. (1988) confirmed this rise, correlating it with a significant increase in membrane rigidity (Hübner et al., 1988). In rabbits, Schwarz et al. (1984) found similar values, with the C:P ratio increasing from 0.56 (14 days-old) to 0.83 (>42-days old) in the jejunum (Schwarz et al., 1992). In contrast, Brasitus et al. (1984) reported that during the first postnatal week, the C:P ratio decreased from ~0.91 at birth to ~0.66 at weaning (Brasitus et al., 1984), while Meddings and Theisen (1989) found that between day 9 and 25 in rats, the C:P ratio remained constant (0.87 ± 0.08 → 0.84 ± 0.04) (Meddings and Theisen, 1989).

However, during this period, the fatty acid composition shifted toward longer and more saturated chains, accompanied by an increase in phosphatidylcholine and sphingomyelin at the expense of phosphatidylethanolamine and phosphatidylinositol. Hübner et al. (1988) and Lindner et al. (1987) both recorded an increase in the saturated:unsaturated fatty-acid ratio with age (Hübner et al., 1988; Lindner et al., 1987), while Schwarz et al. (1985) found that sphingomyelin and phosphatidylinositol contents decrease and phosphatidylcholine increases during maturation—a lipid profile consistent with reduced fluidity (Schwarz et al., 1985). Chu and Walker (1988) further showed that neonatal rat membranes contain higher palmitate/stearate (16:0/18:0) and oleate/linoleate (18:1/18:2) ratios than adults, indicating shorter, more monounsaturated chains that promote greater lipid mobility (Chu and Allan Walker, 1988). In rabbits, Keelan et al. (1985) observed a progressive rise in total lipid per protein and higher brush-border enzyme activities with age, linking biochemical stabilization of the bilayer to functional maturation of the intestinal epithelium (Keelan et al., 1985). Therefore, the high fluidity typical of early development is driven by lipid composition rather than sterol content. Collectively, these findings reveal a consistent developmental trend. The neonatal membrane behaves like warm wax, pliable and dynamic, before hardening into a more rigid seal as development proceeds. This heightened fluidity is not a structural flaw but a physiological feature, in other words, membrane fluidity acts as a developmental gatekeeper, flexible early to permit adaptation, rigid later to ensure protection.

1.2.3. Adaptive Permeability: Tight Junction Plasticity as a Developmental Signal

There is evidence that paracellular transport changes with age. It is accepted that the neonatal intestine differs from adult in both permeability magnitude and selectivity. The following sections summarize functional and molecular evidence describing how paracellular permeability and tight-junction architecture mature postnatally.

Paracellular permeability

In humans, intestinal permeability has been consistently shown to decline with age during infancy. Weaver et al. (1984) measured urinary lactulose:mannitol (L:M) ratios in infants and reported that permeability at 3 months was ~55% higher than at 15 months, indicating progressive barrier closure (Weaver et al., 1984). Kosek et al. (2017) extended these findings, showing that mean lactulose recovery decreased from 0.28 % at 3 months to 0.18 % at 15 months (≈ 55 % reduction), and that the L:M ratio declined from 0.17 → 0.10 (≈ 40 % decrease), reflecting progressive tightening of the paracellular pathway through infancy (Kosek et al., 2017). Johnston et al. (2000) studied 1–12 month-old infants compared with older children and found that the L:M ratio decreased inversely with age, confirming ongoing maturation of paracellular barrier function throughout the first year (Johnston et al., 2000). Extending these data, Faubion et al. (2016) used a urinary lactulose:rhamnose (L:R) assay (HPLC-MS) in children under 5 years from the U.S., Peru, and Zambia. Median L:R ratios were 0.14 in the U.S., 0.75 in Peru, and 2.26 in Zambia, with 82% of Zambian and 53% of Peruvian children above the U.S. 95th percentile, indicating markedly elevated permeability in environmental enteric dysfunction-endemic settings (Faubion et al., 2016).

Large animal data are consistent with human findings. Weström et al. (2020) summarized experimental work in piglets, showing that intestinal uptake of FITC-dextran, immunoglobulins, and lactoferrin is high in neonatal pigs but declines sharply after weaning (7–10 months), reaching values comparable to adults (Weström et al., 2020). In mice, Gleeson et al. (2021) measured *in vivo* FITC-dextran (70 kDa) absorption and found ~4-fold higher uptake in 2-week-old pups compared to 12-week adults, while non-everted gut sacs confirmed a ~2-fold increase in neonatal permeability (Gleeson et al., 2021). In the same study, oral insulin (5.8 kDa) gavage produced a 35% hypoglycemic response relative to injected insulin in neonates, compared to <1% in adults, and lactoferrin (80 kDa) absorption was significantly higher in neonates (Table 1.1).

Collectively, these functional assays demonstrate that the neonatal intestine is markedly more permeable to macromolecules, with permeability progressively declining after weaning.

Table 1.1 Summary of studies asessing age-dependent changes in intestinal paracellular permeability across mammalian species.

The table outlines the experimental models, age ranges, intestinal regions, permeability markers, and analytical methods used to evaluate intestinal barrier function. Abbreviations: L:M, lactulose:mannitol ratio; L:R, lactulose:rhamnose ratio; TEER, transepithelial electrical resistance; HPLC, high-performance liquid chromatography; LC-MS/MS, liquid chromatography–tandem mass spectrometry; HPAE-PAD, high-performance anion-exchange chromatography with pulsed amperometric detection; FITC, fluorescein isothiocyanate; CLDN2, claudin-2; wk, weeks; mo, months; h, hours. Symbols: ↑, increase; ↓, decrease; ≈, approximately.

Reference	Species / Model	Age / Condition	Region / Tissue	Feature / Metric	Methods (brief)	Key Quantitative Results	Interpretation / Key Findings
(Weaver et al., 1984)	Human neonates (preterm vs term)	Preterm (<34 wk) vs late-preterm (34–37 wk) vs term; Days 1–7	Whole small intestine	L:M ratio	Oral L:M solution, 6-h urine collection, high-performance liquid chromatography (HPLC)	L:M ↓ >50 % by Day 4 in late-preterm; preterm ≈ 2–3× > term at Day 1.	Rapid decline in intestinal permeability during the first postnatal week.
(Catassi et al., 1995)	Human infants (full-term)	Day 1 → Day 30	Whole small intestine	L:M ratio	Oral dual-sugar test, urinary HPLC	L:M ↓ 83 % (1.27 ± 0.11 → 0.22 ± 0.02) over 30 d; Day 7: breast = 0.22 vs formula = 0.47 ($p = 0.002$) → ~2× tighter barrier in breast-fed.	Human milk halves intestinal permeability within the first week of life.
(Johnston et al., 2000)	Human preterm infants (≤32 wk gestation)	Days 7–30	Whole small intestine	L:M ratio	Oral L:M test (100 mg lactulose + 40 mg mannitol·kg^{-1}), 6-h urine, enzymatic gas-chromatography assay	≥75 % human milk intake → L:M ↓ 3.8× vs ≤25 %; formula-fed = 2.8× ↑ L:M ($p < 0.05$).	Higher human-milk intake tightens the intestinal barrier.
(Faubion et al., 2016)	Children (USA, Peru, Zambia)	2–36 mo	Small intestine	L:R ratio	60–90 min urine collection, liquid chromatography–(LC-MS/MS	Median L:R — USA 0.14 < Peru 0.75 (×5) < Zambia 2.26 (×16) ($p < 0.001$).	Higher permeability in low-income settings.
(Kosek et al., 2017)	Human infants (MAL-ED, 8 countries)	3, 6, 9, 15 mo	Small intestine	L:M ratio; probe recovery (%)	Standardized 5-h dual-sugar protocol	Median L:M ↓ 40 % (0.17 → 0.10) from 3 → 15 mo; boys +25–30 % higher lactulose recovery vs girls.	Permeability decreases across infancy. Boys had higher permeability than girls.
(Musa et al., 2019)	Human infants	7–26 mo (mean 15 mo)	Small intestine (dual-sugar test)	L:M ratio and sugar recovery (%)	LC-MS/MS vs high-performance anion-exchange (HPAE-PAD); 2-h vs 5-h urine	5 h collection ↑ probe recovery 20–30 %, L:M ↔ (d≈ 0.6, 2 h vs 5 h).	Shorter 2-h urine sampling gives equivalent L:M ratios.
(Adeniyi-Ipadeola et al., 2024)	Human intestinal enteroids	Infant (10–22 wk) vs adult (46–52 yr)	Jejunum and ileum	TEER, fluorescein-dextran flux, tight-junction proteins	Enteroid monolayers; TEER electrode; EGTA challenge;	TEER (infant) ≈ ⅓ adult ($p = 0.0003$); CLDN2 ↑ 2×; FITC–dextran flux 20 vs 6.5 µg/mL	Infant barrier leakier (↓TEER, ↑CLDN2, ↑flux).

					Western blot; RNA sequencing		
(Westrom et al., 1984)	Piglet (newborn)	0–168 h postnatal	Small intestine	Polyethylene glycol-600 (PEG-600) and macromolecule uptake (ovalbumin, bovine serum albumin)	Oral gavage, serum probe quantification	PEG-600 + protein uptake ↑ at birth → ↓ 80–90 % by 24–48 h → baseline by 7 d.	Rapid gut closure within 2 d post-birth.
(Gleeson et al., 2021)	Mouse (juvenile vs adult)	2 wk vs 12 wk	Small intestine and colon	Fluorescein-dextran permeability and oral protein absorption	Non-everted gut sacs, oral gavage, fluorescence and ELISA	FD70 Papp (2 wk) ↑ 2–5× vs adult; serum AUC ↑ 4×; oral insulin (5 IU·kg^{-1}) ↓ glucose >20 % vs <1 %; lactoferrin abs. ↑ 4×.	Infant absorb macromolecules ≈ 4× more than adults.

Tight junctions

In pigs, Pasternak et al. (2015) analyzed jejunum and ileum for tight junction protein location, using immunofluorescence. In neonates (≤2 days), CLDN4 was localized diffusely along the apical membrane of villus epithelial cells, whereas by 6 weeks of age CLDN4 was confined to the lateral tight junction region (Pasternak et al., 2015). In mice, Patel et al. (2012) measured CLDN3 protein localization by immunofluorescence and Western blot. In neonatal epithelium (≤3 weeks), CLDN3 was restricted to crypts, while in adults it was distributed throughout villus epithelium (Patel et al., 2012). Holmes et al. (2006) quantified claudin mRNA and protein in jejunum and ileum from postnatal day 1 to adulthood. CLDN2 expression decreased continuously with age, while CLDN3, CLDN4, CLDN7, and CLDN15 increased. Localization analysis showed CLDN2 was intracellular in neonates but junctional in adults (Holmes et al., 2006). Finally, Gleeson et al. (2021) compared 2-week-old and 12-week-old mice, reporting that mRNA levels of ZO1, OCLN, JAM-A, and CLDN3 were significantly lower in neonates, while CLDN2 and CLDN5 were increased (Gleeson et al., 2021). Unfortunately, no such studies have been performed on humans (Table 1.2).

The developmental choreography of these proteins suggests that the neonatal gut does not aim for impermeability, but for selective permeability: a compromise that allows immune education and nutrient sampling, whilst avoiding pathogen invasion. Thus, tight junction plasticity can be viewed as a molecular signature of the infant's balancing act between openness and defense.

Table 1.2 Developmental differences in tight junction protein expression and localization between infant/newborn and adult intestinal epithelium.

The table presents experimental models, developmental stages, intestinal regions, and methods used to assess tight junction composition, localization, and barrier function. Abbreviations: CLDN, claudin; OCLN, occludin; ZO1, zonula occludens-1; JAM, junctional adhesion molecule; TEER, transepithelial electrical resistance; FITC, fluorescein isothiocyanate; FD4/FD70, fluorescein dextran (4/70 kDa); IHC, immunohistochemistry; qPCR, quantitative polymerase chain reaction; RNA-Seq, RNA sequencing; yr, year; wk, weeks; d, days; h, hours. Symbols: ↑, increase; ↓, decrease; ≈, approximately.

Reference	Species / Model	Age / Condition	Region / Tissue	Feature / Metric	Methods (brief)	Key Quantitative Results	Interpretation / Key Findings
(Adeniyi-Ipadeola et al., 2024)	Human intestinal enteroids (infant vs adult donors)	Infant (10–22 wk) vs adult (46–52 yr)	Jejunal enteroid monolayers	Tight junction proteins (CLDN, OCLN, ZO1); TEER; FITC-dextran flux	RNA-Seq, Western blot, TEER electrodes, FITC-dextran permeability (±EGTA)	CLDN3/4 ↓, CLDN2 ↑ 2× ($p = 0.005$); TEER (infant) = ⅓ adult ($p = 0.0003$); FITC–dextran flux 20 vs 6.5 µg/mL (infant/adult)	Infant TJs are leakier
(Pasternak et al., 2015)	Piglet (conventional and gnotobiotic)	0–2 d, 3–5 d, 6 wk	Jejunum and ileum	CLDN4 localization	Immunohistochemistry (IHC), confocal microscopy, qPCR	CLDN4 apical (0–2 d) → lateral (3–5 d) → strong lateral (6 wk); ileum apical → lateral within 24 h.	CLDN4 rapidly relocalizes apical→lateral, sealing junctions within days.
(Yuan et al., 2021)	Piglet	Neonatal vs weaned	Duodenum, jejunum, ileum	CLDN3,OCLN, ZO1, and E-cadherin mRNA/protein	IHC, quantitative RT-PCR	CLDN3 protein ↑ (duodenum); CLDN + OCLN mRNA ↑ 2–4× (duodenum/jejunum); ZO1 & E-cad =.	Weaning ↑ TJ gene expression
(Holmes et al., 2006)	Mouse	Postnatal Day 1, 14, 28 vs adult (~Day 90)	Jejunum and full intestinal axis	CLDN1–19 transcripts, ZO1, OCLN, JAM	qRT-PCR, immunofluorescence microscopy	CLDN19 ↓ to 0 (Day 1–14 → adult); CLDN3/4 ↑ 2–20×; ZO1, OCLN, JAM = (≤2×).	Postnatal shift from CLDN19 to CLDN3/4 strengthens tight-junction sealing during maturation.
(Patel et al., 2012)	Mouse (C57BL/6)	Neonate (~1–2 wk), 3 wk, adult (8 wk)	Distal small intestine	CLDN3 mRNA/protein; fluorescein-dextran (FD4) permeability	qPCR, immunofluorescence, Western blot, oral FD4 assay	FD4 permeability 14.9 → 3.8 µg/mL (≈4×↓) (neonate→adult); CLDN3 mRNA ↑ 3–11×; LGG probiotic ↑ 2× CLDN3, expands staining crypt → villus..	Infants show higher permeability; probiotic doubles CLDN3 and speeds TJ maturation.
(Bergmann et al., 2013)	Mouse (neonatal necrotizing enterocolitis model) and human NEC tissue	NEC-induced pups (12–72 h stress) vs dam-fed controls	Small intestine and colon	CLDN2, CLDN4, CLDN7, OCLN; tight junction length; permeability	IHC, EM, subcellular fractionation, FD70 flux, qPCR	TJ length ↑ 24 % (0.31 vs 0.25 µm, NEC vs ctrl); CLDN2 ↑ at 6 h, CLDN4/7 ↓ at 24 h, OCLN internalized at 12 h; *B. infantis*	NEC induces leaky TJ pattern; *B. infantis* preserves junction integrity.

						prevented all changes prevented these changes.	
(Gleeson et al., 2021)	Mouse (infant vs adult)	2 wk (infant), 4 wk (juvenile), 12 wk (adult)	Stomach and small intestine	CLDN2, CLDN3, CLDN5, OCLN, ZO1, JAM-A; fluorescein-dextran (FD70) permeability	qPCR, immunofluorescence, permeability assays (Papp), oral pharmacokinetics	FD70 Papp ↑ 2–5×, lactoferrin absorption ↑ 4× (infant vs adult); CLDN3 mRNA ↓ 3–5×, CLDN2 ↑.	Infant barrier leakier (↑permeability, ↑CLDN2, ↓CLDN3)

1.2.4. Enzymatic Maturation: From Milk Digestion to Omnivore Efficiency

During postnatal development, intestinal brush-border enzyme expression is dynamically regulated. In infancy, activities are tailored to efficient milk digestion, whereas following weaning they shift to accommodate a more diverse diet. The following sections summarize the ontogeny of the major brush-border hydrolases, highlighting key differences between infant and adult intestinal function (Table 1.3).

Lactase–phlorizin hydrolase

In humans, lactase activity is already high at 1 month (24 ± 1.6 μmol·min^{-1}·g^{-1} protein) and typically declines thereafter in non-persistent phenotypes, establishing a fall in activity from infant to childhood (Lebenthal and Lee, 1980). In contrast, lactase-persistent populations maintain substantial activity into adulthood, with prevalence highest in parts of northern Europe (Gerbault et al., 2011). This matches milk consumption by adults in northern European countries. At the protein level, infant and adult human lactase are the same enzyme with identical 160 kDa subunits with co-localized phlorizin hydrolase, indicating adult hypolactasia reflects quantitative down-regulation rather than an isoform change (Potter et al., 1985). Transcriptionally, Wang et al. (1998) compared allelic expression of lactase (*LCT* gene) in intestinal biopsies from children aged 3 to 132 months and found that the proportion of mRNA derived from the high-expressing C allele decreased from 49% at 3 months to 27% at 42 months, 20% at 50 months, and 6% at 132 months (Wang et al., 1998). This pattern indicates a progressive transcriptional down-regulation of *LCT* gene during early childhood, consistent with the post-weaning decline in lactase activity. This indicates that enzyme activity declines despite persistent mRNA,

demonstrating post-transcriptional control during the suckling-to-weaning transition (Freund et al., 1991).

In pigs, a progressive decrease in lactase activity occurs across all intestinal segments between weeks 1 and 6 (Shulman et al., 1988). At birth, activity reaches 12–14 μmol·h^{-1}·mg^{-1} protein and declines by 60–70% by day 24 (James et al., 1987). Developmental profiling from birth to 8 weeks confirms high neonatal lactase levels fall as sucrase appears after the first week (Manners and Stevens, 1972).
In rats, a marked postnatal decline in lactase activity is also observed. Jejunal activity decreases by roughly 4–10 fold between birth (day 4) and adulthood (24 months), (Freund et al., 1991). Consistent with this long-term pattern, Meddings and Theisen (1989) quantified lactase in jejunal microvillus membranes during the suckling-to-weaning transition (day 9 to 25), reporting a decline from 1.49 ± 0.11 to 0.53 ± 0.02 U mg^{-1} protein (≈ 65 % reduction) (Meddings and Theisen, 1989). Between 4 and 90 days, lactase mRNA levels in the rat distal ileal is lost while proximal jejunal lactase mRNA persists despite a 5–10-fold fall in enzyme activity, demonstrating region-specific and post-transcriptional regulation during maturation (Duluc et al., 1993).

Sucrase–isomaltase and maltase–glucoamylase

In humans, sucrase–isomaltase and maltase–glucoamylase activities increase from fetal life through infancy into adulthood. Auricchio et al. (1981) showed that sucrase activity rises from 54 ± 27 μmol min^{-1} g^{-1} in fetal intestine to 79 ± 27 μmol min^{-1} g^{-1} in adults, indicating pre- and postnatal maturation (Auricchio et al., 1981). Lebenthal & Lee (1980) reported a substantial duodenal sucrase activity of 51 ± 3

μmol·min^{-1}·g^{-1} protein at 1 month, already approaching adult capacity (Lebenthal and Lee, 1980). Raul et al. (1986) found that by term, sucrase activity is maximal in proximal intestine, and glucoamylase is already detectable in preterm colon, demonstrating that both enzymes are functionally expressed before birth and increase toward term (Raul et al., 1986).

In pigs, sucrase–isomaltase and maltase–glucoamylase activities show a pronounced postnatal rise. Manners & Stevens (1972) observed sucrase absent at birth, appearing by 1 week and reaching mature levels by 8 weeks (Manners and Stevens, 1972), while James et al. (1987) quantified a tenfold increase (0.1 → 1.0 μmol·h^{-1}·mg^{-1} protein) by day 24 (James et al., 1987). Shulman et al. (1988) reported that between weeks 1 and 6, sucrase activity doubled in the ileum and maltase rise 50 % in the jejunum and threefold in the ileum (Shulman et al., 1988). Kinetic studies confirmed this progression: Adeola & King (2006) recorded a 9.2-fold increase in sucrase V_{max} from week 1 to 4, and Fan et al. (2002) found a further 2.7-fold V_{max} increase from days 8 to 70 while affinity ($K_m \approx 15–17$ mM) remained stable (Adeniyi-Ipadeola et al., 2024; Fan et al., 2002). Regional localization also shifts: sucrase–isomaltase I activity peaks proximally early in life and shifts distally with age (Manners and Stevens, 1972).

At the molecular level, Marion et al. (2005) found that early-weaned piglets (weaned at 7 days) exhibited elevated maltase–glucoamylase mRNA but little change in sucrase–isomaltase transcripts. Despite this, both enzyme activities rose sharply after weaning, indicating that sucrase–isomaltase is primarily regulated post-transcriptionally, whereas maltase–glucoamylase responds at both transcriptional and enzymatic levels (Marion et al., 2005).

Similarly, in rats, sucrase–isomaltase activity rises sharply during the suckling–to–weaning transition (from 0.021 ± 0.002 U mg^{-1} protein at day 9 to 0.423 ± 0.020 U mg^{-1} protein at day 25) (Meddings and Theisen, 1989), while lactase activity declines (Cummins et al., 1988). And the gene regulation. At the gene level, Hecht et al. (1997) showed that after weaning in rats, control of the sucrase–isomaltase gene changes: the SIF1 factor is active during suckling, whereas CE-LPH1 takes over in adults to maintain enzyme expression (Hecht et al., 1997).

Peptidases

Auricchio et al. (1981) quantified human intestinal peptidase activities between 8 and 22 weeks of gestation and found that γ-glutamyl transpeptidase was already 2–3 times higher than in adults, while dipeptidyl-aminopeptidase IV and carboxypeptidase had reached adult levels by mid-gestation. Oligoaminopeptidase increased from about 50% to 100% of adult activity by 22 weeks, whereas aminopeptidase A remained at roughly one-third of adult values. In pediatric biopsies (7 months–11 years), enzyme activities were comparable to adults, indicating that most brush-border peptidases attain near-mature levels well before birth (Auricchio et al., 1981). In complementary work, Rubino et al. (1969) detected both glycyl-L-proline and L-glutaminyl-L-proline dipeptidases as early as 14 weeks of gestation, with adult-like activities achieved by 16 weeks. Enzyme activity was consistently higher in the proximal two-thirds of the small intestine and lower distally, and L-glutaminyl-L-proline dipeptidase showed a developmental shift in pH optimum (from 7.2 to 6.3), suggesting a developmental refinement of enzyme function (Rubino et al., 1969).

Moreover, by late gestation, the small intestine already displays an adult-like enzyme pattern, with disaccharidases concentrated proximally (duodenum and jejunum) and peptidases enriched distally (ileum) (Raul et al., 1986; Triadou et al., 1983). This spatial organization is evident even in term infants maintained on parenteral nutrition, indicating that the proximal–distal distribution of digestive enzymes is established before birth and remains stable into adulthood (Raul et al., 1986).

In pigs, aminopeptidase N and dipeptidyl peptidase IV activities rise sharply within days of early weaning (Marion et al., 2005). This shift occurs without parallel mRNA increases for aminopeptidase N or dipeptidyl peptidase IV, indicating post-transcriptional activation during enterocyte maturation. Regionally, aminopeptidase N peaks in the proximal jejunum and is about 40% lower in the duodenum and terminal ileum, with a higher mRNA-to-activity ratio proximally, signifying faster enzyme turnover and post-translational regulation (Torp et al., 1993). In rodents, aminopeptidase N is synthesized as a precursor and processed into its mature brush-border form during differentiation, reinforcing that post-translational maturation is central to peptidase development (Reisenauer et al., 1992).

Intestinal alkaline phosphatase and other lipid hydrolases

Across species, intestinal lipid-hydrolyzing enzymes undergo pronounced developmental changes from the fetal period to adulthood. In humans, intestinal alkaline phosphatase first appears as a fetal isoform that differs kinetically and electrophoretically from the mature enzyme. Fetal and newborn intestinal alkaline phosphatase show substrate inhibition above 2 mM p-nitrophenyl phosphate (p-NPP), whereas the adult enzyme has a Km ≈ 0.1 mM and no inhibition at higher

substrate concentrations (Hernández-Jodra and Gancedo, 1971). In neonates, intestinal alkaline phosphatase carries additional sialic acid residues that increase its negative charge, causing anodal migration during electrophoresis. As these residues are removed postnatally, the enzyme migrates toward the cathode, completing the biochemical "charge switch" from neonatal to adult isoform within the first five days after birth (Kazumasa et al., 1977). Human meconium also contains alkaline sphingomyelinase and neutral ceramidase, with a mean sphingomyelin:cholesterol molar ratio of 0.79 ± 0.06, indicating that sphingolipid-hydrolyzing activity is already functional by 33–42 weeks of gestation (Duan et al., 2007).

In pigs, intestinal alkaline phosphatase activity rises steeply during the suckling-to-weaning transition: jejunal brush-border V_{max} increases from 0.402 to 2.657 μmol mg^{-1} min^{-1}—a 6.6-fold change between weeks 1 and 4 (Adeola and King, 2006). In rodents, alkaline sphingomyelinase and intestinal alkaline phosphatase follow distinct but overlapping developmental patterns. Alkaline sphingomyelinase activity is detectable at fetal day 20 (0.14 ± 0.01 nmol h^{-1} mg^{-1}) and increases about tenfold by day 22, remaining high after birth; parallel rises in protein and mRNA confirm transcriptional induction before birth (Lillienau et al., 2003). In contrast, intestinal alkaline phosphatase peaks briefly between postnatal days 2–7, then declines by weeks 3–4. Western blotting shows higher enzyme protein without a corresponding mRNA increase, indicating mainly post-transcriptional regulation. In contrast, Cummins et al. (1988) measured total alkaline phosphatase activity over a later developmental window (12–30 days) and found a progressive postnatal increase accompanying villus growth and immune maturation, reaching maximal "weaning values" by day 30 (Cummins et al., 1988).

In summary, both intestinal alkaline phosphatase and alkaline sphingomyelinase are active early in life but mature differently. Intestinal alkaline phosphatase peaks soon after birth as a highly glycosylated neonatal isoform, then declines or stabilizes after weaning through post-transcriptional regulation. Alkaline sphingomyelinase, by contrast, is transcriptionally induced before birth, rises about tenfold in late gestation, and remains high into adulthood.

Collectively, these developmental patterns reveal that the infant brush border enzymes are not merely underdeveloped but a finely tuned, stage-specific system optimized for early-life nutrition. High lactase and peptidase activity maximize energy extraction from milk, while the delayed rise of sucrase, maltase, and lipases anticipates the shift to complex foods at weaning. This enzymatic choreography mirrors the infant's shift from a monotypic, milk-based diet to a diversified dietary landscape.

Table 1.3 Summary of studies describing developmental and age-related changes in intestinal brush border enzyme activity and expression between infants/newborns and adults.

The table presents experimental models, developmental stages, intestinal regions, enzyme activities, and analytical methods used to assess brush border maturation. Abbreviations: LPH, lactase-phlorizin hydrolase; DPP-IV, dipeptidyl peptidase IV; GGT, γ-glutamyl transpeptidase; BBM, brush border membrane; ALP, alkaline phosphatase; RT-PCR, reverse transcription polymerase chain reaction; wk, weeks; mo, months; d, days; h, hours. Symbols: ↑, increase; ↓, decrease; ≈, approximately.

Reference	Species / Model	Age / Condition	Region / Tissue	Feature / Metric	Methods (brief)	Key Quantitative Results	Interpretation / Key Findings
(Raul et al., 1986)	Human (preterm and term infants)	28–38 wk gestation; one infant on 12 d total parenteral nutrition (TPN)	Small intestine and colon	Lactase, sucrase, aminopeptidase N, glucoamylase activities	Brush border enzyme assays, histology	Lactase & sucrase ↑ at term vs preterm, maximal proximally; aminopeptidase N & glucoamylase ↑ distally; glucoamylase detectable in preterm colon.	Disaccharidases mature proximally by term, peptidases distally earlier.
(Lebenthal and Lee, 1980)	Human infants (normal vs growth-retarded, 1 mo old)	1 mo	Duodenal mucosa	Disaccharidases (sucrase, maltase, palatinase, lactase)	Crosby–Kugler biopsies, micro-assays	Normal infants — sucrase 51 ± 3, maltase 163 ± 12, palatinase 13.6 ± 1.4, lactase 24 ± 1.6 $\mu mol \cdot min^{-1} \cdot g^{-1}$; growth-retarded: ↓37 %, ↓21 %, ↓36 %, ↓32 % respectively.	Disaccharidase activities near adult levels at 1 mo but reduced by growth retardation.
(Auricchio et al., 1981)	Human fetuses, children, and adults	Fetal 8–22 wk → children (7 mo–14 yr) → adults	Small intestine (whole)	Disaccharidases and peptidases (sucrase, DPP-IV, γ-glutamyl transpeptidase, aminopeptidase A, oligopeptidase)	Homogenate and subcellular fraction assays	Sucrase 54 ± 27 → 79 ± 27 $\mu mol \cdot min^{-1} \cdot g^{-1}$ (fetus→adult); DPP-IV 3.1 ± 2.1 → 23.6 ± 9.8; GGT 26 ± 10 → 41 ± 16.	Brush border enzyme activities appear early in gestation and increase toward adulthood.
(Potter et al., 1985)	Human adults and infants	Infant (biopsy) vs adult	Jejunal membrane extracts	Lactase-phlorizin hydrolase	Immunoassay, electrophoresis, activity measurements	LPH subunits ≈160 kDa; lactase-nonpersistent adults ↓ enzyme activity & ↓ immunoreactivity vs lactase-persistent adults.	Adult hypolactasia reflects reduced LPH quantity, not altered isoform

(Manners and Stevens, 1972)	Pig	Newborn → 8 wk → mature	Six small-intestine sites (5–95 % length)	Lactase-phlorizin hydrolase and sucrase-isomaltase	Mucosal homogenate assays	Sucrase absent at birth → present in all piglets by 1 week; lactase high at birth (max at 20 % intestinal length) → decreased by 8 weeks → stabilized thereafter.	Sucrase appears after birth; lactase declines during early development
(Shulman et al., 1988)	Pig (Hanford miniature)	1 → 6 wk (weekly sampling)	Duodenum, jejunum, ileum	Lactase-phlorizin hydrolase, sucrase, maltase, glucoamylase, acid β-galactosidase	Mucosal enzyme activity assays	Lactase ↓ in all regions; sucrase ↑ ~2× (ileum); maltase ↑ 50 % (jejunum) & 3× (ileum); glucoamylase ↑ slightly (duodenum).	Lactase declines sharply while other disaccharidases rise post-weaning
(Marion et al., 2005)	Piglet (early weaning vs. suckling)	Weaned at 7 d; variable intake post-weaning	Proximal, mid, distal jejunum	Lactase-phlorizin hydrolase, sucrase-isomaltase, maltase-glucoamylase, aminopeptidase N, dipeptidyl peptidase-IV	Disaccharidase assays, p-nitroanilide peptidase assays, RT-PCR	actase mRNA ↓, sucrase / maltase / peptidases ↑; only maltase ↑ at mRNA (transcriptional) level.	Early weaning accelerates brush-border maturation.
(Adeola and King, 2006)	Pig	Weeks 1–4 (2.1 → 6.3 kg BW)	Jejunal brush border membranes (BBM)	Sucrase and alkaline phosphatase	BBM isolation, kinetic enzyme assay	Sucrase Vmax 0.160 → 1.471 mmol·mg⁻¹·min⁻¹ (↑9.2×); ALP Vmax 0.402 → 2.657 µmol·mg⁻¹·min⁻¹ (↑6.6×).	Disaccharidase and alkaline phosphatase activities increase postnatally
(Duluc et al., 1993)	Rat	4 d (neonate) → 14 d (suckling) → 90 d (adult)	Duodenum, jejunum, ileum, colon	Lactase-phlorizin hydrolase mRNA, protein, and enzyme activity	Nuclear run-on, Northern and Western blot	Proximal jejunum Lactase-phlorizin hydrolase mRNA & activity ↓ 9× (day 4 → adult); distal ileum mRNA absent in adults.	Lactase expression declines sharply and becomes regionally restricted with age.
(Lillienau et al., 2003)	Rat	Fetal day 20–22 → 4 wk postnatal	Entire gastrointestinal tract	Alkaline sphingomyelinase (alk-SMase) and alkaline phosphatase	Enzyme activity assays, Western blot	Alk-SMase 0.14 ± 0.01 → ×10 ↑ (fetal day 20 → day 22) → sustained postnatally; alkaline phosphatase ↑ day 2–7 → ↓ by week 4.	Alk-SMase induced prenatally and stable; alkaline phosphatase peaks early then declines.

1.2.5. Nutrient Gateways: Transporter Reprogramming During Early Life

Membrane nutrient transporters form the final barrier to absorption, mediating selective transcellular uptake of monosaccharides, amino acids, peptides, lipids, and micronutrients (Choudhuri and Chanderbhan, 2016; Glatz and Luiken, 2017; Kandasamy et al., 2018; Koepsell, 2020). Their expression and activity are developmentally regulated, and the following sections describe how individual transport systems differ between infants and adults.

Carbohydrates

In pigs, Puchal and Buddington (1992) found that brush-border membrane vesicle uptake of glucose and galactose per mg protein was maximal at birth, then fell sharply after the onset of suckling (from ~15–20 nmol/mg/min to about one-third by day 10), while fructose transport, nearly absent at birth, rose progressively toward weaning (Puchal and Buddington, 1992). Direct quantification of SGLT1 or GLUT proteins across ages is limited in pigs, though functional declines in transport after birth (Puchal and Buddington, 1992) strongly suggest parallel changes at the protein level.

In rodents, Khan et al. (2000) showed that jejunal glucose absorption in weanling rats (22–24 days) was several times greater than in sucklings (16 days) and about twice that of mature animals (6–8 weeks), consistent with a “burst” of SGLT1 activity at weaning (Khan et al., 2000). Earlier work by Lindi et al. (1985) found that net glucose transport across jejunal sacs peaked in young rats (2 months), being significantly higher than in very young (35–45 days), adult (7 months), or old (20 months) animals (Lindi et al., 1985). Similarly, Said et al. (1987) reported that the V_{max} of active glucose transport in jejunum was greatest at day 3 after birth and

declined rapidly, reaching adult levels by ~7 days (Said et al., 1990). Toloza and Diamond (1992) observed that total intestinal uptake capacity for glucose rise during suckling, peaked around weaning, and declined thereafter, while fructose uptake was negligible until weaning, when it increased steeply regardless of dietary fructose, suggesting a hard-wired developmental program (Toloza and Diamond, 1992). Shu et al. (1997) showed that feeding weanling rats high-fructose diets induced a sharp rise in GLUT5 protein in the brush border, confirmed by Western blotting, alongside a several-fold increase in fructose uptake rates (up to ~8–10 nmol/mg/min vs ~2 in controls) (Shu et al., 1997). Castelló et al. (1995) showed that GLUT5 mRNA was nearly undetectable prenatally, rose gradually after birth, and reached adult levels only after weaning, with expression peaking in proximal jejunum (Castelló et al., 1995). Rand et al. (1993) similarly observed that GLUT5 mRNA was low in fetal and neonatal rat intestine and kidney, with rapid postnatal induction (Rand et al., 1993). Shu et al. (1997) demonstrated that fructose feeding accelerated this process, with ~10% dietary fructose sufficient to significantly boost GLUT5 mRNA during weaning (Shu et al., 1997). Finally, Cui et al. (2003) showed that GLUT2 mRNA levels were relatively stable across late suckling, weaning, and adulthood, but could be strongly upregulated by high-glucose or high-fructose diets (Cui et al., 2003).

In humans, Davidson et al. (1992) reported significantly higher mRNA levels of SGLT1, GLUT2, and GLUT5 in adult compared to fetal small intestine (Davidson et al., 1992).

All in all, in infancy, glucose and galactose absorption via SGLT1 is maximal, while fructose transport through GLUT5 is very low or absent. Around weaning, glucose uptake peaks transiently, then declines to adult levels, whereas fructose transport

rises sharply. In adults, SGLT1 activity is lower per unit tissue, but GLUT2 and GLUT5 expression are higher, supporting broader carbohydrate handling.

Peptides

To understand how peptide absorption capacity develops after birth, several studies have examined the ontogeny of dipeptide transport and PEPT1 expression in different mammalian species (Table 1.4).

In miniature pigs, Nosworthy et al. (2012) performed *in situ* perfusion in Yucatan piglets at 1, 2, 3, and 6 weeks. They measured Gly-Sar disappearance and showed that ileal transport was highest at 1 week , decreased at 2–3 weeks, and increased again at 6 weeks post-weaning (Nosworthy et al., 2013). In contrast to pigs, uptake remained minimal at all ages, and kinetic constants were not saturable, unlike amino acid transport. In rabbits, Guandalini and Rubino (1982) examined jejunal and ileal uptake of Gly-Pro at gestational age 25–30 days, in newborns 1–6 days, sucklings at 10–40 days, and adults (>90 days). They found that uptake of 0.5 mM Gly-Pro peaked at birth (V_{max} jejunum 126.7 ± 26.4 pmol·g^{-1}·h^{-1}, Kt 0.98 ± 0.26 mM; ileum V_{max} 59.6 ± 9.2, Kt 0.70 ± 0.10 mM), whereas in adults jejunal uptake was only 3.8 ± 0.5 pmol·g^{-1}·h^{-1}, reflecting an ~12-fold developmental decline (Guandalini and Rubino, 1982). Importantly, uptake of free glycine (0.5 mM) remained constant across ages, confirming that the dipeptide transport system follows a distinct developmental course.

Protein expression studies corroborate these developmental differences. In humans, Mooij et al. (2016) confirmed robust apical PEPT1 staining in intestinal tissue from infants (gestational age 24.7–40 weeks; postnatal age 0–16.6 weeks),

indistinguishable from older children (Mooij et al., 2016). In rats, Hussain et al. (2002) detected PEPT1 immunostaining at embryonic day 18, with diffuse cytoplasmic and basolateral localization at postnatal day 0, which became exclusively apical by day 21 and in adults (3–4 months) (Hussain et al., 2002). Shen et al. (2001) quantified PEPT1 protein abundance, observing a peak at postnatal days 3–5 (~1.4-fold adult values at 60–75 days), a secondary ileal increase at day 24, and complete absence in adult colon despite detectable expression in the first week of life (Shen et al., 2001).

Transcript-level data add further nuance. In human infants (gestational 24.7–40 weeks; postnatal 0–16.6 weeks), Mooij et al. (2016) found that PEPT1 mRNA was 20% lower than in older children, (Mooij et al., 2016). However, Meier (2018) found that PEP1 mRNA was not significant between newborn (gestational 33–41 weeks; postnatal 0–4 days) and adult (41-77 years old). In pigs, Nosworthy et al. (2012) showed colonic PEPT1 mRNA peaked at 1–2 weeks and declined at 6 weeks (Nosworthy et al., 2013). In rats, Miyamoto et al. (1996) demonstrated that jejunal PEPT1 mRNA peaked at day 4 and declined to adult levels by day 28 (Miyamoto et al., 1996). Rome et al. (2002) measured PEPT1 mRNA at days 4–50 and found stable regional expression patterns, suggesting that distribution along the proximal–distal axis is set early and does not change (Rome et al., 2002). Shen et al. (2001) reported transcript levels that paralleled protein profiles, with PEPT1 highest at days 3–5, declining by 2–3 weeks, and transiently increased at day 24 (Shen et al., 2001). Overall, the evidence suggests that PEPT1 is expressed and functional from the earliest stages of intestinal development in humans, pigs, rabbits, and rodents, but its ontogeny differs across species. In humans, expression is already close to adult

levels by late gestation and the neonatal period. In pigs and rabbits, PEPT1 activity is very high around birth, declines during suckling, and shows a secondary rise at weaning. In rodents, a clear early neonatal peak is followed by a decline and transient weaning-associated reinduction.

Table 1.4 Summary of studies describing developmental changes in intestinal peptide transport across mammalian species.

The table presents experimental models, developmental stages, intestinal regions, transport mechanisms, and analytical methods used to assess peptide transport and transporter expression. Abbreviations: PEPT1/2, peptide transporter 1/2; MDR1, multidrug resistance protein 1; OATP2B1, organic anion transporting polypeptide 2B1; MRP2, multidrug resistance-associated protein 2; BBM, brush border membrane; qPCR, quantitative polymerase chain reaction; RT-PCR, reverse transcription polymerase chain reaction; wk, weeks; d, days; h, hours; AA, amino acids. Symbols: ↑, increase; ↓, decrease; ≈, approximately equal; ↔, no significant change.

Reference	Species / Model	Age / Condition	Region / Tissue	Feature / Metric	Methods (brief)	Key Quantitative Results	Interpretation / Key Findings
(Mooij et al., 2016)	Human (pediatric biopsies)	Neonates/infants vs older children	Small intestine	PEPT1 expression and localization; comparison with multidrug resistance protein 1 (MDR1), organic anion transporter (OATP2B1), and multidrug resistance-associated protein 2 (MRP2)	qPCR, immunohistochemistry	PEPT1 mRNA (infant) ≈ 0.8× older children ($p < 0.05$); localization apical = across ages.	PEPT1 expression slightly lower but functionally mature at birth.
(Himukai et al., 1980)	Guinea pig	Suckling (3–4 d), weanling (10–14 d), adult	Jejunum and ileum (everted sleeves)	Intact dipeptide transport (Gly–Gly, Gly–L-Leu) vs free amino acid uptake	One-minute radiotracer uptake; kinetic analysis	Gly–Gly Jmax 51 ± 1.9 → 20 ± 2.4 nmol·cm^{-2}·min^{-1} (sucklings vs. adults ≈2.5× ↓); Km ≈ 2.4 ↔ 2.1 mM; free AA uptake ↔; Ile inhibition 35–38 % (young) < 50 % (adult).	Neonates show ≈2.5× higher peptide transport efficiency vs adults.
(Guandalini and Rubino, 1982)	Rabbit	Newborn 1–6 d → adult	Jejunum and ileum	Dipeptide transport system; Gly–Pro kinetics	Initial-rate uptake, inhibitor assays, sodium dependence	Jejunal Vmax 126.7 ± 26.4 → 3.8 ± 0.5 pmol·g^{-1}·h^{-1} (≈97% ↓); Km 0.98 ± 0.26 mM; Ileal Vmax 59.6 ± 9.2, Km 0.70 ± 0.10; Na^+ removal ½ Vmax.	Neonatal peptide uptake ≈13× higher and Na^+-dependent.
(Shen et al., 2001)	Rat	Embryonic day 17–20 → postnatal day 75	Duodenum, jejunum, ileum, colon	PEPT1/2 mRNA and protein	Northern blot densitometry, brush-border membrane (BBM) immunoblotting	PEPT1 mRNA peaked at day 5 (duodenum/jejunum) and day 3 (ileum/colon); protein levels matched mRNA; expression decreased during week 1–2 →	PEPT1 shows a biphasic pattern—early neonatal peak and weaning rebound

						increased again near day 21 (weaning).	
(Hussain et al., 2002)	Rat (Wistar)	Embryonic day 18, postnatal day 0, day 21, adult	Duodenum	Cellular localization of PEPT1 protein	Confocal immunocytochemistry with anti-PepT1	Day 0: PepT1 apical + basolateral; adult: apical-only.	Transient basolateral PepT1 in neonates enables systemic peptide uptake.
(Rome et al., 2002)	Rat (Sprague–Dawley)	Postnatal days 4, 8, 10, 12, 21, 30, 50	Small intestine (proximal, median, distal)	PEPT1 and other transporters (NBAT, EAAC1)	Semi-quantitative RT-PCR, immunohistochemistry	PepT1 mRNA ↓ at day 50 vs day 21 ($p < 0.05$); distribution uniform along intestine; protein apical (brush border) with crypt–villus gradient, no crypt staining.	PepT1 remains apical and regionally stable despite modest transcript decline.
(Nosworthy et al., 2013)	Pig (Yucatan miniature)	1, 2, 3 wk (suckling) and 6 wk (post-weaning)	Four 10-cm intestinal loops and colon	PEPT1 mRNA and peptide absorption (Gly–Sar)	In vivo perfused loops, radiolabeled Gly–Sar uptake, qRT-PCR	Ileal Gly–Sar transport peak at 1 wk > 2–3 wk ($p < 0.05$); suckling < 6 wk post-wean; colonic PepT1 mRNA max 1–2 wk → min 6 wk.	Ileal peptide transport peaks in early life; colonic PepT1 transient in neonates.

Free amino acids

Understanding the transport system of amino acids through the gut barrier can be complicated because every amino acid can be carried by several systems, and many transporters accept multiple substrates.

In rats, Fitzgerald et al. (1971, 1972) demonstrated that 2-day-old neonates exhibit high rates of neutral amino acid transport (leucine, isoleucine, valine, methionine, tryptophan, phenylalanine, tyrosine, alanine; 3.9–5.6 mM/5 min). Basic amino acids (lysine, arginine, ornithine) were also efficiently transported (1.7–2.0 mM/5 min), whereas acidic amino acids (aspartate, glutamate) were much less active (0.24–0.28 mM/5 min). Sarcosine and betaine (non-proteogenic, methylated derivatives of glycine) uptake (~0.5 mM/5 min) indicated weak imino/glycine pathway activity (Fitzgerald et al., 1972, 1971). Developmental profiling revealed steep postnatal declines: glycine transport decreased ~70% between days 2 and 10, and lysine uptake fell >50% between days 10 and 30 (Fitzgerald et al., 1971).

Younoszai et al. (1985) confirmed that valine transport declined ~55% and lysine ~90% between 2 and 6 weeks, with the largest drop occurring before weaning (Younoszai et al., 1985a). Toloza and Diamond (1992) found proline uptake peaked during suckling and dropped thereafter, lysine increased sharply at weaning, and leucine remained stable, reflecting nutrient-specific regulation (Toloza and Diamond, 1992). Navab and Winter (1988) extended the profile into senescence. In 24-month rats, phenylalanine V_{max} (maximum transport rate) decreased by half (1.03 → 0.51 µmol/g·2 min), while Kt (affinity constant, lower Kt = higher affinity) improved (5.46 → 2.54 mM) with tryptophan showing a similar V_{max} drop (0.38 → 0.25) (Navab and Winter, 1988).

In terms of transporters expression and localization, in humans, Meier et al. (2018) reported that B0AT1 and its partner ACE2 are expressed at the same level in in both newborns (0–4 days) and adults (41–77). In contrast, SIT1 protein, which transports amino acids, proline hydroxyproline and glycine, was not detected in newborns (Meier et al., 2018).

In rats, Rome et al. (2002) showed that EAAC1 and NBAT proteins were regionally distributed (EAAC1 in crypts/villus bases, NBAT proximally), and these patterns remained unchanged from day 4 to 50 (Rome et al., 2002).

At the transcript level, Meier et al. (2018) found that 12 transporters (including B0AT1, LAT1/2, y+LAT1/2, EAAT3, rBAT, PAT1, and 4F2hc) were expressed at similar levels in newborn and adult intestine. Only SIT1 mRNA was significantly reduced (~3-fold lower in newborns) (Meier et al., 2018).

Rodent data indicate more variability. Rome et al. (2002) observed stable expression of EAAC1 and NBAT transcripts across postnatal days 4–50, suggesting that not all transporters undergo ontogenetic shifts (Rome et al., 2002).

Taken together, these studies show that in rodents and rabbits, neonatal intestine exhibits high uptake of essential amino acids, followed by steep declines around weaning. In humans, most free amino acid transporters are already expressed at adult-like levels from birth, with the major exception of SIT1, which is absent in neonates.

Lipids

At the level of direct transport, human infants absorb dietary fat less efficiently than adults. In preterm infants, the coefficient of fat absorption (CFA) is only 68–85% with formula and 74–91% with breast milk, compared with ~90% in term infants and

>95% in adults (Lindquist and Hernell, 2010; Poquet and Wooster, 2016). In rodents, suckling rats (12–14 days, ~25 g) absorb dietary triglycerides at markedly higher rates than adults (10 weeks, 150–250 g): disappearance of [^{14}C]triolein, breath $^{14}CO_2$ output, and plasma triglyceride output were all 2–3 times higher in sucklings than in adults (Flores et al., 1989).

At the level of protein localization and quantification, in piglets, jejunal lipid absorption directly stimulates apolipoprotein A-IV (apoA-IV) synthesis, with jejunal synthesis increasing sevenfold in newborn piglets receiving high-triglyceride infusions compared with baseline fetal levels (2.1% of total protein synthesis) or low-triglyceride/bile-diverted controls (Black et al., 1990).

At the transcript level, in infant FABP6 and SLC10A2, both involved in bile acid binding/transport and fatty acid metabolism, were upregulated compared to adult human enteroids (Adeniyi-Ipadeola et al., 2024). In swine, microsomal triglyceride transfer protein (MTP) mRNA was high in 40-day gestation fetal intestine, peaked at 2 days postnatal with milk feeding, and falled to low steady levels by weaning at 2 months (Lu et al., 2002). g. In rodents, intestinal FAT/CD36 mRNA is expressed in all gut regions (e.g., jejunum 238 ± 17 relative to 18S, ileum 117 ± 14, stomach 45 ± 7) with a fourfold increase from neonatal to adult rats (Chen et al., 2001).

Together, these findings show neonatal absorption is less efficient in humans, accelerated in rodents, and strongly diet- and age-dependent, unlike the stable efficiency of adults.

Minerals and Vitamins

In rat newborns, Ca^{2+} and Mg^{2+} absorption rates are higher than in adolescents, relying more on passive diffusion during suckling and shifting to carrier-mediated transport after weaning (Ghishan et al., 1980; Ghishan and Meneely, 1982; Meneely et al., 1982). Expression of the Ca^{2+} transporter CaT1 (TRPV6) rises at weaning in rats but declines later in development (Song et al., 2003), while Mg^{2+} transport via TRPM (Voets et al., 2004) remains incompletely characterized. Pi absorption, mediated by NaPi-2b, is higher in suckling rats compared to adults but decreases with age (Kirchner et al., 2008; Xu et al., 2002).

For iron, in newborns, DMT1 and ferroportin expression is low and unresponsive to iron status in rats (Leong et al., 2003), mice (Lopez et al., 2006) and humans (Domellöf et al., 2002), resulting in markedly reduced iron absorption until late infancy. Instead, iron absorption in early life may be supported by lactoferrin receptors, which are upregulated soon after birth (Liao et al., 2007; Lopez et al., 2006; Suzuki et al., 2001).

For zinc, transporters such as ZIP4 and ZnT2 show higher expression in the neonatal intestine in rats (Liuzzi et al., 2003) and mice (Huang et al., 2006), with developmental downregulation after weaning, while piglet studies show substrate-dependent regulation (Martin et al., 2013). In contrast, copper absorption in early life is relatively high and largely passive in human infants (Olivares et al., 2002), rats (Bauerly et al., 2004; Lönnerdal et al., 1985), and mice (Varada et al., 1993), while regulatory control of Ctr1 and ATP7A expression is limited compared to adults (Bauerly et al., 2004; Lönnerdal et al., 1985).

Vitamin absorption in infancy shows distinct differences from adulthood, often with higher uptake during the suckling period. Thiamin (B1) absorption via hTHTR-1 and hTHTR-2 is greater in suckling than in adults mice, with declining transporter expression and activity during maturation (Reidling et al., 2006). Biotin (B7) uptake is higher in suckling rats, predominantly localized to the ileum, whereas in adults absorption shifts to the jejunum with increased transporter expression (Nabokina et al., 2003; Said et al., 1990). Folate (B9) absorption is also greater in suckling rats (Balamurugan and Said, 2003; Said et al., 1990) and piglets (Shafizadeh and Halsted, 2009), with reduced uptake and RFC expression in adults (Balamurugan and Said, 2003; Said et al., 1985; Shafizadeh and Halsted, 2009). By contrast, cobalamin (B12) absorption is lower in newborns in piglets (Trugo et al., 1985) and rats (Dieckgraefe et al., 1988; Ramasamy et al., 1989) compared to weanlings and adults, reflecting lower activity of the intrinsic factor–cubilin–megalin system in early life, though milk-derived factors may facilitate neonatal uptake (Trugo et al., 1985). Retinol (vitamin A) absorption is higher in sucklings than in adults rats (Dew and Ong, 1997, 1994; Reboul, 2013; Said et al., 1989, 1988). Overall, most vitamins show enhanced absorption during early infancy compared to adulthood, based primarily on rodent and piglet data, likely reflecting adaptations to neonatal nutritional needs.

Maternal immunoglobulin G (IgG)

Beyond classical nutrient transporters, the neonatal intestine possesses a specialized endocytic and transcytotic pathway dedicated to passive immune protection. During early life, developmentally elevated endocytosis enables the uptake of maternal immunoglobulin G (IgG) from colostrum or amniotic fluid, conferring systemic and

mucosal immunity while the newborn's immune system matures (Weström et al., 2020).

IgG is internalized by enterocytes and M cells via the neonatal Fc receptor (FcRn) expressed on the apical membrane. Within acidic endosomes, FcRn binds the Fc region of IgG and transports it across the epithelial cell to the basolateral surface, where it is released at neutral pH. Once transported across the cell, the antibody can bind luminal antigens or interact with immune cells, thereby supporting immune priming within the developing gut (Harris et al., 2006; Yoshida et al., 2004).

In humans, FcRn is predominantly expressed on the syncytiotrophoblast of the placenta, where it mediates maternal IgG transfer during gestation (Simister et al., 1996; Story et al., 1994). After birth, FcRn expression persists in the intestinal mucosa of infants (Shah et al., 2003) and adults (Dickinson et al., 1999; Israel et al., 1997). However, its precise role in the postnatal gut remains unclear. Current evidence suggests that FcRn primarily contributes to IgG and albumin homeostasis, recycling, and immune surveillance by mediating the bidirectional transport and clearance of IgG–antigen complexes (Baker et al., 2009; Pyzik et al., 2015).

In contrast, in pigs and rodents, FcRn plays a central role in antibody and macromolecule uptake during the suckling period. In piglets, maternal IgG is absorbed exclusively after birth through a combination of non-selective endocytosis and FcRn-mediated transcytosis in the small intestine during a brief "open-gut" window that closes within 24–36 hours postnatally. In rodents, IgG transfer occurs both before and after birth, but the major postnatal phase is mediated by FcRn-dependent transcytosis through enterocytes throughout the suckling period until weaning (~3 weeks) (Weström et al., 2020).

To sum up, across nutrient classes, infant transporters operate as part of a developmental program tailored to a milk-based diet, maximizing rapid uptake of simple sugars, amino acids, and small peptides while relying heavily on passive routes for minerals and vitamins. As the diet diversifies, this permissive, high-capacity system is progressively reprogrammed into a selective and tightly regulated barrier, aligning nutrient absorption with the metabolic and protective needs of the mature intestine. These key differences between infant and adult intestinal transport are summarized in Fig. 1.3.

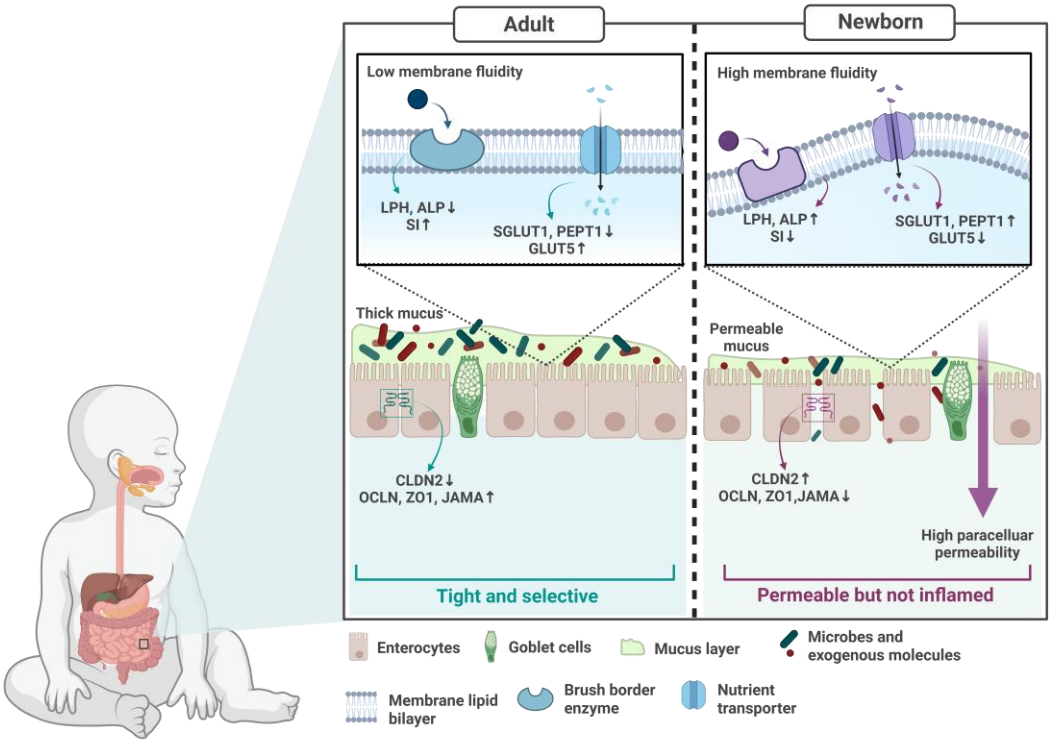


Figure 1.3 Key Differences Between Infant and Adult Small Intestinal Barrier Function. Arrows indicate relative levels in infants compared to adults (↑ higher in infants, ↓ lower in infants). Tight junction proteins: CLDN2 = claudin-2; OCLN = occludin; ZO1 = zonula occludens-1; JAMA = junctional adhesion molecule-A. Brush border enzymes: LPH=lactase–phlorizin hydrolase; SI = sucrase–isomaltase; ALP = alkaline phosphatase. Nutrient transporters: SGLT1 = sodium–glucose co-transporter 1; GLUT5 = fructose transporter; PEPT1 = peptide transporter 1.

1.3. Feeding for Maturity: Human Milk Supports Intestinal Barrier Development

Human milk contains a wide array of bioactive molecules that modulate intestinal epithelial maturation and barrier integrity. In early life, intestinal permeability declines rapidly as the mucosa differentiates, and tight junctions mature. Functional assessments such as sugar absorption tests provide *in vivo* evidence of this process. Catassi et al. (1995) measured urinary L:M ratios in healthy term infants and found values of 0.06 ± 0.01 in breastfed versus 0.14 ± 0.02 in formula-fed infants, indicating significantly lower paracellular permeability and faster epithelial closure in the breastfed group (Catassi et al., 1995). Extending these observations to preterm infants, Roskes et al. (2025) evaluated 158 infants <33 weeks' gestation using the lactulose:rhamnose test at 7–10 days of life and reported mean lactulose:rhamnose ratios of 0.05 ± 0.07 for exclusive mother's milk, 0.06 ± 0.07 for donor ± mother's milk, and 0.11 ± 0.11 for preterm formula ± mother's milk. Infants who received > 150 mL kg^{-1} of human milk during the first week were 2.5 times more likely to exhibit a low-permeability phenotype (lactulose:rhamnose < 0.05). (Roskes et al., 2025). Similarly, Taylor et al. (2009) studied 62 infants <32 weeks and found that those receiving ≥ 75 % of feeds as mother's milk had a 3.8-fold lower composite median lactulose:mannito ratio across the first month (0.25 vs 0.94, $p < 0.01$) compared with infants receiving ≤ 25 %. (Taylor et al., 2009). The clinical relevance of this barrier maturation is underscored by the multicentre trial of Lucas and Cole (1990), where the incidence of necrotizing enterocolitis was 6–10 times higher in exclusively formula-fed and threefold higher in mixed-fed infants compared with those fed mother's own or pasteurized donor milk (Lucas and Cole, 1990).

Mechanistic evidence from *ex vivo* pediatric human enteroids corroborates these findings. Noel et al. (2021) showed that apical exposure to 20 % human colostrum increased transepithelial electrical resistance by ~70 %, reduced FITC-dextran (4 kDa) permeability by ~60 %, and upregulated the tight-junction protein OCLN with apical and junctional redistribution, confirming direct epithelial barrier enhancement by human milk (Noel et al., 2021).

The components of human milk that have been most extensively studied for their beneficial effects on gut maturation and barrier function include Human Milk Oligosaccharides (HMOs), Epidermal Growth Factor (EGF), lactoferrin, and secretory IgA (Andreas et al., 2015; Ballard and Morrow, 2013). HMOs, the third most abundant solid component of milk after lactose and lipids (5–15 g/L in mature milk, up to 25 g/L in colostrum), support intestinal and immune maturation by promoting beneficial bacterial growth, acting as soluble decoy receptors that block pathogen adhesion, strengthening epithelial junctions and mucin production, and modulating inflammatory and systemic immune responses (Bode, 2012).
EGF, present at concentrations up to 200 ng/mL in colostrum, binds epithelial receptors to stimulate enterocyte proliferation and differentiation, enhance mucosal repair, and reduce intestinal permeability—mechanisms that accelerate barrier maturation and protect against NEC (Ballard and Morrow, 2013).
Among milk proteins, lactoferrin, a major whey glycoprotein, chelates iron, exerts antimicrobial effects, and mitigates LPS-induced barrier disruption through cytokine modulation (Ballard and Morrow, 2013). Secretory IgA coats luminal microbes and antigens, limiting epithelial activation and antigen translocation to maintain mucosal tolerance (Andreas et al., 2015; Ballard and Morrow, 2013).

Interestingly, peptides derived from the digestion of human milk proteins have also been shown to exert biological effects beyond their nutritional value. Recent systematic analysis by Biondi Ryan et al. (2025) compiled human and animal data showing that intact milk-derived peptides have been detected in circulation following ingestion, particularly those originating from β-casein and α-lactalbumin. Many of these digestion-resistant fragments correspond to known bioactive peptides with ACE-inhibitory, antimicrobial, antioxidant, or immunomodulatory. While these peptides may act locally within the gastrointestinal tract, their detection in blood suggests the potential for systemic activity, although direct in vivo effects remain to be fully established (Biondi Ryan et al., 2025).

Together, these data underscore the multifactorial nature of human milk's influence on epithelial barrier maturation, while the relative contributions, optimal timing, and interactions of individual bioactives remain active areas of investigation.

1.4. Modeling the Immature Barrier: How Close Are We to the Real Infant Gut?

Given the large differences between an infant and adult intestinal barrier, it is imperative that there are cellular models that represent the infant. This is not only required to understand the developmental transition but also to assist in designing foods for this life stage that support gut maturity. A cell model to mimic the infant should have a more permeable mucus layer, be leaky but not inflamed, have a higher rate of glucose and amino acid transport, and respond to human milk by decreasing permeability. Bridging this gap is key to designing nutritionally relevant and predictive infant gut models.

In recent years, intestinal organoid and enteroid-derived monolayer systems have emerged as state-of-the-art *in vitro* models for investigating intestinal physiology and nutrition (Noel et al., 2021; Taelman et al., 2022). These cultures are derived either from intestinal stem cells biopsies (primary organoids) or from pluripotent stem cells differentiated into intestinal tissue (Taelman et al., 2022). They self-organize into three-dimensional structures containing all major epithelial cell types and can be adapted into two-dimensional monolayers suitable for permeability assays (Taelman et al., 2022). However, their feasibility remains limited. Culturing organoids is costly and requires, access to primary tissue or pluripotent stem cells, (Taelman et al., 2022). Consequently, these models are not yet suitable for routine or high-throughput screening, such as that required to evaluate the safety and efficacy of novel infant foods. For broader screening applications, simplified epithelial or co-culture systems remain more practical, while organoids serve as a translational platform for confirmatory or mechanistic studies.

In accordance with the 3R's principle (Replacement, Reduction, Refinement) included in Directive 2010/63/EU of the European Parliament and of the Council on the protection of animals used for scientific purposes ("Directive 2010/63/EU of the European Parliament and of the Council on the protection of animals used for scientific purposes," n.d.), there is therefore a pressing need to develop refined, cell-line–based *in vitro* systems that can reliably reproduce essential features of the infant intestinal barrier while remaining compatible with scalable, high-throughput experimental workflows. Accordingly, human and animal intestinal epithelial cell lines and co-culture systems currently represent the most feasible platforms for such

research. Table 1.5 and the following paragraphs summarize the key structural and functional characteristics of commonly used *in vitro* intestinal models.

1.4.1. Caco-2 and Co-culture Models

The Caco-2 cell line, derived in 1977 from a human colon adenocarcinoma (Fogh et al., 1977), remains the most widely characterized *in vitro* model of the intestinal epithelium. Upon confluence, Caco-2 cells spontaneously differentiate into enterocyte-like monolayers that display dense microvilli, tight junctions, and brush-border enzymes, such as alkaline phosphatase, sucrase–isomaltase, and aminopeptidase N (Artursson et al., 2012; Gullberg et al., 2000). Cells are typically cultured in DMEM with 10 % FBS and antibiotics, and when grown on semipermeable filters, they reach full polarization after 14–21 days (Lea, 2015). Caco-2 monolayers exhibit high transepithelial electrical resistance (TEER), typically 1,400–2,400 $\Omega \cdot cm^2$, and narrow paracellular pores (~4.5 Å) compared with the small intestine (8–13 Å) (Rubas et al., 1996; Sun et al., 2008). Consequently, their paracellular permeability is approximately 100-fold lower than *in vivo* tissue (Artursson et al., 2012). TEER and differentiation markers vary with passage number. Higher passages increase TEER while decreasing ALP and raising sucrase activity (Briske-Anderson et al., 1997). The membranes are relatively ordered and rigid, indicating low membrane fluidity compared with other intestinal cell lines (Efremov et al., 2023).

Caco-2 cells express a comprehensive panel of nutrient transporters (SGLT1, GLUT2/5, PEPT1, ASCT2, LAT1/2, FATP4, CD36) and efflux systems (P-gp, MRP2, BCRP) (Fedi et al., 2021; Sun et al., 2002). However, the expression of most transporters and metabolic enzymes is markedly lower than in native human

intestinal tissue. For example, SGLT1 and GLUT5 are expressed more than 600-fold and 20-fold higher, respectively, in the human duodenum, whereas GLUT3 is approximately 150-fold higher in Caco-2 cells. Likewise, the peptide transporter hPEPT1 is about 15-fold higher in duodenal tissue (Sun et al., 2002). Notably, Caco-2 cells express the neonatal Fc receptor (FcRn) involved in IgG transcytosis (Shah et al., 2003), suggesting some fetal-type features relevant for modeling immunity. These characteristics make Caco-2 cells invaluable for mechanistic nutrient-transport studies yet emphasize their limitations for modeling the immature, permeable, and dynamically regulated infant intestinal barrier. Consequently, modified systems such as the Caco-2/HT29-MTX co-culture and the Caco-2/HT29-MTX/Raji B triple model have been developed to introduce mucus secretion, paracellular modulation, and transcytosis activity, respectively.

Caco-2/ HT29-MTX Co-Culture

The Caco-2/HT29-MTX co-culture is the most widely adopted multiple-cell intestinal model. The HT29-MTX cell line was derived from the parental HT29 human colon adenocarcinoma (Fogh and Trempe, 1975) through long-term exposure to methotrexate (MTX), which selected for clones capable of differentiating into mucus-secreting goblet-like cells (Lesuffleur et al., 1990). Since its development, HT29-MTX has been extensively used as a model for goblet cells in co-culture with enterocyte-like Caco-2 monolayers.

Morphologically, differentiated HT29-MTX cells are similar in size to Caco-2 but exhibit shorter apical microvilli and looser tight junctions, resulting in a barrier of higher permeability (Hilgendorf et al., 2000; Pontier et al., 2001). The mucus produced by HT29-MTX contains both neutral and acidic glycoconjugates—MUC1

(membrane-bound), MUC3, and MUC5AC (gel-forming)—together with N-acetylgalactosamine, N-acetylglucosamine, galactose, mannose, sialic acid, and sulfate residues (Huet et al., 1995; Lesuffleur et al., 1990). Mucus secretion begins around day 9 post-seeding and reaches maximal thickness at day 23 (Pontier et al., 2001). Although early reports described the HT29-MTX mucus as “gastric-like” and deficient in MUC2 (Deplancke and Gaskins, 2001; Lesuffleur et al., 1990), more recent evidence demonstrates that HT29-MTX-E12 and related subclones do express MUC2 (Elzinga et al., 2021).

The co-culture is established by mixing the two cell lines in defined ratios prior to seeding on semi-permeable filters. The 90:10 (Caco-2:HT29-MTX) and 75:25 ratios are most frequently used (Kleiveland, 2015), but evidence suggests that 90:10 most faithfully reproduces physiological conditions and remains stable after differentiation, whereas increasing the proportion of HT29-MTX cells still results in predominantly Caco-2–dominated monolayers (Araújo & Sarmento, 2013). Functionally, TEER decreases proportionally with the HT29-MTX fraction, from approximately 930 Ω×cm² (10 %), 651 Ω×cm² (30 %), to 482 Ω×cm² (50 %), while HT29-MTX monocultures exhibit values near 180 Ω×cm² (Hilgendorf et al., 2000). In parallel, mannitol permeability increases more than ten-fold—from 0.10×10^{-6} cm/s (Caco-2) to 1.37×10^{-6} cm/s (50 % HT29-MTX) (Hilgendorf et al., 2000). Carrier-mediated transport processes are generally lower than in Caco-2 monocultures. D-glucose uptake (GLUT2/SGLT1), L-phenylalanine (large-neutral amino-acid carriers), and PEPT1 are all reduced (Hilgendorf et al., 2000; Walter et al., 1996).

Because HT29-MTX cells lack P-glycoprotein (MDR1), co-culture with Caco-2 effectively attenuates the overexpression of P-gp found in Caco-2 (Hilgendorf et al., 2000; Oga et al., 2012).

The mucus layer formed in 90:10 co-cultures measures 2–10 µm, approximately 60 % of the duodenal adherent mucus (≈ 15 µm) in adults (Mahler et al., 2009). This thinner layer may improve physiological relevance for modeling the infant intestinal barrier, whose mucus is naturally less developed and more permeable (see section 2.1).

In terms of nutrient processing, brush border enzyme activities (ALP, sucrase-isomaltase, ANPEP) originate mainly from the Caco-2 population, while HT29-MTX contributes little enzymatic activity (Briske-Anderson et al., 1997; Ferruzza et al., 2012).

Overall, absorption rates for actively transported nutrients are underestimated relative to human intestine, whereas paracellular transport and mucus diffusion barriers are more realistic. Considering that paracellular uptake predominates in early life, the Caco-2/HT29-MTX co-culture remains a more appropriate proxy for the immature intestinal epithelium than the Caco-2 monoculture.

Caco-2/ HT-29 MTX/ Raji-B Triple Co-Culture

The Caco-2/HT29-MTX/Raji B triple co-culture further enhances physiological complexity by incorporating an immune component. The Raji B line, established in 1964 from a Burkitt's lymphoma of an 11-year-old boy (Pulvertaft, 1964), consists of human B-lymphoblast-like cells that release soluble factors capable of inducing M-cell differentiation in Caco-2 epithelium (Gullberg et al., 2000; Kernéis et al., 1997; Lo et al., 2004).

In the triple-culture system, Caco-2 or Caco-2/HT29-MTX monolayers are grown for 14 days on Transwell filters, after which Raji B cells are added to the basolateral compartment. Within 5–7 days, approximately 10–15 % of the epithelial cells transform into M-cell-like phenotypes (Antunes et al., 2013; Araújo and Sarmento, 2013). These Caco-2-derived M-cells have the functional properties of the ones in the intestine, with the capacity to transport microparticles across the monolayer through the transcellular pathway (Gullberg et al., 2000).

M-cell induction causes a pronounced TEER decrease—from about 480 $\Omega \cdot cm^2$ (co-culture) to 50–100 $\Omega \times cm^2$—without compromising tight-junction continuity (Araújo and Sarmento, 2013). Functionally, the barrier's permeability to 4 kDa dextran rises from 0.3×10^{-6} cm/s in the co-culture to $\approx 2.6 \times 10^{-6}$ cm/s, a nine-fold increase, reflecting enhanced transcellular transport rather than junctional leakage. Likewise, uptake of 100 nm latex nanoparticles increases by 7–10-fold, while larger (500–1000 nm) particles show 2–3-fold higher transcytosis rates (Araújo and Sarmento, 2013; Kulthong et al., 2021).

Alkaline phosphatase and other brush-border enzymes are markedly downregulated within M-cell regions, reflecting the loss of microvilli and absorptive enterocyte characteristics (Araújo et al., 2013). Consistent with their specialized role in antigen sampling, M-cells are largely devoid of digestive enzymes and exhibit an attenuated apical surface, lacking both a structured brush border and a defined glycocalyx (Niedergang and Jean-Pierre, 2000). Despite this pronounced morphological remodeling, mucus secretion by HT29-MTX cells remains unaffected, and a continuous mucus layer persists across the epithelial surface (Araújo and Sarmento, 2013).

Together, these features generate a multifunctional epithelial model that integrates the principal components of the intestinal barrier: mucus-secreting goblet-like cells, nutrient-absorbing enterocytes, and transcytotic M-cells. A practical limitation, however, is that Raji B cells harbor Epstein–Barr virus (EBV) genomic sequences, requiring the model to be handled under biosafety level 2 conditions (Epstein et al., 1966).

1.4.2. The IPEC-J2 cell line

In contrast to the adult, tumor-derived Caco-2 model, the intestinal porcine enterocyte cell line IPEC-J2 (ACC 701, DSMZ) offers a non-transformed and physiologically relevant alternative that more closely mimics the immature intestinal epithelium. IPEC-J2 was established from the jejunal epithelium of a neonatal, unsuckled piglet (Berschneider, 1989), making it one of the few permanent small-intestinal epithelial cell lines of non-cancerous origin. Owing to the high anatomical, physiological, and functional similarities between pigs and humans, particularly during early postnatal development, IPEC-J2 represents a suitable translational model for studying the infant gut barrier (Darragh and Moughan, 1995).

When cultured on permeable supports in DMEM/F-12 medium supplemented with either fetal bovine serum (FBS) or species-specific porcine serum (PS), epidermal growth factor (EGF), and insulin–transferrin–selenium (ITS), IPEC-J2 cells differentiate within 1–2 weeks into polarized epithelial monolayers exhibiting clear apical–basolateral orientation, brush borders with dense microvilli, and functional tight junctions (Nossol et al., 2015; Schierack et al., 2006; Vergauwen, 2015). They also secrete cytokines such as interleukin-6 (IL-6) and interleukin-8 (IL-8), express toll-like receptors and β-defensins, and thus can respond immunologically to

microbial or dietary stimuli (Brosnahan and Brown, 2012; Mariani et al., 2009). Importantly, IPEC-J2 express the neonatal Fc receptor (FcRn) on the apical surface, enabling bidirectional IgG transport across polarized monolayers and providing a system to investigate mucosal antibody trafficking in early life (Guo et al., 2016). Compared with Caco-2, IPEC-J2 cells form a less restrictive epithelial barrier. TEER values vary markedly depending on culture conditions, from 2,000 $\Omega \cdot cm^2$ in standard FBS media to approximately 200–400 $\Omega \cdot cm^2$ in PS-supplemented media, closely matching ex vivo jejunal tissue of piglets (Bernardini et al., 2021; Zakrzewski et al., 2013). Substituting FBS with PS not only reduces TEER but also promotes taller, more differentiated cells with enhanced tight-junction architecture and improved paracellular permeability (Zakrzewski et al., 2013). These morphological and physiological characteristics make the PS-based culture a more appropriate representation of the neonatal intestinal barrier, which is naturally more permeable than in adults.

IPEC-J2 cells produce a thin mucus layer composed predominantly of neutral mucins, visualized by periodic acid–Schiff (PAS) staining and the expression of MUC1 and MUC3, but not MUC2 (Mariani et al., 2009; Perruchot et al., 2025; Schierack et al., 2006). While this differs from the adult human mucus composition, it parallels the more permeable and less acidic mucus characteristic of newborn intestinal barrier. Together, these properties support IPEC-J2 as a physiologically relevant *in vitro* model for studying the neonatal gut barrier.

From a functional standpoint, IPEC-J2 cells express a broad panel of nutrient transporters, including SGLT1, GLUT2, PEPT1, and several amino-acid transporters such as B^0,+AT, y^+LAT1, and ASCT2 (Chen et al., 2021; Liao et al., 2017; Tang et al., 2022). They also express fatty-acid transport and metabolism genes (FATP1/4,

CD36, FABP3, DGAT1) (Chen et al., 2021; Xu et al., 2023). Their metabolic profile—characterized by both glycolytic and oxidative phosphorylation activity and a shift toward glycolysis upon differentiation (Bernardini et al., 2021; Nossol et al., 2015)—reflects that of normal intestinal tissue rather than the Warburg-type metabolism typical of Caco-2 cells (Vander Heiden et al., 2009).

Despite these advantages, variability in TEER and gene expression remains a limitation, as culture parameters such as serum origin, supplement composition, substrate material, and temperature (37–39 °C) markedly affect epithelial differentiation and TEER. Moreover, passage number is not provided by the culture collection and rarely standardized or reported, complicating cross-study comparisons.

Overall, the IPEC-J2 model combines non-cancerous origin, neonatal derivation, appropriate permeability, and metabolic normality, making it a promising alternative to Caco-2 for investigating the infant intestinal barrier, nutrient absorption, and host–microbe interactions.

1.4.3. Human Fetal Intestinal Cell Lines (FHs 74 Int, HIEC-6)

Human fetal-derived intestinal cell lines provide an intermediate model between immortalized adult tumor cell lines and complex primary organoid cultures. They are non-transformed, preserve several characteristics of the immature intestinal epithelium, and are therefore particularly suited to study early-life epithelial physiology and nutritional effects under controlled conditions.

The FHs 74 Int cell line (ATCC CCL-241) originates from the small intestine of a 12–16-week-gestation human fetus (Owens et al., 1976; Smith, 1979) and represents

one of the few adherent non-transformed fetal intestinal epithelial models available. FHs 74 Int cultures exhibit a population-doubling time of approximately 6–7 days in Dulbecco's modified Eagle's medium (4.5 g/L glucose) supplemented with 10 % fetal calf serum, 10 µg/mL insulin, and non-essential amino acids, maintained at 37 °C in 10 % CO_2 (Owens et al., 1976). When grown on a permeable insert, FHs 74 expresses alkaline phosphatase (Maheshwari et al., 2002), OCLN (Li Lu et al., 2021) and develop a TEER of 500–600 Ω/cm^2 from 2 to 3 weeks (Li Lu et al., 2021). Later cell-bank characterization indicated that the line is keratin and PAS-negative (mucins), suggesting a less mature, incompletely differentiated epithelial phenotype (ATCC CCL-241).

HIEC-6 (ATCC CRL-3266) is a non-tumorigenic human fetal intestinal epithelial line derived from the crypt region of a 17–19-week-gestation small intestine using a thermolysin dissociation protocol developed by Perreault and Beaulieu (1996) (Perreault and Beaulieu, 1996). It exhibits a crypt-like, proliferative morphology, expressing cytokeratins and early enterocytic markers, but remains undifferentiated even at confluence, consistent with an immature phenotype (Gauthier et al., 2001). The cells grow continuously for approximately 28 passages with a doubling time of ~96 h, maintained in OptiMEM I medium supplemented with 4% FBS, 20 mM HEPES, 10 mM GlutaMAX, and 10 ng/mL EGF (ATCC, 2025). Barrier function studies demonstrate that HIEC-6 does not develop measurable TEER above blank levels (≈ 31–32 $\Omega \cdot cm^2$), even at high seeding densities and long culture durations, and that probiotic co-culture fails to enhance TEER (Lopez-Escalera and Wellejus, 2022). Immunofluorescence confirms expression of ZO1 and CLDN1, but OCLN is absent, explaining the lack of tight paracellular sealing (Lopez-Escalera and

Wellejus, 2022). Despite this, HIEC-6 expresses functional brush-border enzymes such as aminopeptidase N and dipeptidyl-peptidase IV, but not sucrase–isomaltase (Perreault and Beaulieu, 1996) and displays lipid absorptive capacity, indicating partial enterocytic functionality (Levy et al., 2000).

Despite their relevance as human fetal intestinal models, FHs 74 Int and HIEC-6 present important limitations. Both exhibit low and unstable barrier integrity, incomplete differentiation, and variable epithelial polarity, which constrain their use in quantitative permeability or absorption studies. They also lack mucus production and fully developed transport systems.

Table 1.5 Summary of commonly used *in vitro* intestinal epithelial cell models and their functional characteristics in relation to infant/newborn gut physiology.

Feature / Metric	Caco-2	Caco-2 + HT29 (co-culture)	Caco-2 + HT29 + Raji B (triple co-culture)	IPEC-J2 (porcine jejunal)	FHs 74 Int and HIEC-6 (human fetal intestinal lines)
Mucus production and composition	Does not form a surface mucus layer (*Artursson et al., 2012*).	Produces acidic (Alcian blue–positive) and neutral (PAS–positive) mucins; expresses MUC1, MUC2, MUC3, and MUC5AC (*Lesuffleur et al., 1990; McCright et al., 2022*). Mucus viscosity and pore size depend on HT29 fraction; 90:10 ratio ≈ 0.034 Pa·s, 390–440 nm², similar to porcine jejunal mucus (*McCright et al., 2022*).	Alcian blue–positive mucus forms only when HT29 cells are present (*Araújo & Sarmento, 2013*).	Expresses MUC1 and MUC3, but lacks MUC2; PAS positive (*Schierack et al., 2006; Vergauwen, 2015*).	FHs 74 = PAS negative (cell line resource) HIC-6 =no mucus secretion *(Beaulieu & Quaroni, 1991)*
Membrane fluidity and stiffness	Laurdan generalized polarization (GP) = 0.45 ± 0.03; AFM Young's modulus = 5.2 ± 0.9 kPa (*Efremov et al., 2023*).	HT29-MTX membranes more fluid: Laurdan GP = 0.34 ± 0.04; AFM modulus = 3.6 ± 0.7 kPa (*Efremov et al., 2023*).	Not reported.	Not reported.	Not reported.
Barrier integrity and paracellular permeability (transepithelial electrical resistance = TEER)	TEER ≈ 1,400–2,400 Ω·cm² at days 14–17 (*Hilgendorf et al., 2000; Artursson et al., 2012*). Tight-junction pore radius ≈ 4.5 Å (vs human intestine = 8–13 Å) (*Sun et al., 2008*). Permeability ≈ 100× lower than in vivo.	TEER decreases as HT29 fraction increases: 10 % HT29 ≈ 930 Ω·cm²; 30 % ≈ 651; 50 % ≈ 482; HT29 alone ≈ 180 Ω·cm² (*Hilgendorf et al., 2000*).	TEER ≈ 50–100 Ω·cm²; apparent permeability (Papp) increases from 0.3 × 10^{-6} cm/s (co-culture) → 2.6 × 10^{-6} cm/s (triple), ≈ 9× increase (*Araújo & Sarmento, 2013; Antunes et al., 2013*).	TEER 1,200–6,500 Ω·cm² (FBS media) or 500–1,000 Ω·cm² (porcine serum) (*Zakrzewski et al., 2013*).	FHs 74 Int = 500–600 Ω·cm² (*Lu et al., 2021*); HIEC-6 = 31–32 Ω·cm² (mean ± SD).
Tight-junction (TJ) proteins and architecture	Expresses ZO1, occludin (OCLN), claudins (CLDN1, 3, 4, 7), junctional adhesion molecule-A (JAM-A), E-cadherin (*Fedi et al., 2021; Artursson et al., 2001*).	TJ strands visible between both Caco-2↔HT29 and Caco-2↔Caco-2 cells; barrier looser than pure Caco-2, consistent with lower TEER and higher paracellular flux (*Hilgendorf et al., 2000; Walter et al., 1996*).	Tight junctions present; Raji B–induced M cells locally reduce microvilli density. CLDN1, 3, 4, 5, 7, 8, 12 expressed; CLDN2 and 15 absent (*Gullberg et al., 2000; Vergauwen, 2015*).	Expresses CLDN1, 3, 4, 5, 7, 8, 12; CLDN2 and 15 absent (*Vergauwen, 2015*).	FHs 74 Int expresses OCLN (*Lu et al., 2021*); HIEC-6 expresses ZO1 and CLDN1 but lacks OCLN.
Nutrient and drug transporters	Expresses transporters including SGLT1, GLUT1–5, PEPT1, organic anion	Transporter expression similar to Caco-2; co-culture yields	Transporter profile dominated by Caco-2; Raji	Expresses SGLT1, GLUT2, PEPT1, amino-	HIEC-6 shows lipid-absorptive

	transporting polypeptide (OATP2B1), monocarboxylate transporter 1 (MCT1), apical sodium–bile acid transporter (ASBT), organic cation transporter (OCTN2), multidrug resistance protein 1 (MDR1/P-gp), and multidrug resistance–associated proteins (MRP2–6) (*Sun et al., 2002; Sambuy et al., 2005*). SGLT1 > 600× higher in duodenum vs Caco-2; GLUT5 ≈ 20× higher in duodenum; GLUT3 ≈ 150× higher in Caco-2 (*Sun et al., 2002*).	permeability and iron absorption values closer to in vivo intestine (*McCright et al., 2022*).	B–induced M cells enhance macromolecule and particle transcytosis (*Araújo & Sarmento, 2013*).	acid transporters (B^0,+AT, y^+LAT1, ASCT2), and lipid-related genes (FATP1/4, CD36, FABP3, DGAT1) (*Chen et al., 2021; Liao et al., 2017; Tang & Xiong, 2022; Xu et al., 2023*).	capacity; FHs 74 Int data limited (*Maheshwari et al., 2002*).
Brush-border enzymes (BBEs)	High alkaline phosphatase (ALP), sucrase–isomaltase (SI), and aminopeptidase N (APN) expression after confluence (*Ferruzza et al., 2012*). CYP3A4 ≈ 160×, CYP2B1 49×, CYP2C9 17×, CYP2J2 20×, CYP PCN3 322× higher in duodenum vs Caco-2 (*Sun et al., 2002*).	Co-culture retains Caco-2 enterocyte BBEs; HT29-MTX has lower SI and ALP expression (*Antunes et al., 2013*).	M-cell induction downregulates ALP; M-cell regions lack BBEs (*Araújo & Sarmento, 2013; Gullberg et al., 2000*).	ALP activity confirmed; BBEs expressed similarly to enterocytes (*Tang & Xiong, 2022*).	FHs 74 Int expresses ALP; HIEC-6 expresses APN and DPP-IV but lacks SI (*Maheshwari et al., 2002*).

1.5. Experimental Strategies for Modelling the Infant Gut Barrier

Although human fetal cell lines and pediatric intestinal organoids provide physiologically relevant insights into the immature intestinal epithelium, their application remains limited by technical complexity, high cost, and restricted accessibility. These constraints make them unsuitable for routine or large-scale nutritional screening. Consequently, researchers continue to rely on more accessible models such as Caco-2, which, despite its adult origin, offers a reproducible and well-characterized epithelial system. However, Caco-2 monolayers typically display high TEER and low paracellular permeability. These traits differ markedly from the naturally leaky neonatal intestine. To address this limitation, several experimental strategies have been developed to modulate tight-junction architecture and thereby increase Caco-2 permeability. The following section summarizes these approaches and the molecular agents used to reproduce a physiologically relevant, infant-like barrier phenotype *in vitro*.

A recently published paper from our group reports that 125 mM sodium butyrate (NaB) increases the Caco-2 paracellular permeability through tight junction modification without causing inflammation (Kondrashina et al., 2021). In particular, NaB at 125 mM decreased the TEER, increased the lactulose and mannitol leakage through the monolayer, increased the transport of the dairy proteins β–lactoglobulin and α–lactalbumin, and modified the tight junction architecture without being cytotoxic or inducing inflammation. NaB is the sodium salt of the corresponding short-chain fatty acid (SCFA), abundantly present in the gut and produced by the intestinal microbiota. Numerous studies have proven that butyrate, at physiological concentrations, has a positive effect on gut health, improving the epithelial barrier

and reducing paracellular permeability (Mariadason et al., 1997). Therefore, it might seem surprising that a high concentration of NaB induces the opposite effect. However, there is evidence *in vitro* (Donohoe et al., 2012; Peng et al., 2007) and *ex vivo* (Mariadason et al., 1999) confirming its dual effect depending on the concentration. Further studies are therefore warranted to confirm whether NaB can be used to create a physiologically relevant, infant-like intestinal model.

Other molecules that can transiently enhance the permeability of the gut barrier without being cytotoxic have been studied in the field of orally delivered drugs and peptides but to date have not been used to create an infant-like gut barrier. The permeability enhancers belong to three categories: (i) surfactants, which enhance the transcellular route by disrupting membranes; (ii) non-surfactants, which increase the paracellular route by modulating tight junctions; and (iii) mixed-action agents, which act on both mechanisms (Maher and Mrsny, 2016). Given that the infant gut barrier is inherently more permeable—both due to looser tight junctions (see Section 2.2) and increased membrane fluidity (see Section 2.3)—permeability enhancers with mixed modes of action are particularly promising for converting a standard Caco-2 monolayer into a leaky but non-inflamed gut barrier.

Among these compounds, medium-chain fatty acids have shown significant potential. Specifically, treatment with the sodium salts of the fatty acids with a chain length from C8 to C12 will result in Caco-2 monolayers with decreased TEER and increased [^{14}C]-mannitol permeability. (Brayden et al., 2014; Lindmark et al., 1995). The EC_{50} for barrier disruption decreases with increasing chain length—C12 having

the lowest (1.8 mM) and C8 the highest (74 mM)—while cytotoxicity increases with chain length (Brayden et al., 2014).

Thus, sodium caprate (C10) has emerged as the most suitable medium-chain fatty acid permeability enhancer, capable of increasing both paracellular and transcellular permeability in Caco-2 monolayers at non-cytotoxic concentrations. At concentrations between 8.5 and 13 mM, C10 perturbs Caco-2 plasma and mitochondrial membranes and increases intracellular calcium, which activates calmodulin and myosin light-chain kinase, leading to peri junctional actomyosin contraction and tight junction opening (Twarog et al., 2019). However, C10 use is restricted to calcium-free buffers, as it precipitates with calcium, limiting its application in cell culture (Lindmark et al., 1998; Twarog et al., 2020; Watson et al., 2001).

Medium-chain fatty acid derivatives, such as sodium N-(8-[2-hydroxybenzoyl]amino) caprylate (SNAC)—a C8 derivative—have received significant attention as permeability enhancers in *in vitro* and *in vivo* studies. SNAC has demonstrated concentration-dependent reductions in barrier TEER and increases in the flux of permeability markers such as [^{3}H]-mannitol, FD4, and heparin, without inducing cytotoxicity (Alani and Robinson, 2008; Brayden et al., 1997; Malkov et al., n.d.; Twarog et al., 2020). However, in Caco-2 monolayers, SNAC primarily enhances transcellular permeability by transiently altering plasma membrane integrity and increasing intracellular calcium levels, rather then affecting the paracellular pathway (Twarog et al., 2020).

In addition to medium-chain fatty acids, bile salts have been investigated as permeability enhancers in *in vitro*, *ex vivo*, and *in vivo* models. Bile salts such as

cholate, taurocholate, chenodeoxycholate, ursodeoxycholate, and glycodeoxycholate enhance the permeability of hydrophilic markers and drugs (Brayden and Stuettgen, 2021; Fricker et al., 1996; Mahalingam et al., 2007; Meaney and O'Driscoll, 2000; Mukaizawa et al., 2009). In the human gut, bile salts exist as conjugated and unconjugated forms. Conjugated bile salts, bound to amino acids such as glycine or taurine, are more water-soluble and generally less toxic (Hofmann and Hagey, 2008). In contrast, unconjugated bile salts, such as sodium cholate, are more effective but more cytotoxic (Meaney and O'Driscoll, 2000).

Among the conjugated bile salts, glycodeoxycholic acid (GDC) is a secondary bile salt conjugated with glycine and synthesized via hepatic and microbial metabolism (Chiang, 2009; Ridlon et al., 2006). GDC has demonstrated strong permeability-enhancing effects. GDC significantly increased macromolecule transport *in vitro* in Caco-2 monolayers (Brayden and Stuettgen, 2021; Song et al., 2005), *ex vivo* (Hoogstraate et al., 1996a), and *in vivo* (Hoogstraate et al., 1996b). Specifically, 2.12 mM GDC increased calcitonin permeability by 10.66-fold and reduced monolayer TEER by 4.57-fold (Song et al., 2005).Treatment of Caco-2 monolayers with 0.5 mM GDC increased [14C]-mannitol apparent permeability (Papp) threefold and decreased TEER 2.5-fold, without cytotoxicity, as confirmed by MTS, CellTox™ Green, and Caspase 3/7 assays (Brayden and Stuettgen, 2021).

In summary, permeability enhancers such as SCFAs (e.g., sodium butyrate), medium-chain fatty acids (e.g., sodium caprate and SNAC), and bile salts (e.g., GDC) represent promising tools for developing *in vitro* models that mimic the naturally leaky yet non-inflamed state of the neonatal intestine.

1.6.Conclusion

The infant intestine represents a transient but critical stage of postnatal development, during which barrier permeability is naturally higher and plays an essential role in early adaptation. This physiological openness allows interactions between luminal components and the developing mucosa, contributing to the maturation of epithelial, microbial, and immune functions. As this “permeable barrier” matures, it evolves into the selective, homeostatic barrier of adulthood, and the tempo of this transformation may influence lifelong metabolic and inflammatory trajectories. Human milk guides this process through a complex combination of nutrients and bioactive molecules that support epithelial maturation, microbial colonization, and immune tolerance. Conventional formulas do not replicate the effects of human milk. Bridging this gap will require innovative formulations informed by physiologically relevant, high-throughput *in vitro* models that capture the dynamic features of the neonatal gut. Ultimately, understanding and recreating the unique properties of the infant intestine offers a blueprint for optimizing early-life nutrition and reducing disease risk across the lifespan.

1.7.References

Adeniyi-Ipadeola, Grace O., Julia D. Hankins, Amal Kambal, et al. 2024. “Infant and Adult Human Intestinal Enteroids Are Morphologically and Functionally Distinct.” mBio 15 (8): e01316-24. https://doi.org/10.1128/mbio.01316-24.

Adeola, O., and D. E. King. 2006. “Developmental Changes in Morphometry of the Small Intestine and Jejunal Sucrase Activity during the First Nine Weeks of Postnatal Growth in Pigs1.” Journal of Animal Science 84 (1): 112–18. https://doi.org/10.2527/2006.841112x.

Alani, Adam W. G., and Joseph R. Robinson. 2008. “Mechanistic Understanding of Oral Drug Absorption Enhancement of Cromolyn Sodium by an Amino Acid Derivative.” Pharmaceutical Research 25 (1): 48–54. https://doi.org/10.1007/s11095-007-9438-6.

Anand, Rahul J., Cynthia L. Leaphart, Kevin P. Mollen, and David J. Hackam. 2007. “THE ROLE OF THE INTESTINAL BARRIER IN THE PATHOGENESIS OF NECROTIZING ENTEROCOLITIS.” Shock 27 (2): 124–33. https://doi.org/10.1097/01.shk.0000239774.02904.65.

Andreas, Nicholas J., Beate Kampmann, and Kirsty Mehring Le-Doare. 2015. “Human Breast Milk: A Review on Its Composition and Bioactivity.” Early Human Development 91 (11): 629–35. https://doi.org/10.1016/j.earlhumdev.2015.08.013.

Antunes, Filipa, Fernanda Andrade, Francisca Araújo, Domingos Ferreira, and Bruno Sarmento. 2013. “Establishment of a Triple Co-Culture in Vitro Cell Models to Study Intestinal Absorption of Peptide Drugs.” European Journal of Pharmaceutics and Biopharmaceutics 83 (3): 427–35. https://doi.org/10.1016/j.ejpb.2012.10.003.

Araújo, Francisca, and Bruno Sarmento. 2013. “Towards the Characterization of an in Vitro Triple Co-Culture Intestine Cell Model for Permeability Studies.” International Journal of Pharmaceutics 458 (1): 128–34. https://doi.org/10.1016/j.ijpharm.2013.10.003.

Artursson, Per, Katrin Palm, and Kristina Luthman. 2012. “Caco-2 Monolayers in Experimental and Theoretical Predictions of Drug Transport.” Advanced Drug Delivery Reviews 64 (December): 280–89. https://doi.org/10.1016/j.addr.2012.09.005.

Auricchio, Salvatore, Antonio Stellato, and Basilio De Vizia. 1981. “Development of Brush Border Peptidases in Human and Rat Small Intestine during Fetal and Neonatal Life.” Pediatric Research 15 (7): 7. https://doi.org/10.1203/00006450-198107000-00003.

Baker, Kristi, Shuo-Wang Qiao, Timothy Kuo, et al. 2009. “Immune and Non-Immune Functions of the (Not so) Neonatal Fc Receptor, FcRn.” Seminars in Immunopathology 31 (2): 223–36. https://doi.org/10.1007/s00281-009-0160-9.

Balamurugan, Krishnaswamy, and Hamid M. Said. 2003. “Ontogenic Regulation of Folate Transport across Rat Jejunal Brush-Border Membrane.” American Journal of Physiology-Gastrointestinal and Liver Physiology 285 (5): G1068–73. https://doi.org/10.1152/ajpgi.00188.2003.

Ballard, Olivia, and Ardythe L. Morrow. 2013. “Human Milk Composition.” Pediatric Clinics of North America 60 (1): 49–74. https://doi.org/10.1016/j.pcl.2012.10.002.

Bauerly, Kathryn A, Shannon L Kelleher, and Bo Lönnerdal. 2004. “Functional and Molecular Responses of Suckling Rat Pups and Human Intestinal Caco-2

Cells to Copper Treatment." The Journal of Nutritional Biochemistry 15 (3): 155–62. https://doi.org/10.1016/j.jnutbio.2003.10.008.

Bein, Amir, Smadar Eventov-Friedman, Dan Arbell, and Betty Schwartz. 2018. "Intestinal Tight Junctions Are Severely Altered in NEC Preterm Neonates." Pediatrics & Neonatology 59 (5): 464–73. https://doi.org/10.1016/j.pedneo.2017.11.018.

Bernardini, Chiara, Cristina Algieri, La Debora Mantia, et al. 2021. "Relationship between Serum Concentration, Functional Parameters and Cell Bioenergetics in IPEC-J2 Cell Line." Histochemistry and Cell Biology 156 (1): 59–67. https://doi.org/10.1007/s00418-021-01981-2.

Berschneider, H. M. 1989. "Development of Normal Cultured Small Intestinal Epithelial Cell Lines Which Transport Na and Cl." Gastroenterology 96 (Suppl. Pt 2): A41.

Bevins, Charles L., and Nita H. Salzman. 2011. "Paneth Cells, Antimicrobial Peptides and Maintenance of Intestinal Homeostasis." Nature Reviews Microbiology 9 (5): 356–68. https://doi.org/10.1038/nrmicro2546.

Biondi Ryan, Marie R, Jillien Zukaitis, Suwimon Sutantawong, and David C Dallas. 2025. "Overall Evidence for Milk-Derived Proteins and Peptides in Blood after Digestion: A Systematic Review." Nutrition Reviews, August 29, nuaf118. https://doi.org/10.1093/nutrit/nuaf118.

Birchenough, G M H, M Ev Johansson, J K Gustafsson, J H Bergström, and G C Hansson. 2015. "New Developments in Goblet Cell Mucus Secretion and Function." Mucosal Immunology 8 (4): 712–19. https://doi.org/10.1038/mi.2015.32.

Birchenough, George M. H., Fatma Dalgakiran, Luci A. Witcomb, et al. 2017. "Postnatal Development of the Small Intestinal Mucosa Drives Age-Dependent, Regio-Selective Susceptibility to Escherichia Coli K1 Infection." Scientific Reports 7 (1): 83. https://doi.org/10.1038/s41598-017-00123-w.

Black, D D, PL Rohwer-Nutter, and NO Davidson. 1990. "Intestinal Apolipoprotein A-IV Gene Expression in the Piglet." Journal of Lipid Research 31 (3): 497–505. https://doi.org/10.1016/S0022-2275(20)43171-2.

Bode, L. 2012. "Human Milk Oligosaccharides: Every Baby Needs a Sugar Mama." Glycobiology 22 (9): 1147–62. https://doi.org/10.1093/glycob/cws074.

Brasitus, T. A., K. Y. Yeh, P. R. Holt, and D. Schachter. 1984. "Lipid Fluidity and Composition of Intestinal Microvillus Membranes Isolated from Rats of Different Ages." Biochimica Et Biophysica Acta 778 (2): 341–48. https://doi.org/10.1016/0005-2736(84)90378-x.

Brayden, D., E. Creed, A. O'Connell, H. Leipold, R. Agarwal, and A. Leone-Bay. 1997. "Heparin Absorption across the Intestine: Effects of Sodium N-[8-(2-Hydroxybenzoyl)Amino]Caprylate in Rat in Situ Intestinal Instillations and in Caco-2 Monolayers." Pharmaceutical Research 14 (12): 1772–79. Scopus. https://doi.org/10.1023/A:1012192115828.

Brayden, David J., John Gleeson, and Edwin G. Walsh. 2014. "A Head-to-Head Multi-Parametric High Content Analysis of a Series of Medium Chain Fatty Acid Intestinal Permeation Enhancers in Caco-2 Cells." European Journal of Pharmaceutics and Biopharmaceutics 88 (3): 830–39. https://doi.org/10.1016/j.ejpb.2014.10.008.

Brayden, David J, and Vivien Stuettgen. 2021. "Sodium Glycodeoxycholate and Sodium Deoxycholate as Epithelial Permeation Enhancers: In Vitro and Ex

Vivo Intestinal and Buccal Bioassays." European Journal of Pharmaceutical Sciences, 12.

Briske-Anderson, M. J., J. W. Finley, and S. M. Newman. 1997. "The Influence of Culture Time and Passage Number on the Morphological and Physiological Development of Caco-2 Cells." Proceedings of the Society for Experimental Biology and Medicine. Society for Experimental Biology and Medicine (New York, N.Y.) 214 (3): 248–57. https://doi.org/10.3181/00379727-214-44093.

Brosnahan, Amanda J., and David R. Brown. 2012. "Porcine IPEC-J2 Intestinal Epithelial Cells in Microbiological Investigations." Veterinary Microbiology 156 (3): 229–37. https://doi.org/10.1016/j.vetmic.2011.10.017.

Castelló, A, A Gumá, L Sevilla, et al. 1995. "Regulation of GLUT5 Gene Expression in Rat Intestinal Mucosa: Regional Distribution, Circadian Rhythm, Perinatal Development and Effect of Diabetes." Biochemical Journal 309 (Pt 1): 271–77.

Catassi, C., A. Bonucci, G. V. Coppa, A. Carlucci, and P. L. Giorgi. 1995. "Intestinal Permeability. Changes during the First Month: Effect of Natural versus Artificial Feeding." Journal of Pediatric Gastroenterology and Nutrition 21 (4): 383–86. https://doi.org/10.1097/00005176-199511000-00003.

Chen, Min, Yingkui Yang, Evan Braunstein, Keith E. Georgeson, and Carroll M. Harmon. 2001. "Gut Expression and Regulation of FAT/CD36: Possible Role in Fatty Acid Transport in Rat Enterocytes." American Journal of Physiology-Endocrinology and Metabolism 281 (5): E916–23. https://doi.org/10.1152/ajpendo.2001.281.5.E916.

Chen, Zhigang, Lihua Zhou, Qiaoling Yuan, Huiyu Chen, Hongyu Lei, and Jianming Su. 2021. “Effect of Fumonisin B1on Oxidative Stress and Gene Expression Alteration of Nutrient Transporters in Porcine Intestinal Cells.” Journal of Biochemical and Molecular Toxicology 35 (4). https://doi.org/10.1002/jbt.22706.

Chiang, John Y.L. 2009. “Bile Acids: Regulation of Synthesis.” Journal of Lipid Research 50 (10): 1955–66. https://doi.org/10.1194/jlr.R900010-JLR200.

Choudhuri, Supratim, and Ronald F. Chanderbhan. 2016. “The Biology of Nutrients.” In Nutraceuticals. Elsevier. https://doi.org/10.1016/B978-0-12-802147-7.00017-6.

Chu, Shu-Heh W., and W. Allan Walker. 1988. “Development of the Gastrointestinal Mucosal Barrier: Changes in Phospholipid Head Groups and Fatty Add Composition of Intestinal Microvillus Membranes from Newborn and Adult Rats.” Pediatric Research 23 (4): 4. https://doi.org/10.1203/00006450-198804000-00020.

Citi, Sandra, Michael Fromm, Mikio Furuse, et al. 2024. “A Short Guide to the Tight Junction.” Journal of Cell Science 137 (9): jcs261776. https://doi.org/10.1242/jcs.261776.

Clark, Jessica A., Robert H. Lane, Nicole K. MacLennan, et al. 2005. “Epidermal Growth Factor Reduces Intestinal Apoptosis in an Experimental Model of Necrotizing Enterocolitis.” American Journal of Physiology-Gastrointestinal and Liver Physiology 288 (4): G755–62. https://doi.org/10.1152/ajpgi.00172.2004.

Cui, Xue-Lin, Lan Jiang, and Ronaldo P. Ferraris. 2003. “Regulation of Rat Intestinal GLUT2 mRNA Abundance by Luminal and Systemic Factors.”

Biochimica Et Biophysica Acta 1612 (2): 178–85. https://doi.org/10.1016/s0005-2736(03)00129-9.

Cummins, A G, T W Steele, J T LaBrooy, and D J Shearman. 1988. “Maturation of the Rat Small Intestine at Weaning: Changes in Epithelial Cell Kinetics, Bacterial Flora, and Mucosal Immune Activity.” Gut 29 (12): 1672–79. https://doi.org/10.1136/gut.29.12.1672.

Darragh, Alison J., and Paul J. Moughan. 1995. “The Three-Week-Old Piglet as a Model Animal for Studying Protein Digestion in Human Infants.” Journal of Pediatric Gastroenterology and Nutrition 21 (4): 387–93. https://doi.org/10.1097/00005176-199511000-00004.

Davidson, N. O., A. M. Hausman, C. A. Ifkovits, et al. 1992. “Human Intestinal Glucose Transporter Expression and Localization of GLUT5.” American Journal of Physiology-Cell Physiology 262 (3): C795–800. https://doi.org/10.1152/ajpcell.1992.262.3.C795.

Deplancke, Bart, and H Rex Gaskins. 2001. “Microbial Modulation of Innate Defense: Goblet Cells and the Intestinal Mucus Layer.” The American Journal of Clinical Nutrition 73 (6): 1131S-1141S. https://doi.org/10.1093/ajcn/73.6.1131S.

Dew, Stephanie E., and David E. Ong. 1994. “Specificity of the Retinol Transporter of the Rat Small Intestine Brush Border.” Biochemistry 33 (40): 12340–45. https://doi.org/10.1021/bi00206a042.

Dew, Stephanie E., and David E. Ong. 1997. “Absorption of Retinol from the Retinol:Retinol-Binding Protein Complex by Small Intestinal Gut Sheets from the Rat.” Archives of Biochemistry and Biophysics 338 (2): 233–36. https://doi.org/10.1006/abbi.1996.9830.

Dickinson, B.L., K. Badizadegan, Z. Wu, et al. 1999. “Bidirectional FcRn-Dependent IgG Transport in a Polarized Human Intestinal Epithelial Cell Line.” Journal of Clinical Investigation 104 (7): 903–11. Scopus. https://doi.org/10.1172/JCI6968.

Dieckgraefe, B. K., B. Seetharam, and D. H. Alpers. 1988. “Developmental Regulation of Rat Intrinsic Factor mRNA.” American Journal of Physiology-Gastrointestinal and Liver Physiology, ahead of print, June 1. Bethesda, MD. https://doi.org/10.1152/ajpgi.1988.254.6.G913.

Directive 2010/63/EU of the European Parliament and of the Council on the Protection of Animals Used for Scientific Purposes. n.d. 47.

Domellöf, Magnus, Bo Lönnerdal, Steven A Abrams, and Olle Hernell. 2002. “Iron Absorption in Breast-Fed Infants: Effects of Age, Iron Status, Iron Supplements, and Complementary Foods.” The American Journal of Clinical Nutrition 76 (1): 198–204. https://doi.org/10.1093/ajcn/76.1.198.

Donohoe, Dallas R., Leonard B. Collins, Aminah Wali, Rebecca Bigler, Wei Sun, and Scott J. Bultman. 2012. “The Warburg Effect Dictates the Mechanism of Butyrate-Mediated Histone Acetylation and Cell Proliferation.” Molecular Cell 48 (4): 612–26. https://doi.org/10.1016/j.molcel.2012.08.033.

Duan, Rui-Dong, Yajun Cheng, Bo A. G. Jönsson, et al. 2007. “Human Meconium Contains Significant Amounts of Alkaline Sphingomyelinase, Neutral Ceramidase, and Sphingolipid Metabolites.” Pediatric Research 61 (1): 1. https://doi.org/10.1203/01.pdr.0000250534.92934.c2.

Duluc, I, B Jost, and J N Freund. 1993. “Multiple Levels of Control of the Stage- and Region-Specific Expression of Rat Intestinal Lactase.” The Journal of Cell Biology 123 (6): 1577–86. https://doi.org/10.1083/jcb.123.6.1577.

Efremov, Yuri M., Liubov Shimolina, Alexander Gulin, et al. 2023. “Correlation of Plasma Membrane Microviscosity and Cell Stiffness Revealed via Fluorescence-Lifetime Imaging and Atomic Force Microscopy.” Cells 12 (21): 2583. https://doi.org/10.3390/cells12212583.

Elzinga, Janneke, Benthe Van Der Lugt, Clara Belzer, and Wilma T. Steegenga. 2021. “Characterization of Increased Mucus Production of HT29-MTX-E12 Cells Grown under Semi-Wet Interface with Mechanical Stimulation.” PLOS ONE 16 (12): e0261191. https://doi.org/10.1371/journal.pone.0261191.

Epstein, M. A., B. G. Achong, Y. M. Barr, B. Zajac, G. Henle, and W. Henle. 1966. “Morphological and Virological Investigations on Cultured Burkitt Tumor Lymphoblasts (Strain Raji).” Journal of the National Cancer Institute 37 (4): 547–59.

Fan, Ming Z., Olayiwola Adeola, Elikplimi K. Asem, and Dale King. 2002. “Postnatal Ontogeny of Kinetics of Porcine Jejunal Brush Border Membrane-Bound Alkaline Phosphatase, Aminopeptidase N and Sucrase Activities.” Comparative Biochemistry and Physiology Part A: Molecular & Integrative Physiology 132 (3): 599–607. https://doi.org/10.1016/S1095-6433(02)00102-2.

Faubion, W A, M Camilleri, J A Murray, et al. 2016. “Improving the Detection of Environmental Enteric Dysfunction: A Lactulose, Rhamnose Assay of Intestinal Permeability in Children Aged under 5 Years Exposed to Poor Sanitation and Hygiene.” BMJ Global Health 1 (1): e000066. https://doi.org/10.1136/bmjgh-2016-000066.

Fedi, Arianna, Chiara Vitale, Giulia Ponschin, Seyoum Ayehunie, Marco Fato, and Silvia Scaglione. 2021. “In Vitro Models Replicating the Human Intestinal

Epithelium for Absorption and Metabolism Studies: A Systematic Review." Journal of Controlled Release 335 (July): 247–68. https://doi.org/10.1016/j.jconrel.2021.05.028.

Ferruzza, Simonetta, Carlotta Rossi, Maria Laura Scarino, and Yula Sambuy. 2012. "A Protocol for in Situ Enzyme Assays to Assess the Differentiation of Human Intestinal Caco-2 Cells." Toxicology in Vitro 26 (8): 1247–51. https://doi.org/10.1016/j.tiv.2011.11.007.

Fitzgerald, J F, S Reiser, and P A Christiansen. 1971. "Developmental Pattern of Sugar and Amino Acid Transport in the Postnatal Rat Small Intestine." Pediatric Research 5 (12): 698–703. https://doi.org/10.1203/00006450-197112000-00007.

Fitzgerald, J F, S Reiser, and P A Christiansen. 1972. "Amino Acid Transport Pathways in the Small Intestine of the Neonatal Rat." Pediatric Research 6 (7): 713–19. https://doi.org/10.1203/00006450-197207000-00004.

Flores, C. A., S. A. Hing, M. A. Wells, and O. Koldovský. 1989. "Rates of Triolein Absorption in Suckling and Adult Rats." The American Journal of Physiology 257 (5 Pt 1): G823-829. https://doi.org/10.1152/ajpgi.1989.257.5.G823.

Fogh, J., W. C. Wright, and J. D. Loveless. 1977. "Absence of HeLa Cell Contamination in 169 Cell Lines Derived from Human Tumors." Journal of the National Cancer Institute 58 (2): 209–14. https://doi.org/10.1093/jnci/58.2.209.

Fogh, Jørgen, and Germain Trempe. 1975. "New Human Tumor Cell Lines." In Human Tumor Cells in Vitro, edited by Jørgen Fogh. Springer US. https://doi.org/10.1007/978-1-4757-1647-4_5.

Freund, J. N., I. Duluc, and F. Raul. 1991. “Lactase Expression Is Controlled Differently in the Jejunum and Ileum during Development in Rats.” Gastroenterology 100 (2): 388–94. https://doi.org/10.1016/0016-5085(91)90207-2.

Fricker, G., A. Fahr, C. Beglinger, T. Kissel, G. Reiter, and J. Drewe. 1996. “Permeation Enhancement of Octreotide by Specific Bile Salts in Rats and Human Subjects: In Vitro, in Vivo Correlations.” British Journal of Pharmacology 117 (1): 217–23. https://doi.org/10.1111/j.1476-5381.1996.tb15177.x.

Gauthier, Rémy, Charlène Harnois, Jean-François Drolet, John C. Reed, Anne Vézina, and Pierre H. Vachon. 2001. “Human Intestinal Epithelial Cell Survival: Differentiation State-Specific Control Mechanisms.” American Journal of Physiology-Cell Physiology 280 (6): C1540–54. https://doi.org/10.1152/ajpcell.2001.280.6.C1540.

Gerbault, Pascale, Anke Liebert, Yuval Itan, et al. 2011. “Evolution of Lactase Persistence: An Example of Human Niche Construction.” Philosophical Transactions of the Royal Society B: Biological Sciences 366 (1566): 863–77. https://doi.org/10.1098/rstb.2010.0268.

Ghishan, F. K., J. T. Jenkins, and M. K. Younoszai. 1980. “Maturation of Calcium Transport in the Rat Small and Large Intestine.” The Journal of Nutrition 110 (8): 1622–28. https://doi.org/10.1093/jn/110.8.1622.

Ghishan, Fayez K., and Raymond L. Meneely. 1982. “Intestinal Maturation: The Effect of Glucocorticoids on in Vivo Net Magnesium and Calcium Transport in the Rat.” Life Sciences 31 (2): 133–38. https://doi.org/10.1016/0024-3205(82)90425-8.

Glatz, Jan F. C., and Joost J. F. P. Luiken. 2017. “From Fat to FAT (CD36/SR-B2): Understanding the Regulation of Cellular Fatty Acid Uptake.” Biochimie, “Pleiotropic physiological roles of PPARs and Fatty Acids” a tribute to Paul Grimaldi’, vol. 136 (May): 21–26. https://doi.org/10.1016/j.biochi.2016.12.007.

Gleeson, John P., Katherine C. Fein, Namit Chaudhary, Rose Doerfler, Alexandra N. Newby, and Kathryn A. Whitehead. 2021. “The Enhanced Intestinal Permeability of Infant Mice Enables Oral Protein and Macromolecular Absorption without Delivery Technology.” International Journal of Pharmaceutics 593: 120120. https://doi.org/10.1016/j.ijpharm.2020.120120.

Gribble, Fiona M., and Frank Reimann. 2019. “Function and Mechanisms of Enteroendocrine Cells and Gut Hormones in Metabolism.” Nature Reviews Endocrinology 15 (4): 226–37. https://doi.org/10.1038/s41574-019-0168-8.

Guandalini, Stefano, and Armido Rubino. 1982. “Development of Dipeptide Transport in the Intestinal Mucosa of Rabbits.” Pediatric Research 16 (2): 2. https://doi.org/10.1203/00006450-198202000-00004.

Gullberg, Elisabet, Maurice Leonard, Johan Karlsson, et al. 2000. “Expression of Specific Markers and Particle Transport in a New Human Intestinal M-Cell Model.” Biochemical and Biophysical Research Communications 279 (3): 808–13. https://doi.org/10.1006/bbrc.2000.4038.

Guo, Jinyue, Fei Li, Qigai He, et al. 2016. “Neonatal Fc Receptor-Mediated IgG Transport Across Porcine Intestinal Epithelial Cells: Potentially Provide the Mucosal Protection.” DNA and Cell Biology 35 (6): 301–9. https://doi.org/10.1089/dna.2015.3165.

Harayama, Takeshi, and Howard Riezman. 2018. “Understanding the Diversity of Membrane Lipid Composition.” Nature Reviews Molecular Cell Biology 19 (5): 281–96. https://doi.org/10.1038/nrm.2017.138.

Harris, Nicola L., Iris Spoerri, Jacqueline F. Schopfer, et al. 2006. “Mechanisms of Neonatal Mucosal Antibody Protection.” HOST DEFENSE. The Journal of Immunology 177 (9): 6256–62. https://doi.org/10.4049/jimmunol.177.9.6256.

Hecht, A, Cf Torbey, Ha Korsmo, and Wa Olsen. 1997. “Regulation of Sucrase and Lactase in Developing Rats: Role of Nuclear Factors That Bind to Two Gene Regulatory Elements.” Gastroenterology 112 (3): 803–12. https://doi.org/10.1053/gast.1997.v112.pm9041242.

Herath, Madushani, Suzanne Hosie, Joel C. Bornstein, Ashley E. Franks, and Elisa L. Hill-Yardin. 2020. “The Role of the Gastrointestinal Mucus System in Intestinal Homeostasis: Implications for Neurological Disorders.” Frontiers in Cellular and Infection Microbiology 10. https://www.frontiersin.org/article/10.3389/fcimb.2020.00248.

Hernández-Jodra, M., and C. Gancedo. 1971. “Isoenzymes of Alkaline Phosphatase in Human Meconium and Small Intestine during Development.” Enzyme 12: 682–87. https://doi.org/10.1159/000459603.

Hickey, John W., Winston R. Becker, Stephanie A. Nevins, et al. 2023. “Organization of the Human Intestine at Single-Cell Resolution.” Nature 619 (7970): 572–84. https://doi.org/10.1038/s41586-023-05915-x.

Hilgendorf, Constanze, Hildegard Spahn-Langguth, Carl G. Regårdh, Elke Lipka, Gordon L. Amidon, and Peter Langguth. 2000. “Caco-2 versus Caco-2/HT29-MTX Co-cultured Cell Lines: Permeabilities Via Diffusion, Inside-

and Outside-Directed Carrier-Mediated Transport." Journal of Pharmaceutical Sciences 89 (1): 63–75. https://doi.org/10.1002/(SICI)1520-6017(200001)89:1<63::AID-JPS7>3.0.CO;2-6.

Hill, R. R. H., H. M. Cowley, and A. Andremont. 1990. "Influence of Colonizing Micro-Flora on the Mucin Histochemistry of the Neonatal Mouse Colon." The Histochemical Journal 22 (2): 102–5. https://doi.org/10.1007/BF01885788.

Hofmann, A. F., and L. R. Hagey. 2008. "Bile Acids: Chemistry, Pathochemistry, Biology, Pathobiology, and Therapeutics." Cellular and Molecular Life Sciences 65 (16): 2461–83. https://doi.org/10.1007/s00018-008-7568-6.

Holmes, Jennifer L., Christina M. Van Itallie, Julia E. Rasmussen, and James M. Anderson. 2006. "Claudin Profiling in the Mouse during Postnatal Intestinal Development and along the Gastrointestinal Tract Reveals Complex Expression Patterns." Gene Expression Patterns 6 (6): 581–88. https://doi.org/10.1016/j.modgep.2005.12.001.

Hoogstraate, A.J., S. Senel, C. Cullander, J. Verhoef, H.E. Junginger, and H.E Boddé. 1996. "Effects of Bile Salts on Transport Rates and Routes of FITC-Labelled Compounds across Porcine Buccal Epithelium in Vitro." Journal of Controlled Release 40 (3): 211–21. https://doi.org/10.1016/0168-3659(95)00187-5.

Hoogstraate, A.J., J.C. Verhoef, B. Tuk, et al. 1996. "In-Vivo Buccal Delivery of Fluorescein Isothiocyanate–Dextran 4400 with Glycodeoxycholate as an Absorption Enhancer in Pigs." Journal of Pharmaceutical Sciences 85 (5): 457–60. https://doi.org/10.1021/js950129k.

Hooton, Diane, Roger Lentle, John Monro, Martin Wickham, and Robert Simpson. 2015. “The Secretion and Action of Brush Border Enzymes in the Mammalian Small Intestine.” In Reviews of Physiology, Biochemistry and Pharmacology, edited by Bernd Nilius, Thomas Gudermann, Reinhard Jahn, Roland Lill, Ole H. Petersen, and Pieter P. de Tombe, vol. 168. Reviews of Physiology, Biochemistry and Pharmacology. Springer International Publishing. https://doi.org/10.1007/112_2015_24.

Horowitz, Arie, Sandra D. Chanez-Paredes, Xenia Haest, and Jerrold R. Turner. 2023. “Paracellular Permeability and Tight Junction Regulation in Gut Health and Disease.” Nature Reviews Gastroenterology & Hepatology 20 (7): 417–32. https://doi.org/10.1038/s41575-023-00766-3.

Huang, Zhixin L., Jodi Dufner-Beattie, and Glen K. Andrews. 2006. “Expression and Regulation of SLC39A Family Zinc Transporters in the Developing Mouse Intestine.” Developmental Biology 295 (2): 571–79. https://doi.org/10.1016/j.ydbio.2006.03.045.

Hübner, C., S. G. Lindner, M. Stern, M. Claussen, and A. Kohlschütter. 1988. “Membrane Fluidity and Lipid Composition of Rat Small Intestinal Brush-Border Membranes during Postnatal Maturation.” Biochimica Et Biophysica Acta 939 (1): 145–50. https://doi.org/10.1016/0005-2736(88)90055-7.

Huet, G., I. Kim, C. de Bolos, et al. 1995. “Characterization of Mucins and Proteoglycans Synthesized by a Mucin-Secreting HT-29 Cell Subpopulation.” Journal of Cell Science 108 (3): 1275–85. https://doi.org/10.1242/jcs.108.3.1275.

Hussain, I., G. Kellett, J. Affleck, E. Shepherd, and C. Boyd. 2002. “Expression and Cellular Distribution during Development of the Peptide Transporter (PepT1)

in the Small Intestinal Epithelium of the Rat." Cell and Tissue Research 307 (1): 139–42. https://doi.org/10.1007/s00441-001-0473-z.

Israel, E.J., S. Taylor, Z. Wu, et al. 1997. "Expression of the Neonatal Fc Receptor, FcRn, on Human Intestinal Epithelial Cells." Immunology 92 (1): 69–74. Scopus. https://doi.org/10.1046/j.1365-2567.1997.00326.x.

James, P S, M W Smith, D R Tivey, and T J Wilson. 1987. "Epidermal Growth Factor Selectively Increases Maltase and Sucrase Activities in Neonatal Piglet Intestine." The Journal of Physiology 393 (1): 583–94. https://doi.org/10.1113/jphysiol.1987.sp016842.

Johansson, Åsa, Mahadevan Venkita Subramani, Bahtiyar Yilmaz, et al. 2025. "Neonatal Microbiota Colonization Primes Maturation of Goblet Cell–Mediated Protection in the Pre-Weaning Colon." Journal of Experimental Medicine 222 (8): e20241591. https://doi.org/10.1084/jem.20241591.

Johansson, Malin E. V., Daniel Ambort, Thaher Pelaseyed, et al. 2011. "Composition and Functional Role of the Mucus Layers in the Intestine." Cellular and Molecular Life Sciences 68 (22): 3635. https://doi.org/10.1007/s00018-011-0822-3.

Johansson, Malin E. V., Jessica M. Holmén Larsson, and Gunnar C. Hansson. 2011. "The Two Mucus Layers of Colon Are Organized by the MUC2 Mucin, Whereas the Outer Layer Is a Legislator of Host–Microbial Interactions." Colloquium Paper. Proceedings of the National Academy of Sciences 108 (Supplement 1): 4659–65. https://doi.org/10.1073/pnas.1006451107.

Johnston, Simon D, Michael Smye, R G Peter Watson, Stanley A McMillan, Elisabeth R Trimble, and A H Gary Love. 2000. "Lactulose-Mannitol Intestinal Permeability Test: A Useful Screening Test for Adult Coeliac

Disease." Annals of Clinical Biochemistry: International Journal of Laboratory Medicine 37 (4): 512–19. https://doi.org/10.1177/000456320003700413.

Kandasamy, Palanivel, Gergely Gyimesi, Yoshikatsu Kanai, and Matthias A. Hediger. 2018. "Amino Acid Transporters Revisited: New Views in Health and Disease." Trends in Biochemical Sciences 43 (10): 752–89. https://doi.org/10.1016/j.tibs.2018.05.003.

Kazumasa, Miki, Suzuki Hiroshi, Uno Shiro, Oda Toshitsugu, Hirano Kazuyuki, and Sugiura Mamoru. 1977. "Human Fetal Intestinal Alkaline Phosphatase." Clinica Chimica Acta 79 (1): 21–30. https://doi.org/10.1016/0009-8981(77)90455-7.

Keelan, M., K. Walker, and A.B.R. Thomson. 1985. "Intestinal Morphology, Marker Enzymes and Lipid Content of Brush Border Membranes from Rabbit Jejunum and Ileum: Effect of Aging." Mechanisms of Ageing and Development 31 (1): 49–68. https://doi.org/10.1016/0047-6374(85)90026-0.

Kernéis, Sophie, Anna Bogdanova, Jean-Pierre Kraehenbuhl, and Eric Pringault. 1997. "Conversion by Peyer's Patch Lymphocytes of Human Enterocytes into M Cells That Transport Bacteria." Science 277 (5328): 949–52. https://doi.org/10.1126/science.277.5328.949.

Khan, J. M., M. A. Wingertzahn, S. Teichberg, I. Vancurova, R. G. Harper, and R. A. Wapnir. 2000. "Development of the Intestinal SGLT1 Transporter in Rats." Molecular Genetics and Metabolism 69 (3): 233–39. https://doi.org/10.1006/mgme.2000.2973.

Kirchner, Séverine, Anjali Muduli, Donatella Casirola, Kannitha Prum, Véronique Douard, and Ronaldo P Ferraris. 2008. "Luminal Fructose Inhibits Rat

Intestinal Sodium-Phosphate Cotransporter Gene Expression and Phosphate Uptake." The American Journal of Clinical Nutrition 87 (4): 1028–38. https://doi.org/10.1093/ajcn/87.4.1028.

Kleiveland, Charlotte R. 2015. "Co-Cultivation of Caco-2 and HT-29MTX." The Impact of Food Bioactives on Health, 135–40.

Koepsell, Hermann. 2020. "Glucose Transporters in the Small Intestine in Health and Disease." Pflügers Archiv - European Journal of Physiology 472 (9): 1207–48. https://doi.org/10.1007/s00424-020-02439-5.

Kondrashina, Alina, Andre Brodkorb, and Linda Giblin. 2021. "Sodium Butyrate Converts Caco-2 Monolayers into a Leaky but Healthy Intestinal Barrier Resembling That of a Newborn Infant." Food & Function 12 (11): 5066–76. https://doi.org/10.1039/D1FO00519G.

Kosek, Margaret N., Gwenyth O. Lee, Richard L. Guerrant, et al. 2017. "Age and Sex Normalization of Intestinal Permeability Measures for the Improved Assessment of Enteropathy in Infancy and Early Childhood: Results From the MAL-ED Study." Journal of Pediatric Gastroenterology and Nutrition 65 (1): 31–39. https://doi.org/10.1097/MPG.0000000000001610.

Krupa, Lukasz, Balazs Bajka, Robert Staroń, et al. 2020. "Comparing the Permeability of Human and Porcine Small Intestinal Mucus for Particle Transport Studies." Scientific Reports 10 (1): 20290. https://doi.org/10.1038/s41598-020-77129-4.

Kulthong, Kornphimol, Guido J. E. J. Hooiveld, Loes Duivenvoorde, et al. 2021. "Transcriptome Comparisons of in Vitro Intestinal Epithelia Grown under Static and Microfluidic Gut-on-Chip Conditions with in Vivo Human

Epithelia." Scientific Reports 11 (1): 3234. https://doi.org/10.1038/s41598-021-82853-6.

Lea, Tor. 2015. "Caco-2 Cell Line." In The Impact of Food Bioactives on Health: In Vitro and Ex Vivo Models, edited by Kitty Verhoeckx, Paul Cotter, Iván López-Expósito, et al. Springer International Publishing. https://doi.org/10.1007/978-3-319-16104-4_10.

Lebenthal, Emanuel, and P.C. Lee. 1980. "Glucoamylase and Disaccharidase Activities in Normal Subjects and in Patients with Mucosal Injury of the Small Intestine." The Journal of Pediatrics 97 (3): 389–93. https://doi.org/10.1016/S0022-3476(80)80187-9.

Leong, Weng-In, Christopher L. Bowlus, Jonas Tallkvist, and Bo Lönnerdal. 2003. "DMT1 and FPN1 Expression during Infancy: Developmental Regulation of Iron Absorption." American Journal of Physiology-Gastrointestinal and Liver Physiology 285 (6): G1153–61. https://doi.org/10.1152/ajpgi.00107.2003.

Lesuffleur, T., A. Barbat, E. Dussaulx, and A. Zweibaum. 1990. "Growth Adaptation to Methotrexate of HT-29 Human Colon Carcinoma Cells Is Associated with Their Ability to Differentiate into Columnar Absorptive and Mucus-Secreting Cells." Cancer Research 50 (19): 6334–43.

Levy, Emile, Jean-François Beaulieu, Edgard Delvin, et al. 2000. "Human Crypt Intestinal Epithelial Cells Are Capable of Lipid Production, Apolipoprotein Synthesis, and Lipoprotein Assembly." Journal of Lipid Research 41 (1): 12–22. https://doi.org/10.1016/S0022-2275(20)32069-1.

Liao, Peng, Meifang Liao, Ling Li, Bie Tan, and Yulong Yin. 2017. "Effect of Deoxynivalenol on Apoptosis, Barrier Function, and Expression Levels of Genes Involved in Nutrient Transport, Mitochondrial Biogenesis and

Function in IPEC-J2 Cells." Toxicology Research 6 (6): 866–77. https://doi.org/10.1039/c7tx00202e.

Liao, Yalin, Veronica Lopez, Tracy B. Shafizadeh, Charles H. Halsted, and Bo Lönnerdal. 2007. "Cloning of a Pig Homologue of the Human Lactoferrin Receptor: Expression and Localization during Intestinal Maturation in Piglets." Comparative Biochemistry and Physiology Part A: Molecular & Integrative Physiology 148 (3): 584–90. https://doi.org/10.1016/j.cbpa.2007.08.001.

Lillienau, Jan, Yajun Cheng, Åke Nilsson, and Rui-Dong Duan. 2003. "Development of Intestinal Alkaline Sphingomyelinase in Rat Fetus and Newborn Rat." Lipids 38 (5): 545–49. https://doi.org/10.1007/s11745-003-1340-1.

Lindi, C., P. Marciani, A. Faelli, and G. Esposito. 1985. "Intestinal Sugar Transport during Ageing." Biochimica Et Biophysica Acta 816 (2): 411–14. https://doi.org/10.1016/0005-2736(85)90509-7.

Lindmark, T., T. Nikkilä, and P. Artursson. 1995. "Mechanisms of Absorption Enhancement by Medium Chain Fatty Acids in Intestinal Epithelial Caco-2 Cell Monolayers." Journal of Pharmacology and Experimental Therapeutics 275 (2): 958–64.

Lindmark, T., N. Schipper, L. Lazorová, A. G. De Boer, and P. Artursson. 1998. "Absorption Enhancement in Intestinal Epithelial Caco-2 Monolayers by Sodium Caprate: Assessment of Molecular Weight Dependence and Demonstration of Transport Routes." Journal of Drug Targeting 5 (3): 215–23. https://doi.org/10.3109/10611869808995876.

Lindner, S G, C Hübner, M Stern, and A Kohlschütter. 1987. “LIPID AND FATTY ACID COMPOSITION OF RAT INTESTINAL BRUSH BORDER MEMBRANES (BBM) DURING MATURATION: THE BIOCHEMICAL CORRELATE TO CHANGES IN MEMBRANE FLUIDITY.” Pediatric Research 22 (2): 235–235. https://doi.org/10.1203/00006450-198708000-00132.

Lindquist, Susanne, and Olle Hernell. 2010. “Lipid Digestion and Absorption in Early Life: An Update:” Current Opinion in Clinical Nutrition and Metabolic Care 13 (3): 314–20. https://doi.org/10.1097/MCO.0b013e328337bbf0.

Liuzzi, Juan P., Jeffrey A. Bobo, Li Cui, Robert J. McMahon, and Robert J. Cousins. 2003. “Zinc Transporters 1, 2 and 4 Are Differentially Expressed and Localized in Rats during Pregnancy and Lactation.” The Journal of Nutrition 133 (2): 342–51. https://doi.org/10.1093/jn/133.2.342.

Lo, David, Wendy Tynan, Janet Dickerson, et al. 2004. “Cell Culture Modeling of Specialized Tissue: Identification of Genes Expressed Specifically by Follicle-associated Epithelium of Peyer’s Patch by Expression Profiling of Caco-2/Raji Co-cultures.” International Immunology 16 (1): 91–99. https://doi.org/10.1093/intimm/dxh011.

Lock, Jaclyn Y., Taylor L. Carlson, Yueyue Yu, Jing Lu, Erika C. Claud, and Rebecca L. Carrier. 2020. “Impact of Developmental Age, Necrotizing Enterocolitis Associated Stress, and Oral Therapeutic Intervention on Mucus Barrier Properties.” Scientific Reports 10 (1): 6692. https://doi.org/10.1038/s41598-020-63593-5.

Lönnerdal, B., and S. L. Kelleher. 2009. “Micronutrient Transfer: Infant Absorption.” Advances in Experimental Medicine and Biology 639: 29–40. https://doi.org/10.1007/978-1-4020-8749-3_3.

Lopez, Veronica, Yasushi A. Suzuki, and Bo Lönnerdal. 2006. “Ontogenic Changes in Lactoferrin Receptor and DMT1 in Mouse Small Intestine: Implications for Iron Absorption during Early lifeThis Paper Is One of a Selection of Papers Published in This Special Issue, Entitled 7th International Conference on Lactoferrin: Structure, Function, and Applications, and Has Undergone the Journal’s Usual Peer Review Process.” Biochemistry and Cell Biology 84 (3): 337–44. https://doi.org/10.1139/o06-059.

Lopez-Escalera, Silvia, and Anja Wellejus. 2022. “Evaluation of Caco-2 and Human Intestinal Epithelial Cells as in Vitro Models of Colonic and Small Intestinal Integrity.” Biochemistry and Biophysics Reports 31 (September): 101314. https://doi.org/10.1016/j.bbrep.2022.101314.

Lu, Li, Weijue Xu, Jiangbin Liu, et al. 2021. “DRG1 Maintains Intestinal Epithelial Cell Junctions and Barrier Function by Regulating RAC1 Activity in Necrotizing Enterocolitis.” Digestive Diseases and Sciences 66 (12): 4237–50. https://doi.org/10.1007/s10620-020-06812-3.

Lu, Song, Mark Huffman, Ying Yao, et al. 2002. “Regulation of MTP Expression in Developing Swine.” Journal of Lipid Research 43 (8): 1303–11.

Lucas, A., and T.J. Cole. 1990. “Breast Milk and Neonatal Necrotising Enterocolitis.” The Lancet 336 (8730–8731): 1519–23. https://doi.org/10.1016/0140-6736(90)93304-8.

Mabbott, N A, D S Donaldson, H Ohno, I R Williams, and A Mahajan. 2013. “Microfold (M) Cells: Important Immunosurveillance Posts in the Intestinal

Epithelium." Mucosal Immunology 6 (4): 666–77. https://doi.org/10.1038/mi.2013.30.

Macierzanka, Adam, Alan R. Mackie, Balazs H. Bajka, Neil M. Rigby, Françoise Nau, and Didier Dupont. 2014. "Transport of Particles in Intestinal Mucus under Simulated Infant and Adult Physiological Conditions: Impact of Mucus Structure and Extracellular DNA." PLOS ONE 9 (4): e95274. https://doi.org/10.1371/journal.pone.0095274.

Mahalingam, Ravichandran, Harish Ravivarapu, Sanjeev Redkar, Xiaoling Li, and Bhaskara R. Jasti. 2007. "Transbuccal Delivery of 5-Aza-2′-Deoxycytidine: Effects of Drug Concentration, Buffer Solution, and Bile Salts on Permeation." AAPS PharmSciTech 8 (3): E28–33. https://doi.org/10.1208/pt0803055.

Maher, Sam, and Randall J. Mrsny. 2016. "Intestinal Permeation Enhancers for Oral Peptide Delivery." Advanced Drug Delivery Reviews, Oral delivery of peptides, vol. 106 (November): 277–319. https://doi.org/10.1016/j.addr.2016.06.005.

Maheshwari, Akhil, Wenge Lu, Atilano Lacson, et al. 2002. "EFFECTS OF INTERLEUKIN-8 ON THE DEVELOPING HUMAN INTESTINE." Cytokine 20 (6): 256–67. https://doi.org/10.1006/cyto.2002.1996.

Mahler, Gretchen J., Michael L. Shuler, and Raymond P. Glahn. 2009. "Characterization of Caco-2 and HT29-MTX Cocultures in an in Vitro Digestion/Cell Culture Model Used to Predict Iron Bioavailability." The Journal of Nutritional Biochemistry 20 (7): 494–502. https://doi.org/10.1016/j.jnutbio.2008.05.006.

Malkov, Dmitry, Robert Angelo, Huai-zhen Wang, Elizabeth Flanders, Heather Tang, and Isabel Gomez-Orellana. n.d. “Oral Delivery of Insulin with the Eligen(®) Technology: Mechanistic Studies.” Current Drug Delivery 2 (2): 191–97.

Managlia, Elizabeth, Xiaocai Yan, and Isabelle G De Plaen. 2022. “Intestinal Epithelial Barrier Function and Necrotizing Enterocolitis.” Newborn 1 (1): 32–43. https://doi.org/10.5005/jp-journals-11002-0003.

Manners, M. J., and J. A. Stevens. 1972. “Changes from Birth to Maturity in the Pattern of Distribution of Lactase and Sucrase Activity in the Mucosa of the Small Intestine of Pigs.” British Journal of Nutrition 28 (1): 113–27. https://doi.org/10.1079/BJN19720014.

Mansbach, Charles M., and Shadab A. Siddiqi. 2010. “The Biogenesis of Chylomicrons.” Annual Review of Physiology 72: 315–33. https://doi.org/10.1146/annurev-physiol-021909-135801.

Mariadason, J. M., D. H. Barkla, and P. R. Gibson. 1997. “Effect of Short-Chain Fatty Acids on Paracellular Permeability in Caco-2 Intestinal Epithelium Model.” American Journal of Physiology-Gastrointestinal and Liver Physiology 272 (4): G705–12. https://doi.org/10.1152/ajpgi.1997.272.4.G705.

Mariadason, John M, Diana Kilias, Anthony Catto-Smith, and Peter R Gibson. 1999. “Effect of Butyrate on Paracellular Permeability in Rat Distal Colonic Mucosa Ex Vivo.” Journal of Gastroenterology and Hepatology 14 (9): 873–79. https://doi.org/10.1046/j.1440-1746.1999.01972.x.

Mariani, Valentina, Simona Palermo, Silvia Fiorentini, Alessandra Lanubile, and Elisabetta Giuffra. 2009. “Gene Expression Study of Two Widely Used Pig

Intestinal Epithelial Cell Lines: IPEC-J2 and IPI-2I." Veterinary Immunology and Immunopathology 131 (3): 278–84. https://doi.org/10.1016/j.vetimm.2009.04.006.

Marion, Julia, Yvette Miata Petersen, Véronique Romé, et al. 2005. "Early Weaning Stimulates Intestinal Brush Border Enzyme Activities in Piglets, Mainly at the Posttranscriptional Level." Journal of Pediatric Gastroenterology and Nutrition 41 (4): 401–10. https://doi.org/10.1097/01.mpg.0000177704.99786.07.

Martin, Lena, Ulrike Lodemann, Angelika Bondzio, et al. 2013. "A High Amount of Dietary Zinc Changes the Expression of Zinc Transporters and Metallothionein in Jejunal Epithelial Cells in Vitro and in Vivo but Does Not Prevent Zinc Accumulation in Jejunal Tissue of Piglets." The Journal of Nutrition 143 (8): 1205–10. https://doi.org/10.3945/jn.113.177881.

McGuckin, Michael A., Sara K. Lindén, Philip Sutton, and Timothy H. Florin. 2011. "Mucin Dynamics and Enteric Pathogens." Nature Reviews Microbiology 9 (4): 265–78. https://doi.org/10.1038/nrmicro2538.

Meaney, C.M, and C.M O'Driscoll. 2000. "A Comparison of the Permeation Enhancement Potential of Simple Bile Salt and Mixed Bile Salt:Fatty Acid Micellar Systems Using the CaCo-2 Cell Culture Model." International Journal of Pharmaceutics 207 (1–2): 21–30. https://doi.org/10.1016/S0378-5173(00)00526-3.

Meddings, J. B., and S. Theisen. 1989. "Development of Rat Jejunum: Lipid Permeability, Physical Properties, and Chemical Composition." American Journal of Physiology-Gastrointestinal and Liver Physiology 256 (5): G931–40. https://doi.org/10.1152/ajpgi.1989.256.5.G931.

Meier, C., S. M. Camargo, S. Hunziker, et al. 2018. “Intestinal IMINO Transporter SIT1 Is Not Expressed in Human Newborns.” American Journal of Physiology-Gastrointestinal and Liver Physiology 315 (5): G887–95. https://doi.org/10.1152/ajpgi.00318.2017.

Meneely, Raymond, Laura Leeper, and Fayez K. Ghishan. 1982. “Intestinal Maturation: In Vivo Magnesium Transport.” Pediatric Research 16 (4): 4. https://doi.org/10.1203/00006450-198204000-00010.

Miyamoto, Ken-ichi, Toshiyuki Shiraga, Kyoko Morita, et al. 1996. “Sequence, Tissue Distribution and Developmental Changes in Rat Intestinal Oligopeptide Transporter.” Biochimica et Biophysica Acta (BBA) - Gene Structure and Expression 1305 (1–2): 34–38. https://doi.org/10.1016/0167-4781(95)00208-1.

Mooij, M. G., B. E. A. de Koning, D. J. Lindenbergh-Kortleve, et al. 2016. “Human Intestinal PEPT1 Transporter Expression and Localization in Preterm and Term Infants.” Drug Metabolism and Disposition 44 (7): 1014–19. https://doi.org/10.1124/dmd.115.068809.

Mortensen, Janni Støvring, Søren S.-R. Bohr, Lasse Skjoldborg Krog, et al. 2024. “Neonatal Intestinal Mucus Barrier Changes in Response to Maturity, Inflammation, and Sodium Decanoate Supplementation.” Scientific Reports 14 (1): 7665. https://doi.org/10.1038/s41598-024-58356-5.

Mukaizawa, Fuyuki, Koji Taniguchi, Masateru Miyake, et al. 2009. “Novel Oral Absorption System Containing Polyamines and Bile Salts Enhances Drug Transport via Both Transcellular and Paracellular Pathways across Caco-2 Cell Monolayers.” International Journal of Pharmaceutics 367 (1–2): 103–8. https://doi.org/10.1016/j.ijpharm.2008.09.027.

Nabokina, Svetlana M., Veedamali S. Subramanian, and Hamid M. Said. 2003. "Comparative Analysis of Ontogenic Changes in Renal and Intestinal Biotin Transport in the Rat." American Journal of Physiology-Renal Physiology 284 (4): F737–42. https://doi.org/10.1152/ajprenal.00364.2002.

Nakshabendi, Imad M., Ruth McKee, Shaun Downie, Robin I. Russell, and Michael J. Rennie. 1999. "Rates of Small Intestinal Mucosal Protein Synthesis in Human Jejunum and Ileum." American Journal of Physiology-Endocrinology and Metabolism 277 (6): E1028–31. https://doi.org/10.1152/ajpendo.1999.277.6.E1028.

Navab, Farhad, and Charles G. Winter. 1988. "Effect of Aging on Intestinal Absorption of Aromatic Amino Acids in Vitro in the Rat." American Journal of Physiology-Gastrointestinal and Liver Physiology, ahead of print, April 1. world. https://doi.org/10.1152/ajpgi.1988.254.4.G630.

Niedergang and Jean-Pierre, Florence. 2000. "Much Ado about M Cells." Trends in Cell Biology 10 (4): 137–41. https://doi.org/10.1016/S0962-8924(00)01731-1.

Noel, Gaelle, Julie G. In, Jose M. Lemme-Dumit, et al. 2021. "Human Breast Milk Enhances Intestinal Mucosal Barrier Function and Innate Immunity in a Healthy Pediatric Human Enteroid Model." Frontiers in Cell and Developmental Biology 9 (July): 685171. https://doi.org/10.3389/fcell.2021.685171.

Nossol, Constanze, Anicò Barta-Böszörményi, Stefan Kahlert, et al. 2015. "Comparing Two Intestinal Porcine Epithelial Cell Lines (IPECs): Morphological Differentiation, Function and Metabolism." PLOS ONE 10 (7): e0132323. https://doi.org/10.1371/journal.pone.0132323.

Nosworthy, Matthew G., Robert F. Bertolo, and Janet A. Brunton. 2013. “Ontogeny of Dipeptide Uptake and Peptide Transporter 1 (PepT1) Expression along the Gastrointestinal Tract in the Neonatal Yucatan Miniature Pig.” British Journal of Nutrition 110 (2): 275–81. https://doi.org/10.1017/S0007114512005041.

Oga, Enoche F., Shuichi Sekine, Yoshihisa Shitara, and Toshiharu Horie. 2012. “P-Glycoprotein Mediated Efflux in Caco-2 Cell Monolayers: The Influence of Herbals on Digoxin Transport.” Journal of Ethnopharmacology 144 (3): 612–17. https://doi.org/10.1016/j.jep.2012.10.001.

Okuyama, Hiroomi, Masahiko Urao, David Lee, et al. 1998. “Changes, with Age, in the Phospholipid Content of the Intestinal Mucus Layer of the Newborn Rabbit.” Journal of Pediatric Surgery 33 (1): 35–38. https://doi.org/10.1016/S0022-3468(98)90356-6.

Olivares, Manuel, Bo Lönnerdal, Steve A. Abrams, Fernando Pizarro, and Ricardo Uauy. 2002. “Age and Copper Intake Do Not Affect Copper Absorption, Measured with the Use of 65Cu as a Tracer, in Young Infants.” The American Journal of Clinical Nutrition 76 (3): 641–45. https://doi.org/10.1093/ajcn/76.3.641.

Otani, Tetsuhisa, and Mikio Furuse. 2020. “Tight Junction Structure and Function Revisited.” Trends in Cell Biology 30 (10): 805–17. https://doi.org/10.1016/j.tcb.2020.08.004.

Owens, R. B., H. S. Smith, W. A. Nelson-Rees, and E. L. Springer. 1976. “Epithelial Cell Cultures From Normal and Cancerous Human Tissues2.” JNCI: Journal of the National Cancer Institute 56 (4): 843–49. https://doi.org/10.1093/jnci/56.4.843.

Pang, Kam-Yee, Jean L. Bresson, and W.Allan Walker. 1983. “Development of the Gastrointestinal Mucosal Barrier. Evidence for Structural Differences in Microvillus Membranes from Newborn and Adult Rabbits.” Biochimica et Biophysica Acta (BBA) - Biomembranes 727 (1): 201–8. https://doi.org/10.1016/0005-2736(83)90385-1.

Parrish, Amy, Marie Boudaud, Annette Kuehn, Markus Ollert, and Mahesh S. Desai. 2022. “Intestinal Mucus Barrier: A Missing Piece of the Puzzle in Food Allergy.” Trends in Molecular Medicine 28 (1): 36–50. https://doi.org/10.1016/j.molmed.2021.10.004.

Pasternak, J. Alex, Coral Kent-Dennis, Andrew G. Van Kessel, and Heather L. Wilson. 2015. “Claudin-4 Undergoes Age-Dependent Change in Cellular Localization on Pig Jejunal Villous Epithelial Cells, Independent of Bacterial Colonization.” Mediators of Inflammation 2015 (1): 263629. https://doi.org/10.1155/2015/263629.

Patel, Ravi M., Loren S. Myers, Ashish R. Kurundkar, Akhil Maheshwari, Asma Nusrat, and Patricia W. Lin. 2012. “Probiotic Bacteria Induce Maturation of Intestinal Claudin 3 Expression and Barrier Function.” The American Journal of Pathology 180 (2): 626–35. https://doi.org/10.1016/j.ajpath.2011.10.025.

Peng, Luying, Zhenjuan He, Wei Chen, Ian R. Holzman, and Jing Lin. 2007. “Effects of Butyrate on Intestinal Barrier Function in a Caco-2 Cell Monolayer Model of Intestinal Barrier.” Pediatric Research 61 (1): 37–41. https://doi.org/10.1203/01.pdr.0000250014.92242.f3.

Perreault, Nathalie, and Jean-François Beaulieu. 1996. “Use of the Dissociating Enzyme Thermolysin to Generate Viable Human Normal Intestinal Epithelial

Cell Cultures.” Experimental Cell Research 224 (2): 354–64. https://doi.org/10.1006/excr.1996.0145.

Perruchot, Marie-Hélène, Gaëlle Boudry, Frédérique Mayeur-Nickel, et al. 2025. “In Vitro Evaluation of Intestinal Barrier Function after Exposure to Digested Pea Ingredients─Food Matrix Effect.” Journal of Agricultural and Food Chemistry 73 (1): 584–94. https://doi.org/10.1021/acs.jafc.4c09963.

Peterson, Lance W., and David Artis. 2014. “Intestinal Epithelial Cells: Regulators of Barrier Function and Immune Homeostasis.” Nature Reviews Immunology 14 (3): 141–53. https://doi.org/10.1038/nri3608.

Pontier, Catherine, Jean Pachot, Roger Botham, Bernard Lenfant, and Philippe Arnaud. 2001. “HT29-MTX and Caco-2/TC7 Monolayers as Predictive Models for Human Intestinal Absorption: Role of the Mucus Layer.” Journal of Pharmaceutical Sciences 90 (10): 1608–19. https://doi.org/10.1002/jps.1111.

Poquet, Laure, and Tim J. Wooster. 2016. “Infant Digestion Physiology and the Relevance of in Vitro Biochemical Models to Test Infant Formula Lipid Digestion.” Molecular Nutrition & Food Research 60 (8): 1876–95. https://doi.org/10.1002/mnfr.201500883.

Potter, Jennifer, Mae-Wan Ho, Hilary Bolton, Anna J. Furth, Dallas M. Swallow, and Beatrice Griffiths. 1985. “Human Lactase and the Molecular Basis of Lactase Persistence.” Biochemical Genetics 23 (5): 423–39. https://doi.org/10.1007/BF00499084.

Puchal, A. A., and R. K. Buddington. 1992. “Postnatal Development of Monosaccharide Transport in Pig Intestine.” American Journal of

Physiology-Gastrointestinal and Liver Physiology 262 (5): G895–902. https://doi.org/10.1152/ajpgi.1992.262.5.G895.

Pulvertaft, R. J. V. 1964. “CYTOLOGY OF BURKITT’S TUMOUR (AFRICAN LYMPHOMA).” The Lancet, Originally published as Volume 1, Issue 7327, vol. 283 (7327): 238–40. https://doi.org/10.1016/S0140-6736(64)92345-1.

Pyzik, Michal, Timo Rath, Wayne I Lencer, Kristi Baker, and Richard S Blumberg. 2015. “FcRn: The Architect Behind the Immune and Nonimmune Functions of IgG and Albumin.” The Journal of Immunology 194 (10): 4595–603. https://doi.org/10.4049/jimmunol.1403014.

Ramasamy, M., D. H. Alpers, C. Tiruppathi, and B. Seetharam. 1989. “Cobalamin Release from Intrinsic Factor and Transfer to Transcobalamin II within the Rat Enterocyte.” The American Journal of Physiology 257 (5 Pt 1): G791-797. https://doi.org/10.1152/ajpgi.1989.257.5.G791.

Rand, E. B., A. M. Depaoli, N. O. Davidson, G. I. Bell, and C. F. Burant. 1993. “Sequence, Tissue Distribution, and Functional Characterization of the Rat Fructose Transporter GLUT5.” The American Journal of Physiology 264 (6 Pt 1): G1169-1176. https://doi.org/10.1152/ajpgi.1993.264.6.G1169.

Raul, Francis, Brigitte Lacroix, and Marc Aprahamian. 1986. “Longitudinal Distribution of Brush Border Hydfolases and Morphological Maturation in the Intestine of the Preterm Infant.” Early Human Development 13 (2): 225–34. https://doi.org/10.1016/0378-3782(86)90010-1.

Ravisankar, Srikanth, Rodney Tatum, Parvesh M. Garg, Maja Herco, Prem S. Shekhawat, and Yan-Hua Chen. 2018. “Necrotizing Enterocolitis Leads to Disruption of Tight Junctions and Increase in Gut Permeability in a Mouse

Model." BMC Pediatrics 18 (1): 372. https://doi.org/10.1186/s12887-018-1346-x.

Reboul, Emmanuelle. 2013. "Absorption of Vitamin A and Carotenoids by the Enterocyte: Focus on Transport Proteins." Nutrients 5 (9): 3563–81. https://doi.org/10.3390/nu5093563.

Reidling, Jack C., Svetlana M. Nabokina, Krishnaswamy Balamurugan, and Hamid M. Said. 2006. "Developmental Maturation of Intestinal and Renal Thiamin Uptake: Studies in Wild-Type and Transgenic Mice Carrying Human THTR-1 and 2 Promoters." Journal of Cellular Physiology 206 (2): 371–77. https://doi.org/10.1002/jcp.20492.

Reisenauer, A. M., E. A. Lee, and R. O. Castillo. 1992. "Ontogeny of Membrane and Soluble Amino-Oligopeptidases in Rat Intestine." American Journal of Physiology-Gastrointestinal and Liver Physiology 262 (1): G178–84. https://doi.org/10.1152/ajpgi.1992.262.1.G178.

Ridlon, Jason M., Dae-Joong Kang, and Phillip B. Hylemon. 2006. "Bile Salt Biotransformations by Human Intestinal Bacteria." Journal of Lipid Research 47 (2): 241–59. https://doi.org/10.1194/jlr.R500013-JLR200.

Rittler, Peter, Hans Demmelmair, Berthold Koletzko, Friedrich W. Schildberg, and Wolfgang H. Hartl. 2000. "Determination of Protein Synthesis in Human Ileum in Situ by Continuous [1-13 C]Leucine Infusion." American Journal of Physiology-Endocrinology and Metabolism 278 (4): E634–38. https://doi.org/10.1152/ajpendo.2000.278.4.E634.

Rome, Sophie, Laurence Barbot, Eugénie Windsor, et al. 2002. "The Regionalization of PepT1, NBAT and EAAC1 Transporters in the Small Intestine of Rats Are

Unchanged from Birth to Adulthood." The Journal of Nutrition 132 (5): 1009–11. https://doi.org/10.1093/jn/132.5.1009.

Roskes, Lisa, Athanasios Chamzas, Bing Ma, et al. 2025. "Early Human Milk Feeding: Relationship to Intestinal Barrier Maturation and Postnatal Growth." Pediatric Research 97 (6): 2065–73. https://doi.org/10.1038/s41390-024-03622-5.

Rubas, W., M. E. M. Cromwell, Z. Shahrokh, et al. 1996. "Flux Measurements across Caco-2 Monolayers May Predict Transport in Human Large Intestinal Tissue." Journal of Pharmaceutical Sciences 85 (2): 165–69. https://doi.org/10.1021/js950267+.

Rubino, A., M. Pierro, G. Torretta, M. Vetrella, D. Martino, and S. Auricchio. 1969. "Studies on Intestinal Hydrolysis of Peptides: II. Dipeptidase Activity Toward L-Glutaminyl-L-Proline and Glycyl-L-Proline in the Small Intestine of the Human Fetus." Pediatric Research, ahead of print. https://doi.org/10.1203/00006450-196907000-00007.

Said, H. M., F. K. Ghishan, and J. E. Murrell. 1985. "Ontogenesis of Intestinal Transport of 5-Methyltetrahydrofolate in the Rat." American Journal of Physiology-Gastrointestinal and Liver Physiology, ahead of print, November 1. Bethesda, MD. https://doi.org/10.1152/ajpgi.1985.249.5.G567.

Said, H. M., D. E. Ong, and J. L. Shingleton. 1989. "Intestinal Uptake of Retinol: Enhancement by Bovine Milk Beta-Lactoglobulin." The American Journal of Clinical Nutrition 49 (4): 690–94. https://doi.org/10.1093/ajcn/49.4.690.

Said, Hamid M., David Ong, and Reyadh Redha. 1988. "Intestinal Uptake of Retinol in Suckling Rats: Characteristics and Ontogeny." Pediatric Research 24 (4): 4. https://doi.org/10.1203/00006450-198810000-00013.

Said, Hamid M., Ali Sharifian, and Amir Bagherzadeh. 1990. “Transport of Biotin in the Ileum of Suckling Rats: Characteristics and Ontogeny.” Pediatric Research 28 (3): 3. https://doi.org/10.1203/00006450-199009000-00023.

Saleem, Waqar, Nathan Carpentier, Charlotte Hinnekens, et al. 2024. “Porcine Ex-Vivo Intestinal Mucus Has Age-Dependent Blocking Activity against Transmissible Gastroenteritis Virus.” Veterinary Research 55 (1): 113. https://doi.org/10.1186/s13567-024-01374-y.

Schaart, Maaike W., Adrianus C. J. M. De Bruijn, Henk Schierbeek, Dick Tibboel, Ingrid B. Renes, and Johannes B. Van Goudoever. 2009. “Small Intestinal MUC2 Synthesis in Human Preterm Infants.” American Journal of Physiology-Gastrointestinal and Liver Physiology 296 (5): G1085–90. https://doi.org/10.1152/ajpgi.90444.2008.

Schierack, Peter, Marcel Nordhoff, Marion Pollmann, et al. 2006. “Characterization of a Porcine Intestinal Epithelial Cell Line for in Vitro Studies of Microbial Pathogenesis in Swine.” Histochemistry and Cell Biology 125 (3): 293–305. https://doi.org/10.1007/s00418-005-0067-z.

Schwarz, S. M., B. Hostetler, S. Ling, M. Mone, and J. B. Watkins. 1985. “Intestinal Membrane Lipid Composition and Fluidity during Development in the Rat.” The American Journal of Physiology 248 (2 Pt 1): G200-207. https://doi.org/10.1152/ajpgi.1985.248.2.G200.

Schwarz, Steven M., Ann S. Lambert, and Marvin S. Medow. 1992. “Ontogeny of Proximal Colon Basolateral Membrane Lipid Composition and Fluidity in the Rabbit.” Biochimica et Biophysica Acta (BBA) - Biomembranes 1107 (1): 70–76. https://doi.org/10.1016/0005-2736(92)90330-O.

Seetharam, Bellur, and Raghunatha R. Yammani. 2003. “Cobalamin Transport Proteins and Their Cell-Surface Receptors.” Expert Reviews in Molecular Medicine 5 (18): 1–18. https://doi.org/10.1017/S1462399403006422.

Shafizadeh, Tracy B., and Charles H. Halsted. 2009. “Postnatal Ontogeny of Intestinal GCPII and the RFC in Pig.” American Journal of Physiology. Gastrointestinal and Liver Physiology 296 (3): G476-481. https://doi.org/10.1152/ajpgi.00446.2007.

Shah, Uzma, Bonny L. Dickinson, Richard S. Blumberg, Neil E. Simister, Wayne I. Lencer, and W. Allan Walker. 2003. “Distribution of the IgG Fc Receptor, FcRn, in the Human Fetal Intestine.” Pediatric Research 53 (2): 295.

Shen, Hong, David E. Smith, and Frank C. Brosius. 2001. “Developmental Expression of PEPT1 and PEPT2 in Rat Small Intestine, Colon, and Kidney.” Pediatric Research 49 (6): 6. https://doi.org/10.1203/00006450-200106000-00013.

Shu, R., E. S. David, and R. P. Ferraris. 1997. “Dietary Fructose Enhances Intestinal Fructose Transport and GLUT5 Expression in Weaning Rats.” The American Journal of Physiology 272 (3 Pt 1): G446-453. https://doi.org/10.1152/ajpgi.1997.272.3.G446.

Shulman, R. J., S. J. Henning, and B. L. Nichols. 1988. “The Miniature Pig as an Animal Model for the Study of Intestinal Enzyme Development.” Pediatric Research 23 (3): 3. https://doi.org/10.1203/00006450-198803000-00016.

Silverman, Jennifer B., Paige N. Vega, Matthew J. Tyska, and Ken S. Lau. 2024. “Intestinal Tuft Cells: Morphology, Function, and Implications for Human Health.” Annual Review of Physiology 86 (1): 479–504. https://doi.org/10.1146/annurev-physiol-042022-030310.

Simister, N. E., C. M. Story, H. L. Chen, and J. S. Hunt. 1996. “An IgG-Transporting Fc Receptor Expressed in the Syncytiotrophoblast of Human Placenta.” European Journal of Immunology 26 (7): 1527–31. https://doi.org/10.1002/eji.1830260718.

Singh, Sudha B., Amanda Carroll-Portillo, Cristina Coffman, Nathaniel L. Ritz, and Henry C. Lin. 2020. “Intestinal Alkaline Phosphatase Exerts Anti-Inflammatory Effects Against Lipopolysaccharide by Inducing Autophagy.” Scientific Reports 10 (1): 1. https://doi.org/10.1038/s41598-020-59474-6.

Smith, Helene S. 1979. “In Vitro Properties of Epithelial Cell Lines Established from Human Carcinomas and Nonmalignant Tissue2.” JNCI: Journal of the National Cancer Institute 62 (2). https://doi.org/10.1093/jnci/62.2.225.

Song, Chunyan, Zhenglong Chai, Si Chen, Hui Zhang, Xiaohong Zhang, and Yuping Zhou. 2023. “Intestinal Mucus Components and Secretion Mechanisms: What We Do and Do Not Know.” Experimental & Molecular Medicine 55 (4): 681–91. https://doi.org/10.1038/s12276-023-00960-y.

Song, Keon-Hyoung, Suk-Jae Chung, and Chang-Koo Shim. 2005. “Enhanced Intestinal Absorption of Salmon Calcitonin (sCT) from Proliposomes Containing Bile Salts.” Journal of Controlled Release 106 (3): 298–308. https://doi.org/10.1016/j.jconrel.2005.05.016.

Song, Yurong, Xiaorong Peng, Angela Porta, et al. 2003. “Calcium Transporter 1 and Epithelial Calcium Channel Messenger Ribonucleic Acid Are Differentially Regulated by 1,25 Dihydroxyvitamin D3 in the Intestine and Kidney of Mice.” Endocrinology 144 (9): 3885–94. https://doi.org/10.1210/en.2003-0314.

Story, C. M., J.E. Mikulska, and N. E. Simister. 1994. “A Major Histocompatibility Complex Class I-like Fc Receptor Cloned from Human Placenta: Possible Role in Transfer of Immunoglobulin G from Mother to Fetus.” The Journal of Experimental Medicine 180 (6): 2377–81. https://doi.org/0.1084/jem.180.6.2377.

Sun, Duxin, Hans Lennernas, Lynda S. Welage, et al. 2002. “Comparison of Human Duodenum and Caco-2 Gene Expression Profiles for 12,000 Gene Sequences Tags and Correlation with Permeability of 26 Drugs.” Pharmaceutical Research 19 (10): 1400–1416. https://doi.org/10.1023/A:1020483911355.

Sun, Huadong, Edwin CY Chow, Shanjun Liu, Yimin Du, and K Sandy Pang. 2008. “The Caco-2 Cell Monolayer: Usefulness and Limitations.” Expert Opinion on Drug Metabolism & Toxicology 4 (4): 395–411. https://doi.org/10.1517/17425255.4.4.395.

Suzuki, Y. A., K. Shin, and B. Lönnerdal. 2001. “Molecular Cloning and Functional Expression of a Human Intestinal Lactoferrin Receptor.” Biochemistry 40 (51): 15771–79. https://doi.org/10.1021/bi0155899.

Taelman, Jasin, Mònica Diaz, and Jordi Guiu. 2022. “Human Intestinal Organoids: Promise and Challenge.” Frontiers in Cell and Developmental Biology 10 (March): 854740. https://doi.org/10.3389/fcell.2022.854740.

Tang, Hengkuan, Chen Wang, Shinuo Cao, and Fengjun Wang. 2022. “Novel Angiotensin I-converting Enzyme (ACE) Inhibitory Peptides from Walnut Protein Isolate: Separation, Identification and Molecular Docking Study.” Journal of Food Biochemistry 46 (12). https://doi.org/10.1111/jfbc.14411.

Taylor, Sarah N., Laura A. Basile, Myla Ebeling, and Carol L. Wagner. 2009. “Intestinal Permeability in Preterm Infants by Feeding Type: Mother’s Milk

versus Formula." Breastfeeding Medicine: The Official Journal of the Academy of Breastfeeding Medicine 4 (1): 11–15. https://doi.org/10.1089/bfm.2008.0114.

Toloza, E. M., and J. Diamond. 1992. "Ontogenetic Development of Nutrient Transporters in Rat Intestine." American Journal of Physiology-Gastrointestinal and Liver Physiology 263 (5): G593–604. https://doi.org/10.1152/ajpgi.1992.263.5.G593.

Torp, N, M Rossi, J T Troelsen, J Olsen, and E M Danielsen. 1993. "Lactase-Phlorizin Hydrolase and Aminopeptidase N Are Differentially Regulated in the Small Intestine of the Pig." Biochemical Journal 295 (Pt 1): 177–82.

Triadou, N., J. Bataille, and J. Schmitz. 1983. "Longitudinal Study of the Human Intestinal Brush Border Membrane Proteins." Gastroenterology 85 (6): 1326–32. https://doi.org/10.1016/S0016-5085(83)80014-6.

Trugo, N. M. F., J. E. Ford, and D. N. Salter. 1985. "Vitamin B12 Absorption in the Neonatal Piglet: 3. Influence of Vitamin B12-Binding Protein from Sows' Milk on Uptake of Vitamin B12 by Microvillus Membrane Vesicles Prepared from Small Intestine of the Piglet." British Journal of Nutrition 54 (1): 269–83. https://doi.org/10.1079/BJN19850110.

Turck, D., A. S. Feste, and C. H. Lifschitz. 1993. "Age and Diet Affect the Composition of Porcine Colonic Mucins." Pediatric Research 33 (6): 564–67. https://doi.org/10.1203/00006450-199306000-00005.

Twarog, Caroline, Sarinj Fattah, Joanne Heade, Sam Maher, Elias Fattal, and David J. Brayden. 2019. "Intestinal Permeation Enhancers for Oral Delivery of Macromolecules: A Comparison between Salcaprozate Sodium (SNAC) and

Sodium Caprate (C10).” Pharmaceutics 11 (2): 2. https://doi.org/10.3390/pharmaceutics11020078.

Twarog, Caroline, Kai Liu, Peter J. O’Brien, et al. 2020. “A Head-to-Head Caco-2 Assay Comparison of the Mechanisms of Action of the Intestinal Permeation Enhancers: SNAC and Sodium Caprate (C10).” European Journal of Pharmaceutics and Biopharmaceutics 152 (July): 95–107. https://doi.org/10.1016/j.ejpb.2020.04.023.

Vancamelbeke, Maaike, and Séverine Vermeire. 2017. “The Intestinal Barrier: A Fundamental Role in Health and Disease.” Expert Review of Gastroenterology & Hepatology 11 (9): 821–34. https://doi.org/10.1080/17474124.2017.1343143.

Vander Heiden, Matthew G., Lewis C. Cantley, and Craig B. Thompson. 2009. “Understanding the Warburg Effect: The Metabolic Requirements of Cell Proliferation.” Science 324 (5930): 1029–33. https://doi.org/10.1126/science.1160809.

Vergauwen, Hans. 2015. “The IPEC-J2 Cell Line.” In The Impact of Food Bioactives on Health: In Vitro and Ex Vivo Models, edited by Kitty Verhoeckx, Paul Cotter, Iván López-Expósito, et al. Springer. http://www.ncbi.nlm.nih.gov/books/NBK500147/.

Voets, Thomas, Bernd Nilius, Susan Hoefs, et al. 2004. “TRPM6 Forms the Mg2+ Influx Channel Involved in Intestinal and Renal Mg2+ Absorption.” Journal of Biological Chemistry 279 (1): 19–25. https://doi.org/10.1074/jbc.M311201200.

Walter, Elke, Sonia Janich, Blake J. Roessler, John M. Hilfinger, and Gordon L. Amidon. 1996. “HT29-MTX/Caco-2 Cocultures as an in Vitro Model for the

Intestinal Epithelium: In Vitro–in Vivo Correlation with Permeability Data from Rats and Humans." Journal of Pharmaceutical Sciences 85 (10): 1070–76. https://doi.org/10.1021/js960110x.

Wang, Yangxi, Clare B. Harvey, Edward J. Hollox, et al. 1998. "The Genetically Programmed Down-Regulation of Lactase in Children." Gastroenterology 114 (6): 1230–36. https://doi.org/10.1016/S0016-5085(98)70429-9.

Watson, C. J., M. Rowland, and G. Warhurst. 2001. "Functional Modeling of Tight Junctions in Intestinal Cell Monolayers Using Polyethylene Glycol Oligomers." American Journal of Physiology-Cell Physiology 281 (2): C388–97. https://doi.org/10.1152/ajpcell.2001.281.2.C388.

Weaver, L T, S Austin, and T J Cole. 1991. "Small Intestinal Length: A Factor Essential for Gut Adaptation." Gut 32 (11): 1321–23. https://doi.org/10.1136/gut.32.11.1321.

Weaver, L T, M F Laker, and R Nelson. 1984. "Intestinal Permeability in the Newborn." Archives of Disease in Childhood 59 (3): 236–41. https://doi.org/10.1136/adc.59.3.236.

Weström, Björn, Ester Arévalo Sureda, Kateryna Pierzynowska, Stefan G. Pierzynowski, and Francisco-José Pérez-Cano. 2020. "The Immature Gut Barrier and Its Importance in Establishing Immunity in Newborn Mammals." Frontiers in Immunology 11. https://www.frontiersin.org/articles/10.3389/fimmu.2020.01153.

Xu, Hua, Liqun Bai, James F. Collins, and Fayez K. Ghishan. 2002. "Age-Dependent Regulation of Rat Intestinal Type IIb Sodium-Phosphate Cotransporter by 1,25-(OH)2 Vitamin D3." American Journal of Physiology-

Cell Physiology 282 (3): C487–93. https://doi.org/10.1152/ajpcell.00412.2001.

Xu, Mengmeng, Long Che, Lizhu Niu, et al. 2023. “Molecular Mechanism of Valine and Its Metabolite in Improving Triglyceride Synthesis of Porcine Intestinal Epithelial Cells.” Scientific Reports 13 (1). https://doi.org/10.1038/s41598-023-30036-w.

Yoshida, Masaru, Steven M Claypool, Jessica S Wagner, et al. 2004. “Human Neonatal Fc Receptor Mediates Transport of IgG into Luminal Secretions for Delivery of Antigens to Mucosal Dendritic Cells.” Immunity 20 (6): 769–83. https://doi.org/10.1016/j.immuni.2004.05.007.

Younoszai, M. Kabir, Carolyn Smith, and Michael H. Finch. 1985. “Comparison of In Vitro Jejunal Uptake of L-Valine and L-Lysine in the Rat During Maturation.” Journal of Pediatric Gastroenterology and Nutrition 4 (6): 992–97. https://doi.org/10.1002/j.1536-4801.1985.tb08998.x.

Zakrzewski, Silke S., Jan F. Richter, Susanne M. Krug, et al. 2013. “Improved Cell Line IPEC-J2, Characterized as a Model for Porcine Jejunal Epithelium.” PLOS ONE 8 (11): e79643. https://doi.org/10.1371/journal.pone.0079643.

Rational and Objectives of the Thesis

Despite growing interest in early-life intestinal development, there remains a lack of reproducible, physiologically relevant *in vitro* models that accurately mimic the structure and function of the infant gut barrier.

Existing systems often reflect adult physiology and fail to capture the unique features of the neonatal epithelium, such as heightened permeability, immature enzymatic activity, and delayed barrier closure. Moreover, while human milk is known to support gut maturation, there is limited comparative data on how infant formulae influence barrier integrity and transporter function relative to breast milk in an infant-like model. A further limitation is the absence of model systems that can track barrier maturation or closure dynamically over time—an essential feature for studying nutritional programming in early life.

The main aim of the thesis is to contribute to the development of more predictive and translational *in vitro* models for early-life nutrition research.

This aim is addressed through a series of experimental studies:

- Chapter 2 builds on published work with sodium butyrate, further testing its suitability to convert Caco-2/HT29-MTX monolayers into an infant-like barrier model.
- Chapter 3 describes an alternative compound GDC. It reports on the development of a reversible, infant-like epithelial barrier using Caco-2/HT29-MTX treated with GDC.
- Chapter 4 investigates the comparative effects of human milk and a range of infant formulae on epithelial structure and function in both infant- and adult-

like Caco-2/HT29-MTX models, highlighting product-specific influences on barrier phenotype.

- Chapter 5 assesses IPEC-J2 cell line as an infant-like model. This chapter focuses on the use of culture media to create a stable IPEC-J2 monolayer for infant nutrition studies.

2. Chapter 2

Modeling Leaky Gut *In Vitro*: Sodium Butyrate-Induced Barrier Disruption of Caco-2 monolayers

A version of this chapter is published in The Journal of Nutritional Physiology:

Bietto, F., Arranz, E., Mechoud, M., Rath, E., Lucey, A.J., Giblin, L., 2026a. Modeling a leaky gut In vitro: Sodium butyrate-induced barrier disruption of Caco-2 monolayers. The Journal of Nutritional Physiology 6, 100021. https://doi.org/10.1016/j.jnphys.2026.100021

The published version of this chapter is presented in **Appendix A**.

Abstract

Butyrate exhibits a dual effect on gut permeability, promoting epithelial health at low concentrations but disrupting barrier integrity at higher levels. This disruption at higher levels can be exploited, *in vitro,* to create gut barrier models with increased permeability. This study aimed to unravel the mechanism of action of sodium butyrate (NaB, 50–125 mM) on enterocyte monolayers (Caco-2). NaB reduced Trans-Epithelial Electrical Resistance (TEER) and increased paracellular permeability in a dose-dependent manner on Caco-2 monolayers, effects that persisted after NaB withdrawal. TEER reductions induced by NaB occurred under hyperosmotic conditions (430.5 ± 4.5 mOsm/kg), however treatment with mannitol, a non-metabolizable osmotic agent used to mimic the osmotic effect, only caused a transient decrease in TEER. NaB was actively transported into cells, with increased mRNA expression of butyrate transporters MCT-1 and SMCT-1. However, NaB did not act as an energy substrate, as evidenced by decreased ATP levels and unchanged cellular reductase activity. Instead, NaB elevated Caspase-3 activity, induced stress markers (p21, HSP-70), and stimulated cytokine production (IL-6, IL-8, TNF). Most importantly, treatment with dexamethasone, a commonly used steroid, restored TEER and reduced stress and inflammation markers in Caco-2 monolayers disrupted by 75 mM NaB. Therefore, NaB treated Caco-2 monolayers are a suitable *in vitro* model for gut barrier dysfunction and inflammation such as Crohn's disease or necrotizing enterocolitis.

Keywords:

Sodium Butyrate, Caco-2 Monolayers, *In vitro* leaky gut, Transepithelial Electrical Resistance (TEER), Hyperosmolarity, Dexamethasone

2.1.Introduction

The intestinal barrier is a highly specialized system that regulates the selective movement of nutrients and metabolites, whilst providing defense against harmful exogenous agents (Groschwitz and Hogan, 2009). This barrier consists of a single layer of intestinal epithelial cells joined by tight junctions, which are complexes of transmembrane proteins such as occludin (OCLN), claudins (CLDN), junctional adhesion molecules (JAM) and zonula occludens (ZO) (Otani and Furuse, 2020). These proteins regulate the pore size and the passage of molecules through the paracellular pathway (Otani and Furuse, 2020). The increased permeability of this barrier, commonly referred to as "leaky gut," is associated with various disorders, including inflammatory bowel diseases (Hollander, 1999), but also with the immature infant gut. Paracellular permeability is higher during early postnatal life (Catassi et al., 1995; Kosek et al., 2017; Weaver et al., 1984), allowing for the uptake of bioactives from milk (Weström et al., 2020). Studies have shown that breast milk, compared to infant formula, contributes to a more rapid reduction in intestinal permeability and therefore gut closure over time (Catassi et al., 1995; Weaver et al., 1984; Weström et al., 2020).

Butyrate is a short-chain fatty acid (SCFA), produced by microbial fermentation of dietary fibers, that has emerged as a key regulator of the intestinal barrier (Liu et al., 2018). Together with acetate and propionate, butyrate comprises the most abundant SCFAs in the gut, typically present in an approximate molar ratio of 60:20:20. The total daily SCFA production in the colon is estimated to range between 500 and 600 mmol (Dalile et al., 2019). Notably, clinical studies have demonstrated that butyrate concentrations up to 100 mM can be safely administered via rectal enema in humans (Hamer et al., 2008). Butyrate can exert its effects either by being transported into

intestinal epithelial cells via monocarboxylate transporters (MCT-1) and sodium-coupled monocarboxylate transporters (SMCT-1) (Dalile et al., 2019; Hamer et al., 2008; Stilling et al., 2016), or by binding to G-protein coupled receptors (GPR41, GPR43, and GPR109A) on the cell surface, thereby triggering intracellular signaling pathways without entering the cell (Brown et al., 2003). Once inside the intestinal cell, butyrate undergoes β-oxidation to produce acetyl-CoA, which serves as an energy substrate for enterocytes, supporting metabolic activity and maintaining barrier integrity (Canani, 2011; Hamer et al., 2008; Stilling et al., 2016). However, when present at high concentration, it can accumulate in the nucleus, where it acts as a histone deacetylase (HDAC) inhibitor, promoting epigenetic modifications (Dalile et al., 2019; Singh et al., 2023) and activating pathways that induce apoptosis and cell cycle arrest in the intestinal barrier (Avivi-Green et al., 2002; Chirakkal et al., 2006; Donohoe et al., 2012; Siavoshian, 2000). While these effects have been reported in various cell types, including colon cancer lines, the specific concentration thresholds and downstream outcomes in differentiated Caco-2 monolayers remain less well defined, particularly under hyperosmotic conditions.

Caco-2 cell monolayers, derived from a human colon adenocarcinoma (Fogh et al., 1977), are widely utilized as an *in vitro* model for studying intestinal barrier function. If grown on a permeable support, they have the ability to differentiate into a polarized barrier with brush border enzymes, nutrient transporters and tight junctions (Lea, 2015). Peng et al. (2007) reported that exposure to 2 mM sodium butyrate significantly increased Caco-2 transepithelial electrical resistance (TEER) and decreased permeability. However, at higher NaB concentrations (8 mM for 96 h), Peng et al. (2007) observed a significant decrease TEER decreasing from 200 ± 21 $\Omega.cm^2$ to 23 ± 18 $\Omega.cm^2$ ($P<0.05$). Monolayer permeability to the large molecule,

inulin-FITC (2-5 kDa), was increased and apoptosis ensued. Similarly, Ruemmele et al. (2003) reported that treatment of Caco-2 cells with butyrate at concentrations ranging from 5 to 100 mM for 16 h significantly increased apoptosis (Ruemmele, 2003). Previously, our laboratory reported that high concentrations of sodium butyrate for 24 h reduced TEER (≥50 mM NaB), increased paracellular permeability to mannitol (Man) (≥150 mM NaB), reduced CLDN1 and CLDN2 mRNA levels (≥50 mM NaB) and caused a redistribution of ZO1 (≥125 mM NaB) in Caco-2 monolayers (Kondrashina et al., 2021). Interestingly, the barrier allowed for a 9.3% increased transport rate of the intact milk protein α-lactalbumin, suggesting that NaB treatment could be used to create an *in vitro* model of the infant gut. However, at these concentrations, the osmolality of the NaB solution in media (200 mM NaB = 790 mOsm/kg) is at the upper limit of Caco-2 cell tolerance (Grauso et al., 2019; Inokuchi et al., 2009), raising the potential for hyperosmotic stress contributing to the observed barrier manipulation.

The objective of this study was to determine whether or not NaB's induction of a 'leaky' barrier is reversible. A transient leaky attribute is critical in any *in vitro* infant gut model as it allows for the assessment of gut closure over time, particularly in the presence of breast milk or infant formula. This study also tracked the metabolism of NaB in Caco-2 cells and monitored apoptotic or stress responses. A further understanding of how NaB interacts with human intestinal enterocytes *in vitro* helps to decipher whether or not NaB should be utilised to create a 'leaky' transient infant gut model or if it would be more suited to represent a 'leaky' model of a diseased barrier.

2.2.Materials and Methods

2.2.1. Materials

Human intestinal epithelial cell lines Caco-2 (EACC 86010202) and HT29-MTX-E12 (EACC 12040401) were purchased from the European Collection of Cell Culture (UK). Six-well plates with polyester permeable-membrane inserts (0.4 μm pore size, 4.5 cm^2 area) and 12 well plates with polyester permeable-membrane inserts (0.4 μm pore size, 1.11 cm^2 area) were purchased from Sarstedt Group (Germany). CellTiter 96™ AQueous One Solution Cell Proliferation Assay (MTS, G3582) and CellTiter-Glo™ Luminescence Viability Assay (G7570) were purchased from Promega (USA). CyQUANT™ LDH Cytotoxicity Assay (C20300) was purchased from Invitrogen (USA). RNeasy mini kit (74104) and RNA-free DNase set (79254) were from Qiagen (Netherlands). SensiFAST cDNA Synthesis Kit (BIO-65053) was from Meridian Bioscience (UK). Light Cycler SYBR GREEN I Master kit (04707516001) was from Roche Diagnostics (Switzerland). Primers for RT-qPCR were synthesized by Eurofins Genomics (Germany). Lucifer yellow (L1177) was supplied by ThermoFisher Scientific (USA).

All the other reagents were purchased from Sigma-Aldrich, unless stated otherwise.

2.2.2. Cell Culture

Caco-2 and HT29-MTX were grown in 75 cm^2 tissue culture flasks at 37°C37ºC, 5% CO_2 in a humidified environment. Thawed cells were passaged three times prior to use. Cells were routinely cultured in Dulbecco's Modified Eagle Medium (DMEM D5796) supplemented with 10% (v/v) fetal bovine serum (FBS, F7524), and 100 U/mL Penicillin-Streptomycin (P4333) (complete DMEM). For HT29-MTX cells or co-cultures, 1% (v/v) MEM Non-essential Amino Acid Solution (M7145) was added to complete DMEM. Cells were passaged at 80% confluence every 4-5 days by

0.25% Trypsin- EDTA solution (T4049). Caco-2 passage numbers were 19-25. HT29-MTX passage numbers were 65-70. Trypan blue staining and a TC20 cell counter (Bio-Rad, USA) were used for cell counting.

2.2.3. 2.3 NADH dehydrogenase activity and ATP levels

Caco-2 cells were seeded into a 96-well plate at a density of 5×10^4 cells/well in complete DMEM (4500 mg/L glucose, L-glutamine and sodium bicarbonate). After 24 h, the cells were washed twice with PBS, and 100 µL of either DMEM D1145 or glucose/glutamine-free DMEM was added (D5030). Cells were incubated for 16 h. The following day, cells were washed twice with PBS and treated with 100 µL of 50, 75, 100 and 125 mM NaB or 100, 150, 200 and 250 mM mannitol (Man) prepared in DMEM D1145 or glucose/glutamine-free DMEM for 4 h.

CellTiter 96™ AQueous One Solution Cell Proliferation Assay (MTS) was performed as per manufacturer's instructions. In brief, MTS solution (20 µL) was added into each well and the plate incubated for 1 h at 37 °C in the dark. Absorbance was measured at 490 nm in a plate reader (Synergy HT, BioTek).

For the ATP assay, CellTiter-Glo® 2.0 Cell Viability Assay was performed, following the manufacturer's instructions. After the 4 h incubation, cell supernatant was removed and 150 µL of reagent containing luciferin was added. Cells were immediately lysed by pipetting. Cell lysate (100 µL) was transferred into a white bottom 96-well plate and allowed to equilibrate at room temperature in the dark for 10 min. Luminescence was measured using a plate reader (Synergy HT, Biotek; excitation = plug, emission = hole, gain = 135).

Control cells were incubated with either DMEM D1145 or glucose/glutamine-free DMEM. To verify the ability of nutrient-starved cells to recover, control cells in

glucose/glutamine-free DMEM were subsequently replenished with DMEM D1145 and allowed to recover for 4 h. Subsequently, MTS and ATP assays were performed to assess recovery.

2.2.4. Caspase-3 activity

Caco-2 cells were initially seeded into a 96-well plate at a density of 5×10^4 cells/well and cultured in complete DMEM. After 24 h, media was replaced with DMEM D1145 and cells were incubated overnight. The next day, cells were washed twice with HBSS and incubated with either DMEM D1145, 75/125 mM NaB or 150/250 mM Man in DMEM D1145. After a 4-h incubation Caspase-3 activity was measured with Caspase-3 assay kit (CASP3F, Sigma-Aldrich) following the manufacturer's instructions. Briefly, the plate was placed on ice and incubated with 25 µL of lysis buffer for 15 minutes. Then, 200 µL of reaction mixture (including peptide substrate acetyl-Asp-Glu-Val-Asp-7-amido-4-methylcoumarin) was added. Subsequently, 200 µL of the mixture were transferred into a black bottom 96-well plate and the fluorescence (excitation – 360 nm, emission – 460 nm) was measured at room temperature in a Biotek Synergy HT plate reader after a 60-minute incubation. The assay positive control was isolated human Caspase-3 (0.5 µg/mL, without cells).

The caspase-3 activity was calculated in nmol of 7-Amino-4-methylcoumarin (fluorescent product) released per minute per mL of cell lysate based on the formula:

Activity, nmol AMC/min/mL = (nmol AMC × d)/ (t × v)

Where: v = volume of sample in mL, d = dilution factor, t = reaction time in minutes.

2.2.5. NaB treatment of Caco-2 or Caco-2/HT29-MTX monolayers

Caco-2 cells were diluted in complete DMEM to a concentration of 1.2×10^5 cells/mL. Cells were then seeded at a density of 6.0×10^4 cells/insert (0.5 mL) into 12 well plates with inserts. The basolateral compartment received 1.5 mL complete DMEM. For the Caco-2/ HT29-MTX co-culture, cells were diluted in complete DMEM media with 1% (v/v) MEM Non-essential Amino Acid at a 90:10 ratio (respectively) in a final concentration of 1.2×10^5 cells/mL for seeding at 6.0×10^4 cells/insert (0.5 mL).

Cells were allowed to differentiate for 20 days with culture media replaced every other day. Monolayer integrity was assessed every 7 days (16 h after media change) by TEER via the Millicell ERS-2 (Millipore, USA) (Fig. S1). TEER values were expressed as $\Omega \times cm^2$- blank (Transwell insert with media in the absence of cells). Only monolayers exhibiting TEER values over 800 $\Omega \times cm^2$ on the experimental day before washing, were used for subsequent permeability studies.

Around 16 h before experimental day, the apical and basolateral compartments were washed twice with Hanks Balanced Salt Solution (HBSS, H8264) and incubated with DMEM (DMEM D1145, *i.e.*, without phenol red and glutamine), without antibiotics and FBS. On experimental day, TEER values were recorded and cells washed twice with HBSS. DMEM D1145 was then added to the apical (0.4 mL) and basolateral compartments (1.5 mL), and the plates were incubated for 30 min for acclimatization.

NaB was freshly prepared as a 5X stock solution in DMEM D1145 and filtered with 0.22 µm PES filter (Sarsted Group). This stock solution (100 µL) was then added to the apical compartment, resulting in a final concentration of 50, 75, 100 and 125 mM NaB in 0.5mL total volume. For experiments with Man, a 2.5X solution was

prepared and 200 µL was added to the apical compartment with 300 µL DMEM D1145 to a final Man concentration of 100, 150, 200 and 250 mM. The osmolality of the samples was measured with OsmoTECH® XT Single-Sample Micro-Osmometer (Advanced Instruments, USA).

Monolayers exposed to NaB or Man were incubated for 24 h. TEER was measured at times 0, 2, 4, 6 and 24 h. Control monolayers contained DMEM D1145 only. At 24 h, apical and basolateral compartments were collected and stored at -20 °C for further analysis. Further experiments were performed on the monolayers, or the monolayers were lysed for RT-PCR.

2.2.6. Monolayer recovery

After the 24 h incubation with NaB or Man, monolayers were washed twice with HBSS and DMEM D1145 was added in the apical (0.5 mL) and basolateral (1.5 mL). Monolayers were incubated for a further 24 h. TEER was measured after 1, 2, 4, 6, and 24 h.

2.2.7. TEER measurements with isosmotic NaB and Man solutions

To obtain isosmotic solutions of NaB and Man, DMEM D1145 was firstly diluted with Milli-Q H_2O; 1 in 1.37 for 50 mM NaB/ 100 mM Man, 1 in 1.678 for 75 mM NaB/ 150 mM Man, 1 in 2.17 for 100 mM NaB/ 200 mM Man and 1 in 3 for 125 mM NaB and 250 mM Man. The diluted media were then used to dissolve NaB or Man. Osmolality of the prepared stock solutions were measured using OsmoTECH® XT Single-Sample Micro-Osmometer (Advanced Instruments).

On day 19, Caco-2 monolayers were washed twice with HBSS and incubated overnight with DMEM D1145. The next day, monolayers were washed twice with HBSS and treated with 0.5 mL of the isosmotic solutions on the apical side for 24 h.

The basolateral side contained fresh 1.5 mL DMEM D1145 (348.6 mOsm/kg). TEER measurements were taken 0, 1, 2, 4, 6 and 24 h using the Millicell ERS-2 (Millipore). DMEM D1145 served as the control condition.

2.2.8. Treatment with dexamethasone

Dexamethasone (D4902) was dissolved in DMSO to a stock concentration of 2 mM, which was sequentially diluted 1 in 200 in DMEM D1145. After 24h incubation with NaB or Man, 21-day Caco-2 monolayers were washed twice with HBSS. Dexamethasone (10 µM in DMEM D1145, 0.5 mL) was added to the apical compartment for 24 h. Basolateral compartment contained 1.5 mL DMEM D1145. TEER was measured at T0 and T24. Apical samples were then collected for LDH release. Monolayers were washed twice with PBS and lysed on ice using 350 µL of RLT buffer for RT-PCR analysis. Lysates were stored at -20°C until use.

2.2.9. Lucifer Yellow permeability

After the 24 h incubation with NaB or Man, Caco-2 monolayers were washed twice with HBSS. The apical side was then exposed to 0.5 mL of 0.5 mg/mL Lucifer Yellow in HBSS for 2 h, while the basolateral side was exposed to 1.5 mL of HBSS. To prepare a standard curve, the stock Lucifer Yellow solution was diluted in HBSS ranging from 7.81 to 0.24 to µg/mL. After incubation, 300 µL of each basolateral sample or standard was transferred to a black, flat-bottom 96-well plate (Corning). Fluorescence was read (excitation – 420 nm, emission – 528 nm, gain = 40) at 37°C using a plate reader (Synergy HT, Biotek, USA). The concentration of Lucifer Yellow in the basolateral side was calculated comparing the measured fluorescence to the standard curve. The apparent permeability (Papp) was calculated with the following formula:

Papp (cm/min) = $(C_{Baso} \times V)/(t \times A \times C_{In})$

Where: C_{Baso} = Concentration of Lucifer yellow in the basolateral compartment (µg/mL); V = Volume of the basolateral compartment (mL); t = incubation time (120 min); A = surface area (1.1 cm^2); C_{In} = initial concentration in the apical (µg/mL).

2.2.10. NaB and Man quantification in apical and basolateral samples

NaB and Man concentrations were quantified using High-Performance Liquid Chromatography (HPLC), employing a Waters Alliance Separation Module e2695 coupled with a Waters 2414 refractive index (RI) detector (Waters, MA, USA).

For NaB analysis, apical samples and initial NaB stock solutions were diluted 1:100 in MilliQ H_2O, while basolateral samples were diluted 1:10 in MilliQ H_2O. For Man analysis, apical samples were diluted 1:100 and basolateral samples 1:25 in MilliQ H_2O. Samples were filtered via 0.22 µm nylon syringe filters.

A 20 µL aliquot of each sample or standard was injected. For NaB detection, separation was carried out on an Aminex HPX-87C ion exchange column (300 × 7.8 mm), operated at 60 °C. Elution was performed using 0.005 N H_2SO_4 as the mobile phase at a flow rate of 0.6 mL/min. NaB quantification was performed by comparing sample peak areas to a standard curve prepared with known NaB concentrations ranging from 10 to 100 µg/mL in MilliQ H_2O.

For Man detection, separation was achieved using an Aminex HPX-87P carbohydrate analysis column (300 × 7.8 mm) equipped with an Aminex HPX-87P guard column (Bio-Rad, cat. no. 1250131), and maintained at 60 °C. The RI detector was operated at 35 °C. Elution was performed with MilliQ H_2O at a flow rate of 0.6 mL/min. Analytical-grade Man was used to prepare standard solutions at

concentrations of 20, 50, 100, and 200 μg/mL. Man quantification was based on retention time matching and comparison of peak areas to the standard curve.

Data are expressed as the amount (μg) of NaB or Man present in 0.5 mL of the apical sample at T0 and T24, and 1.5 mL of the basolateral sample at T24. The percentage of NaB or Man transported was calculated using the following equation:

% transported = $(C_{baso} / C_{T0}) \times 100$

Where C_{baso} = concentration of butyrate in the basolateral compartment (mmol in 1.5 mL); C_{T0}= concentration of butyrate in the solution applied to the apical compartment at T0 (mmol in 0.5 mL)

2.2.11. RT-qPCR

For the RT-qPCR analysis, Caco-2 monolayers were washed twice with PBS and lysed with the addition of 350 μL RLT buffer. After 5 min on ice, cell lysate was collected by pipetting and stored at -80 °C. Lysed cells were thawed at room temperature and RNA extracted using the RNeasy Mini Kit with a DNAse step, following manufactures instructions. Total RNA quantity was measured using Nanodrop 1000 (Thermo Fisher Scientific, MA, USA) and RNA samples with $OD_{260/280} > 1.8$ were progressed to cDNA synthesis. The SensiFAST cDNA Synthesis Kit was used to synthesize cDNA from 0.5 μg Total RNA. Subsequently, quantitative PCR was conducted with the Light Cycler SYBR GREEN I Master kit using a Light Cycler 96 instrument.

Primers were designed based on GenBank sequences (Supplementary Table 2.1). p21 primer was obtained from Ding et al. (2019). The human ribosomal protein lateral stalk subunit P0 (RPLP0) was chosen as a housekeeping gene. Amplification efficiency ranged between 90 and 110%, with optimal annealing temperature of

60°C. The $2^{-\Delta\Delta Ct}$ method was employed to calculate the relative amount of the target, where

$\Delta\Delta Ct = (Ct\ Target\ gene - Ct\ RPLP0)_{test} - (Ct\ Target\ gene - Ct\ RPLP0)_{Control}$. Ct = threshold cycle for either the target gene or RPLP0; test = Man or NaB treated monolayers; control = DMEM D1145 media treated monolayers.

2.2.12. Lactate Dehydrogenase (LDH) cytotoxicity assay

To measure LDH release, 50 µL from the apical chamber of NaB-, Man- or NaB + dexamethasone-treated Caco-2 monolayers were transferred to a 96-well flat-bottom plate and combined with an equal volume of the LDH Cytotoxicity Assay reaction mixture. The plate was incubated in the dark at room temperature for 30 minutes, allowing the LDH-mediated conversion of lactate to pyruvate and subsequent reduction of the formazan dye. Following incubation, 50 µL of stop solution was added to each well, and absorbance was measured at 490 nm and 680 nm using a Synergy HT plate reader (Biotek). LDH activity was determined by subtracting the absorbance at 680 nm from the absorbance at 490 nm for each sample. LDH release was calculated using the formula:

% LDH release = [(Treated LDH activity – Spontaneous LDH activity) / (Maximum LDH activity – Spontaneous LDH activity)] × 100

Where: Treated LDH activity = LDH activity in the supernatant of NaB- or Man-treated monolayers; Spontaneous LDH activity = activity in supernatant of DMEM D1145 control monolayers; Maximum LDH activity = LDH released from 50 µL of lysed control monolayers treated with 500 µL of 1% Triton X-100.

2.2.13. Statistical analysis

All experiments were conducted in triplicate on three independent days, each with technical duplicates. Results are presented as means ± SEM. Statistical analyses were performed using GraphPad Prism 9.1.0 (GraphPad Software, San Diego, California, USA). One-way or two-way ANOVA followed by Tukey's multiple comparisons test was used for normally distributed data, while the Friedman test with Dunn's multiple comparisons test was applied for non-normally distributed data. Statistical significance was defined as $P < 0.05$.

2.3. Results

2.3.1. NaB impairs epithelial barrier integrity monolayers without subsequent recovery

Caco-2 monolayers (20-day old) were treated with either 50, 75, 100, 125 mM NaB or the osmolality equivalent Man concentration (Fig. 2.1). The mean TEER value at day 20 for was 1451.40 ± 33.03 $\Omega \times cm^2$ (Supplementary Fig. 2.1A). The osmolality (mOsm/kg) of NaB-DMEM D1145 solutions applied to the cells are detailed in Table 2.2A and ranged from 348.7 ± 1 mOsm/kg for DMEM D1145 to 579.5 ± 2.5 for 125 mM NaB in DMEM D1145. As Man is not metabolized nor internalized by Caco-2 cells but is transported paracellularly to the basolateral chamber (Ménard et al., 2010), Man with equivalent osmolality to NaB ($P > 0.05$) was included as a control (Table 2.2). Treatment with NaB reduced the Caco-2 monolayer TEER values in a dose-dependent manner, compared to media alone (Fig. 2.1A; T4 = $P < 0.05$, T24 = $P < 0.05$). NaB was then removed and replaced with fresh DMEM D1145 to support recovery. By 24 h recovery, NaB treated monolayers, regardless of dose, had not recovered (T24 vs. Recovery T24 $P < 0.05$). Indeed Caco-2

monolayers treated with 125 mM NaB had a TEER value at recovery T24 of 66.36 ± 21.93 compared to 1742.03 ± 100.24 with DMEM D1145. In contrast, treatment with Man (100, 150, 200, 250 mM) resulted in a significant reduction at 2, 4, 6 h but by 24 h only 250 mM Man was significantly reduced ($P < 0.05$) (Fig. 3.1B). Removal of Man allowed all monolayers to recover to control condition ($P > 0.05$). As TEER is only one measurement of barrier function, paracellular permeability was also assessed using Lucifer Yellow (Fig. 2.1C and D). NaB at 75, 100 and 150 mM induced a dose-dependent increase in Lucifer Yellow Papp compared to DMEM D1145 (75 and 100 mM NaB $P < 0.05$; 125 mM NaB $P<0.01$). Only 250 mM Man (osmolality equivalent to 125 mM NaB) had a significantly higher Papp compared to DMEM D1145 ($P < 0.05$), while the other Man concentrations had no effect ($P > 0.05$). The Papp of DMEM D1145 control monolayers was = $0.51\times10^{-5} \pm 9.82\times10^{-6}$ cm^2/min.

Mucus is known to provide protective effects to monolayers *in vitro* (Sheng and Hasnain, 2022). To evaluate whether monolayers could be protected from NaB, a 20-day co-culture monolayer comprised of Caco-2 with goblet cells, HT29-MTX, at a ratio of 90:10 was treated with NaB or Man (Supplementary Fig. 2.1B and 2.2). The presence of the mucus layer provided no protection from TEER reduction caused by NaB. In addition, no recovery was observed with removal of NaB from the co-cultures. Co-cultures treated with Man recovered to control condition at T24 recovery ($P > 0.05$).

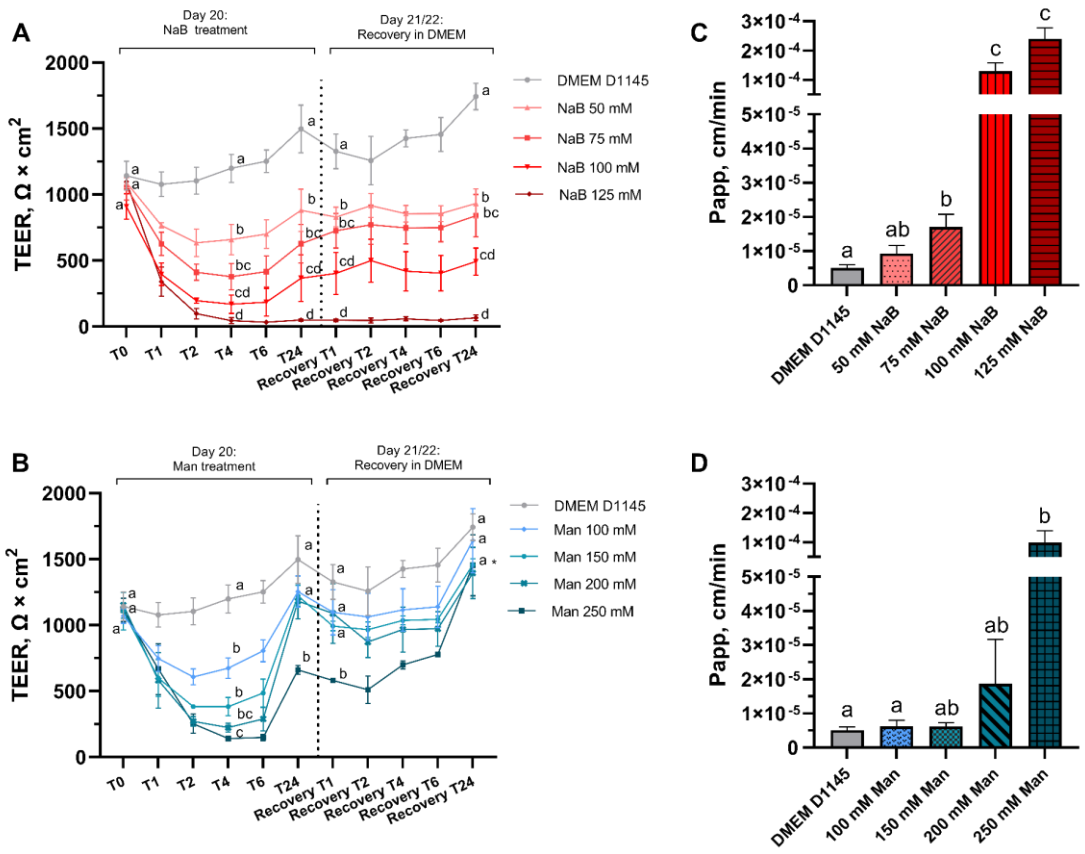


Fig. 2.1 Effects of Sodium Butyrate (NaB) and Mannitol (Man) on Caco-2 Monolayer Permeability.

The mean TEER value at day 20 Caco-2 was 1451.40 ± 33.03 Ω × cm². (A) NaB-treated monolayers in DMEM 1145 or (B) Mannitol-treated monolayers in DMEM 1145. TEER values were recorded before the treatment (T0) and at 1, 2, 4, 6 and 24 h (T1/2/4/6/24). NaB or Man was then removed and TEER values were recorded at Recovery 1, 2, 4, 6, and 24 h. Statistical analysis was performed by two-way ANOVA with Tukey's multiple comparison. Statistical differences between different concentrations, at the same time point, is depicted by different letters. Statistical difference between T24 and Recovery T24 within the same concentration is indicated by an asterisk. (C) Lucifer yellow apparent permeability (Papp) for NaB-treated monolayers and (D) Man-treated monolayers. Lucifer yellow (mM) was added to the apical and quantified in the basolateral after 2 h. Statistical significance between different concentrations, at the same time point, was determined for C by one-way ANOVA with Tukey's Multiple comparisons and for D by Friedman test with Dunn's multiple comparisons. Results are presented as biological triplicates with technical duplicates ± SEM. Different letters indicate statistically significant differences ($P<0.05$).

Table 2.1 Average osmolality (mOsmol/kg) of DMEM D1145, NaB, and Man solutions. Osmolality of DMEM D1145 and NaB/ Man samples dissolved in (A) DMEM D1145 or (B) diluted DMEM D1145 to maintain isosmotic conditions. Osmolality was measured using a cryoscopic osmometer (OsmoTECH® XT). Data represent the mean of biological triplicates ± SEM. Statistical analysis was performed using one-way ANOVA with Tukey's multiple comparisons. Within stock solutions or apical samples, different letters indicate significant differences ($P < 0.05$).

A – Samples in DMEM D1145		**B – Samples in diluted DMEM D1145**	
Sample	**Osmolality (mOsm/kg)**	**Sample**	**Osmolality (mOsm/kg)**
DMEM D1145	348.6667 ± 1^{a}	-	
NaB 50 mM	430.5 ± 4.5^{b}	NaB 50 mM	343.5 ± 5.5^{a}
NaB 75 mM	474.5 ± 1.5^{c}	NaB 75 mM	360.5 ± 20.5^{a}
NaB 100 mM	525 ± 9^{d}	NaB 100 mM	343.0 ± 7^{a}
NaB 125 mM	579.5 ± 2.5^{e}	NaB 125 mM	368.5 ± 2.5^{a}
Man 100 mM	438 ± 4^{b}	Man 100 mM	351 ± 2^{a}
Man 150 mM	484.5 ± 0.5^{c}	Man 150 mM	368.5 ± 6.5^{a}
Man 200 mM	534 ± 1^{d}	Man 200 mM	362.5 ± 1.5^{a}
Man 250 mM	583 ± 1^{e}	Man 250 mM	372.0 ± 11^{a}

2.3.2. NaB does not reduce TEER under isosmotic conditions

Caco-2 monolayers/cells can withstand osmolality ranging from 150-680 mOsm/L and are isotonic at 336 mOsm/L (Grauso et al., 2019; Hubert et al., 2004). To evaluate whether or not the NaB effect on Caco-2 monolayers was due to osmotic stress, the osmolality of 50 (430.5 mOsm/kg), 75 (474.5 mOsm/kg), 100 (525 mOsm/kg) and 125 mM (579 mOsm/kg) NaB solutions were adjusted to 360-368 mOsm/kg by diluting the media, DMEM D1145, in MilliQ H_2O (Table 2.2B). Osmolality was not significantly different among all test solutions ($P > 0.05$). Caco-2 monolayers were then treated for 24 h with these adjusted NaB solutions (Fig. 2A). The average TEER of control monolayers was $1269.03 \pm 118.60\ \Omega \times cm^2$ at the initial time point (T0) and increased to $1841.22 \pm 91.488\ \Omega \times cm^2$ after 24 h (T24).

Under these isosmotic conditions, neither NaB nor Man treatment significantly decreased TEER values over a 24 h period compared to monolayers treated with media alone (Fig. 2.2). This indicates that osmotic stress is playing a major role in Caco-2 response to both NaB and Man but does not explain the inability of Caco-2 monolayers to recover from NaB treatment whilst recovering from Man treatment occurs. Interestingly, 200 mM Man at T24 had a TEER of 2728.92 ± 59.49 $\Omega \times cm^2$, significantly higher compared to control monolayers in DMEM D1145 ($P < 0.05$, Fig. 2.2B).

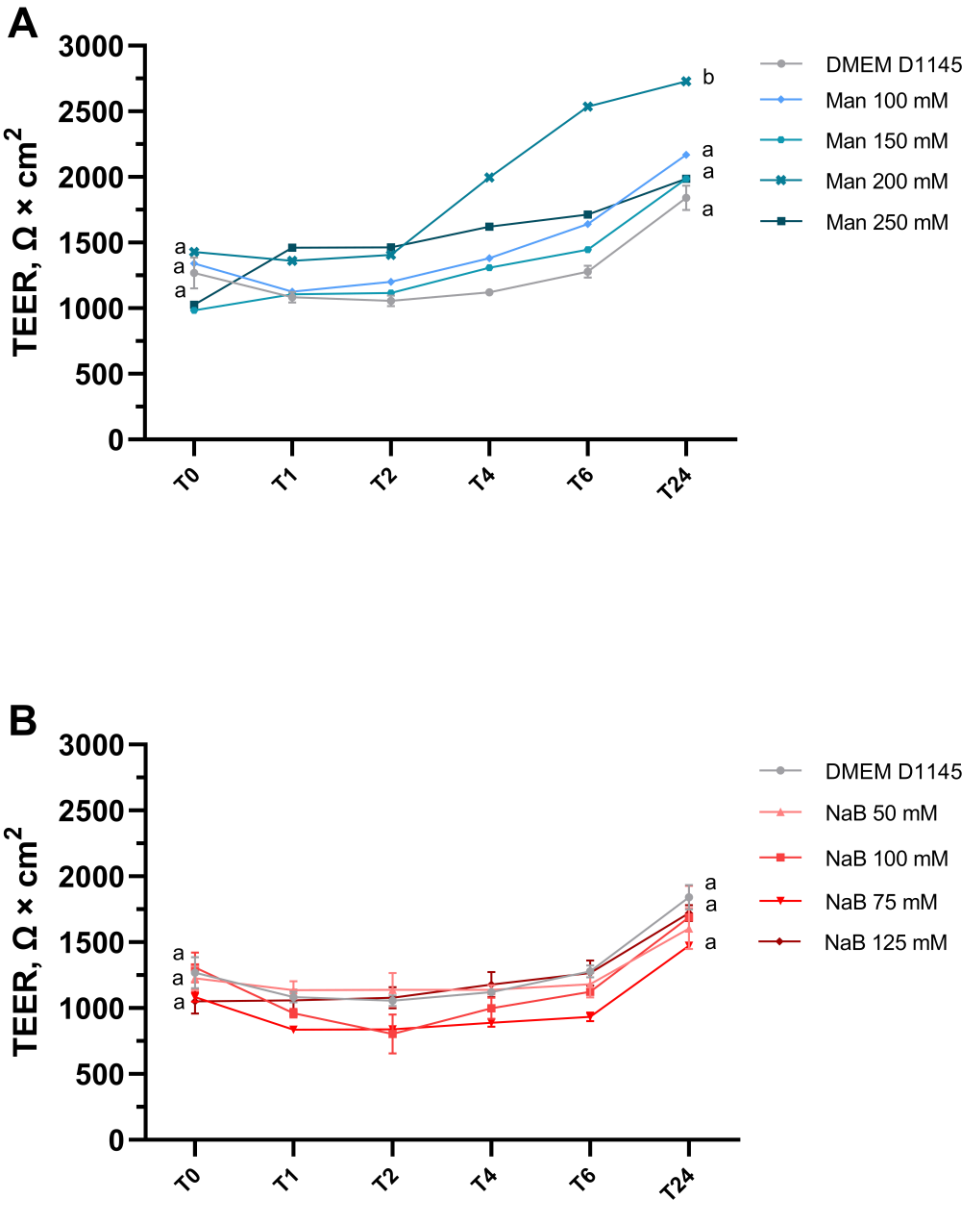


Fig. 2.2 Transepithelial electrical resistance (TEER) values for 20 day Caco-2 monolayers treated with NaB or Man at 367.4 ± 4.86 mOsm/kg.

Differentiated 20 day Caco-2 monolayers were washed with HBSS (T0), and treated for 24 h (T1–T24) with DMEM D1145 (control condition) and (A) NaB at 50, 75, 100 and 125 mM or (B) Man at 100, 150, 200 and 250 mM, with an adjusted osmolality of 371 mOsm/kg. Results are presented as biological triplicates with technical duplicates ± SEM. Statistical significance compared to DMEM D1145 at each time point was determined using two-way ANOVA with Dunnet's multiple comparison test. Different letters indicate statistically significant differences ($P < 0.05$).

2.3.3. NaB is transported across and into Caco-2 monolayers

To determine whether NaB was transported across mature 20-days-old Caco-2 monolayers, concentrations of each compound were quantified in apical and basolateral chambers after 24 h treatment (Fig. 2.3A and B). Similar to Man, NaB was detected in the basolateral compartment, confirming translocation across the monolayer. Notably, the total recovered amount of NaB (apical plus basolateral compartments) was significantly lower than the initial apical concentration ($P < 0.05$), indicating substantial uptake or metabolism by the monolayers. In contrast, the total recovered amount of Man matched the initially applied concentration ($P < 0.05$), confirming no uptake by Caco-2 cells. Specifically, the percentage of NaB transported to the basolateral compartment was: 50 mM NaB = 31.85 ± 0.6%, 75 mM NaB = 33.03 ± 1.9%, 100 mM NaB = 41.41 ± 1.2%, and 125 mM NaB = 53.87 ± 4.03%. In contrast, Man showed comparatively lower transport percentages: 100 mM Man = 3.13 ± 0.49%, 150 mM Man = 8.91 ± 1.04%, 200 mM Man = 20.76 ± 5.45%, and 250 mM Man = 27.13 ± 7.82%.

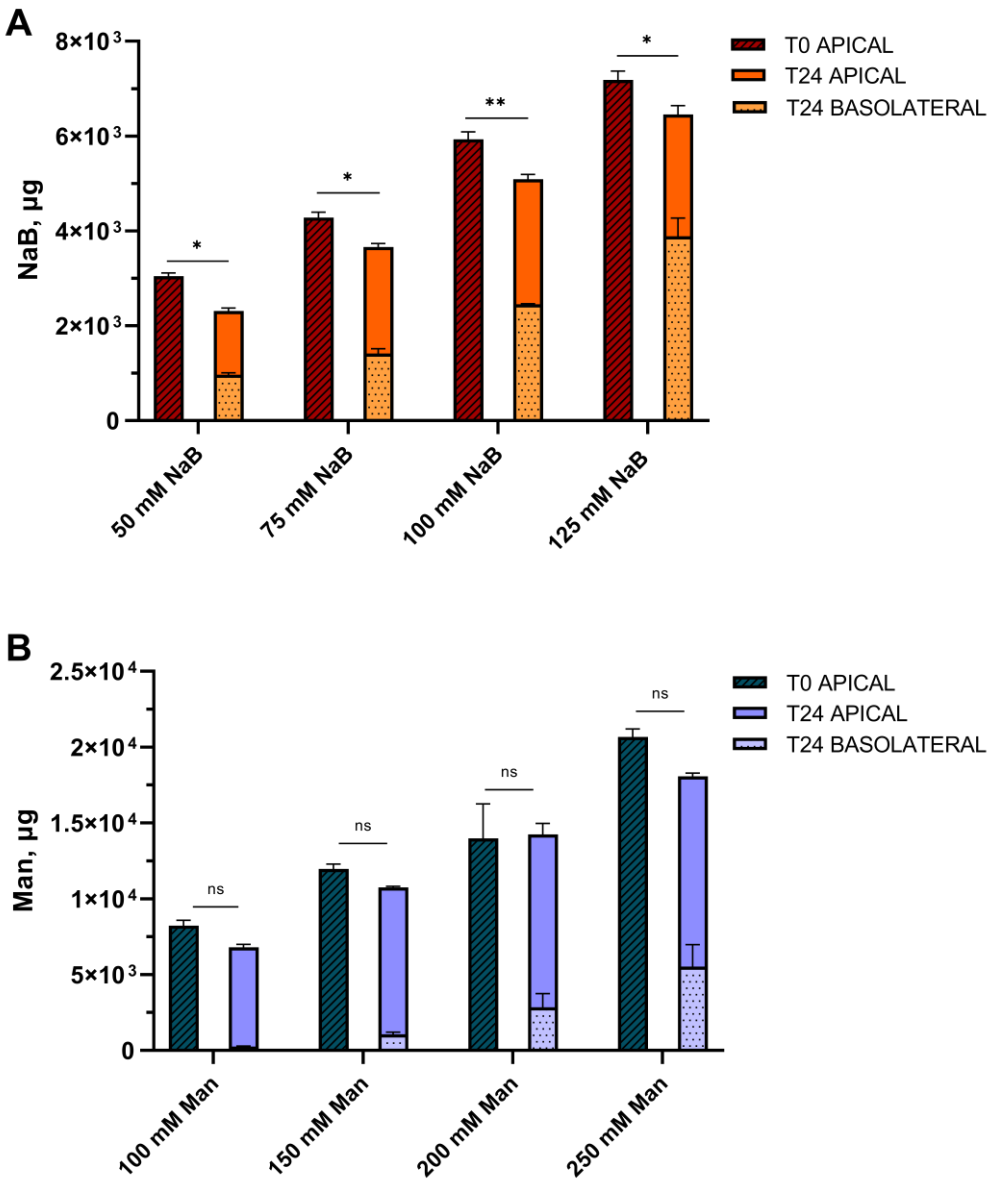


Fig. 2.3 Quantification of NaB and Man solutions applied to Caco-2 Monolayers.
Quantification of (A) NaB and (B) Man by HPLC. T0 apical = solution applied to the apical compartment at T0; T24 apical = apical sample after 24 h incubation T24 basolateral = basolateral sample after 24 h incubation. Results represent the average of three biological and two technical replicates, presented as mean ± SEM. Statistical Analysis was determined using two-way ANOVA with Dunnet's multiple comparison test. Statistical significance ($P<0.05$) between T0 apical and (T24 apical + T24 basolateral) is indicated with an asterisk.

2.3.4. NaB is not utilized as an energy source in Caco-2 cells

To assess whether or not NaB is utilized by Caco-2 cells, NADH dehydrogenase activity (MTS assay) and intracellular ATP levels were measured after cells were starved for 16 h in media in the absence of a carbon source (glucose and sodium pyruvate-free DMEM) (Fig. 4). NaB or Man were then added. Without a carbon source in the media, NADH dehydrogenase activity in the cells was 25.5 ± 0.75 % of the control media with glucose ($P < 0.05$). The addition of NaB or Man to the media, did not restore NADH dehydrogenase activity in the cells, indicating neither NaB nor Man were used as a carbon source. Where cells were cultured in media with glucose, the addition of NaB or Man did not significantly increase NADH dehydrogenase activity ($P > 0.05$).

Intracellular ATP is a marker of metabolically active cells. The levels of intracellular ATP produced in Caco-2 in response to NaB or Man are depicted in Fig. 2.4C and D. In the absence of a carbon source, ATP levels are 25.77 ± 0.85% of the control cells with glucose (DMEM D1145, $P < 0.05$). The addition of NaB or Man did not increase ATP levels. Interestingly when cells were incubated with glucose (DMEM D1145), the addition of 75, 100 and 125 mM NaB or 100, 150, 200 and 250 mM Man significantly reduced ATP levels ($P < 0.05$).

As a positive control, cells incubated in glucose-free DMEM for 16 h, and subsequently transferred to glucose-containing DMEM D1145 for 4 h, exhibited partial metabolic recovery, with NADH dehydrogenase activity and ATP levels reaching 65.60 ± 12.29% and 49.07 ± 0.14% of control values, respectively.

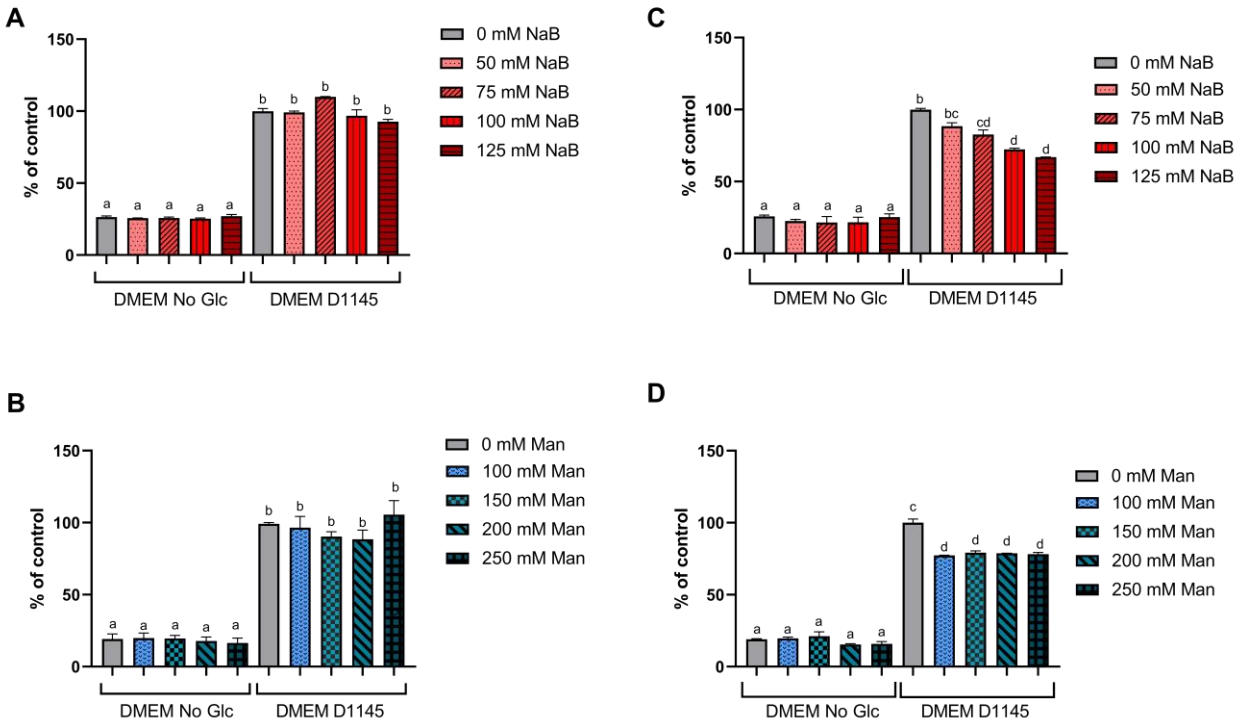


Fig. 2.4 Metabolic activity of undifferentiated Caco-2 cells after treatment with NaB or Man.

Caco-2 cells were seeded at 10^5 cells/well, grown for 24 h, washed with PBS and media changed to DMEM D1145 (no glutamine or sodium pyruvate) or DMEM No Glc (no glutamine, sodium pyruvate or glucose) for 16 h. Cells were then exposed to NaB or Man solutions in DMEM D1145 or DMEM No Glc for 4 h. (A, B) MTS assay (C, D) intracellular ATP expressed as % of control (0 mM NaB/Man in DMEM D1145). Cells exposed to DMEM No Glc for 16 h and subsequently to DMEM D1145 for 4 h were 65.60 ± 12.29 % for the MTS assay and 49.07 ± 0.14 % for the ATP assay. Data represents the mean ± SEM from biological triplicates and technical duplicates. Statistical analysis was assessed by one-way ANOVA with Tukey's multiple comparisons. Significant differences are indicated with different letters ($P<0.05$)

2.3.5. NaB induces apoptosis (Caspase-3 activity)

Since TEER, Papp and ATP levels were adversely affected by 75-125 mM NaB, the activity level of the apoptotic marker, Caspase-3 (Porter and Jänicke, 1999; Ruemmele, 2003), was quantified in undifferentiated Caco-2 cells treated with NaB at these concentrations (Fig. 2.5). Both NaB concentrations induced a significant increase in Caspase-3 activity compared to media alone ($P < 0.05$), with 125 mM NaB treatment causing the highest Caspase 3 activity in Caco-2 cells. ($P < 0.05$), significantly higher than Man at the equivalent osmolality. Noteworthy, there was no statistical difference in the % of cytotoxicity (measured as LDH release in the apical chamber of Caco-2 monolayers) for 75 and 125 mM NaB (Fig. S3A) compared media alone ($P > 0.05$).

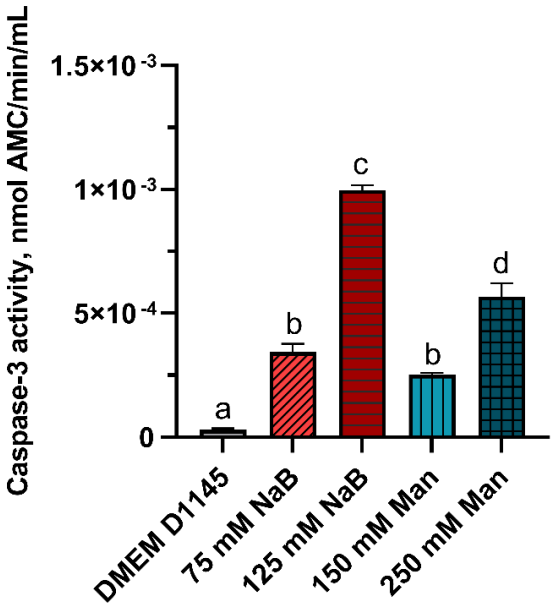


Fig. 2.5 Caspase 3 activity in undifferentiated Caco-2 cells treated with NaB or Man.
Caspase-3 activity in undifferentiated Caco-2 cells treated with NaB or Man for 4 h. Results are expressed as nmol of 7-Amino-4-methylcoumarin—AMC—released per min per mL of cell lysate. DMEM D1145= cells in DMEM. The assay positive control was isolated human Caspase-3 (1 µg/mL, no cells) which gave units of $4.43 \times 10^{-3} \pm 0.75 \times 10^{-3}$ nmol AMC/min/mL. Results are presented as the average of a biological triplicate and a technical duplicate ± SEM. Statistical difference between treatments was assessed by one-way ANOVA with Tukey's multiple comparison and it is indicated by a different letter ($P<0.05$).

2.3.6. NaB induces mRNA expression of butyrate transporters, stress markers and cytokines

To determine whether NaB induces upregulation of butyrate transporters (Monocarboxylate Transporter 1 (MCT-1) and Sodium-Coupled Monocarboxylate Transporter 1 (SMCT-1)) or the first enzyme of β-oxidation Short-Chain Acyl-CoA Dehydrogenase (SCAD), mRNA transcript levels were measured in Caco-2 monolayers treated with NaB at 75 mM and 125 mM (Fig. 2.6). Both 75 and 125 mM NaB significantly increased SMCT-1 mRNA transcript levels compared to the monolayers treated with media alone ($P < 0.05$), whilst only 125 mM NaB significantly upregulated MCT-1 expression ($P < 0.05$). No significant changes were observed in SCAD mRNA levels in NaB-treated monolayers compared to the media control ($P > 0.05$).

To determine whether NaB exposure causes stress or initiates an inflammatory response, mRNA transcript levels of the water transport channel aquaporin 3 (AQP-3) (Grauso et al., 2019; Yde et al., 2021), stress markers p21 (p21^Cip1/Waf1) and 70 kilodalton heat shock protein (HSP-70) (Renis et al., 2008), and pro-inflammatory cytokines, Interleukin 6 (IL-6), Interleukin 8/ CXC chemokine ligand 8 (IL-8) and Tumor Necrosis Factor (TNF) (Iglesias et al., 2020; Jung et al., 1995) were measured. As shown in Fig. 2.6, NaB did not affect AQP-3 mRNA, whereas 250 mM Man (osmolality = 125 mM NaB) significantly reduced AQP-3 mRNA levels compared to media alone ($P < 0.05$). Both 75 mM and 125 mM NaB treatments significantly increased p21, HSP-70, IL-8, and TNF mRNA transcripts compared to monolayers treated with media alone ($P < 0.05$); However, only 125 mM NaB significantly increased IL-6 mRNA expression compared to media control

($P < 0.05$). Treatment with Man at similar osmolality did not significantly alter mRNA levels of p21, HSP-70, IL6, IL8, or TNF ($P > 0.05$).

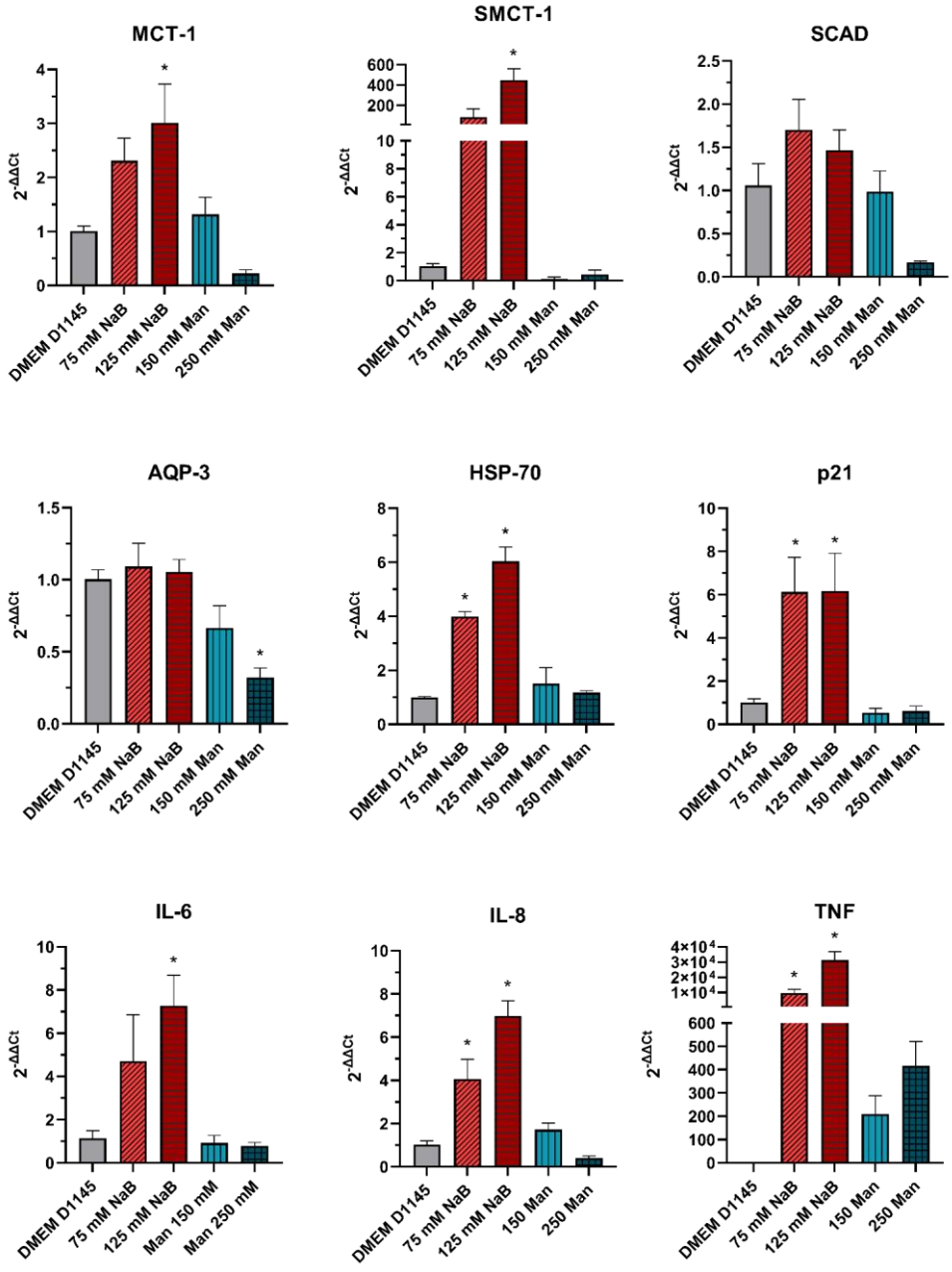


Fig. 2.6 mRNA Expression of MCT-1, SMCT-1, SCAD, AQP-3, HSP-70, IL-6, IL-8, and TNF in Caco-2 Monolayers treated with NaB or Man.

20-day Caco-2 monolayers treated for 24 h with NaB or Man. Messenger RNA transcript levels of Sodium-Coupled Monocarboxylate Transporter 1 (SMCT1), Monocarboxylate Transporter 1 (MCT1), Short-Chain Acyl-Coenzyme A Dehydrogenase (SCAD), Aquaporin-3 (AQP-3), Heat-Shock Protein-70 (HSP-70), cyclin-dependent kinase inhibitor 1 (p21), Interleukin 6 and 8 (IL-6, IL-8) and Tumor Necrosis Factor (TNF) were quantified using RT-PCR and normalized to the housekeeping gene RPLP0 mRNA and the control condition (monolayers in DMEM D1145 only) via the $2^{-\Delta\Delta Ct}$ method. Data represent the mean ± SEM from biological triplicates and technical duplicates. Statistical analysis was conducted using One-way ANOVA with Dunnet's multiple comparisons. The asterisk represents a significant difference to DMEM D1145 ($P < 0.05$).

2.3.7. Dexamethasone promotes recovery of Caco-2 monolayers treated with 75 mM NaB

To assess whether the adverse effects of NaB on epithelial integrity could be reversed, we tested dexamethasone, a synthetic glucocorticoid known to regulate stress markers such as HSPs (Urayama et al., 1998) suppress pro-inflammatory cytokines, and stabilize barrier function in conditions like inflammatory bowel disease (Liu et al., 2009; Schreiber et al., 1998) and necrotizing enterocolitis (Lei Lu et al., 2021). In our study, Caco-2 monolayers were exposed to NaB under hyperosmotic conditions, with osmolality levels exceeding physiological norms, mimicking pathological states like Crohn's disease (Schilli et al., 1982). To evaluate dexamethasone's restorative effect, 10 μM was added during a 24-hour recovery phase following NaB treatment. This concentration of dexamethasone was not cytotoxic, as determined by LDH release (Fig. S3B). Treatment with 75 mM NaB reduced TEER values to 506 ± 117.02 Ω×cm². Subsequent removal of NaB and addition of dexamethasone significantly restored TEER to 931.70 ± 35.59 Ω×cm² at 24 h ($P < 0.05$). However, monolayers treated with 125 mM NaB did not recover with dexamethasone administration. Post-treatment, mRNA analysis (Fig. 2.7B) showed no significant differences in stress marker levels (HSP-70, p21, IL-8) or inflammation (IL-6 or TNF) in Caco-2 monolayers treated with 75 mM NaB + dexamethasone compared to Caco-2 monolayers treated with dexamethasone only ($P<0.05$). However, IL-6 and TNF mRNA expression were significantly elevated in monolayers treated with 125 mM NaB + dexamethasone compared to controls ($P < 0.05$). Notably, expression levels of stress and inflammatory markers were lower in dexamethasone-treated DMEM D1145 control monolayers compared to untreated DMEM D1145. The $2^{-\Delta\Delta Ct}$ normalized values for control Caco-2 monolayers were:

HSP-70 = 47.24 ± 2.06, p21 = 386.7 ± 86.85, IL-6 = 263 ± 119.9, IL-8 = 164.8 ± 27.24, and TNF = 6.28 ± 1.65.

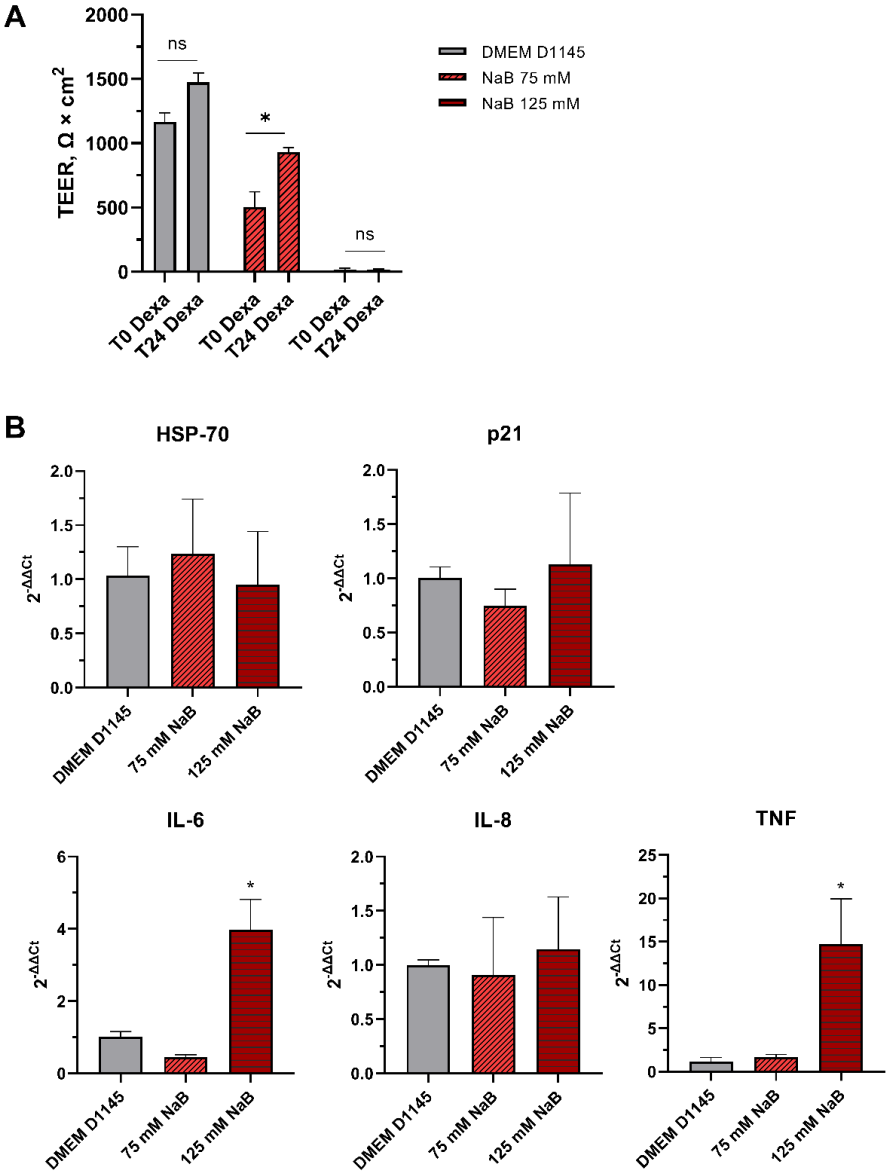


Fig. 2.7 Effect of dexamethasone (Dexa) on NaB-treated Caco-2 monolayers.

Caco-2 monolayers were treated with 75/125 mM NaB for 24 h, washed with HBSS, and exposed to 10 µM dexamethasone in DMEM D1145 for a further 24 h. (A) TEER values were recorded pre (T0 Dexa) and post (T24 Dexa) dexamethasone treatment. DMEM D1145= control monolayers treated with 10 µM dexamethasone. DMEM D1145 TEER at T0 was= 1167.83±69.72Ω×cm^2. (B) mRNA transcript levels of Heat-Shock Protein-70 (HSP-70), cyclin-dependent kinase inhibitor 1 (p21), Interleukin 6 and 8 (IL-6, IL-8) and Tumor Necrosis Factor (TNF) in Caco-2 monolayers post dexameathsone treatment. RT-PCR data was normalized to the housekeeping gene *RPLP0* mRNA and the control condition (DMEM D1145 + dexamethasone) via the $2^{-\Delta\Delta Ct}$ method. Data represents the mean ± SEM from biological triplicates and technical duplicates. Statistical analysis was conducted using (A) two-way ANOVA with Tukey's multiple comparisons or (B) one-way ANOVA with Dunnet's multiple comparisons. The asterisk represents a significant difference to (A) T0 or (B) DMEM D1145+ dexamethasone ($P < 0.05$).

2.4. Discussion

Our study demonstrated that high concentrations of NaB (50–125 mM) significantly reduce TEER and increase paracellular permeability in a dose-dependent manner ($P < 0.05$), with no recovery observed after treatment removal ($P > 0.05$). NaB does not serve as an energy substrate, as shown by reduced ATP levels ($P < 0.05$) and unchanged cellular reductase activity (MTS assay, $P > 0.05$). However, it is actively transported into cells, as evidenced by increased mRNA expression of the butyrate transporters MCT-1 and SMCT-1 at 125 mM ($P < 0.05$). NaB at 75 and 125 mM also activates the apoptosis marker Caspase-3 ($P < 0.05$) and uniquely elevates stress markers (p21, HSP-70) and pro-inflammatory cytokines (IL-6, IL-8, TNF; $P < 0.05$). Importantly, while the induction of stress and inflammation markers was specific to NaB, TEER reductions were observed only under hyperosmotic conditions, suggesting an interplay between NaB-specific effects and hyperosmolarity. Treatment with 75 mM NaB followed by 24 h of dexamethasone restored TEER ($P < 0.05$) and normalized stress and inflammation markers ($P > 0.05$). These findings establish 75 mM NaB-treated Caco-2 monolayers as a robust *in vitro* model for studying a leaky damaged gut.

We initially investigated the impact of NaB on the permeability of Caco-2 monolayers using two key metrics: TEER and Lucifer Yellow (LY) apparent permeability (Papp). High concentrations of NaB (50–125 mM) significantly reduced TEER values ($P < 0.05$), with concentrations ≥75 mM also significantly increasing LY permeability ($P < 0.05$), clearly indicating compromised barrier integrity. Importantly, removal of NaB after treatment did not lead to monolayer recovery. These results align with Kondrashina et al. (2021), who reported reduced TEER at NaB concentrations ranging from 50 to 250 mM and enhanced paracellular

permeability to lactulose and Man at higher concentrations (150-250 mM, $P < 0.05$). Specifically, Kondrashina et al. observed that 125 mM NaB reduced TEER to 408 ± 52 Ω × cm² ($P < 0.05$ vs. control) and notably increased lactulose leakage relative to Man. TEER results at 125 mM NaB (48.77 ± 7.53 Ω × cm²) in the current study were considerably lower, likely due to inherent Caco-2/HT29-MTX clone variabilities (Hevia et al., 2023a). However, our findings at 75 mM NaB (626.82 ± 146.22 Ω × cm²) closely match Kondrashina's results at 125 mM, suggesting that targeting TEER thresholds rather than specific concentrations might yield more consistent results for 'leaky' gut models. Consistent with these observations, Peng et al. (2007) also found that prolonged exposure (96 h) to 8 mM NaB significantly reduced TEER and increased permeability to inulin-FITC. Similarly, *ex vivo* studies by Mariadason et al. (1997) demonstrated increased transepithelial conductance and enhanced [51Cr]-EDTA flux in rat distal colon tissues exposed to 10 mM butyrate for 4 h ($P < 0.05$) (Mariadason et al., 1997).

To delineate whether the barrier disruption imposed by NaB was compound-specific or a consequence of hyperosmotic stress, the NaB effects were compared to osmotically matched Man. While all tested Man concentrations (100-250 mM) transiently reduced TEER within 6 h ($P < 0.05$), complete recovery was observed by 24 h ($P > 0.05$). Notably, when both NaB and Man were tested under strictly controlled, isosmotic conditions (348.67 ± 1.0 mOsm/kg), neither compound reduced TEER ($P > 0.05$). These results together with HSP70 mRNA increases, clearly indicate that osmotic stress plays a role in cell response to >75 mM NaB. Our findings are also consistent with those of Adesina et al. (2023, 2021), who reported elevated HSP-70 protein levels and mRNA expression in Caco-2 cells treated with 10–20 mM NaB for 24 h ($P < 0.05$), suggesting a stress response mechanism induced

by butyrate.(Adesina et al., 2023, 2021). However, stress alone does not explain the sustained barrier disruption after NaB removal. The lack of recovery suggests that NaB induces persistent permeability changes, making it useful for modeling a leaky gut *in vitro*. However, this limits its relevance for simulating normal gut maturation and may instead support its use in this life stage to model pathological conditions like necrotizing enterocolitis.

Our study demonstrates that >75 mM NaB treatment impacts energy metabolism in Caco-2 cells, as evidenced by significantly reduced ATP levels but not cellular reductase activity (MTS assay). This is in agreement with Kondrashina et al. (2021) who observed no significant changes in cellular reductase activity in Caco-2 cells treated for 4 h with NaB (50–250 mM) in DMEM (4500 mg/L glucose). Conversely, Peng et al. (2007) found that 8 mM NaB significantly reduced reductase activity, accompanied by increased cell detachment, indicating cytotoxicity rather than purely metabolic inhibition (Peng et al., 2007). This may be explained by a prolonged exposure of 72 h. Caco-2 cells, like other cancerous cells, predominantly rely on glycolysis rather than oxidative phosphorylation for energy, a phenomenon known as the Warburg effect (Vander Heiden et al., 2009). Our results confirm this metabolic dependency, as glucose deprivation significantly reduced both cellular reductase activity and ATP levels ($P < 0.05$). Interestingly, Caco-2 cells did not use NaB as an alternate oxidative energy substrate. Previous studies highlight a dual metabolic role for butyrate, dependent on concentration and metabolic context. Donohoe et al. (2012) observed that 0.5 mM butyrate promoted cell proliferation under low-glucose conditions (0.5 mM glucose) through β-oxidation in HCT116 colon cancer cells (Etomoxir + BrdU incorporation; $P < 0.05$). Conversely, treatment with higher butyrate concentrations (0.5 mM glucose and 5 mM butyrate) or higher-glucose

levels (25 mM glucose and 0.5-5 mM butyrate) inhibited cell proliferation similarly to the HDAC inhibitor Trichostatin A (Donohoe et al., 2012). Supporting these observations, our data indicate active internalization of NaB by Caco-2 cells, as evidenced by the significantly lower total recovery of NaB from the apical and basolateral compartments after 24-hour incubation. In contrast, HPLC quantification showed that Man was detected in the basolateral compartment, but its total recovery matched the initial apical concentration, indicating it was transported paracellularly without cellular uptake. Consistently, we observed increased mRNA expression of butyrate transporters (MCT-1, SMCT-1; $P < 0.05$) without concurrent changes in the β-oxidation enzyme SCAD ($P > 0.05$), further suggesting that NaB uptake is not directed toward energy metabolism via β-oxidation but may instead exert effects as an epigenetic regulator, potentially through HDAC inhibition.

In our study, treatment with 75 and 125 mM NaB significantly increased the activity of the apoptotic marker Caspase-3 in Caco-2 cells. While osmotic controls using 150 and 250 mM Man also showed elevated Caspase-3 activity ($P < 0.05$), the increase observed with 250 mM Man was less pronounced than that seen with 125 mM NaB ($P < 0.05$). This suggests that the apoptotic effect is not solely attributable to hyperosmotic stress, but rather reflects a NaB-specific response. These findings are consistent with previous studies demonstrating the pro-apoptotic effects of butyrate in Caco-2 cells (Avivi-Green et al., 2002; Chirakkal et al., 2006; Peng et al., 2007; Ruemmele, 2003). Ruemmele et al. (2003) reported a dose-dependent increase in apoptosis (Annexin V/propidium iodide, $P < 0.05$) in Caco-2 cells treated with 5–100 mM butyrate for 48 h, along with activation of caspase-3 and -9 (Ruemmele, 2003). Similarly, Avivi-Green et al. (2002) observed that 5–10 mM butyrate significantly increased apoptosis (cytoplasmic nucleosome concentration, $P < 0.05$)

and upregulated caspase-3 activity (2131 ± 640% above control, $P < 0.05$) and expression (Western blot, $P < 0.05$) (Avivi-Green et al., 2002). Peng et al. (2007) demonstrated that 8 mM NaB induced apoptosis markers, including DNA fragmentation (electrophoresis) and PARP cleavage (immunoblotting) (Peng et al., 2007). Chirakkal et al. also demonstrated that butyrate (≥5 mM, 24 h treatment) induces apoptosis in HCT116 cells (nuclear condensation and PARP cleavage; $P < 0.05$) without significant cellular damage (clonogenic assay, $P > 0.05$) (Chirakkal et al., 2006). This apoptotic effect is mediated by increased binding of the transcription factor Sp3 to Sp1/Sp3 sites, causing upregulation of the transcription of apoptosis-related genes (Chirakkal et al., 2006). Additionally, Donohoe et al. (2012) demonstrated in HCT116 cells that butyrate (3-day exposure to 0.5–5 mM) increased apoptosis (Annexin staining, $P < 0.05$) and histone H3 acetylation (Western blot, $P < 0.05$). Significant increases in p21 mRNA expression were observed in monolayers treated with >75 mM NaB. Previous studies have demonstrated that p21, a key regulator of cell proliferation and apoptosis (Macleod et al., 1995), is upregulated by butyrate (mRNA expression, 5-20 mM; $P < 0.05$) through histone hyperacetylation in HT29 cells (Archer et al., 1998; Siavoshian, 2000). Collectively, these findings reinforce our observation that NaB induces apoptosis in intestinal epithelial cells, likely through mechanisms involving histone acetylation and transcriptional modulation of apoptotic pathways.

Transcript levels of TNF were significantly increased (3000-fold) in monolayers treated with >75 mM NaB. Such a remarkable increase warrants an assessment of a panel of cytokines in the apical and basolateral chambers of Caco-2 monolayers treated with NaB and questions its use to create a non-inflamed barrier. Previously,

Kondrashina et al. (2021) reported a 12-fold increase in TNF secretion in the apical chamber (up to 12-fold at 150 mM NaB, $P < 0.05$).

In our study, Caco-2 monolayers were exposed to NaB under hyperosmotic conditions, with a resulting average osmolality significantly exceeding physiological levels. This mimics pathological scenarios where persistent hyperosmolarity is linked to intestinal barrier dysfunction, such as Crohn's disease (Schilli et al., 1982). It was interesting to observe that 10 μM dexamethasone, a corticosteroid frequently used in managing IBD, assisted the recovery of NaB-treated monolayers (Liu et al., 2009; Schreiber et al., 1998). In the 75 mM NaB-treated monolayers, the treatment with dexamethasone significantly increased TEER (T0 dexamethasone *vs*. T24 dexamethasone, $P < 0.05$) and restored the inflammation/stress markers to control condition (HSP79, p21, TNF, $P > 0.05$). This suggests that 75 mM NaB-treated Caco-2 monolayers could offer a physiologically relevant *in vitro* model of IBD or necrotizing enterocolitis. Future work should include comparisons with IL-1β and TNF or LPS, commonly used to replicate IBD *in vitro* using Caco-2 cells (Mobbs et al., 2024; P. Xu et al., 2019), evaluating tight junction proteins and permeability, as well as inflammation and oxidative stress markers (Macedo et al., 2023).

Interestingly, treatment of Caco-2 monolayers with 100- 250 mM Man (osmolality) resulted in a dose-dependent and temporary decrease in TEER ($P < 0.05$), that allowed full recovery after removal (DMEM D1145 *vs*. Man = $P > 0.05$). Similarly, Inokuchi et al. (2009) reported that hyperosmotic media containing 100 mM Man caused a decline in TEER (90 minutes exposure) with full recovery at lower concentrations (100 mM) (Inokuchi et al., 2009). Notably, 100 and 150 mM Man increased the activity of the apoptotic marker Caspase-3. While no direct studies report mannitol-induced apoptosis in Caco-2 cells, similar effects have been

observed in endothelial cells, where hyperosmolar mannitol induced apoptosis (Malek et al., 1998). Finally, 250 mM Man significantly reduced the mRNA expression of AQP-3, a marker of osmotic stress (Grauso et al., 2019; Yde et al., 2021) ($P < 0.05$). This is consistent with Grauso et al. (2019), who found a similar reduction in AQP-3 expression under hyperosmotic conditions (680 mOsm/L Man; $P < 0.05$) (Grauso et al., 2019). These results collectively support the interpretation that while Man-induced osmotic stress elicits specific responses such as increased Caspase-3 activity and reduced AQP-3 expression, the broader pro-inflammatory and stress marker expression profile observed with NaB is compound-specific and likely mediated by epigenetic and transcriptional regulatory pathways.

The present study demonstrates that NaB increases Caco-2 monolayers permeability, induces apoptosis, and triggers cellular stress and inflammatory responses. Notably, barrier disruption occurred only under hyperosmotic conditions, and no recovery was observed following NaB removal. These features, along with the reversal of barrier dysfunction by dexamethasone, closely mimic aspects of gut diseased states like inflammatory bowel disease or, for the infant, necrotizing enterocolitis. Importantly, because hyperosmotic stress leads to epithelial cell shrinkage and water loss, this model may also serve as a valuable *in vitro* platform for evaluating products designed to support sustained cellular hydration. Future studies should include a co-culture model with immune cells to better elucidate the effect of high concentration of NaB on inflammation. Overall, NaB offers an *in vitro* model which is damaged but stable over 24 h, well-suited for *in vitro* investigations of both barrier repair and hydration support strategies.

2.5.References

Adesina, P. A., Isayama, K., Sitolo, G. C., Yamamoto, Y., & Suzuki, T. (2021). Propionate and Dietary Fermentable Fibers Upregulate Intestinal Heat Shock protein70 in Intestinal Caco-2 Cells and Mouse Colon. Journal of Agricultural and Food Chemistry, 69(30), 8460–8470. https://doi.org/10.1021/acs.jafc.1c03036

Adesina, P. A., Saeki, I., Yamamoto, Y., & Suzuki, T. (2023). N-butyrate increases heat shock protein 70 through heat shock factor 1 and AMP-activated protein kinase pathways in human intestinal Caco-2 cells. Archives of Biochemistry and Biophysics, 736, 109525. https://doi.org/10.1016/j.abb.2023.109525

Archer, S. Y., Meng, S., Shei, A., & Hodin, R. A. (1998). P21 WAF1 is required for butyrate-mediated growth inhibition of human colon cancer cells. Proceedings of the National Academy of Sciences, 95(12), 6791–6796. https://doi.org/10.1073/pnas.95.12.6791

Avivi-Green, C., Polak-Charcon, S., Madar, Z., & Schwartz, B. (2002). Different Molecular Events Account for Butyrate-Induced Apoptosis in Two Human Colon Cancer Cell Lines. The Journal of Nutrition, 132(7), 1812–1818. https://doi.org/10.1093/jn/132.7.1812

Brown, A. J., Goldsworthy, S. M., Barnes, A. A., Eilert, M. M., Tcheang, L., Daniels, D., Muir, A. I., Wigglesworth, M. J., Kinghorn, I., Fraser, N. J., Pike, N. B., Strum, J. C., Steplewski, K. M., Murdock, P. R., Holder, J. C., Marshall, F. H., Szekeres, P. G., Wilson, S., Ignar, D. M., … Dowell, S. J. (2003). The Orphan G Protein-coupled Receptors GPR41 and GPR43 Are Activated by Propionate and Other Short Chain Carboxylic Acids. Journal of

Biological Chemistry, 278(13), 11312–11319. https://doi.org/10.1074/jbc.M211609200

Canani, R. B. (2011). Potential beneficial effects of butyrate in intestinal and extraintestinal diseases. World Journal of Gastroenterology, 17(12), 1519. https://doi.org/10.3748/wjg.v17.i12.1519

Catassi, C., Bonucci, A., Coppa, G. V., Carlucci, A., & Giorgi, P. L. (1995). Intestinal Permeability. Changes during the First Month: Effect of Natural versus Artificial Feeding. Journal of Pediatric Gastroenterology and Nutrition, 21(4), 383–386. https://doi.org/10.1097/00005176-199511000-00003

Chirakkal, H., Leech, S. H., Brookes, K. E., Prais, A. L., Waby, J. S., & Corfe, B. M. (2006). Upregulation of BAK by butyrate in the colon is associated with increased Sp3 binding. Oncogene, 25(54), 7192–7200. https://doi.org/10.1038/sj.onc.1209702

Dalile, B., Van Oudenhove, L., Vervliet, B., & Verbeke, K. (2019). The role of short-chain fatty acids in microbiota–gut–brain communication. Nature Reviews Gastroenterology & Hepatology, 16(8), Article 8. https://doi.org/10.1038/s41575-019-0157-3

Ding, D., Liu, Z., Zhao, L., Geng, H., Liang, Z., & Yu, D. (2019). Role of PI3K/Akt pathway in Benzidine-induced proliferation in SV-40 immortalized human uroepithelial cell. Translational Cancer Research, 8(4), 1301–1310. https://doi.org/10.21037/tcr.2019.07.14

Donohoe, D. R., Collins, L. B., Wali, A., Bigler, R., Sun, W., & Bultman, S. J. (2012). The Warburg Effect Dictates the Mechanism of Butyrate-Mediated

Histone Acetylation and Cell Proliferation. Molecular Cell, 48(4), 612–626. https://doi.org/10.1016/j.molcel.2012.08.033

Fogh, J., Wright, W. C., & Loveless, J. D. (1977). Absence of HeLa cell contamination in 169 cell lines derived from human tumors. Journal of the National Cancer Institute, 58(2), 209–214. https://doi.org/10.1093/jnci/58.2.209

Grauso, M., Lan, A., Andriamihaja, M., Bouillaud, F., & Blachier, F. (2019). Hyperosmolar environment and intestinal epithelial cells: Impact on mitochondrial oxygen consumption, proliferation, and barrier function in vitro. Scientific Reports, 9(1), Article 1. https://doi.org/10.1038/s41598-019-47851-9

Groschwitz, K. R., & Hogan, S. P. (2009). Intestinal barrier function: Molecular regulation and disease pathogenesis. Journal of Allergy and Clinical Immunology, 124(1), 3–20. https://doi.org/10.1016/j.jaci.2009.05.038

Hamer, H. M., Jonkers, D., Venema, K., Vanhoutvin, S., Troost, F. J., & Brummer, R. -J. (2008). Review article: The role of butyrate on colonic function. Alimentary Pharmacology & Therapeutics, 27(2), 104–119. https://doi.org/10.1111/j.1365-2036.2007.03562.x

Hevia, A., Ruas-Madiedo, P., Faria, M. A., Petit, V., Alves, B., Alvito, P., Arranz, E., Bastiaan-Net, S., Corredig, M., Dijk, W., Dupont, D., Giblin, L., Graf, B. A., Kondrashina, A., Ramos, H., Ruiz, L., Santos-Hernández, M., Soriano-Romaní, L., Tomás-Cobos, L., … Miralles, B. (2023). A Shared Perspective on in Vitro and in Vivo Models to Assay Intestinal Transepithelial Transport of Food Compounds. Journal of Agricultural and Food Chemistry, 71(49), 19265–19276. https://doi.org/10.1021/acs.jafc.3c05479

Hollander, D. (1999). Intestinal permeability, leaky gut, and intestinal disorders. Current Gastroenterology Reports, 1(5), 410–416. https://doi.org/10.1007/s11894-999-0023-5

Hubert, A., Cauliez, B., Chedeville, A., Husson, A., & Lavoinne, A. (2004). Osmotic stress, a proinflammatory signal in Caco-2 cells. Biochimie, 86(8), 533–541. https://doi.org/10.1016/j.biochi.2004.07.009

Iglesias, D. E., Cremonini, E., Fraga, C. G., & Oteiza, P. I. (2020). Ellagic acid protects Caco-2 cell monolayers against inflammation-induced permeabilization. Free Radical Biology and Medicine, 152, 776–786. https://doi.org/10.1016/j.freeradbiomed.2020.01.022

Inokuchi, H., Takei, T., Aikawa, K., & Shimizu, M. (2009). The Effect of Hyperosmosis on Paracellular Permeability in Caco-2 Cell Monolayers. Bioscience, Biotechnology, and Biochemistry, 73(2), 328–334. https://doi.org/10.1271/bbb.80538

Jung, H. C., Eckmann, L., Yang, S. K., Panja, A., Fierer, J., Morzycka-Wroblewska, E., & Kagnoff, M. F. (1995). A distinct array of proinflammatory cytokines is expressed in human colon epithelial cells in response to bacterial invasion. Journal of Clinical Investigation, 95(1), 55–65. https://doi.org/10.1172/JCI117676

Kondrashina, A., Brodkorb, A., & Giblin, L. (2021). Sodium butyrate converts Caco-2 monolayers into a leaky but healthy intestinal barrier resembling that of a newborn infant. Food & Function, 12(11), 5066–5076. https://doi.org/10.1039/D1FO00519G

Kosek, M. N., Lee, G. O., Guerrant, R. L., Haque, R., Kang, G., Ahmed, T., Bessong, P., Ali, A., Mduma, E., Peñataro Yori, P., Faubion, W. A., Lima, A.

A. M., Paredes Olortegui, M., Mason, C., Babji, S., Singh, R., Qureshi, S., Kosek, P. S., Samie, A., … Network, the M.-E. (2017). Age and Sex Normalization of Intestinal Permeability Measures for the Improved Assessment of Enteropathy in Infancy and Early Childhood: Results From the MAL-ED Study. Journal of Pediatric Gastroenterology and Nutrition, 65(1), 31–39. https://doi.org/10.1097/MPG.0000000000001610

Lea, T. (2015). Caco-2 Cell Line. In K. Verhoeckx, P. Cotter, I. López-Expósito, C. Kleiveland, T. Lea, A. Mackie, T. Requena, D. Swiatecka, & H. Wichers (Eds.), The Impact of Food Bioactives on Health: In vitro and ex vivo models (pp. 103–111). Springer International Publishing. https://doi.org/10.1007/978-3-319-16104-4_10

Liu, H., Wang, J., He, T., Becker, S., Zhang, G., Li, D., & Ma, X. (2018). Butyrate: A Double-Edged Sword for Health? Advances in Nutrition, 9(1), 21–29. https://doi.org/10.1093/advances/nmx009

Liu, L., Yuan, S., Long, Y., Guo, Z., Sun, Y., Li, Y., Niu, Y., Li, C., & Mei, Q. (2009). Immunomodulation of Rheum tanguticum polysaccharide (RTP) on the immunosuppressive effects of dexamethasone (DEX) on the treatment of colitis in rats induced by 2,4,6-trinitrobenzene sulfonic acid. International Immunopharmacology, 9(13–14), 1568–1577. https://doi.org/10.1016/j.intimp.2009.09.013

Lu, L., Lu, J., Yu, Y., & Claud, E. (2021). Necrotizing enterocolitis intestinal barrier function protection by antenatal dexamethasone and surfactant-D in a rat model. Pediatric Research, 90(4), 768–775. https://doi.org/10.1038/s41390-020-01334-0

Macedo, M. H., Dias Neto, M., Pastrana, L., Gonçalves, C., & Xavier, M. (2023). Recent Advances in Cell-Based In Vitro Models to Recreate Human Intestinal Inflammation. Advanced Science, 10(31), 2301391. https://doi.org/10.1002/advs.202301391

Macleod, K. F., Sherry, N., Hannon, G., Beach, D., Tokino, T., Kinzler, K., Vogelstein, B., & Jacks, T. (1995). P53-dependent and independent expression of p21 during cell growth, differentiation, and DNA damage. Genes & Development, 9(8), 935–944. https://doi.org/10.1101/gad.9.8.935

Malek, A. M., Goss, G. G., Jiang, L., Izumo, S., & Alper, S. L. (1998). Mannitol at Clinical Concentrations Activates Multiple Signaling Pathways and Induces Apoptosis in Endothelial Cells. Stroke, 29(12), 2631–2640. https://doi.org/10.1161/01.STR.29.12.2631

Mariadason, J. M., Barkla, D. H., & Gibson, P. R. (1997). Effect of short-chain fatty acids on paracellular permeability in Caco-2 intestinal epithelium model. American Journal of Physiology-Gastrointestinal and Liver Physiology, 272(4), G705–G712. https://doi.org/10.1152/ajpgi.1997.272.4.G705

Ménard, S., Cerf-Bensussan, N., & Heyman, M. (2010). Multiple facets of intestinal permeability and epithelial handling of dietary antigens. Mucosal Immunology, 3(3), 247–259. https://doi.org/10.1038/mi.2010.5

Mobbs, C. L., Darling, N. J., & Przyborski, S. (2024). An in vitro model to study immune activation, epithelial disruption and stromal remodelling in inflammatory bowel disease and fistulising Crohn's disease. Frontiers in Immunology, 15, 1357690. https://doi.org/10.3389/fimmu.2024.1357690

Otani, T., & Furuse, M. (2020). Tight Junction Structure and Function Revisited. Trends in Cell Biology, 30(10), 805–817. https://doi.org/10.1016/j.tcb.2020.08.004

Peng, L., He, Z., Chen, W., Holzman, I. R., & Lin, J. (2007). Effects of Butyrate on Intestinal Barrier Function in a Caco-2 Cell Monolayer Model of Intestinal Barrier. Pediatric Research, 61(1), 37–41. https://doi.org/10.1203/01.pdr.0000250014.92242.f3

Porter, A. G., & Jänicke, R. U. (1999). Emerging roles of caspase-3 in apoptosis. Cell Death & Differentiation, 6(2), 99–104. https://doi.org/10.1038/sj.cdd.4400476

Renis, M., Calandra, L., Scifo, C., Tomasello, B., Cardile, V., Vanella, L., Bei, R., Fauci, L. L., & Galvano, F. (2008). Response of cell cycle/stress-related protein expression and DNA damage upon treatment of Caco-2 cells with anthocyanins. British Journal of Nutrition, 100(1), 27–35. https://doi.org/10.1017/S0007114507876239

Ruemmele, F. M. (2003). Butyrate induced Caco-2 cell apoptosis is mediated via the mitochondrial pathway. Gut, 52(1), 94–100. https://doi.org/10.1136/gut.52.1.94

Schilli, R., Breuer, R. I., Klein, F., Dunn, K., Gnaedinger, A., Bernstein, J., Paige, M., & Kaufman, M. (1982). Comparison of the composition of faecal fluid in Crohn's disease and ulcerative colitis. Gut, 23(4), 326–332. https://doi.org/10.1136/gut.23.4.326

Schreiber, S., Nikolaus, S., & Hampe, J. (1998). Activation of nuclear factor kappa B in inflammatory bowel disease. Gut, 42(4), 477–484. https://doi.org/10.1136/gut.42.4.477

Sheng, Y. H., & Hasnain, S. Z. (2022). Mucus and Mucins: The Underappreciated Host Defence System. Frontiers in Cellular and Infection Microbiology, 12, 856962. https://doi.org/10.3389/fcimb.2022.856962

Siavoshian, S. (2000). Butyrate and trichostatin A effects on the proliferation/differentiation of human intestinal epithelial cells: Induction of cyclin D3 and p21 expression. Gut, 46(4), 507–514. https://doi.org/10.1136/gut.46.4.507

Singh, V., Lee, G., Son, H., Koh, H., Kim, E. S., Unno, T., & Shin, J.-H. (2023). Butyrate producers, "The Sentinel of Gut": Their intestinal significance with and beyond butyrate, and prospective use as microbial therapeutics. Frontiers in Microbiology, 13, 1103836. https://doi.org/10.3389/fmicb.2022.1103836

Stilling, R. M., Van De Wouw, M., Clarke, G., Stanton, C., Dinan, T. G., & Cryan, J. F. (2016). The neuropharmacology of butyrate: The bread and butter of the microbiota-gut-brain axis? Neurochemistry International, 99, 110–132. https://doi.org/10.1016/j.neuint.2016.06.011

Urayama, S., Musch, M. W., Retsky, J., Madonna, M. B., Straus, D., & Chang, E. B. (1998). Dexamethasone protection of rat intestinal epithelial cells against oxidant injury is mediated by induction of heat shock protein 72. Journal of Clinical Investigation, 102(10), 1860–1865. https://doi.org/10.1172/JCI2235

Vander Heiden, M. G., Cantley, L. C., & Thompson, C. B. (2009). Understanding the Warburg Effect: The Metabolic Requirements of Cell Proliferation. Science, 324(5930), 1029–1033. https://doi.org/10.1126/science.1160809

Weaver, L. T., Laker, M. F., & Nelson, R. (1984). Intestinal permeability in the newborn. Archives of Disease in Childhood, 59(3), 236–241. https://doi.org/10.1136/adc.59.3.236

Weström, B., Arévalo Sureda, E., Pierzynowska, K., Pierzynowski, S. G., & Pérez-Cano, F.-J. (2020). The Immature Gut Barrier and Its Importance in Establishing Immunity in Newborn Mammals. Frontiers in Immunology, 11. https://www.frontiersin.org/articles/10.3389/fimmu.2020.01153

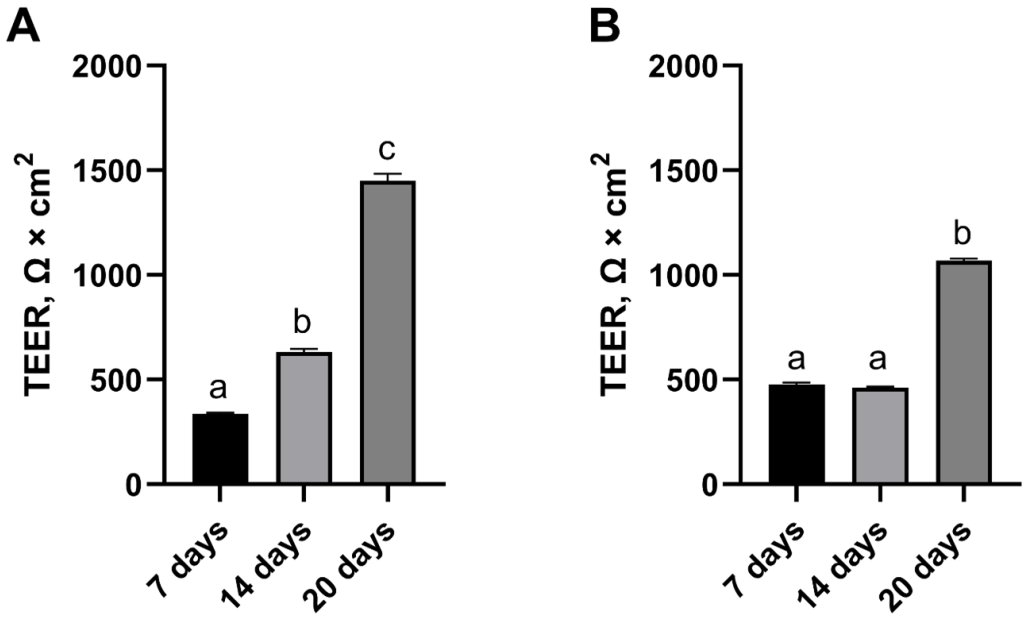
Xu, P., Elamin, E., Elizalde, M., Bours, P. P. H. A., Pierik, M. J., Masclee, A. A. M., & Jonkers, D. M. A. E. (2019). Modulation of Intestinal Epithelial Permeability by Plasma from Patients with Crohn's Disease in a Three-dimensional Cell Culture Model. Scientific Reports, 9(1), 2030. https://doi.org/10.1038/s41598-018-38322-8

Yde, J., Keely, S. J., & Moeller, H. B. (2021). Expression, regulation and function of Aquaporin-3 in colonic epithelial cells. Biochimica et Biophysica Acta (BBA) - Biomembranes, 1863(7), 183619. https://doi.org/10.1016/j.bbamem.2021.183619

2.6.Supplementary Information

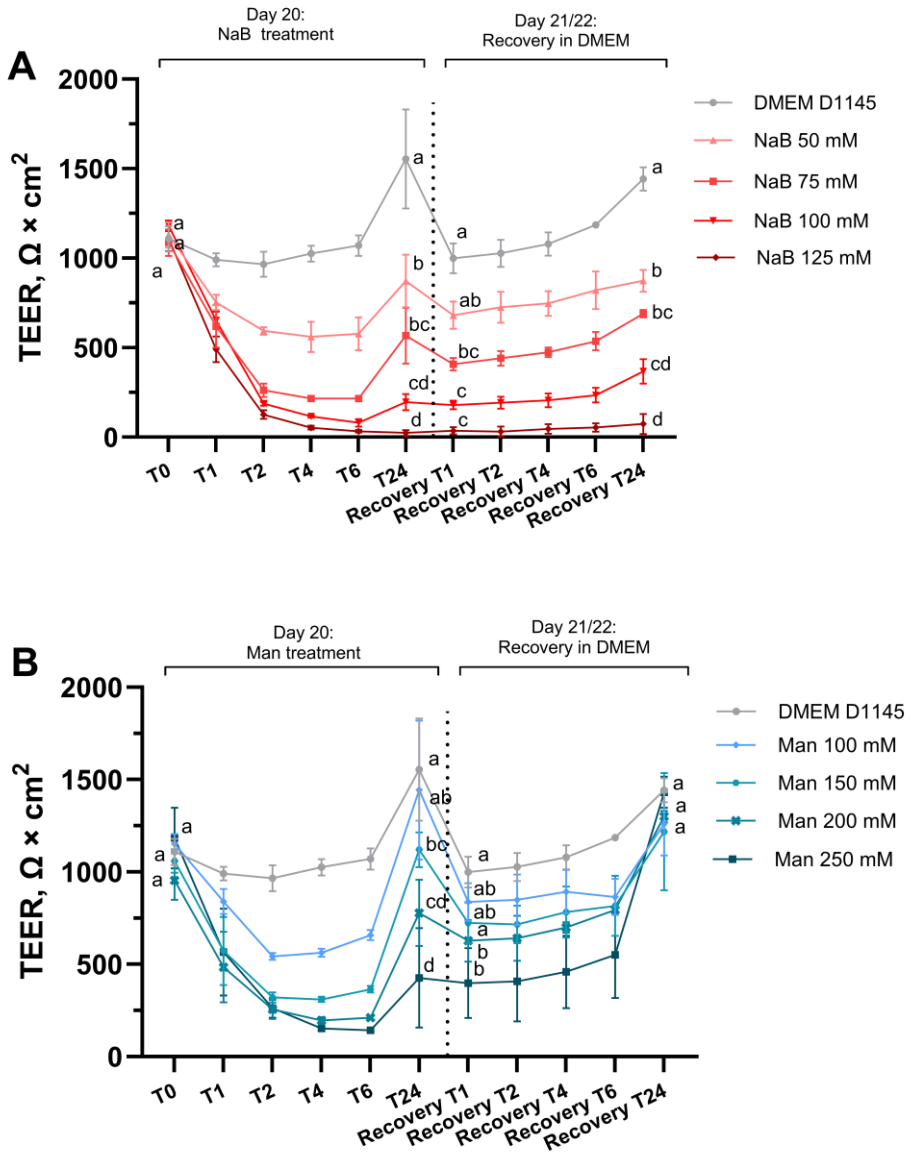
Supplementary Table 2.1 Gene name, protein name, GenBank accession number, primers and annealing temperature (Ta) for RT-PCR analysis.

Gene	Protein	GenBank	Foreward Primer	Reverse Primer	T_a (°C)
SLC5A8	Sodium-coupled monocarboxylate transporter 1 (SMCT1)	NM_145913	GGCGTCACTTATGGGAGCTTTG	GGCAAATCCAGCCATCAGACCA	60
SLC16A1	Monocarboxylate transporter 1 (MCT1)	NM_003051	TTGTTGGTGGCTGCTTGTCAGG	TCATGGTCAGAGCTGGATTCAAG	60
ACADS	Short-chain acyl-coenzyme A dehydrogenase (SCAD)	NM_000017	CACGCCTTTCACCAGTGGTGAC	GGCATTGGTGATCCAGGCTTTG	60
HSPA1A	70 kilodalton heat shock protein (Hsp70)	NM_005345	ACCTTCGACGTGTCCATCCTGA	TCCTCCACGAAGTGGTTCACCA	60
CDKN1A	p21 (p21^Cip1/Waf1)	NM_000389.5	GACACCACTGGAGGGTGACT	CAGGTCCACATGGTCTTCCT	60
AQP3	Aquaporin 3	NM_004925	CCGTGACCTTTGCCATGTGCTT	TTGTCGGCGAAGTGCCAGATTG	60
CXCL8	Interleukin 8/ CXC chemokine ligand 8 (IL-8)	NM_000584.2	GAGAGTGATTGAGAGTGGACCAC	CACAACCCTCTGCACCCAGTTT	60



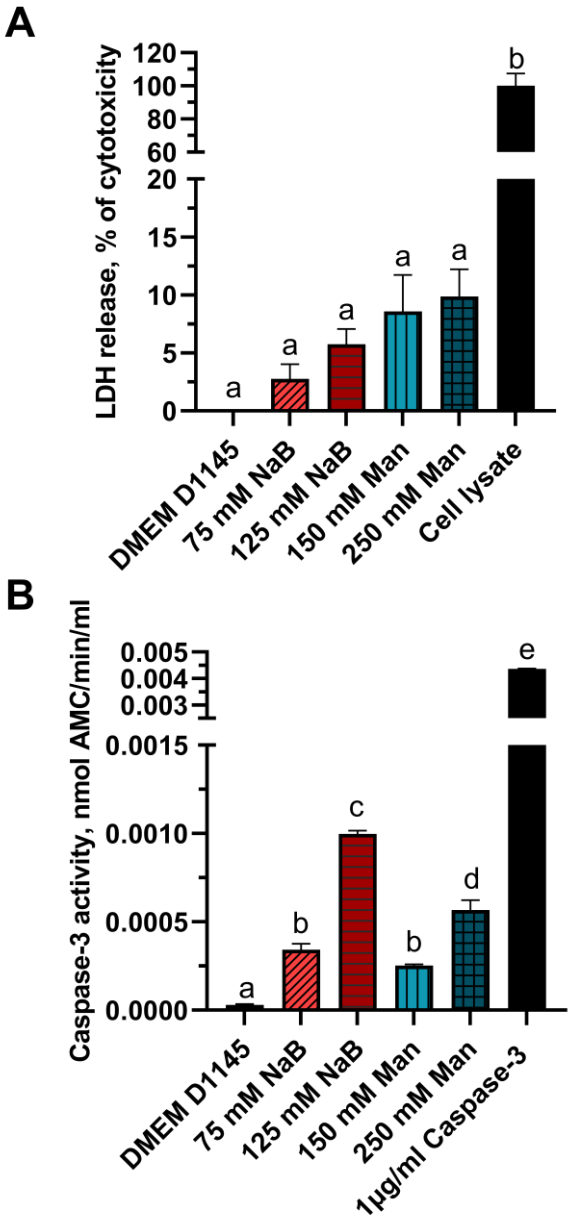
Supplementary Fig 2.1 Transepithelial Electrical Resistance (TEER) of Caco-2 and Caco-2/HT29-MTX (90:10) monolayers from day 7 to day 20.

(A) Caco-2 cells or (B) a co-culture of Caco-2/HT29-MTX at a ratio of 90:10 were seeded at a final concentration of 6×10^4 cells/well in a 12-well Transwell plate. The media was changed every two days, and 16 h before each measurement. TEER values were recorded on days 7, 14 and 20 using a Millicell-ERS Voltohmmeter. The mean TEER value at day 20 for (A) Caco-2 was 1451.40 ± 33.03 Ω × cm² and for (B) Caco-2/HT29-MTX was 1069.04 ± 10.41 Ω × cm². The bar graph represents TEER values, where each bar shows the average of all biological triplicates and technical duplicates for each experimental condition ± SEM. Statistical differences between treatments within a time point were assessed using two-way ANOVA with Tukey's multiple comparison test and are indicated by different letters ($P < 0.05$).



Supplementary Fig 2.2 : Transepithelial electrical resistance (TEER) values of Caco-2/HT29-MTX 90:10 monolayers treated with sodium butyrate (NaB) or mannitol (Man).

Caco-2/HT29-MTX cells were seeded at 6×10^4 cells/well at a 90:10 ratio and cultured for 20 days. The mean TEER value on day 20 was 1069.04 ± 10.41 Ω × cm².(A) NaB-treated monolayers in DMEM 1145 or (B) Mannitol-treated monolayers in DMEM 1145. TEER values were recorded before the treatment (T0) and at 1, 2, 4, 6 and 24 h (T1/2/4/6/24). NaB or Man was then removed and TEER values were recorded at 1, 2, 4, 6, and 24 h (Recovery). Statistical significance between different concentrations, at the same time point, was determined by two-way ANOVA with Tukey's multiple comparison. Control monolayers were treated with DMEM D1145 only. Data represents the mean±SEM from biological triplicates and technical duplicates. Statistical significance between treatments at each time point was determined using two-way ANOVA with Tukey's multiple comparison test. Different letters indicate statistically significant differences ($P < 0.05$).



Supplementary Fig 2.3 % of Cytotoxiciy as LDH release in the apical compartment of 20-day old Caco-2 monolayers.

(A) % of cytotoxicity after 24 h treatment with 75/125 mM NaB or 150/250 mM Man. (B) % of cytotoxicity after 24 h treatment with 75/125 mM NaB or 150/250 mM Man and further 24 h with 10 µM dexamethasone (Dexa).

LDH release in the apical compartment was given by the amount of formazan produced in the enzymatic reaction with the assay mixture. DMEM D1145 = monolayers in DMEM only, (set as 0% cytotoxicity, $Abs_{490\text{-}680}$ = 0.0042 ± 0.00033). Cell Lysate = monolayers lysed with 1% Triton-X (set as 100% cytotoxicity, $Abs_{490\text{-}680}$ = 0.64 ± 0.948). Results are presented as the average of a biological triplicate and a technical duplicate ± SEM. Statistical difference in the treatments was assessed by one-way ANOVA with Tukey's multiple comparison and is indicated with different letters ($P<0.05$).

3. Chapter 3

Using sodium glycodeoxycholate to develop a temporary infant-like gut barrier model, *in vitro*

Part of this work was carried out during a short-term scientific mission at the Institute of Food Science Research (CIAL, CSIC–UAM, Madrid, Spain), under the supervision of Dr. Beatriz Miralles.

A version of this chapter is published in Frontiers in Nutrition:

Bietto, F., Arranz, E., Miralles, B., Gómez-Marín, C., Rath, E., Lucey, A.J., Giblin, L., 2025. Using sodium glycodeoxycholate to develop a temporary infant-like gut barrier model, in vitro. Front. Nutr. 12, 1577369.

https://doi.org/10.3389/fnut.2025.1577369

Published version of this chapter is presented in **Appendix A**.

Abstract

In newborns, the intestinal barrier is permeable but not inflamed. This study aimed to develop an *in vitro* model of the infant gut barrier treating Caco-2/HT29-MTX with 0.5, 0.8, and 1 mM sodium glycodeoxycholate (GDC). Our research demonstrates that GDC decreases Caco-2/HT29-MTX Trans-Epithelial Electrical Resistance (TEER) and increases paracellular permeability, without inflammation or cytotoxicity. Notably, the treatment with 0.8 mM GDC increased lactulose transport rate by 1.63-fold. The treatment also reduced the key tight junction protein, occludin, at the cell membrane, and increased acidic mucins and extracellular alkaline phosphatase activity. Additionally, GDC decreased cAMP, suggesting its mechanism of action was via activation of a G-protein coupled receptor. Of particular importance to nutrition studies, the GDC effect was reversible with TEER recovery within 4 h. Applying digested infant formula to 0.8 mM GDC-treated Caco-2/HT29-MTX monolayers resulted in a higher concentration of amino acids in the basolateral compartment compared to control monolayers.

Keywords: *in vitro* infant gut barrier, sodium glycodeoxycholate, Caco-2/HT29-MTX, tight junctions, intestinal permeability, TEER, infant formula (IF), INFOGEST

3.1. Introduction

The infant gut barrier has a higher paracellular permeability during early development (Catassi et al., 1995; Kosek et al., 2017; Weaver et al., 1984), facilitating the absorption of bioactive molecules from human milk (Weström et al., 2020). Human milk, in turn, matures the gut barrier and gradually reduces its permeability overtime (Catassi et al., 1995). Infant formulae are formulated to provide nutrients similarly to breast milk. However, the ability of breast milk to support the transition from an infant gut barrier to an adult barrier, occurs due to its unique composition of bioactive components (*i.e.* peptides (Su et al., 2017), lipids (Jensen et al., 1978; Michalski et al., 2005) oligosaccharides (Bode, 2012), probiotics and prebiotics).

There are ethical and logistical challenges of conducting clinical trials in early infancy to understand the gut barrier. As an alternative, current models for studying the infant gut barrier include cell lines, enteroids and animal models. Adult-derived colorectal cell lines (Caco-2, HT29-MTX) are widely used (Hilgendorf et al., 2000; Lea, 2015) but differ significantly from neonatal physiology due to differences in paracellular pore size (Sun et al., 2008). The neonatal piglet-derived IPEC-J2 cell line is closer to infant gut characteristics yet limited by species-specific differences (Vergauwen, 2015). Human enteroids closely mimic infant intestinal physiology but face challenges related to culture complexity and scalability (Noel et al., 2021). Animal models (neonatal rodents, piglets) offer valuable physiological insights but ethical concerns and interspecies variations limit direct human applicability (Sangild et al., 2014). These limitations underscore the necessity for developing specialized, reproducible, and infant-specific *in vitro* models of the gut barrier. Furthermore for nutrition research, any infant-like model should be able to transition from infant to

adult within a suitable timeframe, and should be able to generate data on nutrient absorption for both life stages.

The infant intestinal paracellular permeability is measured *in vivo* by quantifying lactulose (radius = 9.5 Å) and mannitol (radius = 6.7 Å) in urine after oral administration (Catassi et al., 1995; Kosek et al., 2017; Weaver et al., 1984). This test represents the only direct method in humans to evaluate intestinal permeability. In healthy adults, the jejunum restricts the passage of molecules > 8 Å (Fine et al., 1995), making lactulose transport an indicator of gut barrier impairment (Johnston et al., 2000). In newborns, lactulose permeability is 55.56% higher than in older infants (3 vs. 15 months = 0.28% vs. 0.18%) (Kosek et al., 2017). Moreover, the lactulose-to-mannitol ratio inversely correlates with age (Johnston et al., 2000; Musa et al., 2019; Weaver et al., 1984), indicating that larger molecules, such as lactulose, can more readily cross the intestinal barrier during infancy compared to older children. Due to the limited research in children, much of our understanding of the infant gut barrier comes from animal models. Studies using mice, for example, show that newborns can absorb big molecules, such as FITC-dextran 70 kDa (4 fold increase in transport at 2 week-old vs. 12 week-old mice) and lactoferrin 80 kDa, (4-fold increase in transport at 2 week-old vs. 12 week-old mice) (Gleeson et al., 2021). Paracellular transport across the epithelial barrier is regulated by tight junction proteins, which form cell-to-cell complexes and depend on calcium for assembly (Otani and Furuse, 2020). Key proteins maintaining barrier integrity and limiting paracellular permeability include Occludin (OCLN), Zonula Occludens (ZO1), several Claudins (CLDN) and Junctional Adhesion Molecules (JAMs). Notably CLDN2 increases paracellular permeability (Otani and Furuse, 2020). In mice, mRNA expression of *Cldn3*, *Ocln*, *Tjp1* (ZO1), and *Jam1* in the small intestine is

lower in newborns (1 day and 2-week-old mice), while the expression of *Cldn2* is higher compared to adults (12-week-old mice) (Gleeson et al., 2021; Holmes et al., 2006).

Intestinal alkaline phosphates is a brush border enzyme expressed and secreted by enterocytes (Lallès, 2019), whose activity is essential for maintaining gut homeostasis and protecting against inflammation (Lallès, 2019) and aging (Kühn et al., 2020). Importantly, this enzyme upregulates tight junction proteins both *in vit*ro (Liu et al., 2016) and *in vivo* (Hamarneh et al., 2014). Interestingly, *in vivo* studies have shown that serum alkaline phosphatase levels are higher in young children (29 days to 1 year, 50^{th} percentile: males = 218.19, females = 210.62 U/L) compared to older children (17 to 18 years, 50^{th} percentile: males = 104.74, females = 75.50 U/L) (Lü et al., 2020), further supporting the enzyme's relevance during early life when the gut barrier is still developing.

Permeability is also influenced by the mucus layer, composed of high-molecular-weight glycoproteins secreted by goblet cells (Paone and Cani, 2020). Studies on mucus development are limited, especially in humans, but *in vivo* data show that at birth colonic mucus in humans, pigs and mice predominantly contains acidic mucins over neutral mucins (Deplancke and Gaskins, 2001). In human, Filipe et al. (1989) reported that acid mucins predominate in the human colon throughout fetal life. While this study does not quantify the acidic-to-neutral mucin ratio, it does suggest a predominance of acidic mucins in the neonatal period (Filipe et al., 1989). In pigs, infant mucus (2-week-old) is less viscous and more permeable compared to adults (7–10-month-old) (Macierzanka et al., 2014).

Differences in paracellular permeability, tight junctions, and mucus properties between infants and adults question the reliability of adult gut models for infant

research. Given the higher incidence of necrotizing enterocolitis in formula-fed versus breastfed infants (Altobelli et al., 2020; Lucas and Cole, 1990), developing an accurate infant gut model is crucial to understanding human milk's benefits to the young gut, and improving formulations of infant formula to mimic these benefits. The Caco-2 monolayer (Fogh et al., 1977) is a standard *in vitro* intestinal model, but it lacks a mucus layer and its tight junctions resemble those of the colon, with narrower pores (4.5 Å) (Rubas et al., 1996; Watson et al., 2001) compared to the small intestine (8-9 Å) (Fine et al., 1995). To address these limitations, the Caco-2/HT29-MTX co-culture was developed, combining enterocytes (Caco-2) and goblet cells (HT29-MTX) (Hilgendorf et al., 2000; Lesuffleur et al., 1990) in a polarized monolayer. The 90:10 seeding ratio simulates small intestine conditions, increasing paracellular permeability and providing a mucus layer (Araújo and Sarmento, 2013). Previous studies have examined methods for increasing the permeability of Caco-2 monolayers whilst preventing inflammation. Our laboratory demonstrated that treating 20-day-old Caco-2 monolayers with 125 mM sodium butyrate effectively increases paracellular permeability without causing inflammation or cytotoxicity (Kondrashina et al., 2021). However, the high concentration of sodium butyrate resulted in an osmolality of 0.79 Osmol/kg (Kondrashina et al., 2021), which is at the upper limit of Caco-2 tolerance (Grauso et al., 2019), possibly initiating stress responses.

For oral drug delivery studies, medium-chain fatty acids, bile salts, bacterial toxins, surfactants and chelating agents have been investigated for their ability to enhance barrier permeability (Brayden et al., 2020; Maher and Mrsny, 2016; Twarog et al., 2019). Among these molecules, sodium N-(8-[2-hydroxybenzoyl]amino) caprylate

(SNAC) (a C8 derivate) and sodium caprate (C10) have been widely tested in Caco-2 monolayers and clinical trials (Twarog et al., 2019).

In Caco-2 (20 to 28 days old monolayers), SNAC primarily modulates the transcellular pathway, enhancing membrane fluidity but not targeting specifically tight junctions (Twarog et al., 2020), which limits its relevance for modeling the paracellular permeability characteristic of the neonatal gut. On the other hand, C10 affects the paracellular permeability but requires calcium-free buffers, as it precipitates with calcium, an essential ion for tight junction maintenance and physiological relevance (Lindmark et al., 1998; Twarog et al., 2020; Watson et al., 2001). Moreover, C10 acts by increasing the number of paracellular pores rather than expanding pore diameter, making it less suitable for mimicking the permeability state of the infant gut barrier (Watson et al., 2001).

Bile salts such as cholate, taurocholate, chenodeoxycholate, usodexycholate and glycodeoxucholate have been used to enhance the permeability of hydrophilic markers and drugs *in vitro* (Brayden and Stuettgen, 2021; Fricker et al., 1996; Meaney and O'Driscoll, 2000; Mukaizawa et al., 2009), *ex-vivo* (Brayden and Stuettgen, 2021; Mahalingam et al., 2007) and *in vivo* (Fricker et al., 1996). Among these, glycodeoxycholic acid (GDC) stands out due to its favorable low toxicity and dose-dependent permeability enhancement. GDC is a secondary bile salt conjugated with glycine, synthesized through the synergistic action of the liver and gut microbiota (Chiang, 2009; Ridlon et al., 2006). In the human intestine, bile salts exist in conjugated (bound to amino acids, such as glycine or taurine) and unconjugated forms. Conjugated bile salts are more water-soluble and generally less toxic (Hofmann and Hagey, 2008), whereas unconjugated forms, such as sodium cholate, tend to be more potent but are more toxic (Meaney and O'Driscoll, 2000).

GDC has been found to effectively increases permeability *in vitro* in Caco-2 monolayers (Brayden and Stuettgen, 2021; Song et al., 2005), *ex-vivo* (Hoogstraate et al., 1996a) and *in vivo* (Hoogstraate et al., 1996b). Specifically, 2.12 mM GDC increased calcitonin permeability in Caco-2 monolayers by 10.66-fold and decreased TEER by 4.57-fold (Song et al., 2005), whilst 0.5 mM GDC increased [^{14}C]-mannitol apparent permeability (Papp) by 3-fold and transiently decreased TEER by 2.5-fold, without reducing cell viability (MTS, CellTox™ Green assay, Caspase 3/7) (Brayden and Stuettgen, 2021).

Although the precise mechanism by which GDC modulates epithelial permeability is unknown, bile salts bind to TGR5 and FXR membrane receptors (Schaap et al., 2014). TGR5 activation can modulate intracellular cAMP levels, which in turn regulate PKA activity (Kawamata et al., 2003). Deoxycholic acid, for example, signals through TGR5, leading to PKA inhibition and has been linked to EGFR activation, ERK1/2 signaling, and occludin redistribution in Caco-2 cells (Raimondi et al., 2008; Yasuda et al., 2007). Compared to permeability enhancers like sodium butyrate (which requires high, hyperosmolar concentrations) or sodium caprate (active only in calcium-free conditions), GDC is effective at low, physiologically relevant doses (0.5–2.12 mM) under standard conditions. These properties make GDC a novel and ideal candidate for transiently inducing a leaky, infant-like epithelial phenotype, a previously unexplored approach for modeling early-life gut barrier function *in vitro.*

An *in vitro* infant model should deliver a barrier with paracellular permeability levels, tight junction and mucus characteristics similar to infants but with the capability to transition overtime to an adult barrier. Importantly, the ability of the model to recover barrier integrity after transient permeability, is essential to provide

a prototype for studying gut maturation overtime, particularly when assessing dietary (bioactive) components for their ability to accelerate this transition. In this study, GDC was evaluated as a candidate for developing an infant gut barrier using Caco-2/HT-29 MTX monolayers. We hypothesized that GDC treatment would produce an infant-like barrier capable of transitioning to an adult state within a reasonably time frame for cell culture experimentation. Therefore, GDC treated monolayers could be employed in nutrition research to develop next generation infant formula.

3.2.2 Materials and Methods

3.2.1. Materials

Human intestinal epithelial cell lines Caco-2 (EACC 86010202) and HT29-MTX-E12 (EACC 12040401) were purchased from the European Collection of Cell Culture (UK). Six and 12-wells plates and polyester permeable-membrane inserts (0.4 μm pore size, 4.5 and 1.11 cm^2 growth area respectively) were purchased from Sarstedt Group (Germany). All pipetting was performed using low-retention, Biosphere® Plus filtered pipette tips (Sarstedt, 70.3050.255). CellTiter 96™ AQueous One Solution Cell Proliferation Assay (MTS, G3582) and cAMP-Glo™ Assay kit (V1501) were purchased from Promega (USA). CyQUANT™ LDH Cytotoxicity Assay (C20300) was purchased from Invitrogen (USA). Milliplex Map Kit (HSTCMAG-28SK, Human High Sensitivity T cell Magnetic Bead Panel, was purchased from Merck Millipore (USA). RNeasy mini kit and RNA-free DNase set were from Qiagen (Netherlands). SensiFAST cDNA Synthesis Kit was from Meridian Bioscience (UK). Light Cycler SYBR GREEN I Master kit was from Roche Diagnostics (Switzerland). Primers for RT-qPCR were synthesised by Eurofins Genomics (Germany). Pierce BCA Protein Assay Kit, Rabbit Occludin

Polyclonal Antibody (71-1500), Alexafluor 488 Donkey Anti-Rabbit Antibody (A-21206,),ProLong™ Glass Antifade Mountant (P36982) and DAPI (62248) were purchased from ThermoFisher Scientific (USA). Dairy Infant Formula (IF) was purchased in a local supermarket. Rabbit gastric extract 15 (RGE 15) was purchased from Lipolyltech (lot number 1201, France). AccQ-Tag Ultra Derivatization Kit, Amino Acid Hydrolysate Standard, AccQ•Tag Ultra Eluent A and AccQ•Tag Ultra Eluent B were purchased from Waters Corporation® (USA). All the other reagents were purchased from Sigma-Aldrich unless stated otherwise.

3.2.2. Cell Culture

Caco-2 and HT29-MTX cell lines were cultured in 75-cm^2 tissue culture flasks at 37°C, 5% CO_2, and humidified atmosphere. After thawing, they were passaged three times before use. The culture medium was Dulbecco's Modified Eagle Medium (DMEM, D5796), supplemented with 10% fetal bovine serum (FBS, F7524), and 100 U/mL Penicillin-Streptomycin (P4333), referred to as 'complete DMEM'. For HT29-MTX cells, 1% MEM Non-essential Amino Acid Solution (M7145,) was also added. Cells were passaged at 80% confluence every 4-5 days using 0.25% Trypsin-EDTA (T4049). Cells were used between passage numbers 22-28 for Caco-2, and 64-68 for HT29-MTX cells. Cells Trypan blue staining and a TC20 cell counter (Bio-Rad, USA) were used for cell counting.

3.2.3. MTS Assay

GDC was dissolved in DMEM D1145 and filter sterilized using 0.22 μm PET syringe filters, (A16532-GUK, Misart Engineering Ltd, New Zealand.), to a concentration of 0.5 to 5 mM. Gastrointestinal digested samples of diary IF were

thawed at room temperature, then diluted to ratios of 1in 10, 1 in 15, and 1 in 20 in HBSS, followed by filtration using a 0.45 nm PES syringe filter. Caco-2 and HT29-MTX cells were seeded in a 96-well plate at a concentration of 10^5 cells/well at a 90:10 ratio (Caco-2:HT29-MTX) in complete DMEM+1% MEM. After approximately 16 h the cells were washed with HBSS and incubated for 30 min with DMEM free from glutamine and phenol red (DMEM D1145). Cells were then washed twice with Hanks Balanced Salt Solution (HBSS, H8264) and incubated with 200 µL GDC (12 concentrations, 0-5mM) in DMEM D1145 or 1% TritonX (X-100). After 2h at 37°C, 20 µL MTS reagent were added to each well and incubated for 1 h. For the digested samples, 200 µL of pre-warmed (37°C) digesta was added for 2 h and then removed, as its turbidity interfered with absorbance readings. Cells were washed twice with HBSS and then 200 µL of MTS reagent diluted 1 in 11 in HBSS (for each reaction: 18 µL of MTS reagent + 182 µL of HBSS) was added for 1 h. Absorbance was read at 490 nm in a microplate reader (Synergy HT BioTek, Winooski, VT, USA). Cell viability was determined by normalizing the absorbance values to DMEM-treated cells (set as 100%) for GDC samples and HBSS-treated cells for digesta samples. The IC_{50} values for GDC were determined using non-linear regression analysis.

3.2.4. Caspase-3 Assay

Caco-2/HT29-MTX (90:10) were seeded 10^5 cells/well in a 96-well plate, cultured overnight and then treated with 0.5, 0.8 and 1 mM GDC for 2 h. Caspase-3 assay was performed according to the manufacturer's guidelines. Briefly, the plate was cooled on ice, media removed, wells rinsed with HBSS. Then, 200 µl reaction mixture (including peptide substrate acetyl-Asp-Glu-Val-Asp-7-amido-4-

methylcoumarin) was added to the wells, mixed by pipetting and transferred into a black, flat bottom 96-well plate. Fluorescence was read (excitation – 360 nm, emission – 460 nm) every min for 60-min at 37°C using a plate reader (Synergy HT, Biotek). Control cells were exposed to DMEM D1145 only, and the assay positive control was isolated human 0.5 µM Caspase-3 (no cells). Caspase-3 activity was quantified in nanomoles of 7-Amino-4-methylcoumarin (the fluorescent product) liberated from acetyl-Asp-Glu-Val-Asp-7-amido-4-methylcoumarin per minute per milliliter of cell lysate, calculated using the formula:

Activity, nmol AMC/min/mL = (nmol AMC×d)/(t×v)

Where v = volume of the sample in milliliters, d = dilution factor, and t = reaction time in min.

3.2.5. Intracellular cAMP quantification

Cyclic AMP levels were assessed using the cAMP-Glo™ Assay (V1501, Promega), according to the manufacturer's instructions. Caco-2/ HT29-MTX (90:10) were seeded in a 96-well plate at 10^5 cells/well and cultured overnight. On the experiment day, 100 mM IBMX (3-isobutyl-1-methylxanthine) was prepared by dissolving 22.2 mg in 100% DMSO and diluted in DMEM D1145 to a final concentration of 500 µM. Cells were washed twice with HBSS and incubated with DMEM D1145+IBMX for 30 min to equilibrate.

During equilibration, 0.5, 0.8, and 1 mM GDC solutions were prepared in DMEM D1145 + IBMX and filter sterilized. DMEM D1145 + IBMX was removed from each well and replaced with 100 µL of the GDC in DMEM D1145 + IBMX. Cells were incubated at 37°C for 2 h. Following the incubation, 80 µL was removed from each well. Cyclic AMP-Glo™ Lysis Buffer (20 µL) was added to the remaining 20

µL volume in the wells. The plate was incubated at room temperature on a shaker for 15 min. Subsequently, a cAMP Detection Solution was prepared by mixing 2.5 µL of Protein Kinase A (PKA) with 1 mL cAMP-Glo™ Reaction Buffer. Next, cAMP Detection Solution (40 µL) was added to each well, and the plate was shaken for 30 s before incubating for 20 min at room temperature. After incubation, 80 µL room-temperature Kinase-Glo® Reagent was added to each well. The plate was shaken for 30 s and incubated for 10 min. Finally, 150 µL from each well was transferred to a white flat-bottom plate, and luminescence was measured using a plate reader (Synergy HT, Biotek) with the following settings: excitation = plug, emission = hole, and gain = 135.

To determine if GDC directly inhibits PKA, GDC solutions were incubated directly with cAMP in the absence of cells. Briefly, 1 µL cAMP (1mM) was diluted in 249 µL DMEM D1145 +I BMX (final cAMP concentration 4 µM). In a 96-well plate, 10 µL of this cAMP solution was mixed with 10 µL of D1145 + IBMX (control condition) or 2X GDC in D1145 + IBMX (GDC = 0.5 0.8, 1 mM). Following this, 20 µL cAMP-Glo™ Lysis Buffer was added to each well, and the plate was incubated for 15 min. The remaining steps were performed as described above for the cell lysate.

3.2.6. GDC treatment of Caco-2/HT29-MTX monolayers

Caco-2 and HT29-MTX cells were diluted separately in complete DMEM with 1% MEM at 1.2×105 cells/mL. A 90:10 cell mix (Caco-2/ HT29-MTX) was added to the apical compartment of 12 well plates containing polyester permeable-membrane inserts (Sarstedt Group) at 6×104 cells/well (500 µL). The basolateral compartment received 1.5 mL complete DMEM with 1% MEM. Media was replaced every two

days and monolayer integrity measured by TEER (Ω×cm², Millicell-ERS Voltohmmeter, Merck Millipore) every 7 days (16 h after media change). To determine the optimal experimental time point for barrier maturity, transepithelial electrical resistance (TEER) was monitored at several intervals (days 7, 14, 21, 24, and 25). Based on these measurements, the monolayer was considered stabilized by day 25, which falls within the widely accepted 21–29 day window for Caco-2 differentiation (Hubatsch et al., 2007). Senescence markers p21 and p53 were monitored by RT-qPCR (see Supplementary Fig. 3.3) to evaluate cell senescence.

At day 24 monolayers were washed twice and incubated with DMEM D1145 for 16 h. Monolayers with TEER > 1000 Ω×cm² on day 25 were used. Monolayers were washed twice with HBSS and incubated with DMEM D1145 (apical = 0.4 mL and basolateral = 1.5 mL) for 30 min for acclimatization. GDC (5X in DMEM D1145) was added to the apical compartment (100 µL) to a final concentration of 0.5, 0.8 and 1 mM. Monolayers were incubated for 2h. TEER was measured at times 0, 1 and 2h. Control monolayers received DMEM D1145 only. Apical and basolateral samples were collected and stored at -20°C for further analysis. Monolayers were either kept for further experiments or lysed for RT-PCR. TEER values are expressed as Ω×cm²- blank (Transwell insert with media in the absence of cells).

3.2.7. Monolayer recovery

On day 25, GDC was removed from Caco-2/HT29-MTX monolayers, which were then washed twice with HBSS. DMEM D1145 was added to the apical (0.5 mL) and basolateral (1.5 mL) compartments, and monolayers were incubated for 24 h. TEER measurements were taken at 1 and 24 h thereafter.

For real-time TEER, Caco-2/HT29-MTX cells (90:10) were seeded at a concentration of 4.8×10^5 cells/well (2 mL/well) in a 6-well plate containing polyester permeable-membrane inserts (basolateral chamber = 3 mL). Media was replaced every 2 days and monolayer integrity tracked by Millicell. On day 24, cells were washed twice with HBSS and incubated for 16 h with DMEM D1145. On day 25, the permeable inserts with monolayers attached were placed into the CellZscope plate (nanoAnalytics GmbH, Germany) for real-time TEER measurements. Only monolayers with a TEER > 1000 $\Omega\times cm^2$ were used. The monolayers were initially washed with HBSS, then equilibrated for 30 min by adding 1.6 mL DMEM D1145 to the apical side and 4 mL to the basolateral side. Then 0.4 mL 5X GDC in DMEM D1145 was added for 2h. Monolayers were washed twice with HBSS and incubated for 24 h with fresh DMEM D1145. The CellZscope system measured TEER every h.

3.2.8. Permeability to Lactulose

The protocol for measuring monolayer permeability to lactulose was adapted from (Kondrashina et al., 2021). Lactulose (61360-25G) was prepared in HBSS (2.5 mg/mL) and filter sterilized. GDC treated monolayers were washed twice and acclimatized for 30 min at 37° in HBSS (0.4 mL in the apical and 1.5 mL in the basolateral). Lactulose (0.5 mg/mL in HBSS, 100 µL) was added to the apical side, and monolayers incubated for 4 h at 37°C. TEER was measured at T0 and T4h. Apical and basolateral samples were collected and stored at -20°.

For the quantification, a high performance anion exchange chromatography with pulsed amperometric detection (HPAEC-PAD) on an ICS3000 system equipped with an electrochemical detector (Dionex, USA) was employed. Apical samples were diluted 1in100 in Milli-Q H_2O while the basolateral samples were analyzed

undiluted. All samples were filtered with a 0.2 μm nylon syringe filter. Separation was conducted using a CarboPac PA100 column (4 × 250 mm) preceded by a guard column (CarboPac PA-100, 4 × 50 mm) at a flow rate of 1 mL/min. Eluent A = 100 mM NaOH; Eluent B = 100 mM NaOH+500 mM sodium acetate (NaOAc). Elution proceeded according to the following gradient: from t = 0 to 6 min, 100% Eluent A; at t = 13 min, 51.4% Eluent A and 48.6% Eluent B; from t = 13.1 to 23.1 minute, equilibrated at 100% Eluent A.

Lactulose levels were quantified by comparing peak areas with known lactulose standards (10 mg/L). The results were expressed as lactulose apparent permeability (Papp) calculated with the following formula:

$$Papp\ (cm/min) = (C_{Baso} \times V)/(t \times A \times C_{In})$$

Where: C_{Baso} = Concentration of lactulose in the basolateral compartment (mg/L); V = Volume of the basolateral compartment (L); t = incubation time (240 min); A = surface area (1.1 cm^2); C_{In} = initial concentration in the apical (mg/L).

3.2.9. Lactate Dehydrogenase (LDH) assay

Briefly, 50 μL from the apical chamber of GDC-treated monolayers were transferred to a 96-well flat-bottom plate, and mixed with equal volume of LDH Cytotoxicity Assay reaction mixture. The plate was incubated at room temperature in the dark for 30 min to allow LDH conversion of lactate to pyruvate, initiating a reduction of formazan dye. After incubation, 50 μL stop solution was added to each well, and absorbance was measured at 490 nm and 680 nm using a Synergy HT plate reader (Biotek). Cytotoxicity was then calculated as follows:

% cytotoxicity = (GDC-treated LDH activity–Spontaneous LDH activity)/(Maxium LDH activity–Spontaneous LDH activity)×100

Where: GDC-treated LDH activity = GDC treated monolayer supernatant; Spontaneous LDH activity = supernatant from control monolayers, Maximum LDH activity = LDH released from 50 µL of cell lysate (control monolayers lysed, with 500 µL of 1% TritonX, by pipetting)

3.2.10. Alkaline phosphatase activity

Caco-2/HT29-MTX monolayers were tested for alkaline phosphatase activity after a 2h treatment with 0, 0.5, 0.8, 1 mM GDC. In each well, the apical fluid was collected and the monolayer was then washed twice with PBS. Monolayers were lysed with 0.2% TritonX (0.5 mL) in Milli-Q H_2O by shaking for 20 min at room temperature. Then 50 µL apical sample or 50 µL cell lysate were transferred into a clear flat-bottom 96-well plate. The activity of alkaline phosphatase was measured with the Alkaline Phosphatase Assay kit (MAK447), in which p-nitrophenyl phosphate is converted into p-nitrophenol and inorganic phosphate. After 4 min of reaction, absorbance was measured at 405 nm using a Synergy HT plate reader. The activity of alkaline phosphatase was calculated with the following formula:

$[(OD_{T4}- OD_{T0})\times RxnVol]/ \varepsilon PNP\times L\times SmplVol\times t$;

Where: OD_{T0} = D value at 405 nm at time 0, OD_{T0} = OD value at 405 nm at time 4 min, RxnVol = reaction volume, εPNP = absorptivity coefficient for p-Nitrophenol (18.75 $mM^{-1}\times cm^{-1}$), L = light path in cm, SmplVol = sample volume, t = reaction time, 4 min. The light path (L) has been calculated with the following formula:

$L = (OD_{Cal}–OD_{Blank})/(\varepsilon C)$;

Where: OD_{Cal} = absorbance at 405 nm of the Calibrator of the kit, OD_{Blank} = absorbance at 405 nm of the blank (well with just media and no cells), ε = molar absorptivity coefficient, C = path length of the plate in cm.

3.2.11. Cytokine Quantification

For the pro-inflammatory cytokines (IL-8, IL-6 and TNF), apical samples were centrifuged at 900 g for 5 min to remove debris. The analysis was performed with 25 µL supernatant using the Human Milliplex Map Kit (HSTCMAG-28SK, Merck Millipore) and MagPix fluorescent detection system (Luminex, The Netherlands), according to the manufacturer's instructions. Milliplex assay detects IL-6 in the concentration range 0.18–750 pg/mL, IL-8 between 0.31–1250 pg/mL and TNF-α between 0.43–1750 pg/mL.

3.2.12. OCLN immunofluorescence

After GDC treatment, monolayers were washed twice with PBS and fixed for 30 min at room temperature by adding 500 µL 75% ethanol in PBS to the apical chamber. Monolayers were washed twice with PBS and kept at 4°C in PBS until use. Monolayers were permeabilized with 75% acetone in PBS for 3 min at room temperature, washed three times with PBS and incubated for 30 min at room temperature with the blocking solution (1% BSA in PBS). The blocking solution was removed and 150 µL primary antibody (71-1500, Rabbit Occludin Polyclonal Antibody, ThermoFisher Scientific) diluted in blocking solution (8.33 µg/mL) was added. Monolayers were incubated overnight at 4°C. The following day, monolayers were washed twice with PBS and 150 µL secondary antibody (A-21206, Alexafluor 488 Donkey anti-rabbit, ThermoFisher Scientific) in blocking solution was added (11 µg/mL). Monolayers were incubated for 1h in the dark at room temperature, washed three times with MilliQ H_2O and incubated with DAPI (62248, ThermoFisher Scientific; 1:500 dilution in MilliQ H_2O) for 2 min, in the dark, at

room temperature. The permeable supports of the Transwell plates were excised with a scalpel and mounted on a microscope slide with 40 µL mounting media (ProLong™ Glass Antifade Mountant).

Microscopy images were captured with Leica TCS SP5 Confocal Laser Scanning Microscope with 405 Diode and Argon lasers (Leica Microsystems, Wetzlar, Germany) and HC PL APO 63x/1,40 OIL CS2 objective. Pinhole size was 85.65 nm. Images were captured with the following settings: scan mode—xyz, format—1024 x 1024, speed—440 Hz, pixel size—240.50 x 240.50 x 713.35 nm, line and frame average—6, z-step size—0.71 µm. Alexa Fluor 488 acquisition parameters were: 520-560 nm (emission range), 929 V (gain) and 100 % (laser intensity). DAPI acquisition parameters were: 410-480 (emission range), 700 V (gain) and 64 % (laser intensity). Images were acquired using the Leica Application Suite AV (v 2.7.3.9723) software (Leica Microsystems). Fiji/ImageJ software (version 1.54f, Java 1.8.0_322) was used for subsequent analysis of OCLN fluoresence intensity. Regions of Interest (ROIs) were manually selected from acquired images based on where the nuclei were well visible. For intensity quantification, the z-plane corresponding to the middle of the nuclei was chosen to ensure consistent measurement across samples. Intensity threshold was determined with the Otsu algorithm. The OCLN fluorescence intensity was calculated as raw integrated density (Raw IntDen), which represents the sum of pixel intensity within each ROI, normalized by the number of nuclei. For improved visualization, contrast adjustments were applied to the images using ImageJ software. The adjustments were performed uniformly across all images.

3.2.13. mRNA Expression by Real Time PCR

Cell monolayers treated with GDC were lysed by the addition of RLT buffer (350 µL) with 1 % β-mercaptoethanol on ice for 5 min. Cell lysate was collected and stored at -80 °C prior to use. Total RNA was extracted with the RNeasy Mini Kit with DNase digestion (Qiagen), following manufacturer's instructions. RNA was quantified with Nanodrop 1000 (Thermo Fisher Scientific) and only the samples meeting the criteria of $OD_{260/280}$ ratios between 1.8 and 2.0 were used for cDNA synthesis. Reverse transcription from 0.5 µg of total RNA to cDNA was conducted using the SensiFAST cDNA Synthesis kit (Bioline, UK). mRNA transcripts were quantified using LightCycler 480 SYBR Green I Master kit (Roche Diagnostics Ltd., UK) using a LightCycler 96 instrument.

Primer sequences and annealing temperatures, for Claudin-2 (CLDN2), Junctional Adhesion Molecule 1 (JAM1), Occludin (OCLN), Zonula Occludens-1 (ZO1), Claudin-4 (CLDN4), Ribosomal Protein Lateral Stalk Subunit (P0-RPLP0), Mucin-1 (MUC1), Mucin 2 (MUC2), Mucin-5AC (MUC5A) cyclin-dependent kinase inhibitor 1 (p21) and tumor protein p53 (p53), are listed in Supplementary Table 3.1. The reaction mixture for each well consisted of 5 µL of master mix, 0.5 µL of each forward and reverse primer (10 µM) and 1 µL of 1 in 10 dilution of cDNA.

The $2^{-\Delta\Delta Ct}$ method was employed to calculate the relative amount of the target gene, where $\Delta\Delta Ct = (Ct_{\text{Target gene}} - Ct_{\text{RPLP0}})_{\text{GDC test}} - (Ct_{\text{Target gene}} - Ct_{\text{RPLP0}})_{\text{Control}}$.

Here, Ct = theshold cycle for either the target gene or RPLP0; test = monolayers treated with 0.5, 0.8 or 1 mM GDC; control = DMEM D1145 media treated monolayers.

3.2.14. Mucus Quantification by Alcian Blue

GDC-treated monolayers were washed twice with PBS. Then, 0.5 mL of 1% Alcian blue (A5268) in 0.16 M sucrose + 0.05 M sodium acetate at pH 5.8 was added to the apical compartment and incubated at 37°C for 30 min. After incubation, the stain was removed and monolayers were washed, at least 3 times, with PBS (until the PBS was clear). Monolayers were then lysed by pipetting with 0.5 mL RIPA buffer with 1% EDTA. Collected cell lysates were briefly spun to remove debris. The supernatant (150 µL) was placed in a clear flat-bottom 96-well plate in duplicate and absorbance measured at 620 nm in a Biotek Synergy HT plate reader. Results are presented as the absorbance at 620 nm–blank (RIPA buffer with 1 % EDTA alone).

3.2.15. Gastrointestinal digestion of Dairy Infant Formula (IF)

Dairy IF was reconstituted following the manufacturer's instructions by dissolving 4.3 g of powder in 30 mL of MilliQ H_2O. The infant simulated gastro-intestinal digestion (SGID) was performed as per Ménard et al. (2018). The protocol was adjusted to ensure full activation of pepsin and trypsin, with a specific focus on protein digestion. As a result, lipase activity was not prioritized in this setup. This approach aligns with INFOGEST recommendations, which support adapting digestion parameters according to the nutrient class being investigated. (Brodkorb et al., 2019). A volume of 5 mL of reconstituted dairy IF was mixed with 2.94 mL infant simulated gastric fluids containing 268 U/mL RGE 15 (pepsin activity = 596 U/mg). The pH was brought to 5.3 with 1 M HCl. Samples were incubated for 1h at 37°C in a shaking incubator (100 rpm). To stop the gastric phase and inhibit pepsin activity, the pH was increased to 7 with 1M NaOH. Then, 4.88 mL of simulated intestinal fluids containing 16 U/mL pancreatin (lot number SLCM8903, trypsin

activity = 8.9 U/mg) and 3.1 mM bovine bile (lot number SLBV1780, bile salts concentration = 440 g/mol) were added. The pH was decreased to 6.6 with 1 M HCl. The samples were incubated again for 1h at 37°C in a shaking incubator. Following the intestinal phase, digestion was stopped by adding the protease inhibitor 4-(2-aminoethyl) benzene sulfonyl fluoride hydrochloride, dissolved in MilliQ H_2O at a final concentration of 1 mM, along with Orlistat dissolved in ethanol at a final concentration of 0.1 mM. An SGID control sample, where MilliQ H_2O replaced the dairy IF, was subjected to gastrointestinal digestion followed by enzyme inactivation (SGID-H_2O). The SGID samples were stored at -80°C until use. The protein content of the digested dairy IF was determined by Pierce BCA Protein Assay Kit (ThermoFisher Scientific).

3.2.16. Caco-2/HT29-MTX monolayers exposure to digested dairy IF

For the monolayer exposure, 0 mM GDC or 0.8 mM GDC-treated Caco-2/HT29-MTX monolayers were washed twice and incubated with HBSS (0.4 mL in the apical and 1.5 mL in the basolateral side) for 15 min at 37°C for acclimatization. The digested dairy IF was defrosted at room temperature, diluted 1in 3 in HBSS, filtered (0.45 µm PES syringe filters, low protein bind, Sarstedt) and pre-warmed to 37°C. Subsequently, 100 µL SGID dairy IF or HBSS (buffer only control) was added to the apical compartment (final dilution 1:15) for 2h at 37°C. TEER values were recorded at T0h (after HBSS wash and acclimatization) and at T2h (after 2h incubation with the digesta). The protein content of the sample applied to the apical side (µg/cm^2) was calculated as follows: protein content of digesta (BCA assay, µg/mL)/ dilution factor (15)/volume on apical side (0.5 mL)/ Transwell filter area (1.1 cm^2). Apical and basolateral samples were collected and stored at -20°C for amino acids analysis.

3.2.17. Quantification of the total amino acid in the basolateral chamber

Basolateral samples were defrosted at room temperature, and 0.5 mL of each technical replicate was pooled. A total volume of 1 mL from this pooled sample was transferred to a glass vial, evaporated using a SpeedVac concentrator, and then re-suspended in 100 µL of hydrolysis solution (6 M HCl). Hydrolysis was conducted for 15 h at 110°C. To quantify the derivative forms of cysteine (XCys), cysteine standards (10 and 1 mmol/L) were also hydrolyzed. Prior to hydrolysis, an internal standard of Norvaline was added to each sample to achieve a final concentration of 250 ρmol/L. After hydrolysis, 20 µL of each sample was neutralized by the addition of 20 µL of 6 M NaOH and 20 µL of 0.2 mM HCl, and then filtered using a 0.45 µm nylon syringe filter. The samples and standards (Amino Acid Hydrolysate Standard, Waters Corporation) were derivatized using the AccQ-Tag Ultra Derivatization Kit (Waters Corporation). Each derivatization reaction consisted of mixing 10 µL of the sample with 70 µL of AccQ•Tag Ultra Borate Buffer and 20 µL of AccQ•Tag Ultra reagent, followed by incubation at 55 °C for 10 min. Amino acids detection was performed with ACQUITY Ultra Performance LC® (UPLC®) equipped with tunable ultraviolet/visible (TUV) detector (Waters Corporation). Separation was performed with AccQ•Tag Ultra Amino Acid Analysis Column (Eluent 1 = AccQ•Tag Ultra Eluent, Eluent 2 = AccQ•Tag Ultra Eluent B, Waters Corporation; flow rate = 0.7 mL/min; injection volume = 1 µl; column temperature = 55°C). The quantification was performed based on a standard three-point curve. The Empower software (version 3.7.0, Waters Corporation) was used to acquire, process, report, and manage chomatographic information.

3.2.18. Statistical analysis

All experiments were conducted in triplicates or quadruplicate across three separate days, each with technical duplicates or triplicates. Results are expressed as means ± SEM. Statistical analyses were performed using GraphPad Prism 9.1.0 (GraphPad Software, USA) via two-way ANOVA with Tukey's multiple comparison or Dunnet's multiple comparison. Statistical significance was determined at a P-value < 0.05.

3.3. Results

3.3.1. IC_{50} of GDC on Caco-2/HT29-MTX is 2.49 mM

The IC_{50} of GDC on the viability of undifferentiated Caco-2/HT29-MTX cells was determined by MTS and non-linear regression analysis (Supplementary Fig. 3.1). The IC_{50} was 2.49 mM, (95% CI = 2.21-3.04 mM). Cell viability was not decreased by GDC concentrations of 0.5, 0.8 and 1 mM GDC compared to the control (cells in DMEM D1145 only; P > 0.05). Cells treated with 1% Triton X served as a positive control, showing a viability of 0.457 ± 0.037%.

3.3.2. GDC decreases TEER with subsequent recovery

To assess the effect of non-cytotoxic GDC on the intestinal barrier integrity, 25-day old differentiated Caco-2/HT29-MTX 90:10 monolayers were exposed for 2 h to 0.5, 0.8 and 1 mM GDC. Initially, development of the barrier overtime was tracked by TEER measurements at 7, 14, 21, 24 and 25 days after seeding (Supplementary Fig. 3.2). At day 21 TEER values were 848 ± 36.54 $\Omega \times cm^2$. It took a further 3 days for the TEER values to stabilize. By day 24, TEER values had increased to 1261 ± 34.67 $\Omega \times cm^2$ and had stabilized, with no significant increase from day 24 to day 25

(1302.81 ± 35.162 Ω×cm^2 , P > 0.05) (Supplementary Fig. 3.2). Although within the range (day 21-29) recommended by Hubatsch et al. 2007, day 25 monolayers were checked for senescence, by quantifying mRNA transcript levels of senescence markers p21 and p53 (Herbig et al., 2004). Transcript levels of p21 and p53 did not significantly change in day 25 monolayers compared to day 21. (P > 0.05; Supplementary Fig. 3.3).

Once day 25 monolayer were treated with GDC, all 3 GDC concentrations resulted in significantly lower TEER values (Fig. 3.1A, P < 0.05) at 2 h compared to monolayers in media alone (0 mM GDC = 1086.071 ± 01.28; 0.5 mM GDC = 573.34 ± 149.69; 0.8 mM GDC = 403.15 ± 155.29; 1mM GDC = 233.26 ± 82.20 Ω×cm^2). The calculated fold decreases in TEER relative to the control were as follows: 0.5 mM GDC = 1.89, 0.8 mM GDC = 2.69, 1 mM GDC = 4.65. Once GDC was removed (recovery phase), monolayers treated with 0.5 mM GDC had similar TEER values to values of control monolayers within 1h (P > 0.05). Monolayers treated with 0.8 or 1 mM GDC were still significantly lower than controls at 1h (P < 0.0001). By 24 h in the recovery phase, 0.5 and 0.8 mM GDC monolayers had TEER value increases similar to control monolayers (0 mM GDC = 1359.05 ± 86.79; 0.5 mM = 1168.2 ± 85.35; 0.8 mM = 1133.55 ± 73.76 Ω×cm^2; P > 0.05), while 1 mM GDC was still struggling to recover (1 mM = 875.29 ± 145.41 Ω×cm^2, P < 0.01).

This recovery is critical to simulate the transient nature of neonatal gut permeability and to enable post-treatment applications, such as digesta exposure or intervention studies that might induce gut barrier restoration. To examine the recovery phase in detail, TEER values were measured every hour for 24 h using a CellZscope real-time cell monitoring system (Fig. 3.1B). At the start of the recovery phase (T0h), TEER values for monolayers treated with 0.8 mM and 1 mM GDC were significantly lower

than those of the control monolayers ($P < 0.05$). CellZcope measurements revealed that monolayers treated with 0.5 mM GDC showed no significant difference from 0 mM GDC at the beginning of the recovery phase. TEER values of 0.8 mM GDC treated monolayers reached levels similar to control monolayers by 4 h of recovery (T4h; $P > 0.05$). By the end of the 24-h recovery period (T24h), TEER values for all GDC-treated monolayers had returned to levels comparable to those of the control condition (0 mM GDC, $P > 0.05$).

3.3.3. GDC-treated monolayers have a higher permeability to lactulose

To evaluate whether decreased TEER values in GDC-treated monolayers corresponded to increased permeability, a lactulose permeability assay was performed on these monolayers (Fig. 3.1C). Caco-2/HT29-MTX monolayers treated with 0.8 mM and 1 mM GDC had a significantly higher lactulose Papp (0.8 mM GDC = $P < 0.05$, 1 mM GDC = $P < 0.001$) compared to 0 mM GDC. The lactulose Papp increased by 0.91-fold for 0.5 mM GDC, 1.64-fold for 0.8 mM GDC and 3.61-fold for 1 mM GDC (Papp 0 mM GDC = 1.79×10^{-8} cm/s ± 1.21×10^{-9}). Mannitol was not included in the permeability assessment, as mannitol is transported paracellularly and transcellularly *in vivo*, while only paracellularly *in vitro* (Ménard et al., 2010).

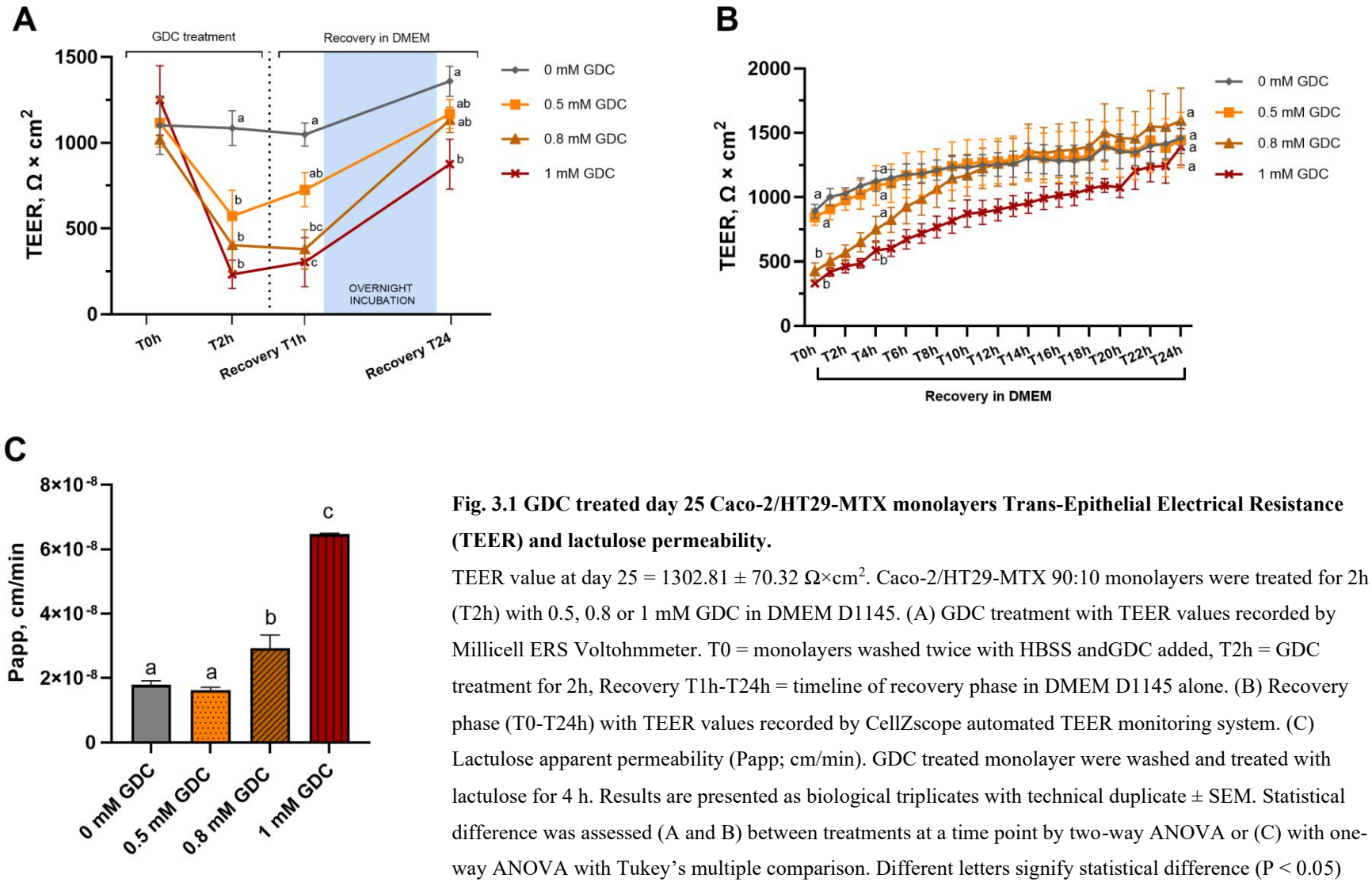


Fig. 3.1 GDC treated day 25 Caco-2/HT29-MTX monolayers Trans-Epithelial Electrical Resistance (TEER) and lactulose permeability.

TEER value at day 25 = 1302.81 ± 70.32 Ω×cm^2. Caco-2/HT29-MTX 90:10 monolayers were treated for 2h (T2h) with 0.5, 0.8 or 1 mM GDC in DMEM D1145. (A) GDC treatment with TEER values recorded by Millicell ERS Voltohmmeter. T0 = monolayers washed twice with HBSS andGDC added, T2h = GDC treatment for 2h, Recovery T1h-T24h = timeline of recovery phase in DMEM D1145 alone. (B) Recovery phase (T0-T24h) with TEER values recorded by CellZscope automated TEER monitoring system. (C) Lactulose apparent permeability (Papp; cm/min). GDC treated monolayer were washed and treated with lactulose for 4 h. Results are presented as biological triplicates with technical duplicate ± SEM. Statistical difference was assessed (A and B) between treatments at a time point by two-way ANOVA or (C) with one-way ANOVA with Tukey's multiple comparison. Different letters signify statistical difference ($P < 0.05$)

3.3.4. GDC treatment does not cause monolayer cytotoxicity

LDH release was measured in the GDC treated monolayers, as LDH leakage indicates cytoplasmic damage. None of the GDC concentrations increased the LDH release, suggesting GDC is not causing cytoplasmic leakage (Fig. 3.2A) ($P > 0.05$).

3.3.5. GDC increases extracellular, but not intracellular, alkaline phosphatase activity

To study the effects of GDC on epithelial function, the intracellular and extracellular alkaline phosphatase activity were measured in GDC treated Caco-2/HT29-MTX monolayers (Fig.3.2B and C). No significant difference was found in the intracellular alkaline phosphatase activity of the GDC treated monolayers compared to the 0 mM GDC (53.99 ± 1.59 μmol/(L x min); $P > 0.05$). However, the 0.8 and 1 mM GDC-treated monolayers showed a significantly increased extracellular activity ($P < 0.05$ and $P < 0.001$) compared to untreated (Fig. 3.2C). The extracellular alkaline phosphatase activity was: 0 mM GDC = 1.478 ± 0.13, 0.8 mM GDC = 5.219 ± 0.79, 1 mM GDC = 11.55 ± 0.02 μmol/(L x min).

3.3.6. GDC treatment does not cause monolayer inflammation

To investigate whether or not GDC treatment resulted in an inflammatory response, cytokines IL-8, IL-6 and TNF were tracked in the apical compartment of GDC-treated monolayers. These cytokines were chosen as they activate the key inflammation pathways such as NF-kB and ERK-MAPK (Iglesias et al., 2020) and are secreted by Caco-2 monolayers under inflammatory conditions (Iglesias et al., 2020; Jung et al., 1995). Secreted IL-6 and TNF could not be detected in the 0 mM GDC nor the GDC-treated monolayers. IL-8 was detected but levels did not

significantly differ with GDC treatment (0 mM GDC = 5.84 ± 0.59; 0.5 mM GDC = 9.54 ± 4.21; 0.8 mM GDC = 8.33 ± 2.81; 1 mM GDC = 11.32 ± 3.81 ρg/mL).

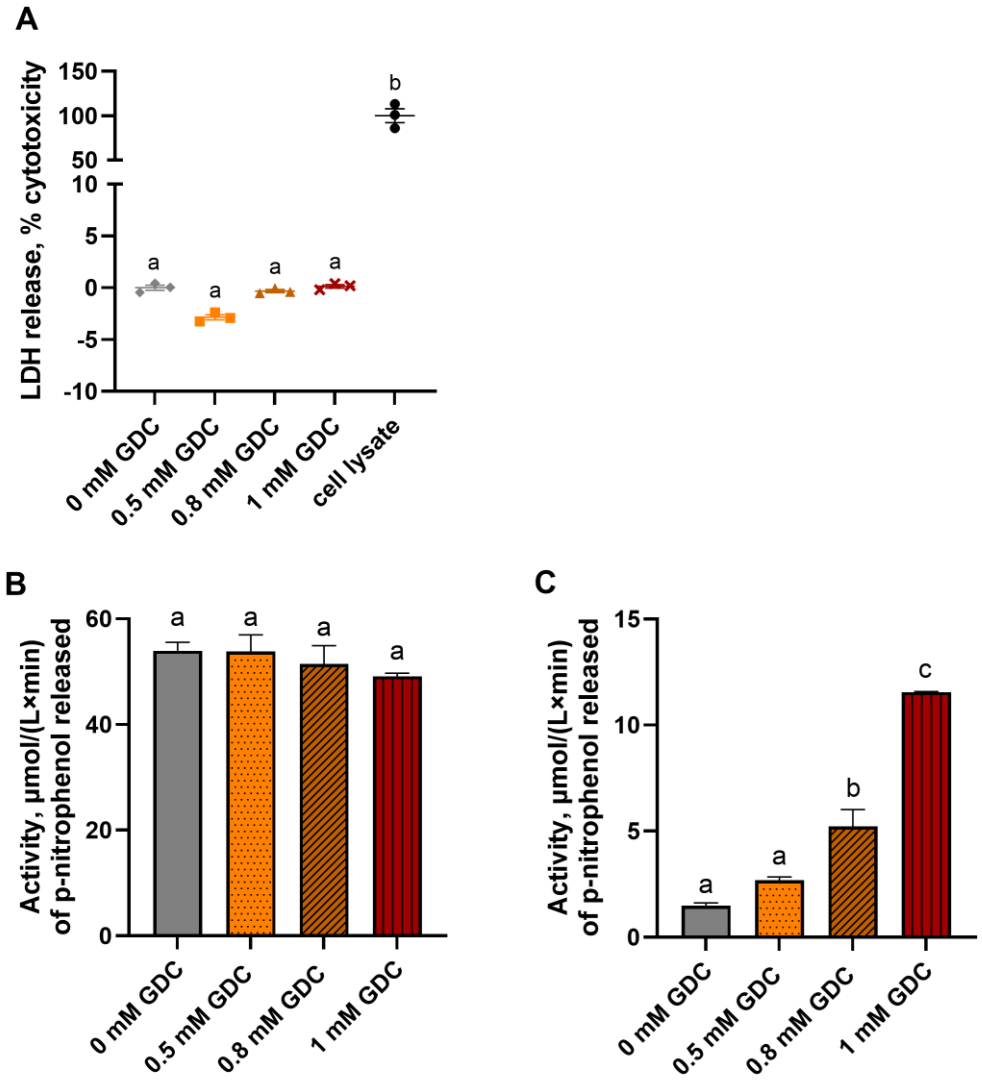


Figure 3.2 Effect of GDC treatment on LDH release, intracellular and extracellular alkaline phosphatase activity in Caco-2/HT29-MTX monolayers.

Caco-2/HT29-MTX 90:10 monolayers were grown for 25 days and exposed for 2 h to 0.5, 0.8 or 1 mM GDC. (A) % of cytotoxicity measured by the release of LDH in the apical compartment, given by the amount of formazan produced in the enzymatic reaction with the assay mixture. LDH was 0 mM GDC = monolayers in DMEM 1145 only (set as 0% cytotoxicity); Cell Lysate = positive control, cells lysed with 1% Triton-X (set as 100% cytotoxicity). (B) Intracellular (cell lysate) and (C) extracellular (apical supernatant) alkaline phosphatase activity was measured using p-nitrophenyl phosphate as substrate. Alkaline phosphatase activity was calculated as µmol/(L x min) of p-nitrophenol released. Results are presented as the average of a biological triplicate and a technical duplicate ± SEM. Statistical difference in the treatments was assessed by one-way ANOVA with Tukey's multiple comparison and is indicated with different letters ($P < 0.05$).

3.3.7. GDC reduces OCLN fluorescence intensity and modulates tight junction proteins mRNA expression

To determine the effect of GDC on the gut barrier integrity, OCLN immunofluorescence was performed on the monolayers treated with 0, 0.5, 0.8 and 1mM GDC (Fig. 3.3A and B). The results revealed a significantly lower fluorescence intensity of OCLN per number of cell nuclei for all GDC treatments (Fig. 3.3B; $P < 0.05$). Specifically, OCLN intensity for 0 mM GDC was 50758 ± 4809, for 0.5 mM GDC was 43214 ± 3716 (85.28 ± 0.89 % of control), for 0.8 mM GDC was 38447 ± 4597 (75.79 ± 5.02 % of control) and for 1 mM GDC was 29783 ± 7740 (57.40 ± 10.26 % of control).

To assess if the lower protein levels was due to lower mRNA transcripts, *OCLN* mRNA and associated tight junction biomarkers (ZO1, CLDN2/4 and JAM1) were measured in GDC-treated Caco-2/HT29-MTX monolayers (Fig. 3.3C). OCLN and ZO1 mRNA levels were significantly higher in 1 mM GDC-treated monolayers (OCLN = $P < 0.01$; ZO1 = $P < 0.05$) compared to 0 mM GDC, whilst treatment of monolayers with 0.5 or 0.8 mM GDC did not alter OCLN or ZO1 mRNA transcript levels ($P > 0.05$). CLDN2, CLDN4 and JAM1 expression was increased in 0.8 mM GDC –treated monolayers ($P < 0.05$), compared to 0 mM GDC.

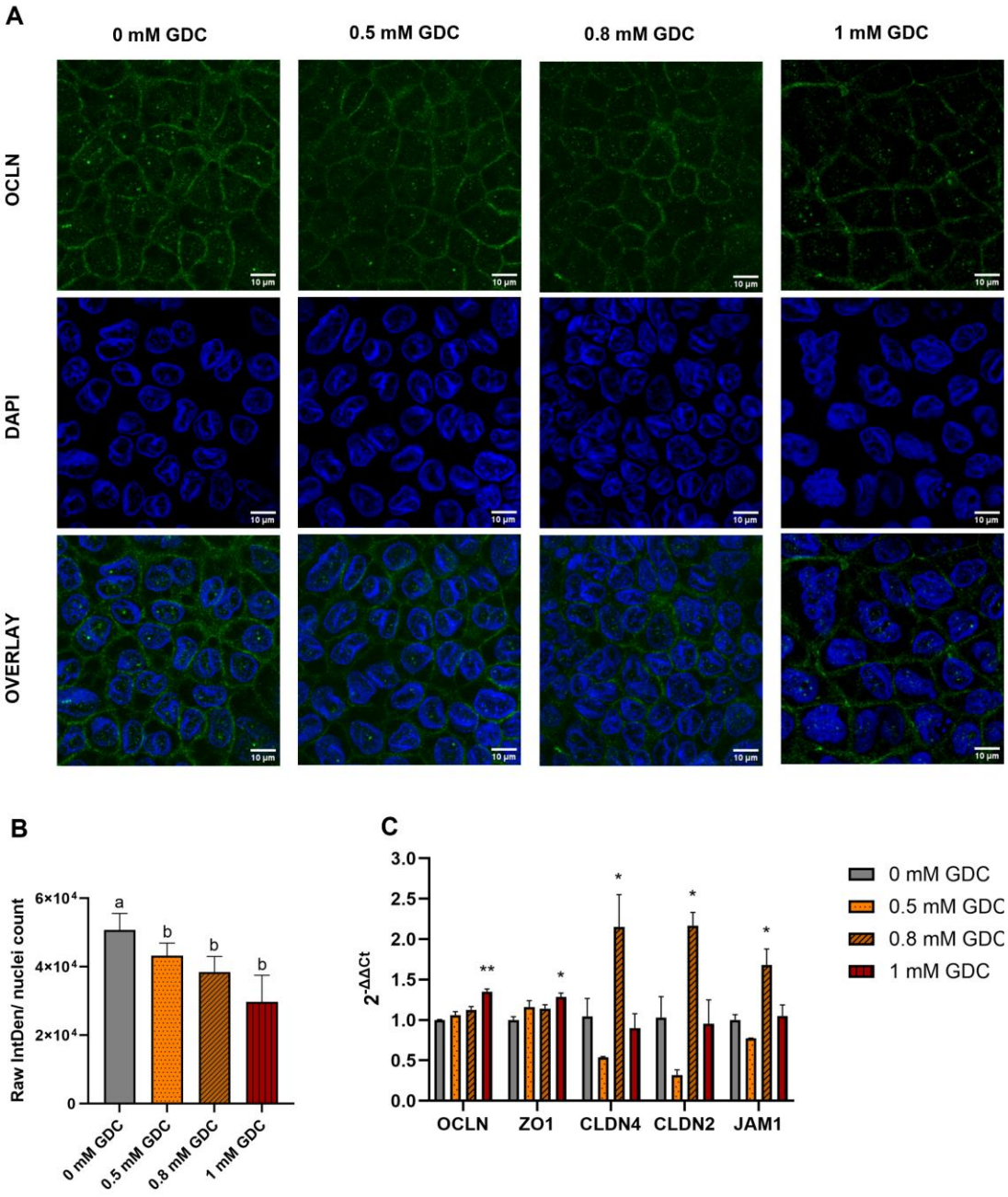


Fig. 3.3 Effect of GDC treatment on occludin (OCLN) localization and tight junction protein expression in Caco-2/HT29-MTX monolayers.

Caco-2/ HT29-MTX 90:10 monolayers were grown for 25 days and treated for 2h with 0.5, 0.8 and 1 mM GDC. (A) Representative confocal microscopy images of monolayers stained with OCLN (Alexa488, green) and nuclei stained with DAPI (blue). Scale bar = 10 µm. (B) Fluorescence intensity of OCLN from images using the Otsu thresholding algorithm in Fiji-ImageJ and normalized to the number of nuclei. Results represent the average of three biological replicates and three images for each replicate (mean ± SEM). Statistical differences ($P < 0.05$) between treatments was evaluated using one-way ANOVA and indicated by different letters. 0 mM GDC = monolayers in DMEM 1145 media only. (C) Relative mRNA expression levels of tight junction proteins *OCLN*, zonulin (ZO1,

TJP1), claudin-4 (*CLDN4*), claudin-2 (*CLDN2*), and junctional adhesion molecule 1 (*JAM1*) in monolayers treated with GDC. Transcript levels were normalized to the housekeeping gene *RPLP0* mRNA and monolayers in DMEM 1145 alone (0 mM GDC), employing the $2^{-\Delta\Delta Ct}$ method. Results represent the average of three biological and four technical replicates, presented as mean ± SEM. Statistical significance was evaluated using one-way ANOVA with Dunnett's multiple comparison test (treatment vs. control). Asterisks denote statistical difference between each treatment and 0 mM GDC ($P < 0.05$).

3.3.8. GDC increases mucus production but not mucins expression

To determine whether GDC treatment affects the mucus layer, GDC-treated monolayers were stained with Alcian blue to quantify acidic mucins. Acidic mucins were selected as the main focus because the neonatal intestinal mucus is enriched in these glycoproteins, particularly sialomucins and sulfomucins, which predominate at birth and play critical roles in early-life gut barrier function and host–microbiota interactions (Deplancke and Gaskins, 2001)

As shown in Fig. 3.4A, 0.8 mM and 1 mM GDC-treated cells exhibited a significant increase in Alcian blue staining intensity compared to 0 mM ($P < 0.05$). Monolayers treated with 0.5 mM GDC had similar Alcian blue staining 0 mM and 0.8 mM GDC-treated monolayers ($P > 0.05$).

The expression of MUC1, MUC2, and MUC5AC was assessed using RT-qPCR (Fig. 3.4B). The analysis revealed that GDC-treated monolayers had a significantly lower mRNA expression of MUC1 (0.5 mM GDC = $P < 0.01$, 0.8/ 1 mM = $P < 0.05$) and MUC2 ($P < 0.05$) compared to 0 mM GDC, with no difference in MUC5AC.

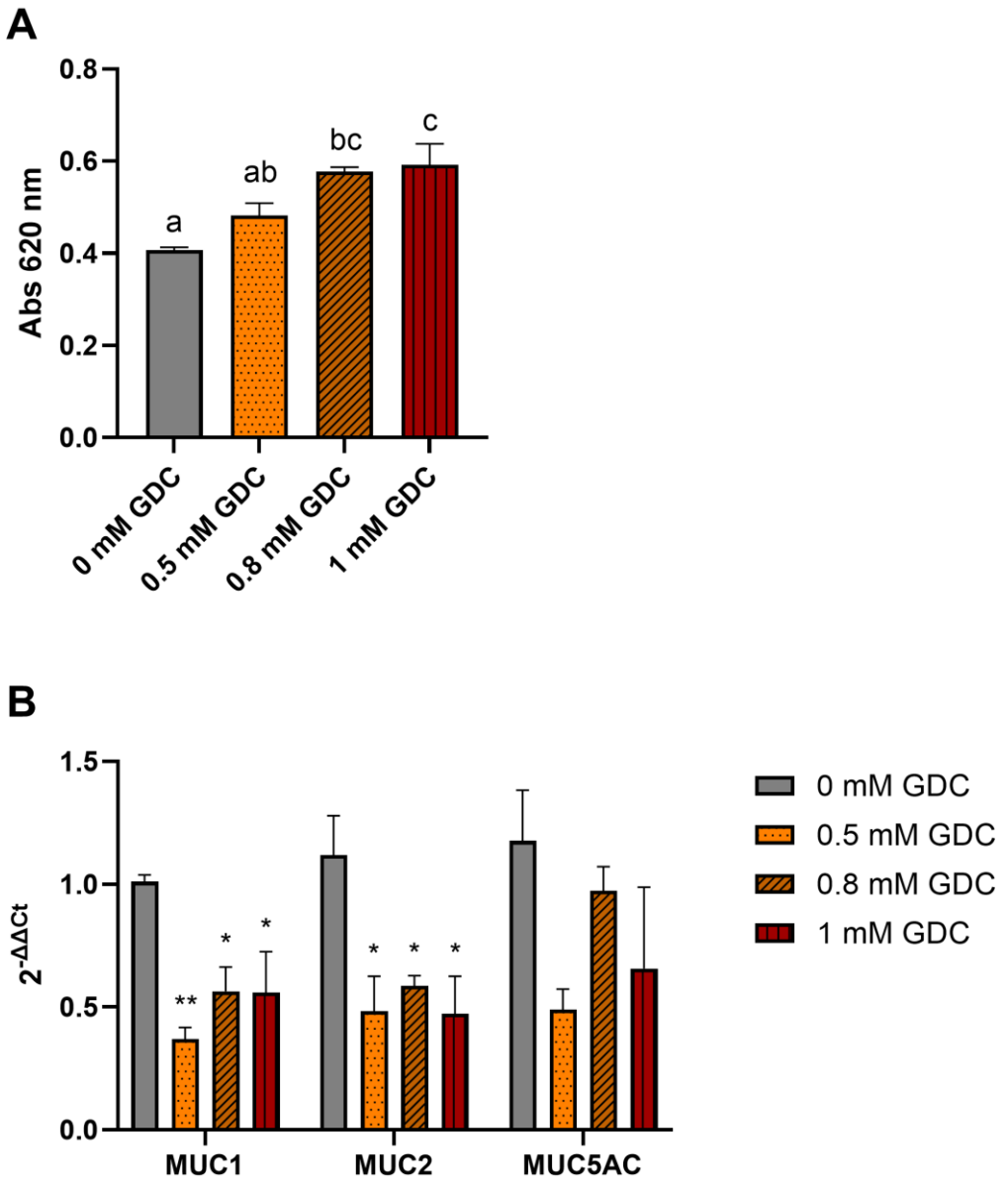


Fig. 3.4 (A) Mucus staining (B) and mucins mRNA expression in Caco-2/HT29-MTX monolayers treated with GDC.

(A) 25-day-old Caco-2/HT29-MTX 90:10 monolayers treated with 0.5, 0.8 and 1 mM GDC for 2h were stained with Alcian Blue, lysed and absorbance at 490 nm recorded. (B) mRNA expression of mucin-1 (*MUC1*), mucin-2 (*MUC2*) and mucin-5AC (*MUC5AC*). Transcript levels were determined using RT-PCR and normalized to the housekeeping gene RPLP0 mRNA and monolayers in media alone (0 mM GDC), employing the $2^{-\Delta\Delta Ct}$ method. Results represent the average of three biological and four technical replicates, presented as mean ± SEM. Statistical significance ($P<0.05$) was evaluated using one-way ANOVA with (A) Dunnet's multiple comparison test (treatment vs. control) or (B) Tukey's multiple comparison. (A) Different letters denote statistical difference between each condition. (B) Asterisks denote statistical difference between each treatment and the control within each gene.

3.3.9. GDC does not activate the apoptotic cascade but decreases cAMP levels

To investigate the mechanism of action of this bile salt, Caspase-3 activity assay was performed on undifferentiated Caco-2/HT29MTX cells, as an indicator of apoptotic pathway activation. No statistical difference was found between GDC treated cells compared to cells in media overnight ($P > 0.05$) (Fig.5A).

To assess whether GDC treatment results in modulation of intracellular cAMP levels, cAMP was measured in undifferentiated Caco-2/HT29-MTX cells following treatment with 0, 0.5, 0.8 and 1 mM GDC (Fig.5B). Cells treated with 0.8 and 1 mM GDC resulted in a significantly higher Relative Luminescence Unit (RLU) (which equates to lower cAMP levels) compared to control cells without GDC (0 mM GDC = DMEM D1145+IBMX only; $P < 0.05$). No statistical difference was found between control and 0.5 mM GDC treated cells ($P > 0.05$). To determine if GDC inhibits PKA activity directly, GDC solutions were mixed with cAMP prior to PKA activity measurement. There was no significant difference ($P > 0.05$) between media only and GDC solutions, indicating that GDC does not inhibit PKA activity (Supplementary Fig. 3.4).

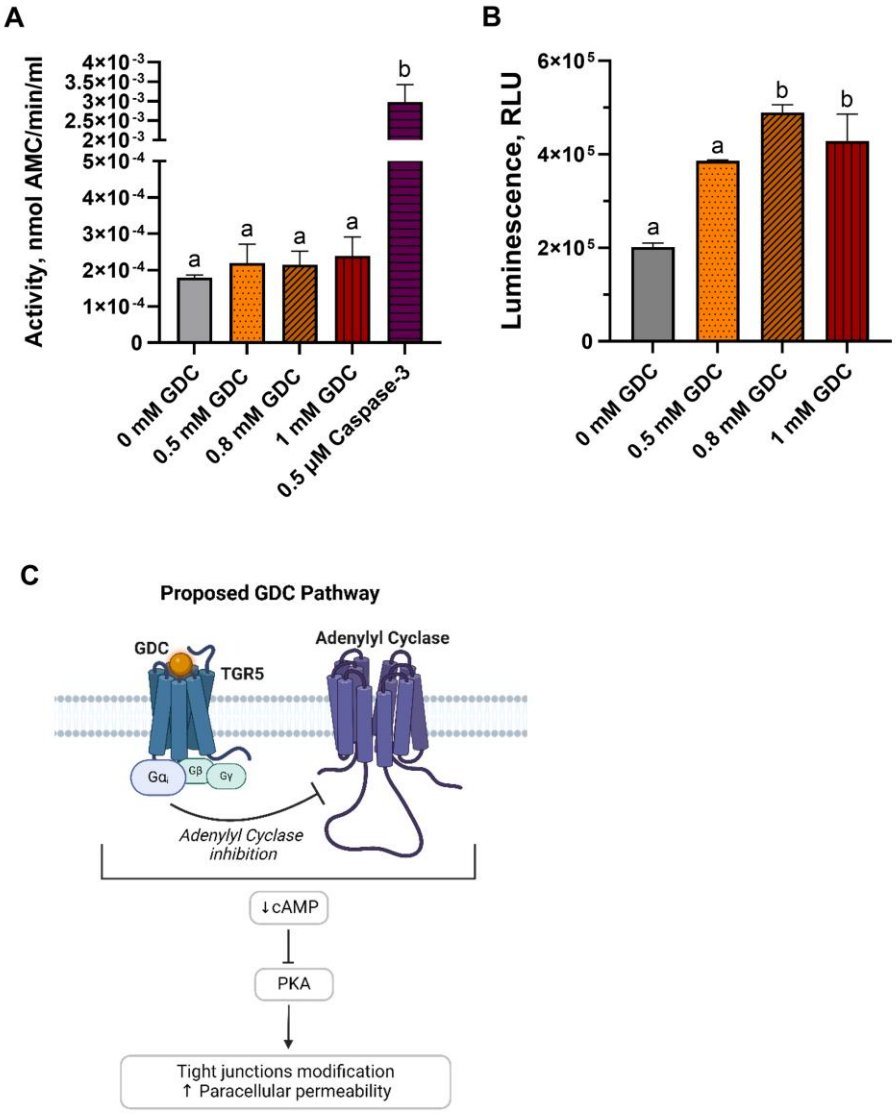


Fig. 3.5 Caspase-3 activity and intracellular cAMP levels in undifferentiated Caco-2/HT29-MTX cells treated with GDC and proposed mechanism of action.

Caco-2/HT29-MTX 90:10 cells were seeded at 10^5 cells/well, grown for 24h and then exposed for 2h to 0.5, 0.8 or 1 mM GDC. (A) Caspase-3 activity, reported as nmol of 7-Amino-4-methylcoumarin—AMC—released per min per mLof cell lysate, was measured usingvacetyl-Asp-Glu-Val-Asp-7-amido-4-methylcoumarin as the reaction substrate. (B) Intracellular cAMP was measured indirectly via protein kinase A activity, where cAMP activates protein kinase A, reducing ATP and thereby decreasing light output in a coupled luciferase reaction. 0 mM GDC = monolayers in DMEM D1145 + IBMX. Results are presented as Relative Light Unit (RLU), which inversely correlates with cAMP levels. 0 mM GDC RLU=201707±8486. The results represent the average of a biological triplicate and a technical duplicate ± SEM. Statistical difference in the treatments was assessed by one-way ANOVA with Tukey's multiple comparison and is indicated with different letters ($P<0.05$). (C) Proposed mechanism of action of GDC. By binding to the G-protein coupled receptor TGR5 (Takeda G protein-coupled Receptor), GDC inhibits adenylate cyclase via the Gαi subunit, leading to reduced cAMP levels and PKA inactivation.

3.3.10. GDC (0.8 mM) increases amino acids transport after exposure to digested dairy IF

Based on permeability, tight junction, mucus data, and timeline to recovery, 0.8 mM GDC was selected as the preferred concentration to create an *in vitro* model of an infant gut barrier. To evaluate whether 0.8 mM GDC-treated monolayers were biocompatible with digested food, dairy IF was subjected to *in vitro* infant gastrointestinal digestion. This digested dairy IF sample (100.55 ± 3.55 µg protein /cm^2) was applied to 0.8 mM GDC treated monolayers (Fig. 3.6). Preliminary experiments indicated that this dairy IF digesta was not toxic to intestinal cells (% of viability = 99.56 ± 2.95, MTS assay, Supplementary Fig. 3.5).

As shown in Fig. 3.6A, no significant differences in TEER values were observed between the T0h and T2h in 0 mM GDC and 0.8 mM GDC monolayers following exposure to digested dairy IF ($P > 0.05$), indicating that the monolayer was unaffected by digesta addition. As a control, monolayers were exposed to HBSS alone for 2 h, and no significant change in TEER was observed (TEER T2h vs. T0h = 97.95 ± 6.19 % for 0 mM GDC; 106 ± 4.98 % for 0.8 mM GDC).

To track nutrient absorption post dairy IF-digesta treatment, total AA concentration in the basolateral chamber was quantified. Interestingly, total AA concentration in the basolateral chamber was significantly higher in GDC treated monolayers compared to control monolayers (80.55 ± 15.45 ρmol/µL compared to 24.09 ± 8.62 ρmol/µL, $P < 0.05$, Fig. 3.6B).

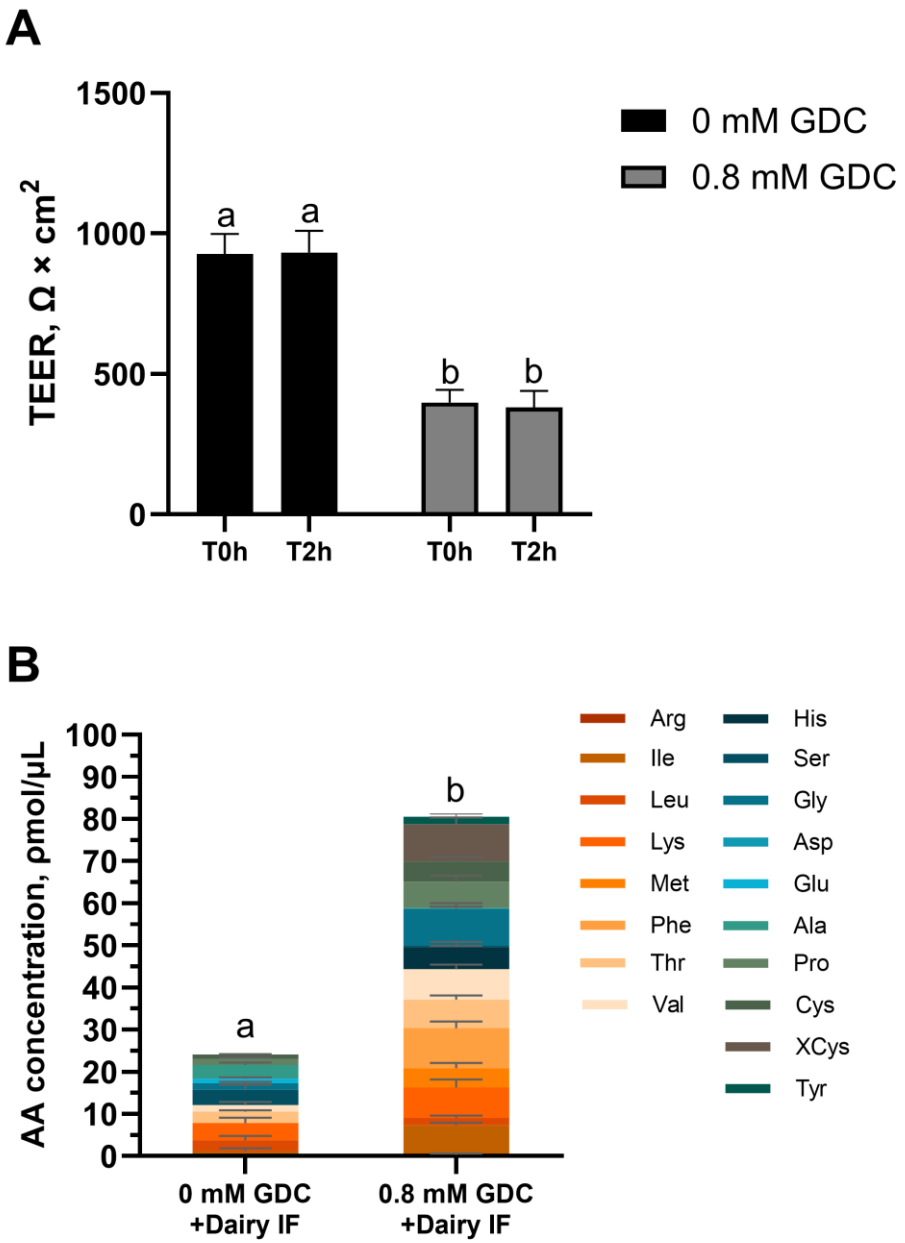


Fig. 3.6 (A) TEER values and (B) total amino acid content in the basolateral side of Caco-2/HT29-MTX monolayers treated with GDC and digested dairy Infant Formula (IF).
25-day-old Caco-2/HT29-MTX 90:10 monolayers treated for 2h with 0.8 mM GDC or DMEM D1145 (0 mM GDC) were washed with HBSS and exposed for 2h to digested dairy IF diluted 1:15 (A) TEER values were recorded by Millicell ERS Voltohmmeter after washing (T0h) and after the incubation with the digested IMF (T2h). (B) After the 2h incubation with the dairy IF digesta, the basolateral samples were subjected to acid hydrolysis and analyzed by UPLC to quantify amino acids. Results represent the average of three biological and two technical replicates ± SEM. Statistical significance ($P<0.05$) was evaluated using two-way ANOVA with Tukey's multiple comparison (A) or Student's t-test (B). Different letters indicate significant difference ($P<0.05$).

3.4. Discussion

In our study, we investigated the potential of GDC in converting Caco-2/HT29-MTX monolayers into a model of the infant gut barrier. GDC is a bile salt that has been studied as an epithelial permeation enhancer for oral macromolecule delivery (Brayden and Stuettgen, 2021; Song et al., 2005). Our main findings are that treatment of Caco-2/HT29-MTX monolayers with 0.8 mM GDC resulted in (a) decreased TEER and increased lactulose paracellular permeability ($P < 0.05$), (b) reduced OCLN at the cell membrane and (c) increased acidic mucins ($P < 0.05$). The monolayer recovered from GDC treatment within 4h ($P > 0.05$). This timely recovery is essential for an *in vitro* infant gut model designed to test digested foods, as it allows experiments to be performed in buffer rather than culture media. In addition, it simulates food transit times in the upper gut. It is likely that the mechanism of action of GDC involves the activation of G-protein coupled receptors, leading to a reduction in cAMP ($P < 0.05$), with a knock-on effect that includes an increase in extracellular alkaline phosphatase activity ($P < 0.05$) and modulation of intracellular signaling pathways that modify tight junctions. Importantly, our results indicate that neither cytotoxicity (as assessed by MTS and LDH assays, $P > 0.05$), apoptosis (caspase-3 activity, $P > 0.05$), nor inflammation (IL-8, IL-6, and TNF secretion, $P > 0.05$) were involved. GDC treated monolayers were biocompatible with infant formula digesta and resulted in higher concentrations of bioavailable amino acids ($P < 0.05$)

Our findings revealed a significant but transient reduction in TEER and an increase in lactulose Papp ($P < 0.05$) and mRNA levels of the permeability enhancer marker CLDN2 upon treatment with 0.8 mM GDC. Brayden et al. (2021) reported a similar TEER reduction of 54 ± 13.1% with 0.5 mM GDC in 21/22-day-old Caco-2 cells,

(our study = 53.34 ± 25.77% with 0.5mM GDC). However, Brayden et al. (2021), reported no recovery after 24 h. The inclusion of a mucus layer provides a protective barrier to Caco-2 monolayers (Antoine et al., 2015; Birch et al., 2018; Wuyts et al., 2015), which possibly supports recovery once GDC is removed.

In agreement with our lactulose Papp data, Song et al. (2005) also observed that treating Caco-2 with 2.15 mM GDC increased salmon calcitonin Papp by 10.66-fold and decreased TEER by 4.57-fold, compared to the control (Song et al., 2005). Moreover, the Papp/TEER was 2.33 ± 0.56, whilst for the unconjugated form (sodium deoxycholate) the Papp/TEER was 1.31 ± 0.25, indicating the conjugated form is less harmful to the plasma membrane (Carubbi et al., 1996). Indeed Brayden et al. (2021) report no significant changes in Caco-2 membrane fluidity after exposure to 0.5 mM GDC using the Laurdan assay (Brayden and Stuettgen, 2021). In our study, lactulose Papp across 0.8 mM GDC treated monolayers was approximately 63.35 ± 22.68% higher than control monolayers. Interestingly *in vivo*, lactulose permeability was reported 55.56% higher in the urine of 3-month-old infants (n of samples = 1715) compared to 15-month infants (n of samples = 1582). In addition, increased *CLDN2* mRNA has been reported in the proximal small intestine of 2-week-old mice compared to 12-week mice ($P < 0.05$), in line with significantly increased permeability of orally administered 4 kDa, 10 kDa, 70 kDa dextran ($P < 0.05$) (Gleeson et al., 2021). However, despite the higher mRNA expression, CLDN2 protein was localized intracellularly in villi of infant mice indicating, together with short villi, an immature villi architecture (Gleeson et al., 2021).

In our study, confocal microscopy revealed that GDC treatment decreased membrane bound OCLN in a dose-dependent manner ($P < 0.05$). Surprisingly, 0.8 mM GDC

significantly increased ($P < 0.05$) mRNA expression of tight junction biomarkers OCLN, Claudin-4, JAM-1 (barrier-forming), and Claudin-2 (permeability-enhancing) (Otani and Furuse, 2020). This suggests that GDC does not downregulate OCLN transcription but instead promotes post-translational modifications, redistribution, and/or internalization of the protein. Similarly, Zeng et al. (2022) and Raimondi et al. (2008) reported that, in Caco-2 cells, unconjugated deoxycholic acid (0.1–0.3 mM and 50 μM, respectively), induced OCLN post-translational redistribution, potentially through EGFR–mediated internalization (Raimondi et al., 2008).

In vivo studies have shown that there is a significantly higher level of OCLN leakage in feces at birth compared to 3 and 6-month-old infants (median values: birth = 2.36; 3 months = 2.25; 6 months = 2.17; 12 months = 2.17 ng/g), indicating an increased intestinal permeability correlated to OCLN localization (Sochaczewska et al., 2022). *In vivo* data from animal models show contrasting findings. Holmes et al. (2006) report no significant changes in ZO1, OCLN, and JAM1 mRNA expression in mice during neonatal development (1, 14, 28, and 90 days-old) (Holmes et al., 2006). Whilst, Gleeson et al. (2021) reported reduced mRNA levels of ZO1, OCLN, and JAM1 in 2-week-old infant mice compared to 12-week-old adults.

Our treatment with 0.8 and 1 mM GDC significantly increased acidic mucins ($P < 0.05$), as shown by Alcian blue staining. This stain, binds to sialic acid and sulfate groups of acidic mucins (Hall et al., 1980). In parallel, the GDC treatment downregulated the expression of mucins MUC1 (0.5 mM, $P < 0.01$; 0.8 and 1 mM, $P < 0.05$) and MUC2 ($P < 0.05$), while MUC5AC remained unchanged ($P > 0.05$). These findings indicate that there was a shift toward increased acidic mucus that occurred independently from mucin expression.

Several previous studies have shown that bile salts can stimulate mucin secretion. For example, Klinkspoor et al. (1999) and Shekels et al. (1996) demonstrated that deoxycholic acid (0.0625 to 0.25 mM and 2.5 mM, respectively) and its taurine-conjugated form (taurodeoxycholic acid—2.5 mM) stimulated mucin secretion in a dose-dependent manner in LS174T and HT29 cells (measured by [^{3}H]-glucosamine labeling) (Klinkspoor et al., 1999; Shekels et al., 1996). This effect is believed to be mediated by intracellular calcium and PKC signaling, pathways known to regulate mucin exocytosis in colonic cell lines such as T84 and HT29-18N2 (Lencer et al., 1990; Marcon et al., 1990; McCool et al., 1990). Thus, the increased Alcian Blue signal in our study may reflect GDC-induced exocytosis of preformed mucins rather than transcriptional upregulation.

It has also been reported that sodium deoxycholate, glycocholate and taurodeoxycholate (0.2, 0.5, 2 and 20 mM) decrease the viscosity of human-isolated mucus (Martin et al., 1978). Given GDC's structural similarity to these bile salts, it is likely that GDC similarly reduces mucus viscosity. This, along with increased acidic mucins, may contribute to the infant-like characteristics of our model. *In vivo* data on colonic mucus in newborn humans, pigs and mice show a predominance of acidic mucins over neutral mucins at birth (Deplancke and Gaskins, 2001). In mice, MUC2 protein levels and *Muc-3/2/5* mRNA expression levels progressively increase from 5 to 15 days and at 6 weeks of age (Zhang et al., 2014). Future work would track mucin expression over the GDC recovery period to investigate its alignment to *in vivo* data.

Bile salts primarily interact with intestinal cells through the surface receptor Takeda G protein-coupled Receptor (TGR5) and the nuclear Farnesoid X Receptor (FXR) (Schaap et al., 2014). TGR5 modulates adenylyl cyclase via the G-protein α subunit

stimulatory ($G\alpha_s$) or inhibitory ($G\alpha_i$) (Pierce et al., 2002). In our research, we observed a decrease in the intracellular cAMP for the 0.8 and 1 mM GDC-treated monolayers ($P < 0.05$), indicating adenylyl cyclase inhibition and downstream suppression of PKA, pointing to $G\alpha_i$ involvement. Interestingly, TGR5 activation by deoxycholic acid has been linked to ERK1/2 activation, EGFR phosphorylation, and reduced OCLN immunofluorescence in Caco-2, without the involvement of muscarinic receptors, another secondary receptor for bile salts (Raimondi et al., 2008; Yasuda et al., 2007). However, conflicting findings from Zeng et al. (2022) report a decrease in ERK1/2 phosphorylation in deoxycholic acid-treated Caco-2 cells (Zeng et al., 2022). Although we cannot rule out that GDC modulation could be via alternative β-arrestin or EGFR pathways, the cAMP reduction we observed favors the hypothesis of $G\alpha_i$ involvement (Fig. 4.5C). Furthermore, although nuclear FXR may play a role in this process, its primary effects are though transcriptional changes (Schaap et al., 2014). Therefore, it is unlikely to be the direct cause of the OCLN redistribution induced by GDC as OCLN mRNA levels were unchanged at 0.8 mM GDC. It is also worth noting that while GDC was selected for its low toxicity and reversible effects, other conjugated bile salts such as taurocholate or glycocholate may offer similar advantages. Future studies could explore whether these alternatives yield comparable or complementary effects on epithelial permeability and mucus modulation.

Interestingly, recent insights suggest that intestinal alkaline phosphatase may regulate tight junction protein expression (Lallès, 2019). Hamarneh et al. (2014) demonstrated that exogenous alkaline phosphatase increases the mRNA levels of ZO1, ZO3, and CLDN3 in Caco-2 cells (Hamarneh et al., 2014). In our study, GDC at all tested concentrations significantly increased the activity of secreted alkaline

phosphatase ($P < 0.05$), suggesting a potential explanation for tight junction mRNA increases observed in our study. This reinforces the idea that alkaline phosphatase may play a role not only in maintaining gut homeostasis, but also in modulating barrier function in early life (Lü et al., 2020).

While infant formulae aim to replicate human milk, the latter offers additional bioactive benefits to the infant barrier. For example, milk proteins and their peptides are known to support gut health and nutrient absorption (Su et al., 2017). Caco-2/HT29-MTX monolayers treated with 0.8 mM GDC were sufficiently robust to withstand infant formula digesta (food components, digestive enzymes and bile salts). Although GDC was removed after 2 h, the barrier remained moderately permeable for at least 4 h, providing a physiologically relevant window for nutrient absorption kinetics, as intestinal transit in infants typically occurs within this timeframe (orocecal transit time in pre-term infants = 3.1 h) (Bodé et al., 2004). No further TEER decline was observed during digesta exposure, confirming the stability of the model for cellular studies. Most importantly, GDC treated monolayers facilitated higher concentration of AA transported in the basolateral compared to control monolayers ($P < 0.05$). Although human data are limited*, in vivo* studies in rats and pigs show that the infant barrier allows higher AA transport (Buddington et al., 2001; Toloza and Diamond, 1992; Younoszai et al., 1985b). This further demonstrates GDC-treated Caco-2/HT29-MTX suitability as an infant gut barrier model for nutrition research.

One of the model's strengths is its adaptability to compact experimental timelines. Advanced *in vitro* systems must be time-efficient to offer a practical alternative to animal studies. Following the Hubatsch et al. protocol, monolayers are viable and functional from day 21 to 29; thus, a complete experimental sequence—including

transient induction of infant-like permeability, followed by repeated exposure to milk components—can be conducted within a focused 8-day window.

While our model provides an infant-like gut barrier, several limitations must be acknowledged. First, compounds can only be tested for a short duration (e.g., 4 h exposure), which may restrict the ability to detect slower or long-term effects on barrier function or improvement. Furthermore, our model currently captures paracellular and amino acids transport only and has not yet been validated for transporter activity or receptor-mediated uptake. It is also crucial to study the potential effects of GDC on brush border enzymes, as well as mucus viscoelastic properties and neutral mucins. Studying neutral mucins will, however, require method development to use Periodic Acid-Schiff with cell lysates. Complementary Alcian Blue and PAS staining post-recovery would help determine if GDC alters acidic and neutral mucin composition through changes in secretion, regulation, or glycosylation. Future studies should also explore whether the conjugated bile salt GDC activates molecular pathways involving β-arrestin, EGFR, and FXR. Additionally, testing the model with breast milk would track its response to breast milk components allowing comparison with *in vivo* data.

3.5.Conclusions

This study proposes 0.8 mM GDC as a suitable treatment for Caco-2/HT29-MTX monolayers to create a reversible, infant-like gut barrier model, which is currently appropriate for infant nutrition research focused on paracellular and AA transport.

3.6.References

Altobelli, E., Angeletti, P.M., Verrotti, A., Petrocelli, R., 2020. The Impact of Human Milk on Necrotizing Enterocolitis: A Systematic Review and Meta-Analysis. Nutrients 12, 1322. https://doi.org/10.3390/nu12051322

Antoine, D., Pellequer, Y., Tempesta, C., Lorscheidt, S., Kettel, B., Tamaddon, L., Jannin, V., Demarne, F., Lamprecht, A., Béduneau, A., 2015. Biorelevant media resistant co-culture model mimicking permeability of human intestine. International Journal of Pharmaceutics 481, 27–36. https://doi.org/10.1016/j.ijpharm.2015.01.028

Araújo, F., Sarmento, B., 2013. Towards the characterization of an in vitro triple co-culture intestine cell model for permeability studies. International Journal of Pharmaceutics 458, 128–134. https://doi.org/10.1016/j.ijpharm.2013.10.003

Birch, D., Diedrichsen, R.G., Christophersen, P.C., Mu, H., Nielsen, H.M., 2018. Evaluation of drug permeation under fed state conditions using mucus-covered Caco-2 cell epithelium. European Journal of Pharmaceutical Sciences 118, 144–153. https://doi.org/10.1016/j.ejps.2018.02.032

Bode, L., 2012. Human milk oligosaccharides: Every baby needs a sugar mama. Glycobiology 22, 1147–1162. https://doi.org/10.1093/glycob/cws074

Bodé, S., Dreyer, M., Greisen, G., 2004. Gastric Emptying and Small Intestinal Transit Time in Preterm Infants: a Scintigraphic Method: Journal of Pediatric Gastroenterology and Nutrition 39, 378–382. https://doi.org/10.1097/00005176-200410000-00014

Brayden, D.J., Hill, T.A., Fairlie, D.P., Maher, S., Mrsny, R.J., 2020. Systemic delivery of peptides by the oral route: Formulation and medicinal chemistry approaches. Advanced Drug Delivery Reviews, Advanced Drug Delivery

2020 - Part 2: Routes of Delivery and Biological Barriers 157, 2–36. https://doi.org/10.1016/j.addr.2020.05.007

Brayden, D.J., Stuettgen, V., 2021. Sodium glycodeoxycholate and sodium deoxycholate as epithelial permeation enhancers: in vitro and ex vivo intestinal and buccal bioassays. European Journal of Pharmaceutical Sciences 12.

Brodkorb, A., Egger, L., Alminger, M., Alvito, P., Assunção, R., Ballance, S., Bohn, T., Bourlieu-Lacanal, C., Boutrou, R., Carrière, F., Clemente, A., Corredig, M., Dupont, D., Dufour, C., Edwards, C., Golding, M., Karakaya, S., Kirkhus, B., Le Feunteun, S., Lesmes, U., Macierzanka, A., Mackie, A.R., Martins, C., Marze, S., McClements, D.J., Ménard, O., Minekus, M., Portmann, R., Santos, C.N., Souchon, I., Singh, R.P., Vegarud, G.E., Wickham, M.S.J., Weitschies, W., Recio, I., 2019. INFOGEST static in vitro simulation of gastrointestinal food digestion. Nat Protoc 14, 991–1014. https://doi.org/10.1038/s41596-018-0119-1

Buddington, R.K., Elnif, J., Puchal-Gardiner, A.A., Sangild, P.T., 2001. Intestinal apical amino acid absorption during development of the pig. American Journal of Physiology-Regulatory, Integrative and Comparative Physiology 280, R241–R247. https://doi.org/10.1152/ajpregu.2001.280.1.R241

Carubbi, F., Guicciardi, M.E., Concari, M., Bozzoli, M., Carulli, N., 1996. Cytotoxic and Protective Effects of Bile Salts in Vitro, in: Gentilini, P., Dianzani, M.U. (Eds.), New Trends in Hepatology. Springer Netherlands, Dordrecht, pp. 133–141. https://doi.org/10.1007/978-94-009-0357-9_15

Catassi, C., Bonucci, A., Coppa, G.V., Carlucci, A., Giorgi, P.L., 1995. Intestinal Permeability. Changes during the First Month: Effect of Natural versus

Artificial Feeding. Journal of Pediatric Gastroenterology and Nutrition 21, 383–386. https://doi.org/10.1097/00005176-199511000-00003

Chiang, J.Y.L., 2009. Bile acids: regulation of synthesis. Journal of Lipid Research 50, 1955–1966. https://doi.org/10.1194/jlr.R900010-JLR200

Deplancke, B., Gaskins, H.R., 2001. Microbial modulation of innate defense: goblet cells and the intestinal mucus layer. The American Journal of Clinical Nutrition 73, 1131S-1141S. https://doi.org/10.1093/ajcn/73.6.1131S

Filipe, M.I., Sandey, A., Carapeti, E.A., 1989. Goblet cell mucin in human foetal colon, its composition and susceptibility to enzyme degradation: a histochemical study. Symp Soc Exp Biol 43, 249–258.

Fine, K.D., Santa Ana, C.A., Porter, J.L., Fordtran, J.S., 1995. Effect of changing intestinal flow rate on a measurement of intestinal permeability. Gastroenterology 108, 983–989. https://doi.org/10.1016/0016-5085(95)90193-0

Fogh, J., Wright, W.C., Loveless, J.D., 1977. Absence of HeLa cell contamination in 169 cell lines derived from human tumors. J Natl Cancer Inst 58, 209–214. https://doi.org/10.1093/jnci/58.2.209

Fricker, G., Fahr, A., Beglinger, C., Kissel, T., Reiter, G., Drewe, J., 1996. Permeation enhancement of octreotide by specific bile salts in rats and human subjects: in vitro, in vivo correlations. British J Pharmacology 117, 217–223. https://doi.org/10.1111/j.1476-5381.1996.tb15177.x

Gleeson, J.P., Fein, K.C., Chaudhary, N., Doerfler, R., Newby, A.N., Whitehead, K.A., 2021. The enhanced intestinal permeability of infant mice enables oral protein and macromolecular absorption without delivery technology.

International Journal of Pharmaceutics 593, 120120. https://doi.org/10.1016/j.ijpharm.2020.120120

Grauso, M., Lan, A., Andriamihaja, M., Bouillaud, F., Blachier, F., 2019. Hyperosmolar environment and intestinal epithelial cells: impact on mitochondrial oxygen consumption, proliferation, and barrier function in vitro. Sci Rep 9, 11360. https://doi.org/10.1038/s41598-019-47851-9

Hall, R.L., Miller, R.J., Peatfield, A.C., Richardson, P.S., Williams, I., Lampert, I., 1980. A colorimetric assay for mucous glycoproteins using Alcian Blue. Biochemical Society Transactions 8, 72–72. https://doi.org/10.1042/bst0080072

Hamarneh, S.R., Mohamed, M.M.R., Economopoulos, K.P., Morrison, S.A., Phupitakphol, T., Tantillo, T.J., Gul, S.S., Gharedaghi, M.H., Tao, Q., Kaliannan, K., Narisawa, S., Millán, J.L., Van Der Wilden, G.M., Fagenholz, P.J., Malo, M.S., Hodin, R.A., 2014. A Novel Approach to Maintain Gut Mucosal Integrity Using an Oral Enzyme Supplement. Annals of Surgery 260, 706–715. https://doi.org/10.1097/SLA.0000000000000916

Herbig, U., Jobling, W.A., Chen, B.P.C., Chen, D.J., Sedivy, J.M., 2004. Telomere Shortening Triggers Senescence of Human Cells through a Pathway Involving ATM, p53, and p21CIP1, but Not p16INK4a. Molecular Cell 14, 501–513. https://doi.org/10.1016/S1097-2765(04)00256-4

Hilgendorf, C., Spahn-Langguth, H., Regårdh, C.G., Lipka, E., Amidon, G.L., Langguth, P., 2000. Caco-2 versus Caco-2/HT29-MTX Co-cultured Cell Lines: Permeabilities Via Diffusion, Inside- and Outside-Directed Carrier-Mediated Transport. Journal of Pharmaceutical Sciences 89, 63–75.

https://doi.org/10.1002/(SICI)1520-6017(200001)89:1<63::AID-JPS7>3.0.CO;2-6

Hofmann, A.F., Hagey, L.R., 2008. Bile Acids: Chemistry, Pathochemistry, Biology, Pathobiology, and Therapeutics. Cell. Mol. Life Sci. 65, 2461–2483. https://doi.org/10.1007/s00018-008-7568-6

Holmes, J.L., Van Itallie, C.M., Rasmussen, J.E., Anderson, J.M., 2006. Claudin profiling in the mouse during postnatal intestinal development and along the gastrointestinal tract reveals complex expression patterns. Gene Expression Patterns 6, 581–588. https://doi.org/10.1016/j.modgep.2005.12.001

Hoogstraate, A.J., Senel, S., Cullander, C., Verhoef, J., Junginger, H.E., Boddé, H.E., 1996a. Effects of bile salts on transport rates and routes of FITC-labelled compounds across porcine buccal epithelium in vitro. Journal of Controlled Release 40, 211–221. https://doi.org/10.1016/0168-3659(95)00187-5

Hoogstraate, A.J., Verhoef, J.C., Tuk, B., Pijpers, A., Van Leengoed, L.A.M.G., Verheijden, J.H.M., Junginger, H.E., Boddé, H.E., 1996b. In-vivo Buccal Delivery of Fluorescein Isothiocyanate–Dextran 4400 with Glycodeoxycholate as an Absorption Enhancer in Pigs. Journal of Pharmaceutical Sciences 85, 457–460. https://doi.org/10.1021/js950129k

Hubatsch, I., Ragnarsson, E.G.E., Artursson, P., 2007. Determination of drug permeability and prediction of drug absorption in Caco-2 monolayers. Nat Protoc 2, 2111–2119. https://doi.org/10.1038/nprot.2007.303

Iglesias, D.E., Cremonini, E., Fraga, C.G., Oteiza, P.I., 2020. Ellagic acid protects Caco-2 cell monolayers against inflammation-induced permeabilization. Free

Radical Biology and Medicine 152, 776–786. https://doi.org/10.1016/j.freeradbiomed.2020.01.022

Jensen, R.G., Hagerty, M.M., McMahon, K.E., 1978. Lipids of human milk and infant formulas: a review. The American Journal of Clinical Nutrition 31, 990–1016. https://doi.org/10.1093/ajcn/31.6.990

Johnston, S.D., Smye, M., Watson, R.G.P., McMillan, S.A., Trimble, E.R., Love, A.H.G., 2000. Lactulose-Mannitol Intestinal Permeability Test: A Useful Screening Test for Adult Coeliac Disease. Ann Clin Biochem 37, 512–519. https://doi.org/10.1177/000456320003700413

Jung, H.C., Eckmann, L., Yang, S.K., Panja, A., Fierer, J., Morzycka-Wroblewska, E., Kagnoff, M.F., 1995. A distinct array of proinflammatory cytokines is expressed in human colon epithelial cells in response to bacterial invasion. J. Clin. Invest. 95, 55–65. https://doi.org/10.1172/JCI117676

Kawamata, Y., Fujii, R., Hosoya, M., Harada, M., Yoshida, H., Miwa, M., Fukusumi, S., Habata, Y., Itoh, T., Shintani, Y., Hinuma, S., Fujisawa, Y., Fujino, M., 2003. A G Protein-coupled Receptor Responsive to Bile Acids. Journal of Biological Chemistry 278, 9435–9440. https://doi.org/10.1074/jbc.M209706200

Klinkspoor, J.H., Mok, K.S., Van Klinken, B.J.-W., Tytgat, G.N.J., Lee, S.P., Groen, A.K., 1999. Mucin secretion by the human colon cell line LS174T is regulated by bile salts. Glycobiology 9, 13–19. https://doi.org/10.1093/glycob/9.1.13

Kondrashina, A., Brodkorb, A., Giblin, L., 2021. Sodium butyrate converts Caco-2 monolayers into a leaky but healthy intestinal barrier resembling that of a

newborn infant. Food Funct. 12, 5066–5076. https://doi.org/10.1039/D1FO00519G

Kosek, M.N., Lee, G.O., Guerrant, R.L., Haque, R., Kang, G., Ahmed, T., Bessong, P., Ali, A., Mduma, E., Peñataro Yori, P., Faubion, W.A., Lima, A.A.M., Paredes Olortegui, M., Mason, C., Babji, S., Singh, R., Qureshi, S., Kosek, P.S., Samie, A., Pascal, J., Shrestha, S., McCormick, B.J.J., Seidman, J.C., Lang, D.R., Zaidi, A., Caulfield, L.E., Gottlieb, M., Network, the M.-E., 2017. Age and Sex Normalization of Intestinal Permeability Measures for the Improved Assessment of Enteropathy in Infancy and Early Childhood: Results From the MAL-ED Study. Journal of Pediatric Gastroenterology and Nutrition 65, 31–39. https://doi.org/10.1097/MPG.0000000000001610

Kühn, F., Adiliaghdam, F., Cavallaro, P.M., Hamarneh, S.R., Tsurumi, A., Hoda, R.S., Munoz, A.R., Dhole, Y., Ramirez, J.M., Liu, E., Vasan, R., Liu, Y., Samarbafzadeh, E., Nunez, R.A., Farber, M.Z., Chopra, V., Malo, M.S., Rahme, L.G., Hodin, R.A., 2020. Intestinal alkaline phosphatase targets the gut barrier to prevent aging. JCI Insight 5, e134049. https://doi.org/10.1172/jci.insight.134049

Lallès, J.-P., 2019. Recent advances in intestinal alkaline phosphatase, inflammation, and nutrition. Nutrition Reviews 77, 710–724. https://doi.org/10.1093/nutrit/nuz015

Lea, T., 2015. Caco-2 Cell Line, in: Verhoeckx, K., Cotter, P., López-Expósito, I., Kleiveland, C., Lea, T., Mackie, A., Requena, T., Swiatecka, D., Wichers, H. (Eds.), The Impact of Food Bioactives on Health: In Vitro and Ex Vivo Models. Springer International Publishing, Cham, pp. 103–111. https://doi.org/10.1007/978-3-319-16104-4_10

Lencer, W.I., Reinhart, F.D., Neutra, M.R., 1990. Interaction of cholera toxin with cloned human goblet cells in monolayer culture. American Journal of Physiology-Gastrointestinal and Liver Physiology 258, G96–G102. https://doi.org/10.1152/ajpgi.1990.258.1.G96

Lesuffleur, T., Barbat, A., Dussaulx, E., Zweibaum, A., 1990. Growth adaptation to methotrexate of HT-29 human colon carcinoma cells is associated with their ability to differentiate into columnar absorptive and mucus-secreting cells. Cancer Res 50, 6334–6343.

Lindmark, T., Schipper, N., Lazorová, L., De Boer, A.G., Artursson, P., 1998. Absorption Enhancement in Intestinal Epithelial Caco-2 Monolayers by Sodium Caprate: Assessment of Molecular Weight Dependence and Demonstration of Transport Routes. Journal of Drug Targeting 5, 215–223. https://doi.org/10.3109/10611869808995876

Liu, W., Hu, D., Huo, H., Zhang, W., Adiliaghdam, F., Morrison, S., Ramirez, J.M., Gul, S.S., Hamarneh, S.R., Hodin, R.A., 2016. Intestinal Alkaline Phosphatase Regulates Tight Junction Protein Levels. Journal of the American College of Surgeons 222, 1009–1017. https://doi.org/10.1016/j.jamcollsurg.2015.12.006

Lü, K.-L., Xie, S.-S., Liu, E., Yu, X.-M., Wang, L., Yang, Z.-Y., Xiong, Q., Luo, X.-G., Yang, W., Liao, W., Zhang, Y.-P., 2020. Age-wise trends in alkaline phosphatase activity in 167,625 Chinese children aged 0–18 years. Clinical Biochemistry 79, 34–40. https://doi.org/10.1016/j.clinbiochem.2020.03.001

Lucas, A., Cole, T.J., 1990. Breast milk and neonatal necrotising enterocolitis. The Lancet 336, 1519–1523. https://doi.org/10.1016/0140-6736(90)93304-8

Macierzanka, A., Mackie, A.R., Bajka, B.H., Rigby, N.M., Nau, F., Dupont, D., 2014. Transport of Particles in Intestinal Mucus under Simulated Infant and Adult Physiological Conditions: Impact of Mucus Structure and Extracellular DNA. PLOS ONE 9, e95274. https://doi.org/10.1371/journal.pone.0095274

Mahalingam, R., Ravivarapu, H., Redkar, S., Li, X., Jasti, B.R., 2007. Transbuccal delivery of 5-Aza-2′-deoxycytidine: Effects of drug concentration, buffer solution, and bile salts on permeation. AAPS PharmSciTech 8, E28–E33. https://doi.org/10.1208/pt0803055

Maher, S., Mrsny, R.J., 2016. Intestinal permeation enhancers for oral peptide delivery. Advanced Drug Delivery Reviews, Oral delivery of peptides 106, 277–319. https://doi.org/10.1016/j.addr.2016.06.005

Marcon, M.A., McCool, D., Forstner, J., Forstner, G., 1990. Inhibition of mucin secretion in a colonic adenocarcinoma cell line by DIDS and potassium channel blockers. Biochimica et Biophysica Acta (BBA) - Molecular Cell Research 1052, 17–23. https://doi.org/10.1016/0167-4889(90)90051-E

Martin, G.P., Marriott, C., Kellaway, I.W., 1978. Direct effect of bile salts and phospholipids on the physical properties of mucus. Gut 19, 103–107. https://doi.org/10.1136/gut.19.2.103

McCool, D.J., Marcon, M.A., Forstner, J.F., Forstner, G.G., 1990. The T84 human colonic adenocarcinoma cell line produces mucin in culture and releases it in response to various secretagogues. Biochemical Journal 267, 491–500. https://doi.org/10.1042/bj2670491

Meaney, C.M., O'Driscoll, C.M., 2000. A comparison of the permeation enhancement potential of simple bile salt and mixed bile salt:fatty acid micellar systems using the CaCo-2 cell culture model. International Journal

of Pharmaceutics 207, 21–30. https://doi.org/10.1016/S0378-5173(00)00526-3

Ménard, S., Cerf-Bensussan, N., Heyman, M., 2010. Multiple facets of intestinal permeability and epithelial handling of dietary antigens. Mucosal Immunology 3, 247–259. https://doi.org/10.1038/mi.2010.5

Michalski, M.C., Briard, V., Michel, F., Tasson, F., Poulain, P., 2005. Size Distribution of Fat Globules in Human Colostrum, Breast Milk, and Infant Formula. Journal of Dairy Science 88, 1927–1940. https://doi.org/10.3168/jds.S0022-0302(05)72868-X

Mukaizawa, F., Taniguchi, K., Miyake, M., Ogawara, K., Odomi, M., Higaki, K., Kimura, T., 2009. Novel oral absorption system containing polyamines and bile salts enhances drug transport via both transcellular and paracellular pathways across Caco-2 cell monolayers. International Journal of Pharmaceutics 367, 103–108. https://doi.org/10.1016/j.ijpharm.2008.09.027

Musa, Md.A., Kabir, M., Hossain, Md.I., Ahmed, E., Siddique, A., Rashid, H., Mahfuz, M., Mondal, D., Ahmed, T., Petri, W.A., Haque, R., 2019. Measurement of intestinal permeability using lactulose and mannitol with conventional five hours and shortened two hours urine collection by two different methods: HPAE-PAD and LC-MSMS. PLoS ONE 14, e0220397. https://doi.org/10.1371/journal.pone.0220397

Noel, G., In, J.G., Lemme-Dumit, J.M., DeVine, L.R., Cole, R.N., Guerrerio, A.L., Campbell, J.D., Kovbasnjuk, O., Pasetti, M.F., 2021. Human Breast Milk Enhances Intestinal Mucosal Barrier Function and Innate Immunity in a Healthy Pediatric Human Enteroid Model. Front. Cell Dev. Biol. 9, 685171. https://doi.org/10.3389/fcell.2021.685171

Otani, T., Furuse, M., 2020. Tight Junction Structure and Function Revisited. Trends in Cell Biology 30, 805–817. https://doi.org/10.1016/j.tcb.2020.08.004

Paone, P., Cani, P.D., 2020. Mucus barrier, mucins and gut microbiota: the expected slimy partners? Gut 69, 2232–2243. https://doi.org/10.1136/gutjnl-2020-322260

Pierce, K.L., Premont, R.T., Lefkowitz, R.J., 2002. Seven-transmembrane receptors. Nat Rev Mol Cell Biol 3, 639–650. https://doi.org/10.1038/nrm908

Raimondi, F., Santoro, P., Barone, M.V., Pappacoda, S., Barretta, M.L., Nanayakkara, M., Apicella, C., Capasso, L., Paludetto, R., 2008. Bile acids modulate tight junction structure and barrier function of Caco-2 monolayers via EGFR activation. American Journal of Physiology-Gastrointestinal and Liver Physiology 294, G906–G913. https://doi.org/10.1152/ajpgi.00043.2007

Ridlon, J.M., Kang, D.-J., Hylemon, P.B., 2006. Bile salt biotransformations by human intestinal bacteria. Journal of Lipid Research 47, 241–259. https://doi.org/10.1194/jlr.R500013-JLR200

Rubas, W., Cromwell, M.E.M., Shahrokh, Z., Villagran, J., Nguyen, T.-N., Wellton, M., Nguyen, T.-H., Mrsny, R.J., 1996. Flux Measurements across Caco-2 Monolayers May Predict Transport in Human Large Intestinal Tissue. Journal of Pharmaceutical Sciences 85, 165–169. https://doi.org/10.1021/js950267+

Sangild, P.T., Ney, D.M., Sigalet, D.L., Vegge, A., Burrin, D., 2014. Animal models of gastrointestinal and liver diseases. Animal models of infant short bowel syndrome: translational relevance and challenges. American Journal of Physiology-Gastrointestinal and Liver Physiology 307, G1147–G1168. https://doi.org/10.1152/ajpgi.00088.2014

Schaap, F.G., Trauner, M., Jansen, P.L.M., 2014. Bile acid receptors as targets for drug development. Nat Rev Gastroenterol Hepatol 11, 55–67. https://doi.org/10.1038/nrgastro.2013.151

Shekels, L.L., Lyftogt, C.T., Ho, S.B., 1996. Bile acid-induced alterations of mucin production in differentiated human colon cancer cell lines. The International Journal of Biochemistry & Cell Biology 28, 193–201. https://doi.org/10.1016/1357-2725(95)00125-5

Sochaczewska, D., Ziętek, M., Dołęgowska, B., Kordek, A., Szczuko, M., 2022. Implications of Indirect Biomarkers of Intestinal Permeability in the Stools of Newborns and Infants with Perinatal Risk Factors for Intestinal Colonization Disorders and Infant Feeding Patterns. Nutrients 14, 2224. https://doi.org/10.3390/nu14112224

Song, K.-H., Chung, S.-J., Shim, C.-K., 2005. Enhanced intestinal absorption of salmon calcitonin (sCT) from proliposomes containing bile salts. Journal of Controlled Release 106, 298–308. https://doi.org/10.1016/j.jconrel.2005.05.016

Su, M.-Y., Broadhurst, M., Liu, C.-P., Gathercole, J., Cheng, W.-L., Qi, X.-Y., Clerens, S., Dyer, J.M., Day, L., Haigh, B., 2017. Comparative analysis of human milk and infant formula derived peptides following in vitro digestion. Food Chemistry 221, 1895–1903. https://doi.org/10.1016/j.foodchem.2016.10.041

Sun, H., Chow, E.C., Liu, S., Du, Y., Pang, K.S., 2008. The Caco-2 cell monolayer: usefulness and limitations. Expert Opinion on Drug Metabolism & Toxicology 4, 395–411. https://doi.org/10.1517/17425255.4.4.395

Toloza, E.M., Diamond, J., 1992. Ontogenetic development of nutrient transporters in rat intestine. American Journal of Physiology-Gastrointestinal and Liver Physiology 263, G593–G604. https://doi.org/10.1152/ajpgi.1992.263.5.G593

Twarog, C., Fattah, S., Heade, J., Maher, S., Fattal, E., Brayden, D.J., 2019. Intestinal Permeation Enhancers for Oral Delivery of Macromolecules: A Comparison between Salcaprozate Sodium (SNAC) and Sodium Caprate (C10). Pharmaceutics 11, 78. https://doi.org/10.3390/pharmaceutics11020078

Twarog, C., Liu, K., O'Brien, P.J., Dawson, K.A., Fattal, E., Illel, B., Brayden, D.J., 2020. A head-to-head Caco-2 assay comparison of the mechanisms of action of the intestinal permeation enhancers: SNAC and sodium caprate (C10). European Journal of Pharmaceutics and Biopharmaceutics 152, 95–107. https://doi.org/10.1016/j.ejpb.2020.04.023

Vergauwen, H., 2015. The IPEC-J2 Cell Line, in: Verhoeckx, K., Cotter, P., López-Expósito, I., Kleiveland, C., Lea, T., Mackie, A., Requena, T., Swiatecka, D., Wichers, H. (Eds.), The Impact of Food Bioactives on Health: In Vitro and Ex Vivo Models. Springer, Cham (CH).

Watson, C.J., Rowland, M., Warhurst, G., 2001. Functional modeling of tight junctions in intestinal cell monolayers using polyethylene glycol oligomers. American Journal of Physiology-Cell Physiology 281, C388–C397. https://doi.org/10.1152/ajpcell.2001.281.2.C388

Weaver, L.T., Laker, M.F., Nelson, R., 1984. Intestinal permeability in the newborn. Arch Dis Child 59, 236–241. https://doi.org/10.1136/adc.59.3.236

Weström, B., Arévalo Sureda, E., Pierzynowska, K., Pierzynowski, S.G., Pérez-Cano, F.-J., 2020. The Immature Gut Barrier and Its Importance in Establishing Immunity in Newborn Mammals. Frontiers in Immunology 11.

Wuyts, B., Riethorst, D., Brouwers, J., Tack, J., Annaert, P., Augustijns, P., 2015. Evaluation of fasted state human intestinal fluid as apical solvent system in the Caco-2 absorption model and comparison with FaSSIF. European Journal of Pharmaceutical Sciences 67, 126–135. https://doi.org/10.1016/j.ejps.2014.11.010

Yasuda, H., Hirata, S., Inoue, K., Mashima, H., Ohnishi, H., Yoshiba, M., 2007. Involvement of membrane-type bile acid receptor M-BAR/TGR5 in bile acid-induced activation of epidermal growth factor receptor and mitogen-activated protein kinases in gastric carcinoma cells. Biochemical and Biophysical Research Communications 354, 154–159. https://doi.org/10.1016/j.bbrc.2006.12.168

Younoszai, M.K., Smith, C., Finch, M.H., 1985. Comparison of In Vitro Jejunal Uptake of L-Valine and L-Lysine in the Rat During Maturation. Journal of Pediatric Gastroenterology and Nutrition 4, 992–997.

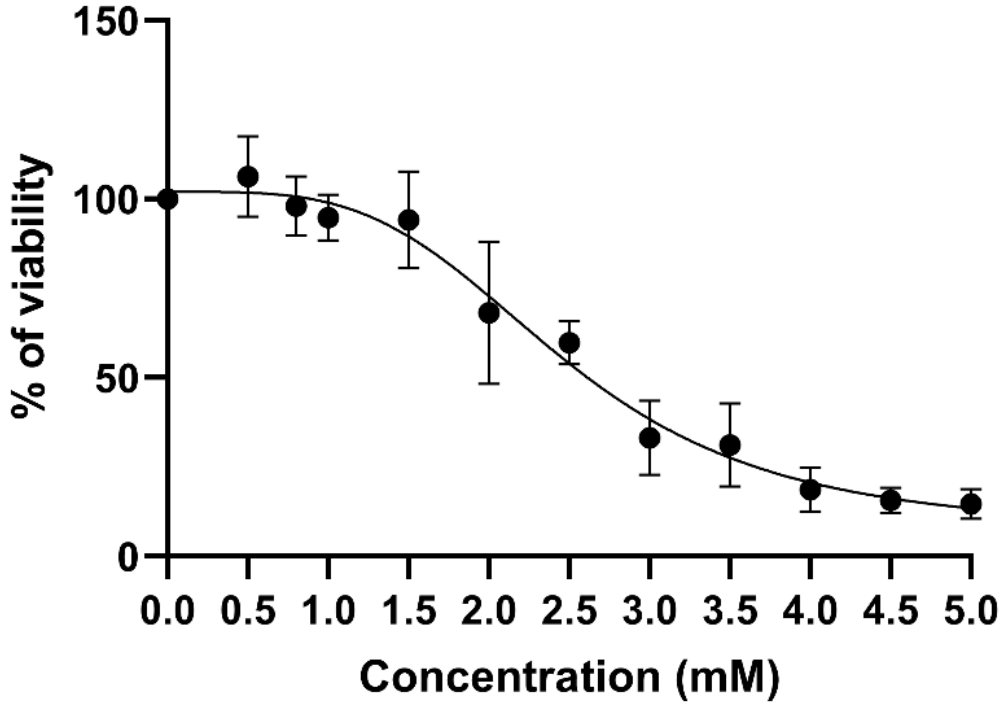
Zeng, H., Safratowich, B.D., Cheng, W.-H., Larson, K.J., Briske-Anderson, M., 2022. Deoxycholic Acid Modulates Cell-Junction Gene Expression and Increases Intestinal Barrier Dysfunction. Molecules 27, 723. https://doi.org/10.3390/molecules27030723

Zhang, K., Dupont, A., Torow, N., Gohde, F., Leschner, S., Lienenklaus, S., Weiss, S., Brinkmann, M.M., Kühnel, M., Hensel, M., Fulde, M., Hornef, M.W., 2014. Age-Dependent Enterocyte Invasion and Microcolony Formation by Salmonella. PLoS Pathog 10, e1004385. https://doi.org/10.1371/journal.ppat.1004385

3.7.Supplementary Materials

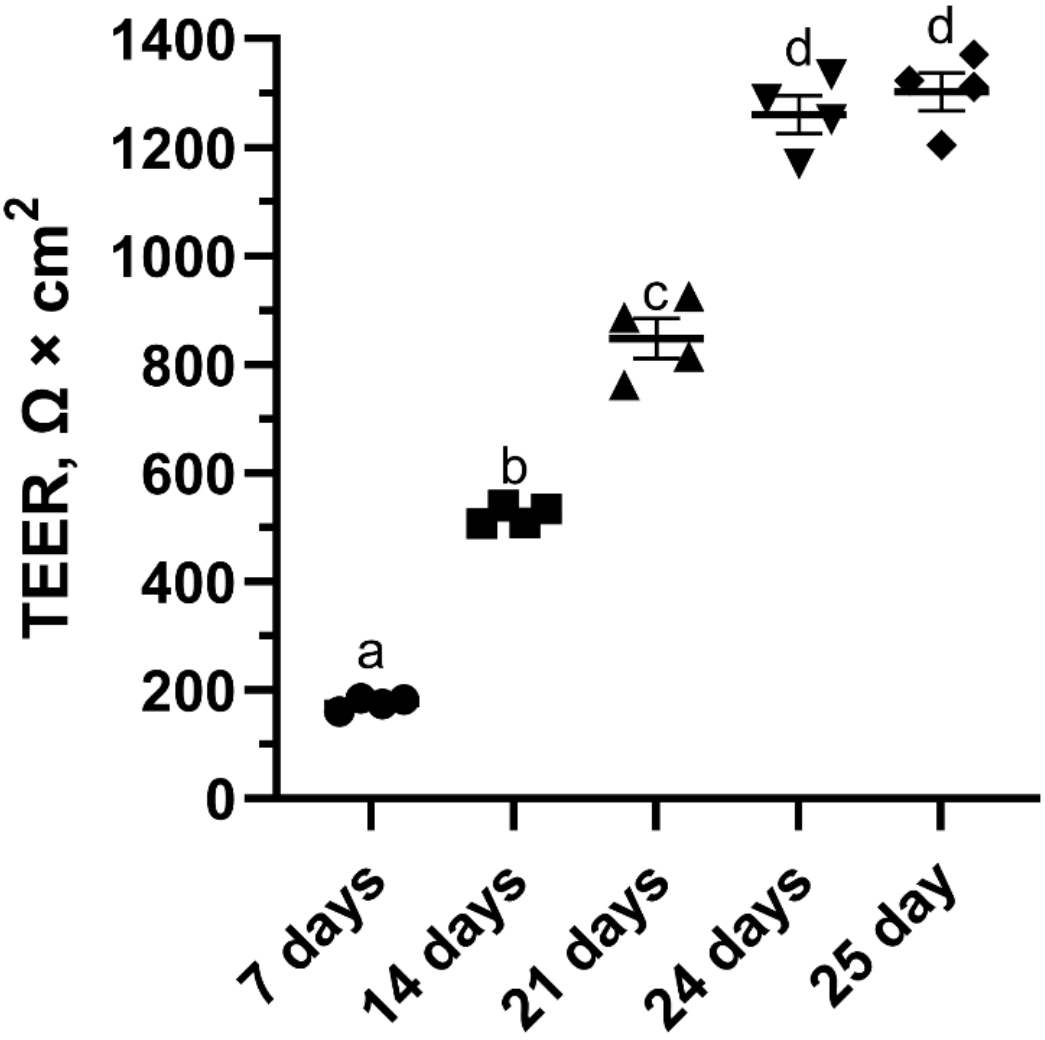
Supplementary Table 3.1 Gene name, protein name, GenBank accession number, primers sequences and annealing temperature (Ta) for RT-PCR analysis.

Gene	Protein	GenBank	Foreword Primer	Reverse Primer	T_a (°C)	Reference
TJP1	Zonulin-1 (ZO1)	NM_003257.4	CATCTCCAGTCCCTTACCTTTC	TCTGCTGGCTTGTTTCTCTAC	57	Kondrashina et al. (2021)
OCLN	Occludin (OCLN)	NM_002538.3	CTGGCCTACAGGAATACAAGAG	TGATGCTCACAGAGGTTTGG	57	Kondrashina et al. (2021)
CLDN2	Claudin-2 (CLDN2)	NM_020384.3	GCTGAGGATAGACTGACTTTGG	GGGAAGCTTGAGAAGTAGGTTAG	57	Kondrashina et al. (2021)
CLDN4	Claudin-4 (CLDN4)	NM_001305.4	CAGGAATCCAGAGAAACTGGTC	CACCGTGAGTCAGGAGATAAAG	60	Kondrashina et al. (2021)
JAM1	Junctional Adhesion Protein-1	AF111713.1	TGTCCTGAATCCCACAACAG	CGGCTATAGGCAAACCAGAT	57	Kondrashina et al. (2021)
RPLP0	Ribosomal Protein Lateral Stalk Subunit P0	NM_001002.4	GCAGCATCTACAACCATGAA	GCAGATGGATCAGCCAAGAA	57	Kondrashina et al. (2021)
MUC1	Mucin-1 (MUC1)	NM_002456.6	CCTACCATCCTATGAGCGAGTAC	GCTGGGTTTGTGTAAGAGAGGC	60	This study
MUC2	Mucin-2 (MUC1)	NM_002457.5	AAGACGGCACCTACCTCG	TTGGAGGAATAAACTGGAGAACC	60	This study
MUC5AC	Mucin 5-AC (MUC5AC)	NM_001304359.2	ACAGCGGTGACTTCGACACA	CCGATGCCTGCTCCCTGTTA	60	This study
CDKN1A	Cyclin-Dependent Kinase Inhibitor 1 (p21)	Not reported	GACACCACTGGAGGGTGACT	CAGGTCCACATGGTCTTCCT	61	(Chen et al., 2012)
TP53	Tumor Protein p53 (p53)	Not reported	GTTCCGAGAGCTGAATGAGG	TGAGTCAGGCCCTTCTGTCT	61	(Chen et al., 2012)



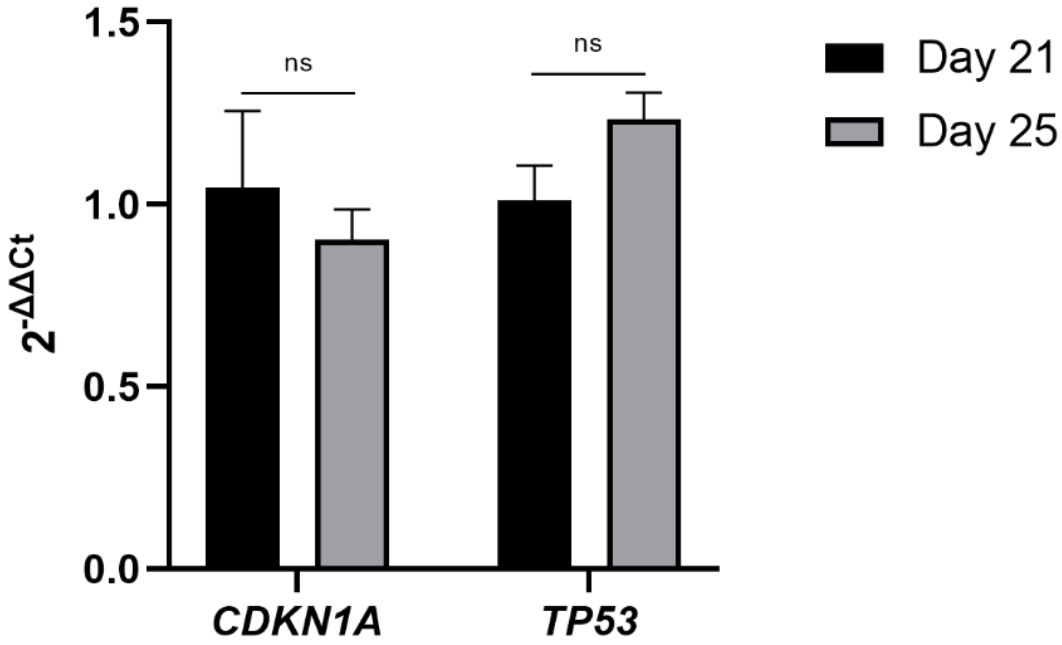
Supplementary Fig 3.1 GDC IC50 on undifferentiated Caco-2/HT29-MTX cells.

Caco-2/ HT29-MTX were seeded at 105 cells/well (90:10) and incubated for 24 h in DMEM D1145. Cells were then treated for 2 h with GDC in DMEM D1145. Cell viability was measured as NADPH dehydrogenase activity (MTS assay). The data are expressed as % untreated cells (0 mM GDC). Results are presented as the average of a biological triplicate and a technical duplicate ± SEM.



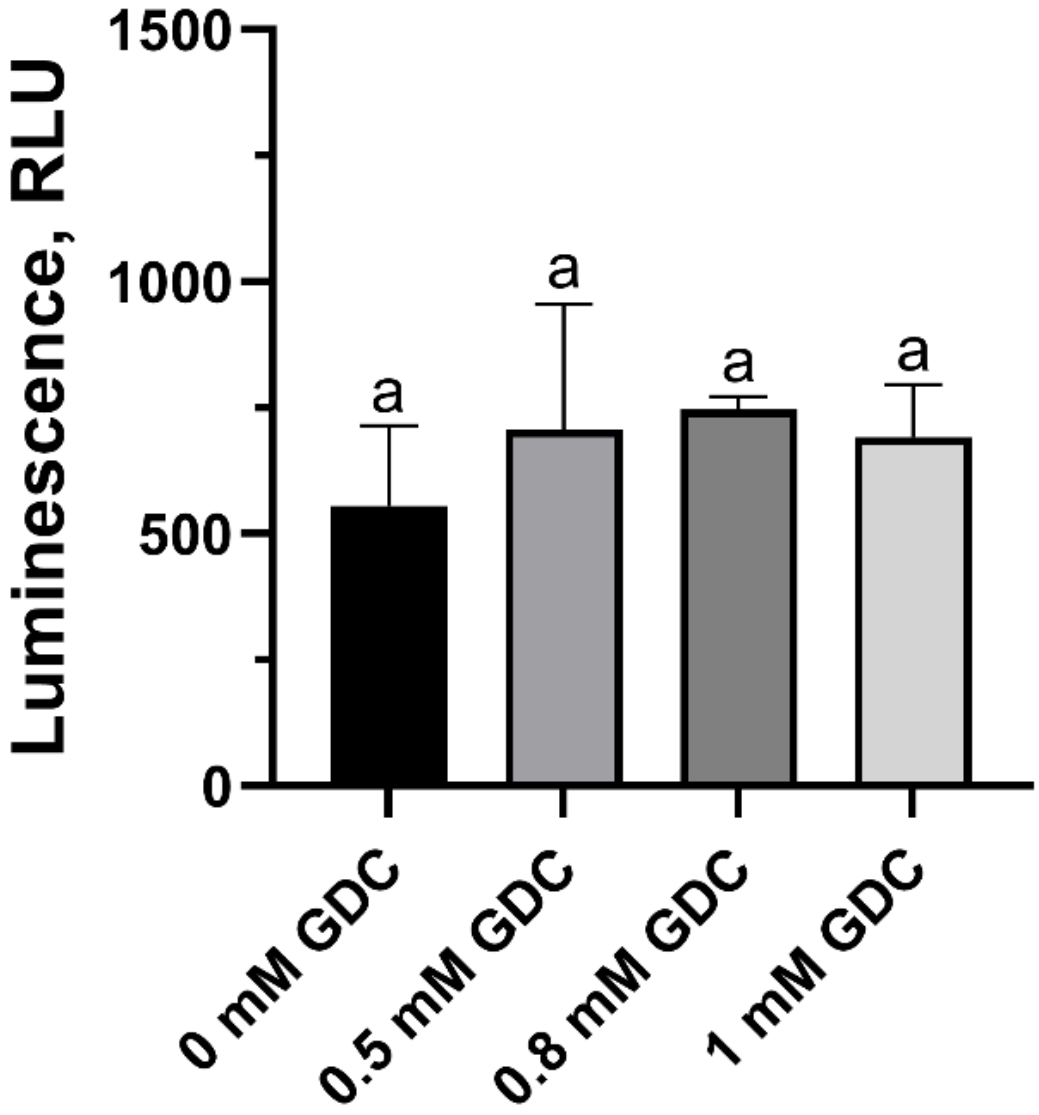
Supplementary Fig 3.2 Trans Epithelial Electrical Resistance (TEER) of the (90:10) Caco-2/HT29-MTX monolayers from day 7 to day 25.

Cells were seeded at a concentration of 6×10^4 cells/ well in a 12-well Transwell plate. Media was changed every two days and 16 h prior to measurement. TEER values were recorded at day 7, 14, 21, 24 and 25 days by Millicell-ERS Voltohmmeter. Mean TEER value at day 25 was 1302.81 ± 70.32 Ω×cm^2. Results are presented as the average of a biological triplicate and a technical duplicate ± SEM. Statistical difference between treatments within a time point was assessed by two-way ANOVA with Tukey multiple comparison and is indicated by a different letter ($P < 0.05$).

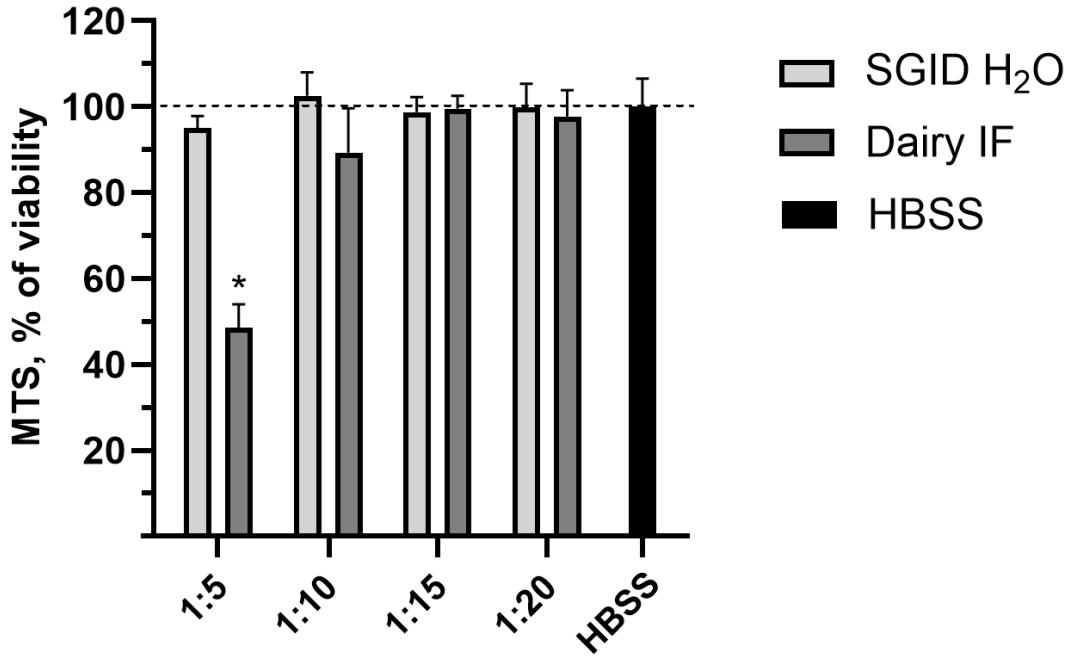


Supplementary Fig 3.3 mRNA expression of p21 and p53 as markers to cellular response to stress.

Caco-2/HT29-MTX monolayers were seeded at a 90:10 ratio and concentration of 6 × 104 cells/ well in a 12-well Transwell plate and cultured for 21 or 25 days. The day prior to the experiment, media was replaced with D1145 and cells were allowed to incubate for approximately 16 hr. Following this, cells were washed with PBS and lysed using RLT buffer. p21 (CDKN1A) and p53 (TP53) mRNA transcript levels in the cell lysate were quantified using RT-PCR and normalized to the housekeeping gene RPLP0 mRNA via the 2-ΔΔCt method. Transcript levels are expressed as the fold change relative to the mean value of day 21. .Data represent the mean ± SEM from biological triplicates and technical duplicates. Statistical analysis was conducted using Student's t-test. ns = non-significant difference ($P < 0.05$).



Supplementary Fig 3.4 Direct inhibition of Protein Kinase A (PKA) by GDC.
GDC solutions (final concentrations = 0.5, 0.8, and 1 mM) were mixed with cAMP (final concentration = 2 µM) in DMEM D1145 + IBMX and incubated with cAMP-Glo™ Assay reagents, including PKA, following the manufacturer instructions. Low cAMP levels signify high PKA activity (increased Relative Light Unit—RLU). Data was generated from a biological triplicate and a technical duplicate ± SEM. Statistical difference in the treatments was assessed by one-way ANOVA with Tukey's multiple comparison and is indicated with different letters ($P < 0.05$).



Supplementary Fig 3.5 MTS viability assay of undifferentiated Caco-2/HT29-MTX after exposure to digesta.

Caco-2/HT29-MTX co-culture (90:10) was seeded at a concentration of 10^5 cells/well in a 96-well plate. After 16 h, cells were treated with IMF (SGID-IMF) or H_2O (SGID H_2O) digesta diluted (1:5, 1:10, 1:15, 1:20) in HBSS for 2 h. Cell viability results are expressed as the mean percentage, with the viability of HBSS-treated cells normalized to 100% (average Abs 490 nm = 0.66 ± 0.017). The mean % of cells in media alone for HBSS-treated cells was 93.79±5.53. SGID IMF = static infant gastrointestinal digestion of Infant milk formula, SGID H_2O = static infant gastrointestinal digestion of water control. Number of biological replicates = 3, technical replicates = 2. Results are mean ± SEM. Asterisk indicates significant difference to HBSS control ($P < 0.05$).

4. Chapter 4

Comparative effects of human milk and infant formulae on peptide transport and epithelial barrier function in infant- and adult-like *in vitro* gut models

Part of this work was carried out during short-term scientific missions at the Institute of Food Science Research (CIAL, CSIC–UAM, Madrid, Spain) under the supervision of Dr. Beatriz Miralles, and at the Institute of Sciences of Food Production (CNR-ISPA, Grugliasco, Italy) under the supervision of Dr. Simona Cirrincione, Dr. Simona Bavaro and Dr. Cristina Lamberti.

A version of this chapter has been published to **Food Research International**: Bietto, F., Cirrincione, S., Gómez-Marín, C., Miralles, B., Romaniello, F., Arranz, E., Lamberti, C., Bavaro, S.L., Cavallarin, L., Rath, E., Lucey, A.J., Giblin, L., 2026. Comparative effects of digested human milk and infant formulas on peptide transport and gut barrier function in infant- and adult-like Caco-2/HT29-MTX models. Food Research International 235, 119071. https://doi.org/10.1016/j.foodres.2026.119071

The published version of this chapter is presented in **Appendix A**.

Abstract

Early postnatal nutrition is critical for gut barrier maturation, yet infant formulae only partially replicate the functional benefits of human milk. Using infant- and adult-like Caco-2/HT29-MTX models, this *in vitro* study compared the effects of gastrointestinal digested human milk, dairy-, soya-, and amino acid–based infant formulae on epithelial barrier integrity and peptide transport. Barrier function was assessed by transepithelial electrical resistance and occludin–actin colocalization, while amino acid and peptide transport were profiled by UHPLC-HRMS/MS operated in data-dependent acquisition mode.

In the infant-like model, human milk uniquely enhanced occludin–actin co-localization ($P < 0.05$) and increased the abundance of basolateral bioactive peptides. Amino acid–based infant formula increased occludin fluorescence intensity ($P < 0.05$) in infant-like monolayers but reduced TEER ($P < 0.05$) in adult-like monolayers. For all digested foods, peptide transport and diversity were significantly greater in infant-like than in adult-like monolayers ($P < 0.05$), with human milk promoting the highest basolateral peptide load.

These findings demonstrate that infant-specific epithelial models reveal unique effects of human milk on tight junction architecture and peptide bioavailability, which is not captured in adult-like systems. This study highlights the need for age-appropriate *in vitro* digestion protocols coupled with gut barrier models, when evaluating the functional properties of foods for infants.

Keywords: human milk; infant formula; infant intestinal barrier; digestion; occludin; amino acid (AA); peptides; Caco-2/HT29-MTX, INFOGEST

4.1.Introduction

Human milk is the gold standard of human infant nutrition, offering not only complete nourishment but also bioactive compounds that support health and development of the infant (Brockway et al., 2024). In the intestinal tract of the infant, human milk plays a critical role in promoting gut barrier integrity (Carr et al., 2021), reducing paracellular permeability (Catassi et al., 1995), and shaping the intestinal microbiome (Bode, 2012; Pannaraj et al., 2017).

The infant gut barrier is characterized by high permeability during early development. In several domestic species (e.g., calves, piglets, lambs), the neonatal small intestine can absorb intact colostral immunoglobulins, predominantly IgG, thereby establishing systemic passive immunity (Weström et al., 2020). In the human, systemic passive immunity is acquired primarily before birth through active FcRn-mediated transplacental transfer of maternal IgG (Atyeo and Alter, 2021). Nevertheless, the human neonatal gut barrier remains highly permeable in early infancy with significantly higher lactulose permeability (Kosek et al., 2017) and a higher lactulose-to-mannitol ratio than adults, indicating predominance of paracellular over transcellular transport pathways (Johnston et al., 2000; Musa et al., 2019; Weaver et al., 1984). These permeability traits are linked to lower expression of tight junction proteins (e.g., Occludin- OCLN, Zonulin-1- ZO1, Tight Junction Protein 1- TJP1) and higher levels of the permeability-enhancing claudin-2 (CLDN2) in early life Intestinal barrier maturation, as reflected by decreasing permeability, continues for up to 15 months after birth in human infants (Kosek et al., 2017). Human milk, promotes this maturation process, as observed by L:M experiments (Catassi et al., 1995). The World Health Organization recommends exclusive breast feeding in the first 6 months of life (World Health Organization., 2014). However,

the choice to breastfeed is deeply personal and can be shaped by a variety of factors (Blum, 1999). Infant formula (IF) can be used as an alternative or supplement for the first 12 months of life (UNICEF., 2003). Dairy-based IF is the most widely used. Soya-based IF offers a plant-based alternative, whereas highly hydrolysed and aminoacid (AA)-based IF are designed for infants with severe protein allergies or gastrointestinal disorders (Martin et al., 2016). Although nutritionally similar to human milk, IFs do not replicate the health benefits of human milk on the gut barrier, particularly in promoting gut maturation, integrity, and reducing the risk of necrotizing enterocolitis (Colaizy et al., 2016; Lucas and Cole, 1990; Quigley et al., 2024).

The Codex Alimentarius (CXS 72-1981), established by FAO/WHO, sets international standards for composition, safety, and labelling of IF products (Codex Alimentarius Commission., 1981). In the EU, Regulation (EU) 2016/127 governs IF, mandating detailed compositional criteria (European Commission, 2016), including adequate protein or AAs, to meet the requirements for growth and development. During digestion, proteins are broken down into peptides and free AAs (Korhonen and Pihlanto, 2006). While free AAs are absorbed directly via specific transporters (Bröer, 2008), small peptides are taken up either via peptide transporters or by paracellular diffusion (Hevia et al., 2023b). Many of these peptides can exert bioactive effects on the gut barrier (Dold et al., 2025; Korhonen and Pihlanto, 2006). Moreover, a recent systematic review also confirms that milk-derived proteins and peptides can be detected in the bloodstream of human infants post-ingestion, supporting their potential for systemic bioactivity (Biondi Ryan et al., 2025)

To study nutrient digestion in the infant gut, the Ménard et al. protocol offers an *in vitro* static gastrointestinal digestion method to track digestion under infant

conditions (Ménard et al., 2018). Recent studies with this protocol have demonstrated comparable overall protein digestibility between human milk and dairy IF, as assessed by free amino acid release, molecular weight distribution and peptidomic analysis (Komatsu et al., 2024; Sánchez-Hernández et al., 2021). Polarized Caco-2/HT29-MTX monolayers are a well-established *in vitro* model of the adult gut barrier (Kleiveland, 2015). Absorption of peptides from human milk and IF has been evaluated using Caco-2 monolayers following *in vitro* digestion of these matrices (Bavaro et al., 2021; Liang et al., 2022). Although few studies have evaluated the effects of human milk–derived peptides on Caco-2/HT29-MTX monolayers´ gut barrier properties, peptides released from IF during digestion increased mRNA transcripts of mucins within these monolayers (Dold et al., 2025). The substantial differences between the infant and adult gut barrier in terms of permeability warrant an age-appropriate transient model to simulate gut maturation and nutrient uptake from human milk and from the various IFs. However, *in vitro* gut barrier models for this life stage remain scarce. Current models, including cell lines (Sun et al., 2008; Vergauwen, 2015), enteroids (Noel et al., 2021), and animal models (Sangild et al., 2014), are constrained by physiological, ethical, or scalability limitations. In our previous work (Bietto et al., 2025), we developed a reversible gut barrier model by treating Caco-2/HT29-MTX monolayers with 0.8 mM sodium glycodeoxycholate (GDC). These monolayers mirrored key aspects of the *in vivo* infant barrier with significantly reduced barrier integrity, altered OCLN localization, and increased paracellular permeability without inflammation or toxicity. Notably, treating these monolayers with digested dairy IF led to enhanced basolateral AA transport compared to adult-like monolayers (Bietto et al., 2025).

The objective of this *in vitro* study was to compare human milk to dairy IF, soya IF and AA IF, using infant-like models of gastrointestinal digestion and gut barrier function. Specifically, we aimed (i) to evaluate the effects of these foods on barrier maturation by tracking OCLN localization in infant- and adult-like Caco-2/HT29-MTX monolayers and (ii) to quantify free AAs and identify individual dietary peptides in the basolateral chambers of these monolayers.

4.2.Materials and Methods

4.2.1. Materials

Dairy-based, soya-based IF and AA-based IF were shop-bought. Human milk samples were collected from six healthy lactating women approved by the ethics committee of the Hospital Universitario Virgen de las Nieves (Granada, Spain) and registered on ClinicalTrials.gov (accessed 15 April 2019; NCT02811172). Mature milk (≥17 days postpartum) from each donor was pooled to create a composite sample. Rabbit gastric extract 15 (RGE 15; lot no. 1201) was obtained from Lipolyltech. Bicinchoninic acid assay (BCA) kit was purchased from Pierce® (Ireland). XT MES Running Buffer, Precision Plus Protein™ Unstained Standard were sourced from Bio-Rad. AccQ-Tag Ultra Derivatization Kit, Ultra AA Analysis Column, and AA Hydrolysate Standard were purchased from Waters® (MA, USA). Transwell inserts with polyester permeable membranes were obtained from Sarstedt Group (Germany). CellTiter 96® AQueous One Solution Cell Proliferation Assay was supplied by Promega. Rabbit anti-Occludin (Sigma-Aldrich), Alexa Fluor 488 Donkey anti-Rabbit (A-21206), Alexa Fluor 555 Phalloidin (A-34055), DAPI (268298), and ProLong™ Glass Antifade Mountant (P36980) were supplied by Thermo Fisher Scientific (MA, USA). Strata C18-E SPE Solid Phase Extraction and

Luna C18 column were purchased from Phenomenex (Torrance, USA). Human intestinal epithelial cell lines Caco-2 (EACC 86010202) and HT29-MTX-E12 (EACC 12040401) were purchased from the European Collection of Cell Culture (UK). All other reagents were purchased from Sigma-Aldrich, unless otherwise stated.

4.2.2. Simulated static infant gastrointestinal digestion (SGID)

IFs were reconstituted following the manufacturer's instructions. For dairy and soya IF, 4.3 g of powder was dissolved in 30 mL MilliQ water; while for AA IF, 4.5 g of powder was dissolved in 30 mL MilliQ water. Human milk samples were thawed at 4°C. Crude protein content was determined in duplicate using the Kjeldahl method (FOSS Scrubber 2501 / Kjeltec Sampler 8420 / Kjeltec 8400) on freeze-dried samples. Crude protein was calculated using the standard factor (N × 6.25). Simulated gastrointestinal digestion (SGID) was performed as per Ménard et al. 2018 protocol (Ménard et al., 2018). An oral phase was not included. Initially, 5 mL reconstituted IF or human milk was mixed with 2.94 mL infant simulated gastric fluids containing 268 U/mL RGE 15 (pepsin activity determined in-house = 596 U/mg). Milli-Q water (5 mL) subjected to the same digestion conditions served as negative control. The pH was brought to 5.3 with 1 M HCl. Samples were incubated for 1 h at 37°C in a shaking incubator (100 rpm). To stop the gastric phase, pH was increased to 7 with 1M NaOH. For the intestinal phase, 4.88 mL of simulated intestinal fluids containing 16 U/mL pancreatin (lot no. SLCM8903; trypsin activity determined in-house = 8.9 U/mg) and 3.1 mM bovine bile (lot no. SLBV1780; concentration of bile salts = 440 g/mol) were added to the gastric phase. The pH was decreased to 6.6 with 1 M HCl. The samples were incubated again for 1 h at 37°C in

a shaking incubator. Digestion was then stopped by adding the protease inhibitor, 4-(2-aminoethyl) benzene sulfonyl fluoride hydrochloride, dissolved in MilliQ water at a final concentration of 1 mM, along with Orlistat dissolved in ethanol at a final concentration of 0.1 mM. The digesta were aliquoted and stored at -20 °C until use. Samples were collected at 3 time points; before the gastric phase (G0), at the end of the gastric phase (G60), and at the end of the intestinal phase (I60). Each food was digested on 3 separate occasions (n=3).

4.2.3. SDS-PAGE

Digested (G0, G60, and I60) and undigested IF and human milk, were analyzed using SDS-PAGE with 12% Bis-tris–polyacrylamide gels (Criterion XT, Bio-Rad, Hercules, California, USA). Protein content was determined by bicinchoninic acid assay (BCA) kit, following the manufacturer's instructions. Dairy, soya, and human milk samples were diluted at a protein concentration of 0.8 mg/mL in loading buffer and heated at 95 °C for 5 min. The loading buffer was 0.05 M Tris-HCL pH 6.8, SDS 1.6% w:v, glycerol 8% w:w, Bromophenol blue 0.002% w:v, β-mercaptoethanol 2% v:v. AA IF was diluted using the same factor as the dairy and soya IF to ensure consistency across conditions (undigested sample = 1:10.25; G0 = 1:12.33; G60 = 1:9, and I60 = 1:3.44). SGID H_2O was loaded undiluted. Precision Plus Protein™ Unstained Standards (15 µL) was loaded as the M_w standard. Electrophoresis was performed at 150 V for 60 min with XT MES running buffer, and gels were stained overnight with InstantBlue™ solution followed by de-staining with Milli-Q water.

4.2.4. Total nitrogen content by o-phthaldialdehyde (OPA) assay

The degree of protein hydrolysis was measured through the concentration of free NH_2 groups, determined by the o-phthaldialdehyde (OPA) assay (Nielsen et al., 2001). The G0, G60, and I60 samples were defrosted on ice, precipitated with 5% trichloroacetic acid (0.5 mL sample in 0.83 mL TCA) and centrifuged for 30 min at 1000 g. The supernatants were then diluted 1:1 (dairy, soya IF and human milk G0 and G60), 1:4 (I60) or 1:9 (AA IF G0, G60) in 0.1 mol/L borate solution. The OPA reagent was prepared with 0.1 mol/L borate, 10% SDS, 40 g/L OPA in ethanol and 200 g/L N-Acetyl-L-Methionine Ethyl Ester. Samples (8 µL) were transferred into a UV 96-well plate and incubated for 10 min at 30°C in the dark with 232 µL OPA solution. Absorbance at 340 nm was measured using a microplate reader (PowerWave XS, BioTek Instruments, Winooski, Vermont, USA). A standard curve of glutamic acid (0-8 mmol/L) was used for quantification. Hydrolysis % was calculated as follows:

Hydrolysis (%) = 100 - [(mmol NH_2 G0 / mmol NH_2 I0) × 100]

4.2.5. Size Exclusion Chromatography (SEC)

Digesta samples (I60) were first clarified by centrifugation at 10,000 × g for 10 min at 4 °C. The resulting supernatant was diluted 1:1 and filtered through a 0.22 µm nylon syringe filter. A 20 µL aliquot was injected into two TSKgel columns connected in series (TSKgel G2000SW, 7.5 mm × 30 cm; TSKgel G2000SWXL, 7.8 mm × 30 cm) with a TSKgel SW guard column (7.5 mm × 7.5 cm) upstream. SEC was performed on a Waters HPLC system (Waters 2695 separation module) equipped with a Waters 2487 dual-wavelength absorbance detector set to 214 nm. Separation was achieved by isocratic elution at 0.7 mL/min for 55 min, using a

mobile phase of 0.1 M phosphate buffer (pH 6.7) containing 0.1 M Na_2SO_4 and 10% (v/v) methanol.

Molecular-size calibration was carried out by applying the same conditions to a series of standards spanning the protein–peptide range: bovine serum albumin (67 kDa), equine carbonic anhydrase (29 kDa), β-lactoglobulin (18.4 kDa), α-lactalbumin (14.4 kDa), cytochrome c (12.4 kDa), bacitracin (1.4 kDa), H-Tyr-Leu-OH (0.29 kDa) and phenylalanine (0.17 kDa). Retention times of these standards were plotted against the logarithm of their molecular weights to generate a calibration curve, which was then used to estimate the size distribution of analytes present in the digesta samples.

4.2.6. Free and total AAs analysis in the digested samples

Digested samples (I60) were defrosted on ice, and methanol was added for a final concentration of 80% to precipitate proteins (5 mL final volume). Each sample was centrifuged for 30 min at 1000 g. The supernatant (220 µL) was subjected to SpeedVac evaporation (SC200, Savant) to eliminate methanol. To quantify free AA, the pellet was re-suspended in 500 µL 0.1 mM HCl. To quantify total AA, the pellet was hydrolysed in 6 M HCl for 15 h at 110°C in a glass vial. Cys (10 and 1 mmol/L) was also hydrolysed to quantify the derivative forms (Cys2). An internal standard of 25 mM (final concentration) Norvaline was added to the samples prior to hydrolysis. All samples were derivatized using the AccQ-Tag Ultra Derivatization Kit following the manufacturer's instructions. Briefly, the samples were neutralized, filtered with a 0.2 µm nylon filter, mixed with 70 µL AccQ•Tag Ultra Borate Buffer and 20 µL AccQ•Tag Ultra reagent, and incubated at 55ºC for 10 min. The derivatized samples were separated using ACQUITY Ultra Performance UPLC® (Waters Corporation,

USA) with a tunable ultraviolet/visible (TUV) detector with a flow cell. Separation was performed with AccQ•Tag Ultra AA Analysis Column (Eluent 1 = AccQ•Tag Ultra Eluent A, Eluent 2= AccQ•Tag Ultra Eluent B; flow rate = 0.7 mL/min; injection volume = 1 μL). The quantification was performed based on a standard three-point curve (AA Hydrolysate Standard). The Empower software (version 3.7.0, Waters Corporation) was used to acquire, process, report and manage chromatographic information.

4.2.7. Cell Culture

Caco-2 and HT29-MTX cell lines were cultured in 75-cm^2 tissue culture flasks maintained at 37°C, 5% CO_2, in a humidified atmosphere. Following thawing, the cells underwent three passages before use. 'Complete DMEM' media consisted of Dulbecco's Modified Eagle Medium (DMEM, D5796) supplemented with 10% heat-inactivated fetal bovine serum (FBS, F7524), 100 U/mL Penicillin-Streptomycin (P4333) and 2.5 μg/mL amphotericin B (A2942). Additionally, for HT29-MTX cells and for co-culture monolayers, 1% MEM Non-essential AA Solution (M7145) was added to complete DMEM. Passaging of the cells occurred at 80% confluence every 4-5 days using 0.25% Trypsin-EDTA solution (T4049). After trypsinization, cells were stained with trypan blue and counted with the TC20 cell counter (Bio-Rad, USA). Cells were used between passage numbers 21-25 for Caco-2, and 64-68 for HT29-MTX cells.

4.2.8. MTS Assay

Digesta samples (I60) were defrosted on ice, diluted in HBSS (1:4, 1:9, 1:14, 1:19), filter sterilized (0.2 μm syringe filter) and warmed up at 37°C. Caco-2/HT29-MTX

were seeded in a 96-well plate (Corning® CellBIND®) at a concentration of 5 x 10^4 cells/well and incubated for 24 h. Cells were then washed twice with HBSS and incubated for 2 h with diluted digested samples (150 µL). After the incubation period, the digesta was removed cells were washed twice with HBSS and incubated for 1 h at 37°C with the MTS reagent (100 µL), diluted 1:10 in HBSS following the CellTiter 96® AQueous One Solution Cell Proliferation Assay kit instructions. Absorbance was read at 490 nm in a multi-plate reader (BioTek Cytation 5 multimode reader) and the viability was calculated as a % of the control cells (cells incubated with HBSS only). Viability of control cells was >88% of cells cultured in complete DMEM.

4.2.9. Caco-2/HT29-MTX monolayers exposure to GDC and digesta

A 90:10 ratio (Caco-2:HT29-MTX) was seeded in the apical chamber (500 µL) of 12-well plates containing polyester permeable-membrane inserts (Sarstedt Group), reaching a final density of 6×10^4 cells/well. The basolateral chamber received 1.5 mL of complete DMEM with 1% MEM Non-essential AA. The culture medium was refreshed every two days. Transepithelial electrical resistance (TEER) was monitored weekly using a Millicell-ERS Voltohmmeter (Merck Millipore, USA), with background TEER values obtained from Transwells without cells. Following our protocol (Bietto et al., 2025), monolayers were washed twice on day 24 and incubated with serum-free DMEM D1145 for 16 h. Only monolayers exhibiting TEER values >800 $\Omega \times cm^2$ were selected for experiments (Bietto et al., 2025). Monolayers were washed with HBSS and pre-equilibrated in DMEM D1145 (0.4 mL apical, 1.5 mL basolateral) for 30 min at 37 °C. To create the infant-like barrier, monolayers were incubated for 2 h at 37 °C with GDC (0.8 mM). Firstly, GDC (4

mM) was freshly prepared and sterile-filtered in DMEM D1145. A volume of 100 µL was added to the apical compartment with 400 µL DMEM. TEER values were recorded at 0 and 2 h. Control 'adult-like' monolayers were treated with DMEM D1145 during the same timeframe. Following treatment, monolayers were washed twice and incubated with HBSS (0.4 mL apical, 1.5 mL basolateral) for 15 min at 37 °C for acclimatization. Digested IF and human milk samples were thawed on ice, diluted 1:2 in HBSS, sterile-filtered (0.2 µm PES syringe filters), and prewarmed to 37 °C. Subsequently, 100 µL sample was added to the apical chamber, achieving a final ratio of 1:14. TEER values were recorded before and after the 2 h incubation period. Apical and basolateral media were collected after the incubation period (T2-apical, T2-basolateral) and stored at –20 °C for subsequent AA and peptide analysis. Monolayers were fixed for immunofluorescence and confocal microscopy.

4.2.10. Immunofluorescence and confocal microscopy

Monolayers were washed twice with PBS and fixed for 30 min at room temperature by adding 500 µL 75% ethanol (prepared in PBS) into the apical chamber. Monolayers were then washed twice with PBS and kept at 4 °C in PBS until use (max 1 week). Monolayers were permeabilized with 75% acetone in PBS for 3 min at room temperature, washed and incubated for 30 min at room temperature with blocking solution (1% BSA in PBS). The primary antibody (Rabbit anti-Occludin, Sigma Aldrich) was added (1:149 dilution) in blocking solution (150 µL) and incubated overnight at 4°C. Fixed monolayers were washed twice with PBS. Then, secondary antibody (A-21206, Alexafluor 488 Donkey anti-rabbit, Thermo Fisher Scientific;1:499 dilution) plus actin binder, phalloidin 555 (bindso F-actin, A-34055,

Alexa Fluor 555 Phalloidin, Thermo Fisher Scientific; 1:499 dilution), was added in the blocking solution (150 µL). Monolayers were incubated for 1 h in the dark at room temperature, washed three times with PBS and incubated with DAPI (268298, Merk; 1:4999 dilution in MilliQ water) for 2 min, in the dark at room temperature to stain cell nuclei. The permeable supports of the Transwell plates were excised with a scalpel and mounted on a microscopy glass slide with 40 µL of mounting media (ProLong™ Glass Antifade Mountant).

Samples were imaged using STED and FALCON (FLIM) coupled to an inverted DMi8 microscope (Leica Microsystems, Germany) equipped with a white light laser (440-790 nm). The objective used was Plan-Apochsomat 63x/1.4 Oil DIC N2. Pinhole size was set to 85.6 nm. Images were captured through Power HyD S detectors (Leica) with a pixel size of 0.7 µm for the Z dimension and 0.18 µm for the X and Y dimensions. Alexa Fluor 488 acquisition parameters were: 512- 542 nm (emission range), 0.4 µs (dwell time), 3.9 (gain), and 56.89 % (laser intensity). Alexa Fluor 555 acquisition parameters were: 565- 605 (emission range), 0.4µs (dwell time), 35.5 (gain), and 68.10 % (laser intensity). DAPI acquisition parameters were: 450-490 nm (emission range), 0.4 µs (dwell time), 5 (gain), and 14.67 % (laser intensity) Line average of 2 was applied to every channel.

Fiji/ImageJ software was used to determine OCLN fluorescence intensity, number of nuclei, colocalization with actin, orthogonal view, and monolayer thickness. Intensity threshold was determined with the Otsu algorithm for intensity quantification. The colocalization between OCLN (Alexa 488) and actin (Alexa 555) was calculated with JACoP Fiji/ImageJ plugin with a threshold set to 7000 for the Alexa 488 and 8000 for Alexa 555. For each test sample, 3 slides and 3 pictures per slide were analyzed.

4.2.11. Free AAs transported in the basolateral side

Free AAs were quantified in the digesta and T2-basolateral compartment using an untargeted UHPLC-HRMS method optimized for hydrophilic compounds. The separation was performed using a Thermo Vanquish Flex UHPLC system with a Thermo Accucore™ Amide-HILIC column (150 × 2.1 mm, 2.6 µm particle size) maintained at 30 °C. Sample (1 µL) was injected and separated under a flow rate of 400 µL/min using a binary gradient composed of solvent A (H_2O with 10% ammonium formate, 20 mM, pH 2.8) and solvent B (ACN with 10% ammonium formate, 20 mM, pH 2.8). The gradient started at 0% A and ramped to 60% A over 22 min, followed by re-equilibration back to initial conditions for a total run time of 45 min.

UHPLC was coupled to a high-resolution Orbitrap mass spectrometer (Q Exactive Plus, Thermo Fisher Scientific) via a Heated Electrospray Ionization (H-ESI) source. Full MS data were acquired in positive ionization mode with the following parameters: spray voltage 2.80 kV, capillary temperature 150°C, sheath gas 35 AU, auxiliary gas 10 AU, sweep gas 1 AU, and auxiliary gas heater temperature 150°C. The S-Lens RF level was set to 50.0. Full MS scans were acquired at a resolution of 70,000, with an AGC target of 3.0e6 and maximum injection time of 100 ms, across an m/z range of 65–250. Data-dependent MS/MS (dd-MS^2) was performed using an isolation window of 2 m/z, resolution 17,500, collision energy of 20 eV, AGC target of 5.0×10^4, and maximum IT of 50 ms, with an intensity threshold of 4.0×10^4. Quantification of AAs was based on external calibration curves generated at 7 concentration levels ranging from 0.5 to 80 mg/L. Isotopically labelled internal

standards were used at 10 mg/L, and the peak areas of each analyte were normalized to its corresponding internal standard.

4.2.12. Peptide Profiling by UHPLC-HRMS/MS

Sample Preparation for UHPLC-HRMS/MS

Peptides from digesta, T2-apical and T2-basolateral compartments were purified using solid-phase extraction (SPE) with C18 cartridges. For digesta samples, the digesta was prepared by diluting 1:2 Milli-Q water and filtered using 0.2 µm PES syringe filter. A further 1:4 dilution in Milli-Q water was performed to achieve 1:14 dilution used in cell exposure studies. A 483 µL aliquot was then processed using C18 SPE and reconstituted in 120 µL Milli-Q H_2O. For T2-apical samples, 2 technical replicates were pooled (1.0 mL total). A 483 µL aliquot was purified using C18 SPE. The eluate was dried and reconstituted in 120 µL Milli-Q H_2O. For T2-basolateral samples, 1.5 mL from each of 2 technical replicates (3.0 mL total) were pooled. A 2.9 mL aliquot was subjected to C18 SPE. After peptide elution and drying, the sample was reconstituted in 12 µL of Milli-Q water. All samples were stored at –20 °C until analysis. A 10 µL injection was used for UHPLC-HRMS/MS analysis.

UHPLC-HRMS/MS analysis

Peptide analysis was performed using an Orbitrap Q Exactive Plus mass spectrometer (Thermo Fisher Scientific) coupled to a Vanquish Flex UHPLC binary pump system. Separation was achieved on a Luna C18 reversed-phase column (150 × 1 mm, 3 µm of particle size). The mobile phases consisted of 0.1% (v/v) formic acid in Milli-Q water (solvent A) and 0.1 % (v/v) formic acid in 30% acetonitrile 70% methanol (solvent B), delivered at a flow rate of 70.0 µL/min. The elution

gradient was programmed to increase solvent B from 3% to 50%, over 80 min and with 70% in 5 min, and 100% in 1 min, for 5 min, and after reconditioned at 3% of B for 15 min. The injection volume was 2.0 µL. Column temperature was maintained at 55 °C, and the autosampler was set at 4 °C to preserve sample integrity.

UHPLC was coupled to a high-resolution mass spectrometer via a H-ESI source. Full MS data were acquired in positive ionization mode with the following parameters: spray voltage 3.50 kV, capillary temperature 350 °C, sheath gas 35 AU, auxiliary gas 10 AU, sweep gas 1 AU, and auxiliary gas heater temperature 250 °C. The S-Lens RF level was set to 50.0

Mass spectra were acquired in data-dependent acquisition mode (Full MS-ddMS^2). Full scan spectra were recorded over an *m/z* range of 250–1500 with a resolution of 70,000, an AGC (automatic gain control) target of 3×10^6, and a maximum injection time of 200 ms. Up to 6 of the most intense ions in MS1 were selected for fragmentation in the MS/MS mode. The fragmentation spectra resolution was set at 17,500, with a dynamic exclusion of 10 s and an isolation window of 2.0 m/z, the normalized collision energy was set at 28 (eV), the maximum IT at 110 ms and the AGC target at 1x105.

4.2.13. Peptide identification

Raw LC-MS/MS data were processed using MaxQuant (v2.6.6.0) (Cox, Jürgen and Mann, 2008) with an unspecific digestion mode and a minimum peptide length of 2 AAs, suitable for naturally occurring peptides. The main search mass tolerance was set to 4.5 ppm for precursors and 20 ppm for fragment ions. Variable modifications included oxidation (M), acetylation (protein N-term), phosphorylation (STY), and pyro-glutamate formation (Q/E). No fixed modifications or enzyme constraints were

applied. The "second peptide" and "match between runs" features were enabled, with a match time window of 0.7 min. Label-free quantification (LFQ) was enabled with an LFQ minimum ratio count of 2 and stabilization of large ratios. Intensity normalization was based on FastLFQ.

Database searches were performed against custom UniProtKB FASTA files corresponding to Bos taurus (dairy, 402 entries), Glycine max (soy, 109 entries) or Homo sapiens (human milk, 1142 entries) and a manually added contaminants FASTA file (124 entries), retaining only reviewed sequences. Decoy sequences were automatically generated for FDR estimation using the revert mode. Peptide-spectrum match (PSM), peptide, and protein FDR thresholds were each set to 1%. Additional filtering required a minimum Andromeda score of 40 for modified peptides and a minimum delta score of 6. All MS/MS data were searched using Andromeda, with up to 15 candidate matches per spectrum and deisotoping enabled.

4.2.14. Bioinformatics analysis

Raw and annotated peptide data from MaxQuant output files (evidence.txt, peptides.txt) were post-processed using Python (v3.10) (Python Software Foundation, n.d.) within a Google Colab (Google Research, n.d.) environment. Data manipulation and filtering were conducted using the pandas (v1.5.3) (McKinney, 2010) and numpy (v1.23.5) (Harris et al., 2020) libraries. Peptides were retained only if they had at least one MS/MS count, belonged to a single protein group, and showed non-zero intensity in ≥2 biological replicates per condition. Peptides identified in T2-apical and T2-basolateral compartments were further filtered to ensure their source protein was also detected in the corresponding digesta dataset. Reverse hits and known contaminants were excluded from all analyses.

Shared and unique peptides were identified using set-based comparisons and classified as follows: peptides detected in only one compartment were labeled "compartment-unique," while those in both were "shared." Within each compartment-unique set, we further classified by age group: "exclusive" label was used for those peptides that were present in only one age group (Infant or Adult), whereas "shared" when peptides were present in both. Overlaps were visualized via Venn diagrams using matplotlib-venn (Tretyakov, 2012). For count-based statistics, per-peptide PSM counts across Infant and Adult were subjected to equal-variance t-tests. For intensity-based analysis, raw intensities were $\log_2$-transformed then imputed from a left-shifted normal distribution (mean = μ–1.8σ, σ = 0.3·global σ); per-peptide $\log_2$ means and Welch's t-tests were computed on the imputed data. A parallel workflow was applied to modified peptides (grouped by Sequence + Modification). Significantly enriched peptides ($P < 0.05$) were annotated by source protein and mapped across compartments.

To assess peptide transformation by brush border enzymes, apical-only peptides were analyzed using a classification pipeline. A breadth-first search matched them to longer digesta-derived precursors based on cleavage motifs: Dipeptidyl peptidase-4 /8/9: N-terminal dipeptides, X–P/A; Aminopeptidase N: N-terminal single residues, L/I/V/M/A; Aminopeptidase A: N-terminal E/D; Aminopeptidase B: N-terminal R/K; Enteropeptidase: N-terminal D/E/R/K; Carboxypeptidase A: C-terminal F/L/I/W/Y/V/M; Carboxypeptidase B: C-terminal R/K; Dipeptidyl carboxypeptidase: C-terminal dipeptides, G/S/D; Tripeptidyl peptidase II: N-terminal tripeptides.

Bioactivity annotation was conducted via cross-referencing with BIOPEP (Minkiewicz et al., 2019), the Milk Bioactive Peptide Database (MBPD) (Nielsen et

al., 2017), and PeptideRanker (Mooney et al., 2012) (score threshold ≥ 0.5). Volcano plots were generated using scikit-learn (v1.2.2) (Pedregosa, 2011), matplotlib (Hunter, 2007), and seaborn (Waskom, 2021) for dimensionality reduction and visual inspection of condition-driven separation.

All outputs were exported using xlsxwriter (McNamara, 2023), and the entire pipeline was modular, script-based, and reproducible.

4.2.15. Statistical analysis

All experiments were conducted in triplicates or quadruplicates across three separate days, each with technical duplicates or triplicates. Results are expressed as means ± SEM. Statistical analyses for cellular and functional assays were performed using GraphPad Prism 10.4.2 (GraphPad Software, USA), employing two-way ANOVA with Tukey's or Dunnett's multiple comparison test, as appropriate. Statistical significance was defined as $P < 0.05$.

For peptidomic data, statistical analysis was conducted in Python (v3.10) using Welch's t-test via the scipy.stats module (Virtanen, 2020). Peptide-level comparisons were based on $\log_2$-transformed intensity values across conditions, and peptides with $P < 0.05$ were considered significantly differentially enriched.

4.3. Results

4.3.1. IF and human milk exhibit similar protein hydrolysis with differences in molecular size distribution and amino acid profiles

Human milk and 3 commercially available IFs (dairy, soya and AA-based) were subjected to static gastrointestinal digestion adapted to the infant gut (Ménard et al., 2018). Prior to digestion, crude protein content determined by Kjeldahl was 9.41%

for dairy IF, 13.25% for soya IF, 14.16% for AA IF (expressed as protein equivalents from free AAs) and 10.11% for human milk. To mimic consumption of these liquid foods *in vivo*, protein content was not standardised before digestion. However, no significant differences in total protein content were found between dairy IF, soya IF and human milk, at the end of the intestinal phase (3556 ± 314.4 µg/mL, BCA assay, $P < 0.05$, Supplementary Fig. 4.1A).

SDS-PAGE revealed distinct digestion patterns. Dairy IF and human milk showed progressive loss of intact proteins such as caseins and α-lactalbumin, with human milk preserving lactoferrin (Supplementary Fig. 4.1B). Soya IF displayed a diffuse smear indicative of extensive hydrolysis and AA IF showed no bands, consistent with its composition of free AAs (Supplementary Fig. 4.1B).

OPA assay confirmed progressive proteolysis across all samples, with similar degrees of hydrolysis (~82–85%) in dairy IF, soya IF and human milk. AA IF showed higher initial free NH_2 due to its formulation, decreasing upon dilution during digestion (Fig. 4.1A).

Size exclusion chromatography at I60 timepoint (after gastric and intestinal digestion) revealed that digested AA IF consisted almost entirely of <0.5 kDa molecules (88%), while dairy IF, soya IF, and human milk revealed that the majority (90%) of compounds were <5kDa in size. Human milk uniquely retained a small fraction (>5%) of >50 kDa proteins, suggestive of digestion-resistant proteins (Fig. 4.1B).

To evaluate the nutritional quality of digested proteins, the concentrations of total hydrolyzed (Fig. 4.1C) and free (Fig. 4.1D) AAs in the bioaccessible fraction of the digesta (I60) were quantified and grouped as branched-chain AAs (BCAAs), essential AAs (EAAs), and non-essential AAs (NEAAs).

Among digested dairy IF, soya IF, and human milk, total AA concentrations ranged from 357,060.6 ± 4180.8 µmol/L (human milk) to 430,180.2 ± 10,823.3 µmol/L (soya IF), with dairy IF at 394,794.6 ± 8488.2 µmol/L. Digested soya IF had significantly higher total AA content compared to digested human milk ($P < 0.05$). In digested dairy IF, soya IF and human milk, NEAAs represented the majority of the total pool. EAAs ($P > 0.05$) and BCAA ($P > 0.05$) were similar across these digested samples.

Glutamic acid was the most abundant AA in dairy IF (51,845.7 ± 1325.9 µmol/L), soya IF (62,339.6 ± 14,38.66 µmol/L; $P < 0.05$) and human milk at I60 timepoint (50,277.0 ± 699.0 µmol/L) (Fig. 4.1C and Supplementary Table 4.1). Digested dairy IF had the highest leucine (39,956.1 ± 11,45.6 µmol/L; $P < 0.05$) and lysine content (29,784.0 ± 573.34 µmol/L; $P< 0.05$). Soya IF had the highest arginine (24,264.6 ± 735.9 µmol/L; $P< 0.05$), glycine (50,334.3 ± 656.4 µmol/L; $P< 0.05$), serine (27,974.4 ± 905.7 µmol/L; $P< 0.05$) and aspartic acid content (41,279.4 ± 10,33.28 µmol/L; $P< 0.05$). Digested human milk contained the highest concentration of proline (32,463.9 ± 514.1 µmol/L; $P< 0.05$) (Fig. 4.1C and Supplementary Table 4.1).

Total free AA values were not significantly different among digested dairy IF (80,016.3 ± 8284.9 µmol/L), soya IF (88,309.6 ± 4960.9 µmol/L) and human milk (88,140.1 ± 5478.3 µmol/L; $P > 0.05$). Free EAAs and BCAA were similar in digested dairy IF, soya IF, and human milk ($P > 0.05$) (Fig. 4.1D).

Notably, digested soya IF showed significantly higher free arginine compared to dairy IF and human milk (20,914.9 ± 1024.6 µmol/L, $P < 0.05$), while digested human milk had significantly more free glutamic acid (7542.4 ± 588.1 µmol/L) than

both dairy IF (2642.8 ± 367.2 μmol/L) and soya IF (2699.9 ± 155.0 μmol/L, $P < 0.05$) (Fig. 4.1D and Supplementary Table 4.2).

Digested AA IF had significantly higher concentrations of AAs across all categories ($P < 0.05$) (Fig. 4.1 and Supplementary Table 4.1 and 4.2). Total AAs were 610,221.0 ± 13,721.7 μmol/L, with NEAAs and EAA at 214,226. ± 3,090.7 μmol/L and 14,2834.5 ± 1,135.39 μmol/L respectively, exceeding all other samples. Free AAs were equally elevated (343,283.8 ± 27,830.0 μmol/L), with glycine, leucine, and arginine ranking as the top three free residues (Supplementary Table 4.2).

The total AA content and free AA content of SGID H_2O control were 99,888.9 ± 14,587.4 μmol/L and 25,382.0 ± 8797.2 μmol/L, respectively, indicating minimum AA contribution from digestive enzyme autolysis. In summary, human milk and infant formulae showed similar overall hydrolysis but differed in molecular size distribution and amino acid composition, reflecting matrix-specific digestion patterns.

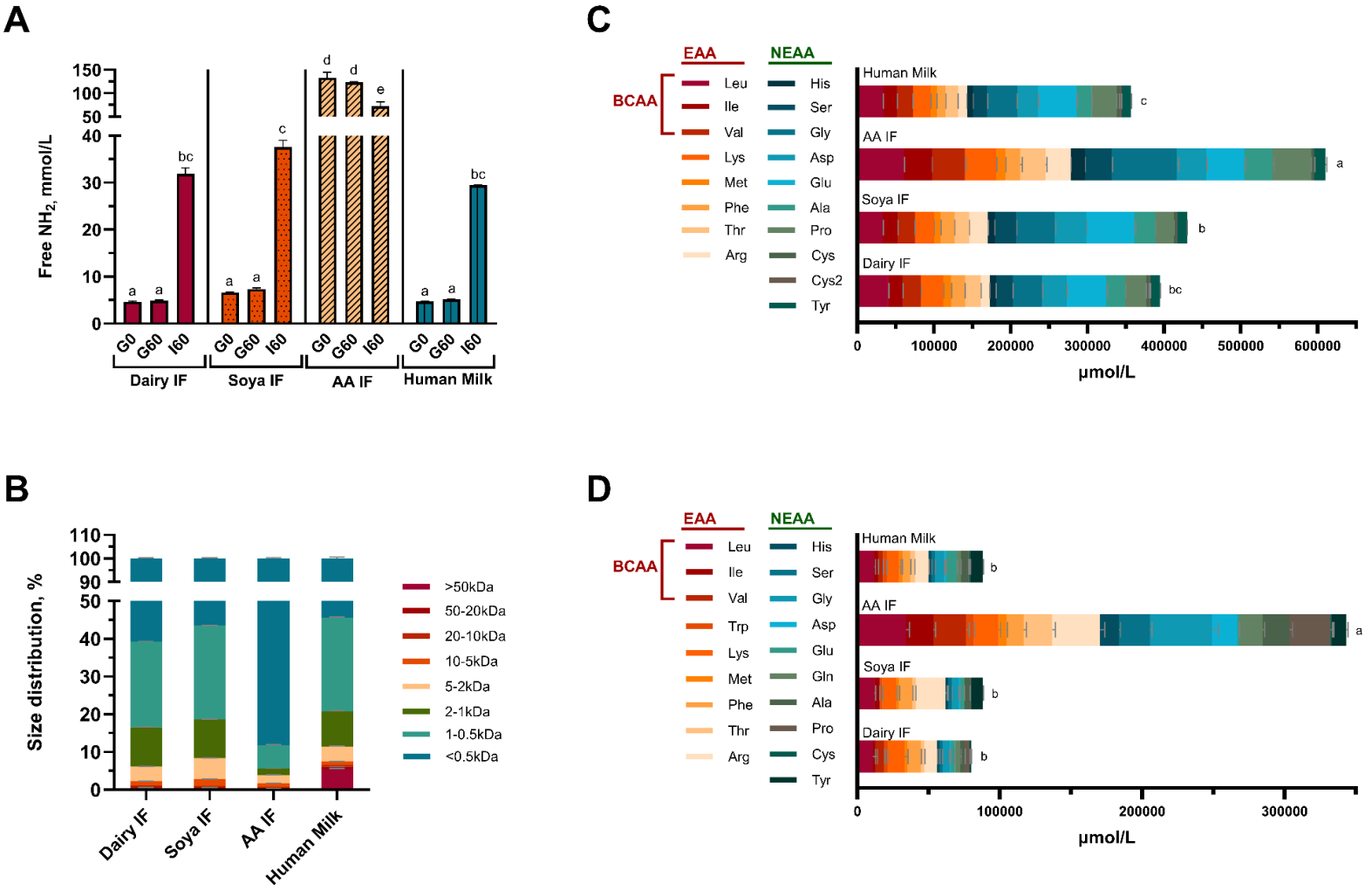

A
Free NH2, mmol/L
150
100
50
40
30
20
10
0
a
a
bc
a
a
c
d
d
e
a
a
bc
G0
G60
I60
Dairy IF
Soya IF
AA IF
Human Milk
B
Size distribution, %
110
100
90
50
40
30
20
10
0
Dairy IF
Soya IF
AA IF
Human Milk
>50kDa
50-20kDa
20-10kDa
10-5kDa
5-2kDa
2-1kDa
1-0.5kDa
<0.5kDa
C
EAA
NEAA
BCAA
Leu
Ile
Val
Lys
Met
Phe
Thr
Arg
His
Ser
Gly
Asp
Glu
Ala
Pro
Cys
Cys2
Tyr
Human Milk
AA IF
Soya IF
Dairy IF
c
a
b
bc
0
100000
200000
300000
400000
500000
600000
µmol/L
D
EAA
NEAA
BCAA
Leu
Ile
Val
Trp
Lys
Met
Phe
Thr
Arg
His
Ser
Gly
Asp
Glu
Gln
Ala
Pro
Cys
Tyr
Human Milk
AA IF
Soya IF
Dairy IF
b
a
b
b
0
100000
200000
300000
µmol/L

Fig. 4.1 Infant gastrointestinal digestion of Dairy, Soya and amino acid-based (AA) infant formulae (IF) and human milk.

(A) Degree of protein hydrolysis, assessed by OPA, at G0 (before gastric phase), G60 (after gastric phase) and I60 (after intestinal phase) timepoints. (B) Size exclusion chromatography of the soluble fraction at I60 timepoint. (C) I60 digesta Total amino acids, quantified by UPLC. (D) I60 digesta free amino acids quantified by UPLC. Data represent mean values from three independent digestions performed on separate days. Statistical analysis was performed using one-way ANOVA followed by Tukey's multiple comparisons test (A-C), or (D) Welch's one-way ANOVA followed by pairwise comparisons with Benjamini–Hochberg false discovery rate (FDR) correction. Different letters indicate statistically significant differences ($P < 0.05$). Amino acids are color-coded as follows: red = branched-chain amino acids (BCAA), red + orange = essential amino acids (EAA), blue/green = non-essential amino acids (NEAA).

4.3.2. Digested IF and human milk maintain infant-like barrier integrity

To assess the impact of digested IF and human milk on intestinal barrier integrity, an infant-like epithelial monolayer was treated with digested samples. For comparison purposese Caco-2/HT29 monolayers were included, representing an adult barrier (Hidalgo et al., 1989).

Initially, MTS assay was employed to determine the appropriate dilution to ensure biocompatibility of the digested samples with Caco-2/HT29-MTX co-cultures (Supplementary Fig. 4.3). Dilutions ≥1:14 of dairy IF, soya IF, AA IF, and human milk did not significantly affect cell viability compared to the SGID H_2O control ($P > 0.05$), whereas dilutions ≤1:9 resulted in a significant decrease in viability ($P < 0.05$). Therefore, 1:14 was selected as the highest non-toxic concentration for subsequent experiments.

To create an infant-like barrier, day 25 Caco-2/HT29-MTX monolayers were treated with 0.8 mM GDC, leading to the expected and significant reduction in TEER (Bietto et al., 2025) from 1165 ± 11.85 Ω × cm^2 to 412.15 ± 18.98 Ω × cm^2 (experiment baseline TEER) (Fig. 4.2A). Following 2 h exposure to digesta (T2), infant-like cultures maintained stable TEER values regardless of milk formulation (Fig. 4.2A; $P > 0.05$).

At baseline (T0), adult-like monolayers had a TEER value of 1010.90 ± 96.96 Ω × cm^2. No significant TEER reduction was observed in adult-like monolayers with the digested dairy IF, soya IF or human milk samples for 2 h (T2) ($P > 0.05$). Treatment with digested AA IF resulted in a significant drop in TEER in adult like monolayers (Fig. 4.2B; $P < 0.05$).

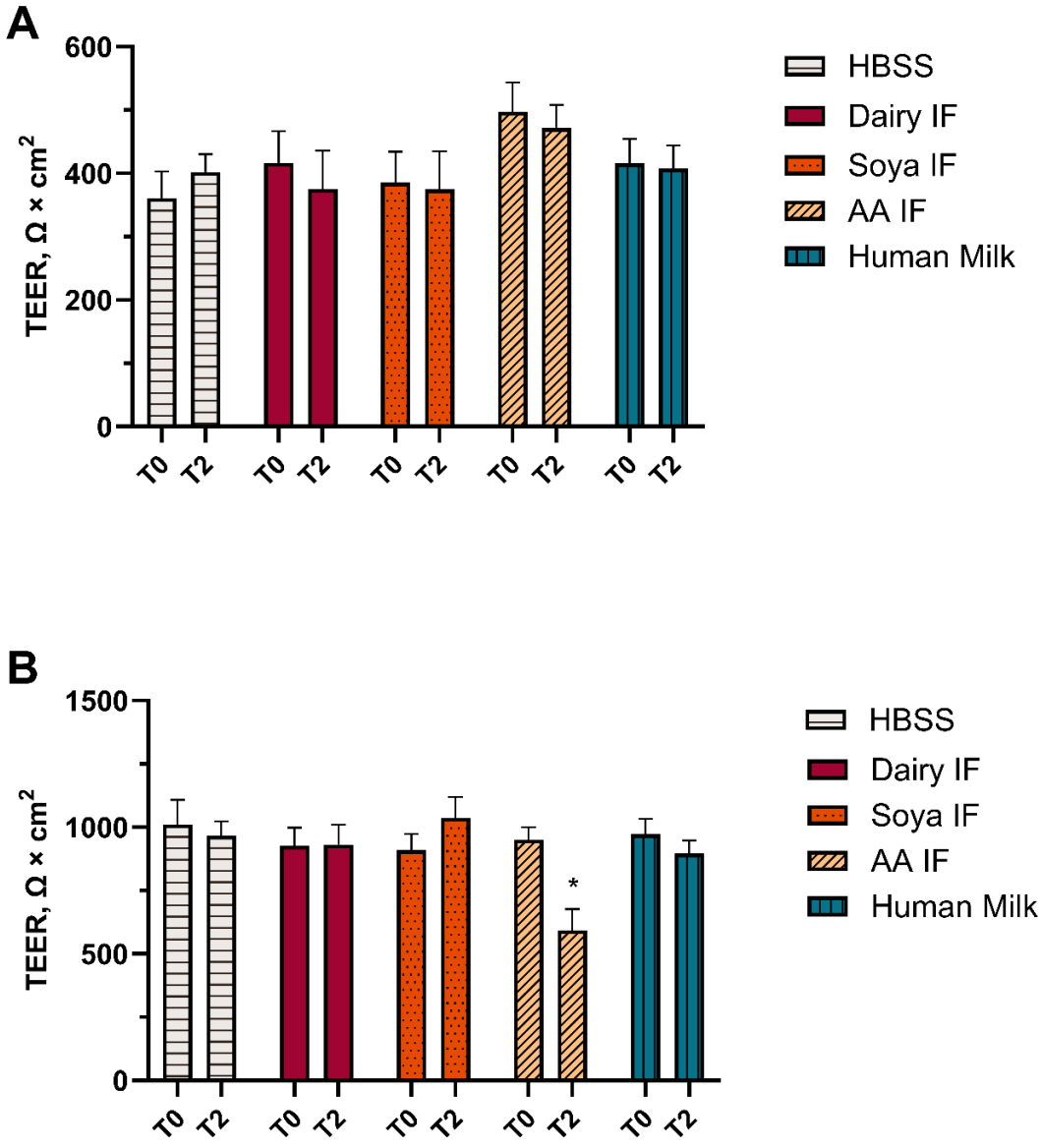


Fig. 4.2 Transepithelial electrical resistance (TEER) of Caco-2/HT29-MTX monolayers treated with digested infant formulae (IF) or Human Milk.

(A) Infant-like and (B) adult-like monolayers (90:10) were exposed for 2 h to digested Dairy IF, Soya IF, amino acid-based (AA) IF, and Human Milk (1:15 in HBSS). TEER at day 25 = 1165 ± 11.85 Ω × cm². T0 = Before digesta addiction; T2 = post-treatment. Data are mean ± SEM from six biological replicates (three digestions × two exposures × duplicate wells; n = 12). One-way ANOVA with Tukey's test; *P < 0.05 vs. HBSS.

4.3.3. Digested human milk enhances OCLN–actin co-localization in infant-like monolayers

To investigate whether exposure to digested IF or human milk promotes gut barrier maturation, tight junction protein OCLN was labelled in Caco-2/HT29-MTX co-cultures under infant- and adult-like conditions after 2 h treatment. OCLN localization was assessed by fluorescence intensity normalized to nuclei count (Fig. 4.3, Supplementary Fig. 4.4). Its spatial relationship with the actin cytoskeleton was evaluated through co-localization analysis (Fig. 4.4).

Infant-like monolayers treated with digested human milk exhibited a distinct pattern of OCLN distribution, characterized by focal accumulation of OCLN at cell junctions, visible as dot-like structures (Fig. 4.3A, white arrows), which were not present in adult monolayers. In the adult-like model, treatment with either digesta of dairy IF, AA IF or human milk resulted in lower OCLN intensity compared to soya IF ($P < 0.05$). Digested AA IF significantly increased OCLN fluorescence intensity in infant-like monolayers, compared to digested dairy IF ($P < 0.05$).

When comparing infant- vs. adult-like conditions within each treatment, baseline OCLN fluorescence under HBSS control was significantly lower in infant-like monolayers (120,127 ± 9,556) than in adult-like monolayers (201,627 ± 2,397; $P < 0.05$, Fig. 4.3B). Soya IF treatment induced significantly higher OCLN intensity in adult-like monolayers compared to intensity in the infant-like model ($P < 0.05$).

To further examine the interaction between OCLN and the actin cytoskeleton, Pearson's and Manders' co-localization coefficients were calculated for OCLN and actin signals (Fig. 4.4). Pearson's coefficient, which indicates overall spatial correlation, was significantly increased by digested human milk on infant-like monolayers compared to the infant HBSS control (0.32 ± 0.02 vs. 0.37 ± 0.01; $P <$

0.05, Fig. 4.4A). In contrast, both soya IF and human milk significantly reduced Pearson's coefficient in the adult-like model relative to HBSS ($P < 0.05$).

When comparing across developmental models, HBSS-treated infant monolayers exhibited a significantly lower Pearson's coefficient than adult monolayers (0.27 ± 0.02 vs. 0.40 ± 0.01; $P < 0.05$). Interestingly, both soya IF and human milk significantly increased this coefficient in the infant-like model compared to their adult counterparts ($P < 0.05$), suggesting increased alignment between OCLN and actin under infant conditions.

These findings were supported by Manders' coefficient M1, which reflects the fraction of OCLN signal overlapping with actin. M1 was increased in infant-like monolayers treated with soya IF compared to HBSS control ($P < 0.05$, Fig. 4.4B). In the adult model, M1 was significantly reduced following exposure of monolayers to dairy IF and human milk compared to HBSS control ($P<0.05$, Fig. 4.4B). Among all treatments, HBSS-treated infant monolayers displayed significantly lower M1 values than adults (0.33 ± 0.03 vs. 0.65 ± 0.04; $P < 0.05$, Fig.4B).

M2 (fraction of actin overlapping OCLN) was less biologically informative, as actin is broadly distributed and its overlap with OCLN does not specifically reflect tight junction structure. Nevertheless, M2 was significantly reduced in soya and AA IF groups for infant and dairy and AA IF for adult compared to HBSS (infant coefficient = 0.14 ± 0.03; adult coefficent = 0.25 ± 0.04, $P < 0.05$). No significant difference was found in M2 for adult and infant monolayer with HBSS treatment.

Interestingly, orthogonal views of z-stack images revealed a significant increase in monolayer thickness, reflective of greater cell height, in our infant-like model with HBSS treatment versus the standard Caco-2/HT29-MTX monolayer with HBSS (13.54 ± 0.34 μm vs. 12.12 ± 0.41 μm; $P < 0.05$) (Supplementary Fig. 4.4).

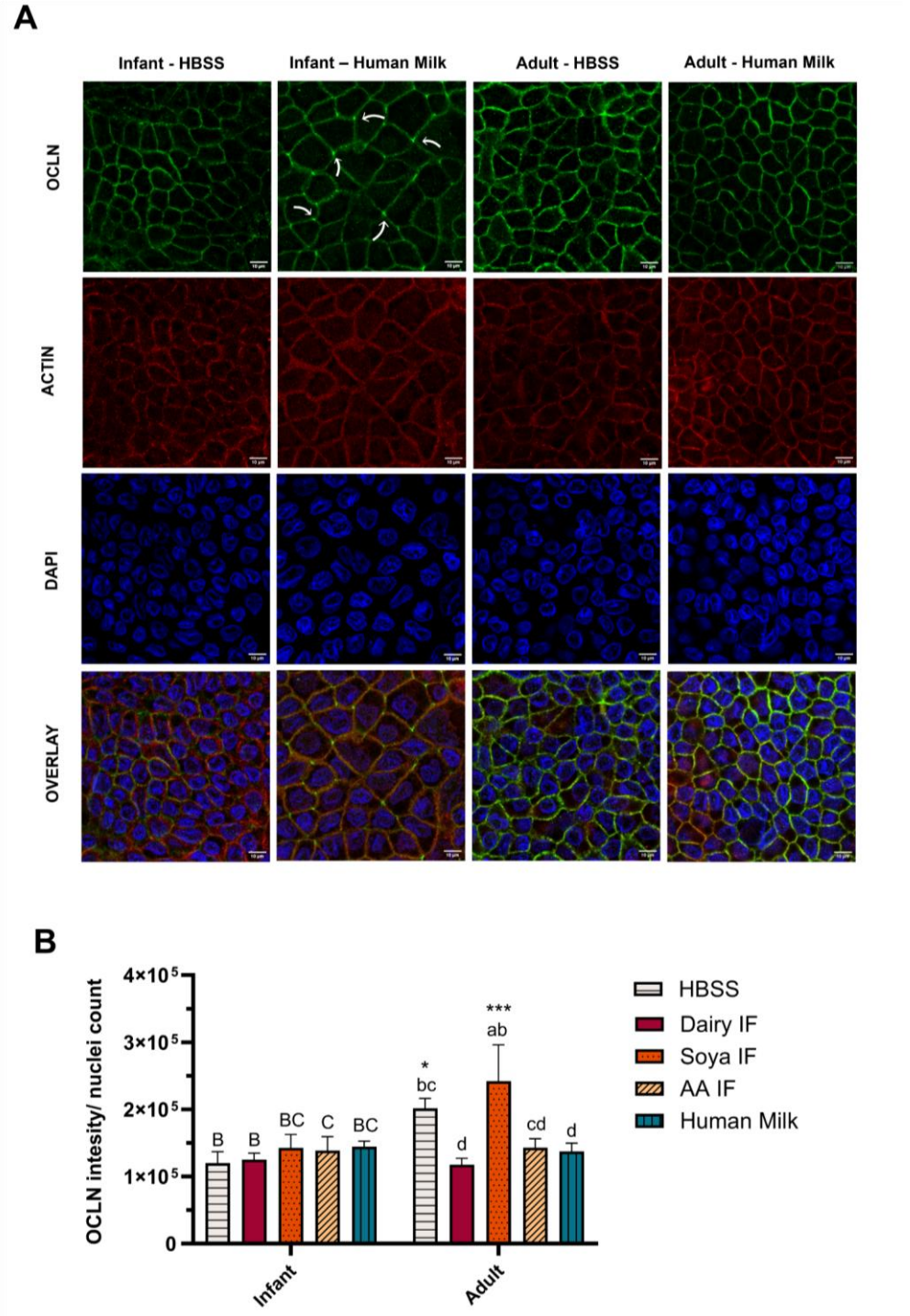


Fig. 4.3 Occludin (OCLN) localization in infant and adult-like Caco-2/HT29-MTX monolayers treated with digested Human Milk.

Monolayers (90:10) were cultured for 25 days and treated for 2 h with HBSS (control) or digested Human Milk. (A) Representative confocal images showing OCLN (green), actin (red), and nuclei (blue); white arrows highlight membrane OCLN with Human Milk. Scale = 10 µm. (B) OCLN fluorescence intensity normalized to nuclei count. Data are mean ± SEM from three biological replicates (n = 9). One-way ANOVA with Tukey's test: different letters indicate significant differences within infant (uppercase) or adult (lowercase) models; asterisks indicate significant differences between infant and adult models within the same treatment ($P < 0.05$).

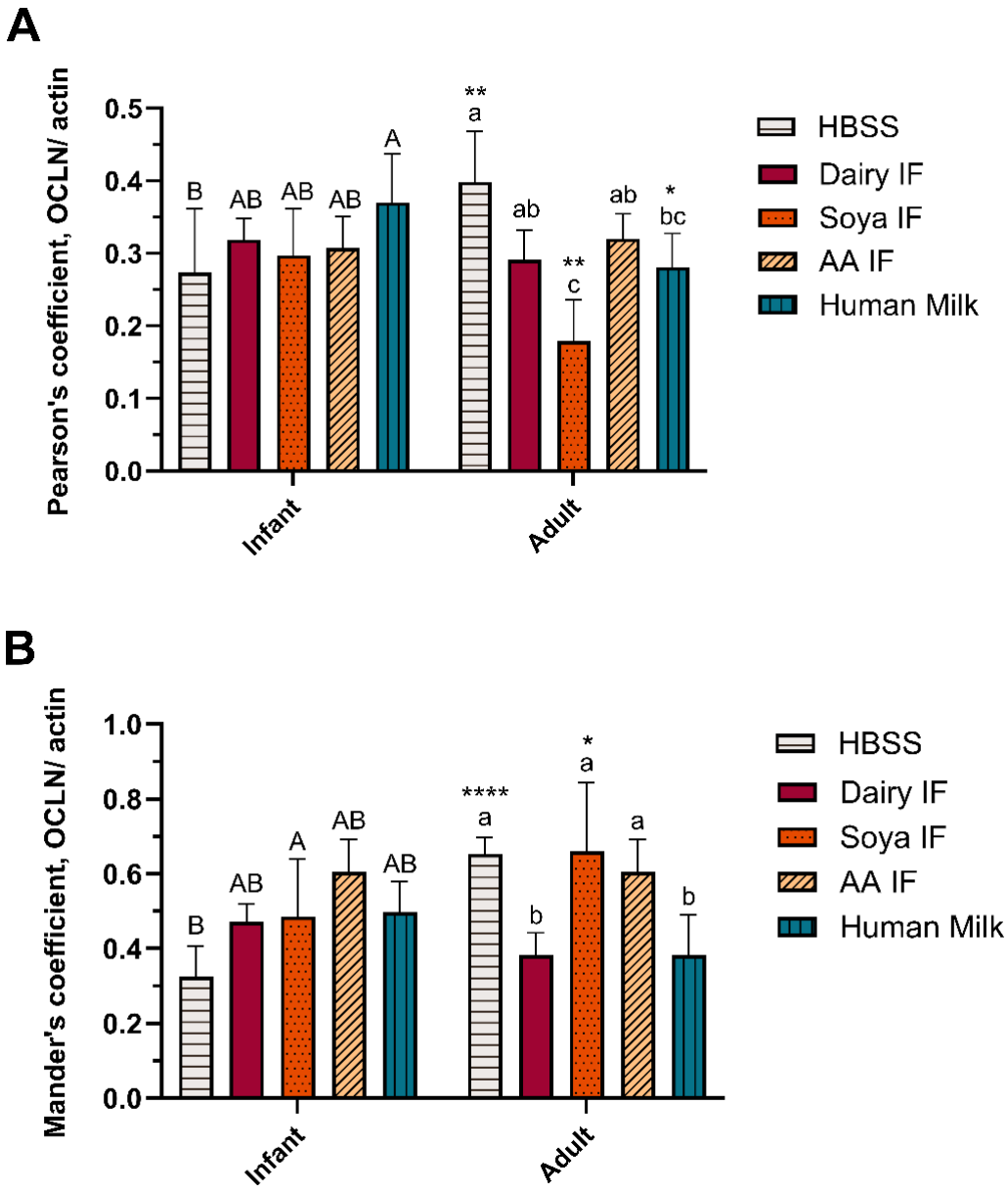


Fig. 4.4 Colocalization of occludin (OCLN) and actin in infant- and adult-like Caco-2/HT29-MTX monolayers exposed to digested infant formulae (IF) and Human Milk.

Adult- and infant-like Caco-2/HT29-MTX (90:10) monolayers (day 25) were treated for 2 h with digested Dairy, Soya, or amino acid-based (AA) IF or Human Milk. Confocal images were analyzed in FIJI (ImageJ). (A) Pearson's coefficient quantifies overall OCLN–actin co-localization. (B) Manders' M1 coefficient shows the fraction of OCLN overlapping with actin. Data are mean ± SEM from three biological replicates (n = 9). One-way ANOVA with Tukey's test: different letters indicate differences between treatments within infant (uppercase) or adult (lowercase) models; asterisks indicate significant differences between infant and adult models ($P < 0.05$).

4.3.4. AA IF shows the highest basolateral free AA levels

Fig. 4.5 depicts the free AA concentration found in the basolateral compartment of Caco-2/ HT29-MTX monolayers after 2 h exposure to digesta (T2-basolateral). Supplementary Tables 4.3 report the specific concentrations and statistical comparisons for all free AAs measured in the T2-basolateral compartment. Across all conditions, the five most abundant AAs present in the T2-basolateral samples were lysine, aspartic acid, arginine, threonine, and serine. These five AAs accounted for approximately 50–58% of the total free AAs found in the T2-basolateral compartment across all samples.

In the infant model, treatment with AA IF resulted in a mean free AA concentration of 8.275 ± 0.362 mg/L, which was higher ($P < 0.05$) than that observed for soya IF (6.444 ± 0.335 mg/L), dairy IF (6.634 ± 0.279 mg/L), and human milk (6.915 ± 0.326 mg/L) treatments. In the adult-like model, treatment with AA IF again led to the highest free AA levels (7.712 ± 0.360 mg/L), exceeding those from soya IF (6.182 ± 0.094 mg/L), dairy IF (5.728 ± 0.015 mg/L), and human milk (6.275 ± 0.308 mg/L) treatments.

Interestingly, the total amount of free AAs found in the T2-basolateral side was significantly higher in the infant-like model than in the adult for dairy IF (6.64 ± 0.09 vs. 5.73 ± 0.01 mg/L; $P < 0.05$), driven largely by increased transport of glycine (0.27 ± 0.02 mg/L) and serine (0.62 ± 0.11 mg/L) in the infant model ($P < 0.05$). Supplementary Fig. 4.6 shows the total free AA concentrations in the T2-basolateral compartment of the HBSS control condition, which were not significantly different ($P > 0.05$) between infant-like (3.41 ± 0.52 mg/L) and adult-like (3.97 ± 0.17 mg/L) monolayers. Importantly, these background levels were ~2-fold lower than the T2-

basolateral free AA concentrations measured after exposure to digested dairy IF, soya IF, AA IF, and human milk (Fig. 4.5), indicating that the AAs detected in the transport experiments originated from the formulations rather than the buffer or cell system. As free AA in basolateral T2 samples were quantified by UHPLC–HRMS/MS Supplementary Fig. 4.6 and Supplementary Table 4.3 also include UHPLC–HRMS/MS data of digesta samples, for comparison purposes.

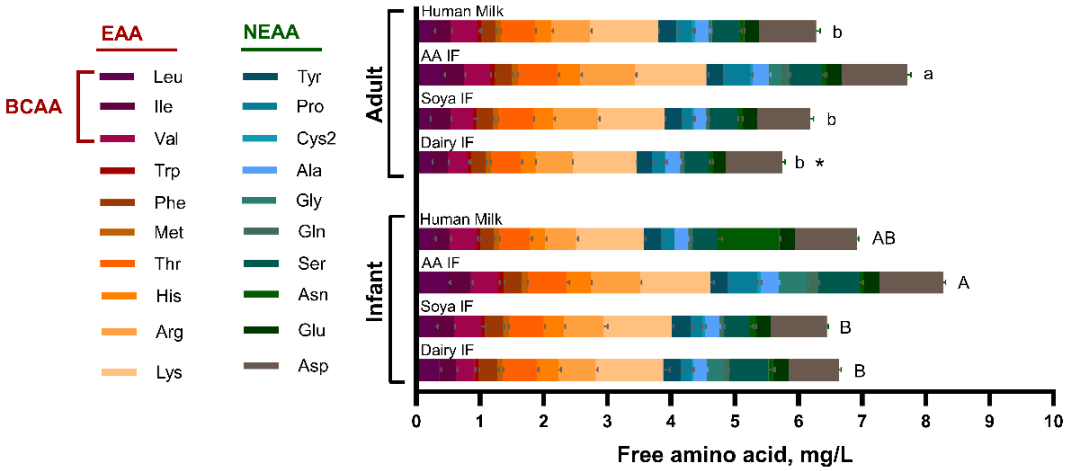


Figure 4.5 Free Amino Acid Concentrations in the basolateral compartments of Caco-2/HT29-MTX monolayers treated with digested Infant Formulas (IF) and Human Milk.

Free amino acid concentrations (mg/L) in the basolateral compartment of infant-like and adult-like monolayers exposed for 2 h to digested Dairy IF, Soya IF, amino-acid (AA) IF, and Human Milk, measured by UHPLC–HRMS/MS. Data are mean ± SEM from three biological replicates (technical duplicates). One-way ANOVA with Tukey's test: different letters indicate differences between treatments within infant (uppercase) or adult (lowercase) models; asterisks indicate adult vs. infant differences ($P < 0.05$). Amino acids: red = BCAA, red + orange = EAA, blue/green = NEAA.

4.3.5. Infant-like monolayers exhibit higher peptide transport and higher sequence diversity

To identify peptides present post-digestion and post-absorption, UHPLC–HRMS/MS was performed in the digesta (I60), T2-apical and T2-basolateral samples for all foods (dairy IF, soya IF and human milk). Database searches were performed against custom UniProtKB FASTA files corresponding to *Bos taurus* (dairy), *Glycine max* (soya) or *Homo sapiens* (human milk), allowing only data comparisons between infant and adult-like monolayers

Fig. 4.6 depicts total unique peptide counts in digesta, infant (A, C, E) and adult (B, D, F) models. Detailed counts of unique and shared peptides across digesta, T2-apical, and T2-basolateral samples for each formulation and model are provided in Appendix Tables B1, B2 and B3.

For dairy IF, 170 unique peptides were identified in the digesta, while 206 and 182 were detected in the T2-basolateral compartments of infant- and adult-like models, respectively. This suggests that the infant-like model absorbed a broader range of peptides than the adult monolayer. In the T2-apical compartments, 310 unique peptides were detected in the infant model and 289 in the adult. In the infant model, 139 unique peptides were common to both T2-apical and T2-basolateral samples, 52 of which were not present in the digesta. In the adult monolayer treated with dairy IF digesta, the T2-apical and T2- basolateral samples had 131 peptides in common, of which 54 were not present in the digesta. Additionally, 67 peptides were found in the infant T2-basolateral compartment only (not detected in T2-apical or digesta), compared with 47 in the adult T2-basolateral compartment only.

For soya IF, 229 unique peptides were detected in the digesta. The infant- and adult-like models yielded 163 and 127 unique peptides in the T2-basolateral compartment

and 335 and 366 in the T2-apical compartment, respectively. Of these, 124 (infant) and 96 (adult) were shared across compartments, while 39 and 31 were in the T2-basolateral sample only. Thirty-four peptides (infant) and 25 (adult) were shared between apical and basolateral compartments but were not present in the digesta.

For human milk, 129 unique peptides were detected in the digesta. The infant- and adult-like models yielded 206 and 167 unique peptides in the T2-apical compartment and 51 and 50 in the T2-basolateral compartment, respectively. Of these, 45 (infant) and 42 (adult) were shared across compartments. Notably, 10 (infant) and 8 (adult) of these shared peptides were absent from the digesta. Six (infant) and 8 (adult) peptides were found in the T2-basolateral side only.

When examining peptides exclusive to one model (*i.e.*, peptides detected only in either the infant or adult condition in the T2- apical and T2-basolateral samples), a higher number of individual peptides were observed in the infant-like model. Specifically, 62 peptides were exclusive to the infant model with dairy IF treatment, compared to 25 in the adult; 35 versus 16 with soya IF treatment, and 43 versus 6 with human milk treatment.

In all cases the number of peptides identified in the T2-apical samples exceeded those in the original digesta. Moreover, each formula showed a subset of peptides shared between T2-apical and T2-basolateral compartments but absent from the digesta. Together, these findings suggest that brush border enzymes further cleave dietary peptides during the 2h incubation, generating new fragments capable of transepithelial transport.

Interestingly, the peptides exclusive to the infant-like monolayer with dairy IF treatment had a lower median length (3.5 AAs) than those in the adult-like monolayer (4 AAs) and included a notably higher number of tripeptides (39 *vs.* 14 in

adults). In contrast, peptides exclusive to the infant-like monolayer with soya IF or human milk treatments were generally longer (soya IF: median infant = 9, adult = 8; human milk: median infant = 8, adult = 4.5), suggesting less hydrolysis.

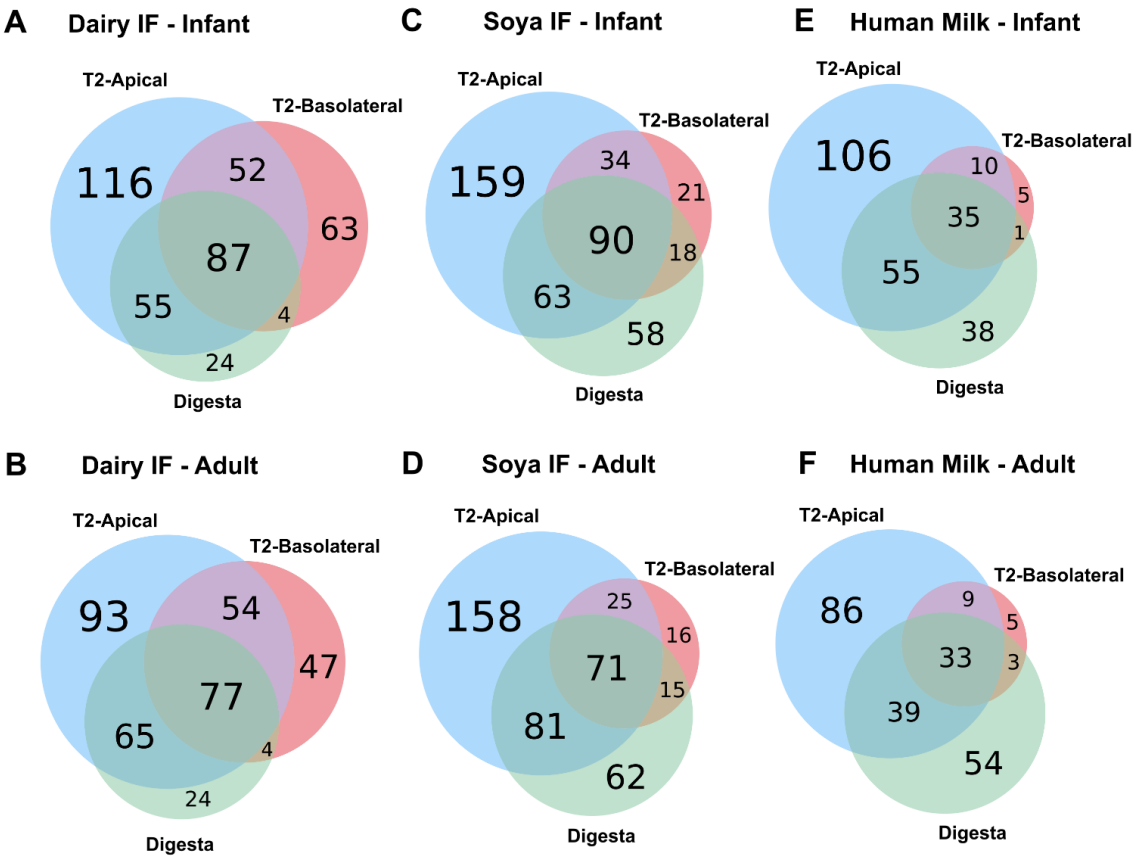


Fig. 4.6 Venn diagrams of unique peptides detected in infant- and adult-like monolayers treated with digested Dairy IF, Soya IF or Human Milk.

Infant- and adult-like monolayers were treated for 2 h (T2) with digested Dairy IF, Soya IF, or Human Milk. Peptides identified by UHPLC–HRMS/MS in digesta (green), in T2-apical (blue) and in T2-basolateral (red) compartments Panels: (A–B) Dairy IF, (C–D) Soya IF, (E–F) Human Milk in infant and adult models.

4.3.6. Apical peptides reflect active brush border enzyme cleavage

With dairy IF, soya IF and human milk treatments, a substantial number of unique peptides were detected in the T2-apical compartment that were not present in the digesta, suggesting further processing by epithelial peptidase enzymes. To explore whether the peptides identified in the apical compartment were as a result of brush border enzyme activity, peptides present in the T2-apical chamber were assigned to parental digesta peptides with cleavage sites mapped of known intestinal brush border enzymes. Fig.7 illustrates the total number of times each brush border enzyme was involved in cleaving apical peptides, with higher event counts indicating greater predicted brush border activity. When including both 1-step and multi-step cleavage events, the infant-like model had 51 (dairy IF treatment), 61 (soya IF treatment) and 31 (human milk treatment) cleavage events. The adult-like model had 52 (dairy IF treatment), 59 (soya IF treatment) and 27 (human milk treatment) cleavage events. Tripeptidyl peptidase II, aminopeptidase N, and dipeptidyl peptidase-4 were the most commonly assigned brush border enzymes across all conditions, collectively accounting for the majority of predicted cleavage events.

In terms of peptide counts, the T2-apical sample collected with dairy IF treatment showed 36 single-step and 11 multi-step peptides in the infant-like model, compared to 36 single-step and 10 multi-step in the adult-like model. With soya-IF treatment, the T2-apical sample of infant monolayers had 41 single-step and 12 multi-step peptides, while the T2-apical sample from adult-like monolayers had 38 single-step and 12 multi-step peptides. With human milk treatment, the T2-apical sample of infant-like monolayers yielded 26 single-step and 4 multi-step peptides, compared with 22 and 4 in the T2-apical sample of adult-like model.

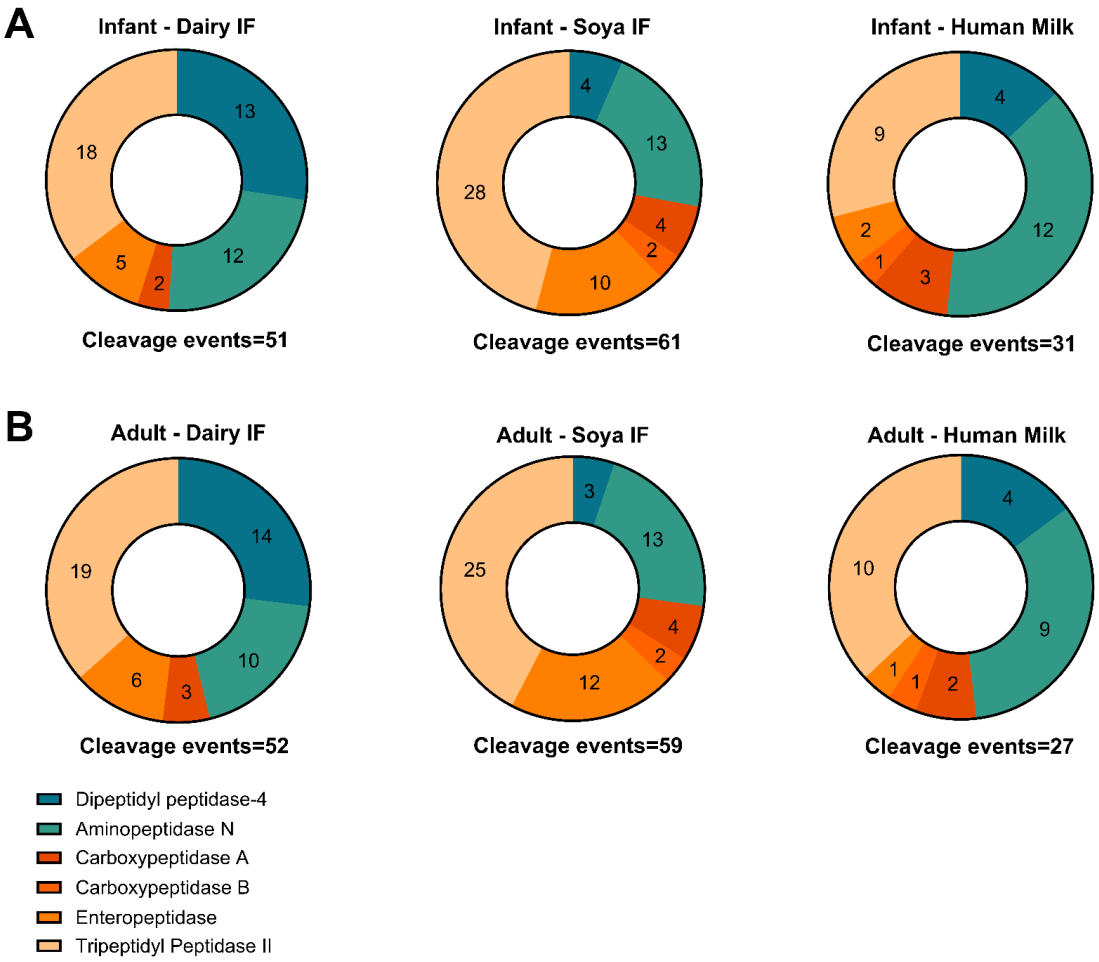


Fig. 4.7 Cleavage events attributed to specific brush border enzymes.

(A) Infant-like and (B) adult-like Caco-2/HT29-MTX monolayers were treated for 2 h (T2) with digested Dairy IF, Soya IF, and Human Milk. Peptides identified in the T2-apical compartment (UHPLC–HRMS/MS) were compared with those in digesta to map new cleavage sites. Cleavage motifs were matched to specific enzymes, with higher event counts indicating greater predicted brush border activity.

4.3.7. Infant-like monolayers show enhanced basolateral peptide load in response to human milk

To study the total load of peptides transported across the intestinal barrier, both the total peptide intensity (log_2-normalized) and the total number of peptides (including repeated detections of the same sequence) in T2-apical (Fig. 4.8A, B) and T2-basolateral (Fig. 4.8C, D) samples were quantified.

In the T2-basolateral compartment, both the total peptide intensity and count were significantly higher in the infant model treated with digested human milk compared to the adult model ($P < 0.05$). Peptide intensity was 30.10 ± 0.24 in infants versus 28.58 ± 0.22 in adults, and peptide count was 68.67 ± 0.67 vs. 60 ± 1, respectively. With dairy and soya IF treatments, no significant differences were detected in peptide intensity or count between infant and adult models in the T2-basolateral side ($P > 0.05$). In the T2-apical compartment, no significant differences in peptide intensity (reflecting relative abundance) and count were observed between infant and adult monolayers for any of the food conditions ($P > 0.05$).

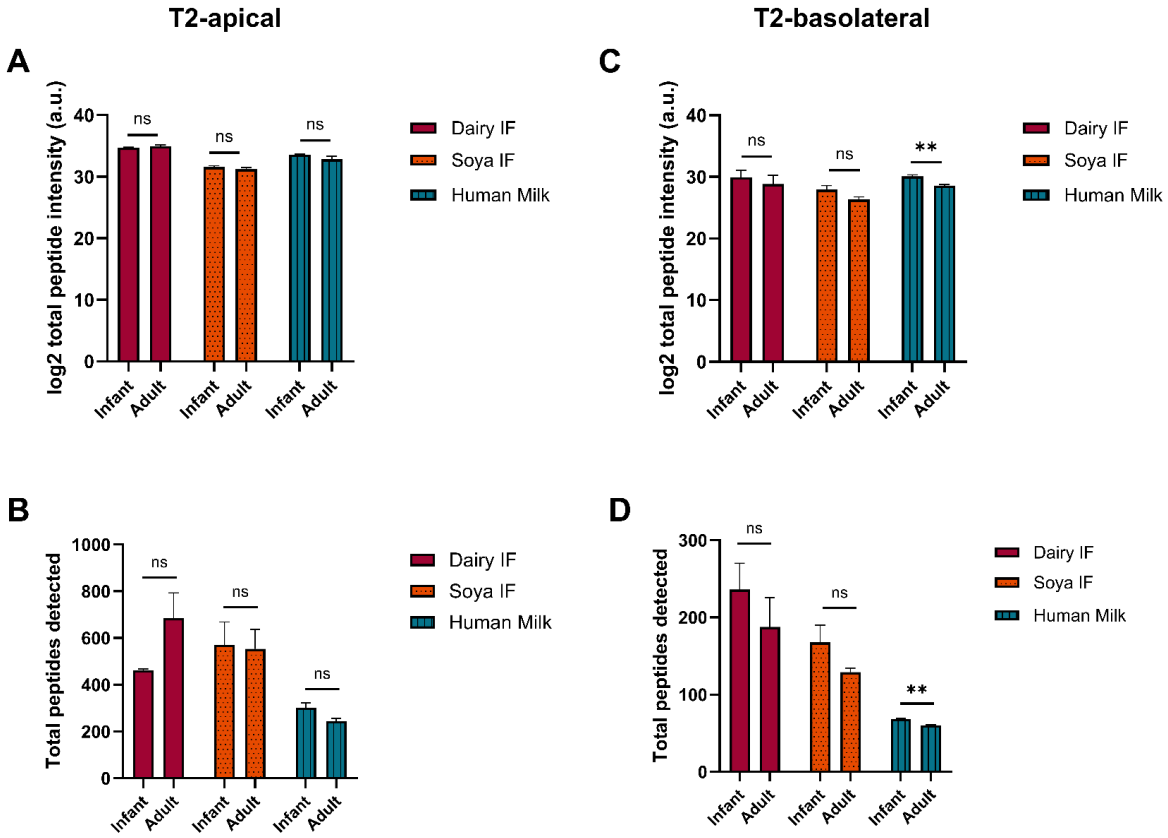


Fig. 4.8 Peptide transport across infant- and adult-like monolayers after exposure to digested infant formulae (IFs) and Human Milk.

Infant-like and adult-like monolayers (day 25, Caco-2/HT29-MTX 90:10) were treated for 2 h (T2) with digested Dairy IF, Soya IF, and Human Milk. UHPLC–HRMS/MS was used to measure: (A, C) log_2-transformed total peptide intensity and (B, D) total peptide count in apical and basolateral compartments at T2. Data are mean ± SEM from three biological replicates. Unpaired t-tests compare infant and adult models; asterisks indicate significant differences ($P < 0.05$).

4.3.8. Human milk-derived bioactive peptides are more abundant in infant-like monolayers

To assess whether peptides present in the T2-apical and T2-basolateral compartments exhibited bioactivity, PeptideRanker was employed to predict bioactivity scores based on sequence motifs (Mooney et al., 2012). The results were, matched against the BIOPEP and MBPD databases, which catalogue experimentally validated and predicted bioactive peptides. Fig. 4.9 displays volcano plots of $\log_2$ intensity differences (infant – adult) for individual peptides, highlighting those with predicted or confirmed bioactivities. All identified bioactive peptides, their predicted functions, and statistical comparisons are reported in Appendix Tables 4 (dairy IF), 5 (soya IF), 6 (human milk). Peptides with multiple predicted bioactivities were included in the count for each functional category to capture their multifunctional potential.

In the T2-apical compartment, monolayers treated with dairy IF yielded the highest number of bioactive peptides (n = 86), primarily linked to ACE inhibition (n = 45), antioxidative activity (n = 21), DPP-IV inhibition (n = 12), immunomodulation (n = 11), and AChE inhibition (n = 8). Among these, three peptides with antioxidant, DPP-IV inhibitory, and hypouricemic functions were more abundant in the infant model, while two antiamnestic and ACE-inhibitory peptides were higher in adult-like monoaleyrs. T2-apical samples from monolayers treated with human milk contained 11 bioactive peptides, mostly ACE inhibitors (n = 6) and DPP-II inhibitors (n = 3), with individual peptides also associated with antioxidant, anticancer, opioid, cholesterol-regulating, and growth-promoting activities (n = 1 each). Two ACE-inhibitory peptides were significantly higher in infant monolayers. T2-apical samples

form monolayers treated with soya IF contained only one identified bioactive peptide with both ACE-inhibitory and antioxidant potential.

In the absorbed fraction (T2-basolateral), monolayers treated with dairy IF contained 54 bioactive peptides, with functional classifications including ACE inhibition (n = 26), antioxidant (n = 14), and DPP-IV inhibition (n = 12). One opioid peptide (β-casein ^{75}YPF^{77}) was more abundant in T2-basolateral from infant monolayers, while one ACE-inhibitory peptide (κ-casein ^{77}LPYP^{80}) was higher in adult T2-basolateral. T2-basolateral samples from monolayers treated with soya IF yielded a single antioxidant peptide (β -conglycinin ^{267}SLVNNDDRDS^{276}). T2-basolateral samples from monolayers treated with human milk contained five bioactive peptides: two with ACE-inhibitory activity, one with antioxidant activity, one with both ACE-inhibitory and antioxidant activity, and one with cholesterol-regulating activity. Notably, four of the five peptides were detected at significantly higher intensity in the infant model than in the adult ($P < 0.05$).

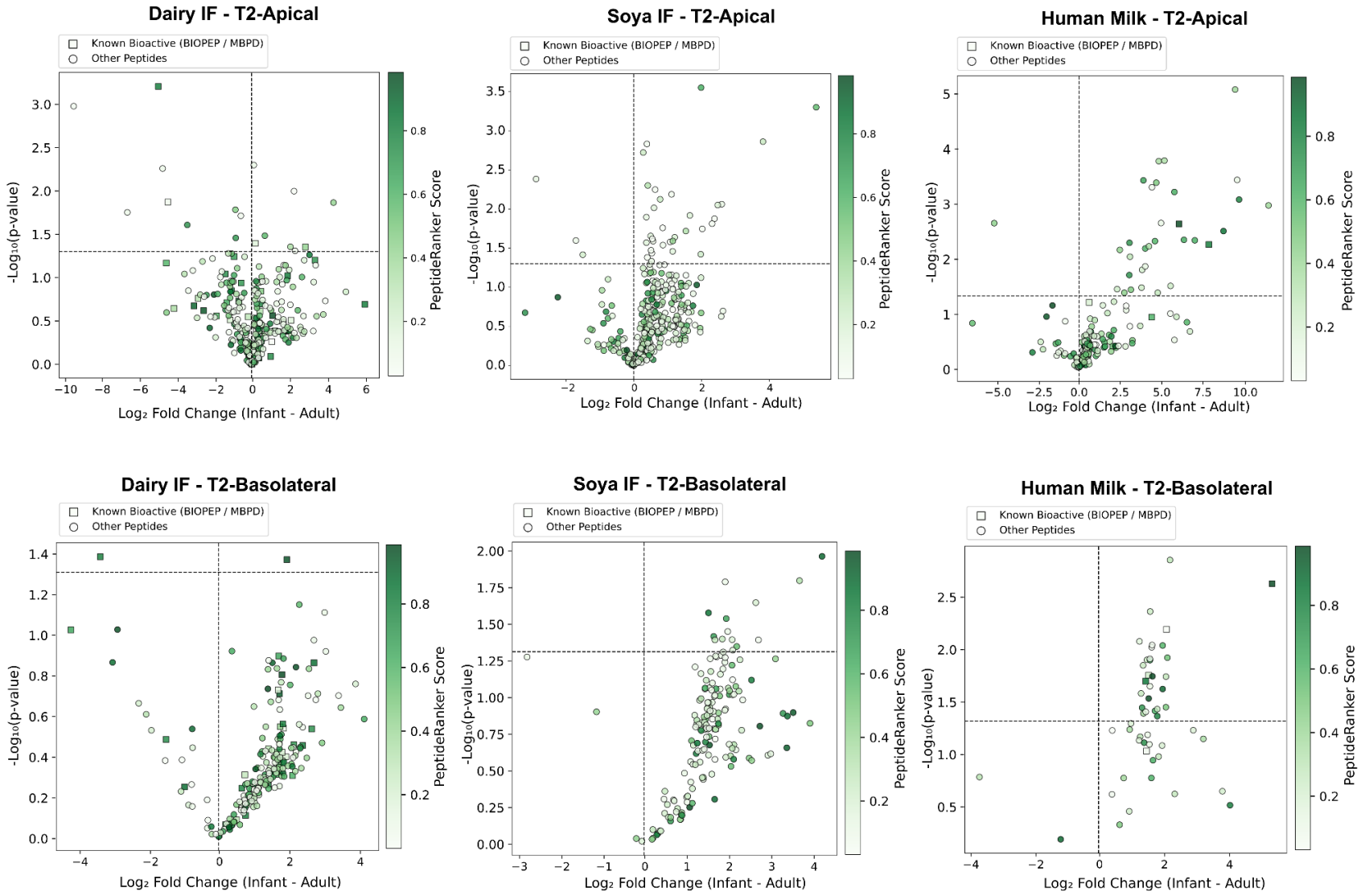

Dairy IF - T2-Apical
Soya IF - T2-Apical
Human Milk - T2-Apical
Dairy IF - T2-Basolateral
Soya IF - T2-Basolateral
Human Milk - T2-Basolateral
Known Bioactive (BIOPEP / MBPD)
Other Peptides
-Log₁₀(p-value)
Log₂ Fold Change (Infant - Adult)
PeptideRanker Score

Figure 4.9 Volcano plots of peptide abundance differences between infant- and adult-like models after exposure to digested infant formulas (IF) and Human Milk.

Infant- and adult-like Caco-2/HT29-MTX monolayers were treated for 2 h (T2) with digested Dairy IF, Soya IF, and Human Milk. Peptides identified by UHPLC–HRMS/MS in the (A) T2-apical and (B) T2-basolateral samples are shown. Each point represents a peptide; X-axis = $\log_2$ fold change (infant − adult), Y-axis = $-\log_{10}$(P-value) from unpaired t-tests. Horizontal line indicates P = 0.05. The vertical line at $\log_2$ fold change = 0 separates peptides enriched in the infant model (right side, positive values) from those enriched in the adult model (left side, negative values). The upper-right quadrant highlights peptides significantly more abundant in infants, while the upper-left quadrant highlights peptides significantly more abundant in adults. Color intensity reflects predicted bioactivity (PeptideRanker); darker green = higher bioactivity. Squares = peptides matched to known bioactive sequences (BIOPEP/MBPD), circles = unmatched peptides.

4.4. Discussion

In this study, infant- and adult-like Caco-2/HT29-MTX models were treated with gastrointestinal digests of human milk, dairy IF, soya IF or AA IF. The main findings were (i) human milk uniquely enhanced OCLN–actin co-localization and increased basolateral bioactive peptides in the infant-like model, (ii) IFs showed limited effects on both models, with AA–based formula increasing OCLN intensity in infant-like monolayers whilst lowering TEER in adult-like monolayers, and (iii) dietary peptide transport and diversity were consistently higher in infant- than adult-like models, highlighting the value of age-appropriate systems for infant nutrition research.

The primary finding for human milk was that treatment of the infant-like monolayer resulted in significantly increased OCLN/actin co-localization (Fig. 4.4, $P < 0.05$), indicating tight junction remodeling despite no overall change in OCLN expression or TEER values (Fig. 4.2; $P > 0.05$). Confocal imaging confirmed brighter OCLN staining at intercellular junctions. Importantly, these effects were unique to the infant-like model and absent in the adult-like condition. These structural changes observed in our infant-like model are interesting in the context of Noel et al. study, who reported that human colostrum induced a granular OCLN pattern in pediatric enteroids, particularly co-localizing with goblet (trefoil factor 3 +) and Paneth (lysozyme +) cells (Noel et al., 2021). Kondrashina et al. (2024) observed no OCLN upregulation ($P > 0.05$) after 4 h exposure to digested human milk and dairy IF (500 $\mu g/cm^2$) in Caco-2/HT29-MTX monolayers, although TEER was significantly increased compared with HBSS controls ($664 \pm 72\ \Omega \cdot cm^2$; $P < 0.05$) (Kondrashina et al., 2024). Kondrashina et al. used an adult-like Caco-2/HT29-MTX model, whereas

our study and that of Noel et al. employed infant-like or pediatric enteroid systems, which may better capture age-specific responses. OCLN participates in maintaining epithelial barrier function by modulating paracellular permeability and coordinating tight junction assembly through its interactions with cytoplasmic adaptors (e.g., ZO1) and the actin cytoskeleton (Cummins, 2012). Although human milk is complex, the peptide and AA profile post gastrointestinal digestion may play a role in this OCLN response. SEC revealed large proteins/peptides remaining at the end of the intestinal phase (MW > 50 kDa; Fig. 4.1B). SDS-PAGE had a persistent ~80 kDa band likely to be glycosylated lactoferrin, known to be resistant to digestion (Ma et al., 2021; Van Berkel et al., 1995). Lactoferrin has been shown to directly improve gut barrier function and tight junctions (Conesa et al., 2023). Specifically, in Caco-2 monolayers, Zhao et al. (2019) demonstrated that treatment with bovine lactoferrin significantly increased both mRNA and protein levels of OCLN, and promoted its redistribution to the cell membrane, as shown by immunofluorescence (Zhao et al., 2019). Moreover, digested human milk contains significantly higher levels of free glutamic acid. *In vitro*, glutamic acid improves TEER in infant pig IPEC-J2 monolayers (0.5 mmol/L) (Jiao et al., 2015). As both a precursor and product of glutamine, glutamic acid also contributes indirectly to gut barrier maturation, since glutamine upregulates tight junction proteins (OCLN, CLDN1/4, ZO1/2/3) and restores barrier integrity (improved TEER and reduced ^{14}C-mannitol and FITC-dextran flux) in Caco-2 monolayers (Kim and Kim, 2017).

Peptide profiling of human milk revealed greater T2-basolateral transport and diversity in the infant- compared to the adult-like model (51 vs. 50 unique T2-basolateral peptides, UHPLC–HRMS/MS intensity 30.10 ± 0.24 $\log_2$ vs. 28.58 ± 0.22; total counts 68.67 ± 0.67 vs. 60.00 ± 1.00; Fig. 4.6 and 8; $P < 0.05$). The T2-

apical compartment yielded 206 unique milk peptides for infant and 167 for adult. Previously, Liang et al. (2022) identified 169 peptides in the apical chamber and 44 peptides in the basolateral chamber after applying a digested human milk extract (10 µg/mL) to Caco-2 monolayers for 12 h. There was overlap with our data, including β-casein ^{138}NLHLPLP^{144} (ACE-inhibitory activity) and additional β-casein fragments such as ^{126}FDPQIPK^{132}, ^{210}PVTQPLAPV^{220} and ^{96}PEIMEVPKA^{104}. In contrast, Kondrashina et al. (2024) reported only 17 basolateral peptides after 4 h exposure to human milk, from which 6 peptides were common to our study. In terms of peptide abundance in the T2-basolateral compartment, the most abundant peptide for human milk was β-casein ^{126}FDPQIPK^{132} (1.17-fold higher in the infant-like model; $P > 0.05$), followed by β-casein ^{176}VLPIPQ^{181} (1.06-fold higher in the infant-like model; $P < 0.05$), with proven *in vitro* ACE-inhibitory effects (Kohmura et al., 1989). Notably, T2-basolateral peptides from the infant-like model carried a higher functional load. Five bioactive peptides were identified, four of which were more abundant in the infant-like condition. These included β-casein ^{176}VLPIPQ^{181}, β-casein ^{138}NLHLPLP^{144}, and β-casein ^{169}WSVPQPK^{175}, all exhibiting ACE-inhibitory activity (Hernández-Ledesma et al., 2007; Kohmura et al., 1989), as well as β-casein ^{90}VLPVPQ^{95}, which has been linked to cholesterol-regulating activity (Jiang et al., 2020). Interestingly, ^{169}WSVPQPK^{175} was also found in the gastric digesta of *in vivo* infants (Nielsen et al., 2018).

For the IF foods, no significant differences were observed in the response of infant-like monolayers to either dairy IF or soya IF, in terms of TEER (Fig. 4.2), OCLN intensity (Fig. 4.3) and OCLN/β-actin Pearson's co-localization coefficient (Fig 4; $P < 0.05$). Consistent findings to our study were also reported by our group previously

where dairy IF digesta did not significantly alter TEER or OCLN levels in Caco-2/HT29-MTX monolayers (Dold et al., 2025). Similarly, Paparo et al. (2020) demonstrated that soya IF digesta did not impair TEER in Caco-2 cells, although it did upregulate OCLN mRNA expression (Paparo et al., 2021).

Notably, AA IF elicited a distinct response in the infant-like model: it significantly increased OCLN fluorescence intensity (Fig. 4.3B; $P < 0.05$) without a corresponding rise in TEER (Fig. 4.1A; $P > 0.05$) compared to HBSS. This may suggest that treatment with AA IF causes a selective tightening of the OCLN-regulated leak pathway, while the ion-conductive pore pathway that determines TEER remained unaffected (Al-Sadi et al., 2011). This finding aligns with *in vivo* data showing that extensively hydrolyzed formulae (no intact proteins) reduce intestinal paracellular permeability in infants (lactulose/mannitol ratio, $P = 0.003$) compared with conventional cow's milk-based formula (Koivusaari et al., 2023). In contrast, Paparo et al. (2020) found no upregulation of OCLN mRNA nor differences in TEER with AA IF in Caco-2 cells.

In the adult-like model, barrier responses to formula digesta diverged from the infant-like phenotype. Dairy IF reduced OCLN fluorescence intensity and Mander's coefficient for OCLN–actin co-localization (Fig. 4.3B and 4B; $P < 0.05$), Soya IF decreased Pearson's coefficient for OCLN–actin spatial correlation (Fig. 4.3A; $P < 0.05$), and AA IF significantly lowered TEER (Fig. 4.2B; $P < 0.05$) without affecting OCLN intensity (Fig. 4.3; $P > 0.05$). The TEER reduction observed with AA IF may reflect increased amino acid transport activity, as amino acid uptake is coupled to proton and ion fluxes (Bröer, 2008) that transiently influence TEER. This interpretation is supported by the higher basolateral amino acid levels measured for AA IF compared with the other samples ($P < 0.05$).

In terms of unique dairy or soya peptides transported to the T2-basolateral compartment, the infant-like monolayers consistently exhibited higher unique peptide counts (Fig. 4.6). For the dairy IF, we identified 206 unique peptides in the T2-basolateral and 314 in the T2-apical compartments for the infant-like model and 182 and 289 for the adult-like model. Similarly, Bavaro et al. (2021) identified 105 unique peptides in the basolateral and 585 in the apical compartments following 4 h exposure to 200 μg protein/cm² of digested heat-treated dairy infant formula (Bavaro et al., 2021). Of these, 132 apical peptides and 25 basolateral peptides matched to our data. In contrast, Kondrashina et al. (2024) identified only 17 peptides in the T2-basolateral side of Caco-2/HT29-MTX monolayers exposed for 4 h to dairy IF (Kondrashina et al., 2024). From their dataset, we identified 11 peptides in common from dairy IF (distributed across both compartments). In a milk protein study, Zenker et al. (2020) treated Caco-2 monolayers with gastrointestinal digested micellar casein and whey (80:20) for 2 h (Zenker et al., 2020). Assessment of milk peptide transport revealed 181 peptides on the basolateral side, including several peptides exhibiting sIgE-binding epitopes. When comparing their dataset with ours, we found four epitope-containing peptides in common—β-casein ^{98}VVPPFLQPE^{106}, ^{96}PVVVPPFLQPEV^{107}, ^{98}VVPPFLQPEV^{107}, and β-lactoglobulin ^{58}YVEELKPTPEGDLE^{71}. These bovine milk peptides were detected in both T2-apical and T2-basolateral compartments but absent in the digesta. With dairy IF treatment the most abundant peptide in the infant model was β-lactoglobulin ^{59}VEELKPTPE^{67} (1.04-fold higher in the infant model; $P > 0.05$), followed by β-casein ^{88}NIPPLTQTPV^{97} (1.08-fold higher; $P > 0.05$), which is also known for its ACE-inhibitory activity (Gobbetti et al., 2000). While dairy IF treatment produced

the highest number of total bioactive peptides in the Transwell chambers (54 in T2-basolateral, 86 in T2-apical), these were more evenly distributed between models. Where the infant-like model was treated with digested soya IF, 163 soya unique peptides were identified in the T2-basolateral and 346 in the T2-apical peptides. For the adult-like model, 127 soya unique peptides were identified in the basolateral and 335 in the apical. Martineau-Côté et al. (2024) identified 17 peptides in the basolateral and 55 in the apical fractions after exposing Caco-2/HT29-MTX monolayers for 2 h to digested soy flour (2240 µg of peptide/mL). When comparing their dataset with ours, we found five peptides in common: β-conglycinin ^{86}EPQQPGEKEEDEDEQPRPI^{104} (detected in both our T2-basolateral and T2-apical compartments), and seed linoleate 9S-lipoxygenase ^{208}NDLGDPDKGENH^{219}, Glycinin G4 ^{309}EQDEDEDEDEDKPRPS^{324} and ^{278}EEEEEEEDEKPQ^{287}, and sucrose-binding protein ^{309}TEVGPDDDEK^{338} (detected in our T2-apical compartment). Notably, these peptides were absent from our soya IF digesta.

The most abundant soya peptides in the Transwell chambers were glycinin ^{263}SVIKPPTDEQ^{272} (1.07-fold higher in the infant-like model; $P > 0.05$) and β-conglycinin ^{578}FVDAQPK^{584} (1.09-fold higher; $P > 0.05$).

Only one known bioactive peptide from soya was identified in the T2-apical compartment (Seed linoleate 13S-lipoxygenase-1 ^{306}TIIPLPV^{312}, ACE inhibitor and antioxidant (Minkiewicz et al., 2019)) and one in the T2-basolateral ^{267}β-conglycinin^{276} SLVNNDDRDS, antioxidant), with no significant difference between the infant and adult models ($P > 0.05$).

From our dataset, Caco-2/HT29-MTX brush border enzymes contributed to substantial protein digestion, as demonstrated by the higher number of peptides identified in the apical chamber after a 2 h incubation with monolayers but which

were not present in the digesta (Fig. 4.7). In the infant model, 46 peptides from dairy IF, 53 from soya IF, and 30 from human milk matched cleavage motifs. The main enzymes implicated were tripeptidyl peptidase II, aminopeptidase N, and dipeptidyl peptidase-4, which is consistent with brush border proteolytic activity. Similarly, Lacroix et al. (2017) studied five bioactive milk peptides and found that all underwent partial degradation by Caco-2 peptidases, with only ~70–90% remaining intact in the apical chamber after 2 h (Lacroix et al., 2017). Picariello et al. (2015) further showed that, after digestion of whey protein isolate, addition of brush border enzymes from porcine jejunum increased the degree of hydrolysis from 53.3% to 70.7%, underscoring the crucial role of brush border enzymes in shaping the final peptide pool (Picariello et al., 2015).

Interestingly, peptides exclusively found in T2-apical of infant-like monolayers, post treatment with dairy-IF were shorter in length. This suggests more extensive cleavage by monolayer brush border enzymes or intracellular processing in response to dairy IF. This enhanced breakdown likely contributed to the higher T2-basolateral free AA levels observed in the infant-like condition compared with the adult model with dairy IF treatment.

The infant-like and adult-like barriers differed in their responses to the foods. Only the infant-like model responded to AA IF with increased OCLN fluorescence, and responded to human milk with enhanced OCLN–actin co-localization. By contrast, the adult model showed a TEER reduction with AA IF treatment and lower OCLN fluorescence intensity with dairy IF and human milk treatments. Compared to the adult-like model, the infant-like monolayer also exhibited greater dietary peptide transport and diversity, with human milk in particular delivering a higher T2-basolateral load of bioactive peptides. Consistently, AA transport in the T2-

basolateral was higher in the infant-like than in the adult-like model for dairy IF. These observations agree with *in vivo* data showing greater intestinal permeability in neonates, driven by enhanced paracellular transport (Catassi et al., 1995), a key route for peptide absorption (Q. Xu et al., 2019). Thus, the adult Caco-2/HT29-MTX was less representative of the infant epithelium.

Limitations of this study include the absence of immune cells, short exposure windows, and a focus only on protein-derived bioactives. Additionally, peptide identification and bioactivity annotation are inherently limited by biases in available databases. Bovine milk proteins are overrepresented in proteomic and bioactive peptide databases compared to soya and human milk proteins. This may lead to underestimation of peptide diversity or function in soya IF and human milk samples, and overrepresentation of bioactive hits in dairy IF. Expanding and diversifying peptide reference databases will be critical for accurate cross-formulation comparisons. Moreover, we could not differentiate active amino acid and peptide transport from paracellular flux, since transporter perturbation assays (e.g. competitive inhibition) were not conducted to quantify each pathway. Future work should assess long-term exposure effects, test lipid and carbohydrate fractions, and incorporate co-cultures with immune or mucus-producing cells. Nonetheless, our model offers a reproducible and efficient platform for early-life nutrition research.

4.5.Conclusions

In summary, the infant-like model revealed that digested human milk altered tight junctions' architecture by increasing OCLN–actin co-localization and delivered a more diverse set of absorbed bioactive peptides. For all foods, infant-like monolayer transported more dietary peptides with greater diversity, than the adult-like

monolayers. For dairy IF, AA levels in the T2-basolateral were higher in the infant-like than in the adult-like model. These observations agree with *in vivo* data and support our view that *in vitro* barrier models mimicking the infant should be used in line with digestion protocols tailored for this life stage. Although, unexpectedly, both Caco-2/HT29-MTX models showed similar responses to dairy and soya IF and human milk for the limited biomarkers assessed here, future work should expand the biomarker panel. Formula development should continue to prioritize mimicking the bioactive and barrier-supportive properties of human milk.

4.6.References

Al-Sadi, R., Khatib, K., Guo, S., Ye, D., Youssef, M., Ma, T., 2011. Occludin regulates macromolecule flux across the intestinal epithelial tight junction barrier. American Journal of Physiology-Gastrointestinal and Liver Physiology 300, G1054–G1064. https://doi.org/10.1152/ajpgi.00055.2011

Atyeo, C., Alter, G., 2021. The multifaceted roles of breast milk antibodies. Cell 184, 1486–1499. https://doi.org/10.1016/j.cell.2021.02.031

Bavaro, S.L., Mamone, G., Picariello, G., Callanan, M.J., Chen, Y., Brodkorb, A., Giblin, L., 2021. Thermal or membrane processing for Infant Milk Formula: Effects on protein digestion and integrity of the intestinal barrier. Food Chemistry 347, 129019. https://doi.org/10.1016/j.foodchem.2021.129019

Bietto, F., Arranz, E., Miralles, B., Gómez-Marín, C., Rath, E., Lucey, A.J., Giblin, L., 2025. Using sodium glycodeoxycholate to develop a temporary infant-like gut barrier model, in vitro. Front. Nutr. 12, 1577369. https://doi.org/10.3389/fnut.2025.1577369

Biondi Ryan, M.R., Zukaitis, J., Sutantawong, S., Dallas, D.C., 2025. Overall Evidence for Milk-Derived Proteins and Peptides in Blood after Digestion: A Systematic Review. Nutrition Reviews nuaf118. https://doi.org/10.1093/nutrit/nuaf118

Blum, L.M., 1999. At the Breast: Ideologies of Breastfeeding and Motherhood in the Contemporary United States. Beacon Press.

Bode, L., 2012. Human milk oligosaccharides: Every baby needs a sugar mama. Glycobiology 22, 1147–1162. https://doi.org/10.1093/glycob/cws074

Brockway, M. (Merilee), Daniel, A.I., Reyes, S.M., Gauglitz, J.M., Granger, M., McDermid, J.M., Chan, D., Refvik, R., Sidhu, K.K., Musse, S., Patel, P.P., Monnin, C., Lotoski, L., Geddes, D.T., Jehan, F., Kolsteren, P., Bode, L., Eriksen, K.G., Allen, L.H., Hampel, D., Rodriguez, N., Azad, M.B., 2024. Human Milk Bioactive Components and Child Growth and Body Composition in the First 2 Years: A Systematic Review. Advances in Nutrition 15, 100127. https://doi.org/10.1016/j.advnut.2023.09.015

Bröer, S., 2008. Amino Acid Transport Across Mammalian Intestinal and Renal Epithelia. Physiological Reviews 88, 249–286. https://doi.org/10.1152/physrev.00018.2006

Carr, L.E., Virmani, M.D., Rosa, F., Munblit, D., Matazel, K.S., Elolimy, A.A., Yeruva, L., 2021. Role of Human Milk Bioactives on Infants' Gut and Immune Health. Front. Immunol. 12. https://doi.org/10.3389/fimmu.2021.604080

Catassi, C., Bonucci, A., Coppa, G.V., Carlucci, A., Giorgi, P.L., 1995. Intestinal Permeability. Changes during the First Month: Effect of Natural versus Artificial Feeding. Journal of Pediatric Gastroenterology and Nutrition 21, 383–386. https://doi.org/10.1097/00005176-199511000-00003

Codex Alimentarius Commission., 1981. Codex Alimentarius Commission. Standard for Infant Formula and Formulas for Special Medical Purposes Intended for Infants (CXS 72-1981). Rome: FAO/WHO; Revised 2023.

Colaizy, T.T., Bartick, M.C., Jegier, B.J., Green, B.D., Reinhold, A.G., Schaefer, A.J., Bogen, D.L., Schwarz, E.B., Stuebe, A.M., Jobe, A.H., Oh, W., Vohr, B.R., Walden, R.V., Alksninis, B., Hensman, A.M., Leonard, M.R., Noel, L., Leach, T.M., Watson, V.E., Fanaroff, A.A., Walsh, M.C., Wilson-Costello,

D.E., Newman, N.S., Siner, B.S., Friedman, H.G., Donovan, E.F., Schibler, K., Steichen, J.J., Alexander, B., Grisby, C., Mersmann, M.W., Mincey, H.L., Hessling, J., Gratton, T.L., Stoll, B.J., Adams-Chapman, I., Hale, E.C., LaRossa, M.M., Carter, S., Higgins, R.D., Wright, L.L., McClure, E.M., Poindexter, B.B., Lemons, J.A., Dusick, A.M., Kardatzke, D., Lytle, C., Appel, D.D., Bohnke, L.G., Eaken, G., Herron, D.E., Miller, L.C., Richard, L., Wilson, L.D., Das, A., Poole, W.K., Wrage, L.A., Hastings, B.K., McClure, E.M., O'Donnell Auman, J., Taylor, S., Stevenson, D.K., Hintz, S.R., Ball, M.B., Kohn, J.G., Baran, J.M., Lee-Ancajas, J.C., St. John, N.H., Carlo, W.A., Ambalavanan, N., Nelson, K.G., Peralta-Carcelen, M., Bailey, K.J., Biasini, F.J., Chopko, S.A., Collins, M.V., Cosby, S.S., Phillips, V.A., Rector, R.V., Finer, N.N., Vaucher, Y.E., Anderson, J.M., Rasmussen, M.R., Arnell, K., Demetrio, C., Fuller, M.G., Henderson, C., Posin, D., Bell, E.F., Colaizy, T.T., Bauer, C.R., Duara, S., Worth, A.M., Everett-Thomas, R., Diaz, A.N., Mathews, E.O., Hamlin-Smith, K., Jean-Gilles, L., Calejo, M., Frade, S.M., Hiriart-Fajardo, S., Gideon, Y., Korones, S.B., Bada, H.S., Hudson, T., Yolton, K., Williams, M.G., Laptook, A.R., Salhab, W.A., Broyles, R.S., Madison, S., Hickman, J.F., Guzman, A., Adams, S.S., Madden, L.A., Heyne, E.T., Dooley, C., Shankaran, S., Delaney-Black, V., Johnson, Y.R., Bara, R., Muran, G., Kennedy, D., Goldston, L.A., Ehrenkranz, R.A., Gettner, P., Konstantino, M., Romano, E., Close, N., Gilliam, W.S., Poulsen, J., 2016. Impact of Optimized Breastfeeding on the Costs of Necrotizing Enterocolitis in Extremely Low Birthweight Infants. The Journal of Pediatrics 175, 100-105.e2. https://doi.org/10.1016/j.jpeds.2016.03.040

Conesa, C., Bellés, A., Grasa, L., Sánchez, L., 2023. The Role of Lactoferrin in Intestinal Health. Pharmaceutics 15, 1569. https://doi.org/10.3390/pharmaceutics15061569

Cox, Jürgen, Mann, M., 2008. MaxQuant.

Cummins, P.M., 2012. Occludin: One Protein, Many Forms. Molecular and Cellular Biology 32, 242–250. https://doi.org/10.1128/MCB.06029-11

Dold, C.A., Sahin, A.W., Lawlor, P.G., Hickey, R.M., Giblin, L., 2025. Employing membrane filtration technology during infant milk formula processing, will improve intestinal barrier function in vitro. International Dairy Journal 167, 106283. https://doi.org/10.1016/j.idairyj.2025.106283

European Commission, 2016. Commission Delegated Regulation (EU) 2016/127 of 25 September 2015 supplementing Regulation (EU) No 609/2013 as regards the specific compositional and information requirements for infant formula and follow-on formula.

Gobbetti, M., Ferranti, P., Smacchi, E., Goffredi, F., Addeo, F., 2000. Production of Angiotensin-I-Converting-Enzyme-Inhibitory Peptides in Fermented Milks Started by Lactobacillus delbrueckii subsp. bulgaricus SS1 and Lactococcus lactis subsp. cremoris FT4. Appl Environ Microbiol 66, 3898–3904. https://doi.org/10.1128/AEM.66.9.3898-3904.2000

Google Research, n.d. Google Colaboratory.

Harris, C.R., Millman, K.J., Van Der Walt, S.J., Gommers, R., Virtanen, P., Cournapeau, D., Wieser, E., Taylor, J., Berg, S., Smith, N.J., Kern, R., Picus, M., Hoyer, S., Van Kerkwijk, M.H., Brett, M., Haldane, A., Del Río, J.F., Wiebe, M., Peterson, P., Gérard-Marchant, P., Sheppard, K., Reddy, T., Weckesser, W., Abbasi, H., Gohlke, C., Oliphant, T.E., 2020. Array

programming with NumPy. Nature 585, 357–362. https://doi.org/10.1038/s41586-020-2649-2

Hernández-Ledesma, B., Quirós, A., Amigo, L., Recio, I., 2007. Identification of bioactive peptides after digestion of human milk and infant formula with pepsin and pancreatin. International Dairy Journal 17, 42–49. https://doi.org/10.1016/j.idairyj.2005.12.012

Hevia, A., Ruas-Madiedo, P., Faria, M.A., Petit, V., Alves, B., Alvito, P., Arranz, E., Bastiaan-Net, S., Corredig, M., Dijk, W., Dupont, D., Giblin, L., Graf, B.A., Kondrashina, A., Ramos, H., Ruiz, L., Santos-Hernández, M., Soriano-Romaní, L., Tomás-Cobos, L., Vivanco-Maroto, S.M., Recio, I., Miralles, B., 2023. A Shared Perspective on in Vitro and in Vivo Models to Assay Intestinal Transepithelial Transport of Food Compounds. J. Agric. Food Chem. 71, 19265–19276. https://doi.org/10.1021/acs.jafc.3c05479

Hidalgo, I.J., Raub, T.J., Borchardt, R.T., 1989. Characterization of the Human Colon Carcinoma Cell Line (Caco-2) as a Model System for Intestinal Epithelial Permeability. Gastroenterology 96, 736–749. https://doi.org/10.1016/S0016-5085(89)80072-1

Hunter, J.D., 2007. matplotlib.

Jiang, X., Pan, D., Zhang, T., Liu, C., Zhang, J., Su, M., Wu, Z., Zeng, X., Sun, Y., Guo, Y., 2020. Novel milk casein–derived peptides decrease cholesterol micellar solubility and cholesterol intestinal absorption in Caco-2 cells. Journal of Dairy Science 103, 3924–3936. https://doi.org/10.3168/jds.2019-17586

Jiao, N., Wu, Z., Ji, Y., Wang, B., Dai, Z., Wu, G., 2015. L-Glutamate Enhances Barrier and Antioxidative Functions in Intestinal Porcine Epithelial Cells,.

The Journal of Nutrition 145, 2258–2264. https://doi.org/10.3945/jn.115.217661

Johnston, S.D., Smye, M., Watson, R.G.P., McMillan, S.A., Trimble, E.R., Love, A.H.G., 2000. Lactulose-Mannitol Intestinal Permeability Test: A Useful Screening Test for Adult Coeliac Disease. Ann Clin Biochem 37, 512–519. https://doi.org/10.1177/000456320003700413

Kim, M.-H., Kim, H., 2017. The Roles of Glutamine in the Intestine and Its Implication in Intestinal Diseases. IJMS 18, 1051. https://doi.org/10.3390/ijms18051051

Kleiveland, C.R., 2015. Co-cultivation of Caco-2 and HT-29MTX. The impact of food bioactives on health 135–140.

Kohmura, M., Nio, N., Kubo, K., Minoshima, Y., Munekata, E., Ariyoshi, Y., 1989. Inhibition of Angiotensin-converting Enzyme by Synthetic Peptides of Human β-Casein. Agricultural and Biological Chemistry 53, 2107–2114. https://doi.org/10.1080/00021369.1989.10869621

Koivusaari, K., Niinistö, S., Nevalainen, J., Honkanen, J., Ruohtula, T., Koreasalo, M., Ahonen, S., Åkerlund, M., Tapanainen, H., Siljander, H., Miettinen, M.E., Alatossava, T., Ilonen, J., Vaarala, O., Knip, M., Virtanen, S.M., 2023. Infant Feeding, Gut Permeability, and Gut Inflammation Markers. Journal of Pediatric Gastroenterology & Nutrition 76, 822–829. https://doi.org/10.1097/MPG.0000000000003756

Komatsu, Y., Wada, Y., Shibasaki, T., Kitamura, Y., Ehara, T., Nakamura, H., Miyaji, K., 2024. Comparison of protein digestibility of human milk and infant formula using the INFOGEST method under infant digestion

conditions. Br J Nutr 132, 351–358. https://doi.org/10.1017/S0007114524001260

Kondrashina, A., Mamone, G., Giblin, L., Lane, J.A., 2024. Infant Milk Formula Enriched in Dairy Cream Brings Its Digestibility Closer to Human Milk and Supports Intestinal Health in Pre-Clinical Studies. Nutrients 16, 3065. https://doi.org/10.3390/nu16183065

Korhonen, H., Pihlanto, A., 2006. Bioactive peptides: Production and functionality. International Dairy Journal 16, 945–960. https://doi.org/10.1016/j.idairyj.2005.10.012

Kosek, M.N., Lee, G.O., Guerrant, R.L., Haque, R., Kang, G., Ahmed, T., Bessong, P., Ali, A., Mduma, E., Peñataro Yori, P., Faubion, W.A., Lima, A.A.M., Paredes Olortegui, M., Mason, C., Babji, S., Singh, R., Qureshi, S., Kosek, P.S., Samie, A., Pascal, J., Shrestha, S., McCormick, B.J.J., Seidman, J.C., Lang, D.R., Zaidi, A., Caulfield, L.E., Gottlieb, M., Network, the M.-E., 2017. Age and Sex Normalization of Intestinal Permeability Measures for the Improved Assessment of Enteropathy in Infancy and Early Childhood: Results From the MAL-ED Study. Journal of Pediatric Gastroenterology and Nutrition 65, 31–39. https://doi.org/10.1097/MPG.0000000000001610

Lacroix, I.M.E., Chen, X.-M., Kitts, D.D., Li-Chan, E.C.Y., 2017. Investigation into the bioavailability of milk protein-derived peptides with dipeptidyl-peptidase IV inhibitory activity using Caco-2 cell monolayers. Food Funct. 8, 701–709. https://doi.org/10.1039/C6FO01411A

Liang, N., Kim, B.J., Dallas, D.C., 2022. Bioavailability of Peptides Derived from the In Vitro Digestion of Human Milk Assessed by Caco-2 Cell Monolayers.

J. Agric. Food Chem. 70, 7077–7084. https://doi.org/10.1021/acs.jafc.2c01246

Lucas, A., Cole, T.J., 1990. Breast milk and neonatal necrotising enterocolitis. The Lancet 336, 1519–1523. https://doi.org/10.1016/0140-6736(90)93304-8

Ma, Y., Hou, Y., Xie, K., Zhang, L., Zhou, P., 2021. Digestive differences in immunoglobulin G and lactoferrin among human, bovine, and caprine milk following in vitro digestion. International Dairy Journal 120, 105081. https://doi.org/10.1016/j.idairyj.2021.105081

Martin, C., Ling, P.-R., Blackburn, G., 2016. Review of Infant Feeding: Key Features of Breast Milk and Infant Formula. Nutrients 8, 279. https://doi.org/10.3390/nu8050279

McKinney, W., 2010. pandas.

McNamara, J., 2023. XlsxWriter: A Python module for creating Excel XLSX files.

Ménard, O., Bourlieu, C., De Oliveira, S.C., Dellarosa, N., Laghi, L., Carrière, F., Capozzi, F., Dupont, D., Deglaire, A., 2018. A first step towards a consensus static in vitro model for simulating full-term infant digestion. Food Chemistry 240, 338–345. https://doi.org/10.1016/j.foodchem.2017.07.145

Minkiewicz, P., Iwaniak, A., Darewicz, M., 2019. BIOPEP-UWM Database of Bioactive Peptides: Current Opportunities. IJMS 20, 5978. https://doi.org/10.3390/ijms20235978

Mooney, C., Haslam, N.J., Pollastri, G., Shields, D.C., 2012. Towards the Improved Discovery and Design of Functional Peptides: Common Features of Diverse Classes Permit Generalized Prediction of Bioactivity. PLoS ONE 7, e45012. https://doi.org/10.1371/journal.pone.0045012

Musa, Md.A., Kabir, M., Hossain, Md.I., Ahmed, E., Siddique, A., Rashid, H., Mahfuz, M., Mondal, D., Ahmed, T., Petri, W.A., Haque, R., 2019. Measurement of intestinal permeability using lactulose and mannitol with conventional five hours and shortened two hours urine collection by two different methods: HPAE-PAD and LC-MSMS. PLoS ONE 14, e0220397. https://doi.org/10.1371/journal.pone.0220397

Nielsen, P.M., Petersen, D., Dambmann, C., 2001. Improved Method for Determining Food Protein Degree of Hydrolysis. Journal of Food Science 66, 642–646. https://doi.org/10.1111/j.1365-2621.2001.tb04614.x

Nielsen, S.D., Beverly, R.L., Qu, Y., Dallas, D.C., 2017. Milk bioactive peptide database: A comprehensive database of milk protein-derived bioactive peptides and novel visualization. Food Chemistry 232, 673–682. https://doi.org/10.1016/j.foodchem.2017.04.056

Nielsen, S.D., Beverly, R.L., Underwood, M.A., Dallas, D.C., 2018. Release of functional peptides from mother's milk and fortifier proteins in the premature infant stomach. PLoS ONE 13, e0208204. https://doi.org/10.1371/journal.pone.0208204

Noel, G., In, J.G., Lemme-Dumit, J.M., DeVine, L.R., Cole, R.N., Guerrerio, A.L., Campbell, J.D., Kovbasnjuk, O., Pasetti, M.F., 2021. Human Breast Milk Enhances Intestinal Mucosal Barrier Function and Innate Immunity in a Healthy Pediatric Human Enteroid Model. Front. Cell Dev. Biol. 9, 685171. https://doi.org/10.3389/fcell.2021.685171

Pannaraj, P.S., Li, F., Cerini, C., Bender, J.M., Yang, S., Rollie, A., Adisetiyo, H., Zabih, S., Lincez, P.J., Bittinger, K., Bailey, A., Bushman, F.D., Sleasman, J.W., Aldrovandi, G.M., 2017. Association Between Breast Milk Bacterial

Communities and Establishment and Development of the Infant Gut Microbiome. JAMA Pediatr 171, 647. https://doi.org/10.1001/jamapediatrics.2017.0378

Paparo, L., Picariello, G., Bruno, C., Pisapia, L., Canale, V., Sarracino, A., Nocerino, R., Carucci, L., Cosenza, L., Cozzolino, T., Berni Canani, R., 2021. Tolerogenic Effect Elicited by Protein Fraction Derived From Different Formulas for Dietary Treatment of Cow's Milk Allergy in Human Cells. Front. Immunol. 11, 604075. https://doi.org/10.3389/fimmu.2020.604075

Pedregosa, F., 2011. scikit-learn.

Picariello, G., Miralles, B., Mamone, G., Sánchez-Rivera, L., Recio, I., Addeo, F., Ferranti, P., 2015. Role of intestinal brush border peptidases in the simulated digestion of milk proteins. Molecular Nutrition Food Res 59, 948–956. https://doi.org/10.1002/mnfr.201400856

Python Software Foundation, n.d. Python Language Reference, Version 3.10.

Quigley, M., Embleton, N.D., Meader, N., McGuire, W., 2024. Donor human milk for preventing necrotising enterocolitis in very preterm or very low-birthweight infants. Cochrane Database of Systematic Reviews 2024. https://doi.org/10.1002/14651858.CD002971.pub6

Sánchez-Hernández, S., Théron, L., Jiménez-Barrios, P., Olalla-Herrera, M., Recio, I., Miralles, B., 2021. Protein Profile and Simulated Digestive Behavior of Breast Milk from Overweight and Normal Weight Mothers. Foods 10, 887. https://doi.org/10.3390/foods10040887

Sangild, P.T., Ney, D.M., Sigalet, D.L., Vegge, A., Burrin, D., 2014. Animal models of gastrointestinal and liver diseases. Animal models of infant short bowel syndrome: translational relevance and challenges. American Journal of

Physiology-Gastrointestinal and Liver Physiology 307, G1147–G1168. https://doi.org/10.1152/ajpgi.00088.2014

Sun, H., Chow, E.C., Liu, S., Du, Y., Pang, K.S., 2008. The Caco-2 cell monolayer: usefulness and limitations. Expert Opinion on Drug Metabolism & Toxicology 4, 395–411. https://doi.org/10.1517/17425255.4.4.395

Tretyakov, K., 2012. matplotlib-venn: A Python library for plotting Venn diagrams.

UNICEF., W.H.O., 2003. Global Strategy for Infant and Young Child Feeding. World Health Organization, Geneva.

Van Berkel, P.H.C., Geerts, M.E.J., Van Veen, H.A., Kooiman, P.M., Pieper, F.R., De Boer, H.A., Nuijens, J.H., 1995. Glycosylated and unglycosylated human lactoferrins both bind iron and show identical affinities towards human lysozyme and bacterial lipopolysaccharide, but differ in their susceptibilities towards tryptic proteolysis. Biochemical Journal 312, 107–114. https://doi.org/10.1042/bj3120107

Vergauwen, H., 2015. The IPEC-J2 Cell Line, in: Verhoeckx, K., Cotter, P., López-Expósito, I., Kleiveland, C., Lea, T., Mackie, A., Requena, T., Swiatecka, D., Wichers, H. (Eds.), The Impact of Food Bioactives on Health: In Vitro and Ex Vivo Models. Springer, Cham (CH).

Virtanen, P., 2020. SciPy.

Waskom, M., 2021. seaborn.

Weaver, L.T., Laker, M.F., Nelson, R., 1984. Intestinal permeability in the newborn. Arch Dis Child 59, 236–241. https://doi.org/10.1136/adc.59.3.236

Weström, B., Arévalo Sureda, E., Pierzynowska, K., Pierzynowski, S.G., Pérez-Cano, F.-J., 2020. The Immature Gut Barrier and Its Importance in Establishing Immunity in Newborn Mammals. Frontiers in Immunology 11.

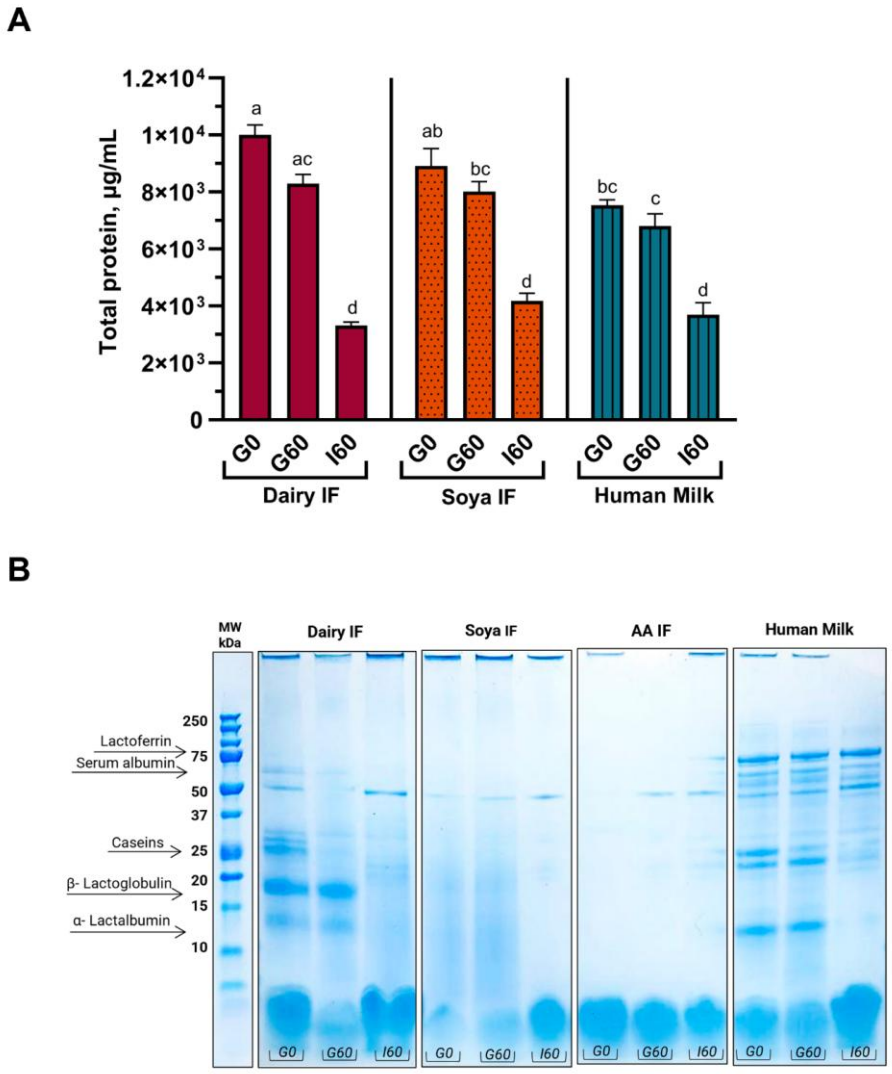
World Health Organization., 2014. Global Nutrition Targets 2025: Breastfeeding Policy Brief.

Xu, Q., Hong, H., Wu, J., Yan, X., 2019. Bioavailability of bioactive peptides derived from food proteins across the intestinal epithelial membrane: A review. Trends in Food Science & Technology 86, 399–411. https://doi.org/10.1016/j.tifs.2019.02.050

Zenker, H.E., Wichers, H.J., Tomassen, M.M.M., Boeren, S., De Jong, N.W., Hettinga, K.A., 2020. Peptide Release after Simulated Infant In Vitro Digestion of Dry Heated Cow's Milk Protein and Transport of Potentially Immunoreactive Peptides across the Caco-2 Cell Monolayer. Nutrients 12, 2483. https://doi.org/10.3390/nu12082483

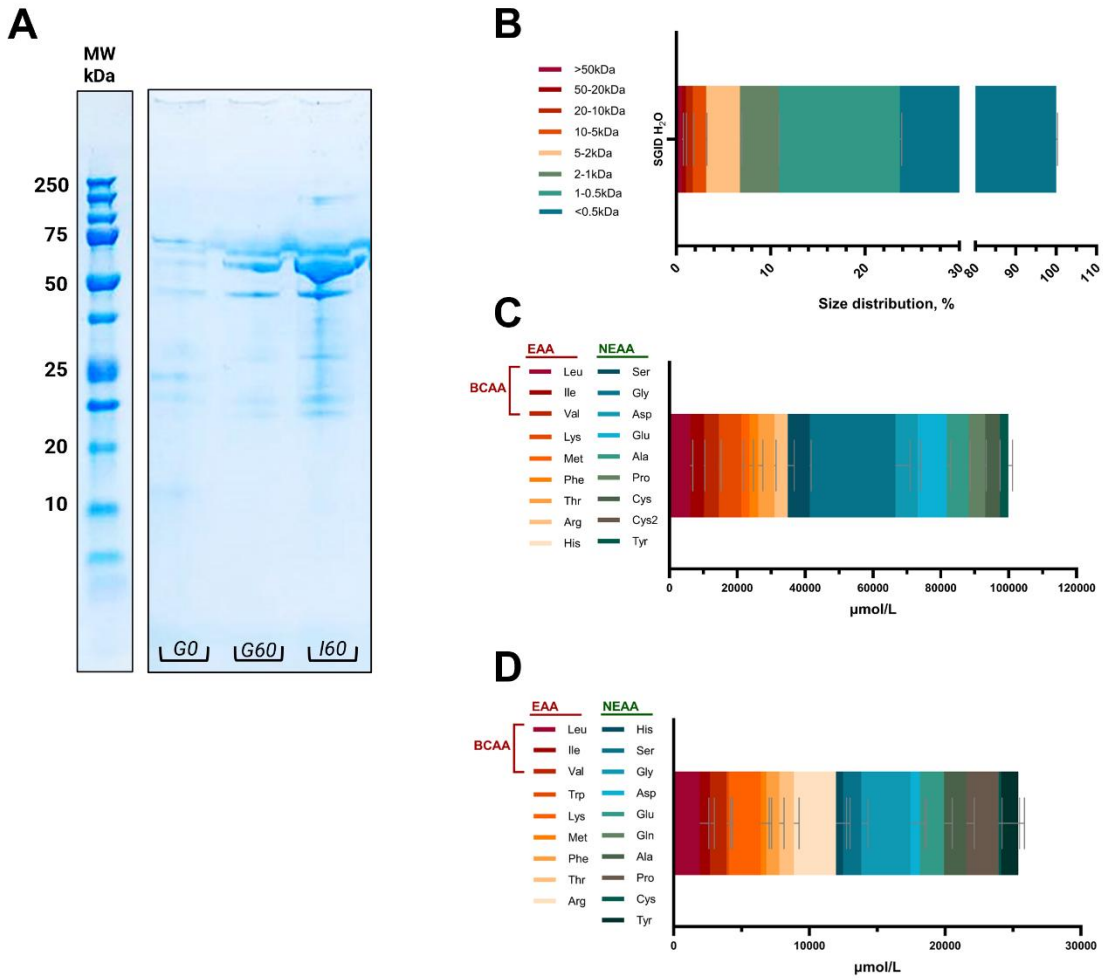
Zhao, X., Xu, X.-X., Liu, Y., Xi, E.-Z., An, J.-J., Tabys, D., Liu, N., 2019. The In Vitro Protective Role of Bovine Lactoferrin on Intestinal Epithelial Barrier. Molecules 24, 148. https://doi.org/10.3390/molecules24010148

4.7.Supplementary Materials



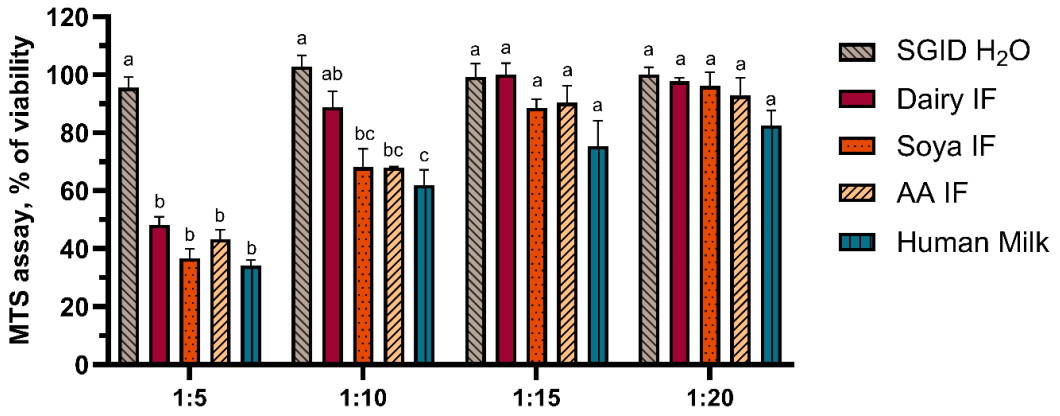
Supplementary Fig 4.1 Protein concentration and profile of digested samples measured by BCA assay and SDS page.

(A) BCA assay of soluble protein (µg/mL) of simulated gastrointestinal digestion of Dairy infant formula (IF), Soya IF, and Human Milk. Data represent mean ± SEM from three independent digestions performed on separate days. Statistical analysis was conducted using two-way ANOVA followed by Tukey's multiple comparisons test. Different letters indicate statistically significant differences ($P < 0.05$). (B) SDS-PAGE of digested samples (0.8 mg/mL loaded for Dairy IF, Soya IF, and Human Milk; amino acid-based (AA) IF (diluted equivalently). Digestion phases: G0 = before gastric phase, G60 = after gastric phase (60 min), I60 = after intestinal phase (60 min).



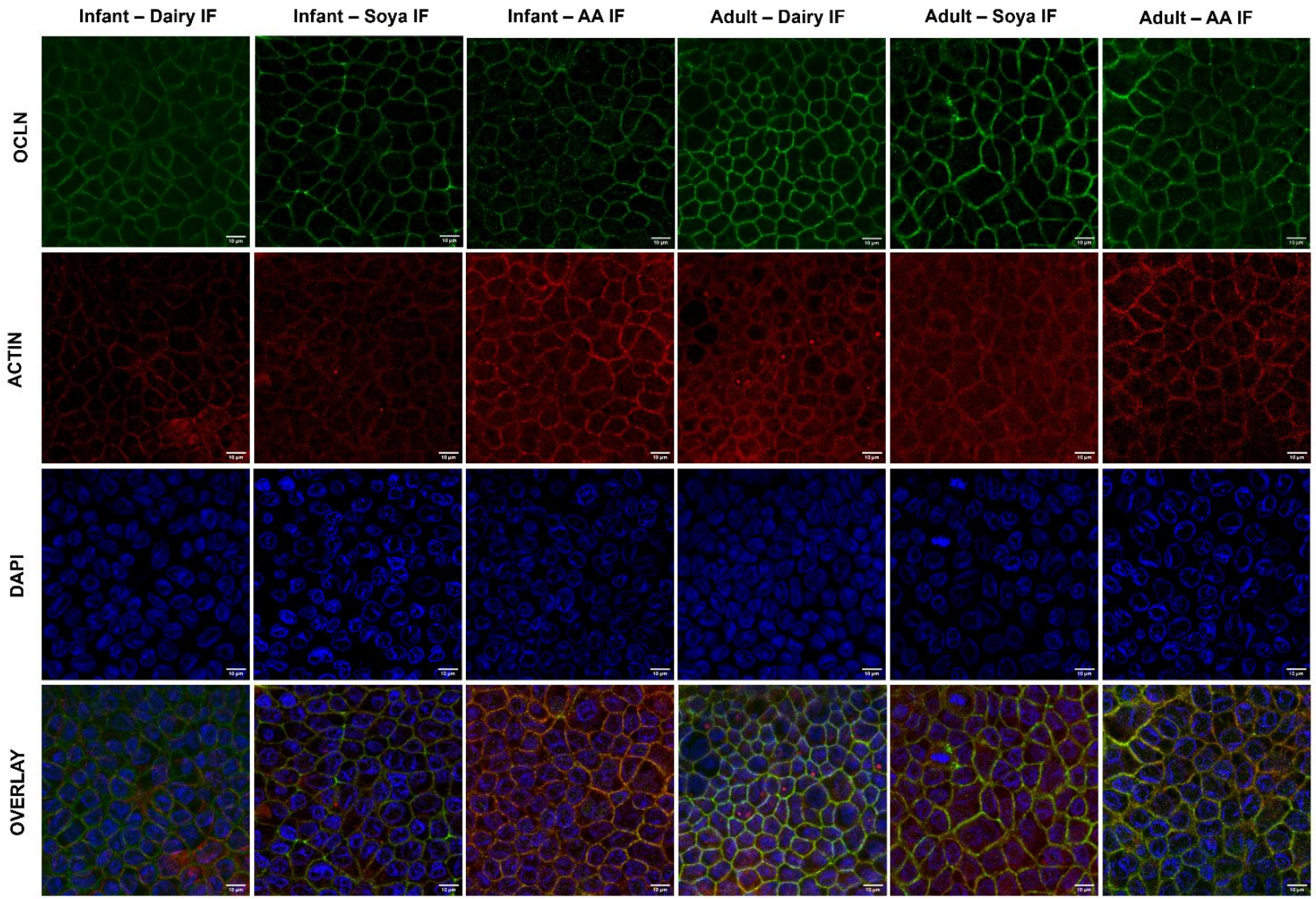
Supplementary Fig 4.2 Characterization of the simulated gastrointestinal digestion (SGID) water control (SGID H_2O).

(A) SDS-PAGE of SGID H_2O at gastric (G0, G60) and intestinal (I60) phases using RGE (gastric) and pancreatin + bile (intestinal). MW = molecular weight marker. (B) HPLC-SEC of soluble fraction from I60 SGID H_2O showing molecular size distribution (% of total eluted material). (C) Total amino acids (µmol/L) measured post-hydrolysis of methanol-precipitated supernatant. (D) Free amino acids (µmol/L) measured directly in the same supernatant. All data from three independent digestions. Amino acids: red = BCAA, red + orange = EAA, blue/green = NEAA.



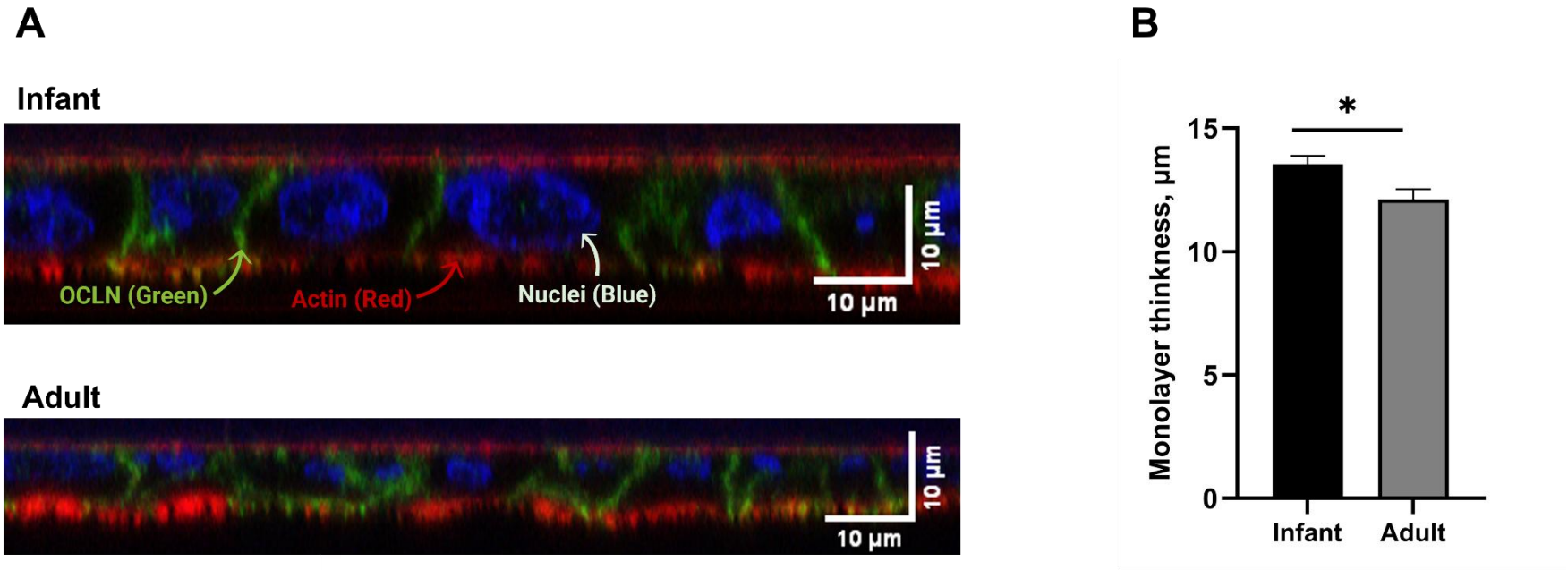
Supplementary Fig 4.3 Cell viability of Caco-2/HT29-MTX treated with digested infant formulae (IF) and Human Milk.

Undifferentiated Caco-2/HT29-MTX cells were treated for 2 h with digested Dairy, Soya and amino acid-based (AA) IF and Human Milk (diluted 1:5, 1:10, 1:15, 1:20 in HBSS). Viability was measured by MTS. Viability was calculated as a % of cells treated with HBSS (assigned 100% viability). SGID H_2O= cells treated with water subjected to the digestion process. Results represent the mean of three replicates performed on three different days in duplicate. Statistical analysis was performed by one-way ANOVA with Tukey's multiple comparison. Samples with different letters were significantly different ($P < 0.05$). Viability of cells in HBSS was 93.79 ± 5.53 % of cells in complete DMEM media.


Infant – Dairy IF
Infant – Soya IF
Infant – AA IF
Adult – Dairy IF
Adult – Soya IF
Adult – AA IF
OCLN
ACTIN
DAPI
OVERLAY

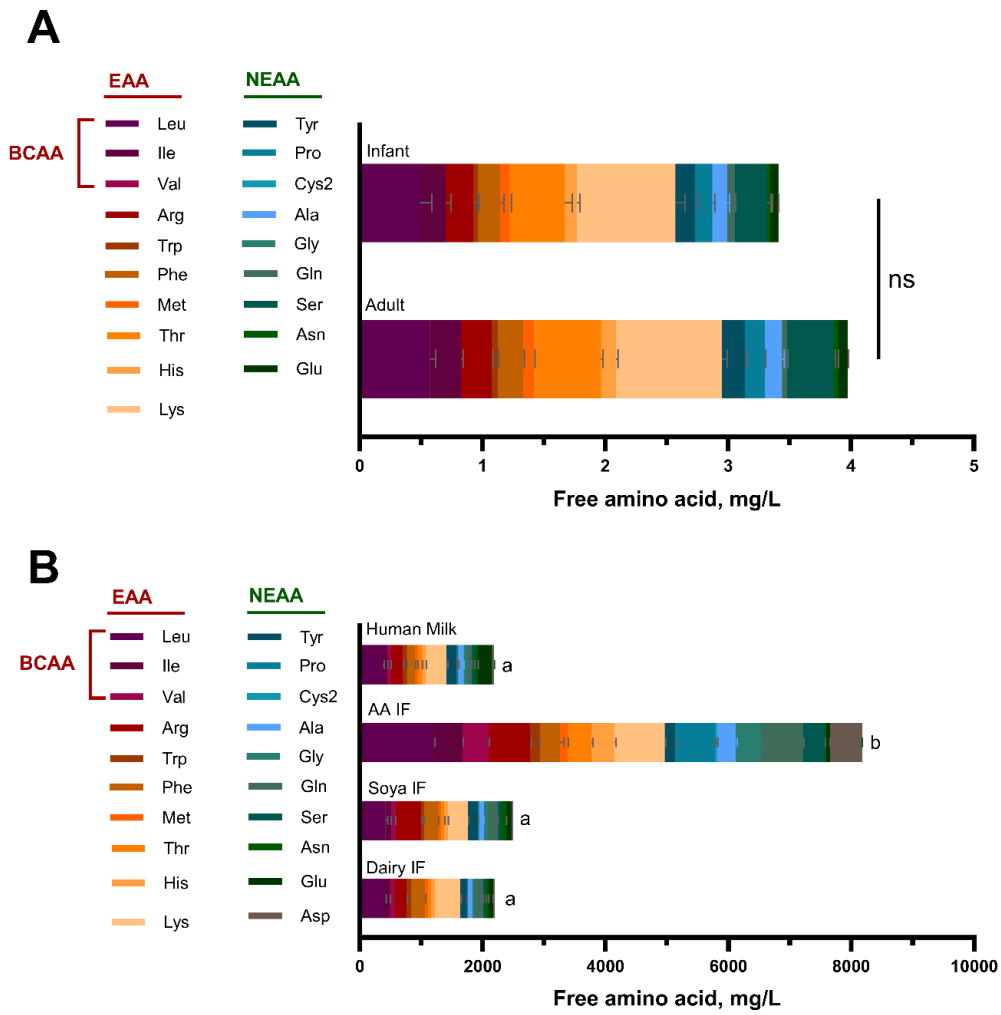
Supplementary Fig 4.4 Occludin (OCLN) localization in adult-like and infant-like Caco-2/HT29-MTX monolayers following exposure to digested infant formulae (IF).

Adult-like and infant-like Caco-2/HT29-MTX (90:10) monolayers were cultured for 25 days and treated for 2 h with digested Dairy, Soya, and amino acid-based (AA) IF. Representative confocal microscopy images show staining for OCLN (Alexa Fluor 488, green), actin (Phalloidin 555, red), and nuclei (DAPI, blue), with overlay images presented for each condition. Scale bar = 10 µm. These images correspond to the treatments analyzed in Figure 4 and are shown here to illustrate OCLN localization across all dietary exposures in both adult-like and infant-like intestinal models.



Supplementary Fig 4.5 Monolayer thickness of control adult-like and infant-like intestinal models.

Adult-like and infant-like Caco-2/HT29-MTX (90:10) monolayers were cultured for 25 days and treated with HBSS for 2 h. Monolayers were analyzed by confocal microscopy to assess structural differences between the two models at control condition. (A) Representative confocal images showing OCLN (OCLN, green, Alexa Fluor 488), actin (red, Rhodamine Phalloidin 555), and nuclei (blue, DAPI) staining. Arrows indicate specific structures: red arrows = actin; green arrows = OCLN; white arrows = nuclei. (B) Quantification of monolayer thickness (µm) based on z-stack confocal imaging, calculated as the average of measurements from both XY and XZ reconstructions. Data represent mean ± SEM from three biological replicates, with three images analyzed per replicate. Statistical analysis was performed using an unpaired t-test; asterisks indicate statistically significant differences ($P < 0.05$).



Supplementary Fig 4.6 Free amino acids in the basolateral compartment of HBSS-treated monolayers and digesta.

Free amino acid concentrations (mg/L) were measured by UHPLC–HRMS/MS. (A) Basolateral compartment after 2 h exposure of adult- and infant-like Caco-2/HT29-MTX monolayers to HBSS, included as a control to assess background amino acid levels without digesta. (B) Digested Dairy IF, Soya IF, amino acid-based (AA) IF, and Human Milk. Data are mean ± SEM from three biological replicates (technical duplicates). Statistical analysis: (A) unpaired t-tests, ns = not significant ($P > 0.05$); (B) one-way ANOVA with Tukey's multiple comparison, different letters indicate significant differences ($P < 0.05$). Amino acids: red = BCAA, red + orange = EAA, blue/green = NEAA.

Supplementary Table 4.1 Concentrations (ρmol/µL) of total amino acids in post-intestinal (I60) digesta of infant formulae and human milk, measured by UPLC.

Data shown as mean ± SEM for n = 3 per group.

	SGID H_2O		SGID Dairy IF		SGID Soya IF		SGID AA IF		SGID Human Milk	
	Mean	**SEM**	**Mean**	**SEM**	**Mean**	**SEM**	**Mean**	**SEM**	**Mean**	**SEM**
Leu	6101.1	771.212	39956.1	1145.641	32942.1	1068.657	61014.3	631.5231	33652.5	394.7436
Ile	4095.3	287.8389	18966.3	729.8322	19520.1	436.0711	36243	527.5753	18212.1	192.9602
Val	4380.3	671.108	23419.5	1010.203	22556.7	498.8764	42834.9	1639.87	20499.9	134.4813
Lys	6607.5	723.6142	29784	573.3488	24944.1	538.9834	40824	769.9616	23594.1	326.5584
Met	2393.7	1200.28	10596.9	176.5716	8984.1	294.2791	12283.8	489.125	8071.5	71.00373
Phe	2640	1320.774	17722.2	426.5185	17825.4	490.6117	18937.5	2915.282	11264.7	128.1695
Thr	4810.5	399.0686	20503.5	523.419	19055.7	589.7262	33575.1	1364.362	15909.3	65.47771
Arg	3840.3	1921.742	11841.6	136.5831	24264.6	735.8604	32268.6	819.7935	11630.4	61.14336
His	0	0	8319.3	233.8675	9321.9	187.8115	18741	500.0449	8193.6	96.49886
Ser	6495.6	441.0861	21562.8	490.0777	27974.4	904.685	34712.7	1540.951	18321.9	581.9005
Gly	25250.7	4348.048	38664.6	656.3998	50334.3	1006.163	84741.3	2826.841	38981.1	294.1207
Asp	6691.2	723.0088	31728.6	684.6051	41279.4	1033.28	38690.1	1162.935	27410.4	448.8294
Glu	8430.6	1150.842	51845.7	1325.945	62339.7	1438.664	49854	1461.55	50277	698.9761
Ala	6428.4	480.608	24421.2	453.8804	27231.3	777.746	36873.9	2015.752	19597.8	270.1501
Pro	4889.1	337.9027	26971.5	680.9082	24076.2	659.8856	50307	579.3322	32463.9	514.0539
Cys	4362.6	38.19201	3917.1	108.1715	3811.5	34.88395	3690.3	74.24742	3995.4	80.27229
Cys2	0	0	2006.7	60.70906	1094.1	7.280797	407.1	407.1	2202.6	74.38004
Tyr	2472	1246.722	12567	234.6144	12624.6	395.687	14222.4	1633.697	12782.4	360.8676

Supplementary Table 4.2 Concentrations (ρmol/μL) of free amino acids in post-intestinal (I60) digesta of infant formulae and human milk, measured by UPLC.

Data shown as mean ± SEM for n = 3 per group.

	SGID H_2O		SGID Dairy IF		SGID Soya IF		SGID AA IF		SGID Human Milk	
	Mean	**SEM**	**Mean**	**SEM**	**Mean**	**SEM**	**Mean**	**SEM**	**Mean**	**SEM**
Leu	1924.033	677.0016	11057.87	1557.448	12101.7	801.9466	34018.22	2460.604	11764.07	880.5469
Ile	781.3167	293.8766	1683.333	1440.672	3539.683	286.5996	19424.92	1475.358	2878.517	142.4357
Val	1205.367	436.1665	5832.883	773.1026	406.5	36.69346	22983.55	2248.337	3371.85	170.1718
Lys	2326.75	799.2933	11826.73	2698.421	9519.05	799.9022	17311.9	1537.833	8682.667	1062.691
Met	402.8333	218.3661	2227.533	215.8774	2317.433	117.3012	5441.333	553.9881	2210.283	122.7277
Phe	970.7	334.5902	9420.867	484.8091	9028	391.7885	11970.52	2003.089	5629.7	266.9903
Thr	1060.733	377.8052	2491.867	219.3224	2706.383	168.8986	20171.68	2041.622	3051.067	127.2861
Arg	3103.217	1035.456	8585.383	520.7583	20914.9	1024.597	33651.75	3295.11	9620.817	536.8884
Trp	185.25	94.91257	2647.867	67.60107	1524.517	66.52007	5482.217	453.3166	2723.817	121.1886
His	520.8167	266.0714	2009.183	103.6411	1730.483	76.08349	13335.22	1116.867	2156.5	83.16454
Ser	1349.867	494.216	1990.483	163.1516	2580.483	169.0062	21445.32	1606.728	2569.367	66.95562
Gly	3614.983	1219.932	4960.983	162.3362	4836.933	148.594	43812.93	4517.679	6372.317	397.6701
Asp	699.8667	350.4146	1147.75	109.0987	1189.4	66.16434	17725.77	1612.506	1210.367	84.35215
Glu	1760.233	621.9885	2642.783	367.1625	2699.85	154.9704	1347.45	117.0627	7542.417	588.1177
Gln	0	0	3828.5	595.7071	0	0	16614.97	1233.726	3005.583	149.6206
Ala	1644.25	595.7736	2904.917	510.046	3909.217	293.461	18677.68	2235.034	5052.4	355.1267
Pro	2383.133	1549.57	3467.467	1537.868	520.2333	33.35521	28873.87	2202.774	664.0167	44.24658
Cys	167.8667	86.45466	310.4167	64.15846	436.8167	22.06599	784.55	340.1721	936.3	80.84635
Tyr	1280.767	457.9459	979.45	151.8583	8348	365.9186	10209.95	1222.533	8698	391.8101

Supplementary Table 4.3 Concentrations (mg/L) of free amino acids in the basolateral compartment after exposure of Adult-like and Infant-like Caco-2/HT29-MTX monolayers to infant formulae and human milk, measured by UHPLC-HRMS.

Data shown as mean ± SEM for n = 3 per group.

	Adult Dairy		Infant Dairy		Adult Soya		Infant Soya		Adult AA		Infant AA		Adult Human Milk		Infant Human Milk	
	Mean	SEM	Mean	SEM	Mean	SEM	Mean	SEM	Mean	SEM	Mean	SEM	Mean	SEM	Mean	SEM
Leu	0.2538	0.0018	0.3606	0.0331	0.2218	0.0070	0.2959	0.0395	0.4217	0.0285	0.4924	0.0476	0.2724	0.0320	0.2789	0.0356
Ile	0.2458	0.0113	0.2605	0.0245	0.3121	0.0128	0.2927	0.0251	0.3336	0.0185	0.3638	0.0327	0.2640	0.0265	0.2388	0.0343
Val	0.3078	0.0263	0.2900	0.0163	0.3601	0.0693	0.4252	0.0705	0.4023	0.0192	0.4310	0.0242	0.4208	0.0448	0.4290	0.0335
Trp	0.0524	0.0010	0.0698	0.0095	0.0609	0.0025	0.0681	0.0054	0.0803	0.0063	0.0908	0.0045	0.0622	0.0068	0.0648	0.0025
Phe	0.2327	0.0107	0.2853	0.0333	0.2518	0.0115	0.2827	0.0234	0.2643	0.0144	0.2709	0.0055	0.2257	0.0226	0.2113	0.0141
Met	0.0770	0.0011	0.0957	0.0100	0.0822	0.0045	0.0931	0.0027	0.0948	0.0033	0.1004	0.0064	0.0828	0.0075	0.0811	0.0086
Thr	0.4732	0.0218	0.5308	0.0318	0.5513	0.0129	0.5406	0.0293	0.6184	0.0269	0.6120	0.0478	0.5329	0.0148	0.4819	0.0335
His	0.2316	0.0035	0.3418	0.0384	0.3120	0.0283	0.3168	0.0237	0.3549	0.0354	0.3772	0.0140	0.2631	0.0271	0.2304	0.0275
Arg	0.5850	0.0042	0.5809	0.0331	0.6958	0.0321	0.6310	0.0568	0.8567	0.0331	0.7785	0.0210	0.6064	0.0296	0.4942	0.0354
Lys	1.0022	0.0023	1.0595	0.1129	1.0449	0.0175	1.0636	0.0375	1.1258	0.0353	1.0974	0.0601	1.0637	0.0177	1.0660	0.0288
Tyr	0.2364	0.0250	0.2761	0.0299	0.2740	0.0093	0.2985	0.0368	0.2664	0.0051	0.2701	0.0392	0.2931	0.0231	0.2631	0.0176
Pro	0.1933	0.0089	0.1719	0.0130	0.1767	0.0037	0.1772	0.0107	0.4137	0.0424	0.4629	0.0200	0.2364	0.0280	0.2098	0.0006
Cys2	0.0241	0.0241	0.0227	0.0125	0.0172	0.0172	0.0415	0.0184	0.0466	0.0024	0.0569	0.0158	0.0506	0.0016	0.0000	0.0000
Ala	0.2281	0.0065	0.2148	0.0181	0.1836	0.0080	0.2269	0.0242	0.2496	0.0352	0.2887	0.0065	0.2140	0.0319	0.2196	0.0066
Gly	0.0000	0.0000	0.2687	0.0239	0.0000	0.0000	0.0000	0.0000	0.2062	0.1037	0.4351	0.0293	0.0000	0.0000	0.0000	0.0000
Gln	0.0568	0.0027	0.0807	0.0047	0.0592	0.0021	0.0795	0.0115	0.1225	0.0173	0.1852	0.0157	0.0492	0.0056	0.0607	0.0025
Ser	0.3919	0.0249	0.6175	0.1050	0.4392	0.0139	0.4041	0.0583	0.5130	0.0434	0.6475	0.0567	0.4354	0.0375	0.3969	0.0817
Asn	0.0617	0.0050	0.0728	0.0120	0.0795	0.0032	0.0928	0.0048	0.0700	0.0036	0.0584	0.0025	0.0741	0.0106	0.9707	0.0248
Glu	0.2101	0.0003	0.2463	0.0258	0.2263	0.0093	0.2297	0.0150	0.2371	0.0147	0.2505	0.0125	0.2307	0.0086	0.2473	0.0197
Asp	0.8789	0.0440	0.7869	0.0366	0.8337	0.0536	0.8842	0.0282	1.0344	0.0503	1.0054	0.0344	0.8980	0.0587	0.9707	0.0248

Supplementary Table 4.4 Concentrations (mg/L) of free amino acids in post-intestinal (I60) digesta of infant formulae and human milk, measured by UHPLC-HRMS.

Data shown as mean ± SEM for n = 3 per group.

	Dairy IF		Soya IF		AA IF		Human Milk	
	Mean	**SEM**	**Mean**	**SEM**	**Mean**	**SEM**	**Mean**	**SEM**
Leu	420.677	10.362	415.127	40.101	1204.092	15.667	373.439	22.846
Ile	73.549	2.468	90.343	3.875	464.459	14.148	74.794	6.124
Val	79.330	1.679	77.821	2.815	426.865	18.352	60.208	3.015
Trp	70.415	1.691	47.487	1.344	155.691	2.802	73.849	5.627
Phe	230.455	10.062	229.964	5.937	327.893	64.511	128.802	7.908
Met	45.502	0.941	47.544	1.298	124.438	8.103	48.194	3.849
Thr	53.581	0.424	52.448	1.553	389.792	18.101	64.793	4.948
His	59.997	0.377	59.190	3.333	380.213	13.539	63.847	4.960
Arg	188.025	7.403	419.156	6.869	679.804	21.574	187.787	13.423
Lys	415.239	15.768	326.036	7.047	812.254	16.789	337.634	18.973
Tyr	107.781	3.787	162.239	9.989	164.465	26.607	161.955	10.165
Pro	10.997	0.368	13.959	0.429	653.508	15.098	28.309	2.632
Cys2	8.895	0.296	6.393	0.127	29.957	14.667	11.873	0.658
Ala	67.258	1.139	75.521	2.597	307.198	20.028	77.832	4.109
Gly	37.928	0.249	55.692	0.919	412.044	18.858	58.208	4.368
Gln	140.071	4.392	161.875	5.730	688.197	12.646	66.339	5.998
Ser	42.450	1.647	55.989	0.522	351.991	12.825	50.321	5.961
Asn	39.992	1.590	91.372	3.434	21.374	0.692	54.272	4.087
Glu	79.778	2.304	80.847	0.659	56.566	1.076	230.319	17.776
Asp	24.285	0.093	21.984	0.510	526.804	4.826	33.842	3.367

5. Chapter 5

Culture Optimization of the IPEC-J2 Piglet Jejunum Cell Line for Applications in Infant Nutrition Research

A version of this chapter has been submitted to **Molecular Nutrition and Food Research**:

Bietto F.[a,b], Grundy M.[c], Arranz E.[d,e], Wiart-Letort S.[c], Rath E.[e], Lucey A. J.[b], Giblin L.[a]. Culture Optimization of the IPEC-J2 Piglet Jejunum Cell Line for Applications in Infant Nutrition Research.

[a]*Teagasc Food Research Centre, Moorepark, Fermoy, Co. Cork, Ireland*
[b]*School of Food and Nutritional Sciences, University College Cork, Cork, Ireland*
[c]*INRAE, French National Research Institute for Agriculture, Food and Environment, UMR PEGASE, Institut Agro, 35590, Saint Gilles, France*
[d]*Sección Departamental de Ciencias de la Alimentación, Universidad Autónoma de Madrid (UAM), Madrid, Spain*
[e]*Institute of Food Science Research CIAL (CSIC-UAM), Madrid, Spain*
[f]*Chair of Nutrition and Immunology, School of Life Sciences, Technische Universität München, Freising, Germany*

Abstract

The intestinal porcine epithelial cell line (IPEC-J2) is a non-transformed jejunal model derived from unsuckled piglets that forms a polarized monolayer. It is increasingly used in gut physiology research, yet its application to digested food components and nutrient absorption remains underexplored.

Four media types were assessed for their ability to support IPEC-J2 barrier integrity, maturation and permeability: Dulbecco's modified Eagle medium/Ham's F-12 with 10% fetal bovine serum (FBS10), 10% porcine serum (PS10), PS10 supplemented with Wnt3a/R-spondin/Noggin conditioned medium (PS5+L-WRN), and 5% porcine serum with epidermal growth factor and insulin–transferrin–selenium (PS5+EGF+ITS).

Culture medium profoundly influenced the epithelial phenotype, with more than a 30-fold range in transepithelial electrical resistance (TEER) and plateauing evident by day 12. PS10 supported the most balanced profile, characterized by intermediate TEER ($2395.00 \pm 485.51\ \Omega \times cm^2$), lowest lactulose and mannitol permeability ($P < 0.05$), high lactate dehydrogenase activity ($P < 0.05$ vs. PS5+L-WRN and FBS10), enhanced membrane localization of zonula occludens-1 ($P < 0.05$ vs. PS5+EGF+ITS), and reduced fibroblast marker S100A4 ($P < 0.05$ vs. PS5+EGF+ITS). After exposure to digested infant milk formula, PS10 monolayers TEER values were stable if not enhanced and free AA quantified in the basolateral chamber

These findings support IPEC-J2, particularly under PS10 conditions, as a physiologically relevant alternative to Caco-2 cells for studying nutrient bioavailability and dietary effects in infant gut models.

Keywords:

IPEC-J2, Transepithelial Electrical Resistance (TEER), Infant milk formula, Amino acid transport, Tight junctions, Cell differentiation, *In vitro* digestion, INFOGEST

5.1.Introduction

The intestinal epithelium plays a central role in nutrient absorption, barrier integrity, and immune signaling within the gastrointestinal tract. It acts as a selective interface between the external environment (digested food) and the systemic system, facilitating the uptake of nutrients while restricting the translocation of antigens, toxins, and pathogens (Chelakkot et al., 2018). The barrier's integrity is maintained by a highly organized structure of polarized epithelial cells joined by tight junction proteins, such as zonula occludens-1 (ZO1), occludin (OCLN), and claudins (CLDN1/2/4), which control paracellular permeability and maintain separation between apical and basolateral compartments (Otani and Furuse, 2020). The apical surface is coated with mucins, such as glycoproteins MUC1 and MUC2, which form a protective mucus layer that supports microbial balance and limits microbial contact with the epithelium (Paone and Cani, 2020). Embedded within the epithelial membrane are nutrient transporters that mediate the selective uptake of carbohydrates, peptides, amino acids (AA), and lipids critical for host metabolism (Kiela and Ghishan, 2016). Additionally, the epithelial barrier plays an active role in immune defense by producing cytokines such as interleukin-6 (IL-6), interleukin-8 (IL-8), and tumor necrosis factor (TNF), which orchestrate responses to infection and inflammation (Meyer et al., 2023). Together, these components define the structural and immunological integrity of the epithelial barrier.

Due to the complexity, cost, and ethical constraints of *in vivo* studies, *in vitro* models of intestinal epithelial cells are often the first choice for investigating nutrient absorption, gut function and responses to dietary or microbial stimuli (Sangild et al., 2014).

Despite their widespread use, standard models of the gut barrier, such as the human-derived Caco-2 cell line, present significant limitations. Originating from a colonic adenocarcinoma, Caco-2 cells are tumorigenic, of adult origin, and have a low permeability similar to colon (Lea, 2015). Their phenotype does not accurately recapitulate the morphology, permeability, or immune responsiveness of the small intestinal epithelium (Sun et al., 2008). One widely used *in vitro* metric of barrier integrity is transepithelial electrical resistance (TEER), a quantitative, non-invasive method for evaluating the tightness of the cell monolayer and its capacity to restrict passive ion flow (Srinivasan et al., 2015). Caco-2 monolayers cultured for 21 days typically develop TEER values in the range of ~200–4000 Ω×cm², which is considerably higher than the adult human small intestine, where TEER values measured in Ussing chambers are only ~50–100 Ω×cm² (Srinivasan et al., 2015) These limitations are particularly problematic in the context of infant nutrition, where the gut barrier is naturally more permeable (Catassi et al., 1995; Kosek et al., 2017; Weaver et al., 1984). As such, Caco-2 cells may not be suitable for studying the effects of digested infant formulae or modelling the unique characteristics of the neonatal intestinal barrier.

In contrast, the intestinal porcine enterocyte cell line IPEC-J2, isolated from the jejunum of an unsuckled neonatal piglet (Berschneider, 1989), offers several advantages. It is non-transformed and is morphologically and functionally similar to primary small intestinal epithelial cells. If grown on a permeable support for 14 days, IPEC-J2 cells grow into tightly adherent, columnar epithelial monolayers that exhibit clear apical-basal polarity, forming dense brush borders composed of microvilli (Geens and Niewold, 2011; Nossol et al., 2015; Schierack et al., 2006; Zakrzewski et al., 2013). The differentiated nature of this epithelial barrier is further supported by

the expression of tight junction proteins such as OCLN, claudins (e.g., CLDN1, 3, 4), and ZO1 (Brosnahan and Brown, 2012). IPEC-J2 cells also produce mucins such as MUC1 (Schierack et al., 2006) and MUC3 (Liu et al., 2010) but MUC2 is limited, and not always detected (Perruchot et al., 2025; Schierack et al., 2006; Støy et al., 2013). IPEC-J2 express a repertoire of nutrient transporters including the sodium-glucose co-transporter 1 (SGLT1) (Chen et al., 2021; Liao et al., 2017; Støy et al., 2013; Tang and Xiong, 2022), and glucose transporter 2 (GLUT2) (Chen et al., 2021; Liao et al., 2017; Tang and Xiong, 2022), the peptide transporter 1 (PEPT1) (Chen et al., 2021; Liao et al., 2017) and several AA transporters such as the neutral and cationic AA transporter $B^{0,+}$ ($B^{0,+}AT$), cationic AA transporter y^+L (y^+LAT1), alanine-serine-cysteine transporter 2 (ASCT2) (Chen et al., 2021; Liao et al., 2017). They also express key fatty acid transport and metabolism genes, including fatty acid transport proteins 1 and 4 (FATP1/4), cluster of differentiation 36 (CD36), fatty acid-binding protein 3 (FABP3), and diacylglycerol O-acyltransferase 1 (DGAT1) (Chen et al., 2021; Xu et al., 2023). This broad expression of nutrient transporters makes IPEC-J2 a valuable model for investigating intestinal nutrient absorption and the bioavailability of dietary components.Furthermore, IPEC-J2 cells function as an immunocompetent epithelial model, expressing interleukin-6 (IL6), interleukin-8 (IL8), tumor necrosis factor (TNF), chemokines, toll-like receptors, and β-defensins in response to stimuli such as lipopolysaccharide (LPS) or live pathogens (Brosnahan and Brown, 2012; Mariani et al., 2009). This makes them a useful system for studying immune-epithelial interactions and the impact of diet on intestinal immunity. Moreover, IPEC-J2 cells express the neonatal Fc receptor (FcRn) on the apical surface, which mediates bidirectional transport of immunoglobulin G (IgG) across polarized monolayers (Guo et al., 2016), offering a

valuable model to study mucosal antibody trafficking in the infant intestinal epithelium.

In terms of metabolism, IPEC-J2 cells rely on both oxidative phosphorylation and glycolysis (Nossol et al., 2015), but will favor glycolysis upon reaching confluence (Bernardini et al., 2021). The capacity to utilize both pathways, indicates IPEC-J2 are more physiologically relevant to study normal intestinal energy metabolism than Caco-2 cells, which depend solely on glycolysis (Vander Heiden et al., 2009),

However, despite its biological relevance, there is a lack of standardized culture protocols for IPEC-J2 monolayers. Moreover, the passage number is not provided by the culture collection, making it difficult to assess how subculturing influences barrier development. Reproducibility is therefore an issue across experiments and between laboratories. This variability is particularly evident in measurements of TEER where IPEC-J2 monolayers develop TEER values that vary depending on serum conditions. When grown in Dulbecco's Modified Eagle Medium/Ham's F12 supplemented with 10% FBS, TEER values at day 14 can vary from 2,000 to over 15,000 Ω×cm² (Bernardini et al., 2021; Saaby et al., 2016; Zakrzewski et al., 2013). IPEC-J2 cells culture in 10% porcine serum (PS) typically yields lower and therefore more physiologically relevant TEER values by day 14 (~300–500 Ω×cm²) (Zakrzewski et al., 2013). Additional studies have employed supplementation with epidermal growth factor (EGF) and insulin-transferrin-selenium (ITS). EGF functions to stimulate cell proliferation (mitogenic EGFR signaling) and differentiation (Orofiamma et al., 2022).ITS acts as a defined serum substitute (Mainzer et al., 2014). Culturing IPEC-J2 cells in 5% FBS supplemented with EGF and ITS (Hu et al., 2020; Lu et al., 2002) or with 5% FBS+EGF alone results in

monolayers exhibiting TEER values of around 7,000 Ω×cm² by day 10 (Nossol et al., 2015). Combining 5% PS with EGF and ITS can achieve lower TEER values (240–330 Ω×cm²) in monolayers that have taller epithelial cells, increased microvilli density, and improved tight junction structure. These features closely resemble native jejunal architecture (Zakrzewski et al., 2013). In contrast, Perruchot et al. (2025) reported a 5% PS + EGF + ITS formulation yielding monolayers with markedly higher TEER values (3,100 ± 684 Ω×cm²) (Perruchot et al., 2025). Recently, L-WRN conditioned medium (DMEM/F12 + L-WRN supplement), used for intestinal organoid culture, has also been applied to IPEC-J2 monolayers. These supplements provide niche signals that maintain epithelial cells in a proliferative, less differentiated state by stimulating Wnt signaling (Wnt3a, R-spondin) and inhibiting BMP-driven differentiation (Noggin) (Li et al., 2018). When grown for 12 days in this medium, the IPEC-J2 cells reached a TEER of 50.3 ± 2.3 Ω×cm² (Boger et al., 2023).

Despite the widespread use of IPEC-J2 for studying microbial interactions, its application to digested food components has been extremely limited, with only one prior report using pea flour digesta (Perruchot et al., 2025). However, the origin of IPEC-J2 from the neonatal piglet makes it particularly suited to infant nutrition studies, as the gastrointestinal tract of a 3-4 week old piglet closely mimics that of the 3-month-old human infant (Darragh and Moughan, 1995). In addition, IPEC-J2 cells were harvested from the jejunum, making this cell line highly relevant to dietary protein absorption studies, as free AAs and small peptides are absorbed at this location in the gastro-intestinal tract. The present study represents a pioneering

effort to characterize IPEC-J2 responses to digested infant formula and to optimize culture conditions for nutrient absorption research in infant nutrition

The objective of this study was to evaluate media compositions for their ability to support IPEC-J2 monolayers with reproducible TEER and to assess their biocompatibility with digested foods. We hypothesized that a good medium for IPEC-J2 should sustain a stable and reproducible TEER, maintain metabolic activity and differentiation, and preserve an enterocyte-like phenotype compatible with exposure to digested foods.

5.2. Materials and Methods

5.2.1. Materials

The cell line IPEC-J2 (ACC 701) was purchased from the Leibniz Institute DSMZ-German Collection of Microorganisms and Cell Cultures. Six-well plates with polyester permeable-membrane inserts (0.4 μm pore size, 4.5 cm^2 area), 12 well plates with polyester permeable-membrane inserts (0.4 μm pore size, 1.11 cm^2 area) and 96-wells tissue culture-treated plates (3300, CellBIND®) were purchased from Corning (USA). The Lactate Dehydrogenase Colorimetric Activity Kit (EEA013) was supplied by Invitrogen (MA, USA). CellTiter 96™ AQueous One Solution Cell Proliferation Assay (MTS, G3582). RNeasy mini kit (74104) and RNA-free DNase set (79254) were from Qiagen (Netherlands). SensiFAST cDNA Synthesis Kit (BIO-65053) was from Meridian Bioscience (UK). Light Cycler SYBR GREEN I Master kit (04707516001) was from Roche Diagnostics (Switzerland). Primers for RT-qPCR were synthesized by Eurofins Genomics (Germany). All the other reagents were purchased from Sigma-Aldrich, unless stated otherwise.

5.2.2. Cell Culture

Culture resuscitation and maintenance

IPEC-J2 cells were maintained in 75 cm² tissue culture flasks at 37 °C in a humidified incubator with 5% CO_2. Routine culture was performed according to the recommendations from the DSMZ cell line collection (ACC 701) in Dulbecco's Modified Eagle Medium/Nutrient Mixture F-12 (DMEM/F-12, D8437), supplemented with heat-inactivated 10% (v/v) FBS (F7524) and 100 U/mL Penicillin-Streptomycin (P4333), referred to as FBS10. Cells were passaged at 80% confluence every 2–3 days using 0.25% Trypsin-EDTA solution (T4049). Cells were used at passages 2–5 (with passage 1 defined as the first passage after resuscitating the stock received from the supplier). Cell counting was performed using Trypan blue exclusion and a TC20™ automated cell counter (Bio-Rad, USA).

Experimental Media

For experimental assays, IPEC-J2 cells in FBS10 were seeded onto appropriate supports depending on the experimental condition. After a 16-h attachment period, cells were washed twice with HBSS and the culture medium was replaced with one of the following:

(i) DMEM/F-12 + 10% PS + 100 U/mL Penicillin-Streptomycin, referred to as PS10 (Zakrzewski et al., 2013); (ii) DMEM/F-12 + 5% PS + 100 U/mL Penicillin-Streptomycin + 1× Insulin-Transferrin-Selenium (ITS, I3146) + 5 ng/mL Epidermal Growth Factor (EGF, E5036), referred to as PS5+EGF+ITS (Zakrzewski et al., 2013) (iii) a 1:1 (v/v) mixture of PS10 and L-WRN conditioned medium (SCM105; Sigma-Aldrich) resulting in a final serum concentration of 5%, referred to as PS5 (L-WRN); or (iv) DMEM/F-12 + 10% PS + 100 U/mL Penicillin-Streptomycin, referred

to as FBS10. Prior to use, PS was heat inactivated (60ºC for 30 min) and filtered via 0.45 μm syringe filter (Filtropur S, PES, Sarsted) before use.

5.2.3. TEER

Real-Time TEER Monitoring

For real-time TEER measurements, IPEC-J2 cells were seeded at a density of 1.2×10^5 cells/mL in 2 mL FBS10 onto polyester permeable membrane inserts (6-well format; apical chamber: 2 mL, basolateral chamber: 3 mL). After 16 h of incubation at 37 °C, the cells were washed with HBSS and the medium was replaced with one of the following: PS10, PS5+EGF+ITS, PS5+L-WRN, or FBS10 (one insert per condition). The inserts were transferred to the CellZscope system (nanoAnalytics GmbH, Germany) for continuous TEER measurements ($\Omega \times cm^2$). Both apical and basolateral chambers received 4 mL of the corresponding medium. One insert without cells was included as a blank control for TEER background values. TEER was recorded every 24 h for 14 days. Culture medium was replaced 16 h prior to each TEER measurement. The experiment was independently repeated four times on separate days.

Endpoint TEER Measurements

For experiments involving differentiated monolayers, IPEC-J2 cells were seeded at 1.2×10^5 cells/mL in 12-well Transwell plates, with 0.5 mL FBS10 in the apical chamber and 1.5 mL FBS10 added to the basolateral chamber. After a 16-h incubation, cells were washed twice with HBSS and the medium was replaced with PS10, PS5+EGF+ITS, PS5+L-WRN, or FBS10 at the same volumes. Media was changed every two days, and 16 h prior to TEER measurements. TEER was

measured at day 7 and day 14 using a Millicell-ERS Voltohmmeter (Ω × cm^2; Merck Millipore). One insert without cells was included as a blank control. Each culture condition was tested in duplicate in at least three independent experiments.

5.2.4. Alkaline phosphates (ALP) and lactate dehydrogenase (LDH) activity

IPEC-J2 monolayers were cultured for 7 or 14 days in 12-well Transwell® plates and assessed for ALP and LDH activity. After incubation, cells were washed twice with PBS and lysed in 0.5 mL of 0.2% Triton X-100 (prepared in Milli-Q H_2O) by shaking at room temperature for 20 min. Total protein concentration in cell lysates was determined using the bicinchoninic acid (BCA) assay (Pierce™, Thermo Fisher Scientific) according to the manufacturer's instructions, and enzyme activities were normalized to total protein content.

ALP Activity Assay

For ALP activity, 50 µL of cell lysate was transferred to a clear, flat-bottom 96-well plate. The assay was performed using the Alkaline Phosphatase Assay Kit (MAK447), which is based on the enzymatic conversion of p-nitrophenyl phosphate into p-nitrophenol and inorganic phosphate. Absorbance was measured at 405 nm using a Synergy HT plate reader at timepoints 0 and 4 min. A reagent blank was included, and its absorbance was subtracted to correct for background color.

ALP activity was calculated using the following formula:

$[(OD_{T4} - OD_{T0}) \times RxnVol] / \varepsilon PNP \times L \times SmplVol \times t$;

Where: OD_{t0} = absorbance at 405 nm at time 0, OD_{t4} = absorbance at 405 nm at time 4 min; RxnVol = reaction volume; εPNP = molar absorptivity of p-nitrophenol

(18.75 $mM^{-1} \cdot cm^{-1}$); L = path length in cm; SmplVol = sample volume; t = reaction time (4 min)

The optical path length (L) was calculated as:

$L = (OD_{Cal} – OD_{Blank})/(\varepsilon C)$;

Where: ODCal = absorbance at 405 nm of the kit calibrator; ODBlank = absorbance at 405 nm of the blank (medium only); ε = molar absorptivity; C = path length of the plate

LDH Activity Assay

For lactate dehydrogenase (LDH) activity, 5 µL of cell lysate was transferred to a clear, flat-bottom 96-well plate. The assay was performed using the Lactate Dehydrogenase Colorimetric Activity Kit, which measures the conversion of lactate to pyruvate. Pyruvate reacts with 2,4-dinitrophenylhydrazine to form a coloured pyruvate-hydrazone product. Absorbance at 450 nm was recorded at 3 and 6 min using a Synergy HT plate reader. Absorbance values were blank-corrected to account for reagent background. LDH activity was calculated as:

LDH activity = B/ (T × V) × Sample Dilution Factor (20)

Where: B = nmoles of NADH generated between timepoints T_3 and T_6, calculated from a standard curve; T = reaction time (3 min); V = sample volume (5 µL); Dilution Factor = 20.

5.2.5. Lactulose: Mannitol Permeability Assay

The protocol for assessing paracellular permeability using lactulose and mannitol was adapted from Kondrashina et al. (2021). Lactulose (25 mg/mL, 61360-25G) and mannitol (5 mg/mL, M9546-250G) were dissolved in HBSS, mixed in a 1:1 volume

ratio (1 part lactulose solution to 1 part mannitol solution) to generate a 2.5× working stock, and filter-sterilized (0.2 µm). IPEC-J2 monolayers were cultured for 14 days in 12-well Transwell® inserts and washed twice with HBSS. Monolayers were equilibrated at 37 °C for 30 minutes in HBSS (apical: 0.3 mL; basolateral: 1.5 mL). After equilibration, 200 µL of the lactulose/mannitol solution was added to the apical chamber, and cells were incubated for 4 h at 37 °C. TEER was recorded at time 0 and after 4 h to monitor barrier integrity. Apical and basolateral samples were collected post-incubation and stored at –20 °C for analysis. Lactulose and mannitol concentrations were measured using high-performance anion-exchange chromatography with pulsed amperometric detection (HPAEC-PAD) on an ICS-3000 system (Dionex, USA) equipped with an electrochemical detector. Apical samples were diluted 1:99 in Milli-Q water, while basolateral samples were diluted 1:1. All samples were filtered through a 0.2 µm nylon syringe filter prior to injection. Separation was performed on a CarboPac PA100 analytical column (4 × 250 mm) preceded by a PA100 guard column (4 × 50 mm), with a flow rate of 1 mL/min. The mobile phases consisted of: Eluent A = 100 mM NaOH; Eluent B = 100 mM NaOH+500 mM sodium acetate (NaOAc). The elution gradient was as follows: from t = 0 to 6 min, 100% Eluent A; at t = 13 min, 51.4% Eluent A and 48.6% Eluent B; from t = 13.1 to 23.1 minute, equilibrated at 100% Eluent A.

Lactulose and mannitol levels were quantified by comparing peak areas with known standards (10 mg/L). The results were expressed as lactulose and mannitol apparent permeability (Papp) calculated with the following formula:

$$\text{Papp (cm/min)} = (C_{Baso} \times V)/(t \times A \times C_{In})$$

Where: C_{Baso} = Concentration of lactulose/ mannitol in the basolateral compartment (mg/L); V = Volume of the basolateral compartment (L); t = incubation time (14400 sec); A = surface area (1.1 cm^2); C_{In} = initial concentration in the apical (mg/L). The L:M ratio (L:M) was also calculated in the 1X stock solution and in both apical and basolateral compartments after 4 h of incubation to evaluate changes in selective permeability.

5.2.6. Reverse Transcription Quantitative PCR (RT-qPCR)

IPEC-J2 monolayers cultured for 14 days, in 12-well Transwell® inserts with the various test media, were washed twice with PBS and lysed by adding 350 µL of RLT buffer (Qiagen). After 5 minutes on ice, the lysates were collected by pipetting and stored at –80 °C. RNA extraction was performed using the RNeasy Mini Kit (Qiagen), including an on-column DNase digestion step, according to the manufacturer's instructions. Total RNA concentration and purity were assessed using a NanoDrop 1000 spectrophotometer (Thermo Fisher Scientific, MA, USA). Only samples with an $OD_{260/280}$ ratio > 1.8 were used for downstream analysis. Complementary DNA (cDNA) was synthesized from 0.5 µg of total RNA using the SensiFAST™ cDNA Synthesis Kit (Bioline). In addition, cDNA harvested from jejunal mucosal scrapings of two male and two female aged 56 days, was kindly provided by Dold et al. (2024). Quantitative PCR was carried out using the LightCycler® SYBR Green I Master Kit (Roche) on a LightCycler® 96 instrument. Primer sequences are listed in Supplementary Table 5.1. Where necessary, primers were designed using Primer-BLAST (Ye et al., 2012) based on porcine gene sequences from GenBank. The RPLP0 gene, encoding ribosomal protein lateral stalk subunit P0, was used as the housekeeping reference. Gene expression levels were

normalized to the FBS10 condition, which represents the standard medium supplied with the cell line collection. Amplification efficiency ranged between 90–110%, and the optimal annealing temperature was 60 °C. Relative gene expression was calculated using the ΔΔCt method:

$\Delta\Delta Ct = (Ct\ Target\ gene - Ct\ RPLP0)_{test} - (Ct\ Target\ gene - Ct\ RPLP0)_{Control}$. Ct = threshold cycle for either the target gene or RPLP0; test refers to any experimental condition, control refers to FBS10 monolayers. Relative expression levels are presented as fold changes ($2^{-\Delta\Delta Ct}$), while statistical analyses were performed on the ΔΔCt values.

5.2.7. Immunofluorescence Staining of ZO1

IPEC-J2 monolayers cultured for 14 days in PS10 or PS5+EGF+ITS were fixed directly in Transwell® inserts. Fixation was performed by adding 1 mL of ice-cold methanol to both the apical and basolateral chambers for 10 min. Following fixation, cells were washed twice with PBS (1 mL per chamber) using a transfer pipette. Permeabilization was carried out for 5 mins at room temperature with 0.5% Triton X-100 in PBS (1 mL per chamber), followed by two additional PBS washes. Monolayers were then incubated for 1.5 h at 37 °C, on the apical side, with 100 µL ZO1 primary antibody directly conjugated to Alexa Fluor 594 (Ref. 3391914, Lot 1364021A; 1:99 dilution in 0.2% BSA in PBS). Inserts were then washed twice with PBS and rinsed briefly in Milli-Q water. The membrane inserts were carefully excised from the Transwell supports and mounted onto microscope glass slides using 15 µL of ProLong™ Gold Antifade Mountant with DAPI (Thermo Fisher Scientific, P36931). Coverslips were applied and sealed. Fluorescence imaging was performed using a Zeiss Axio Observer equipped with an ApoTome.2 structured illumination

system and a Plan-Apochromat 40×/1.3 Oil objective. Images were acquired using fixed exposure times: DAPI (50 ms, blue channel) and Alexa Fluor 594 (100 ms, red channel). Image processing and analysis were performed using Fiji/ImageJ software. For each field of view, a region of interest (ROI) was manually selected to include areas with well-defined nuclei. The Otsu thresholding algorithm was applied to the ZO1 channel to distinguish signal from background, and the integrated fluorescence intensity within the ROI was measured. ZO1 intensity was then normalized to the number of nuclei within the same ROI. Nuclei were counted from the DAPI channel and nuclear density was expressed as the number of nuclei per 1000 μm^2.

5.2.8. Preparation and Characterization of Dairy Infant Formula (IF) Digesta

Simulated Gastro-Intestinal Digestion

A dairy-based IF was reconstituted according to the manufacturer's instructions by dissolving 4.3 g of powder in 30 mL of Milli-Q water. Simulated infant gastrointestinal digestion was performed based on the protocol by Ménard et al. (2018), with modifications. For each digestion, 5 mL of reconstituted DAIRY IF or Milli-Q water (negative control) was mixed with 2.94 mL of infant gastric simulated fluid containing 268 U/mL pepsin (RGE15, pepsin activity: 596 U/mg). The pH was adjusted to 5.3 with 1 M HCl, and samples were incubated at 37 °C for 1 h in a rotating wheel (100 rpm). Following the gastric phase, the pH was raised to 7.0 using 1 M NaOH to inactivate pepsin. Next, 4.88 mL of simulated intestinal fluid was added, containing 16 U/mL pancreatin (trypsin activity: 8.9 U/mg) and 3.1 mM bovine bile salts. The pH was adjusted to 6.6 with 1 M HCl, and samples were incubated again at 37 °C for 1 h in the rotating wheel. After the intestinal phase, digesta were inactivated by either (i) heating at 95 °C for 10 minutes (HI), or (ii)

addition of 4-(2-aminoethyl)benzenesulfonic fluoride hydrochloride (Pefabloc; final concentration: 1 mM) and Orlistat (final concentration: 0.1 mM in ethanol) (P+O). Reconstituted dairy IF with the addition of gastric enzymes, followed by immediate inactivation with heat at 95 °C for 10 minutes represented dairy IF before digestion (dairy IF-G0). All gastrointestinal digestions were performed in triplicate on separate days. Digested dairy IF samples plus water controls—H_2O G0, H_2O (HI) and H_2O (P+O)—were aliquoted and stored at –20 °C until further analysis.

SDS PAGE

Protein profiles of the dairy IF samples (dairy IF G0, dairy IF (HI) and dairy IF (P+O)) were analyzed by SDS-PAGE. Protein concentration was determined using the bicinchoninic acid (BCA) assay (Pierce®, Thermo Fisher Scientific, Ireland), according to the manufacturer's instructions. For each condition, 10 µg protein was prepared under reducing conditions in loading buffer and loaded onto a NuPAGE™ 10% Bis-Tris gel (Thermo Fisher Scientific) with MOPS running buffer. Samples were heated at 95 °C for 5 minutes prior to loading. Electrophoresis was performed using an XCell SureLock™ Mini-Cell system at 150 V for 60 minutes.
A pre-stained protein ladder (PageRuler™, 10–180 kDa, Thermo Fisher Scientific) was used as a molecular weight marker. After electrophoresis, gels were stained overnight with InstantBlue™ Protein Stain (Expedeon) and destained in Milli-Q water.

Degree of Protein Hydrolysis – o-Phthaldialdehyde (OPA) Assay

The extent of protein hydrolysis was also assessed by measuring free amino groups using the o-phthaldialdehyde (OPA) assay. dairy IF-G0, dairy IF (HI) and dairy IF

(P+O) samples were thawed on ice and precipitated with 5% trichloroacetic acid (TCA) by mixing 0.5 mL of sample with 0.83 mL of TCA. After centrifugation at 1000 g for 30 minutes, the supernatants were collected and diluted 1:1 (dairy IF G0) or 1:4 (dairy IF (HI)/ P+O) in 0.1 M borate buffer. The OPA reagent was freshly prepared using 0.1 M borate, 10% SDS, 40 g/L OPA in ethanol, and 200 g/L N-acetyl-L-methionine ethyl ester. For each sample, 8 µL was added to 232 µL of OPA reagent in a UV 96-well plate, followed by incubation in the dark at 30 °C for 10 minutes. Absorbance was measured at 340 nm using a PowerWave XS microplate reader (BioTek Instruments, USA). Quantification was based on a glutamic acid standard curve (0–8 mmol/L). The percentage of hydrolysis was calculated using the following formula:

Hydrolysis (%) = 100 - [(mmol NH_2 G0 / mmol NH_2 I0) × 100]

5.2.9. IPEC-J2 Exposure to Digesta

MTS assay

To assess the cytotoxicity of digested dairy IF samples, IPEC-J2 cells were seeded in 96-well tissue culture-treated plates at a density of 1×10^5 cells/mL in either PS10 or PS5+EGF+ITS medium (150 µL per well) and incubated for 16 h at 37 °C in 5% CO_2.

dairy IF (HI) and dairy IF (P+O) were thawed at room temperature, diluted in HBSS to final concentrations corresponding to 400, 350, 300, 250, 200, 150, and 100 µg protein/cm², and filter-sterilized using 0.2 µm syringe filters. Media was removed from overnight cultures. IPEC-J2 cells were then washed with HBSS. Diluted dairy IF digested samples (150 µL) were then added to the cells and incubated for 2 h at 37 °C. After exposure, the digesta was removed, cells were gently washed with

HBSS, and cell viability was assessed using the CellTiter 96® AQueous One Solution Cell Proliferation Assay (Promega).

Briefly, 100 µL of MTS reagent, diluted 1:10 in HBSS, was added to each well, and cells were incubated for 1 h at 37 °C. Absorbance was then measured at 490 nm using a BioTek Cytation 5 multimode plate reader. Cell viability was expressed as a percentage relative to control wells treated with HBSS alone. Cells in HBSS buffer were 84.26 ± 6.10% viability of cells in PS10 or PS5+EGF+ITS alone.

Transwell Exposure

For monolayer exposure, IPEC-J2 cells cultured for 14 days on 12-well Transwell® inserts were washed twice with HBSS and incubated in HBSS for 30 minutes at 37 °C to allow acclimatization (0.5 mL in the apical and 1.5 mL in the basolateral compartments). Digested dairy IF samples (HI and P+O) were thawed at room temperature, diluted in HBSS to final concentrations of 550 µg protein/mL and 330 µg protein/mL, respectively. Samples were then filtered through low protein-binding 0.45 µm PES syringe filters (Sarstedt), and pre-warmed to 37 °C. Next, 0.5 mL of each sample or HBSS (untreated control) was applied to the apical compartment, resulting in final surface loading concentrations of 250 µg protein/cm² for dairy IF (HI) and 150 µg protein/cm² for dairy IF (P+O). H_2O (HI) and (P+O) were included as negative controls. TEER was measured immediately after acclimatization (T0) and again after 2 h of treatment with digesta samples (T2). Apical and basolateral samples were then collected, aliquoted, and stored at –20 °C for subsequent AA analysis.

Free Amino Acid Analysis

For each dairy IF treatment, two technical replicates were pooled from the apical and basolateral chambers. Basolateral samples were concentrated using a vacuum concentrator (miVac quattro concentrator, Genevac™) at 40 °C and resuspended in 600 µL of Milli-Q water. dairy IF (HI) and (P+O) samples were diluted 1:9 (v/v) in Milli-Q water prior to analysis. Samples were deproteinized by mixing equal volumes of 24% (w/v) trichloroacetic acid (TCA) with sample, followed by incubation at room temperature for 10 minutes. The mixtures were then centrifuged at 14,400 × g for 10 minutes (Microcentaur, MSE, UK). Supernatants were collected and diluted 1:15 with 0.2 M sodium citrate buffer (pH 2.2) containing the internal standard norleucine at a final concentration of 125 nmol/mL. Quantification of free AAs was performed using a Jeol JLC-500/V AA analyser (Jeol (UK) Ltd., Garden City, Herts, UK) equipped with a Jeol Na^+ high-performance cation exchange column. Amino acid concentrations were expressed in nmol/mL. The basolateral AA (AA) concentration was expressed as a ratio of the apical concentration using the following formula:

Ratio = (basolateral concentration at 2 h) / (apical concentration at time 0)

5.2.10. Statistical analysis

All experiments were conducted at least in triplicate on three independent days, each with technical duplicates unless stated otherwise. Results are presented as means ± SEM. Statistical analyses were performed using GraphPad Prism 10.4.2 (GraphPad Software, San Diego, California, USA). One-way or two-way ANOVA followed by Tukey's multiple comparisons test was used for normally distributed data, while the Friedman or Kruskal–Wallis test with Dunn's multiple comparisons test was applied

for non-normally distributed data. For direct pairwise comparisons, Student's t-test was applied. Statistical significance was defined as $P < 0.05$.

5.3. Results

Four media were evaluated for their ability to support stable IPEC-JC monolayers, based on producing monolayers with a wide range of TEER values: (1) PS10, a species-specific media producing more physiologically relevant TEER values (~300–500 Ω·cm²; Zakrzewski et al., 2013); (2) PS5+EGF+ITS, reported to maintain low TEER (240–330 Ω·cm²) together with epithelial morphology resembling native jejunum (Zakrzewski et al., 2013); and (3) PS5+L-WRN, where supplementation with Wnt3a, R-spondin, and Noggin reduces TEER to ~50 Ω·cm² and promotes a more proliferative state in IPEC-J2 (Boger et al., 2023) and (4) FBS10, is recommended by the culture collection supplier but is known to yield very high and variable TEER (2,000–15,000 Ω·cm²; Saaby et al., 2016; Zakrzewski et al., 2013);

5.3.1. Media dictates TEER values of IPEC-J2 monolayers

IPEC-J2 cells were cultured for 14 days on permeable Transwell inserts in PS10, PS5 + EGF/ITS, PS10 + L-WRN, or FBS10 media. As a 1st step in media assessment, barrier integrity of monolayers was assessed by TEER in real-time (CellZScope) and by endpoint (Millicell) (Fig. 5.1A and B). Using the CellZScope system, monolayer TEER values at day 7 were: PS10 = 963.11 ± 318.66, PS5+EGF+ITS = 566.11 ± 528.82, PS5+L-WRN = 3560.51 ± 979.54, and FBS10 = 7241.50 ± 186.85 Ω·× cm² (Fig. 5.1A) At this time point, values for monolayers in PS10 and PS5+EGF+ITS were not significantly different from each other ($P > 0.05$), whilst culturing in PS5+L-WRN was significantly higher than both PS10 and

PS5+EGF+ITS ($P < 0.05$), and culturing in FBS10 was significantly higher again ($P < 0.05$). By day 14, IPEC-J2 TEER had increased with 3 of the media: PS10 = 5178.61 ± 675.74, PS5+L-WRN = 11,931.56 ± 740.28, and FBS10 = 14,412.56 ± 1798.99 Ω ×·cm². However, monolayer TEER values cultured in PS5+EGF+ITS was not significantly different to day7 (943.13 ± 487.39 Ω ×·cm²; $P > 0.05$). At this stage, IPEC-J2 TEER values for PS5+L-WRN and FBS10 were similar ($P > 0.05$) and significantly higher than for PS10 and PS5 +EGF/ITS ($P < 0.05$). Notably, monolayers cultured in PS10 had significantly higher TEER values than monolayers in PS5+EGF+ITS ($P > 0.05$). Importantly, TEER values at day 12 were not significantly different from those at day 14 within each condition ($P > 0.05$), indicating that the epithelial barrier had stabilized by day 12 (Fig. 5.1A).

Using the Millicell-ERS system revealed IPEC-J2 TEER values at day 7 of 978.08 ± 314.45 cultured in PS10, 176.53 ± 40.81 in PS5+EGF+ITS, 3937.52 ± 485.51 in PS5+L-WRN, and 6620.78 ± 1997.03 Ω×cm² in FBS10 (Fig. 5.1B). By day 14, TEER values further increased to: PS10 = 2395.00 ± 485.51, PS5+L-WRN = 9600.00 ± 2150.94, and FBS10 = 12,660.27 ± 1495.01 Ω·× cm². In contrast, IPEC-J2 cultured in PS5+EGF+ITS displayed significantly lower TEER values (327.58 ± 71.58; $P < 0.05$) compared with all other treatments, and these did not increase significantly from day 7 to day 14. Among the other conditions, TEER values were highest in FBS10 and PS5+L-WRN, with no significant difference between the two ($P > 0.05$). Monolayers cultured in PS10 also exhibited significantly higher TEER values than those in PS5+EGF+ITS ($P < 0.05$).

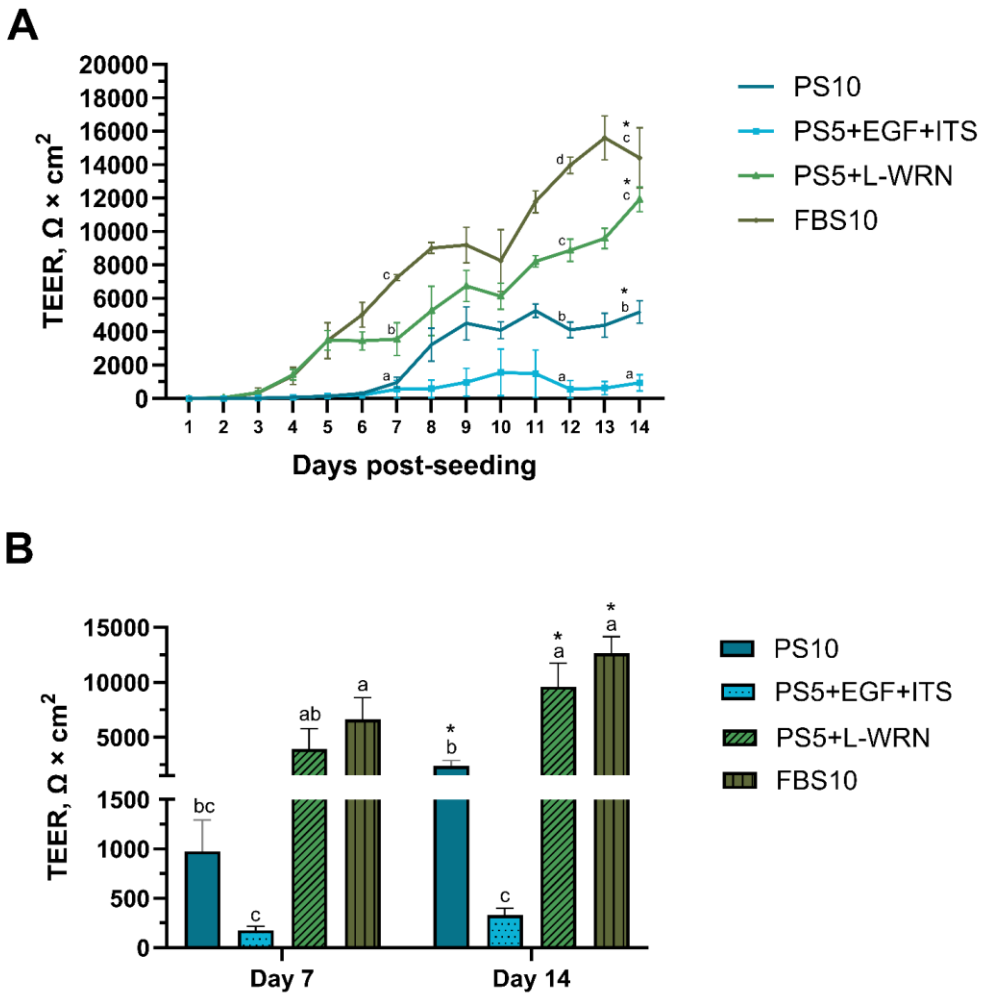


Fig. 5.1 Transepithelial electrical resistance (TEER) measurements in IPEC-J2 monolayers cultured under different media conditions.

(A) TEER values monitored over time using the real-time CellZScope system. (B) Endpoint TEER values measured at selected timepoints using the Millicell-ERS voltameter. Data represent mean ± SEM from three biological replicates, each measured in technical duplicates. Statistical analysis was performed using one-way ANOVA followed by Tukey's post hoc test. Different letters indicate statistically significant differences between conditions at the same timepoint; asterisks denote significant differences between day 7 and day 14 within the same condition. ($P < 0.05$).

5.3.2. ALP and LDH Activity Reflect Media-Dependent IPEC-J Differentiation

To evaluate enterocyte differentiation and metabolic activity in IPEC-J2 monolayers cultured in the various media, ALP and LDH activity were measured on days 7 and 14 (Fig. 5.2). ALP is well known marker of epithelial differentiation (Matsumoto et al., 1990) and LDH is a key enzyme in anaerobic glycolysis. On day 7, FBS10 had the highest ($P < 0.05$) ALP activity in IPEC-J2 monolayers (FBS10 = 16.06 ±1.9 IU/mg of protein; PS10 = 5.72±1.02 IU/mg of protein, PS5+EGF+ITS = 7.75±1.72 IU/mg of protein, PS5+L-WRN = 5.17± 1.31 IU/mg of protein; Fig. 5.2A). By day 14, ALP activity significantly increased in monolayers cultured in PS5+EGF+ITS (15.92 ±3.02 IU/mg of protein; $P < 0.05$ vs. day 7). ALP levels in monolayers cultured in PS10 (8.01 ± 1.54 IU/mg of protein) were not significantly different from those in PS5+EGF+ITS ($P > 0.05$), whereas activity in monolayers with PS5+L-WRN (5.47 ± 1.10 IU/mg of protein) or FBS10 (6.06 ± 1.60 IU/mg of protein) were significantly lower than monolayers cultured in PS5+EGF+ITS ($P < 0.05$) (Fig. 5.2A). Notably, monolayers cultured in FBS10 exhibited a significant decrease in ALP activity from day 7 to day 14 ($P < 0.05$).

LDH activity showed a similar media-dependent pattern (Fig. 5.2B). On day 7, the highest activity was observed in monolayers cultured in PS5+EGF+ITS (0.14±0.007 mU/mg of protein; $P < 0.05$), followed by PS5+L-WRN (0.10 ±0.01 mU/mg of protein) and PS10 (0.10 ± 0.003 mU/mg of protein), which were both significantly higher than monolayers cultured in FBS10 (0.07 ±0.003 mU/mg of protein; $P < 0.05$). By day 14, LDH activity remained highest in monolayers in PS5+EGF+ITS (0.14±0.004 mU/mg of protein) and PS10 (0.12±0.01 mU/mg of protein; $P < 0.05$). In contrast, LDH activity were significantly lower in monolayers cultured in PS5+L-WRN (0.07±0.005 mU/ mg of protein; $P < 0.05$ vs. day 7). LDH activity in IPEC-J2

monolayers cultured in FBS10 remained low at day 14 with values similar to day 7 (0.06 ±0.008 mU/ mg of protein; $P > 0.05$).

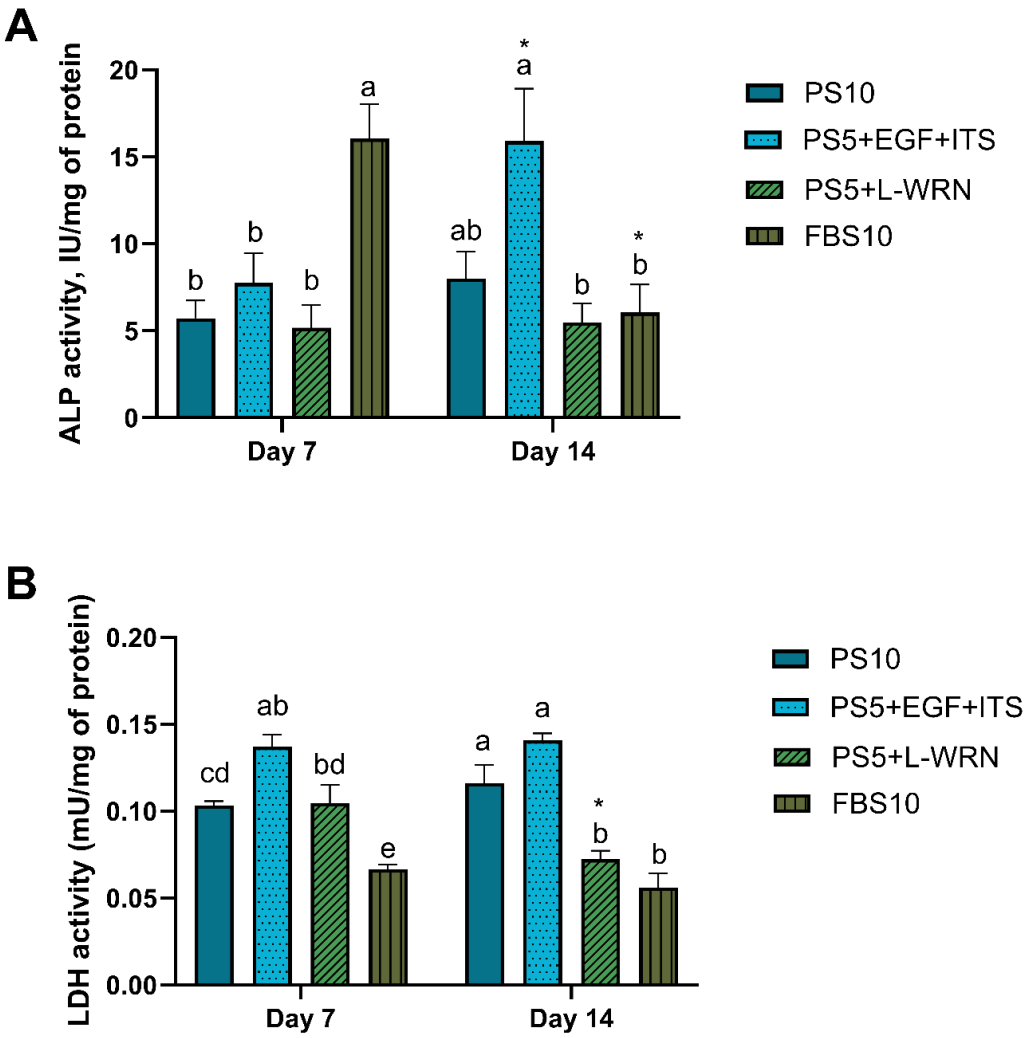


Fig. 5.2 Alkaline phosphatase (ALP) and lactase dehydrogenase (LDH) activity in IPEC-J2 monolayers at days 7 and 14.

IPEC-J2 cells were cultured in PS5+EGF+ITS, PS10, PS5+L-WRN, or FBS10 media for 14 days on permeable Transwell inserts. (A) ALP activity (p-nitrophenol release) and (B) LDH activity (formation of pyruvate dinitrophenylhydrazone) were measured in cell lysates on days 7 and 14. Data represent mean ± SEM from three biological replicates. Statistical analysis was performed using one-way ANOVA followed by Tukey's post hoc test to assess differences between treatments at the same time point. Asterisks indicate statistically significant differences between day 7 and day 14 within the same condition, determined by t-test ($P < 0.05$).

5.3.3. PS5+EGF+ITS Increases Lactulose and Mannitol Permeability in IPEC-J2 Monolayers

To assess the permeability of monolayers at day 14, lactulose (radius = 9.5 Å) and mannitol (radius = 6.7 Å) were simultaneously added to apical chambers. After 4h, levels were quantified in basolateral chambers (Fig. 5.3). Papp of lactulose in IPEC-J2 monolayers revealed that culturing in PS10 resulted in the lowest Papp value ($9.66 \times 10^{-7} \pm 1.97 \times 10^{-7}$ cm/s), significantly lower than culturing in PS5+EGF+ITS ($4.26 \times 10^{-6} \pm 1.53 \times 10^{-7}$ cm/s; $P < 0.05$), and FBS10 ($2.47 \times 10^{-6} \pm 4.69 \times 10^{-7}$ cm/s; $P < 0.05$), albeit similar to PS5+L-WRN ($2.32 \times 10^{-6} \pm 3.70 \times 10^{-7}$ cm/s; $P > 0.05$) (Fig. 5.3A).

The Papp for mannitol in monolayers was significantly lower in PS10 ($1.15 \times 10^{-6} \pm 2.75 \times 10^{-7}$ cm/s) compared to monolayers cultured in either PS5+EGF+ITS and FBS10. PS5+EGF+ITS exhibited the highest mannitol permeability ($6.37 \times 10^{-6} \pm 2.33 \times 10^{-7}$ cm/s; $P < 0.05$ vs. all others), while PS5+L-WRN ($3.23 \times 10^{-6} \pm 7.41 \times 10^{-7}$ cm/s) and FBS10 ($3.31 \times 10^{-6} \pm 5.19 \times 10^{-7}$ cm/s) were not significantly different from each other ($P > 0.05$) (Fig. 5.3A)

The L:M (L:M) ratio of the stock solution applied apically at T_0 was 1:5.27 ± 0.19 (Fig. 5.3B). This served as a reference point, with lower L:M ratios indicative of preferential mannitol (transcellular) transport, and higher ratios suggestive of increased lactulose (paracellular) transport. In the apical compartment after 4h, L:M ratios were significantly lower than the stock solution in monolayers cultured in PS10 (1:4.46 ± 0.056), PS5+EGF+ITS (1:4.47 ± 0.038) and PS5+L-WRN (1:4.33 ± 0.083; $P < 0.05$ for all vs. stock), indicating preferential mannitol uptake over lactulose. L:M ratio in monolayers cultured in FBS10 (5.22 ± 0.087) was not

significantly different from the stock ($P > 0.05$) (Fig. 5.3 B). In the basolateral compartment, the L:M ratio was 1:4.41 ± 0.20 in monolayers cultured in PS10, 1:3.69 ± 0.064 with PS5+EGF+ITS, 1:4.13 ± 0.12; with FBS10), and 1:4.36 ± 0.16 with PS5+L-WRN. Notably, only the L:M ratio in basolateral chambers of monolayers cultured in FBS10 were similar to L:M ratio in the stock solution ($P > 0.05$; Fig. 5.3 B).

Interestingly, treatment with the L:M solution resulted in drop in monolayer TEER values across all media conditions. The most pronounced reduction was observed in FBS10 (93.19 ± 5.39%) and PS5+L-WRN (87.78 ± 0.56%), indicating a loss of barrier resistance. In contrast, PS10 (51.81 ± 24.84%) and PS5+EGF+ITS (23.27 ± 19.2%) showed significantly smaller decreases, suggesting greater resilience and maintenance of epithelial integrity in these conditions.

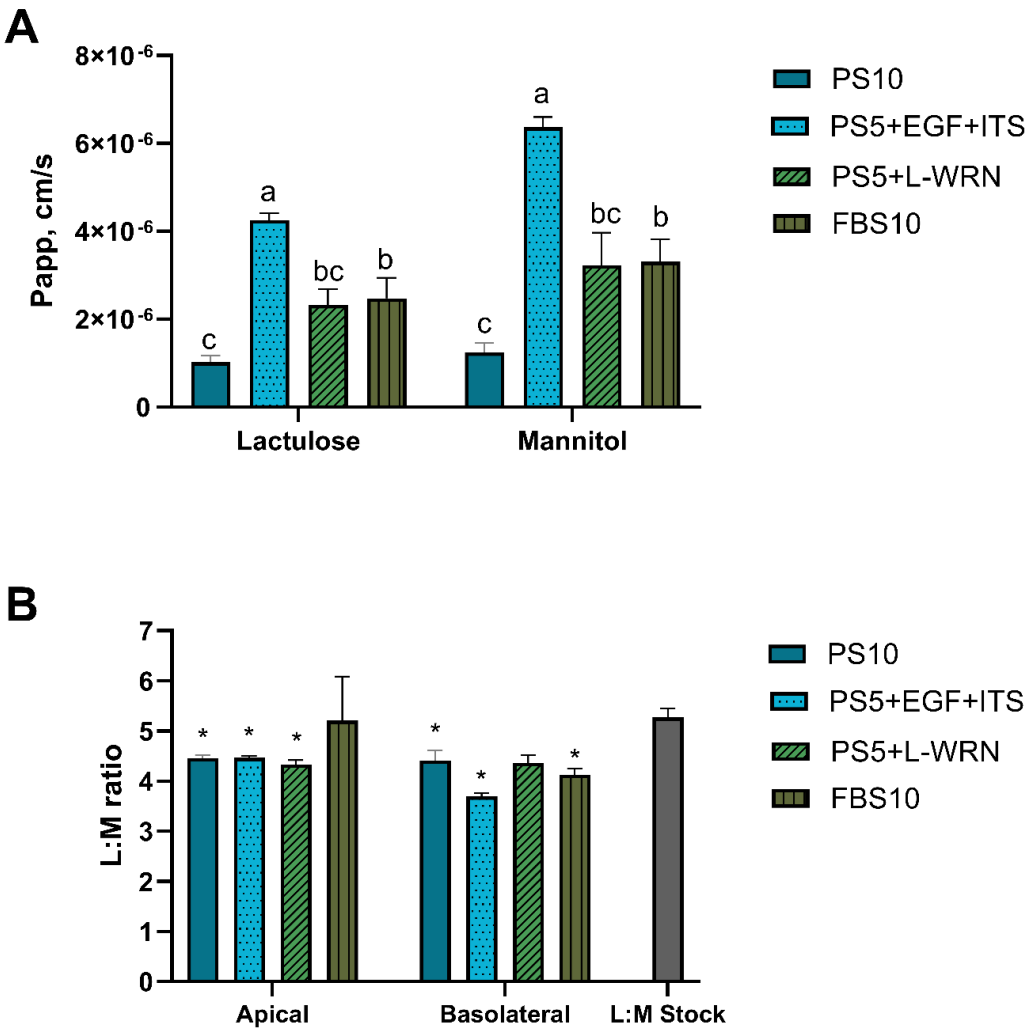


Fig. 5.3 Media-dependent permeability to lactulose and mannitol in IPEC-J2 monolayers. IPEC-J2 cells were cultured for 14 days in PS10, PS5+EGF+ITS, PS5+L-WRN, or FBS10 media on permeable Transwell inserts. (A) Apparent permeability coefficients (Papp) of lactulose and mannitol in HBSS were calculated after a 4 h incubation to assess paracellular and transcellular transport, respectively. (B) Lactulose:mannitol (L:M) ratios were determined in the apical and basolateral compartments at 4 h. L:M stock ratio (5.27 ± 0.19) = initial input solution applied to the apical side at time 0. Data represent mean ± SEM from three biological replicates. Statistical analysis was performed using one-way ANOVA followed by Tukey's post hoc test, with different letters indicating statistically significant differences ($P<0.05$) between treatments within the same sugar Asterisk indicates significant difference with L:M stock. Student's t-tests were employed to compare treatment groups to the L:M stock ratio

5.3.4. Media Modulates mRNA levels of Transport, Barrier and Immune Genes in IPEC-J2 monolayers

To investigate the mRNA transcript levels of genes involved in nutrient transport, epithelial structure, and cell type identity, RT-qPCR was performed on IPEC-J2 monolayers cultured for 14 days in various media (Fig. 5.4). For *in vivo* comparison purposes, RT-qPCR was also performed in jejunal scrapings from young pigs. Cell mRNA levels were normalized to the housekeeping gene RPLP0 and analyzed using the ΔΔCt method, with FBS10 as the reference condition since it is the medium recommended by theIPEC-J2 supplier. Fig. 5.4 shows the relative fold changes ($2^{-\Delta\Delta Ct}$) of IPEC-J2 cells under the different culture media conditions, while Table 1 presents the corresponding mRNA levels present in porcine jejunal tissue of young pigs.

Among nutrient transporters, FATP4 and SGLT1 mRNA transcript levels in monolayers cultured in PS5+EGF+ITS (0.40 ± 0.04-fold and 0.45 ± 0.05-fold, respectively) was lower than levels observed in monolayers in FBS10 ($P > 0.05$). The glucose transporter GLUT2 mRNA was higher in monolayers in PS10 (1.05 ± 0.03-fold vs. FBS10) compared with those cultured in PS5+EGF+ITS (0.29 ± 0.08-fold vs. FBS10). For the lipid uptake gene, CD36, mRNA levels were significantly increased ($P < 0.05$) in monolayers cultured in PS10 (11.47 ±3.71-fold) and PS5+L-WRN (8.56± 0.15-fold), in contrast to those cultured in FBS10 and PS5+EGF+ITS. LAT2 (neutral AA transporter at the basolateral membrane; Bröer and Fairweather, 2019) mRNA was higher ($P < 0.05$) in monolayers in PS5+EGF+ITS (185.96 ± 60.04-fold) and PS10 (42.35 ± 7.10-fold) compared to monolayers in FBS10 media, while mRNA transcripts levels of rBAT(cationic and neutral AAs transporter at the apical membrane; Bröer and Fairweather, 2019) and y+LAT1 (cationic AAs

transporter at the basolateral membrane; Bröer and Fairweather, 2019) were lower ($P < 0.05$) in monolayers in PS5+EGF+ITS (0.26 ± 0.01-fold and 2.55 ± 0.05-fold, respectively) compared to all other conditions. In addition, LAT4 mRNA (neutral branched-chain and aromatic AAs at the basolateral membrane; Bröer and Fairweather, 2019) was higher in monolayers with PS5+L-WRN (1.56 ± 0.31-fold vs. FBS10) compared to PS5+EGF+ITS (0.33 ± 0.03 vs. FBS10; $P < 0.05$).

Regarding epithelial barrier-related biomarkers, OCLN mRNA levels were significantly lower in monolayers cultured in PS10 (0.67 ± 0.04-fold), PS5-EGF/ITS (0.48 ± 0.03-fold), and PS5+L-WRN (0.70 ± 0.08-fold) compared to those in FBS10 media (1.00 ± 0.05, $P < 0.05$). Tight junction ZO1 and CLDN1 mRNA levels were significantly lower in monolayers cultured in PS5+EGF+ITS (0.52 ± 0.01-fold and 0.59 ± 0.09-fold, respectively; $P < 0.05$) relative to those monolayers in FBS10. CLDN2 mRNA was significantly higher ($P > 0.05$) in IPEC-J2 cultured in PS5+L-WRN (23.25 ± 1.21-fold, $P < 0.05$) and PS10 (77.53 ± 69.5-fold, $P < 0.05$) compared to FBS10 and PS5+EGF+ITS (1.61 ± 0.90-fold).

For mucin expression, MUC2 mRNA was significantly higher in monolayers in PS5+L-WRN (7.11 ± 1.17-fold, $P < 0.05$) compared to PS10 (0.48 ± 0.07). MUC1 mRNA was significantly lower in IPEC-J2 cultured in PS5+EGF+ITS (0.56 ± 0.04-fold) compared to P10, PS5+L-WRN and FBS10 ($P < 0.05$).

The biomarkers PEP1, ASCT2, CLDN4, IL6, IL8, and TNF were similar in monolayers regardless of test media. The lineage-specific markers CHGA (enteroendocrine cells; Rindi et al., 2004), CD163 (macrophages; Fabriek et al., 2005), CD45 (leukocytes; Hermiston et al., 2003), as well as the AA transporters B^0AT1, IMINO, ATB^{0+}, were not detected in IPEC-J2 regardless of media conditions. In contrast, these markers were readily expressed in porcine jejunal

tissue, with ΔCt values of CHGA = 5.93 ± 0.17, CD163 = 11.73 ± 1.07, CD45 = 4.17 ± 0.26, B^0AT1 = 2.06 ± 0.24, IMINO = 3.98 ± 0.29, ATB^{0+} = 12.47 ± 0.9. The fibroblast-associated marker S100A4 (Fei et al., 2017) was expressed in all media conditions, with highest absolute levels in PS5+EGF+ITS (1.49 ± 0.08-fold vs. FBS10). This marker was also present in tissue, but at significantly lower levels (Table 1; 0.03 ± 0.01-fold vs. FBS10; $P < 0.05$).

Compared to porcine jejunal scrapings (Table 5.1), IPEC-J2 cultures showed markedly reduced expression of most absorptive and structural genes. PEP1 (220,011-fold), SGLT1 (14,628-fold), GLUT2 (3-fold), FATP4 (307-fold), CD36 (14-fold), y+LAT1 (13-fold), LAT2 (153,074-fold), LAT4 (1150-fold) and rBAT (45-fold) mRNA were all substantially higher in tissue than in IPEC-J2 (FBS10; $P < 0.05$). Messenger RNA levels of structural genes, such as CLDN2 and CLDN4, were elevated 389,089-fold and 4.68-fold, respectively, in tissue compared to IPEC-J2 cells (FBS10, $P < 0.05$). In contrast, ZO1 and CLDN1 mRNA were 0.41-fold and 0.01-fold lower in tissue, respectively, compared to FBS10 ($P < 0.05$). Interestingly, MUC2, IL8, and TNF mRNA were 1,212-fold, 4.44-fold, and 77.55-fold higher in tissue, while MUC1 and IL6 mRNA were 0.02-fold and 0.16-fold lower, respectively ($P < 0.05$). The ASCT2 (neutral AA transporter at the apical membrane; Bröer and Fairweather, 2019) mRNA was not significantly different between tissue and FBS10 ($P > 0.05$).

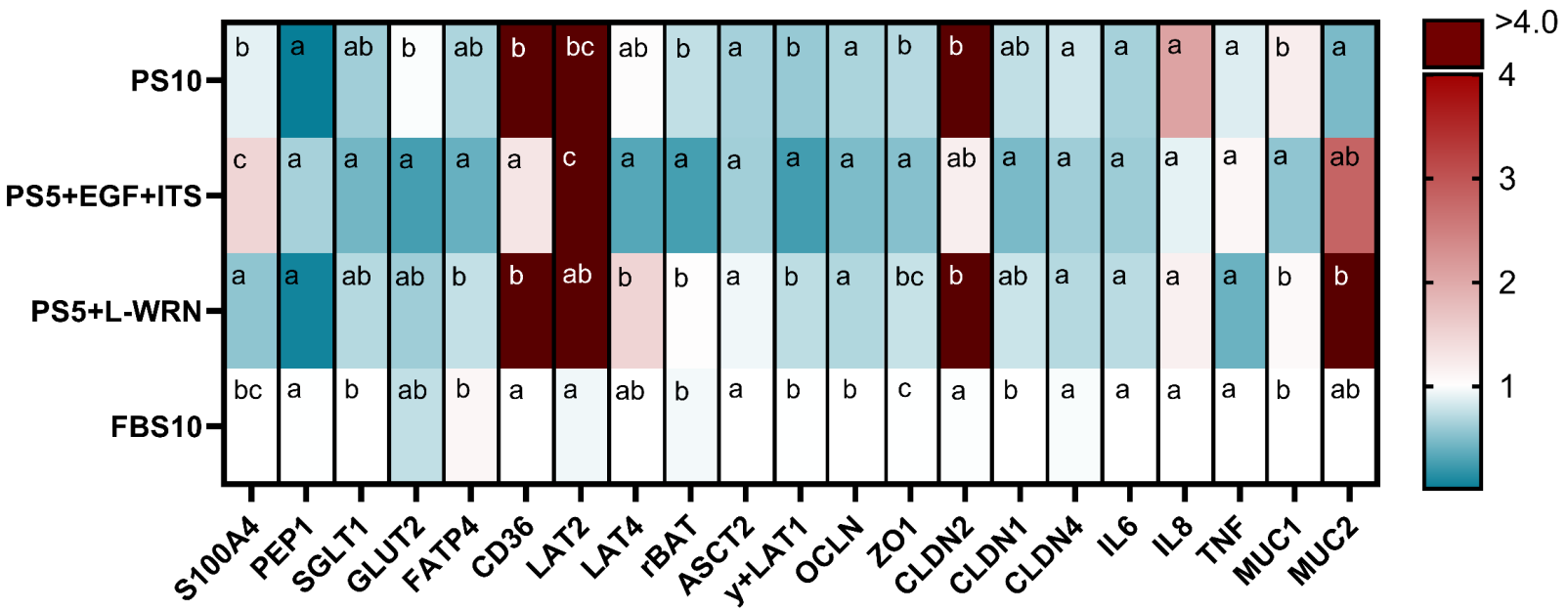


Fig. 5.4 Relative mRNA expression in IPEC-J2 monolayers under different culture media.

IPEC-J2 were grown on Transwell inserts for 14 days in four media (PS10, PS5+EGF+ITS, PS5+L-WRN, FBS10). Messenger RNA was quantified by RT–qPCR, normalised to the housekeeping gene *RPLP0*, and expressed relative to FBS10 using the $2^{-\Delta\Delta Ct}$ method (FBS10 = 1). FBS10 represents the reference medium recommended by the cell line collection. Statistics were performed on ΔΔCt values: one-way ANOVA with Tukey's post hoc test or Kruskal–Wallis with Dunn's multiple comparisons (where normality was not met). Different letters indicate groups that differ significantly ($P < 0.05$). Colour bar: blue < 1 fold(< FBS10), white ≈ 1 fold (= FBS), red > 1 fold (> FBS10), dark red ≥ 4 fold (≥ 4× FBS10).

Table 5.1 mRNA expression in porcine jejunal scrapings relative to IPEC-J2 monolayers cultured in FBS10.

mRNA was quantified by RT–qPCR, normalised to *RPLP0*, and expressed as fold change using the $2^{-\Delta\Delta Ct}$ method (FBS10 = 1). Values are reported as geometric mean ($2^{-\Delta\Delta Ct}$) with 95% CI. p-values correspond to the jejunum vs FBS10 comparison from a Student's t-test performed on ΔΔCt (log_2) values. Significance: *P < 0.05, **P < 0.01, ***P < 0.001, ****P < 0.0001 (n = 4 biologically independent samples; 2 female pigs, 2 male pigs, age 56 days).

Gene	Common name	Gene function	Fold change (FBS10 =1)	SEM	p-value (vs. FBS10)	Significance
S100A4	S100 calcium-binding protein A4 (S100A4/FSP1)	Fibroblast marker, calcium-binding protein linked to cytoskeletal remodelling (Strutz et al., 1995)	0.03	0.01	0.0002	***
SLC15A1	Peptide transporter 1 (PEPT1)	Proton-coupled peptide transporter (apical) (Spanier and Rohm, 2018)	220011.48	37753.33	<0.0001	****
SLC5A1	Sodium/glucose cotransporter 1 (SGLT1)	Na^+/glucose co-transporter (apical) (Gromova et al., 2021)	14628.12	2766.30	<0.0001	****
SLC2A2	Glucose transporter 2 (GLUT2)	Facilitative glucose transporter (basolateral) (Gromova et al., 2021)	3.06	0.57	0.0115	*
SLC27A4	Fatty acid transport protein 4 (FATP4)	Long-chain fatty acid transporter and acyl-CoA synthetase (apical) (Cifarelli and Abumrad, 2018)	307.64	35.33	<0.0001	****
CD36	Cluster of differentiation 36 (CD36/FAT)	Fatty acid translocase (apical) (Cifarelli and Abumrad, 2018)	14.79	6.10	0.0019	**
LAT2	L-type amino acid transporter 2 (LAT2)	Neutral AA exchanger (basolateral) (Bröer and Fairweather, 2019)	153074.28	45294.51	<0.0001	****
LAT4	L-type amino acid transporter 4 (LAT4)	Neutral branched-chain/aromatic AA transporter (basolateral) (Bröer and Fairweather, 2019)	1150.03	200.94	<0.0001	****
rBAT	Related to b0,+ amino acid transporter (rBAT)	Cationic and neutral AAs transporter (apical) (Bröer and Fairweather, 2019)	45.49	10.32	<0.0001	****
ASCT2	Alanine–serine–cysteine transporter 2 (ASCT2)	Neutral AA transporter (apical) (Bröer and Fairweather, 2019)	1.52	0.43	0.4329	ns
SLC7A7	y^+L amino acid transporter 1 (y^+LAT1)	Cationic/neutral AA exchanger (basolateral) (Bröer and Fairweather, 2019)	13.50	5.25	0.0024	**
OCLN	Occludin (OCLN)	Tight junction protein, barrier integrity (Otani and Furuse, 2020)	2.14	0.32	0.0176	*
TJP1	Zonula occludens 1 (ZO1)	Tight junction protein, barrier integrity (Otani and Furuse, 2020)	0.41	0.04	0.0010	**

CLDN2	Claudin-2 (CLDN2)	Tight junction protein' forming paracellular cation-selective channels (Otani and Furuse, 2020)	389089.69	112159.24	<0.0001	****
CLDN1	Claudin-1 (CLDN1)	Tight junction protein, barrier integrity (Otani and Furuse, 2020)	0.01	0.01	0.0012	**
CLDN4	Claudin-4 (CLDN4)	Tight junction protein, barrier integrity (Otani and Furuse, 2020)	4.68	0.89	0.0057	**
IL6	Interleukin-6 (IL-6)	Cytokine (Andrews et al., 2018)	0.16	0.05	0.0048	**
IL8	Interleukin-8 (IL8)	Cytokine (Andrews et al., 2018)	6.44	1.80	0.0022	**
TNF	Tumor necrosis factor (TNF)	Cytokine (Andrews et al., 2018)	77.55	8.38	<0.0001	****
MUC1	Mucin-1 (MUC1)	Membrane-bound mucin (Grondin et al., 2020)	0.02	0.01	<0.0001	****
MUC2	Mucin-2 (MUC2)	Secreted mucin (Grondin et al., 2020)	1212.78	679.12	0.0001	***

5.3.5. Media Influences ZO1 Distribution and Cell Density in IPEC-J2 Monolayers

PS10 and PS5+EGF+ITS were selected for subsequent analyses, as (1) they produced monolayers with lower but stable TEER values at day 14 compared to FBS10 and PS5+L-WRN; (2) both PS10 and PS5+EGF+ITS supported the highest monolayer ALP and LDH activity at day 14, indicating stronger enterocyte differentiation and sustained metabolic activity; (3) RT–qPCR showed lower expression of OCLN and ZO1 compared with FBS10, consistent with a more immature intestinal barrier phenotype characterized by less developed tight junctions (Gleeson et al., 2021); (4) monolayers cultured in either PS10 or PS5+EGF+ITS were resilient to a 4-h incubation in HBSS buffer, as indicated by the smallest TEER reduction during the L:M assay. Because HBSS is the buffer of choice for food bioavailability studies in polarized monolayers, maintenance of barrier integrity during incubation is an important attribute. Selecting both PS10 and PS5+EGF+ITS therefore allowed inclusion of monolayers representing a broad and physiologically relevant range of paracellular permeability.

To investigate the impact of PS10 and PS5 +EGF/ITS on tight junction architecture, ZO1 immunofluorescence staining was performed on day 14 monolayers (Fig. 5.5). ZO1 is a tight junction protein that links CLDNs and OCLN to the actin cytoskeleton and regulates epithelial barrier integrity and paracellular permeability (González-Mariscal et al., 2003). Representative images of ZO1 staining in monolayers grown in PS10 and PS5+EGF+ITS conditions are depicted in Fig. 5.5A. Quantification of the raw integrated density of the ZO1 signal, normalized to the number of nuclei, revealed significantly higher expression in monolayers cultured in PS10 compared to PS5+EGF+ITS (277,086 ± 18,412 vs. 171,298 ± 5,215raw IntDen/ nuclei count,

respectively; $P < 0.05$; Fig. 5.5B). Interestingly, the cell density, expressed as nuclei per 1000 μm^2, was significantly greater in monolayers with PS5+EGF+ITS compared to PS10 (2.26 ± 0.32 vs. 0.91 ± 0.11; $P < 0.05$; Fig. 5.5C), suggesting a higher cell proliferation or seeding efficiency in this condition. Taken together, there were more cells in the monolayers cultured in PS5+EGF+ITS but more ZO1 in monolayers cultured in PS10.

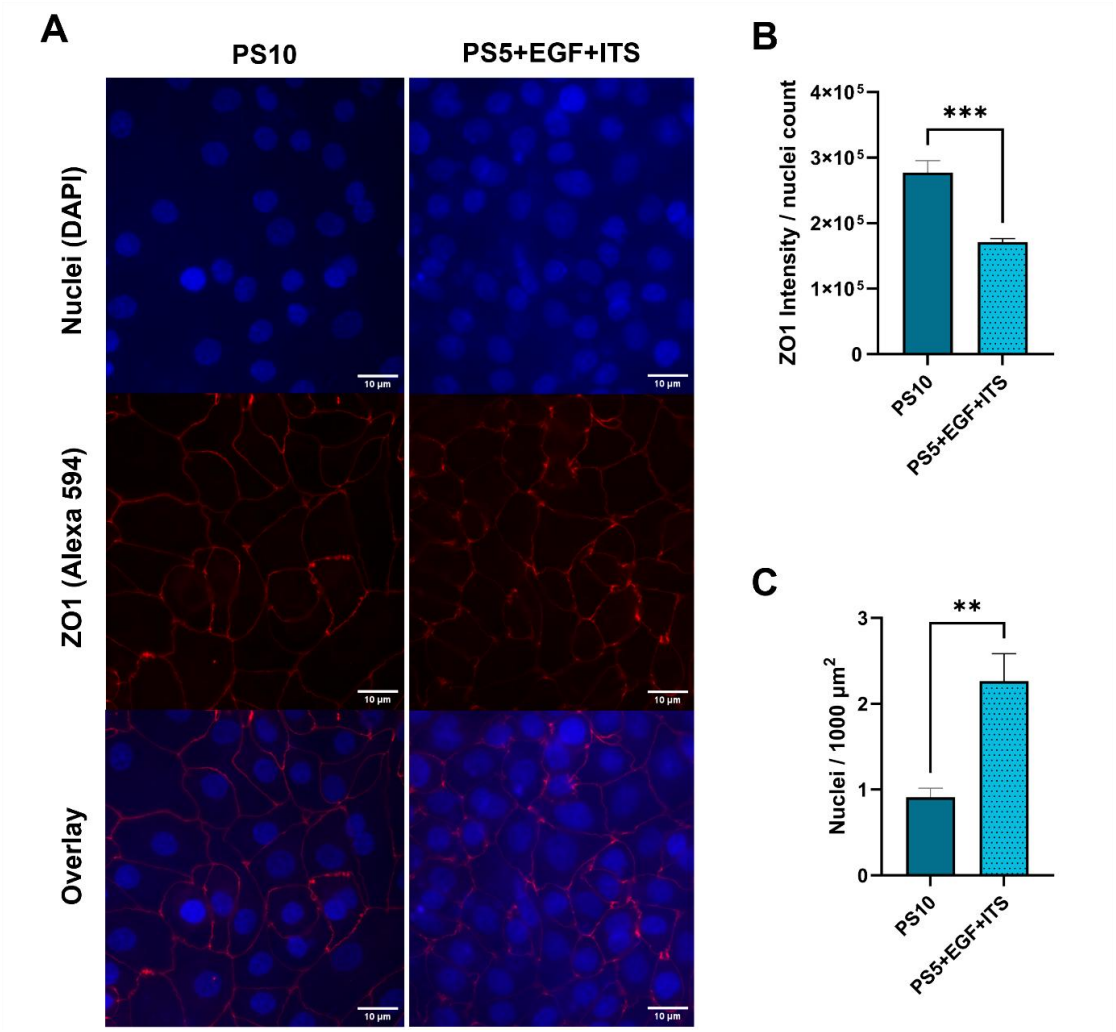


Fig. 5.5 Effect of media composition on ZO1 localization and epithelial cell density in IPEC-J2 monolayers.

IPEC-J2 were cultured for 14 days in either PS10 or PS5+EGF+ITS medium. (A) Representative fluorescence microscopy images of monolayers stained for ZO1 (Alexa Fluor 555, red) and nuclei (DAPI, blue). Scale bar = 10 µm. (B) Fluorescence intensity of ZO 1 from images using the Otsu thresholding algorithm in Fiji-ImageJ and normalized to the number of nuclei. (C) Nuclei count per 1000 µm² used as a proxy for cell density. Results represent the average of three biological replicates with three non-overlapping images per replicate (mean ± SEM). Statistical differences were evaluated using unpaired t-tests ($P < 0.05$).

5.3.6. IPEC-J2 Viability Is Maintained After Exposure to Inactivated Digesta

To assess the biocompatibility of IPEC-J2 monolayers with digested food, infant formula was first subjected to static gastrointestinal digestion using the INFOGEST protocol mimicking the infant gut. At the end of the intestinal phase, heat—dairy IF (HI)—or protease inhibitors—dairy IF (P+O)—were added to digesta to inactivate digestive enzyme, and samples diluted to assist in biocompatibility with IPEC-J2 monolayers (concentration ranging from 400 to 100 µg protein/cm²). The degree of gastrointestinal digestion of proteins was tracked by SDS-PAGE and o-phthaldialdehyde (OPA) assay (Supplementary Fig. 5.1). A significant increase in free amino groups was observed from G0 (pre-gastric phase) to I60 (post-intestinal phase) ($P < 0.05$), confirming effective digestion.

To study the tolerance of IPEC-J2 cells to digested dairy IF, digesta at various protein concentrations were applied to undifferentiated IPEC-J2 cells cultured overnight in PS10 or PS5+EGF+ITS, and cell viability assessed by MTS assay (Fig. 5.6). For cells cultured in PS10 medium, a 2 h treatment with dairy IF (HI), at <350 µg protein /cm², showed no significant difference in viability compared to the cell in HBSS buffer (Fig. 5.6A; $P > 0.05$). Inactivation of digestive enzymes via P+O, was less biocompatible with IPEC-J2 cells. In this instance, dairy IF P+0 at <150 µg protein/cm² was safe for use on IPEC-J2 cells. For PS5+EGF+ITS medium, IPEC-J2 cells treated for 2 h with 250 µg/cm² for dairy IF (HI) or150 µg/cm² for dairy IF (P+O) had similar viability to cells in HBSS for 2 h (96.66 ± 5.58%; $P > 0.05$). Digesta control samples, where H_2O is used in the digestion rather than dairy IF, were non-toxic to IPEC-J2 cells at any dilution tested ($P > 0.05$ compared to cells in HBSS).

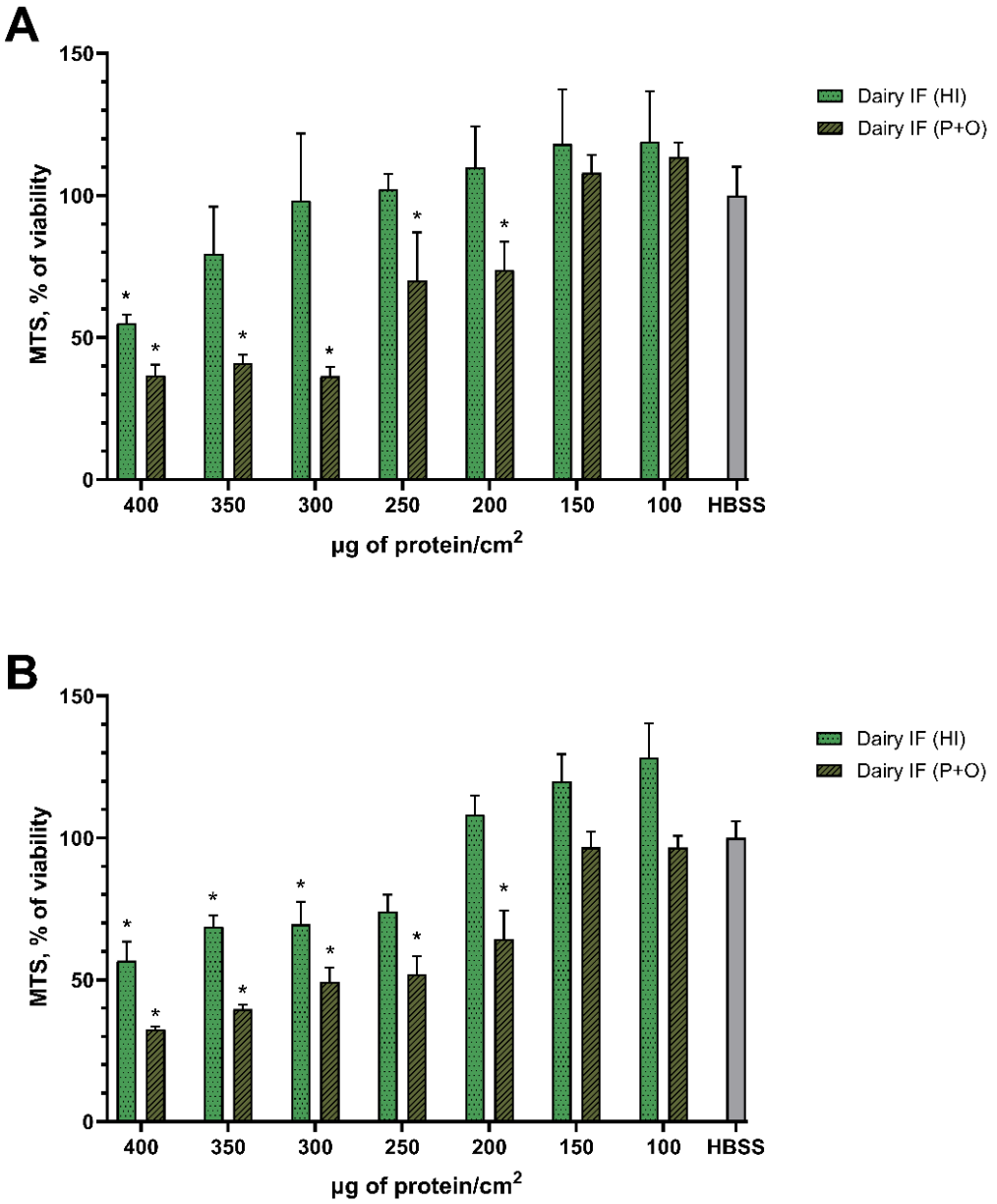


Fig. 5.6 Viability of undifferentiated IPEC-J2 cells exposed to dairy infant formula (IF) digesta. Dairy IF was subjected to simulated infant gastrointestinal digestion and inactivated by either heat inactivation (HI) or enzymatic inhibition using Pefabloc and Orlistat (P+O). Undifferentiated IPEC-J2 cells were cultured for 24 hours in either PS10 or PS5+EGF+ITS medium. Cells were then treated with dairy IF digesta for 2 h and viability assessed using MTS. Results were normalized to cells in HBSS control (100% viable). (A) PS10-cultured cells treated with a range of concentrations of dairy IF (HI) or (P+O) digesta. (B) PS5+EGF+ITS-cultured cells treated with a range of concentrations of dairy IF (HI) or (P+O) digesta. Data are presented as mean ± SEM from three independent experiments. Statistical significance was determined using one-way ANOVA followed by Tukey's post hoc test. $P < 0.05$ indicates a significant difference from the HBSS control and is denoted by an asterisk. Cells in HBSS were 84.26 ± 6.10% viability of cells in PS10 or PS5+EGF+ITS alone.

5.3.7. Heat-inactivated digested dairy IF (HI) increases TEER in IPEC-J2 monolayers cultured in PS10 medium

To assess barrier integrity after exposure to digested dairy IF, IPEC-J2 monolayers were cultured for 14 days in PS5+EGF+ITS or PS10 medium and then treated with digested dairy IF for 2h. Monolayer TEER was measured at baseline (T0) and after 2 h (T2, Fig. 5.7).Monolayers cultured in PS10 exhibited a significant increase in TEER after treatment with dairy IF (HI) (T0 = 1175.5 ± 162.7 vs. T2 = 1595.7 ± 107.0 Ω·× cm²; $P < 0.05$). At T2, these monolayers also exhibited significantly higher TEER compared with HBSS controls (HBSS = 942.15 ± 109.25 Ω·× cm²; $P < 0.05$). When these monolayers were treated with dairy IF (P+O), TEER remained unchanged from T0 to T2 (T0 = 1023 ± 153.66 vs. T2 = 1175.90 ± 189.68 Ω·× cm²; $P > 0.05$). Where monolayers were cultured in PS5+EGF/IT medium for 14 days, TEER values remained stable pre- and post-treatment with dairy IF (HI) and dairy IF P+0 ($P > 0.05$).

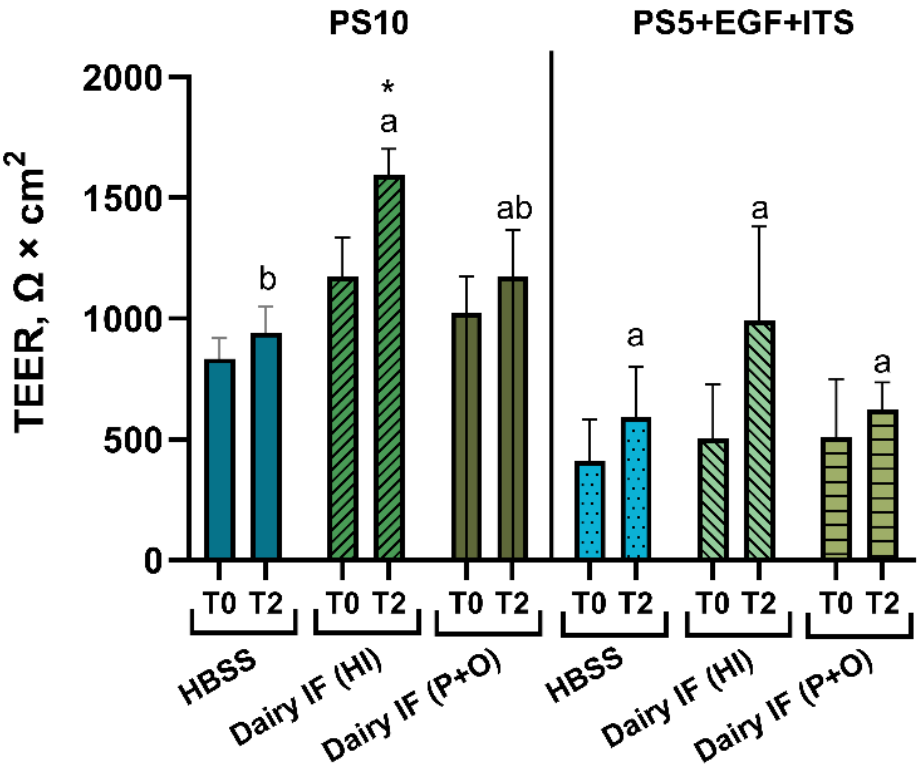


Fig. 5.7 TEER values of undifferentiated IPEC-J2 cells before and after exposure to dairy infant formula (IF) digesta.

IPEC-J2 cells were cultured for 14 days in either PS10 or PS5+EGF+ITS medium and then treated for 2 h with gastrointestinally digested dairy IF heat treated (HI) or with Pefablock and Orlistat (P+O). Transepithelial electrical resistance (TEER) was measured at T0 (after washing monolayers, immediately before digesta addition) and T2 (2 hours post-treatment). Asterisks indicate significant changes between T0 and T2 within the same condition ($P < 0.05$; paired *t*-test). TEER values at T2 were compared across all conditions using one-way ANOVA with Tukey's post hoc test; different letters indicate significant differences between groups ($P < 0.05$). TEER values at T0 did not differ significantly across conditions (one-way ANOVA, $P > 0.05$). Data are presented as mean ± SEM from three independent experiments.

5.3.8. PS10 increases basolateral free AA after exposure to dairy IF digesta

Next, the concentration of free AAs, in the basolateral chambers of monolayers, were quantified to assess media influence on the absorption capability of IPEC-J2 monolayers to digested dairy IF (Fig. 5.8). Individual amino acid concentrations for the digesta and basolateral samples are presented in Supplementary Tables 5.2 and 5.3, respectively. Fig. 5.8A shows the free AA concentration in the digested dairy IF (HI) (1838 ± 34.85 nmol/mL) was not significantly different to dairy IF (P+O) (2065 ± 96.81 nmol/mL; $P > 0.05$). Significant differences were observed in the basolateral compartment of IPEC-J2 monolayers cultured with either PS10 or PS5+EGF+ITS, and subsequently treated with either dairy IF (HI) or dairy IF (P+O) (Fig. 5.8B). Monolayers cultured in PS10 showed higher total free AA concentrations after treatment with dairy IF (P+O) compared to monolayers in PS5+EGF+ITS (117.8 ± 7.90 vs. 72.82 ± 12.53 nmol/1.5 mL; $P < 0.05$). This was also evident for essential AAs (PS10 = 70.53 ± 4.81 vs. PS5+EGF+ITS = 49.79 ± 8.19 nmol/1.5 mL; $P < 0.05$) and branched-chain AAs (PS10 = 28.79 ± 1.61 vs. PS5+EGF+ITS = 16.81 ± 3.84 nmol/1.5 mL; $P < 0.05$). No significant differences were observed in free AAs levels in IPEC-J2 basolateral chambers, between media types following dairy IF (HI) treatment (PS10 = 111.3 ± 15.1; PS5+EGF+ITS = 90.17 ± 25.05 nmol/1.5 mL; $P > 0.05$).

Following 2 h of incubation, the apical compartment of IPEC-J2 retained similar levels of free AAs across all conditions (Supplementary Fig. 5.2): PS10 dairy IF (HI) = 757.5 ± 64.34, PS5+EGF+ITS dairy IF (HI) = 738.6 ± 23.22, PS10 dairy IF (P+O) = 511.3 ± 40.76, PS5+EGF+ITS dairy IF (P+O) = 499.1 ± 50.02 nmol/0.5 mL ($P > 0.05$).

Although the dairy IF derived AA were not labelled, Supplementary Fig. 5.2 presents (B) apical-to-basolateral ratios illustrating AA distribution across the monolayer and (C–D) apical and basolateral concentrations in HBSS-treated controls. Treatment of day 14 IPEC-J2 monolayers cultured in PS10 with 150 μg protein/cm² dairy IF P+0 resulted in significantly enhanced basolateral-to-apical AA ratios, indicating greater trans-epithelial transfer compared with PS5+EGF+ITS. In particular, branched-chain AAs (Val, Ile, Leu) and Thr, as well as non-essential AAs (Arg, Ser, Gly, Ala, and Cysteic acid), showed markedly higher basolateral/apical ratios in monolayers grown in PS10 ($P < 0.05$).

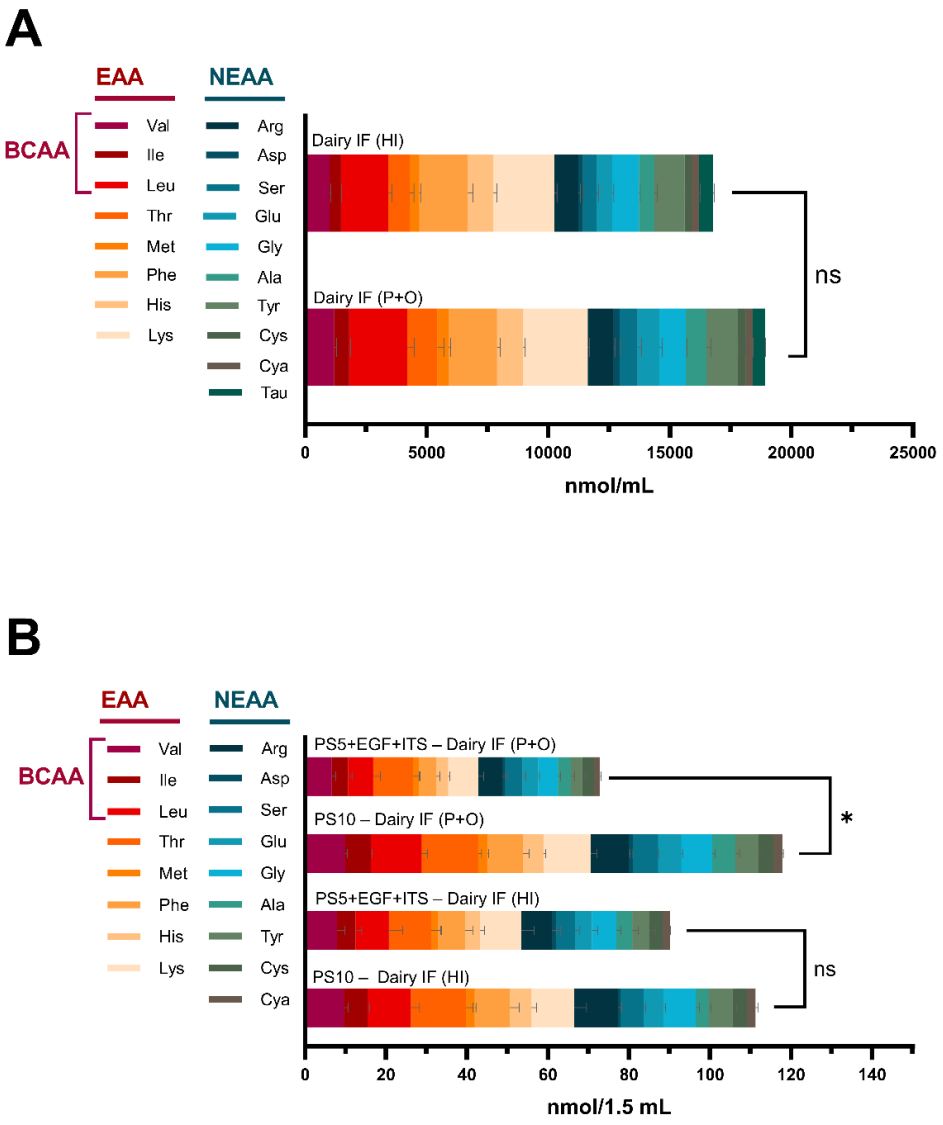


Fig. 5.8 Free amino acid (AA) in basolateral chamber of IPEC-J2 monolayers treated with dairy infant formula (IF) digesta.

IPEC-J2 monolayers were cultured for 14 days in either PS10 or PS5+EGF+ITS medium and then exposed for 2 hours to dairy IF digesta (dairy IF) inactivated by heat (HI; 200 µg protein/cm² in HBSS) or by enzymatic inhibition using Pefabloc and Orlistat (P+O; 150 µg protein/cm² in HBSS). (A) Total free AA content in the undiluted digesta. (B) Free AAs in the basolateral compartment. Colors indicate AA classification: red = branched-chain AAs (BCAA), orange/red = essential AAs (EAA), and blue/green = non-essential AAs (NEAA). Cya = cysteic acid, oxidation product of cysteine. Data represent mean ± SEM from three independent experiments. Statistical analysis was performed using (A) unpaired *t*-tests or (B) two-way ANOVA with FDR correction. Asterik indicates significant difference ($P < 0.05$) between IMF samples within the same cell media, whereas 'ns' denotes not significant.

5.4. Discussion

Previously, IPEC-J2 monolayers were cultured under diverse conditions, such as FBS (Bernardini et al., 2021; Saaby et al., 2016; Zakrzewski et al., 2013), PS (Zakrzewski et al., 2013), or growth factor–supplemented formulations, such as EGF/ITS (Hu et al., 2020; Lu et al., 2002; Nossol et al., 2015; Zakrzewski et al., 2013) or L-WRN conditioned media (Boger et al., 2023). This variability has contributed to wide differences in reported TEER values from monolayers and limited reproducibility between laboratories. To address this, out study compared side by side four widely used media: FBS10 (medium recommended by the cell line supplier), PS10 (species-specific medium), PS5+EGF+ITS (expected to generate monolayers with low TEER, 240–330 Ω·× cm², and displaying epithelial-like morphology) (Zakrzewski et al., 2013), and PS5+L-WRN (expected to generate monolayers with very low TEER, ~50 Ω·cm²butpromoting cell proliferation) (Boger et al., 2023). The goal was to identify one media that provides a reproducible balance of barrier integrity, differentiation, and nutrient absorption, thereby advancing IPEC-J2 as a standardized and physiologically relevant model for infant nutrition research. In the assessment of the four media types, our primary findings are that (a) monolayer TEER values varied substantially with culture media, ranging from 327.58 ± 71.5 Ω×cm² in PS5+EGF+ITS to 6620.78 ± 1997.03 Ω×cm² in FBS10; however, this did not overly influence monolayer paracellular or transcellular permeability; (b) media composition strongly influenced the expression of IPEC-J2 nutrient transporters and tight junction proteins and was associated with distinct cellular traits, with PS5+EGF+ITS encouraging more mesenchymal-like characteristics in IPEC-J2, while FBS10 and PS5+L-WRN supported IPEC-J2 tight barriers but with reduced resilience.

PS10 emerged as the most balanced condition. Monolayers cultured in PS10 displayed TEER values = 2395.0 ± 485.5 Ω × cm² (Fig. 5.1), high ALP and LDH activity (8.01 ± 1.54 IU/mg of protein and 0.12 ± 0.01 mU/mg of protein; Fig. 5.2), and the lowest lactulose permeability (Papp = $9.66 \times 10^{-7} \pm 1.97 \times 10^{-7}$ cm/s; Fig. 5.3). Immunofluorescence indicated that ZO1 displayed an organized distribution at the cell membrane (Fig. 5.5), and mRNA levels of CD36, LAT2, and CLDN2 more closely resembled pig jejunum (Fig. 5.4 and Table 5.1). Moreover, S100A4 expression was lower than in PS5+EGF+ITS and PS5+L-WRN, consistent with a less fibroblast-like phenotype. Functionally, monolayers cultured in PS10 were compatible with both HBSS buffer and digested dairy IF, showing a stable TEER or even a TEER increase after a 2 h treatment with dairy IF (HI) (≈ +36%; Fig. 5.7). These monolayers had a substantial concentration of free AAs in their basolateral chambers post dairy IF apical treatment (dairy IF (P+O) = 117.8 ± 7.9; dairy IF (HI) = 111.3 ± 15.1 nmol/1.5 mL), with PS10 monolayers treated with dairy IF (P+O) exhibiting significantly higher basolateral AA levels than PS5+EGF+ITS ($P < 0.05$). These findings highlight PS10 as the most suitable culture condition for generating robust and functional IPEC-J2 monolayers for food absorption studies.

In agreement with earlier reports, culturing IPEC-J2 in FBS10 yielded the highest TEER values, comparable to those described by Zakrzewski et al. (2013), Saaby et al. (2016), and Bernardini et al. (2021). Zakrzewski et al. (2013) observed a monolayer TEER of 2111 ± 356 Ω×cm² in 10% FBS and only 241 ± 28 Ω×cm² in 5% PS+EGF/ITS (Zakrzewski et al., 2013). Similarly, Saaby et al. recorded 15,833 ± 1596 Ω×cm² for monolayers cultured in 10% FBS, along with a mannitol Papp of 0.04×10^{-6} cm/s (Saaby et al., 2016). Bernardini et al. reported lower TEER values

of approximately ~4500 Ω×cm² for monolayers in 10% FBS and ~1550 Ω×cm² for 5% FBS (Bernardini et al., 2021).

In our study, remarkably, IPEC-J2 cultured in PS5+L-WRN performed similarly to culturing in FBS10, despite lacking bovine serum. This likely reflects the effects provided by Wnt3a, R-spondin, and Noggin, which are known to promote cell proliferation by activating canonical Wnt signaling pathways (Aly et al., 2013). In contrast, PS10 alone supported monolayers with moderate TEER (2395.00 ± 485.51 Ω×cm²), whereas PS5+EGF+ITS media produced monolayers with the weakest barrier (327.58 ± 71.58 Ω×cm²). Notably, real-time CellZScope analysis confirmed that monolayer TEER plateaued around day 12 for all conditions, suggesting that epithelial barrier maturation was complete by this time point.

Moreover, in the present study, IPEC-J2 monolayers exhibited a marked TEER decrease following exposure to L:M in HBSS. Monolayers cultured in FBS10 and PS5+L-WRN showed the greatest TEER loss ($93.19 \pm 5.39\%$ and $87.78 \pm 0.56\%$, respectively), whereas those cultured in PS5+EGF+ITS were the least affected. In contrast, Perruchot et al. (2025) reported a significant TEER reduction in IPEC-J2 monolayers cultured in PS5+EGF+ITS after HBSS washing (from 3100 ± 684 Ω×cm² to 1342 ± 297 Ω×cm²; $P < 0.05$) (Perruchot et al., 2025). Importantly, a decline in TEER did not necessarily indicate increased permeability: lactulose and mannitol fluxes were highest in PS5+EGF+ITS ($3.31 \times 10^{-6} \pm 5.19 \times 10^{-7}$ cm/s), followed by PS5+L-WRN and FBS10, confirming that higher TEER values do not always correspond to reduced paracellular transport. This divergence may be partially explained by differences in epithelial differentiation and metabolic activity. ALP activity, a marker of enterocyte maturation (Matsumoto et al., 1990), and LDH activity, indicative of glycolytic metabolism (Sharma et al., 2022), were both higher

in IPEC-J2 cultured in PS10 and PS5+EGF+ITS compared to FBS10 and PS5+L-WRN ($P < 0.05$). Together, these findings suggest that although FBS10 and PS5+L-WRN support the formation of IPEC-J2 tight epithelial barriers, as reflected by high baseline TEER, they may preferential encourage cell proliferation over maturation In contrast, PS10 and PS5+EGF+ITS promoted lower TEER values in day 14 IPEC-J2 but higher ALP and LDH activity, indicating greater metabolic activity, enhanced differentiation, and potentially a more physiologically relevant epithelial phenotype.

Gene expression and structural characterization of IPEC-J2 under different media revealed distinct phenotypes ranging from proliferative to differentiated epithelial states (Fig. 5.4). In PS10, GLUT2 and CD36 mRNA were higher than in PS5+EGF+ITS, while CD36 and LAT2 were elevated compared with FBS10; CLDN2 was also increased relative to both FBS10 and PS5+EGF+ITS ($P < 0.05$), indicating enhanced nutrient transport capacity. In PS5+L-WRN, CD36 was higher than in FBS10 or PS5+EGF+ITS, and GLUT2 and LAT4 were increased relative to PS5+EGF+ITS; CLDN2 was higher than in FBS10, and MUC2 exceeded levels in PS10 ($P < 0.05$), reflecting additional goblet-like features. In contrast, PS5+EGF+ITS monolayers showed the highest S100A4 but reduced FATP4, SGLT1, rBAT, y^+LAT1, and MUC1 compared with all other media, while LAT2 was higher than in FBS10 ($P < 0.05$). This mRNA pattern is consistent with a fibroblast-like, less differentiated phenotype. Finally, FBS10 cultures expressed higher OCLN, ZO1, and CLDN1 than any other medium ($P < 0.05$), whereas CD36 and LAT2 were lower than in PS10 and PS5+EGF+ITS, respectively, indicating greater barrier integrity but reduced nutrient transporter activity.

To validate these transcriptional trends at the protein level, ZO1 immunofluorescence staining revealed significantly greater membrane-associated ZO1 signal in monolayers cultured in PS10 compared to PS5+EGF+ITS. Conversely, nuclear density was significantly greater in PS5+EGF+ITS than in PS10 (2.26 ± 0.32 vs. 0.91 ± 0.11 nuclei/1000 μm^2; $P < 0.05$), consistent with increased proliferative activity in the PS5+EGF+ITS-based condition.

The only published study directly comparing different media in IPEC-J2 is Zakrzewski et al. (2013), who reported that CLDN4 was significantly upregulated ($P < 0.05$) in IPEC-J2 under PS5+EGF+ITS compared to FBS10, while CLDN2 was absent at both the mRNA and protein level. For us, CLDN4 was detectable under all tested conditions but not significantly different ($P > 0.05$), while CLDN2 expression was clearly present and significantly increased only in monolayers cultured in PS10-based media ($P < 0.05$) compared to FBS10. Zakrzewski et al. also reported significantly higher protein levels of GLUT2 ($P < 0.01$), SGLT1 ($P < 0.05$), and the mesenchymal marker vimentin ($P < 0.01$) in cells grown in PS5+EGF+ITS compared to FBS10-grown cells. In our study, SGLT1 and GLUT2 mRNA were not significantly different between conditions, with SGLT1 expressed at a low level (approximately 20,000-fold lower than in jejunal tissue). While Zakrzewski identified vimentin as a mesenchymal marker upregulated in IPEC-J2 with PS5+EGF+ITS, we observed S100A4 to be similarly expressed in monolayers in either FBS10 or PS5+EGF+ITS media. Nevertheless, expression remained 13- to 37-fold higher than in jejunal tissue across all conditions ($P < 0.05$), indicating a persistent mesenchymal-like phenotype *in vitro*. Regarding mucins, their study showed MUC2 was undetectable in monolayers cultured in FBS but inducible with

PS, which is consistent with our observation that MUC2 mRNA was significantly upregulated in monolayers with PS5+EGF+ITS compared to FBS10.

When compared to porcine jejunum (Table 5.1), all *in vitro* conditions showed markedly reduced mRNA transcripts ($P < 0.05$) of nutrient transporters (PEP1, SGLT1, GLUT2, FATP4, LATs, rBAT, CD36) structural genes (CLDN2, CLDN4), mucin and cytokine genes (MUC2, IL8, TNF), while ZO1, CLDN1, MUC1, and IL6 were higher ($P < 0.05$) in culture. Furthermore, immune, lineage-specific markers and AA transporters such as CHGA, CD163, CD45, B0AT1, IMINO, and ATB0+ were absent from IPEC-J2 cultures but readily detected in tissue, underscoring the restricted cell-type diversity of this model. Thus, although media composition strongly influences the balance between barrier, absorptive, and secretory phenotypes in IPEC-J2, none of the *in vitro* conditions fully replicate the transcriptional complexity of jejunal epithelium.

These observations are further contextualized by the findings of Støy et al. (2013), who compared gene expression profiles between IPEC-J2 cells and preterm pig jejunal tissue under colostrum or formula feeding (Støy et al., 2013). Their principal component analysis (PCA) revealed a clear separation between IPEC-J2 and native tissue, indicating substantial transcriptional divergence. Notably, they reported that MUC2 and ALPI were not expressed in IPEC-J2 under any tested condition. In contrast, we detected low but consistent expression of MUC2. More importantly, ALP enzymatic activity was present in IPEC-J2 cultured in equal 4 media, particularly in PS10 and PS5+EGF+ITS. These discrepancies may reflect phenotypic drift and genomic instability known to affect IPEC-J2, including documented

aneuploidies and structural rearrangements (De Vos et al., 2023) as well as differences in cell handling or unknown passage histories between studies. Regarding immune-related genes, both our data and Støy et al. confirmed expression of IL8, IL6, and TNF in IPEC-J2, with IL6 consistently higher in IPEC-J2 than in jejunal tissue.

A recent study characterized the genomic architecture of IPEC-J2 and reported multiple chromosomal abnormalities, including whole-chromosome and segmental aneuploidies (De Vos et al., 2023). Notably, chromosome 9 was found to be fully triploid, which encompasses both IL6 (SSC9: ~91.5 Mb) and CD36 (SSC9: ~99.7 Mb). In addition, the distal half of chromosome 8 showed a clear copy number gain, which includes IL8 (SSC8: ~69.9 Mb). While the IL6 pattern is consistent with the dosage effects of chromosomal gains, these results also indicate that additional mechanisms, such as altered chromatin accessibility and epigenetic regulation, further influence transcriptional outcomes in this model (De Vos et al., 2023). Similar discrepancies have also been reported in other well-established intestinal cell lines. For example, Sun et al. (2002) demonstrated that Caco-2 cells diverge markedly from human duodenal tissue, with SGLT1 expressed more than 600-fold higher in the duodenum, while GLUT3 was 150-fold higher in Caco-2 (Sun et al., 2002).

The suitability of IPEC-J2 monolayers to food digesta studies was demonstrated with dairy IF. From MTS and TEER data, it was evident that heat inactivation with dilution of digested dairy IF was preferable to the use of protease inhibitors (Fig. 5.6 and 5.7). Indeed, previous studies have reported adverse effects of Pefabloc on Caco-2 epithelial integrity (Kondrashina et al., 2023), supporting the interpretation that

enzymatic inhibitors are harmful. Consistent with our findings, Perruchot et al. (2025) also reported no significant TEER change in IPEC-J2 monolayers after 2 h exposure to heat-inactivated digested pea flour ($P > 0.05$) (Perruchot et al., 2025). Quantification of free AAs in the basolateral chambers of IPEC-J2 monolayers treated with digested dairy IF showed that dairy IF (P+O) treatment enhanced basolateral AA transport in PS10-grown cells compared with PS5+EGF+ITS (Fig. 5.8), consistent with higher expression of apical (rBAT) and basolateral (y^+LAT1) transporters and a more functionally differentiated epithelial phenotype. To our knowledge, this is among the pioneering studies exposing IPEC-J2 monolayers to digested food matrices, demonstrating that PS10-cultured monolayers maintain barrier integrity and nutrient transport following exposure to infant formula digesta.

Despite the valuable insights gained from this study, several limitations warrant consideration. Passage number evaluation was not possible in our study because this information is not provided by the cell culture collection. Although transcript and protein expression of several key markers were evaluated, functional confirmation of transporter activity beyond AA flux remains to be established. Lastly, our study focused on a relatively narrow set of nutrient types and digestion states; expanding the analysis to include additional nutrient classes—such as carbohydrates, vitamins or essential minerals—would further enhance the translational relevance of the model.

5.5. Conclusions

In conclusion, culture medium composition markedly affected IPEC-J2 barrier integrity, differentiation, and responses to digested food. Among the tested

conditions, PS10 provided the most physiologically relevant balance, supporting moderate yet stable TEER, elevated ALP and LDH activity, and tighter junctional organization with reduced S100A4 expression—indicating lower fibroblast-like activity and greater epithelial differentiation. These characteristics suggest that PS10-grown monolayers best replicate the functional balance between barrier selectivity and nutrient absorption observed *in vivo*. The expression of key nutrient transporters and tight junction proteins further validates this model for studying nutrient transport and gut barrier responses. Finally, heat inactivation proved preferable to enzyme inhibition for maintaining digesta biocompatibility. Together, these results establish IPEC-J2 as a robust, non-cancerous alternative to Caco-2 for evaluating dietary protein absorption and epithelial resilience, particularly in the context of infant nutrition.

5.6. References

Aly, H., Rohatgi, N., Marshall, C.A., Grossenheider, T.C., Miyoshi, H., Stappenbeck, T.S., Matkovich, S.J., McDaniel, M.L., 2013. A Novel Strategy to Increase the Proliferative Potential of Adult Human β-Cells While Maintaining Their Differentiated Phenotype. PLoS ONE 8, e66131. https://doi.org/10.1371/journal.pone.0066131

Bernardini, C., Algieri, C., Mantia, L.D., Zannoni, A., Salaroli, R., Trombetti, F., Forni, M., Pagliarani, A., Nesci, S., 2021. Relationship between serum concentration, functional parameters and cell bioenergetics in IPEC-J2 cell line. Histochem Cell Biol 156, 59–67. https://doi.org/10.1007/s00418-021-01981-2

Berschneider, H.M., 1989. Development of normal cultured small intestinal epithelial cell lines which transport Na and Cl. Gastroenterology 96, A41.

Boger, K.D., Sheridan, A.E., Ziegler, A.L., Blikslager, A.T., 2023. Mechanisms and modeling of wound repair in the intestinal epithelium. Tissue Barriers 11, 2087454. https://doi.org/10.1080/21688370.2022.2087454

Bröer, S., Fairweather, S.J., 2019. Amino Acid Transport Across the Mammalian Intestine. Comprehensive Physiology 9, 343–373. https://doi.org/10.1002/j.2040-4603.2019.tb00056.x

Brosnahan, A.J., Brown, D.R., 2012. Porcine IPEC-J2 intestinal epithelial cells in microbiological investigations. Veterinary Microbiology 156, 229–237. https://doi.org/10.1016/j.vetmic.2011.10.017

Catassi, C., Bonucci, A., Coppa, G.V., Carlucci, A., Giorgi, P.L., 1995. Intestinal Permeability. Changes during the First Month: Effect of Natural versus

Artificial Feeding. Journal of Pediatric Gastroenterology and Nutrition 21, 383–386. https://doi.org/10.1097/00005176-199511000-00003

Chelakkot, C., Ghim, J., Ryu, S.H., 2018. Mechanisms regulating intestinal barrier integrity and its pathological implications. Exp Mol Med 50, 1–9. https://doi.org/10.1038/s12276-018-0126-x

Chen, Z., Zhou, L., Yuan, Q., Chen, H., Lei, H., Su, J., 2021. Effect of fumonisin B1on oxidative stress and gene expression alteration of nutrient transporters in porcine intestinal cells. J Biochem & Molecular Tox 35. https://doi.org/10.1002/jbt.22706

Darragh, A.J., Moughan, P.J., 1995. The Three-Week-Old Piglet as a Model Animal for Studying Protein Digestion in Human Infants. Journal of Pediatric Gastroenterology and Nutrition 21, 387–393. https://doi.org/10.1097/00005176-199511000-00004

De Vos, J., Crooijmans, R.P.M.A., Derks, M.F.L., Kloet, S.L., Dibbits, B., Groenen, M.A.M., Madsen, O., 2023. Detailed molecular and epigenetic characterization of the pig IPEC-J2 and chicken SL-29 cell lines. iScience 26, 106252. https://doi.org/10.1016/j.isci.2023.106252

Dold, C. A., Bavaro, S. L., Chen, Y., Callanan, M. J., Kennedy, D., Cassidy, J., Tobin, J., Sahin, A. W., Lawlor, P. G., Brodkorb, A., & Giblin, L. (2024). Infant milk formula, produced by membrane filtration, promotes mucus production in the upper small intestine of young pigs. Food Research International, 187, 114343

Fabriek, B.O., Dijkstra, C.D., Van Den Berg, T.K., 2005. The macrophage scavenger receptor CD163. Immunobiology 210, 153–160. https://doi.org/10.1016/j.imbio.2005.05.010

Fei, F., Qu, J., Li, C., Wang, X., Li, Y., Zhang, S., 2017. Role of metastasis-induced protein S100A4 in human non-tumor pathophysiologies. Cell Biosci 7. https://doi.org/10.1186/s13578-017-0191-1

Geens, M.M., Niewold, T.A., 2011. Optimizing culture conditions of a porcine epithelial cell line IPEC-J2 through a histological and physiological characterization. Cytotechnology 63, 415–423. https://doi.org/10.1007/s10616-011-9362-9

Gleeson, J.P., Fein, K.C., Chaudhary, N., Doerfler, R., Newby, A.N., Whitehead, K.A., 2021. The enhanced intestinal permeability of infant mice enables oral protein and macromolecular absorption without delivery technology. International Journal of Pharmaceutics 593, 120120. https://doi.org/10.1016/j.ijpharm.2020.120120

González-Mariscal, L., Betanzos, A., Nava, P., Jaramillo, B.E., 2003. Tight junction proteins. Progress in Biophysics and Molecular Biology 81, 1–44. https://doi.org/10.1016/s0079-6107(02)00037-8

Guo, J., Li, F., He, Q., Jin, H., Liu, M., Li, S., Hu, S., Xiao, Y., Bi, D., Li, Z., 2016. Neonatal Fc Receptor-Mediated IgG Transport Across Porcine Intestinal Epithelial Cells: Potentially Provide the Mucosal Protection. DNA and Cell Biology 35, 301–309. https://doi.org/10.1089/dna.2015.3165

Hermiston, M.L., Xu, Z., Weiss, A., 2003. CD45: A Critical Regulator of Signaling Thresholds in Immune Cells. Annu. Rev. Immunol. 21, 107–137. https://doi.org/10.1146/annurev.immunol.21.120601.140946

Hu, Z., Li, Y., Du, H., Ren, J., Zheng, X., Wei, K., Liu, J., 2020. Transcriptome analysis reveals modulation of the STAT family in PEDV-infected IPEC-J2 cells. BMC Genomics 21, 891. https://doi.org/10.1186/s12864-020-07306-2

Kiela, P.R., Ghishan, F.K., 2016. Physiology of Intestinal Absorption and Secretion. Best Practice & Research Clinical Gastroenterology 30, 145–159. https://doi.org/10.1016/j.bpg.2016.02.007

Kondrashina, A., Arranz, E., Cilla, A., Faria, M.A., Santos-Hernández, M., Miralles, B., Hashemi, N., Rasmussen, M.K., Young, J.F., Barberá, R., Mamone, G., Tomás-Cobos, L., Bastiaan-Net, S., Corredig, M., Giblin, L., 2023. Coupling in vitro food digestion with in vitro epithelial absorption; recommendations for biocompatibility. Critical Reviews in Food Science and Nutrition 1–19. https://doi.org/10.1080/10408398.2023.2214628

Kosek, M.N., Lee, G.O., Guerrant, R.L., Haque, R., Kang, G., Ahmed, T., Bessong, P., Ali, A., Mduma, E., Peñataro Yori, P., Faubion, W.A., Lima, A.A.M., Paredes Olortegui, M., Mason, C., Babji, S., Singh, R., Qureshi, S., Kosek, P.S., Samie, A., Pascal, J., Shrestha, S., McCormick, B.J.J., Seidman, J.C., Lang, D.R., Zaidi, A., Caulfield, L.E., Gottlieb, M., Network, the M.-E., 2017. Age and Sex Normalization of Intestinal Permeability Measures for the Improved Assessment of Enteropathy in Infancy and Early Childhood: Results From the MAL-ED Study. Journal of Pediatric Gastroenterology and Nutrition 65, 31–39. https://doi.org/10.1097/MPG.0000000000001610

Lea, T., 2015. Caco-2 Cell Line, in: Verhoeckx, K., Cotter, P., López-Expósito, I., Kleiveland, C., Lea, T., Mackie, A., Requena, T., Swiatecka, D., Wichers, H. (Eds.), The Impact of Food Bioactives on Health: In Vitro and Ex Vivo Models. Springer International Publishing, Cham, pp. 103–111. https://doi.org/10.1007/978-3-319-16104-4_10

Li, Y., Liu, Y., Liu, B., Wang, J., Wei, S., Qi, Z., Wang, S., Fu, W., Chen, Y.-G., 2018. A growth factor-free culture system underscores the coordination

between Wnt and BMP signaling in Lgr5+ intestinal stem cell maintenance. Cell Discov 4, 49. https://doi.org/10.1038/s41421-018-0051-0

Liao, P., Liao, M., Li, L., Tan, B., Yin, Y., 2017. Effect of deoxynivalenol on apoptosis, barrier function, and expression levels of genes involved in nutrient transport, mitochondrial biogenesis and function in IPEC-J2 cells. Toxicol. Res. 6, 866–877. https://doi.org/10.1039/c7tx00202e

Liu, F., Li, G., Wen, K., Bui, T., Cao, D., Zhang, Y., Yuan, L., 2010. Porcine Small Intestinal Epithelial Cell Line (IPEC-J2) of Rotavirus Infection As a New Model for the Study of Innate Immune Responses to Rotaviruses and Probiotics. Viral Immunology 23, 135–149. https://doi.org/10.1089/vim.2009.0088

Lu, S., Huffman, M., Yao, Y., Mansbach, C.M., Cheng, X., Meng, S., Black, D.D., 2002. Regulation of MTP expression in developing swine. J Lipid Res 43, 1303–1311.

Mainzer, C., Barrichello, C., Debret, R., Remoué, N., Sigaudo-Roussel, D., Sommer, P., 2014. Insulin–transferrin–selenium as an alternative to foetal serum for epidermal equivalents. Intern J of Cosmetic Sci 36, 427–435. https://doi.org/10.1111/ics.12141

Mariani, V., Palermo, S., Fiorentini, S., Lanubile, A., Giuffra, E., 2009. Gene expression study of two widely used pig intestinal epithelial cell lines: IPEC-J2 and IPI-2I. Veterinary Immunology and Immunopathology 131, 278–284. https://doi.org/10.1016/j.vetimm.2009.04.006

Matsumoto, H., Erickson, R.H., Gum, J.R., Yoshioka, M., Gum, E., Kim, Y.S., 1990. Biosynthesis of Alkaline Phosphatase During Differentiation of the

Human Colon Cancer Cell Line Caco-2. Gastroenterology 98, 1199–1207. https://doi.org/10.1016/0016-5085(90)90334-w

Meyer, F., Wendling, D., Demougeot, C., Prati, C., Verhoeven, F., 2023. Cytokines and intestinal epithelial permeability: A systematic review. Autoimmunity Reviews 22, 103331. https://doi.org/10.1016/j.autrev.2023.103331

Nossol, C., Barta-Böszörményi, A., Kahlert, S., Zuschratter, W., Faber-Zuschratter, H., Reinhardt, N., Ponsuksili, S., Wimmers, K., Diesing, A.-K., Rothkötter, H.-J., 2015. Comparing Two Intestinal Porcine Epithelial Cell Lines (IPECs): Morphological Differentiation, Function and Metabolism. PLoS ONE 10, e0132323. https://doi.org/10.1371/journal.pone.0132323

Orofiamma, L.A., Vural, D., Antonescu, C.N., 2022. Control of cell metabolism by the epidermal growth factor receptor. Biochimica et Biophysica Acta (BBA) - Molecular Cell Research 1869, 119359. https://doi.org/10.1016/j.bbamcr.2022.119359

Otani, T., Furuse, M., 2020. Tight Junction Structure and Function Revisited. Trends in Cell Biology 30, 805–817. https://doi.org/10.1016/j.tcb.2020.08.004

Paone, P., Cani, P.D., 2020. Mucus barrier, mucins and gut microbiota: the expected slimy partners? Gut 69, 2232–2243. https://doi.org/10.1136/gutjnl-2020-322260

Perruchot, M.-H., Boudry, G., Mayeur-Nickel, F., Grondin, M., Wiart-Letort, S., Giblin, L., Grundy, M.M.-L., 2025. In Vitro Evaluation of Intestinal Barrier Function after Exposure to Digested Pea Ingredients─Food Matrix Effect. J. Agric. Food Chem. 73, 584–594. https://doi.org/10.1021/acs.jafc.4c09963

Rindi, G., Leiter, A.B., Kopin, A.S., Bordi, C., Solcia, E., 2004. The “Normal” Endocrine Cell of the Gut: Changing Concepts and New Evidences. Annals

of the New York Academy of Sciences 1014, 1–12. https://doi.org/10.1196/annals.1294.001

Revilla, M., Puig-Oliveras, A., Crespo-Piazuelo, D., Criado-Mesas, L., Castelló, A., Fernández, A. I., Ballester, M., & Folch, J. M. (2018). Expression analysis of candidate genes for fatty acid composition in adipose tissue and identification of regulatory regions. Scientific Reports, 8(1). https://doi.org/10.1038/s41598-018-20473-3

Saaby, L., Helms, H.C.C., Brodin, B., 2016. IPEC-J2 MDR1, a Novel High-Resistance Cell Line with Functional Expression of Human P-glycoprotein (ABCB1) for Drug Screening Studies. Mol. Pharmaceutics 13, 640–652. https://doi.org/10.1021/acs.molpharmaceut.5b00874

Sangild, P.T., Ney, D.M., Sigalet, D.L., Vegge, A., Burrin, D., 2014. Animal models of gastrointestinal and liver diseases. Animal models of infant short bowel syndrome: translational relevance and challenges. American Journal of Physiology-Gastrointestinal and Liver Physiology 307, G1147–G1168. https://doi.org/10.1152/ajpgi.00088.2014

Schierack, P., Nordhoff, M., Pollmann, M., Weyrauch, K.D., Amasheh, S., Lodemann, U., Jores, J., Tachu, B., Kleta, S., Blikslager, A., Tedin, K., Wieler, L.H., 2006. Characterization of a porcine intestinal epithelial cell line for in vitro studies of microbial pathogenesis in swine. Histochem Cell Biol 125, 293–305. https://doi.org/10.1007/s00418-005-0067-z

Sharma, D., Singh, M., Rani, R., 2022. Role of LDH in tumor glycolysis: Regulation of LDHA by small molecules for cancer therapeutics. Seminars in Cancer Biology 87, 184–195. https://doi.org/10.1016/j.semcancer.2022.11.007

Srinivasan, B., Kolli, A.R., Esch, M.B., Abaci, H.E., Shuler, M.L., Hickman, J.J., 2015. TEER Measurement Techniques for In Vitro Barrier Model Systems. SLAS Technology 20, 107–126. https://doi.org/10.1177/2211068214561025

Støy, A.C.F., Heegaard, P.M.H., Sangild, P.T., Østergaard, M.V., Skovgaard, K., 2013. Gene Expression Analysis of the IPEC-J2 Cell Line: A Simple Model for the Inflammation-Sensitive Preterm Intestine. ISRN Genomics 2013, e980651. https://doi.org/10.1155/2013/980651

Sun, D., Lennernas, H., Welage, L.S., Barnett, J.L., Landowski, C.P., Foster, D., Fleisher, D., Lee, K.-D., Amidon, G.L., 2002. Comparison of Human Duodenum and Caco-2 Gene Expression Profiles for 12,000 Gene Sequences Tags and Correlation with Permeability of 26 Drugs. Pharm Res 19, 1400–1416. https://doi.org/10.1023/A:1020483911355

Sun, H., Chow, E.C., Liu, S., Du, Y., Pang, K.S., 2008. The Caco-2 cell monolayer: usefulness and limitations. Expert Opinion on Drug Metabolism & Toxicology 4, 395–411. https://doi.org/10.1517/17425255.4.4.395

Tang, X., Xiong, K., 2022. Epidermal growth factor activates EGFR/AMPK signalling to up-regulate the expression of SGLT1 and GLUT2 to promote intestinal glucose absorption in lipopolysaccharide challenged IPEC-J2 cells and piglets. Italian Journal of Animal Science 21, 943–954. https://doi.org/10.1080/1828051x.2022.2073832

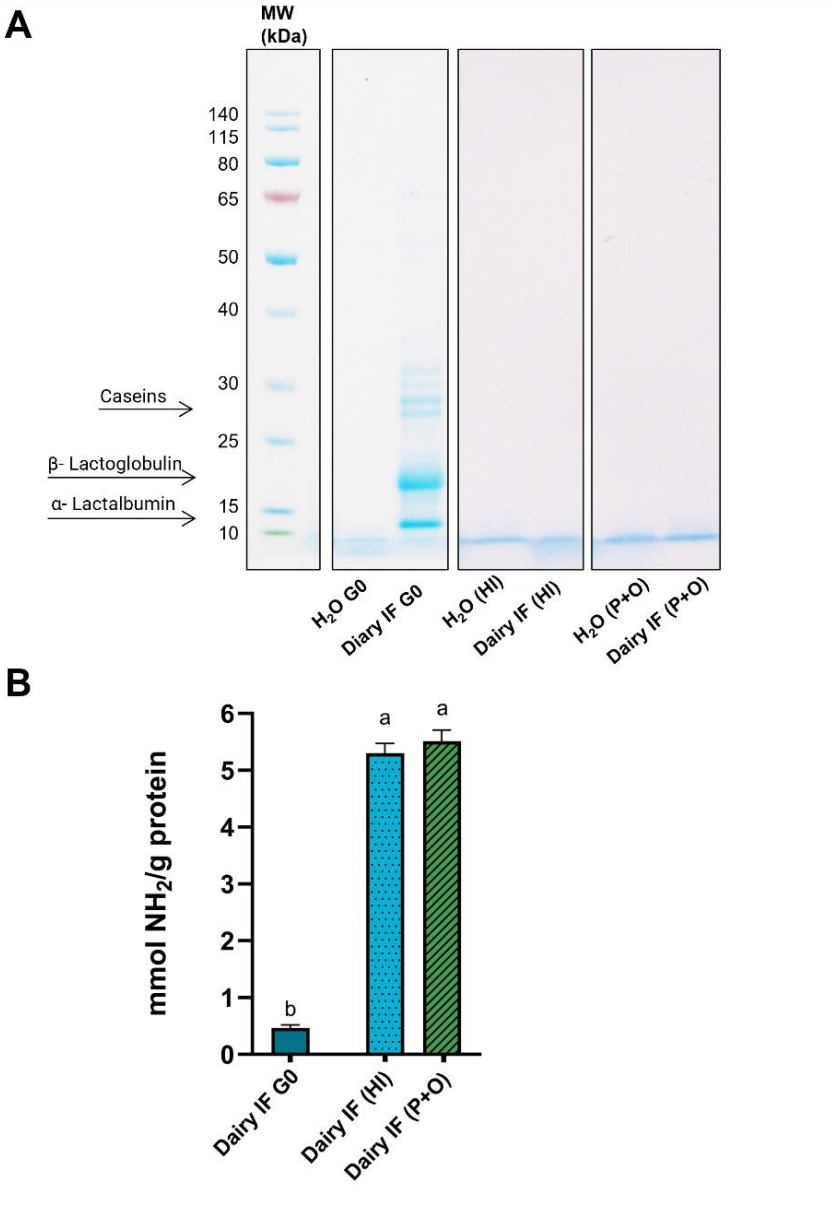
Vander Heiden, M.G., Cantley, L.C., Thompson, C.B., 2009. Understanding the Warburg Effect: The Metabolic Requirements of Cell Proliferation. Science 324, 1029–1033. https://doi.org/10.1126/science.1160809

Weaver, L.T., Laker, M.F., Nelson, R., 1984. Intestinal permeability in the newborn. Arch Dis Child 59, 236–241. https://doi.org/10.1136/adc.59.3.236

Xu, M., Che, L., Niu, L., Wang, L., Li, M., Jiang, D., Deng, H., Chen, W., Jiang, Z., 2023. Molecular mechanism of valine and its metabolite in improving triglyceride synthesis of porcine intestinal epithelial cells. Sci Rep 13. https://doi.org/10.1038/s41598-023-30036-w

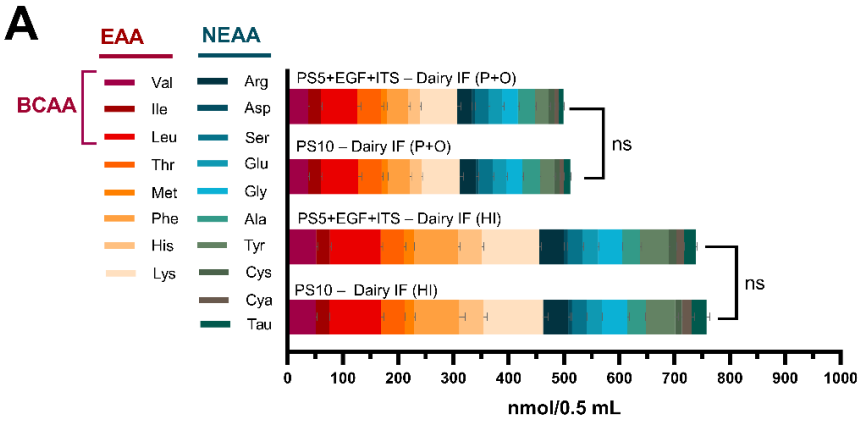
Zakrzewski, S.S., Richter, J.F., Krug, S.M., Jebautzke, B., Lee, I.-F.M., Rieger, J., Sachtleben, M., Bondzio, A., Schulzke, J.D., Fromm, M., Günzel, D., 2013. Improved Cell Line IPEC-J2, Characterized as a Model for Porcine Jejunal Epithelium. PLOS ONE 8, e79643. https://doi.org/10.1371/journal.pone.0079643

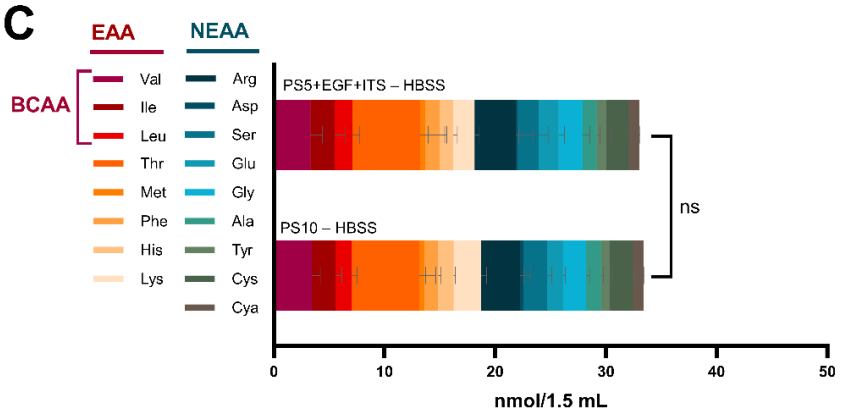
5.7.Supplementary Materials

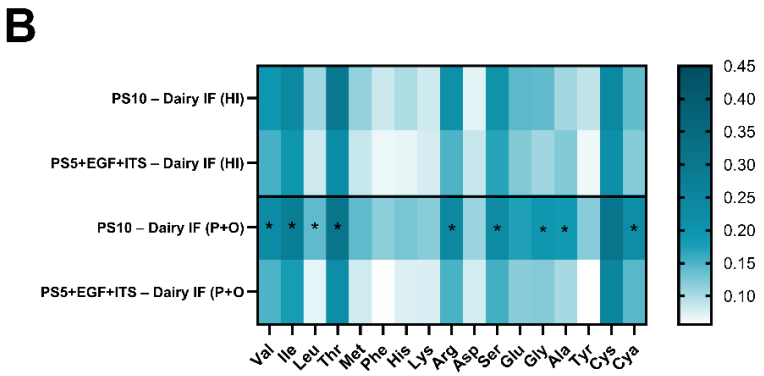


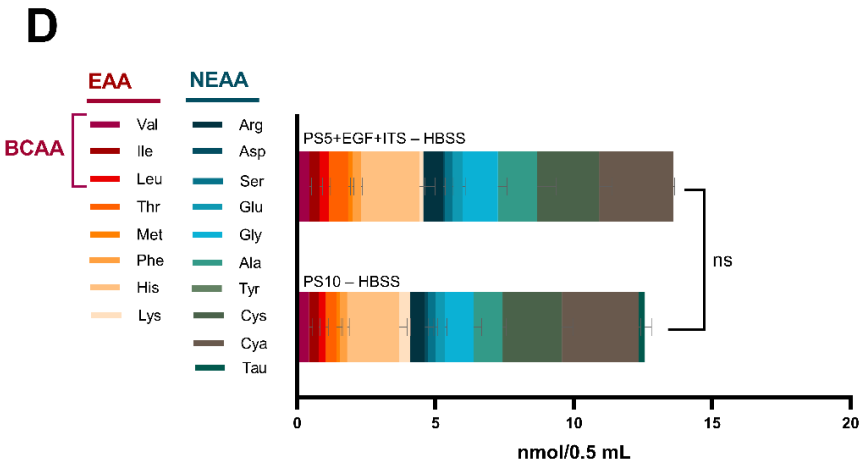
Supplementary Fig 5.1 Tracking protein digestion during simulated gastrointestinal digestion of dairy infant formula (IF).

(A) SDS–PAGE profiles of dairy IF before digestion (G0) and after GI digestion, followed by enzyme inactivation by either heat (HI) or Pefabloc + Orlistat (P+O). Each lane contained 10 µg of total protein, separated on a NuPAGE™ 10% Bis–Tris gel under reducing conditions using MOPS running buffer. (B) Degree of protein hydrolysis in dairy IF-G0 (pre-gastric phase) and digested samples (HI and P+O), determined by o-phthaldialdehyde (OPA) assay and expressed as free amine concentration (µmol NH_2/g protein). Data represent mean ± SEM from three independent digestions (two technical replicates each). Statistical analysis was performed by one-way ANOVA with Tukey's post hoc test; bars with different letters differ significantly ($P < 0.05$).


A
EAA
NEAA
BCAA
Val
Ile
Leu
Thr
Met
Phe
His
Lys
Arg
Asp
Ser
Glu
Gly
Ala
Tyr
Cys
Cya
Tau
PS5+EGF+ITS – Dairy IF (P+O)
PS10 – Dairy IF (P+O)
PS5+EGF+ITS – Dairy IF (HI)
PS10 – Dairy IF (HI)
ns
ns
0
100
200
300
400
500
600
700
800
900
1000
nmol/0.5 mL


C
EAA
NEAA
BCAA
Val
Ile
Leu
Thr
Met
Phe
His
Lys
Arg
Asp
Ser
Glu
Gly
Ala
Tyr
Cys
Cya
PS5+EGF+ITS – HBSS
PS10 – HBSS
ns
0
10
20
30
40
50
nmol/1.5 mL


B
PS10 – Dairy IF (HI)
PS5+EGF+ITS – Dairy IF (HI)
PS10 – Dairy IF (P+O)
PS5+EGF+ITS – Dairy IF (P+O
Val
Ile
Leu
Thr
Met
Phe
His
Lys
Arg
Asp
Ser
Glu
Gly
Ala
Tyr
Cys
Cya
0.45
0.40
0.35
0.30
0.25
0.20
0.15
0.10


D
EAA
NEAA
BCAA
Val
Ile
Leu
Thr
Met
Phe
His
Lys
Arg
Asp
Ser
Glu
Gly
Ala
Tyr
Cys
Cya
Tau
PS5+EGF+ITS – HBSS
PS10 – HBSS
ns
0
5
10
15
20
nmol/0.5 mL

Supplementary Fig 5.2 : Free amino acid (AA) levels in IPEC-J2 monolayers exposed to digested dairy infant formula (IF) or HBSS.

IPEC-J2 cells were cultured for 14 days in either PS10 or PS5+EGF+ITS medium and exposed for 2 hours to dairy IF digesta inactivated by heat (HI; 200 µg protein/cm²) or by enzymatic inhibition using Pefabloc and Orlistat (P+O; 150 µg protein/cm²) or to HBSS. (A) Apical free AA concentrations after incubation with dairy IF digesta. (B) Apical-to-basolateral ratios illustrating AA distribution. Color code: blue = higher ratio (greater relative basolateral abundance), white = 0. (C) Apical free amino AA concentrations in HBSS-treated monolayers. (D) Basolateral free AA concentrations in HBSS-treated monolayers. Color code: red = branched-chain AAs (BCAA), orange/red = essential AAs (EAA), and blue/green = non-essential AAs (NEAA). Cya refers to cysteic acid. Data represent mean ± SEM from three independent experiments. Statistical analysis was performed using unpaired *t*-tests. Asterisk indicates significant difference ($P < 0.05$) between IMF samples within the same media, whereas 'ns' denotes not significant.

Supplementary Table 5.1 Gene name, protein name, GenBank accession number, primers sequences and annealing temperature (Ta) for RT-PCR analysis.

Gene Symbol	Protein Name	Accession Number	Forward Primer	Reverse Primer	Ta (°C)	Source
RPLP0	60S acidic ribosomal protein P0	NM_001098598.1	GACAAAGTGGGAGCCAGTGA	CAGGGTTGTAGATGCTGCCA	56	Dold et al., 2024
MUC1	Mucin-1 (MUC1)	XM_021089729.1	AGTCCATGTTGGCACCTCC	GGAGTACCTTTGCTGACTGG	55	Dold et al., 2024
MUC2	Mucin-2 (MUC2)	XM_013989745.1	TCTGGATCCGCAGCTCTCTGG	CACTGGGCTGGGAGACAGGT	60	Dold et al., 2024
CLDN2	Claudin-2 (CLDN2)	NM_001244539.1	ACCGTGTGGGAACAACCAGA	ACACATGAAAATGGCTTCCCTCC	62	Dold et al., 2024
CLDN1	Claudin-1 (CLDN1)	NM_001161638.1	GCATCATTTCCTCCCTGTT	TCTTGGCTTTGGGTGGTT	60	Dold et al., 2024
CLDN4	Claudin-4 (CLDN4)	NM_001161637.1	CAACTGCGTGGATGATGAGA	CCAGGGGATTGTAGAAGTCG	60	Dold et al., 2024
OCLN	Occludin (OCLN)	NM_001163647.2	TCCTGGGTGTGATGGTGTTC	CGTAGAGTCCAGTCACCGCA	63	Dold et al., 2024
TJP1	Zonula occludens 1 (ZO1)	XM_003353439.2	ATGGCGGAAAGTGAACCTCG	TCACACCCTGCTTAGAATCCG	55	Dold et al., 2024
IL6	Interleukin-6 (IL-6)	NM_214399.1	TGGCTACTGCCTTCCCTACC	CAGAGATTTTGCCGAGGATG	60	Dold et al., 2024
IL8	Interleukin-8 (IL8)	NM_213867.1	GAAGAGAACTGAGAAGCAACAACA	TTGTGTTGGCATCTTTACTGAGA	60	Dold et al., 2024
TNF	Tumor necrosis factor (TNF)	NM_214022.1	CACGTTGTAGCCAATGTCAAAG	GAGGTACAGCCCATCTGTCG	60	Dold et al., 2024
CD163	Cluster of differentiation 163 (CD163)	NM_213976.1	CACATGTGCCAACAAAATAAGAC	CACCACCTGAGCATCTTCAA	60	Støy et al., 2013
S100A4	S100 calcium-binding protein A4 (S100A4/FSP1)	NM_001252605.1	GGCCCTCGATGTGATGGTGT	CATCCGTCCTTTTCCCCAGGA	60	This study
CHGA	Chromogranin A (CHGA)	NM_001164005.2	GCAAGTCATTGCCCTCCCTG	GAGGATCCGTTCATCTCCTCGG	60	This study
LGR5	Leucine-rich repeat-containing G protein-coupled receptor 5 (LGR5)	NM_001315762.1	GCCTTTGTAGGCAACCCTTCT	AGGCACCATTCAAAGTCAGTGT	60	This study
PTPRC	Protein tyrosine phosphatase receptor type C (CD45)	XM_003130596	AAAGCTCGGCCAGGAATGGT	TGGGGCACTTGGTGAACTGA	60	This study
SLC5A1	Sodium/glucose cotransporter 1 (SGLT1)	NM_001098598.1	CTGCAAGAGAGTCAATGAGGAG	CCGGTTCCATAGGCAAACT	60	Støy et al., 2013

SLC2A2	Glucose transporter 2 (GLUT2)	NM_001097417	ACGCAACCATTGGAGTTGGC	AGCACAAGTCCCACCGACAT	60	This study
SLC27A4	Fatty acid transport protein 4 (FATP4)	XM_021069609.1	GCTGCATAAAACAGGGACTTTCA	AACAGCGGGTCTTTCACGACT	60	Revilla et al., 2018
CD36	Cluster of differentiation 36 (CD36/FAT)	NM_001044622.1	GGTCCTTACACGTACAGAGTTCGTT	CCATTGGGCTGTAGGAAAGAGA	60	Revilla et al., 2018
SLC15A1	Peptide transporter 1 (PEPT1)	NM_214347.1	GGCTTCCATGGCTTTCGTGG	TCAAGGGTCACCGTCGTTCC	60	This study
SLC6A20	IMINO	XM_021068640.1	TCGTGTCCCTCATCAACAG	AGGAAGCCATCTTCAAGGTC	60	This study
SLC6A19	Neutral amino acid transporter B0AT1 (B0AT1)	XM_003359855.4	CTTTCATCTTCACCCTGAACTC	GATGTCGCTGTTGAACCTG	60	This study
SLC3A1	Related to b0,+ amino acid transporter (rBAT)	NM_001123042.1	CAATGCAGTGGGACAACAG	GGCGTGAAGCAAACTTAATTC	60	This study
SLC6A14	Amino acid transporter B0,+ (ATB^{0},+)	NM_001348402.1	CTGTGGCTTGGGGTGGTTTA	AACCAAGCAGCAACCCAAAG	60	This study
SLC1A5	Alanine–serine–cysteine transporter 2 (ASCT2)	NM_001444293.1	CGATTCGTTCCTGGA TCTTG	TAGGACGTCGCGTATGAG	60	This study
SLC7A8	L-type amino acid transporter 2 (LAT2)	XM_021099239.1	ACTACCTCTTCTATGGCATCAC	GCAAGTAGATGATGGGGAACAG	60	This study
SLC7A7	y^{+}L amino acid transporter 1 (y^{+}LAT1)	NM_001110421	CTCTGCTGTTCAATGGTCTC	ATAGAGCTGACCCACGATAG	60	This study
SLC43A2	L-type amino acid transporter 4 (LAT4)	XM_021067563.1	CAGATCCAGAAGATCACCAAC	TGAAGGAGAGAATCTGTAGGG	60	This study

Supplementary Table 5.2 Free amino acid concentrations in dairy infant formula (IF) digesta. Free amino acid (AA) concentrations (mean and SEM, nmol/mL) in dairy IF digesta inactivated by either heat (HI) or by enzymatic inhibition using Pefabloc and Orlistat (P+O). Samples were analyzed in triplicate independent digestions (two technical replicates each).

Amino acid	**Digesta - Dairy IF (HI)**		**Digesta - Dairy IF (P+O)**	
	Mean (nmol/mL)	**SEM**	**Mean (nmol/1.5 mL)**	**SEM**
Val	999.27	55.74	1191.16	96.63
Ile	463.19	48.23	611.22	78.03
Leu	1955.019	146.03	2407.35	268.79
Thr	899.09	150.13	1222.05	264.29
Met	374.20	51.10	466.43	75.565
Phe	2001.63	204.49	1988.09	141.82
His	1051.41	131.05	1079.07	84.7
Lys	2506.28	107.25	2659.74	62.07
Arg	982.51	84.04	1063.41	50.95
Asp	196.51	8.23	237.89	24.58
Ser	541.85	97.43	738.73	174.07
Glu	672.19	50.44	889.58	132.39
Gly	1087.77	58.08	1101.29	41.20
Ala	631.57	121.63	851.25	191.98
Tyr	1245.85	80.81	1293.38	12.08
Cys	290.39	4.97	321.15	8.65
Cya	310.57	47.13	276.36	30.36
Tau	557.94	69.18	518.70	16.98

Supplementary Table 5.3 Free amino acid concentrations in the basolateral chamber of IPEC-J2 monolayers exposed to dairy IF digesta.

Basolateral free amino acid (AA) concentrations (mean ± SEM, nmol/mL) in IPEC-J2 monolayers cultured for 14 days in either PS10 or PS5 + EGF + ITS medium and exposed for 2 h to dairy IF digesta inactivated by heat (HI; 200 µg protein/cm²) or enzymatic inhibition (P+O; 150 µg protein/cm²). Data = 3 independent experiments (n=6).

Amino acid	**PS10 – Diary IF (HI)**		**PS5+EGF+ITS – Diary IF (HI)**		**PS10 – Diary IF (P+O)**		**PS5+EGF+ITS – Diary IF (P+O)**	
	Mean (nmol/mL)	**SEM**	**Mean (nmol/mL)**	**SEM**	**Mean (nmol/mL)**	**SEM**	**Mean (nmol/mL)**	**SEM**
Val	9.63	0.98	7.90	2.00	10.02	0.39	6.59	1.04
Ile	5.79	0.51	4.55	1.54	6.28	0.21	4.02	0.96
Leu	10.68	2.17	8.22	3.41	12.49	1.43	6.21	1.86
Thr	13.62	1.70	10.43	2.61	13.91	0.91	9.87	1.46
Met	2.19	0.26	1.67	0.64	2.42	0.20	1.40	0.32
Phe	8.64	2.38	6.83	1.77	8.63	1.54	4.25	0.96
His	5.36	1.27	3.70	1.04	5.07	0.60	2.99	0.41
Lys	10.51	3.07	10.14	3.19	11.71	1.43	7.47	1.38
Arg	10.80	1.01	7.57	2.14	9.37	0.35	5.97	1.19
Asp	0.73	0.10	0.87	0.19	0.97	0.10	0.70	0.07
Ser	5.68	0.46	4.77	1.22	6.30	0.14	4.22	0.76
Glu	4.93	0.48	4.21	1.38	5.69	0.31	3.86	0.37
Gly	7.78	1.06	5.97	1.16	7.71	0.65	4.90	0.63
Ala	3.42	0.42	3.99	1.39	5.67	1.08	3.24	0.89
Tyr	5.73	1.13	4.17	1.61	5.72	1.00	2.71	0.83
Cys	3.56	0.58	3.26	0.30	3.65	0.44	2.95	0.26
Cya	2.21	0.68	1.91	0.10	2.24	0.28	1.47	0.21

6. Chapter 6

General discussion

6.1.General discussion

The overall objective of this thesis was to develop and validate *in vitro* models that better reflect the physiological characteristics of the infant gut barrier and to apply these models to evaluate digestion, peptide transport and gut barrier modulation by human milk and IF. Chapter 1 comprehensively reviewed the differences between the newborn intestinal barrier and the adult's, highlighting the markedly higher paracellular permeability of the infant gut. Chapter 2 explored NaB as a potential means to induce a "leaky" phenotype in epithelial monolayers. Given its activation of apoptotic and inflammatory pathways and the absence of recovery, it was deemed unsuitable for use as an infant model. Chapter 3 then identified GDC as a non-toxic, reversible agent capable of transiently reproducing the increased permeability typical of early infancy. In Chapter 4, these optimized infant-like monolayers were used to investigate the comparative effects of gastrointestinal digested human milk and different IF formulations on tight junctions and peptide transport. Finally, Chapter 5 characterized the porcine intestinal epithelial cell line IPEC-J2 as a physiologically relevant, non-transformed model as an alternative to Caco-2/HT29-MTX.

Together, these studies demonstrated that (i) NaB induces a "leaky," inflammation-associated phenotype useful for disease modelling; (ii) GDC induces a reversible, non-inflammatory increase in paracellular permeability resembling the neonatal state; (iii) human milk uniquely triggers OCLN redistribution and higher peptide delivery in the infant-like barrier; and (iv) IPEC-J2 cultured in porcine serum provides a robust, species-specific model to study nutrient absorption from IF.

The intestinal barrier of infants differs profoundly from that of adults. Early-life permeability is physiologically high, allowing passive transfer of bioactive macromolecules that support immune and tissue maturation (Catassi et al., 1995). Permeability, measured by the urinary L:M ratio, decreases by about 50 % between 3 and 15 months (Kosek et al., 2017), reflecting gradual barrier closure. This developmental process is characterized by reduced expression of certain tight junction proteins (e.g., OCLN, ZO1) and junctional adhesion molecules, alongside increased levels of CLDN (Gleeson et al., 2021; Holmes et al., 2006). The mucus layer is thinner, less viscous, and dominated by acidic mucins, while in adults it becomes denser and more sialylated (Johansson et al., 2025; Macierzanka et al., 2014). Neonatal enterocytes also exhibit greater membrane fluidity, which declines with increasing cholesterol and saturated lipids (Lindner et al., 1987; Meddings and Theisen, 1989).

Digestive and transport capacities mature postnatally. Lactase and peptidase activities are high at birth, whereas sucrase, maltase, and lipase rise later during weaning (Auricchio et al., 1981; Meddings and Theisen, 1989). Nutrient transporters PEPT1 and SGLT1 are active from birth, supporting peptide and glucose uptake, while GLUT5-mediated fructose absorption increases only after weaning (Miyamoto et al., 1996; Shu et al., 1997).

However, widely used intestinal cell models, such as Caco-2 and Caco-2/HT29-MTX co-cultures, reproduce the structural and functional properties of the *adult* small intestine rather than the infant gut. These monolayers develop high transepithelial electrical resistance (typically 800–4000 $\Omega \times cm^2$) and low paracellular permeability, reflecting the tight junction morphology of mature

enterocytes (Hubatsch et al., 2007; Kleiveland, 2015). To advance our understanding of how early nutrition influences epithelial development, there is a critical need for improved, age-appropriate *in vitro* models that capture the transiently permeable, non-inflammatory phenotype of the infant gut. Such models would provide a reliable yet accessible platform for evaluating how dietary components—particularly human milk and emerging infant formula formulations—affect gut barrier maturation, nutrient uptake, and protection against inflammation. Ultimately, these systems could guide the design of next-generation IFs that more effectively mimic the biological functions of human milk and support healthy intestinal development in early life.

Human milk is the gold standard of human infant nutrition, offering not only complete nourishment but also bioactive compounds that support growth, immune protection, and the functional maturation of the infant intestine (Ballard and Morrow, 2013). Within the intestinal tract, human milk strengthens epithelial integrity reduces paracellular permeability, promotes mucosal network maturation (Catassi et al., 1995). Human milk contains lipids, oligosaccharides, immunoglobulins, and proteins such as α-lactalbumin, lactoferrin, and caseins, which release bioactive peptides that modulate immune and epithelial signalling (Dold et al., 2025; Korhonen and Pihlanto, 2006). Peptides and amino acids derived from human milk have been detected in infant plasma (Biondi Ryan et al., 2025), demonstrating systemic absorption. These properties explain the lower intestinal permeability and reduced necrotizing enterocolitis (NEC) risk observed in breastfed compared with formula-fed infants (Colaizy et al., 2016; Lucas and Cole, 1990).

The World Health Organization recommends exclusive breastfeeding for the first six months of life (World Health Organization., 2014). However, when breastfeeding is not possible, IFs serves as an alternative or supplement (Blum, 1999). Dairy-based IFs are the most widely used, whereas soya-based IFs provide a plant-derived option, and highly hydrolysed or amino acid (AA)-based IFs are designed for infants with protein allergies or gastrointestinal disorders (Martin et al., 2016). IFs are produced under strict safety and nutritional regulations. The Codex Alimentarius (Codex Alimentarius Commission., 1981) establishes global standards for composition and IFs are strictly regulated for composition and safety (Codex Alimentarius Commission., 1981; European Commission, 2016). However, during digestion peptide release and profile differ substantially between human milk and IF (Komatsu et al., 2024). Human milk generates shorter, functionally diverse peptides—many with antioxidant, ACE-inhibitory, or barrier-protective activity—whereas dairy and soya IFs yield a less diverse set with limited bioactivity (Dold et al., 2025; Hernández-Ledesma et al., 2007).

Consequently, IFs only partially reproduce the biological effects of human milk on epithelial maturation, leaving formula-fed infants with a more permeable barrier (Catassi et al., 1995) and higher NEC risk (Weström et al., 2020).

Building upon previous work in our laboratory that identified NaB, a short-chain fatty acid, as a potential modulator of epithelial permeability (Kondrashina et al., 2023), Chapter 2 further examined its mechanism of action and suitability for developing an infant-like intestinal barrier model. NaB decreased TEER and increased paracellular permeability in a dose-dependent manner (50–125 mM). It was transported via MCT-1/SMCT-1 but did not act as an energy substrate.

Intracellular accumulation confirmed its role as an epigenetic regulator (Dalile et al., 2019; Donohoe et al., 2012; Singh et al., 2023). NaB induced caspase-3 activation, upregulated stress markers (p21, HSP70), and increased the secretion of inflammatory cytokines (IL6, IL8, TNF) (Adesina et al., 2023; Ruemmele, 2003). At 75 mM, NaB produced a reversible, steroid-responsive inflamed “leaky” barrier. Moreover, the hyperosmolarity associated with NaB mimicks conditions reported in intestinal inflammatory states, where luminal hyperosmotic stress contributes to epithelial injury and cytokine activation (Ruemmele, 2003). Collectively, these findings suggest that 75 mM NaB treatment models an inflamed intestinal phenotype resembling the epithelial dysfunction observed in necrotizing enterocolitis (NEC) or early inflammatory bowel disease Thus, NaB provides a model for studying inflammation-induced leakiness and therapeutic interventions.

In Chapter 3, GDC, a conjugated bile salt, was evaluated as a physiological modulator of paracellular permeability. GDC was selected because bile salts have been shown to increase paracellular permeability *in vitro*, *ex vivo*, and *in vivo* (Brayden and Stuettgen, 2021; Fricker et al., 1996; Hoogstraate et al., 1996b; Meaney and O’Driscoll, 2000; Song et al., 2005), whilst also acting as mild surfactants that enhance membrane fluidity (Hofmann and Hagey, 2008)—both features of the infant gut (Lindner et al., 1987; Meddings and Theisen, 1989). In Caco-2/HT29-MTX co-cultures, 0.8 mM GDC reduced TEER by 2.7-fold and increased lactulose flux 1.6-fold without cytotoxicity or inflammation. Removal of GDC allowed monolayers to recover, as demonstrated by TEER, within four hours. GDC decreased junctional OCLN, upregulated CLDN2/CLDN4, and increased acidic mucins and alkaline phosphatase activity. Reduced intracellular cAMP

suggested GPCR involvement, likely TGR5 signalling (Pierce et al., 2002). These responses closely reflect neonatal intestinal features, including lower occludin and higher CLDN2 expression (Gleeson et al., 2021; Holmes et al., 2006), developmental re-localization of CLDN4 to junctional sites (Pasternak et al., 2015), predominance of acidic mucins in early life (Macierzanka et al., 2014; Turck et al., 1993), and elevated neonatal alkaline phosphatase activity (Adeola and King, 2006; Hernández-Jodra and Gancedo, 1971).

This transient and recoverable "open" state is particularly relevant for studying how nutritional factors contribute to the postnatal sealing of the gut barrier—an adaptive process promoted by human milk *in vivo* (Ballard and Morrow, 2013; Catassi et al., 1995).

Chapter 4 applied the GDC-treated Caco-2/HT29-MTX monolayers to food experiments (human milk and different IF formulations). Initially human milk, dairy, soya and AA IF were subjected to INFOGEST gastrointestinal digestion, adapted to the infant gut (Ménard et al., 2018). The study showed that human milk uniquely enhanced gut barrier OCLN–actin co-localization and increased basolateral transport of peptides across this infant-like barrier, compared with all IFs. Similar junctional remodelling was observed in human fetal enteroids treated with human milk (Noel et al., 2021). The elevated transport of bioactive peptides in our infant-like model is consistent with *in vivo* detection of milk-derived peptides in breastfed infants, (Biondi Ryan et al., 2025). This reflects the greater intestinal permeability to bioactive compounds that characterizes early life (Ballard and Morrow, 2013). The higher number of apical peptides observed in the infant-like monolayers likely reflects efficient brush-border hydrolysis of milk proteins, consistent with early high

peptidase activity (Auricchio et al., 1981). Collectively, human milk induced a maturation-like effect marked by OCLN redistribution, while the model retained infant characteristics such as high brush-border enzyme activity and enhanced peptide transport.

Chapter 5 extended the work to the porcine IPEC-J2 cell line, one of the few non-transformed small-intestinal epithelial cell lines derived from neonatal gut (Schierack et al., 2006; Vergauwen, 2015). Unlike fetal cell lines HIEC and FHs 74 Int, which show poor polarization, low TEER (<100 Ω × cm²), and lack brush-border enzymes and mature junctions (Beaulieu and Quaroni, 1991; Perreault and Beaulieu, 1996; Zhang et al., 1997), IPEC-J2 forms polarized monolayers with organized ZO1/OCLN, moderate to high TEER (200–4000 Ω × cm²), active ALP and aminopeptidase N, and nutrient transporters PEPT1 and SGLT1 (Brosnahan and Brown, 2012; Vergauwen, 2015). As the neonatal piglet is the gold-standard preclinical model for IF testing (Sangild et al., 2014; Weström et al., 2020), screening nutritional effects in IPEC-J2 offers a rational *in vitro* step before piglet trials. Despite their potential, IPEC-J2 cells are cultured under widely variable conditions, leading to large differences in reported barrier properties. In the literature, TEER values range from <200 Ω×cm² to >4000 Ω×cm², depending on serum concentration, passage number, and differentiation medium (Brosnahan and Brown, 2012; Geens and Niewold, 2011; Vergauwen, 2015). This variability limits reproducibility and comparability across studies.

To address this, four culture media were systematically evaluated and demonstrated that supplementation with 10 % porcine serum (PS10) yielded stable TEER (~2400 Ω × cm²), low paracellular flux, strong ZO1 localization, and reduced S100A4

expression. Exposure to digested IF increased TEER and basolateral amino acid transport, confirming barrier responsiveness. This study also pioneered exposure of IPEC-J2 monolayers to digested foods, showing that physiologically digested IF modulates barrier and transport in a non-transformed, species-relevant system.

In conclusion, the NaB study clarified the mode of action of this short-chain fatty acid in inducing a “leaky” barrier model, emphasizing the importance of osmotic control and the distinction between physiological and pathological permeability. The GDC study introduced a novel, reversible method to generate a physiologically relevant permeable barrier that emulates the transient, non-inflammatory permeability characteristic of the neonatal intestine. Application of this model revealed the unique effects of human milk on tight-junction organization and peptide absorption, which were not captured in conventional adult-like monolayers. The IPEC-J2 study validated a species-specific, non-transformed model for investigating digestion and amino acid transport, confirming its suitability for comparative infant nutrition research.

Collectively, these models embody the infant intestinal barrier differences from the adult in structure, permeability, and responsiveness to nutrition. The results highlight the need for age-specific *in vitro* systems to capture the unique benefits of human milk compared with IFs

Despite these advances, some physiological traits of the infant gut remain unaccounted for in our models. Defining the physiological “infant gut” remains challenging. The only *in vivo* human data available come from L:M tests measuring overall permeability, whereas detailed information on tight junction composition,

mucus characteristics, membrane properties, transporter expression, and brush-border enzyme activity derives mainly from animal studies. This knowledge gap limits the precision with which *in vitro* models can replicate early-life intestinal physiology.

In the context of these broader uncertainties, several model-specific methodological limitations must be acknowledged. The transcellular transport pathway was not examined; therefore, the increased amino acid and peptide flux we observed after exposure to the digested foods cannot be attributed solely to tight junction opening or enhanced transporter activity. Membrane fluidity, which is higher in infants and contributes to epithelial permeability (Meddings and Theisen, 1989), was also not evaluated. Although GDC increased acidic mucins, the rheological and permeability properties of the mucus layer were not characterized, even though infant mucus is typically thinner and more permeable (Macierzanka et al., 2014). In addition, nutrient metabolism could not be evaluated, as Caco-2/HT29-MTX cells are cancer-derived and rely mainly on glycolysis rather than the mixed oxidative–glycolytic metabolism typical of enterocytes. In contrast, IPEC-J2 cells possess both oxidative and glycolytic capacity but are non-human and develop high TEER, limiting their translational relevance.

To address these gaps, future research should define the molecular mechanism of GDC more precisely by testing TGR5/FXR involvement and downstream cAMP/PKA–ERK/EGFR signalling. Functional validation should confirm that the infant-like state extends beyond permeability by including assays for brush-border enzyme activities (lactase, sucrase–isomaltase, aminopeptidase N, intestinal ALP), transporter function (PEPT1, SGLT1, GLUT2/5, LAT systems), and membrane fluidity. Future work should also include a detailed characterization of mucus

properties, combining rheological and permeability assays. Physiological relevance could be enhanced by incorporating immune co-cultures (e.g., Raji B–induced M cells or macrophages) and a microbiota component, and by benchmarking results against infant intestinal organoids. These additions would also allow investigation of immune priming by human milk and enable direct comparison with IFs.
Moreover, this study focused primarily on milk proteins and peptides, but future work should also investigate the transport and functional effects of other nutrients and bioactives present in human milk, including human milk oligosaccharides (HMOs), lipids and milk fat globule membrane (MFGM) components, extracellular vesicles, hormones, immunoglobulins, and micronutrients. These compounds contribute collectively to immune protection, microbial colonization, and epithelial maturation (Andreas et al., 2015; Ballard and Morrow, 2013; Bode, 2012). Finally, linking *in vitro* findings with clinical data from feeding studies and circulating biomarkers (e.g., plasma milk peptides) will determine whether formulae designed using these models truly support gut maturation, immune resilience, and metabolic development comparable to human milk-fed infants. (Andreas et al., 2015; Ballard and Morrow, 2013; Bode, 2012). Finally, linking *in vitro* findings with clinical data from feeding studies and circulating biomarkers (e.g., plasma milk peptides) will determine whether formulae designed using these models truly support gut maturation, immune resilience, and metabolic development comparable to human milk-fed infants.

In conclusion, this thesis provides a cohesive experimental and conceptual framework for studying the infant intestinal barrier. By developing reversible, physiologically relevant, and non-inflammatory models, it bridges a key

methodological gap between *in vitro* experimentation and early-life physiology. The insights gained lay the foundation for the rational design of next-IFs that more closely reproduce the protective and developmental benefits of human milk.

6.2. References

Adeola, O., King, D.E., 2006. Developmental changes in morphometry of the small intestine and jejunal sucrase activity during the first nine weeks of postnatal growth in pigs1. Journal of Animal Science 84, 112–118. https://doi.org/10.2527/2006.841112x

Adesina, P.A., Saeki, I., Yamamoto, Y., Suzuki, T., 2023. N-butyrate increases heat shock protein 70 through heat shock factor 1 and AMP-activated protein kinase pathways in human intestinal Caco-2 cells. Archives of Biochemistry and Biophysics 736, 109525. https://doi.org/10.1016/j.abb.2023.109525

Andreas, N.J., Kampmann, B., Mehring Le-Doare, K., 2015. Human breast milk: A review on its composition and bioactivity. Early Human Development 91, 629–635. https://doi.org/10.1016/j.earlhumdev.2015.08.013

Auricchio, S., Stellato, A., Vizia, B.D., 1981. Development of Brush Border Peptidases in Human and Rat Small Intestine during Fetal and Neonatal Life. Pediatr Res 15, 991–995. https://doi.org/10.1203/00006450-198107000-00003

Ballard, O., Morrow, A.L., 2013. Human Milk Composition. Pediatric Clinics of North America 60, 49–74. https://doi.org/10.1016/j.pcl.2012.10.002

Beaulieu, J.F., Quaroni, A., 1991. Clonal analysis of sucrase-isomaltase expression in the human colon adenocarcinoma Caco-2 cells. Biochemical Journal 280, 599–608. https://doi.org/10.1042/bj2800599

Biondi Ryan, M.R., Zukaitis, J., Sutantawong, S., Dallas, D.C., 2025. Overall Evidence for Milk-Derived Proteins and Peptides in Blood after Digestion: A Systematic Review. Nutrition Reviews nuaf118. https://doi.org/10.1093/nutrit/nuaf118

Blum, L.M., 1999. At the Breast: Ideologies of Breastfeeding and Motherhood in the Contemporary United States. Beacon Press.

Bode, L., 2012. Human milk oligosaccharides: Every baby needs a sugar mama. Glycobiology 22, 1147–1162. https://doi.org/10.1093/glycob/cws074

Brayden, D.J., Stuettgen, V., 2021. Sodium glycodeoxycholate and sodium deoxycholate as epithelial permeation enhancers: in vitro and ex vivo intestinal and buccal bioassays. European Journal of Pharmaceutical Sciences 12.

Brosnahan, A.J., Brown, D.R., 2012. Porcine IPEC-J2 intestinal epithelial cells in microbiological investigations. Veterinary Microbiology 156, 229–237. https://doi.org/10.1016/j.vetmic.2011.10.017

Castelló, A., Gumá, A., Sevilla, L., Furriols, M., Testar, X., Palacín, M., Zorzano, A., 1995. Regulation of GLUT5 gene expression in rat intestinal mucosa: regional distribution, circadian rhythm, perinatal development and effect of diabetes. Biochem J 309, 271–277.

Catassi, C., Bonucci, A., Coppa, G.V., Carlucci, A., Giorgi, P.L., 1995. Intestinal Permeability. Changes during the First Month: Effect of Natural versus Artificial Feeding. Journal of Pediatric Gastroenterology and Nutrition 21, 383–386. https://doi.org/10.1097/00005176-199511000-00003

Codex Alimentarius Commission., 1981. Codex Alimentarius Commission. Standard for Infant Formula and Formulas for Special Medical Purposes Intended for Infants (CXS 72-1981). Rome: FAO/WHO; Revised 2023.

Colaizy, T.T., Bartick, M.C., Jegier, B.J., Green, B.D., Reinhold, A.G., Schaefer, A.J., Bogen, D.L., Schwarz, E.B., Stuebe, A.M., Jobe, A.H., Oh, W., Vohr, B.R., Walden, R.V., Alksninis, B., Hensman, A.M., Leonard, M.R., Noel, L.,

Leach, T.M., Watson, V.E., Fanaroff, A.A., Walsh, M.C., Wilson-Costello, D.E., Newman, N.S., Siner, B.S., Friedman, H.G., Donovan, E.F., Schibler, K., Steichen, J.J., Alexander, B., Grisby, C., Mersmann, M.W., Mincey, H.L., Hessling, J., Gratton, T.L., Stoll, B.J., Adams-Chapman, I., Hale, E.C., LaRossa, M.M., Carter, S., Higgins, R.D., Wright, L.L., McClure, E.M., Poindexter, B.B., Lemons, J.A., Dusick, A.M., Kardatzke, D., Lytle, C., Appel, D.D., Bohnke, L.G., Eaken, G., Herron, D.E., Miller, L.C., Richard, L., Wilson, L.D., Das, A., Poole, W.K., Wrage, L.A., Hastings, B.K., McClure, E.M., O'Donnell Auman, J., Taylor, S., Stevenson, D.K., Hintz, S.R., Ball, M.B., Kohn, J.G., Baran, J.M., Lee-Ancajas, J.C., St. John, N.H., Carlo, W.A., Ambalavanan, N., Nelson, K.G., Peralta-Carcelen, M., Bailey, K.J., Biasini, F.J., Chopko, S.A., Collins, M.V., Cosby, S.S., Phillips, V.A., Rector, R.V., Finer, N.N., Vaucher, Y.E., Anderson, J.M., Rasmussen, M.R., Arnell, K., Demetrio, C., Fuller, M.G., Henderson, C., Posin, D., Bell, E.F., Colaizy, T.T., Bauer, C.R., Duara, S., Worth, A.M., Everett-Thomas, R., Diaz, A.N., Mathews, E.O., Hamlin-Smith, K., Jean-Gilles, L., Calejo, M., Frade, S.M., Hiriart-Fajardo, S., Gideon, Y., Korones, S.B., Bada, H.S., Hudson, T., Yolton, K., Williams, M.G., Laptook, A.R., Salhab, W.A., Broyles, R.S., Madison, S., Hickman, J.F., Guzman, A., Adams, S.S., Madden, L.A., Heyne, E.T., Dooley, C., Shankaran, S., Delaney-Black, V., Johnson, Y.R., Bara, R., Muran, G., Kennedy, D., Goldston, L.A., Ehrenkranz, R.A., Gettner, P., Konstantino, M., Romano, E., Close, N., Gilliam, W.S., Poulsen, J., 2016. Impact of Optimized Breastfeeding on the Costs of Necrotizing Enterocolitis in Extremely Low Birthweight Infants.

The Journal of Pediatrics 175, 100-105.e2. https://doi.org/10.1016/j.jpeds.2016.03.040

Dalile, B., Van Oudenhove, L., Vervliet, B., Verbeke, K., 2019. The role of short-chain fatty acids in microbiota–gut–brain communication. Nat Rev Gastroenterol Hepatol 16, 461–478. https://doi.org/10.1038/s41575-019-0157-3

Dold, C.A., Sahin, A.W., Lawlor, P.G., Hickey, R.M., Giblin, L., 2025. Employing membrane filtration technology during infant milk formula processing, will improve intestinal barrier function in vitro. International Dairy Journal 167, 106283. https://doi.org/10.1016/j.idairyj.2025.106283

Donohoe, D.R., Collins, L.B., Wali, A., Bigler, R., Sun, W., Bultman, S.J., 2012. The Warburg Effect Dictates the Mechanism of Butyrate-Mediated Histone Acetylation and Cell Proliferation. Molecular Cell 48, 612–626. https://doi.org/10.1016/j.molcel.2012.08.033

European Commission, 2016. Commission Delegated Regulation (EU) 2016/127 of 25 September 2015 supplementing Regulation (EU) No 609/2013 as regards the specific compositional and information requirements for infant formula and follow-on formula.

Fricker, G., Fahr, A., Beglinger, C., Kissel, T., Reiter, G., Drewe, J., 1996. Permeation enhancement of octreotide by specific bile salts in rats and human subjects: in vitro, in vivo correlations. British J Pharmacology 117, 217–223. https://doi.org/10.1111/j.1476-5381.1996.tb15177.x

Geens, M.M., Niewold, T.A., 2011. Optimizing culture conditions of a porcine epithelial cell line IPEC-J2 through a histological and physiological

characterization. Cytotechnology 63, 415–423. https://doi.org/10.1007/s10616-011-9362-9

Gleeson, J.P., Fein, K.C., Chaudhary, N., Doerfler, R., Newby, A.N., Whitehead, K.A., 2021. The enhanced intestinal permeability of infant mice enables oral protein and macromolecular absorption without delivery technology. International Journal of Pharmaceutics 593, 120120. https://doi.org/10.1016/j.ijpharm.2020.120120

Hernández-Jodra, M., Gancedo, C., 1971. Isoenzymes of Alkaline Phosphatase in Human Meconium and Small Intestine during Development. EZD 12, 682–687. https://doi.org/10.1159/000459603

Hernández-Ledesma, B., Quirós, A., Amigo, L., Recio, I., 2007. Identification of bioactive peptides after digestion of human milk and infant formula with pepsin and pancreatin. International Dairy Journal 17, 42–49. https://doi.org/10.1016/j.idairyj.2005.12.012

Hofmann, A.F., Hagey, L.R., 2008. Bile Acids: Chemistry, Pathochemistry, Biology, Pathobiology, and Therapeutics. Cell. Mol. Life Sci. 65, 2461–2483. https://doi.org/10.1007/s00018-008-7568-6

Holmes, J.L., Van Itallie, C.M., Rasmussen, J.E., Anderson, J.M., 2006. Claudin profiling in the mouse during postnatal intestinal development and along the gastrointestinal tract reveals complex expression patterns. Gene Expression Patterns 6, 581–588. https://doi.org/10.1016/j.modgep.2005.12.001

Hoogstraate, A.J., Verhoef, J.C., Tuk, B., Pijpers, A., Van Leengoed, L.A.M.G., Verheijden, J.H.M., Junginger, H.E., Boddé, H.E., 1996. In-vivo Buccal Delivery of Fluorescein Isothiocyanate–Dextran 4400 with

Glycodeoxycholate as an Absorption Enhancer in Pigs. Journal of Pharmaceutical Sciences 85, 457–460. https://doi.org/10.1021/js950129k

Hubatsch, I., Ragnarsson, E.G.E., Artursson, P., 2007. Determination of drug permeability and prediction of drug absorption in Caco-2 monolayers. Nat Protoc 2, 2111–2119. https://doi.org/10.1038/nprot.2007.303

Johansson, Å., Venkita Subramani, M., Yilmaz, B., Nyström, E.E.L., Layunta, E., Arike, L., Sommer, F., Rosenstiel, P., Vereecke, L., Mannerås-Holm, L., Wullaert, A., Pelaseyed, T., Johansson, M.E.V., Birchenough, G.M.H., 2025. Neonatal microbiota colonization primes maturation of goblet cell–mediated protection in the pre-weaning colon. Journal of Experimental Medicine 222, e20241591. https://doi.org/10.1084/jem.20241591

Kleiveland, C.R., 2015. Co-cultivation of Caco-2 and HT-29MTX. The impact of food bioactives on health 135–140.

Komatsu, Y., Wada, Y., Shibasaki, T., Kitamura, Y., Ehara, T., Nakamura, H., Miyaji, K., 2024. Comparison of protein digestibility of human milk and infant formula using the INFOGEST method under infant digestion conditions. Br J Nutr 132, 351–358. https://doi.org/10.1017/S0007114524001260

Kondrashina, A., Arranz, E., Cilla, A., Faria, M.A., Santos-Hernández, M., Miralles, B., Hashemi, N., Rasmussen, M.K., Young, J.F., Barberá, R., Mamone, G., Tomás-Cobos, L., Bastiaan-Net, S., Corredig, M., Giblin, L., 2023. Coupling in vitro food digestion with in vitro epithelial absorption; recommendations for biocompatibility. Critical Reviews in Food Science and Nutrition 1–19. https://doi.org/10.1080/10408398.2023.2214628

Korhonen, H., Pihlanto, A., 2006. Bioactive peptides: Production and functionality. International Dairy Journal 16, 945–960. https://doi.org/10.1016/j.idairyj.2005.10.012

Kosek, M.N., Lee, G.O., Guerrant, R.L., Haque, R., Kang, G., Ahmed, T., Bessong, P., Ali, A., Mduma, E., Peñataro Yori, P., Faubion, W.A., Lima, A.A.M., Paredes Olortegui, M., Mason, C., Babji, S., Singh, R., Qureshi, S., Kosek, P.S., Samie, A., Pascal, J., Shrestha, S., McCormick, B.J.J., Seidman, J.C., Lang, D.R., Zaidi, A., Caulfield, L.E., Gottlieb, M., Network, the M.-E., 2017. Age and Sex Normalization of Intestinal Permeability Measures for the Improved Assessment of Enteropathy in Infancy and Early Childhood: Results From the MAL-ED Study. Journal of Pediatric Gastroenterology and Nutrition 65, 31–39. https://doi.org/10.1097/MPG.0000000000001610

Lebenthal, E., Lee, P.C., 1980. Glucoamylase and disaccharidase activities in normal subjects and in patients with mucosal injury of the small intestine. The Journal of Pediatrics 97, 389–393. https://doi.org/10.1016/S0022-3476(80)80187-9

Lindner, S.G., Hübner, C., Stern, M., Kohlschütter, A., 1987. LIPID AND FATTY ACID COMPOSITION OF RAT INTESTINAL BRUSH BORDER MEMBRANES (BBM) DURING MATURATION: THE BIOCHEMICAL CORRELATE TO CHANGES IN MEMBRANE FLUIDITY. Pediatr Res 22, 235–235. https://doi.org/10.1203/00006450-198708000-00132

Lucas, A., Cole, T.J., 1990. Breast milk and neonatal necrotising enterocolitis. The Lancet 336, 1519–1523. https://doi.org/10.1016/0140-6736(90)93304-8

Macierzanka, A., Mackie, A.R., Bajka, B.H., Rigby, N.M., Nau, F., Dupont, D., 2014. Transport of Particles in Intestinal Mucus under Simulated Infant and

Adult Physiological Conditions: Impact of Mucus Structure and Extracellular DNA. PLOS ONE 9, e95274. https://doi.org/10.1371/journal.pone.0095274

Manners, M.J., Stevens, J.A., 1972. Changes from birth to maturity in the pattern of distribution of lactase and sucrase activity in the mucosa of the small intestine of pigs. Br J Nutr 28, 113–127. https://doi.org/10.1079/BJN19720014

Martin, C., Ling, P.-R., Blackburn, G., 2016. Review of Infant Feeding: Key Features of Breast Milk and Infant Formula. Nutrients 8, 279. https://doi.org/10.3390/nu8050279

Meaney, C.M., O'Driscoll, C.M., 2000. A comparison of the permeation enhancement potential of simple bile salt and mixed bile salt:fatty acid micellar systems using the CaCo-2 cell culture model. International Journal of Pharmaceutics 207, 21–30. https://doi.org/10.1016/S0378-5173(00)00526-3

Meddings, J.B., Theisen, S., 1989. Development of rat jejunum: lipid permeability, physical properties, and chemical composition. American Journal of Physiology-Gastrointestinal and Liver Physiology 256, G931–G940. https://doi.org/10.1152/ajpgi.1989.256.5.G931

Ménard, O., Bourlieu, C., De Oliveira, S.C., Dellarosa, N., Laghi, L., Carrière, F., Capozzi, F., Dupont, D., Deglaire, A., 2018. A first step towards a consensus static in vitro model for simulating full-term infant digestion. Food Chemistry 240, 338–345. https://doi.org/10.1016/j.foodchem.2017.07.145

Miyamoto, K., Shiraga, T., Morita, K., Yamamoto, H., Haga, H., Taketani, Y., Tamai, I., Sai, Y., Tsuji, A., Takeda, E., 1996. Sequence, tissue distribution and developmental changes in rat intestinal oligopeptide transporter.

Biochimica et Biophysica Acta (BBA) - Gene Structure and Expression 1305, 34–38. https://doi.org/10.1016/0167-4781(95)00208-1

Mooij, M.G., Schwarz, U.I., Koning, B.A.E. de, Leeder, J.S., Gaedigk, R., Samsom, J.N., Spaans, E., Goudoever, J.B. van, Tibboel, D., Kim, R.B., Wildt, S.N. de, 2014. Ontogeny of Human Hepatic and Intestinal Transporter Gene Expression during Childhood: Age Matters. Drug Metab Dispos 42, 1268–1274. https://doi.org/10.1124/dmd.114.056929

Noel, G., In, J.G., Lemme-Dumit, J.M., DeVine, L.R., Cole, R.N., Guerrerio, A.L., Campbell, J.D., Kovbasnjuk, O., Pasetti, M.F., 2021. Human Breast Milk Enhances Intestinal Mucosal Barrier Function and Innate Immunity in a Healthy Pediatric Human Enteroid Model. Front. Cell Dev. Biol. 9, 685171. https://doi.org/10.3389/fcell.2021.685171

Pasternak, J.A., Kent-Dennis, C., Van Kessel, A.G., Wilson, H.L., 2015. Claudin-4 Undergoes Age-Dependent Change in Cellular Localization on Pig Jejunal Villous Epithelial Cells, Independent of Bacterial Colonization. Mediators of Inflammation 2015, 263629. https://doi.org/10.1155/2015/263629

Perreault, N., Beaulieu, J.-F., 1996. Use of the Dissociating Enzyme Thermolysin to Generate Viable Human Normal Intestinal Epithelial Cell Cultures. Experimental Cell Research 224, 354–364. https://doi.org/10.1006/excr.1996.0145

Pierce, K.L., Premont, R.T., Lefkowitz, R.J., 2002. Seven-transmembrane receptors. Nat Rev Mol Cell Biol 3, 639–650. https://doi.org/10.1038/nrm908

Ruemmele, F.M., 2003. Butyrate induced Caco-2 cell apoptosis is mediated via the mitochondrial pathway. Gut 52, 94–100. https://doi.org/10.1136/gut.52.1.94

Sangild, P.T., Ney, D.M., Sigalet, D.L., Vegge, A., Burrin, D., 2014. Animal models of gastrointestinal and liver diseases. Animal models of infant short bowel syndrome: translational relevance and challenges. American Journal of Physiology-Gastrointestinal and Liver Physiology 307, G1147–G1168. https://doi.org/10.1152/ajpgi.00088.2014

Schierack, P., Nordhoff, M., Pollmann, M., Weyrauch, K.D., Amasheh, S., Lodemann, U., Jores, J., Tachu, B., Kleta, S., Blikslager, A., Tedin, K., Wieler, L.H., 2006. Characterization of a porcine intestinal epithelial cell line for in vitro studies of microbial pathogenesis in swine. Histochem Cell Biol 125, 293–305. https://doi.org/10.1007/s00418-005-0067-z

Shu, R., David, E.S., Ferraris, R.P., 1997. Dietary fructose enhances intestinal fructose transport and GLUT5 expression in weaning rats. Am J Physiol 272, G446-453. https://doi.org/10.1152/ajpgi.1997.272.3.G446

Singh, V., Lee, G., Son, H., Koh, H., Kim, E.S., Unno, T., Shin, J.-H., 2023. Butyrate producers, “The Sentinel of Gut”: Their intestinal significance with and beyond butyrate, and prospective use as microbial therapeutics. Front. Microbiol. 13, 1103836. https://doi.org/10.3389/fmicb.2022.1103836

Song, K.-H., Chung, S.-J., Shim, C.-K., 2005. Enhanced intestinal absorption of salmon calcitonin (sCT) from proliposomes containing bile salts. Journal of Controlled Release 106, 298–308. https://doi.org/10.1016/j.jconrel.2005.05.016

Turck, D., Feste, A.S., Lifschitz, C.H., 1993. Age and diet affect the composition of porcine colonic mucins. Pediatr Res 33, 564–567. https://doi.org/10.1203/00006450-199306000-00005

Vergauwen, H., 2015. The IPEC-J2 Cell Line, in: Verhoeckx, K., Cotter, P., López-Expósito, I., Kleiveland, C., Lea, T., Mackie, A., Requena, T., Swiatecka, D., Wichers, H. (Eds.), The Impact of Food Bioactives on Health: In Vitro and Ex Vivo Models. Springer, Cham (CH).

Weaver, L.T., Laker, M.F., Nelson, R., 1984. Intestinal permeability in the newborn. Arch Dis Child 59, 236–241. https://doi.org/10.1136/adc.59.3.236

Weström, B., Arévalo Sureda, E., Pierzynowska, K., Pierzynowski, S.G., Pérez-Cano, F.-J., 2020. The Immature Gut Barrier and Its Importance in Establishing Immunity in Newborn Mammals. Frontiers in Immunology 11.

World Health Organization., 2014. Global Nutrition Targets 2025: Breastfeeding Policy Brief.

Zhang, H., Malo, C., Buddington, R.K., 1997. Suckling Induces Rapid Intestinal Growth and Changes in Brush Border Digestive Functions of Newborn Pigs. J Nutr 127, 418–426. https://doi.org/10.1093/jn/127.3.418

Appendix A

Publications from this thesis

The Journal of Nutritional Physiology 6 (2026) 100021

Contents lists available at ScienceDirect

The Journal of Nutritional Physiology

journal homepage: www.sciencedirect.com/journal/the-journal-of-nutritional-physiology

Research Article

Modeling a leaky gut *In vitro*: Sodium butyrate-induced barrier disruption of Caco-2 monolayers

Francesca Bietto [a,b], Elena Arranz [c,d], Monica Mechoud [a], Eva Rath [e], Alice J. Lucey [b], Linda Giblin [a,*]

[a] Teagasc Food Research Centre, Moorepark, Co. Cork, Fermoy, Ireland
[b] School of Food and Nutritional Sciences, University College Cork, Cork, Ireland
[c] Sección Departamental de Ciencias de La Alimentación, Universidad Autónoma de Madrid (UAM), Madrid, Spain
[d] Institute of Food Science Research CIAL (CSIC-UAM), Madrid, Spain
[e] Chair of Nutrition and Immunology, School of Life Sciences, Technische Universität München, Freising, Germany

ARTICLE INFO

Keywords:
Sodium butyrate
Caco-2
Leaky gut
Hyperosmolarity
Dexamethasone

ABSTRACT

Butyrate exhibits a dual effect on gut permeability, promoting epithelial health at low concentrations but disrupting barrier integrity at higher levels. This disruption at higher concentrations can be exploited, *in vitro,* to create gut barrier models with increased permeability. This study aimed to unravel the mechanism of action of sodium butyrate (NaB, 50–125 mM) on human intestinal enterocyte monolayers using the Caco-2 cell model. NaB reduced trans-epithelial electrical resistance (TEER) and increased lucifer yellow paracellular flux in a dose-dependent manner on Caco-2 monolayers, effects that persisted after NaB withdrawal. TEER reductions induced by NaB occurred under hyperosmotic conditions (430.5 ± 4.5 mOsm/kg). In contrast, treatment with mannitol, a non-metabolizable osmotic agent used to mimic the osmotic effect, only caused a transient decrease in TEER. NaB was actively transported into cells, with increased mRNA expression of butyrate transporters MCT-1 and SMCT-1. However, NaB did not act as an energy substrate, as evidenced by decreased ATP levels and unchanged cellular reductase activity. Instead, NaB elevated Caspase-3 activity, induced stress markers (p21, HSP-70), and stimulated cytokine production (IL-6, IL-8, TNF). Most importantly, treatment with dexamethasone, a commonly used steroid, restored TEER and reduced stress and inflammation markers in Caco-2 monolayers disrupted by 75 mM NaB. Therefore, NaB treated Caco-2 monolayers are a suitable *in vitro* model for gut barrier dysfunction and inflammation such as Crohn's disease or necrotizing enterocolitis.

1. Introduction

The intestinal barrier is a highly specialized system that regulates the selective movement of nutrients and metabolites, whilst providing defense against harmful exogenous agents (Groschwitz & Hogan, 2009). This barrier consists of a single layer of intestinal epithelial cells joined by tight junctions, which are complexes of transmembrane proteins, such as occludin (OCLN), claudins (CLDN), junctional adhesion molecules (JAM) and zonula occludens (ZO) (Otani & Furuse, 2020). These proteins regulate the pore size and the passage of molecules through the paracellular pathway (Otani & Furuse, 2020). Increased permeability of this barrier, commonly referred to as "leaky gut," is associated with various disorders, including inflammatory bowel diseases (Hollander, 1999), but also with the immature infant gut. Paracellular permeability is higher during early postnatal life (Catassi et al., 1995; Kosek et al., 2017; Weaver et al., 1984), allowing for the uptake of bioactives from milk (Weström et al., 2020). Studies have shown that human milk, compared to infant formula, contributes to a more rapid reduction in intestinal permeability and therefore gut closure over time (Catassi et al., 1995; Weaver et al., 1984; Weström et al., 2020).

Butyrate is a short-chain fatty acid (SCFA), produced by microbial fermentation of dietary fibers, that has emerged as a key regulator of the intestinal barrier (H. Liu et al., 2018). Together with acetate and propionate, butyrate comprises the most abundant SCFAs in the gut, typically present in an approximate molar ratio of 60:20:20 (acetate: propionate: butyrate). The total daily SCFA production in the colon is estimated to range between 500 and 600 mmol (Dalile et al., 2019). Butyrate can exert its barrier effects either by being transported into

* Corresponding author.
E-mail address: Linda.Giblin@teagasc.ie (L. Giblin).

https://doi.org/10.1016/j.jnphys.2026.100021
Received 23 July 2025; Received in revised form 13 March 2026; Accepted 18 March 2026
Available online 20 March 2026
3050-6247/© 2026 The Authors. Published by Elsevier Ltd on behalf of The Physiological Society. This is an open access article under the CC BY license (http://creativecommons.org/licenses/by/4.0/).

intestinal epithelial cells via monocarboxylate transporters (MCT-1) and sodium-coupled monocarboxylate transporters (SMCT-1) (Dalile et al., 2019; Hamer et al., 2008; Stilling et al., 2016), or by binding to G-protein coupled receptors (GPR41, GPR43, and GPR109A) on the cell surface, thereby triggering intracellular signaling pathways without entering the cell (Brown et al., 2003). Once inside the intestinal cell, butyrate undergoes β-oxidation to produce acetyl-CoA, which serves as an energy substrate for enterocytes, supporting metabolic activity and maintaining barrier integrity (Canani, 2011; Hamer et al., 2008; Stilling et al., 2016). However, when present at high concentrations, it can accumulate in the nucleus, where it acts as a histone deacetylase (HDAC) inhibitor, promoting epigenetic modifications (Dalile et al., 2019; Singh et al., 2023) and activating pathways that induce apoptosis and cell cycle arrest in the intestinal barrier (Avivi-Green et al., 2002; Chirakkal et al., 2006; Donohoe et al., 2012; Siavoshian, 2000).

Caco-2 cell monolayers, derived from a human colon adenocarcinoma (Fogh et al., 1977), are widely utilized as an *in vitro* model for studying intestinal barrier function. If grown on a permeable support, they have the ability to differentiate over a 3 week period into a polarized barrier with brush border enzymes, nutrient transporters and tight junctions (Lea, 2015). Interestingly, butyrate displays a clear concentration-dependent dual effect on Caco-2 permeability. At low concentrations (2 mM), it strengthens the epithelial barrier by increasing transepithelial electrical resistance (TEER), reducing paracellular permeability (Peng et al., 2007; Suzuki et al., 2008), and enhancing tight-junction protein expression (Peng et al., 2009). However, at higher concentrations, butyrate disrupts Caco-2 barrier integrity and induces a "leaky" phenotype. Peng et al. (2007) reported that prolonged exposure to 8 mM sodium butyrate (NaB) markedly reduced TEER, increased inulin-FITC permeability and induced apoptosis ($P < 0.05$) (Peng et al., 2007). Similarly, Ruemmele et al. (2003) reported that treatment of Caco-2 cells with butyrate at concentrations ranging from 5 to 100 mM significantly increased apoptosis (Ruemmele, 2003). Previously, our laboratory reported that high concentrations of NaB for 24 h reduced TEER, increased paracellular permeability to mannitol (Man), reduced CLDN-1 and CLDN-2 mRNA levels and caused a redistribution of ZO1 in Caco-2 monolayers (Kondrashina et al., 2021). Interestingly, the barrier increased the transport rate of the intact milk protein α-lactalbumin, suggesting that NaB treatment could be used to create an *in vitro* model of the infant gut. However, at these concentrations, the osmolality of the NaB solution in media (200 mM NaB = 790 mOsm/kg) is at the upper limit of Caco-2 cell tolerance (Grauso et al., 2019; Inokuchi et al., 2009), raising the potential for hyperosmotic stress contributing to the observed barrier manipulation. Moreover, an important feature of an infant gut barrier model is reversibility, as this allows assessment of barrier closure over time, particularly in the assessment of human milk or infant formula. Therefore, the objectives of this study were: (i) to determine whether NaB-induced leakiness in Caco-2 barriers is reversible; (ii) to evaluate the contribution of hyperosmolality to this effect; and (iii) to investigate NaB metabolism and health status of Caco-2 cells. Collectively, this study aimed to explore whether NaB treatment of Caco-2 monolayers is better suited to represent a transient "leaky" healthy infant gut barrier, or whether it more accurately represents a persistently disrupted, disease-associated epithelial barrier.

2. Materials and Methods

2.1. Materials

Human intestinal epithelial cell lines Caco-2 (EACC 86010202) and HT29-MTX-E12 (EACC 12040401) were purchased from the European Collection of Cell Culture (UK). Six-well plates with polyester permeable-membrane inserts (0.4 μm pore size, 4.5 cm^2 area) and 12 well plates with polyester permeable-membrane inserts (0.4 μm pore size, 1.11 cm^2 area) were purchased from Sarstedt Group (Germany). CellTiter 96™ AQueous One Solution Cell Proliferation Assay (MTS, G3582) and CellTiter-Glo™ Luminescence Viability Assay (G7570) were purchased from Promega (USA). CyQUANT™ LDH Cytotoxicity Assay (C20300) was purchased from Invitrogen (USA). RNeasy mini kit (74104) and RNA-free DNase set (79254) were from Qiagen (Netherlands). SensiFAST cDNA Synthesis Kit (BIO-65053) was from Meridian Bioscience (UK). Light Cycler SYBR GREEN I Master kit (04707516001) was from Roche Diagnostics (Switzerland). Primers for RT-qPCR were synthesized by Eurofins Genomics (Germany). Lucifer yellow (L1177) was supplied by ThermoFisher Scientific (USA). All the other reagents were purchased from Sigma-Aldrich, unless stated otherwise.

2.2. Cell Culture

Caco-2 and HT29-MTX were grown in 75 cm^2 tissue culture flasks at 37 °C, 5% CO_2 in a humidified environment. Thawed cells were passaged three times prior to use. Cells were routinely cultured in Dulbecco's Modified Eagle Medium (DMEM D5796) supplemented with 10% (v/v) fetal bovine serum (FBS, F7524), and 100 U/mL Penicillin-Streptomycin (P4333) (complete DMEM). For HT29-MTX cells or co-cultures, 1% (v/v) MEM Non-essential Amino Acid Solution (M7145) was added to complete DMEM. Cells were passaged at 80% confluence every 4-5 days by 0.25% Trypsin- EDTA solution (T4049). Caco-2 passage numbers were 19-25. HT29-MTX passage numbers were 65-70. Trypan blue staining and a TC20 cell counter (Bio-Rad, USA) were used for cell counting.

2.3. NAD(P)H dehydrogenase activity and ATP levels

Caco-2 cells were seeded into a 96-well plate at a density of 5×10^4 cells/well in complete DMEM (4500 mg/L glucose, L-glutamine and sodium bicarbonate). After 24 h, the cells were washed twice with PBS, and 100 μL of either DMEM D1145 or glucose/glutamine-free DMEM was added (D5030). Cells were incubated for 16 h. The following day, cells were washed twice with PBS and treated with 100 μL of 50, 75, 100 and 125 mM NaB or 100, 150, 200 and 250 mM Man prepared in DMEM D1145 or glucose/glutamine-free DMEM for 4 h.

CellTiter 96™ AQueous One Solution Cell Proliferation Assay (MTS) was performed as per manufacturer's instructions. In brief, MTS solution (20 μL) was added into each well and the plate incubated for 1 h at 37 °C in the dark. Absorbance was measured at 490 nm in a plate reader (Synergy HT, BioTek).

For the ATP assay, CellTiter-Glo® 2.0 Cell Viability Assay was performed, following the manufacturer's instructions. After the 4 h incubation, cell supernatant was removed and 150 μL of reagent containing luciferin was added. Cells were immediately lysed by pipetting. Cell lysate (100 μL) was transferred into a white bottom 96-well plate and allowed to equilibrate at room temperature in the dark for 10 min. Luminescence was measured using a plate reader (Synergy HT, Biotek; excitation = plug, emission = hole, gain = 135).

Control cells were incubated with either DMEM D1145 or glucose/glutamine-free DMEM. To verify the ability of nutrient-starved cells to recover, control cells in glucose/glutamine-free DMEM were subsequently replenished with DMEM D1145 and allowed to recover for 4 h. Subsequently, MTS and ATP assays were performed to assess recovery.

2.4. Caspase-3 activity

Caco-2 cells were initially seeded into a 96-well plate at a density of 5×10^4 cells/well and cultured in complete DMEM. After 24 h, media was replaced with DMEM D1145 and cells were incubated overnight. The next day, cells were washed twice with Hanks Balanced Salt Solution (HBSS, H8264) and incubated with either DMEM D1145, 75 mM NaB, 125 mM NaB, 150 mM Man or 250 mM Man in DMEM D1145. After a 4-h incubation Caspase-3 activity was measured with Caspase-3 assay

kit (CASP3F, Sigma-Aldrich), following the manufacturer's instructions. Briefly, the plate was placed on ice and incubated with 25 µL of lysis buffer for 15 min. Then, 200 µL of reaction mixture (including peptide substrate acetyl-Asp-Glu-Val-Asp-7-amido-4-methylcoumarin) was added. Subsequently, 200 µL of the mixture were transferred into a black bottom 96-well plate and the fluorescence (excitation – 360 nm, emission – 460 nm) was measured at room temperature in a Biotek Synergy HT plate reader after a 60-min incubation. The assay positive control was isolated human Caspase-3 (0.5 µg/mL, without cells).

The caspase-3 activity was calculated in nmol of 7-Amino-4-methylcoumarin (fluorescent product) released per minute per mL of cell lysate based on the formula:

$$\text{Activity, nmol AMC / min/mL} = (\text{nmol AMC} \times \text{d}) / (\text{t} \times \text{v})$$

Where: v = volume of sample in mL, d = dilution factor, t = reaction time in minutes.

2.5. NaB treatment of Caco-2 or Caco-2/HT29-MTX monolayers

Caco-2 cells were diluted in complete DMEM to a concentration of 1.2×10^5 cells/mL. Cells were then seeded at a density of 6.0×10^4 cells/insert (0.5 mL) into 12 well plates with inserts. The basolateral compartment received 1.5 mL complete DMEM. For the Caco-2/HT29-MTX co-culture, cells were diluted in complete DMEM media with 1% (v/v) MEM Non-essential Amino Acid at a 90:10 ratio (respectively) in a final concentration of 1.2×10^5 cells/mL for seeding at 6.0×10^4 cells/insert (0.5 mL).

Cells were allowed to differentiate for 20 days with culture media replaced every other day. Monolayer integrity was assessed every 7 days (16 h after media change) by TEER via the Millicell ERS-2 (Millipore, USA) (Fig. S1). TEER values were expressed as $\Omega \times cm^2$-blank (Transwell insert with media in the absence of cells). Only monolayers exhibiting TEER values over 800 $\Omega \times cm^2$ on the experimental day before washing, were used for subsequent permeability studies.

Around 16 h before the experimental day, the apical and basolateral compartments were washed twice with HBSS and incubated with DMEM (DMEM D1145, i.e. without phenol red and glutamine), without antibiotics and FBS. On experimental day, TEER values were recorded and cells washed twice with HBSS. DMEM D1145 was then added to the apical (0.4 mL) and basolateral compartments (1.5 mL), and the plates were incubated for 30 min for acclimatization.

NaB was freshly prepared as a 5X stock solution in DMEM D1145 and filtered with 0.22 µm PES filter (Sarstedt Group). This stock solution (100 µL) was then added to the apical compartment, resulting in a final concentration of 50, 75, 100 and 125 mM NaB in 0.5 mL total volume. For experiments with Man, a 2.5X solution was prepared and 200 µL was added to the apical compartment with 300 µL DMEM D1145 to a final Man concentration of 100, 150, 200 and 250 mM. The osmolality of the samples was measured with OsmoTECH® XT Single-Sample Micro-Osmometer (Advanced Instruments, USA).

Monolayers treated with NaB or Man were incubated for 24 h. TEER was measured at times 0, 2, 4, 6 and 24 h. Control monolayers contained DMEM D1145 only. At 24 h, apical and basolateral compartments were collected and stored at −20 °C for further analysis. Further experiments were performed on the monolayers, or the monolayers were lysed for RT-qPCR.

2.6. Monolayer recovery

After the 24 h incubation with NaB or Man, the apical and basolateral chambers were emptied, monolayers were washed twice with HBSS, and DMEM D1145 was added to the apical (0.5 mL) and basolateral (1.5 mL) chambers. Monolayers were incubated for a further 24 h. TEER was measured after 1, 2, 4, 6, and 24 h.

2.7. TEER measurements with isosmotic NaB and Man solutions

To obtain isosmotic solutions of NaB and Man, DMEM D1145 was firstly diluted with MilliQ H_2O: 1 in 1.37 for 50 mM NaB or 100 mM Man, 1 in 1.678 for 75 mM NaB or 150 mM Man, 1 in 2.17 for 100 mM NaB or 200 mM Man, and 1 in 3 for 125 mM NaB or 250 mM Man. The diluted media were then used to dissolve NaB or Man. Osmolality of the prepared stock solutions were measured using OsmoTECH® XT Single-Sample Micro-Osmometer (Advanced Instruments).

On day 19, Caco-2 monolayers were washed twice with HBSS and incubated overnight with DMEM D1145. The next day, monolayers were washed twice with HBSS and treated with 0.5 mL of the isosmotic solutions on the apical side for 24 h. The basolateral side contained fresh 1.5 mL DMEM D1145 (348.6 mOsm/kg). TEER measurements were taken 0, 1, 2, 4, 6 and 24 h using the Millicell ERS-2 (Millipore). Monolayers in DMEM D1145 served as the control condition.

2.8. Treatment with dexamethasone

Dexamethasone (D4902) was dissolved in DMSO to a stock concentration of 2 mM, which was sequentially diluted 1 in 200 in DMEM D1145. After 24 h incubation with NaB or Man, 21-day Caco-2 monolayers were washed twice with HBSS. Dexamethasone (10 µM in DMEM D1145, 0.5 mL) was added to the apical compartment. Fresh 1.5 mL DMEM D1145 was added to the basolateral chamber. Monolayers were incubated for 24 h at 37 °C, 5% CO_2. TEER was measured at T0 and T24. Apical samples were then collected for LDH release. Monolayers were washed twice with PBS and lysed on ice using 350 µL of RLT buffer for RT-qPCR analysis. Lysates were stored at −20 °C until use.

2.9. Lucifer Yellow permeability

After the 24 h incubation with NaB or Man, Caco-2 monolayers were washed twice with HBSS. The apical side was then treated with 0.5 mL Lucifer Yellow (0.5 mg/mL) in HBSS for 2 h, while HBSS (1.5 mL) was added to the basolateral side. To prepare a standard curve, the stock Lucifer Yellow solution was diluted in HBSS ranging from 7.81 to 0.24 to µg/mL. After incubation, 300 µL of each basolateral sample or standard was transferred to a black, flat-bottom 96-well plate (Corning). Fluorescence was read (excitation – 420 nm, emission – 528 nm, gain = 40) at 37 °C using a plate reader (Synergy HT, Biotek, USA). The concentration of Lucifer Yellow in the basolateral side was calculated comparing the measured fluorescence to the standard curve. The apparent permeability (Papp) was calculated with the following formula:

$$\text{Papp (cm / min)} = (C_{Baso} \times V) / (t \times A \times C_{In})$$

Where: C_{Baso} = Concentration of Lucifer yellow in the basolateral compartment (µg/mL); V = Volume of the basolateral compartment (mL); t = incubation time (120 min); A = surface area (1.1 cm^2); C_{In} = initial concentration in the apical (µg/mL).

2.10. NaB and Man quantification in apical and basolateral samples

NaB and Man concentrations were quantified using High-Performance Liquid Chromatography (HPLC), employing a Waters Alliance Separation Module e2695 coupled with a Waters 2414 refractive index (RI) detector (Waters, MA, USA).

For NaB analysis, apical samples and initial NaB stock solutions were diluted 1 in 100 in MilliQ H_2O, while basolateral samples were diluted 1 in10 in MilliQ H_2O. For Man analysis, apical samples were diluted 1 in 100 and basolateral samples 1 in 25 in MilliQ H_2O. Samples were filtered via 0.22 µm nylon syringe filters.

A 20 µL aliquot of each sample or standard was injected. For NaB detection, separation was carried out on an Aminex HPX-87C ion

exchange column (300 × 7.8 mm), operated at 60 °C. Elution was performed using 0.005 N H_2SO_4 as the mobile phase at a flow rate of 0.6 mL/min. NaB quantification was performed by comparing sample peak areas to a standard curve prepared with known NaB concentrations ranging from 10 to 100 μg/mL in MilliQ H_2O.

For Man detection, separation was achieved using an Aminex HPX-87P carbohydrate analysis column (300 × 7.8 mm) equipped with an Aminex HPX-87P guard column (Bio-Rad, cat. no. 1250131), and maintained at 60 °C. The RI detector was operated at 35 °C. Elution was performed with MilliQ H_2O at a flow rate of 0.6 mL/min. Analytical-grade Man was used to prepare standard solutions at concentrations of 20, 50, 100, and 200 μg/mL. Man quantification was based on retention time matching and comparison of peak areas to the standard curve.

Data are expressed as the amount (μg) of NaB or Man present in 0.5 mL of the apical sample at T0 and T24, and 1.5 mL of the basolateral sample at T24. The percentage of NaB or Man transported was calculated using the following equation:

$$\% \text{ transported} = (C_{baso} \ / \ C_{T0}) \times 100$$

Where C_{baso} = concentration of butyrate in the basolateral compartment (mmol in 1.5 mL); C_{T0} = concentration of butyrate in the solution applied to the apical compartment at T0 (mmol in 0.5 mL)

2.11. RT-qPCR

For the RT-qPCR analysis, Caco-2 monolayers were washed twice with PBS and lysed with the addition of 350 μL RLT buffer. After 5 min on ice, cell lysate was collected by pipetting and stored at −80 °C. Lysed cells were thawed at room temperature and RNA extracted using the RNeasy Mini Kit with a DNAse step, following manufactures instructions. Total RNA quantity was measured using Nanodrop 1000 (Thermo Fisher Scientific, MA, USA) and RNA samples with $OD_{260/280} > 1.8$ were progressed to cDNA synthesis. The SensiFAST cDNA Synthesis Kit was used to synthesize cDNA from 0.5 μg Total RNA. Subsequently, qPCR was conducted with the Light Cycler SYBR GREEN I Master kit using a Light Cycler 96 instrument.

Primers were designed based on GenBank sequences (Table 1). P21 primer was obtained from Ding et al. (2019). The human ribosomal protein lateral stalk subunit P0 (RPLP0) was chosen as a housekeeping gene. Amplification efficiency ranged between 90 and 110%, with optimal annealing temperature of 60 °C. The $2^{-\Delta\Delta Ct}$ method was employed to calculate the relative amount of the target, where.

$\Delta\Delta Ct$ = (Ct Target gene − Ct RPLP0)$_{test}$ − (Ct Target gene − Ct RPLP0)$_{Control}$. Ct = threshold cycle for either the target gene or RPLP0; test = Man or NaB treated monolayers; control = DMEM D1145 media treated monolayers.

2.12. Lactate dehydrogenase (LDH) cytotoxicity assay

To measure LDH release, 50 μL from the apical chamber of NaB-, Man- or NaB + dexamethasone-treated Caco-2 monolayers were transferred to a 96-well flat-bottom plate and combined with an equal volume of the LDH Cytotoxicity Assay reaction mixture. The plate was incubated in the dark at room temperature for 30 min, allowing the LDH-mediated conversion of lactate to pyruvate and subsequent reduction of the formazan dye. Following incubation, 50 μL of stop solution was added to each well, and absorbance was measured at 490 nm and 680 nm using a Synergy HT plate reader (Biotek). LDH activity was determined by subtracting the absorbance at 680 nm from the absorbance at 490 nm for each sample. LDH release was calculated using the formula:

$$\% \text{ LDH release} = [(\text{Treated LDH activity} - \text{Spontaneous LDH activity}) \ / \ (\text{Maximum LDH activity} - \text{Spontaneous LDH activity})] \times 100$$

Where: Treated LDH activity = LDH activity in the supernatant of NaB- or Man-treated monolayers; Spontaneous LDH activity = activity in supernatant of DMEM D1145 control monolayers; Maximum LDH activity = LDH released from 50 μL of lysed control monolayers treated with 500 μL of 1% Triton X-100.

2.13. Statistical analysis

All experiments were conducted in triplicate on three independent days, each with technical duplicates. Results are presented as means ± SEM. Statistical analyses were performed using GraphPad Prism 9.1.0 (GraphPad Software, San Diego, California, USA). One-way or two-way ANOVA followed by Tukey's multiple comparisons test was used for normally distributed data, while the Friedman test with Dunn's multiple comparisons test was applied for non-normally distributed data. Statistical significance was defined as $P < 0.05$.

3. Results

3.1. NaB impairs epithelial barrier integrity monolayers without subsequent recovery

Caco-2 monolayers (20-day old) were treated with either 50, 75, 100, 125 mM NaB or the osmolality equivalent Man concentration (Fig. 1). The osmolality (mOsm/kg) of NaB-DMEM D1145 solutions applied to the cells are detailed in Table 2A and ranged from 348.7 ± 1 mOsm/kg for DMEM D1145 to 579.5 ± 2.5 for 125 mM NaB in DMEM D1145. As Man is not metabolized nor internalized by Caco-2 cells but is

Table 1
Gene name, GenBank accession number, primers and annealing temperature (T_a) for RT-PCR analysis.

Protein	Gene	GenBank	Forward Primer	Reverse Primer	T_a (°C)
Sodium-coupled monocarboxylate transporter 1 (SMCT1)	*SLC5A8*	NM_145913	GGCGTCACTTATGGGAGCTTTG	GGCAAATCCAGCCATCAGACCA	60
Monocarboxylate transporter 1 (MCT1)	*SLC16A1*	NM_003051	TTGTTGGTGGCTGCTTGTCAGG	TCATGGTCAGAGCTGGATTCAAG	60
Short-chain acyl-coenzyme A dehydrogenase (SCAD)	*ACADS*	NM_000017	CACGCCTTTCACCAGTGGTGAC	GGCATTGGTGATCCAGGCTTTG	60
70 kDa heat shock protein (Hsp70)	*HSPA1A*	NM_005345	ACCTTCGACGTGTCCATCCTGA	TCCTCCACGAAGTGGTTCACCA	60
p21 (p21ˆCip1/Waf1)	*CDKN1A*	NM_000389.5	GACACCACTGGAGGGTGACT	CAGGTCCACATGGTCTTCCT	60
Aquaporin 3	*AQP3*	NM_004925	CCGTGACCTTTGCCATGTGCTT	TTGTCGGCGAAGTGCCAGATTG	60
Interleukin 8/CXC chemokine ligand 8 (IL-8)	*CXCL8*	NM_000584.2	GAGAGTGATTGAGAGTGGACCAC	CACAACCCTCTGCACCCAGTTT	60
Tumor Necrosis factor (TNF)	*TNF*	NM_000594	CTCTTCTGCCTGCTGCACTTTG	ATGGGCTACAGGCTTGTCACTC	60
Interleukin 6 (IL-6)	*IL6*	NM_000600	AGACAGCCACTCACCTCTTCAG	TTCTGCCAGTGCCTCTTTGCTG	60

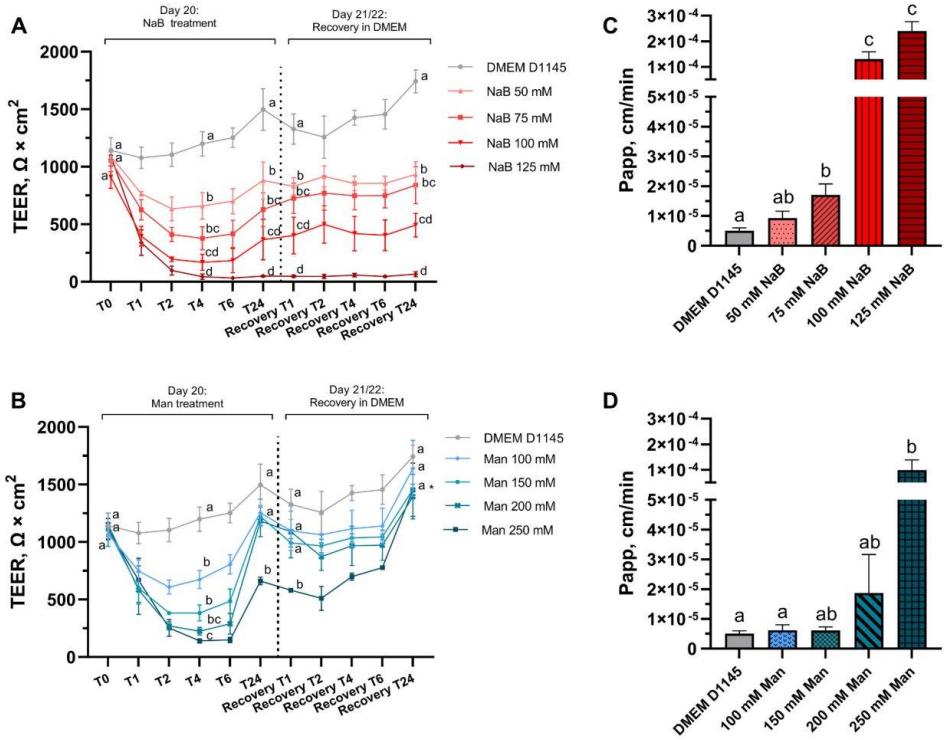


Fig. 1. Sodium butyrate (NaB) impairs epithelial barrier integrity monolayers without subsequent recovery. The mean transepithelial electrical resistance (TEER) value at day 20 Caco-2 was 1451.40 ± 33.03 Ω × cm^2. (A) NaB-treated monolayers in DMEM 1145 or (B) mannitol (Man)-treated monolayers in DMEM D1145 at osmolality ranging from 349 to 580 mOsm/kg. TEER values were recorded before the treatment (T0) and at 1, 2, 4, 6 and 24 h (T1/2/4/6/24). NaB or Man was then removed and TEER values were recorded at Recovery T1, T2, T4, T6 and T24 h. Statistical analysis was performed by two-way ANOVA with Tukey's multiple comparison. Statistical differences between different concentrations, at the same time point, is depicted by different letters. Statistical difference between T24 and Recovery T24 within the same concentration is indicated by an asterisk. (C) Lucifer yellow apparent permeability (Papp) for NaB-treated monolayers and (D) Man-treated monolayers. Lucifer yellow (mM) was added to the apical and quantified in the basolateral after 2 h. Statistical significance between different concentrations, at the same time point, was determined for (C) by one-way ANOVA with Tukey's Multiple comparisons and for (D) by Friedman test with Dunn's multiple comparisons. Results are presented as biological triplicates with technical duplicates ± SEM. Different letters indicate statistically significant differences ($P < 0.05$).

Table 2
Average osmolality (mOsmol/kg) of DMEM D1145, sodium butyrate (NaB) and mannitol (Man) solutions. Osmolality of DMEM D1145 and NaB/Man samples dissolved in (A) DMEM D1145 or (B) diluted DMEM D1145 to maintain isosmotic conditions. Osmolality was measured using a cryoscopic osmometer (OsmoTECH® XT). Data represent the mean of biological triplicates ± SEM. Statistical analysis was performed using one-way ANOVA with Tukey's multiple comparisons. Within stock solutions or apical samples, different letters indicate significant differences ($P < 0.05$).

A – Samples in DMEM D1145		B – Samples in diluted DMEM D1145	
Sample	Osmolality (mOsm/kg)	Sample	Osmolality (mOsm/kg)
DMEM D1145	348.6667 ± 1^a	-	
NaB 50 mM	430.5 ± 4.5^b	NaB 50 mM	343.5 ± 5.5^a
NaB 75 mM	474.5 ± 1.5^c	NaB 75 mM	360.5 ± 20.5^a
NaB 100 mM	525 ± 9^d	NaB 100 mM	343.0 ± 7^a
NaB 125 mM	579.5 ± 2.5^e	NaB 125 mM	368.5 ± 2.5^a
Man 100 mM	438 ± 4^b	Man 100 mM	351 ± 2^a
Man 150 mM	484.5 ± 0.5^c	Man 150 mM	368.5 ± 6.5^a
Man 200 mM	534 ± 1^d	Man 200 mM	362.5 ± 1.5^a
Man 250 mM	583 ± 1^e	Man 250 mM	372.0 ± 11^a

transported paracellularly to the basolateral chamber (Ménard et al., 2010), Man with equivalent osmolality to NaB ($P > 0.05$) was included as a control (Table 2). Treatment with NaB reduced the Caco-2 monolayer TEER values in a dose-dependent manner, compared to media alone (Fig. 1A; T4 = $P < 0.05$, T24 = $P < 0.05$). NaB was then removed and replaced with fresh DMEM D1145 to support recovery. By recovery T24 timepoint, NaB treated monolayers, regardless of dose, had not recovered (T24 vs. Recovery T24 $P < 0.05$). Indeed Caco-2 monolayers treated with 125 mM NaB had a TEER value at recovery T24 of 66.36 ± 21.93 compared to 1742.03 ± 100.24 with DMEM D1145. In contrast, treatment with Man (100, 150, 200, 250 mM) resulted in a significant reduction initially 2, 4, 6 h but by 24 h only 250 mM Man was significantly reduced ($P < 0.05$) (Fig. 1B). Removal of Man allowed all monolayers to recover to control condition ($P > 0.05$).

As TEER is only one measurement of barrier function, paracellular permeability was also assessed using Lucifer Yellow (Fig. 1C and D). NaB at 75, 100 and 150 mM induced a dose-dependent increase in Lucifer Yellow Papp compared to DMEM D1145 (75 and 100 mM NaB $P < 0.05$; 125 mM NaB $P < 0.01$). Only 250 mM Man (osmolality equivalent to 125 mM NaB) had a significantly higher Papp compared to DMEM D1145 ($P < 0.05$), while the other Man concentrations had no effect ($P > 0.05$). The Papp of DMEM D1145 control monolayers was = 0.51 ×

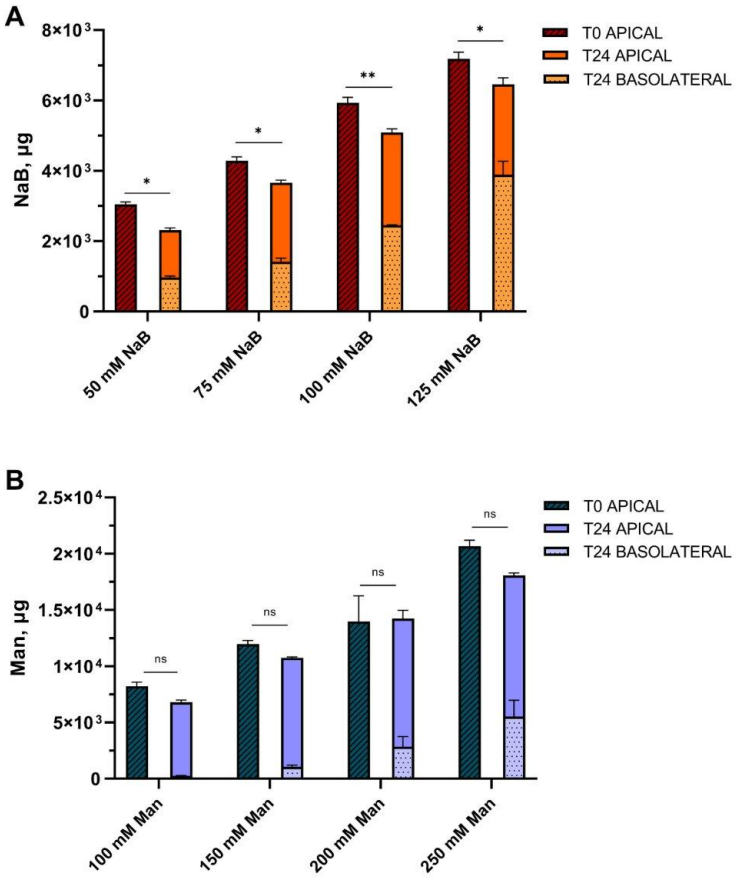


Fig. 3. Sodium butyrate (NaB) is transported across and into Caco-2 monolayers. Quantification of (A) NaB and (B) mannitol (Man) by HPLC. T0 apical = solution applied to the apical compartment at T0; T24 apical = apical sample after 24 h incubation. T24 basolateral = basolateral sample after 24 h incubation. Results represent the average of three biological and two technical replicates, presented as mean ± SEM. Statistical analysis was determined using two-way ANOVA with Dunnet's multiple comparison test. Statistical significance ($P < 0.05$) between T0 apical and (T24 apical + T24 basolateral) is indicated with an asterisk.

Caco-2 monolayers, NaB was quantified in apical and basolateral chambers after 24 h treatment (Fig. 3A and B). Similar to Man, NaB was detected in the basolateral compartment, confirming translocation across the monolayer. Notably, the total recovered amount of NaB (apical plus basolateral compartments) was significantly lower than the initial apical concentration ($P < 0.05$), indicating substantial uptake or metabolism by the monolayers. In contrast, the total recovered amount of Man matched the initially applied concentration ($P < 0.05$), confirming no uptake by Caco-2 cells. Specifically, the percentage of NaB transported to the basolateral compartment was: 31.85 ± 0.6% with 50 mM NaB applied, 33.03 ± 1.9% for 75 mM NaB, 41.41 ± 1.2% for 100 mM NaB, and 53.87 ± 4.03% for 125 mM NaB. In contrast, Man showed comparatively lower transport percentages: 100 mM Man = 3.13 ± 0.49%, 150 mM Man = 8.91 ± 1.04%, 200 mM Man = 20.76 ± 5.45%, and 250 mM Man = 27.13 ± 7.82%.

3.4. NaB is not utilized as an energy source in Caco-2 cells

To assess whether or not NaB is utilized by Caco-2 cells, NAD(P)H dehydrogenase activity (MTS assay) and intracellular ATP levels were measured after cells were starved for 16 h in media in the absence of a carbon source (glucose and sodium pyruvate-free DMEM) (Fig. 4). NaB or Man were then added. Without a carbon source in the media, NAD(P)H dehydrogenase activity in the cells was 25.5 ± 0.75 % of the control media with glucose ($P < 0.05$). The addition of NaB or Man to the media, did not restore NAD(P)H dehydrogenase activity in the cells, indicating neither NaB nor Man were used as a carbon source. Where cells were cultured in media with glucose, the addition of NaB or Man did not significantly increase NADH dehydrogenase activity ($P > 0.05$).

Intracellular ATP is a marker of metabolically active cells. The levels of intracellular ATP produced in Caco-2 in response to NaB or Man are depicted in Fig. 4C and D. In the absence of a carbon source, ATP levels were 25.77 ± 0.85% of the control cells with glucose (DMEM D1145, $P < 0.05$). The addition of NaB or Man did not increase ATP levels. Interestingly when cells were incubated with glucose (DMEM D1145), the addition of 75, 100 and 125 mM NaB or 100, 150, 200 and 250 mM Man significantly reduced ATP levels ($P < 0.05$).

As a positive control, cells were incubated in glucose-free DMEM for 16 h, and subsequently transferred to glucose-containing DMEM D1145 for 4 h. This resulted in partial metabolic recovery, with NAD(P)H dehydrogenase activity and ATP levels reaching 65.60 ± 12.29% and 49.07 ± 0.14% of control values, respectively.

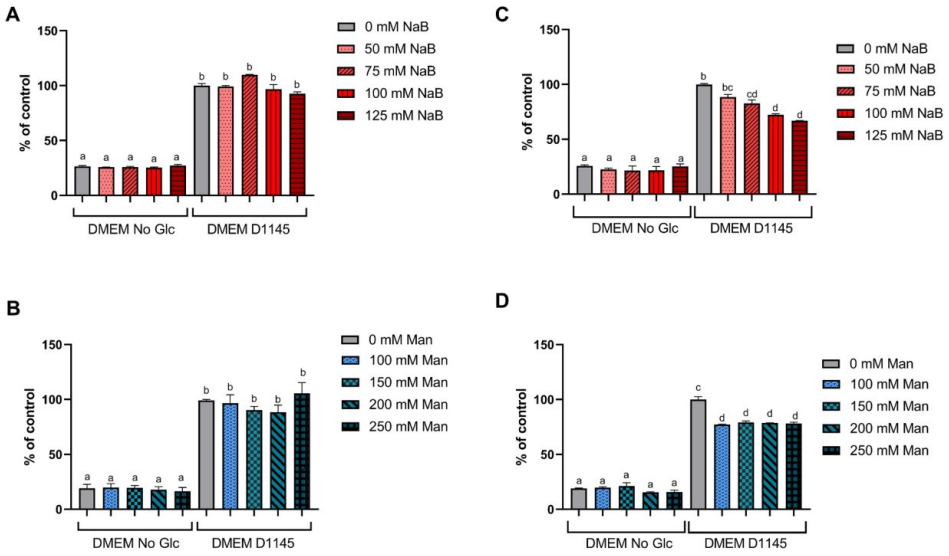


Fig. 4. Sodium butyrate (NaB) is not utilized as an energy source in Caco-2 cells. Caco-2 cells were seeded at 1×10^5 cells/well, grown for 24 h, washed with PBS and media changed to DMEM D1145 (no glutamine or sodium pyruvate) or DMEM No Glc (no glutamine, sodium pyruvate or glucose) media for 16 h. Cells were then treated with NaB or mannitol (Man) solutions in DMEM D1145 or DMEM No Glc for 4 h. (A, B) MTS assay and (C, D) intracellular ATP expressed as % of control (0 mM NaB/Man in DMEM D1145). Cells treated with DMEM No Glc for 16 h and subsequently to DMEM D1145 for 4 h were 65.60 ± 12.29 % for the MTS assay and 49.07 ± 0.14 % for the ATP assay. Data represents the mean ± SEM from biological triplicates and technical duplicates. Statistical analysis was assessed by one-way ANOVA with Tukey's multiple comparisons. Significant differences are indicated with different letters ($P < 0.05$).

3.5. NaB increases Caspase-3 (an early apoptosis indicator)

Since TEER, Papp and ATP levels were adversely affected by 75-125 mM NaB, the activity level of the early apoptotic marker, Caspase-3 (Porter & Jänicke, 1999; Ruemmele, 2003), was quantified in undifferentiated Caco-2 cells treated with NaB at these concentrations (Fig. 5). Both NaB concentrations induced a significant increase in Caspase-3 activity compared to media alone ($P < 0.05$), with 125 mM NaB treatment causing the highest Caspase 3 activity in Caco-2 cells. ($P < 0.05$), significantly higher than Man at the equivalent osmolality. There was no statistical difference in the % of cytotoxicity (measured as LDH release in the apical chamber of Caco-2 monolayers) for 75 and 125 mM NaB (Fig. S3A) compared to monolayers in media alone ($P > 0.05$).

3.6. NaB induces mRNA expression of butyrate transporters, stress markers and cytokines

To determine whether NaB induces upregulation of butyrate transporters (Monocarboxylate Transporter 1 (MCT-1) and Sodium-Coupled Monocarboxylate Transporter 1 (SMCT-1) or the first enzyme of β-oxidation Short-Chain Acyl-CoA Dehydrogenase (SCAD), mRNA transcript levels were measured in Caco-2 monolayers treated with NaB at 75 mM and 125 mM (Fig. 6). Both 75 and 125 mM NaB significantly increased SMCT-1 mRNA transcript levels compared to the monolayers treated with media alone ($P < 0.05$), whilst only 125 mM NaB significantly upregulated MCT-1 expression ($P < 0.05$). No significant changes were observed in SCAD mRNA levels in NaB-treated monolayers compared to the media control ($P > 0.05$).

To determine whether NaB treatment causes stress or initiates an inflammatory response, mRNA transcript levels of the water transport channel aquaporin 3 (AQP-3) (Grauso et al., 2019; Yde et al., 2021), stress markers p21 ($p21^{Cip1/Waf1}$) and 70 kDa heat shock protein (HSP-70) (Renis et al., 2008), and pro-inflammatory cytokines, Interleukin 6 (IL-6), Interleukin 8/CXC chemokine ligand 8 (IL-8) and Tumor Necrosis Factor (TNF) (Iglesias et al., 2020; Jung et al., 1995) were measured. As shown in Fig. 6, NaB did not affect AQP-3 mRNA, whereas 250 mM Man (osmolality = 125 mM NaB) significantly reduced AQP-3 mRNA levels compared to media alone ($P < 0.05$). Both 75 mM and 125 mM NaB treatments significantly increased p21, HSP-70, IL-8, and TNF mRNA transcripts compared to monolayers treated with media alone ($P < 0.05$); However, only 125 mM NaB significantly increased IL-6 mRNA expression compared to media control ($P < 0.05$). Treatment with Man at similar osmolality did not significantly alter mRNA levels of p21, HSP-70, IL-6, IL-8, or TNF ($P > 0.05$).

3.7. Dexamethasone promotes recovery of Caco-2 monolayers treated with 75 mM NaB

To assess whether the adverse effects of NaB on epithelial integrity could be reversed, we tested dexamethasone, a synthetic glucocorticoid known to regulate stress markers such as HSPs (Urayama et al., 1998), suppress pro-inflammatory cytokines, and stabilize barrier function in conditions like inflammatory bowel disease (L. Liu et al., 2009; Schreiber et al., 1998) and necrotizing enterocolitis (Lu et al., 2021). In our study, Caco-2 monolayers were treated with NaB under hyperosmotic conditions, with osmolality levels exceeding physiological norms, mimicking pathological states like Crohn's disease. To evaluate dexamethasone's restorative effect, 10 μM was added during a 24-h recovery phase following NaB treatment. This concentration of dexamethasone was not cytotoxic, as determined by LDH release (Fig. S3B). Treatment with 75 mM NaB reduced TEER values to 506 ± 117.02 Ω × cm^2. Subsequent removal of NaB and addition of dexamethasone significantly restored TEER to 931.70 ± 35.59 Ω × cm^2 at 24 h ($P < 0.05$). However, monolayers treated with 125 mM NaB did not recover with dexamethasone administration. Post-treatment, mRNA analysis (Fig. 7B) showed no significant differences in stress marker levels (HSP-70, p21, IL-8) or inflammation (IL-6 or TNF) in Caco-2 monolayers treated with 75 mM NaB + dexamethasone compared to Caco-2

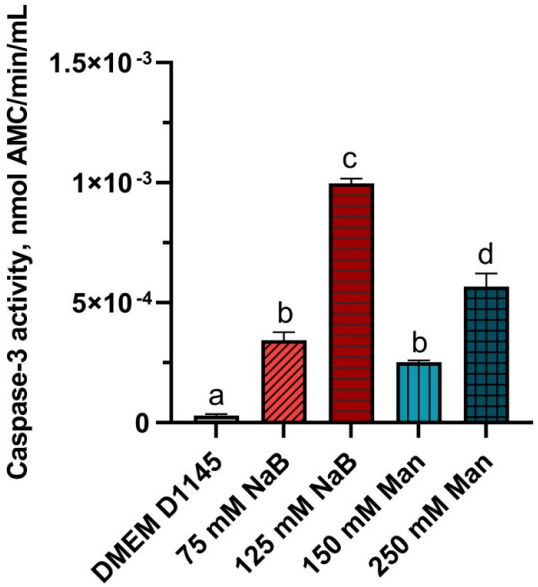


Fig. 5. Sodium butyrate (NaB) increases early apoptosis activity (Caspase-3). Caspase-3 activity in undifferentiated Caco-2 cells treated with NaB or mannitol (Man) for 4 h. Results are expressed as nmol of 7-Amino-4-methyl-coumarin—AMC—released per min per mL of cell lysate. DMEM D1145 = cells in DMEM. The assay positive control was isolated human Caspase-3 (1 μg/mL, without cells) which gave units of $4.43 \times 10^{-3} \pm 0.75 \times 10^{-3}$ nmol AMC/min/mL. Results are presented as the average of a biological triplicate and a technical duplicate ± SEM. Statistical difference between treatments was assessed by one-way ANOVA with Tukey's multiple comparison and it is indicated by a different letter ($P < 0.05$).

monolayers treated with dexamethasone only ($P < 0.05$). However, IL-6 and TNF mRNA expression were significantly elevated in monolayers treated with 125 mM NaB + dexamethasone compared to controls ($P < 0.05$). Notably, expression levels of stress and inflammatory markers were lower in dexamethasone-treated DMEM D1145 control monolayers compared to untreated DMEM D1145. The $2^{-\Delta\Delta Ct}$ normalized values for control Caco-2 monolayers were: HSP-70 = 47.24 ± 2.06, p21 = 386.7 ± 86.85, IL-6 = 263 ± 119.9, IL-8 = 164.8 ± 27.24, and TNF = 6.28 ± 1.65.

4. Discussion

Our study demonstrated that high concentrations of NaB (50–125 mM) significantly reduced TEER and increased paracellular permeability in a dose-dependent manner in Caco-2 barriers, with no recovery observed after treatment removal. NaB does not serve as an energy substrate, as shown by reduced ATP levels and unchanged cellular NAD(P)H-dependent oxidoreductase activity (MTS assay). However, it is actively transported into Caco-2 cells, as evidenced by increased mRNA expression of the butyrate transporters MCT-1 and SMCT-1 at 125 mM. NaB at 75 and 125 mM also activates the early apoptosis marker, Caspase-3, and uniquely elevates stress markers (p21, HSP-70) and pro-inflammatory cytokines (IL-6, IL-8, TNF). Importantly, while the induction of stress and inflammation markers was specific to NaB, TEER reductions were observed only under hyperosmotic conditions, suggesting an interplay between NaB-specific effects and hyperosmolarity. Treatment with 75 mM NaB followed by 24 h of dexamethasone restored TEER, reduced stress and quenched inflammation. These findings establish 75 mM NaB-treated Caco-2 monolayers as a robust *in vitro* model for studying a leaky, damaged gut.

We initially investigated the impact of NaB on the permeability of Caco-2 monolayers using two key metrics: TEER and Lucifer Yellow apparent permeability (Papp). High concentrations of NaB (50–125 mM) significantly reduced TEER values, with concentrations ≥75 mM also significantly increasing Lucifer Yellow permeability, clearly indicating compromised barrier integrity. Importantly, removal of NaB after treatment did not lead to monolayer recovery. These results align with Kondrashina et al. (2021), who reported reduced TEER at NaB concentrations ranging from 50 to 250 mM and enhanced paracellular permeability to lactulose and Man at higher concentrations (150-250 mM). Specifically, Kondrashina et al. observed that 125 mM NaB reduced TEER to 408 ± 52 Ω × cm^2 and notably increased lactulose leakage relative to Man. TEER results at 125 mM NaB in the current study were considerably lower, likely due to inherent Caco-2/HT29-MTX clone variabilities (Hevia et al., 2023). However, our findings at 75 mM NaB closely match Kondrashina's results at 125 mM, suggesting that targeting TEER thresholds rather than specific compound concentrations might yield more consistent results for "leaky" gut models. Consistent with these observations, Peng et al. (2007) also found that prolonged treatment (96 h) to 8 mM NaB significantly reduced TEER and increased permeability to inulin-FITC. Similarly, *ex vivo* studies by Mariadason et al. (1997) demonstrated increased transepithelial conductance and enhanced [51Cr]-EDTA flux in rat distal colon tissues treated with 10 mM butyrate for 4 h (Mariadason et al., 1997). Together, these findings show that NaB induces a pronounced and non-reversible loss of barrier integrity.

To delineate whether the barrier disruption imposed by NaB was compound-specific or a consequence of hyperosmotic stress, the NaB effects were compared to osmotically matched Man. While all tested Man concentrations (100-250 mM) transiently reduced TEER within 6 h, complete barrier recovery was observed by 24 h. Notably, when both NaB and Man were tested under strictly controlled, isosmotic conditions (348.67 ± 1.0 mOsm/kg), neither compound reduced monolayer TEER. These results together with HSP70 mRNA increases, clearly indicate that osmotic stress plays a role in cellular responses to >75 mM NaB. Our findings are also consistent with those of Adesina et al. (2023, 2021), who reported elevated HSP70 protein levels and mRNA expression in Caco-2 cells treated with 10–20 mM NaB for 24 h, suggesting a stress response mechanism induced by butyrate (Adesina et al., 2021, 2023). However, stress alone does not explain the sustained barrier disruption after NaB removal. The lack of recovery suggests that NaB induces persistent permeability changes, making it useful for modeling a stable leaky gut *in vitro*. However, this limits its relevance for simulating normal gut closure and may instead support its use to model pathological conditions like necrotizing enterocolitis in the infant.

Our study demonstrates that >75 mM NaB treatment impacts energy metabolism in Caco-2 cells, as evidenced by significantly reduced ATP levels but not cellular NAD(P)H-dependent oxidoreductases activity (MTS assay). This is in agreement with Kondrashina et al. (2021) who observed no significant changes in cellular reductase activity in Caco-2 cells treated for 4 h with NaB (50–250 mM) in DMEM (4500 mg/L glucose). Conversely, Peng et al. (2007) found that 8 mM NaB significantly reduced reductase activity after prolonged treatment (72 h), accompanied by increased cell detachment, indicating cytotoxicity rather than purely metabolic inhibition (Peng et al., 2007).

Caco-2 cells, like other cancerous cells, predominantly rely on glycolysis rather than oxidative phosphorylation for energy, a phenomenon known as the Warburg effect (Vander Heiden et al., 2009). Our results confirm this metabolic dependency, as glucose deprivation significantly reduced both cellular reductase activity and ATP levels, demonstrating that NaB was not used as an alternative oxidative substrate.

Previous studies have highlighted that butyrate's effects depend on concentration and nutrient conditions. Donohoe et al. (2012) observed

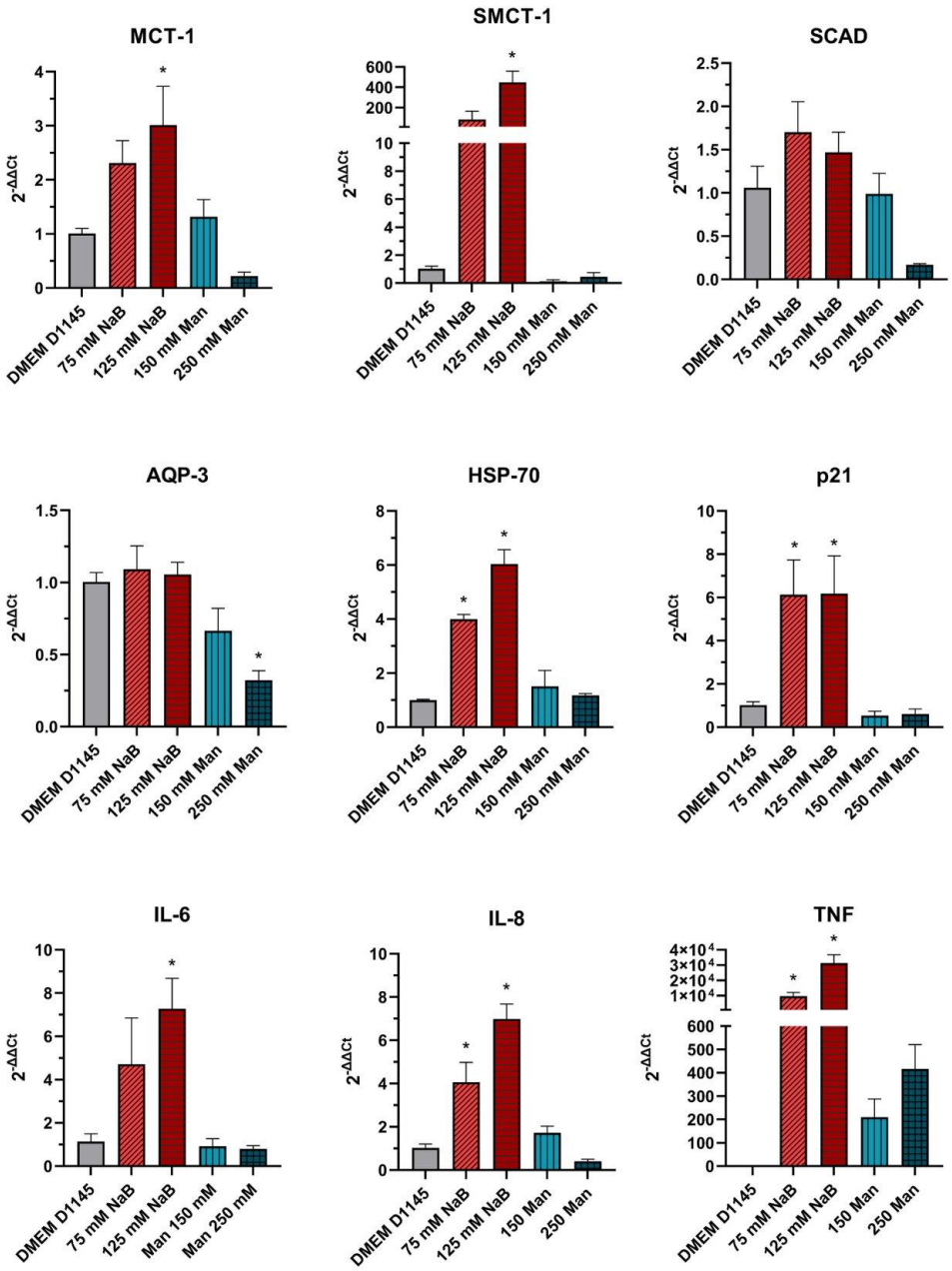


Fig. 6. Sodium butyrate (NaB) induces mRNA expression of butyrate transporters, stress markers and cytokines. 20-day Caco-2 monolayers treated for 24 h with NaB or mannitol (Man). Messenger RNA transcript levels of Sodium-Coupled Monocarboxylate Transporter 1 (SMCT1), Monocarboxylate Transporter 1 (MCT1), Short-Chain Acyl-Coenzyme A Dehydrogenase (SCAD), Aquaporin-3 (AQP-3), Heat-Shock Protein-70 (HSP-70), cyclin-dependent kinase inhibitor 1 (p21), Interleukin 6 and 8 (IL-6, IL-8) and Tumor Necrosis Factor (TNF) were quantified using RT-qPCR and normalized to the housekeeping gene RPLP0 mRNA and the control condition (monolayers in DMEM D1145 only) via the $2^{-\Delta\Delta Ct}$ method. Data represent the mean ± SEM from biological triplicates and technical duplicates. Statistical analysis was conducted using One-way ANOVA with Dunnet's multiple comparisons. The asterisk represents a significant difference to DMEM D1145 ($P < 0.05$).

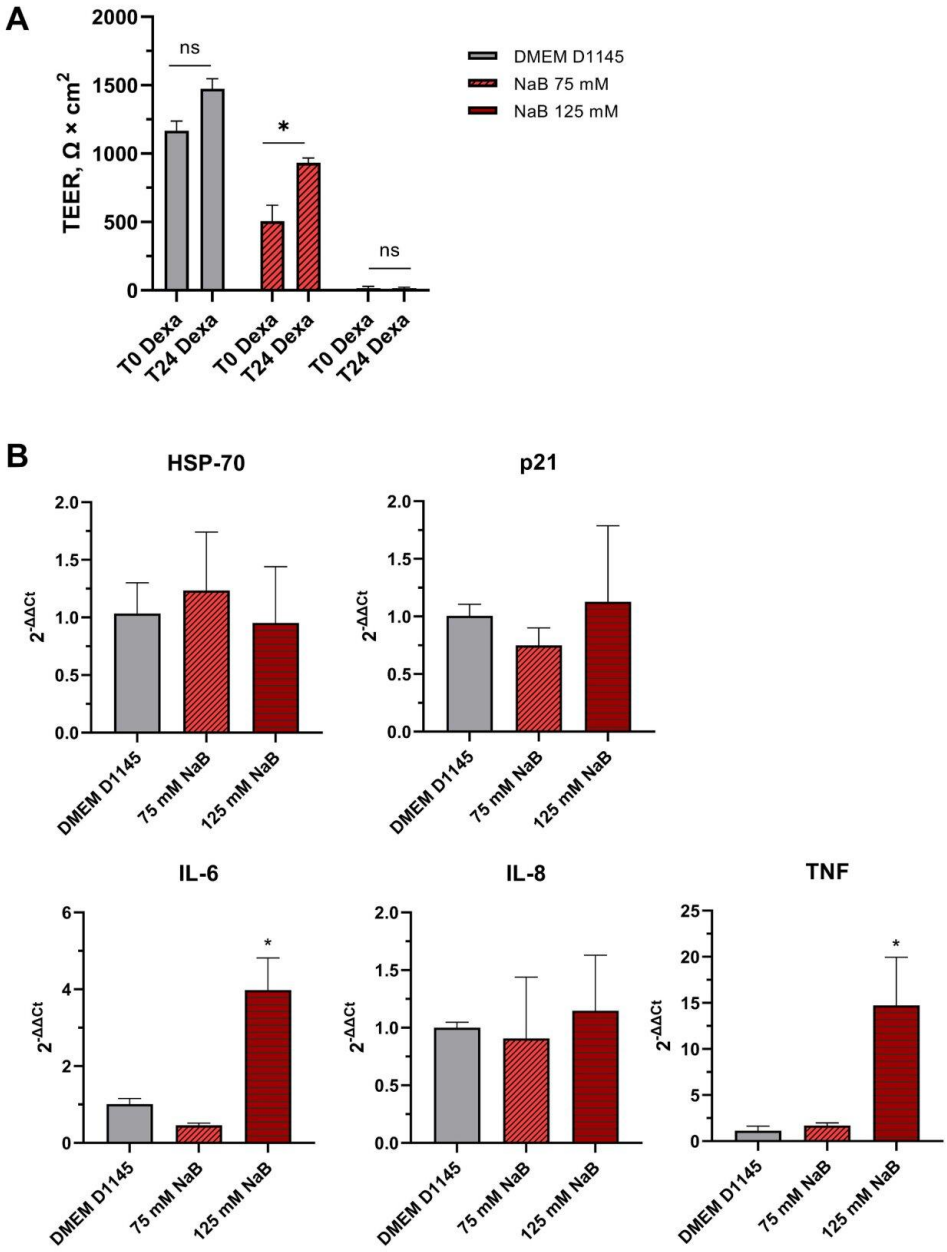


Fig. 7. Dexamethasone (Dexa) promotes recovery of Caco-2 monolayers treated with 75 mM sodium butyrate (NaB). Caco-2 monolayers were treated with 75/125 mM NaB for 24 h, washed with HBSS, and treated with 10 μM dexamethasone in DMEM D1145 for a further 24 h. (A) TEER values were recorded pre- (T0 Dexa) and post- (T24 Dexa) dexamethasone treatment. DMEM D1145 = control monolayers treated with 10 μM dexamethasone. DMEM D1145 TEER at T0 was = 1167.83 ± 69.72 Ω × cm^2. (B) mRNA transcript levels of Heat-Shock Protein-70 (HSP-70), cyclin-dependent kinase inhibitor 1 (p21), Interleukin 6 and 8 (IL-6, IL-8) and Tumor Necrosis Factor (TNF) in Caco-2 monolayers post dexameathsone treatment. RT-qPCR data was normalized to the housekeeping gene *RPLP0* mRNA and the control condition (DMEM D1145 + dexamethasone) via the $2^{-\Delta\Delta Ct}$ method. Data represents the mean ± SEM from biological triplicates and technical duplicates. Statistical analysis was conducted using (A) two-way ANOVA with Tukey's multiple comparisons or (B) one-way ANOVA with Dunnet's multiple comparisons. The asterisk represents a significant difference to (A) T0 or (B) DMEM D1145 + dexamethasone ($P < 0.05$).

in HCT116 colon cancer cells that low butyrate concentrations (0.5 mM) promoted cell proliferation under low-glucose conditions (0.5 mM glucose) through β-oxidation (Etomoxir + BrdU incorporation). Conversely, treatment with higher butyrate concentrations (0.5 mM glucose and 5 mM butyrate) or higher-glucose levels (25 mM glucose and 0.5-5 mM butyrate) inhibited cell proliferation similarly to the HDAC inhibitor Trichostatin A (Donohoe et al., 2012). In our model, NaB did not serve as an alternative fuel source for Caco-2 cells, and the dose-dependent reduction in ATP is therefore consistent with its HDAC-inhibitory activity. This interpretation is supported by Gommers et al. (2022), who also reported reduced ATP levels in Caco-2 cells following NaB (8 mM) treatment (Gommers et al., 2022). Hyperosmotic stress may additionally contribute, as Man controls caused a smaller ATP decrease, and hyperosmolarity has been shown to reduce ATP content in epithelial cells (Grauso et al., 2019).

Supporting this interpretation, our data also indicate active internalization of NaB by Caco-2 cells, as evidenced by the significantly lower total recovery of NaB from the apical and basolateral compartments after 24 h incubation. In contrast, HPLC quantification showed that Man was detected in the basolateral compartment, but its total recovery matched the initial apical concentration, indicating it was transported paracellularly without cellular uptake. Consistently, NaB treatment increased mRNA expression of the butyrate transporters MCT1 and SMCT1 without altering expression of the β-oxidation enzyme SCAD. These findings further suggest that intracellular NaB is not directed toward oxidative metabolism but instead may exert effects as an epigenetic regulator, potentially through HDAC inhibition.

In our study, treatment with 75 and 125 mM NaB significantly increased the activity of the early apoptotic marker, Caspase-3, in Caco-2 cells. While osmotic controls using 150 and 250 mM Man also showed elevated Caspase-3 activity, the increase observed with 250 mM Man was less pronounced than that seen with 125 mM NaB. This suggests that this effect is not solely attributable to hyperosmotic stress but rather reflects a NaB-specific response. Caspase-3 activation represents the initiation of apoptotic signaling and is not, by itself, evidence of completed apoptotic cell death. Consistent with this, LDH release did not increase, and MTS activity remained unchanged in Caco-2 cells, demonstrating preserved membrane integrity and metabolic viability. Nevertheless, we acknowledge that early apoptotic events may influence epithelial permeability.

Nonetheless, previous studies demonstrated the pro-apoptotic effects of butyrate in Caco-2 cells (Avivi-Green et al., 2002; Chirakkal et al., 2006; Peng et al., 2007; Ruemmele, 2003). Ruemmele et al. (2003) reported a dose-dependent increase in apoptosis (Annexin V/propidium iodide) in Caco-2 cells treated with 5–100 mM butyrate for 48 h, along with activation of caspase-3 and -9 (Ruemmele, 2003). Similarly, Avivi-Green et al. (2002) observed that 5–10 mM butyrate significantly increased apoptosis (cytoplasmic nucleosome concentration) and upregulated caspase-3 activity (2131 ± 640% above control) and expression (Western blot) (Avivi-Green et al., 2002). Peng et al. (2007) demonstrated that 8 mM NaB induced apoptosis markers, including DNA fragmentation (electrophoresis) and PARP cleavage (immunoblotting) (Peng et al., 2007). Chirakkal et al. also demonstrated that butyrate (≥5 mM, 24 h treatment) induces apoptosis in HCT116 cells (nuclear condensation and PARP cleavage) without significant cellular damage (clonogenic assay) (Chirakkal et al., 2006). This apoptotic effect is mediated by increased binding of the transcription factor Sp3 to Sp1/Sp3 sites, causing upregulation of the transcription of apoptosis-related genes (Chirakkal et al., 2006). Additionally, Donohoe et al. (2012) demonstrated in HCT116 cells that butyrate (3-day exposure to 0.5–5 mM) increased apoptosis (Annexin staining, $P < 0.05$) and histone H3 acetylation (Western blot, $P < 0.05$). In our study, significant increases in p21 mRNA expression were observed in Caco-2 monolayers treated with >75 mM NaB. Previous studies have demonstrated that p21, a key regulator of cell proliferation and apoptosis (Macleod et al., 1995), is upregulated by butyrate (mRNA expression, 5-20 mM; $P < 0.05$) through histone hyperacetylation in HT29 cells (Archer et al., 1998; Siavoshian, 2000). Collectively, these findings reinforce our observation that NaB induces apoptosis pathways in intestinal epithelial cells, likely through mechanisms involving histone acetylation and transcriptional modulation. Transcript levels of TNF were significantly increased in monolayers treated with >75 mM NaB. Such a remarkable increase warrants an assessment of a panel of cytokines in the apical and basolateral chambers of Caco-2 monolayers treated with NaB and questions its use to create a non-inflamed barrier. Previously, Kondrashina et al. (2021) reported a 12-fold increase in TNF secretion in the apical chamber (up to 12-fold at 150 mM NaB).

It was interesting to observe that 10 μM dexamethasone, a corticosteroid frequently used in managing IBD, supported the recovery of NaB-treated monolayers (L. Liu et al., 2009; Schreiber et al., 1998). In the 75 mM NaB-treated monolayers, the treatment with dexamethasone significantly increased TEER (T0 dexamethasone *vs.* T24 dexamethasone) and restored the inflammation/stress markers to the control condition (HSP70, p21, TNF). This suggests that 75 mM NaB-treated Caco-2 monolayers could offer a physiologically relevant *in vitro* model of IBD or necrotizing enterocolitis.

Traditional *in vitro* models of intestinal inflammation most frequently use pro-inflammatory cytokines such as TNF, IL-1β, IFN-γ (Macedo et al., 2023a) or chemical inducers such as dextran sulfate sodium to disrupt epithelial barrier integrity (Araki et al., 2012; Uemura et al., 2024). Cytokine-induced permeability occurs through NF-κB– and MLCK-dependent contraction of the perijunctional actomyosin ring, leading to tight-junction remodeling (Meyer et al., 2023; Turner, 2009) and, in some cases a reversible decrease in TEER (Droessler et al., 2021; Marr et al., 2023). We have no evidence that this inflammatory pathway induces HSP70 or activate its receptor HSF1 (Dayalan Naidu & Dinkova-Kostova, 2017). Indeed, TNF has been shown to inhibit HSF1 and reduce HSP70 synthesis (Schett et al., 2003). This is important, as HSP70 is increased in both IBD (Samborski & Grzymisławski, 2015) and NEC (Afrazi et al., 2012). Dextran sulfate sodium, although widely used *in vivo*, is predominantly cytotoxic rather than inflammatory in epithelial monocultures (Araki et al., 2012) and is incompatible with PCR-based analyses due to inhibition of DNA polymerases (Lin et al., 2025), limiting its utility for mechanistic studies of epithelial signaling.

In contrast, high-concentration NaB induces a multifactorial injury phenotype that integrates (i) sustained TEER loss with no recovery, (ii) apoptosis, (iii) cytokine induction, and (iv) robust activation of stress-response pathways including HSP70. Moreover, in our study, Caco-2 monolayers were treated with NaB under hyperosmotic conditions, with a resulting average osmolality significantly exceeding physiological levels. This mimics pathological scenarios where persistent hyperosmolarity is linked to intestinal barrier dysfunction, such as Crohn's disease (Schilli et al., 1982). This combination integrates inflammatory, osmotic, and metabolic stress and therefore captures aspects of chronic epithelial injury not reproduced by cytokines or dextran sodium sulfate. Together, these features position the NaB model as a mechanistically distinct and complementary tool for studying IBD and necrotizing enterocolitis.

Future work should include comparisons with IL-1β and TNF or LPS, commonly used to replicate IBD *in vitro* using Caco-2 cells (Mobbs et al., 2024; Xu et al., 2019), evaluating tight junction proteins and permeability, as well as inflammation and oxidative stress markers (Macedo et al., 2023b). Additionally, future studies should include a co-culture model with immune cells to better elucidate the effect of high concentration of NaB on inflammation.

Interestingly, treatment of Caco-2 monolayers with 100- 250 mM Man (osmolality) resulted in a dose-dependent and temporary decrease in TEER, that allowed full recovery after removal. Similarly, Inokuchi et al. (2009) reported that hyperosmotic media containing 100 mM Man caused a decline in TEER (90 min exposure) with full recovery at lower concentrations (100 mM) (Inokuchi et al., 2009). Notably, 100 and 150 mM Man increased the activity of the apoptotic marker Caspase-3. While

no direct studies report Man-induced apoptosis in Caco-2 cells, similar effects have been observed in endothelial cells, where hyperosmolar Man induced apoptosis (Malek et al., 1998). Finally, 250 mM Man significantly reduced the mRNA expression of AQP-3, a marker of osmotic stress (Grauso et al., 2019; Yde et al., 2021). This is consistent with Grauso et al. (2019), who found a similar reduction in AQP-3 expression under hyperosmotic conditions (680 mOsm/L Man; $P < 0.05$) (Grauso et al., 2019).

Although Man treatment produced a reversible increase in paracellular permeability, its effects are limited to hyperosmotic stress. Elevated luminal osmolality is more characteristic of pathological conditions than normal infant physiology, and Man alone does not recapitulate the multifactorial features of either the immature intestinal barrier or an inflamed gut. However, because hyperosmotic stress leads to epithelial cell shrinkage and water loss, this model may also serve as a valuable *in vitro* platform for evaluating products designed to support sustained cellular hydration. These results collectively support the interpretation that the Caco-2 response to NaB is compound-specific and likely mediated by epigenetic and transcriptional regulatory pathways.

The work demonstrates that NaB treatment induces a sustained, multifactorial dysfunction in differentiated Caco-2 monolayers, creating a stable damaged barrier phenotype persisting for 24 h. This phenotype involves the activation of apoptotic, inflammatory, and stress-response pathways. This NaB-induced gut barrier model provides a novel and suitable *in vitro* barrier for investigating mechanisms underlying barrier repair, rehydration, and anti-inflammatory interventions using various compounds.

CRediT authorship contribution statement

Francesca Bietto: Writing – review & editing, Writing – original draft, Visualization, Validation, Investigation, Formal analysis, Data curation, Conceptualization. **Elena Arranz:** Writing – review & editing, Supervision, Methodology. **Monica Mechoud:** Writing – review & editing, Methodology, Investigation. **Eva Rath:** Writing – review & editing, Validation, Supervision, Methodology. **Alice J. Lucey:** Writing – review & editing, Validation, Supervision, Methodology. **Linda Giblin:** Writing – review & editing, Validation, Supervision, Resources, Project administration, Methodology, Funding acquisition, Conceptualization.

Data availability statement

All data supporting the findings of this study are included in the article's Results and Supplementary Material sections, including all figures and tables. No additional data were generated or analyzed beyond what is presented in this publication.

Declaration of competing interest

The authors declare that they have no known competing financial interests or personal relationships that could have appeared to influence the work reported in this paper.

Acknowledgements

This research was supported by Teagasc (InfBar MDBY1370). Francesca Bietto is in receipt of a Teagasc Walsh Scholarship 2021007.

Appendix A. Supplementary data

Supplementary data to this article can be found online at https://doi.org/10.1016/j.jnphys.2026.100021.

References

Adesina, P. A., Isayama, K., Sitolo, G. C., Yamamoto, Y., & Suzuki, T. (2021). Propionate and dietary fermentable fibers upregulate intestinal heat shock protein70 in intestinal Caco-2 cells and mouse Colon. *Journal of Agricultural and Food Chemistry, 69*(30), 8460–8470. https://doi.org/10.1021/acs.jafc.1c03036

Adesina, P. A., Saeki, I., Yamamoto, Y., & Suzuki, T. (2023). N-butyrate increases heat shock protein 70 through heat shock factor 1 and AMP-activated protein kinase pathways in human intestinal Caco-2 cells. *Archives of Biochemistry and Biophysics, 736*, Article 109525. https://doi.org/10.1016/j.abb.2023.109525

Afrazi, A., Sodhi, C. P., Good, M., Jia, H., Siggers, R., Yazji, I., Ma, C., Neal, M. D., Prindle, T., Grant, Z. S., Branca, M. F., Ozolek, J., Chang, E. B., & Hackam, D. J. (2012). Intracellular heat shock Protein-70 negatively regulates TLR4 signaling in the newborn intestinal epithelium. *The Journal of Immunology, 188*(9), 4543–4557. https://doi.org/10.4049/jimmunol.1103114

Araki, Y., Bamba, T., Mukaisho, K.-I., Kanauchi, O., Ban, H., Bamba, S., Andoh, A., Fujiyama, Y., Hattori, T., & Sugihara, H. (2012). Dextran sulfate sodium administered orally is depolymerized in the stomach and induces cell cycle arrest plus apoptosis in the colon in early mouse colitis. *Oncology Reports, 28*(5), 1597–1605. https://doi.org/10.3892/or.2012.1969

Archer, S. Y., Meng, S., Shei, A., & Hodin, R. A. (1998). P21 ^{WAF1} is required for butyrate-mediated growth inhibition of human colon cancer cells. *Proceedings of the National Academy of Sciences, 95*(12), 6791–6796. https://doi.org/10.1073/pnas.95.12.6791

Avivi-Green, C., Polak-Charcon, S., Madar, Z., & Schwartz, B. (2002). Different molecular events account for butyrate-induced apoptosis in two human Colon cancer cell lines. *The Journal of Nutrition, 132*(7), 1812–1818. https://doi.org/10.1093/jn/132.7.1812

Brown, A. J., Goldsworthy, S. M., Barnes, A. A., Eilert, M. M., Tcheang, L., Daniels, D., Muir, A. I., Wigglesworth, M. J., Kinghorn, I., Fraser, N. J., Pike, N. B., Strum, J. C., Steplewski, K. M., Murdock, P. R., Holder, J. C., Marshall, F. H., Szekeres, P. G., Wilson, S., Ignar, D. M., … Dowell, S. J. (2003). The orphan G Protein-coupled Receptors GPR41 and GPR43 are activated by propionate and other short chain carboxylic acids. *Journal of Biological Chemistry, 278*(13), 11312–11319. https://doi.org/10.1074/jbc.M211609200

Canani, R. B. (2011). Potential beneficial effects of butyrate in intestinal and extraintestinal diseases. *World Journal of Gastroenterology, 17*(12), 1519. https://doi.org/10.3748/wjg.v17.i12.1519

Catassi, C., Bonucci, A., Coppa, G. V., Carlucci, A., & Giorgi, P. L. (1995). Intestinal permeability. Changes during the first month: Effect of natural versus artificial feeding. *Journal of Pediatric Gastroenterology and Nutrition, 21*(4), 383–386. https://doi.org/10.1097/00005176-199511000-00003

Chirakkal, H., Leech, S. H., Brookes, K. E., Prais, A. L., Waby, J. S., & Corfe, B. M. (2006). Upregulation of BAK by butyrate in the colon is associated with increased Sp3 binding. *Oncogene, 25*(54), 7192–7200. https://doi.org/10.1038/sj.onc.1209702

Dalile, B., Van Oudenhove, L., Vervliet, B., & Verbeke, K. (2019). The role of short-chain fatty acids in microbiota–gut–brain communication. *Nature Reviews Gastroenterology & Hepatology, 16*(8). https://doi.org/10.1038/s41575-019-0157-3. Article 8.

Dayalan Naidu, S., & Dinkova-Kostova, A. T. (2017). Regulation of the mammalian heat shock factor 1. *FEBS Journal, 284*(11), 1606–1627. https://doi.org/10.1111/febs.13999

Ding, D., Liu, Z., Zhao, L., Geng, H., Liang, Z., & Yu, D. (2019). Role of PI3K/Akt pathway in Benzidine-induced proliferation in SV-40 immortalized human uroepithelial cell. *Translational Cancer Research, 8*(4), 1301–1310. https://doi.org/10.21037/tcr.2019.07.14

Donohoe, D. R., Collins, L. B., Wali, A., Bigler, R., Sun, W., & Bultman, S. J. (2012). The warburg effect dictates the mechanism of butyrate-mediated histone acetylation and cell proliferation. *Molecular Cell, 48*(4), 612–626. https://doi.org/10.1016/j.molcel.2012.08.033

Droessler, L., Cornelius, V., Markov, A. G., & Amasheh, S. (2021). Tumor necrosis factor alpha effects on the porcine intestinal epithelial barrier include enhanced expression of TNF receptor 1. *International Journal of Molecular Sciences, 22*(16), 8746. https://doi.org/10.3390/ijms22168746

Fogh, J., Wright, W. C., & Loveless, J. D. (1977). Absence of HeLa cell contamination in 169 cell lines derived from human tumors. *Journal of the National Cancer Institute, 58*(2), 209–214. https://doi.org/10.1093/jnci/58.2.209

Gommers, L. M. M., Leermakers, P. A., Van Der Wijst, J., Roig, S. R., Adella, A., Van De Wal, M. A. E., Bindels, R. J. M., De Baaij, J. H. F., & Hoenderop, J. G. J. (2022). Butyrate reduces cellular magnesium absorption independently of metabolic regulation in Caco-2 human colon cells. *Scientific Reports, 12*(1), Article 18551. https://doi.org/10.1038/s41598-022-21683-6

Grauso, M., Lan, A., Andriamihaja, M., Bouillaud, F., & Blachier, F. (2019). Hyperosmolar environment and intestinal epithelial cells: Impact on mitochondrial oxygen consumption, proliferation, and barrier function in vitro. *Scientific Reports, 9*(1). https://doi.org/10.1038/s41598-019-47851-9. Article 1.

Groschwitz, K. R., & Hogan, S. P. (2009). Intestinal barrier function: Molecular regulation and disease pathogenesis. *Journal of Allergy and Clinical Immunology, 124*(1), 3–20. https://doi.org/10.1016/j.jaci.2009.05.038

Hamer, H. M., Jonkers, D., Venema, K., Vanhoutvin, S., Troost, F. J., & Brummer, R.-J. (2008). Review article: The role of butyrate on colonic function. *Alimentary Pharmacology & Therapeutics, 27*(2), 104–119. https://doi.org/10.1111/j.1365-2036.2007.03562.x

Hevia, A., Ruas-Madiedo, P., Faria, M. A., Petit, V., Alves, B., Alvito, P., Arranz, E., Bastiaan-Net, S., Corredig, M., Dijk, W., Dupont, D., Giblin, L., Graf, B. A., Kondrashina, A., Ramos, H., Ruiz, L., Santos-Hernández, M., Soriano-Romaní, L., Tomás-Cobos, L., … Miralles, B. (2023). A shared perspective on *in Vitro* and *In Vivo* models to assay intestinal transepithelial transport of food compounds. *Journal of*

Agricultural and Food Chemistry, 71(49), 19265–19276. https://doi.org/10.1021/acs.jafc.3c05479
Hollander, D. (1999). Intestinal permeability, leaky gut, and intestinal disorders. *Current Gastroenterology Reports, 1*(5), 410–416. https://doi.org/10.1007/s11894-999-0023-5
Hubert, A., Cauliez, B., Chedeville, A., Husson, A., & Lavoinne, A. (2004). Osmotic stress, a proinflammatory signal in Caco-2 cells. *Biochimie, 86*(8), 533–541. https://doi.org/10.1016/j.biochi.2004.07.009
Iglesias, D. E., Cremonini, E., Fraga, C. G., & Oteiza, P. I. (2020). Ellagic acid protects Caco-2 cell monolayers against inflammation-induced permeabilization. *Free Radical Biology and Medicine, 152*, 776–786. https://doi.org/10.1016/j.freeradbiomed.2020.01.022
Inokuchi, H., Takei, T., Aikawa, K., & Shimizu, M. (2009). The effect of hyperosmosis on paracellular permeability in Caco-2 cell monolayers. *Bioscience, Biotechnology, and Biochemistry, 73*(2), 328–334. https://doi.org/10.1271/bbb.80538
Jung, H. C., Eckmann, L., Yang, S. K., Panja, A., Fierer, J., Morzycka-Wroblewska, E., & Kagnoff, M. F. (1995). A distinct array of proinflammatory cytokines is expressed in human colon epithelial cells in response to bacterial invasion. *Journal of Clinical Investigation, 95*(1), 55–65. https://doi.org/10.1172/JCI117676
Kondrashina, A., Brodkorb, A., & Giblin, L. (2021). Sodium butyrate converts Caco-2 monolayers into a leaky but healthy intestinal barrier resembling that of a newborn infant. *Food & Function, 12*(11), 5066–5076. https://doi.org/10.1039/D1FO00519G
Kosek, M. N., Lee, G. O., Guerrant, R. L., Haque, R., Kang, G., Ahmed, T., Bessong, P., Ali, A., Mduma, E., Peñataro Yori, P., Faubion, W. A., Lima, A. A. M., Paredes Olortegui, M., Mason, C., Babji, S., Singh, R., Qureshi, S., Kosek, P. S., Samie, A., … Network, the M.-E. (2017). Age and sex normalization of intestinal permeability measures for the improved assessment of enteropathy in infancy and early childhood: Results from the MAL-ED Study. *Journal of Pediatric Gastroenterology and Nutrition, 65*(1), 31–39. https://doi.org/10.1097/MPG.0000000000001610
Lea, T. (2015). Caco-2 cell line. In K. Verhoeckx, P. Cotter, I. López-Expósito, C. Kleiveland, T. Lea, A. Mackie, T. Requena, D. Swiatecka, & H. Wichers (Eds.), *The Impact of Food Bioactives on health: In vitro and ex vivo models* (pp. 103–111). Springer International Publishing. https://doi.org/10.1007/978-3-319-16104-4_10.
Lin, J., Zhang, J., Santiago, A. M., & Sun, Q. (2025). Optimized TRIzol–silica column RNA extraction for DSS-colitis: Resolving PCR inhibition. *Agricultural Products Processing and Storage, 1*(1), 24. https://doi.org/10.1007/s44462-025-00030-8
Liu, H., Wang, J., He, T., Becker, S., Zhang, G., Li, D., & Ma, X. (2018). Butyrate: A double-edged sword for health? *Advances in Nutrition, 9*(1), 21–29. https://doi.org/10.1093/advances/nmx009
Liu, L., Yuan, S., Long, Y., Guo, Z., Sun, Y., Li, Y., Niu, Y., Li, C., & Mei, Q. (2009). Immunomodulation of Rheum tanguticum polysaccharide (RTP) on the immunosuppressive effects of dexamethasone (DEX) on the treatment of colitis in rats induced by 2,4,6-trinitrobenzene sulfonic acid. *International Immunopharmacology, 9*(13–14), 1568–1577. https://doi.org/10.1016/j.intimp.2009.09.013
Lu, L., Lu, J., Yu, Y., & Claud, E. (2021). Necrotizing enterocolitis intestinal barrier function protection by antenatal dexamethasone and surfactant-D in a rat model. *Pediatric Research, 90*(4), 768–775. https://doi.org/10.1038/s41390-020-01334-0
Macedo, M. H., Dias Neto, M., Pastrana, L., Gonçalves, C., & Xavier, M. (2023a). Recent advances in cell-based in vitro models to recreate human intestinal inflammation. *Advanced Science, 10*(31), Article 2301391. https://doi.org/10.1002/advs.202301391
Macedo, M. H., Dias Neto, M., Pastrana, L., Gonçalves, C., & Xavier, M. (2023b). Recent advances in cell-based in vitro models to recreate human intestinal inflammation. *Advanced Science, 10*(31), Article 2301391. https://doi.org/10.1002/advs.202301391
Macleod, K. F., Sherry, N., Hannon, G., Beach, D., Tokino, T., Kinzler, K., Vogelstein, B., & Jacks, T. (1995). P53-dependent and independent expression of p21 during cell growth, differentiation, and DNA damage. *Genes & Development, 9*(8), 935–944. https://doi.org/10.1101/gad.9.8.935
Malek, A. M., Goss, G. G., Jiang, L., Izumo, S., & Alper, S. L. (1998). Mannitol at clinical concentrations activates multiple signaling pathways and induces apoptosis in endothelial cells. *Stroke, 29*(12), 2631–2640. https://doi.org/10.1161/01.STR.29.12.2631
Mariadason, J. M., Barkla, D. H., & Gibson, P. R. (1997). Effect of short-chain fatty acids on paracellular permeability in Caco-2 intestinal epithelium model. *American Journal of Physiology - Gastrointestinal and Liver Physiology, 272*(4), G705–G712. https://doi.org/10.1152/ajpgi.1997.272.4.G705
Marr, E. E., Mulhern, T. J., Welch, M., Keegan, P., Caballero-Franco, C., Johnson, B. G., Kasaian, M., Azizgolshani, H., Petrie, T., Charest, J., & Wiellette, E. (2023). A platform to reproducibly evaluate human colon permeability and damage. *Scientific Reports, 13*(1), 8922. https://doi.org/10.1038/s41598-023-36020-8
Ménard, S., Cerf-Bensussan, N., & Heyman, M. (2010). Multiple facets of intestinal permeability and epithelial handling of dietary antigens. *Mucosal Immunology, 3*(3), 247–259. https://doi.org/10.1038/mi.2010.5
Meyer, F., Wendling, D., Demougeot, C., Prati, C., & Verhoeven, F. (2023). Cytokines and intestinal epithelial permeability: A systematic review. *Autoimmunity Reviews, 22*(6), Article 103331. https://doi.org/10.1016/j.autrev.2023.103331
Mobbs, C. L., Darling, N. J., & Przyborski, S. (2024). An in vitro model to study immune activation, epithelial disruption and stromal remodelling in inflammatory bowel disease and fistulising Crohn's disease. *Frontiers in Immunology, 15*, Article 1357690. https://doi.org/10.3389/fimmu.2024.1357690
Otani, T., & Furuse, M. (2020). Tight junction structure and function revisited. *Trends in Cell Biology, 30*(10), 805–817. https://doi.org/10.1016/j.tcb.2020.08.004
Peng, L., He, Z., Chen, W., Holzman, I. R., & Lin, J. (2007). Effects of butyrate on intestinal barrier function in a Caco-2 cell monolayer model of intestinal barrier. *Pediatric Research, 61*(1), 37–41. https://doi.org/10.1203/01.pdr.0000250014.92242.f3
Peng, L., Li, Z.-R., Green, R. S., Holzmanr, I. R., & Lin, J. (2009). Butyrate enhances the intestinal barrier by facilitating tight junction assembly via activation of AMP-activated protein kinase in Caco-2 cell monolayers. *The Journal of Nutrition, 139*(9), 1619–1625. https://doi.org/10.3945/jn.109.104638
Porter, A. G., & Jänicke, R. U. (1999). Emerging roles of caspase-3 in apoptosis. *Cell Death & Differentiation, 6*(2), 99–104. https://doi.org/10.1038/sj.cdd.4400476
Renis, M., Calandra, L., Scifo, C., Tomasello, B., Cardile, V., Vanella, L., Bei, R., Fauci, L. L., & Galvano, F. (2008). Response of cell cycle/stress-related protein expression and DNA damage upon treatment of CaCo2 cells with anthocyanins. *British Journal of Nutrition, 100*(1), 27–35. https://doi.org/10.1017/S0007114507876239
Ruemmele, F. M. (2003). Butyrate induced Caco-2 cell apoptosis is mediated via the mitochondrial pathway. *Gut, 52*(1), 94–100. https://doi.org/10.1136/gut.52.1.94
Samborski, P., & Grzymisławski, M. (2015). The role of HSP70 heat shock proteinsin the pathogenesis and treatmentof inflammatory bowel diseases. *Advances in Clinical and Experimental Medicine, 24*(3), 525–530. https://doi.org/10.17219/acem/44144
Schett, G., Steiner, C.-W., Xu, Q., Smolen, J. S., & Steiner, G. (2003). TNFα mediates susceptibility to heat-induced apoptosis by protein phosphatase-mediated inhibition of the HSF1/hsp70 stress response. *Cell Death & Differentiation, 10*(10), 1126–1136. https://doi.org/10.1038/sj.cdd.4401276
Schilli, R., Breuer, R. I., Klein, F., Dunn, K., Gnaedinger, A., Bernstein, J., Paige, M., & Kaufman, M. (1982). Comparison of the composition of faecal fluid in Crohn's disease and ulcerative colitis. *Gut, 23*(4), 326–332. https://doi.org/10.1136/gut.23.4.326
Schreiber, S., Nikolaus, S., & Hampe, J. (1998). Activation of nuclear factor kappa B in inflammatory bowel disease. *Gut, 42*(4), 477–484. https://doi.org/10.1136/gut.42.4.477
Sheng, Y. H., & Hasnain, S. Z. (2022). Mucus and mucins: The underappreciated host defence system. *Frontiers in Cellular and Infection Microbiology, 12*, Article 856962. https://doi.org/10.3389/fcimb.2022.856962
Siavoshian, S. (2000). Butyrate and trichostatin A effects on the proliferation/differentiation of human intestinal epithelial cells: Induction of cyclin D3 and p21 expression. *Gut, 46*(4), 507–514. https://doi.org/10.1136/gut.46.4.507
Singh, V., Lee, G., Son, H., Koh, H., Kim, E. S., Unno, T., & Shin, J.-H. (2023). Butyrate producers, "the sentinel of Gut": Their intestinal significance with and beyond butyrate, and prospective use as microbial therapeutics. *Frontiers in Microbiology, 13*, Article 1103836. https://doi.org/10.3389/fmicb.2022.1103836
Stilling, R. M., Van De Wouw, M., Clarke, G., Stanton, C., Dinan, T. G., & Cryan, J. F. (2016). The neuropharmacology of butyrate: The bread and butter of the microbiota-gut-brain axis? *Neurochemistry International, 99*, 110–132. https://doi.org/10.1016/j.neuint.2016.06.011
Suzuki, T., Yoshida, S., & Hara, H. (2008). Physiological concentrations of short-chain fatty acids immediately suppress colonic epithelial permeability. *British Journal of Nutrition, 100*(2), 297–305. https://doi.org/10.1017/S0007114508888733
Turner, J. R. (2009). Intestinal mucosal barrier function in health and disease. *Nature Reviews Immunology, 9*(11), 799–809. https://doi.org/10.1038/nri2653
Uemura, I., Takahashi-Suzuki, N., Kita, F., & Satoh, T. (2024). Establishment of an in-vitro inflammatory bowel disease model using immunological differentiation of Caco-2 cells. *MethodsX, 13*, Article 102952. https://doi.org/10.1016/j.mex.2024.102952
Urayama, S., Musch, M. W., Retsky, J., Madonna, M. B., Straus, D., & Chang, E. B. (1998). Dexamethasone protection of rat intestinal epithelial cells against oxidant injury is mediated by induction of heat shock protein 72. *Journal of Clinical Investigation, 102*(10), 1860–1865. https://doi.org/10.1172/JCI2235
Vander Heiden, M. G., Cantley, L. C., & Thompson, C. B. (2009). Understanding the warburg effect: The metabolic requirements of cell proliferation. *Science, 324*(5930), 1029–1033. https://doi.org/10.1126/science.1160809
Weaver, L. T., Laker, M. F., & Nelson, R. (1984). Intestinal permeability in the newborn. *Archives of Disease in Childhood, 59*(3), 236–241. https://doi.org/10.1136/adc.59.3.236
Weström, B., Arévalo Sureda, E., Pierzynowska, K., Pierzynowski, S. G., & Pérez-Cano, F.-J. (2020). The immature gut barrier and its importance in establishing immunity in newborn mammals. *Frontiers in Immunology, 11*. https://www.frontiersin.org/articles/10.3389/fimmu.2020.01153.
Xu, P., Elamin, E., Elizalde, M., Bours, P. P. H. A., Pierik, M. J., Masclee, A. A. M., & Jonkers, D. M. A. E. (2019). Modulation of intestinal epithelial permeability by plasma from patients with Crohn's disease in a three-dimensional cell culture model. *Scientific Reports, 9*(1), 2030. https://doi.org/10.1038/s41598-018-38322-8
Yde, J., Keely, S. J., & Moeller, H. B. (2021). Expression, regulation and function of Aquaporin-3 in colonic epithelial cells. *Biochimica et Biophysica Acta (BBA) - Biomembranes, 1863*(7), Article 183619. https://doi.org/10.1016/j.bbamem.2021.183619

frontiers | Frontiers in Nutrition

TYPE Original Research
PUBLISHED 09 June 2025
DOI 10.3389/fnut.2025.1577369

Check for updates

OPEN ACCESS

EDITED BY
Giacomo Di Matteo,
Sapienza University of Rome, Italy

REVIEWED BY
Massimo Frangiamone,
Université de Lausanne, Switzerland
Tamara Hoppenbrouwers,
Wageningen University and
Research, Netherlands

*CORRESPONDENCE
Linda Giblin
✉ Linda.Giblin@teagasc.ie

RECEIVED 15 February 2025
ACCEPTED 07 May 2025
PUBLISHED 09 June 2025

CITATION
Bietto F, Arranz E, Miralles B, Gómez-Marín C, Rath E, Lucey AJ and Giblin L (2025) Using sodium glycodeoxycholate to develop a temporary infant-like gut barrier model, *in vitro*. *Front. Nutr.* 12:1577369.
doi: 10.3389/fnut.2025.1577369

COPYRIGHT
© 2025 Bietto, Arranz, Miralles, Gómez-Marín, Rath, Lucey and Giblin. This is an open-access article distributed under the terms of the Creative Commons Attribution License (CC BY). The use, distribution or reproduction in other forums is permitted, provided the original author(s) and the copyright owner(s) are credited and that the original publication in this journal is cited, in accordance with accepted academic practice. No use, distribution or reproduction is permitted which does not comply with these terms.

Using sodium glycodeoxycholate to develop a temporary infant-like gut barrier model, *in vitro*

Francesca Bietto[1,2], Elena Arranz[3,4], Beatriz Miralles[4], Cristina Gómez-Marín[4], Eva Rath[5], Alice J. Lucey[2] and Linda Giblin[1]*

[1]Teagasc Food Research Centre, Moorepark, Cork, Ireland, [2]School of Food and Nutritional Sciences, University College Cork, Cork, Ireland, [3]Sección Departamental de Ciencias de la Alimentación, Universidad Autónoma de Madrid (UAM), Madrid, Spain, [4]Institute of Food Science Research CIAL (CSIC-UAM), Madrid, Spain, [5]Chair of Nutrition and Immunology, School of Life Sciences, Technische Universität München, Freising, Germany

Introduction: In newborns, the intestinal barrier is permeable but not inflamed. Understanding this unique state is essential for developing models relevant to infant gut physiology.

Methods: This study aimed to develop an *in vitro* model of the infant gut barrier treating Caco-2/HT29-MTX with 0.5, 0.8, and 1 mM sodium glycodeoxycholate (GDC).

Results: Our research demonstrates that GDC decreases Caco-2/HT29-MTX Trans-Epithelial Electrical Resistance (TEER) and increases paracellular permeability, without inflammation or cytotoxicity. Notably, the treatment with 0.8 mM GDC increased lactulose transport rate by 1.63-fold. The treatment also reduced the key tight junction protein, occludin, at the cell membrane, and increased acidic mucins and extracellular alkaline phosphatase activity. Additionally, GDC decreased cAMP, suggesting its mechanism of action was via activation of a G-protein coupled receptor. Of particular importance to nutrition studies, the GDC effect was reversible with TEER recovery within 4 h. Applying digested infant formula to 0.8 mM GDC-treated Caco-2/HT29-MTX monolayers resulted in a higher concentration of amino acids in the basolateral compartment compared to control monolayers.

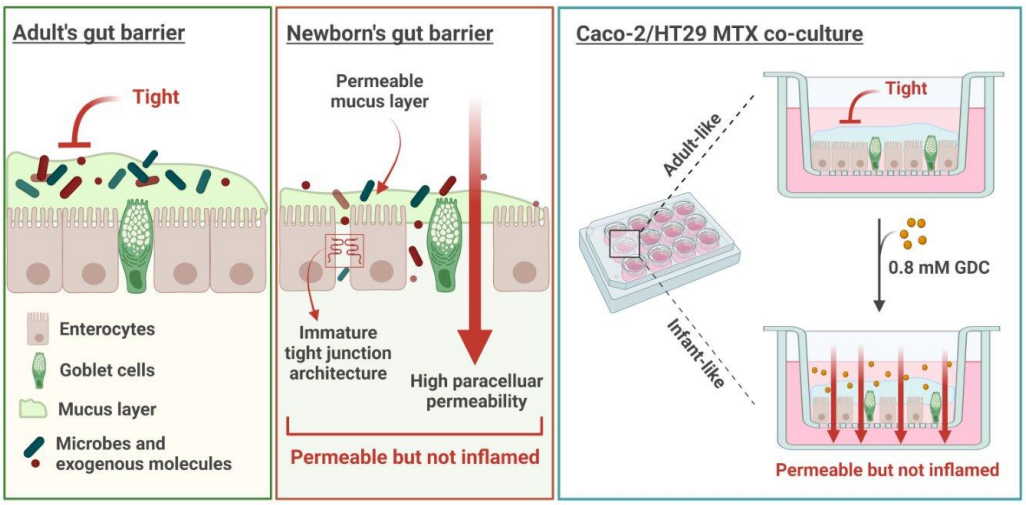
Discussion: These findings suggest that GDC can modulate gut barrier properties in a controled, reversible manner, offering a valuable model for studying nutrient absorption and gut physiology in early life.

KEYWORDS

***in vitro* infant gut barrier, sodium glycodeoxycholate, Caco-2/HT29-MTX, tight junctions, intestinal permeability, TEER, infant milk formula digesta**

Highlights

- GDC temporarily decreases TEER in Caco-2/HT29-MTX monolayers, without cytotoxicity
- GDC decreases OCLN fluorescence intensity and increases lactulose paracellular transport
- GDC increases acidic mucins production and decreases intracellular cAMP
- GDC treated monolayers are biocompatible with Infant Formula digesta



GRAPHICAL ABSTRACT
Created with BioRender.com.

1 Introduction

The infant gut barrier has a higher paracellular permeability during early development (1–3), facilitating the absorption of bioactive molecules from human milk (4). Human milk, in turn, matures the gut barrier and gradually reduces its permeability overtime (1). Infant formulas are formulated to provide nutrients similarly to breast milk. However, the ability of breast milk to support the transition from an infant gut barrier to an adult barrier, occurs due to its unique composition of bioactive components [ie peptides (5), lipids (6, 7) oligosaccharides (8), probiotics and prebiotics].

There are ethical and logistical challenges of conducting clinical trials in early infancy to understand the gut barrier. As an alternative, current models for studying the infant gut barrier include cell lines, enteroids and animal models. Adult-derived colorectal cell lines (Caco-2, HT29-MTX) are widely used (9, 10) but differ significantly from neonatal physiology due to differences in paracellular pore size (11). The neonatal piglet-derived IPEC-J2 cell line is closer to infant gut characteristics yet limited by species-specific differences (12). Human enteroids closely mimic infant intestinal physiology but face challenges related to culture complexity and scalability (13). Animal models (neonatal rodents, piglets) offer valuable physiological insights but ethical concerns and interspecies variations limit direct human applicability (14). These limitations underscore the necessity for developing specialized, reproducible, and infant-specific *in vitro* models of the gut barrier. Furthermore, for nutrition research, any infant-like model should be able to transition from infant to adult within a suitable timeframe, and should be able to generate data on nutrient absorption for both life stages.

The infant intestinal paracellular permeability is measured *in vivo* by quantifying lactulose (radius = 9.5 Å) and mannitol (radius = 6.7 Å) in urine after oral administration (1–3). This test represents the only direct method in humans to evaluate intestinal permeability. In healthy adults, the jejunum restricts the passage of molecules > 8 Å (15), making lactulose transport an indicator of gut barrier impairment (16). In newborns, lactulose permeability is 55.56% higher than in older infants (3 vs. 15 months = 0.28% vs. 0.18%) (2). Moreover, the lactulose-to-mannitol ratio inversely correlates with age (3, 16, 17), indicating that larger molecules, such as lactulose, can more readily cross the intestinal barrier during infancy compared to older children.

Due to the limited research in children, much of our understanding of the infant gut barrier comes from animal models. Studies using mice, for example, show that newborns can absorb big molecules, such as FITC-dextran 70 kDa (4 fold increase in transport at 2 week-old vs. 12 week-old mice) and lactoferrin 80 kDa, (4-fold increase in transport at 2 week-old vs. 12 week-old mice) (18).

Paracellular transport across the epithelial barrier is regulated by tight junction proteins, which form cell-to-cell complexes and depend on calcium for assembly (19). Key proteins maintaining barrier integrity and limiting paracellular permeability include Occludin (OCLN), Zonula Occludens (ZO-1), several Claudins (CLDN) and Junctional Adhesion Molecules (JAMs). Notably CLDN-2 increases paracellular permeability (19). In mice, mRNA expression of *Cldn3*, *Ocln*, *Tjp1* (ZO-1), and *Jam1* in the small intestine is lower in newborns (1 day and 2-week-old mice), while the expression of *Cldn2* is higher compared to adults (12-week-old mice) (18, 20).

Intestinal alkaline phosphates is a brush border enzyme expressed and secreted by enterocytes (21), whose activity is

essential for maintaining gut homeostasis and protecting against inflammation (21) and aging (22). Importantly, this enzyme upregulates tight junction proteins both *in vit*ro (23) and *in vivo* (24). Interestingly, *in vivo* studies have shown that serum alkaline phosphatase levels are higher in young children (29 days to 1 year, 50^{th} percentile: males = 218.19, females = 210.62 U/L) compared to older children (17 to 18 years, 50^{th} percentile: males = 104.74, females = 75.50 U/L) (25), further supporting the enzyme's relevance during early life when the gut barrier is still developing.

Permeability is also influenced by the mucus layer, composed of high-molecular-weight glycoproteins secreted by goblet cells (26). Studies on mucus development are limited, especially in humans, but *in vivo* data show that at birth colonic mucus in humans, pigs and mice predominantly contains acidic mucins over neutral mucins (27). In human, Filipe et al. reported that acid mucins predominate in the human colon throughout fetal life. While this study does not quantify the acidic-to-neutral mucin ratio, it does suggest a predominance of acidic mucins in the neonatal period (28). In pigs, infant mucus (2-week-old) is less viscous and more permeable compared to adults (7–10-month-old) (29).

Differences in paracellular permeability, tight junctions, and mucus properties between infants and adults question the reliability of adult gut models for infant research. Given the higher incidence of necrotizing enterocolitis in formula-fed vs. breastfed infants (30, 31), developing an accurate infant gut model is crucial to understanding human milk's benefits to the young gut, and improving formulations of infant formula to mimic these benefits.

The Caco-2 monolayer (32) is a standard *in vitro* intestinal model, but it lacks a mucus layer and its tight junctions resemble those of the colon, with narrower pores (4.5 Å) (33, 34) compared to the small intestine (8–9 Å) (15). To address these limitations, the Caco-2/HT29-MTX co-culture was developed, combining enterocytes (Caco-2) and goblet cells (HT29-MTX) (10, 35) in a polarized monolayer. The 90:10 seeding ratio simulates small intestine conditions, increasing paracellular permeability and providing a mucus layer (36).

Previous studies have examined methods for increasing the permeability of Caco-2 monolayers whilst preventing inflammation. Our laboratory demonstrated that treating 20-day-old Caco-2 monolayers with 125 mM sodium butyrate effectively increases paracellular permeability without causing inflammation or cytotoxicity (37). However, the high concentration of sodium butyrate resulted in an osmolality of 0.79 Osmol/kg (37), which is at the upper limit of Caco-2 tolerance (38), possibly initiating stress responses.

For oral drug delivery studies, medium-chain fatty acids, bile salts, bacterial toxins, surfactants and chelating agents have been investigated for their ability to enhance barrier permeability (39–41). Among these molecules, sodium N-(8-[2-hydroxybenzoyl]amino) caprylate (SNAC; a C8 derivate) and sodium caprate (C10) have been widely tested in Caco-2 monolayers and clinical trials (39).

In Caco-2 (20 to 28 days old monolayers), SNAC primarily modulates the transcellular pathway, enhancing membrane fluidity but not targeting specifically tight junctions (42), which limits its relevance for modeling the paracellular permeability characteristic of the neonatal gut. On the other hand, C10 affects the paracellular permeability but requires calcium-free buffers, as it precipitates with calcium, an essential ion for tight junction maintenance and physiological relevance (34, 42, 43). Moreover, C10 acts by increasing the number of paracellular pores rather than expanding pore diameter, making it less suitable for mimicking the permeability state of the infant gut barrier (34).

Bile salts such as cholate, taurocholate, chenodeoxycholate, usodexycholate and glycodeoxucholate have been used to enhance the permeability of hydrophilic markers and drugs *in vitro* (44–47), *ex-vivo* (44, 48) and *in vivo* (45). Among these, glycodeoxycholic acid (GDC) stands out due to its favorable low toxicity and dose-dependent permeability enhancement. GDC is a secondary bile salt conjugated with glycine, synthesized through the synergistic action of the liver and gut microbiota (49, 50). In the human intestine, bile salts exist in conjugated (bound to amino acids, such as glycine or taurine) and unconjugated forms. Conjugated bile salts are more water-soluble and generally less toxic (51), whereas unconjugated forms, such as sodium cholate, tend to be more potent but are more toxic (46). GDC has been found to effectively increases permeability *in vitro* in Caco-2 monolayers (44, 52), *ex-vivo* (53) and *in vivo* (54). Specifically, 2.12 mM GDC increased calcitonin permeability in Caco-2 monolayers by 10.66-fold and decreased TEER by 4.57-fold (52), whilst 0.5 mM GDC increased [^{14}C]-mannitol apparent permeability (Papp) by 3-fold and transiently decreased TEER by 2.5-fold, without reducing cell viability (MTS, CellTox^{TM} Green assay, Caspase 3/7) (44).

Although the precise mechanism by which GDC modulates epithelial permeability is unknown, bile salts bind to TGR5 and FXR membrane receptors (55). TGR5 activation can modulate intracellular cAMP levels, which in turn regulate PKA activity (56). Deoxycholic acid, for example, signals through TGR5, leading to PKA inhibition and has been linked to EGFR activation, ERK1/2 signaling, and occludin redistribution in Caco-2 cells (57, 58). Compared to permeability enhancers like sodium butyrate (which requires high, hyperosmolar concentrations) or sodium caprate (active only in calcium-free conditions), GDC is effective at low, physiologically relevant doses (0.5–2.12 mM) under standard conditions. These properties make GDC a novel and ideal candidate for transiently inducing a leaky, infant-like epithelial phenotype, a previously unexplored approach for modeling early-life gut barrier function *in vitro*.

An *in vitro* infant model should deliver a barrier with paracellular permeability levels, tight junction and mucus characteristics similar to infants but with the capability to transition overtime to an adult barrier. Importantly, the ability of the model to recover barrier integrity after transient permeability, is essential to provide a prototype for studying gut maturation overtime, particularly when assessing dietary (bioactive) components for their ability to accelerate this transition. In this study, GDC was evaluated as a candidate for developing an infant gut barrier using Caco-2/HT-29 MTX monolayers. We hypothesized that GDC treatment would produce an infant-like barrier capable of transitioning to an adult state within a reasonably time frame for cell culture experimentation. Therefore, GDC treated monolayers could be employed in nutrition research to develop next generation infant formula.

2 Materials and methods

2.1 Materials

Human intestinal epithelial cell lines Caco-2 (EACC 86010202) and HT29-MTX-E12 (EACC 12040401) were purchased from the European Collection of Cell Culture (UK). Six and 12-wells plates and polyester permeable-membrane inserts (0.4 μm pore size, 4.5 and 1.11 cm^2 growth area respectively) were purchased from Sarstedt Group (Germany). All pipetting was performed using low-retention, Biosphere® Plus filtered pipette tips (Sarstedt, 70.3050.255). CellTiter 96™ AQueous One Solution Cell Proliferation Assay (MTS, G3582) and cAMP-Glo™ Assay kit (V1501) were purchased from Promega (USA). CyQUANT™ LDH Cytotoxicity Assay (C20300) was purchased from Invitrogen (USA). Milliplex Map Kit (HSTCMAG-28SK, Human High Sensitivity T cell Magnetic Bead Panel, was purchased from Merck Millipore (USA). RNeasy mini kit and RNA-free DNase set were from Qiagen (Netherlands). SensiFAST cDNA Synthesis Kit was from Meridian Bioscience (UK). Light Cycler SYBR GREEN I Master kit was from Roche Diagnostics (Switzerland). Primers for RT-qPCR were synthesized by Eurofins Genomics (Germany). Pierce BCA Protein Assay Kit, Rabbit Occludin Polyclonal Antibody (71–1,500), Alexafluor 488 Donkey Anti-Rabbit Antibody (A-21206), and DAPI (62,248) were purchased from ThermoFisher Scientific (USA). Infant Milk Formula (IMF) was purchased in a local supermarket. Rabbit gastric extract 15 (RGE 15) was purchased from Lipolyltech (lot number 1201, France). AccQ-Tag Ultra Derivatization Kit, Amino Acid Hydrolysate Standard, AccQ•Tag Ultra Eluent A and AccQ•Tag Ultra Eluent B were purchased from Waters Corporation® (USA). All the other reagents were purchased from Sigma-Aldrich unless stated otherwise.

2.2 Cell culture

Caco-2 and HT29-MTX cell lines were cultured in 75-cm^2 tissue culture flasks at 37°C, 5% CO_2, and humidified atmosphere. After thawing, they were passaged three times before use. The culture medium was Dulbecco's Modified Eagle Medium (DMEM, D5796), supplemented with 10% fetal bovine serum (FBS, F7524), and 100 U/mL Penicillin-Streptomycin (P4333), referred to as "complete DMEM." For HT29-MTX cells, 1% MEM Non-essential Amino Acid Solution (M7145,) was also added. Cells were passaged at 80% confluence every 4–5 days using 0.25% Trypsin-EDTA (T4049). Cells were used between passage numbers 22–28 for Caco-2, and 64–68 for HT29-MTX cells. Cells Trypan blue staining and a TC20 cell counter (Bio-Rad, USA) were used for cell counting.

2.3 MTS assay

GDC was dissolved in DMEM D1145 and filter sterilized using 0.22 μm PET syringe filters, (A16532-GUK, Misart Engineering Ltd, New Zealand), to a concentration of 0.5 to 5 mM. Gastrointestinal digested samples of infant milk formula (IMF) were thawed at room temperature, then diluted to ratios of 1 in 10, 1 in 15, and 1 in 20 in HBSS, followed by filtration using a 0.45 nm PES syringe filter. Caco-2 and HT29-MTX cells were seeded in a 96-well plate at a concentration of 10^5 cells/well at a 90:10 ratio (Caco-2:HT29-MTX) in complete DMEM+1% MEM. After ~16 h the cells were washed with HBSS and incubated for 30 min with DMEM free from glutamine and phenol red (DMEM D1145). Cells were then washed twice with Hanks Balanced Salt Solution (HBSS, H8264) and incubated with 200 μL GDC (12 concentrations, 0–5 mM) in DMEM D1145 or 1% TritonX (X-100). After 2 h at 37°C, 20 μL MTS reagent were added to each well and incubated for 1 h. For the digested samples, 200 μL of pre-warmed (37°C) digesta was added for 2 h and then removed, as its turbidity interfered with absorbance readings. Cells were washed twice with HBSS and then 200 μL of MTS reagent diluted 1 in 11 in HBSS (for each reaction: 18 μL of MTS reagent + 182 μL of HBSS) was added for 1 h. Absorbance was read at 490 nm in a microplate reader (Synergy HT BioTek, Winooski, VT, USA). Cell viability was determined by normalizing the absorbance values to DMEM-treated cells (set as 100%) for GDC samples and HBSS-treated cells for digesta samples. The IC_{50} values for GDC were determined using non-linear regression analysis.

2.4 Caspase-3 assay

Caco-2/HT29-MTX (90:10) were seeded 10^5 cells/well in a 96-well plate, cultured overnight and then treated with 0.5, 0.8 and 1 mM GDC for 2 h. Caspase-3 assay was performed according to the manufacturer's guidelines. Briefly, the plate was cooled on ice, media removed, wells rinsed with HBSS. Then, 200 μl reaction mixture (including peptide substrate acetyl-Asp-Glu-Val-Asp-7-amido-4-methylcoumarin) was added to the wells, mixed by pipetting and transferred into a black, flat bottom 96-well plate. Fluorescence was read (excitation—360 nm, emission—460 nm) every min for 60-min at 37°C using a plate reader (Synergy HT, Biotek). Control cells were exposed to DMEM D1145 only, and the assay positive control was isolated human 0.5 μM Caspase-3 (no cells). Caspase-3 activity was quantified in nanomoles of 7-Amino-4-methylcoumarin (the fluorescent product) liberated from acetyl-Asp-Glu-Val-Asp-7-amido-4-methylcoumarin per minute per milliliter of cell lysate, calculated using the formula:

$$\text{Activity, nmol AMC/min/mL} = (\text{nmol AMC} \times d)/(t \times v)$$

Where v = volume of the sample in milliliters, d = dilution factor, and t = reaction time in min.

2.5 Intracellular cAMP quantification

Cyclic AMP levels were assessed using the cAMP-Glo™ Assay (V1501, Promega), according to the manufacturer's instructions. Caco-2/ HT29-MTX (90:10) were seeded in a 96-well plate at 10^5 cells/well and cultured overnight. On the experiment day, 100 mM IBMX (3-isobutyl-1-methylxanthine) was prepared by dissolving 22.2 mg in 100% DMSO and diluted in DMEM D1145 to a final

concentration of 500 μM. Cells were washed twice with HBSS and incubated with DMEM D1145 + IBMX for 30 min to equilibrate.

During equilibration, 0.5, 0.8, and 1 mM GDC solutions were prepared in DMEM D1145 + IBMX and filter sterilized. DMEM D1145 + IBMX was removed from each well and replaced with 100 μL of the GDC in DMEM D1145 + IBMX. Cells were incubated at 37°C for 2 h. Following the incubation, 80 μL was removed from each well. Cyclic AMP-Glo™ Lysis Buffer (20 μL) was added to the remaining 20 μL volume in the wells. The plate was incubated at room temperature on a shaker for 15 min. Subsequently, a cAMP Detection Solution was prepared by mixing 2.5 μL of Protein Kinase A (PKA) with 1 mL cAMP-Glo™ Reaction Buffer. Next, cAMP Detection Solution (40 μL) was added to each well, and the plate was shaken for 30 s before incubating for 20 min at room temperature. After incubation, 80 μL room-temperature Kinase-Glo® Reagent was added to each well. The plate was shaken for 30 s and incubated for 10 min. Finally, 150 μL from each well was transferred to a white flat-bottom plate, and luminescence was measured using a plate reader (Synergy HT, Biotek) with the following settings: excitation = plug, emission = hole, and gain = 135.

To determine if GDC directly inhibits PKA, GDC solutions were incubated directly with cAMP in the absence of cells. Briefly, 1 μL cAMP (1 mM) was diluted in 249 μL DMEM D1145 + IBMX (final cAMP concentration 4 μM). In a 96-well plate, 10 μL of this cAMP solution was mixed with 10 μL of D1145 + IBMX (control condition) or 2X GDC in D1145 + IBMX (GDC = 0.5 0.8, 1 mM). Following this, 20 μL cAMP-Glo™ Lysis Buffer was added to each well, and the plate was incubated for 15 min, prior to the addition of PKA and cAMP-Glo™ Reaction Buffer, and the procedure above followed.

2.6 GDC treatment of caco2/HT29-MTX monolayers

Caco-2 and HT29-MTX cells were diluted separately in complete DMEM with 1% MEM at 1.2×105 cells/mL. A 90:10 cell mix (Caco-2/ HT29-MTX) was added to the apical compartment of 12 well plates containing polyester permeable-membrane inserts (Sarstedt Group) at 6×104 cells/well (500 μL). The basolateral compartment received 1.5 mL complete DMEM with 1% MEM. Media was replaced every 2 days and monolayer integrity measured by TEER ($\Omega \times cm^2$, Millicell-ERS Voltohmmeter, Merck Millipore) every 7 days (16 h after media change). To determine the optimal experimental time point for barrier maturity, transepithelial electrical resistance (TEER) was monitored at several intervals (days 7, 14, 21, 24, and 25). Based on these measurements, the monolayer was considered stabilized by day 25, which falls within the widely accepted 21–29 day window for Caco-2 differentiation (59). Senescence markers p21 and p53 were monitored by RT-qPCR (see Supplementary Figure 3) to evaluate cell senescence.

At day 24 monolayers were washed twice and incubated with DMEM D1145 for 16 h. Monolayers with TEER > 1,000 $\Omega \times cm^2$ on day 25 were used. Monolayers were washed twice with HBSS and incubated with DMEM D1145 (apical = 0.4 mL and basolateral = 1.5 mL) for 30 min for acclimatization. GDC (5X in DMEM D1145) was added to the apical compartment (100 μL) to a final concentration of 0.5, 0.8 and 1 mM. Monolayers were incubated for 2 h. TEER was measured at times 0, 1 and 2 h. Control monolayers received DMEM D1145 only. Apical and basolateral samples were collected and stored at −20°C for further analysis. Monolayers were either kept for further experiments or lysed for RT-PCR. TEER values are expressed as $\Omega \times cm^2$- blank (Transwell insert with media in the absence of cells).

2.7 Monolayer recovery

On day 25, GDC was removed from Caco-2/HT29-MTX monolayers, which were then washed twice with HBSS. DMEM D1145 was added to the apical (0.5 mL) and basolateral (1.5 mL) compartments, and monolayers were incubated for 24 h. TEER measurements were taken at 1 and 24 h thereafter.

For real-time TEER, Caco-2/HT29-MTX cells (90:10) were seeded at a concentration of 4.8×10^5 cells/well (2 mL/well) in a 6-well plate containing polyester permeable-membrane inserts (basolateral chamber = 3 mL). Media was replaced every 2 days and monolayer integrity tracked by Millicell. On day 24, cells were washed twice with HBSS and incubated for 16 h with DMEM D1145. On day 25, the permeable inserts with monolayers attached were placed into the CellZscope plate (nanoAnalytics GmbH, Germany) for real-time TEER measurements. Only monolayers with a TEER > 1,000 $\Omega \times cm^2$ were used. The monolayers were initially washed with HBSS, then equilibrated for 30 min by adding 1.6 mL DMEM D1145 to the apical side and 4 mL to the basolateral side. Then 0.4 mL 5X GDC in DMEM D1145 was added for 2 h. Monolayers were washed twice with HBSS and incubated for 24 h with fresh DMEM D1145. The CellZscope system measured TEER every h.

2.8 Permeability to lactulose

The protocol for measuring monolayer permeability to lactulose was adapted from (37). Lactulose (61360-25G) was prepared in HBSS (2.5 mg/mL) and filter sterilized. GDC treated monolayers were washed twice and acclimatized for 30 min at 37° in HBSS (0.4 mL in the apical and 1.5 mL in the basolateral). Lactulose (0.5 mg/mL in HBSS, 100 μL) was added to the apical side, and monolayers incubated for 4 h at 37°C. TEER was measured at T0 and T4h. Apical and basolateral samples were collected and stored at −20°.

For the quantification, a high performance anion exchange chromatography with pulsed amperometric detection (HPAEC-PAD) on an ICS3000 system equipped with an electrochemical detector (Dionex, USA) was employed. Apical samples were diluted 1 in 100 in Milli-Q H_2O while the basolateral samples were analyzed undiluted. All samples were filtered with a 0.2 μm nylon syringe filter. Separation was conducted using a CarboPac PA100 column (4 × 250 mm) preceded by a guard column (CarboPac PA-100, 4 × 50 mm) at a flow rate of 1 mL/min. Eluent A = 100 mM NaOH; Eluent B = 100 mM NaOH+500 mM sodium acetate (NaOAc). Elution proceeded according to the following

gradient: from t = 0 to 6 min, 100% Eluent A; at t = 13 min, 51.4% Eluent A and 48.6% Eluent B; from t = 13.1 to 23.1 min, equilibrated at 100% Eluent A.

Lactulose levels were quantified by comparing peak areas with known lactulose standards (10 mg/L). The results were expressed as lactulose apparent permeability (Papp) calculated with the following formula:

$$\text{Papp (cm/min)} = (C_{Baso} \times V)/(t \times A \times C_{In})$$

Where: C_{Baso} = Concentration of lactulose in the basolateral compartment (mg/L); V = Volume of the basolateral compartment (L); t = incubation time (240 min); A = surface area (1.1 cm^2); C_{In} = initial concentration in the apical (mg/L).

2.9 Lactate dehydrogenase (LDH) assay

Briefly, 50 μL from the apical chamber of GDC-treated monolayers were transferred to a 96-well flat-bottom plate, and mixed with equal volume of LDH Cytotoxicity Assay reaction mixture. The plate was incubated at room temperature in the dark for 30 min to allow LDH conversion of lactate to pyruvate, initiating a reduction of formazan dye. After incubation, 50 μL stop solution was added to each well, and absorbance was measured at 490 nm and 680 nm using a Synergy HT plate reader (Biotek). Cytotoxicity was then calculated as follows:

$$\begin{aligned}\%\ \text{cytotoxicity} = {} & (\text{GDC} - \text{treated LDH activity} \\ & - \text{Spontaneous LDH activity})/(\text{Maxium LDH} \\ & \text{activity} - \text{Spontaneous LDH activity}) \times 100\end{aligned}$$

Where: GDC-treated LDH activity = GDC treated monolayer supernatant; Spontaneous LDH activity = supernatant from control monolayers, Maximum LDH activity = LDH released from 50 μL of cell lysate (control monolayers lysed, with 500 μL of 1% TritonX, by pipetting).

2.10 Alkaline phosphatase activity

Caco-2/HT29-MTX monolayers were tested for alkaline phosphatase activity after a 2 h treatment with 0, 0.5, 0.8, 1 mM GDC. In each well, the apical fluid was collected and the monolayer was then washed twice with PBS. Monolayers were lysed with 0.2% TritonX (0.5 mL) in Milli-Q H_2O by shaking for 20 min at room temperature. Then 50 μL apical sample or 50 μL cell lysate were transferred into a clear flat-bottom 96-well plate. The activity of alkaline phosphatase was measured with the Alkaline Phosphatase Assay kit (MAK447), in which p-nitrophenyl phosphate is converted into p-nitrophenol and inorganic phosphate. After 4 min of reaction, absorbance was measured at 405 nm using a Synergy HT plate reader. The activity of alkaline phosphatase was calculated with the following formula:

$$[(OD_{T4} - OD_{T0}) \times \text{RxnVol}]/\varepsilon\text{PNP} \times L \times \text{SmplVol} \times t;$$

Where: OD_{T0} = D value at 405 nm at time 0, OD_{T0} = OD value at 405 nm at time 4 min, RxnVol = reaction volume, εPNP = absorptivity coefficient for p-Nitrophenol (18.75 $mM^{-1} \times cm^{-1}$), L = light path in cm, SmplVol = sample volume, t = reaction time, 4 min. The light path (L) has been calculated with the following formula:

$$L = (OD_{Cal} - OD_{Blank})/(\varepsilon C);$$

Where: OD_{Cal} = absorbance at 405 nm of the Calibrator of the kit, OD_{Blank} = absorbance at 405 nm of the blank (well with just media and no cells), ε = molar absorptivity coefficient, C = path length of the plate in cm.

2.11 Cytokine quantification

For the pro-inflammatory cytokines (IL-8, IL-6 and TNF), apical samples were centrifuged at 900 g for 5 min to remove debris. The analysis was performed with 25 μL supernatant using the Human Milliplex Map Kit (HSTCMAG-28SK, Merck Millipore) and MagPix fluorescent detection system (Luminex, The Netherlands), according to the manufacturer's instructions. Milliplex assay detects IL-6 in the concentration range 0.18–750 pg/mL, IL-8 between 0.31 and 1,250 pg/mL and TNF between 0.43 and 1,750 pg/mL.

2.12 OCLN immunofluorescence

After GDC treatment, monolayers were washed twice with PBS and fixed for 30 min at room temperature by adding 500 μL 75% ethanol in PBS to the apical chamber. Monolayers were washed twice with PBS and kept at 4°C in PBS until use. Monolayers were permeabilized with 75% acetone in PBS for 3 min at room temperature, washed three times with PBS and incubated for 30 min at room temperature with the blocking solution (1% BSA in PBS). The blocking solution was removed and 150 μL primary antibody (71–1,500, Rabbit Occludin Polyclonal Antibody, ThermoFisher Scientific) diluted in blocking solution (8.33 μg/mL) was added. Monolayers were incubated overnight at 4°C. The following day, monolayers were washed twice with PBS and 150 μL secondary antibody (A-21206, Alexafluor 488 Donkey anti-rabbit, ThermoFisher Scientific) in blocking solution was added (11 μg/mL). Monolayers were incubated for 1 h in the dark at room temperature, washed three times with MilliQ H_2O and incubated with DAPI (62,248, ThermoFisher Scientific; 1:500 dilution in MilliQ H_2O) for 2 min, in the dark, at room temperature. The permeable supports of the Transwell plates were excised with a scalpel and mounted on a microscope slide with 40 μL mounting media (P36930, ProLong™ Gold Antifade Mountant, ThermoFisher Scientific).

Microscopy images were captured with Leica TCS SP5 Confocal Laser Scanning Microscope with 405 Diode and Argon lasers (Leica Microsystems, Wetzlar, Germany) and HC PL APO 63x/1,40 OIL CS2 objective. Pinhole size was 85.65 nm. Images were captured with the following settings: scan mode—xyz, format—1,024 ×

1,024, speed—440 Hz, pixel size—240.50 x 240.50 x 713.35 nm, line and frame average—6, z-step size—0.71 μm. Alexa Fluor 488 acquisition parameters were: 520–560 nm (emission range), 929 V (gain) and 100% (laser intensity). DAPI acquisition parameters were: 410–480 (emission range), 700 V (gain) and 64% (laser intensity). Images were acquired using the Leica Application Suite AV (v 2.7.3.9723) software (Leica Microsystems). Fiji/ImageJ software (version 1.54f, Java 1.8.0_322) was used for subsequent analysis of OCLN fluoresence intensity. Regions of Interest (ROIs) were manually selected from acquired images based on where the nuclei were well visible. For intensity quantification, the z-plane corresponding to the middle of the nuclei was chosen to ensure consistent measurement across samples. Intensity threshold was determined with the Otsu algorithm. The OCLN fluorescence intensity was calculated as raw integrated density (Raw IntDen), which represents the sum of pixel intensity within each ROI, normalized by the number of nuclei. For improved visualization, contrast adjustments were applied to the images using ImageJ software. The adjustments were performed uniformly across all images.

2.13 mRNA expression by real time PCR

Cell monolayers treated with GDC were lysed by the addition of RLT buffer (350 μL) with 1% β-mercaptoethanol on ice for 5 min. Cell lysate was collected and stored at −80°C prior to use. Total RNA was extracted with the RNeasy Mini Kit with DNase digestion (Qiagen), following manufacturer's instructions. RNA was quantified with Nanodrop 1,000 (Thermo Fisher Scientific) and only the samples meeting the criteria of $OD_{260/280}$ ratios between 1.8 and 2.0 were used for cDNA synthesis. Reverse transcription from 0.5 μg of total RNA to cDNA was conducted using the SensiFAST cDNA Synthesis kit (Bioline, UK). mRNA transcripts were quantified using LightCycler 480 SYBR Green I Master kit (Roche Diagnostics Ltd., UK) using a LightCycler 96 instrument.

Primer sequences and annealing temperatures, for Claudin-2 (CLDN-2), Junctional Adhesion Molecule 1 (JAM-1), Occludin (OCLN), Zonula Occludens-1 (ZO-1), Claudin-4 (CLDN-4), Ribosomal Protein Lateral Stalk Subunit (P0-RPLP0), Mucin-1 (MUC-1), Mucin-2 (MUC-2), Mucin-5AC (MUC-5A) cyclin-dependent kinase inhibitor 1 (p21) and tumor protein p53 (p53), are listed in Supplementary Table 1. The reaction mixture for each well consisted of 5 μL of master mix, 0.5 μL of each forward and reverse primer (10 μM) and 1 μL of 1 in 10 dilution of cDNA.

The $2^{-\Delta\Delta Ct}$ method was employed to calculate the relative amount of the target gene, where $\Delta\Delta Ct = (Ct_{\text{Target gene}} - Ct_{\text{RPLP0}})_{\text{GDC test}} - (Ct_{\text{Target gene}} - Ct_{\text{RPLP0}})_{\text{Control}}$.

Here, Ct = theshold cycle for either the target gene or RPLP0; test = monolayers treated with 0.5, 0.8 or 1 mM GDC; control = DMEM D1145 media treated monolayers.

2.14 Mucus quantification by Alcian blue

GDC-treated monolayers were washed twice with PBS. Then, 0.5 mL of 1% Alcian blue (A5268) in 0.16 M sucrose + 0.05 M sodium acetate at pH 5.8 was added to the apical compartment and incubated at 37°C for 30 min. After incubation, the stain was removed and monolayers were washed, at least 3 times, with PBS (until the PBS was clear). Monolayers were then lysed by pipetting with 0.5 mL RIPA buffer with 1% EDTA. Collected cell lysates were briefly spun to remove debris. The supernatant (150 μL) was placed in a clear flat-bottom 96-well plate in duplicate and absorbance measured at 620 nm in a Biotek Synergy HT plate reader. Results are presented as the absorbance at 620 nm–blank (RIPA buffer with 1% EDTA alone).

2.15 Gastrointestinal digestion of infant milk formula (IMF)

Infant milk formula (IMF) was reconstituted following the manufacturer's instructions by dissolving 4.3 g of powder in 30 mL of MilliQ H_2O. The infant simulated gastro-intestinal digestion (SGID) was performed as per Ménard et al. (84). The protocol was adjusted to ensure full activation of pepsin and trypsin, with a specific focus on protein digestion. As a result, lipase activity was not prioritized in this setup. This approach aligns with INFOGEST recommendations, which support adapting digestion parameters according to the nutrient class being investigated (60). A volume of 5 mL of reconstituted IMF was mixed with 2.94 mL infant simulated gastric fluids containing 268 U/mL RGE 15 (pepsin activity = 596 U/mg). The pH was brought to 5.3 with 1 M HCl. Samples were incubated for 1 h at 37°C in a shaking incubator (100 rpm). To stop the gastric phase and inhibit pepsin activity, the pH was increased to 7 with 1 M NaOH. Then, 4.88 mL of simulated intestinal fluids containing 16 U/mL pancreatin (lot number SLCM8903, trypsin activity = 8.9 U/mg) and 3.1 mM bovine bile (lot number SLBV1780, bile salts concentration = 440 g/mol) were added. The pH was decreased to 6.6 with 1 M HCl. The samples were incubated again for 1 h at 37°C in a shaking incubator. Following the intestinal phase, digestion was stopped by adding the protease inhibitor 4-(2-aminoethyl) benzene sulfonyl fluoride hydrochloride, dissolved in MilliQ H_2O at a final concentration of 1 mM, along with Orlistat dissolved in ethanol at a final concentration of 0.1 mM. An SGID control sample, where MilliQ H_2O replaced the IMF, was subjected to gastrointestinal digestion followed by enzyme inactivation (SGID-H_2O). The SGID samples were stored at −80°C until use. The protein content of the digested IMF was determined by Pierce BCA Protein Assay Kit (ThermoFisher Scientific).

2.16 Caco-2/HT29-MTX monolayers exposure to digested IMF

For the monolayer exposure, 0 mM GDC or 0.8 mM GDC-treated Caco-2/HT29-MTX monolayers were washed twice and incubated with HBSS (0.4 mL in the apical and 1.5 mL in the basolateral side) for 15 min at 37°C for acclimatization. The SGID IMF was defrosted at room temperature, diluted 1 in

3 in HBSS, filtered (0.45 μm PES syringe filters, low protein bind, Sarstedt) and pre-warmed to 37°C. Subsequently, 100 μL SGID IMF or HBSS (buffer only control) was added to the apical compartment (final dilution 1 in 15) for 2 h at 37°C. TEER values were recorded at T0h (after HBSS wash and acclimatization) and at T2h (after 2 h incubation with the digesta). The protein content of the sample applied to the apical side (μg/cm^2) was calculated as follows: protein content of digesta (BCA assay, μg/mL)/ dilution factor [15]/volume on apical side (0.5 mL)/ Transwell filter area (1.1 cm^2). Apical and basolateral samples were collected and stored at −20°C for amino acids analysis.

2.17 Quantification of the total amino acid in the basolateral chamber

Basolateral samples were defrosted at room temperature, and 0.5 mL of each technical replicate was pooled. A total volume of 1 mL from this pooled sample was transferred to a glass vial, evaporated using a SpeedVac concentrator, and then re-suspended in 100 μL of hydrolysis solution (6 M HCl). Hydrolysis was conducted for 15 h at 110°C. To quantify the derivative forms of cysteine (XCys), cysteine standards (10 and 1 mmol/L) were also hydrolyzed. Prior to hydrolysis, an internal standard of Norvaline was added to each sample to achieve a final concentration of 250 ρmol/L. After hydrolysis, 20 μL of each sample was neutralized by the addition of 20 μL of 6 M NaOH and 20 μL of 0.2 mM HCl, and then filtered using a 0.45 μm nylon syringe filter. The samples and standards (Amino Acid Hydrolysate Standard, Waters Corporation) were derivatized using the AccQ-Tag Ultra Derivatization Kit (Waters Corporation). Each derivatization reaction consisted of mixing 10 μL of the sample with 70 μL of AccQ•Tag Ultra Borate Buffer and 20 μL of AccQ•Tag Ultra reagent, followed by incubation at 55 °C for 10 min. Amino acids detection was performed with ACQUITY Ultra Performance LC® (UPLC®) equipped with tunable ultraviolet/visible (TUV) detector (Waters Corporation). Separation was performed with AccQ•Tag Ultra Amino Acid Analysis Column (Eluent 1 = AccQ•Tag Ultra Eluent, Eluent 2 = AccQ•Tag Ultra Eluent B, Waters Corporation; flow rate = 0.7 mL/min; injection volume = 1 μl; column temperature = 55°C). The quantification was performed based on a standard three-point curve. The Empower software (version 3.7.0, Waters Corporation) was used to acquire, process, report, and manage chomatographic information.

2.18 Statistical analysis

All experiments were conducted in triplicates or quadruplicate across three separate days, each with technical duplicates or triplicates. Results are expressed as means ± SEM. Statistical analyses were performed using GraphPad Prism 9.1.0 (GraphPad Software, USA) via two-way ANOVA with Tukey's multiple comparison or Dunnet's multiple comparison. Statistical significance was determined at a P-value < 0.05.

3 Results

3.1 IC_{50} of GDC on Caco-2/HT29-MTX is 2.49 mM

The IC_{50} of GDC on the viability of undifferentiated Caco-2/HT29-MTX cells was determined by MTS and non-linear regression analysis (Supplementary Figure 1). The IC_{50} was 2.49 mM, (95% CI = 2.21-3.04 mM). Cell viability was not decreased by GDC concentrations of 0.5, 0.8 and 1 mM GDC compared to the control (cells in DMEM D1145 only; $P > 0.05$). Cells treated with 1% Triton X served as a positive control, showing a viability of 0.457 ± 0.037%.

3.2 GDC decreases TEER with subsequent recovery

To assess the effect of non-cytotoxic GDC on the intestinal barrier integrity, 25-day old differentiated Caco-2/HT29-MTX 90:10 monolayers were exposed for 2 h to 0.5, 0.8 and 1 mM GDC. Initially, development of the barrier overtime was tracked by TEER measurements at 7, 14, 21, 24 and 25 days after seeding (Supplementary Figure 2). At day 21 TEER values were 848 ± 36.54 Ω × cm^2. It took a further 3 days for the TEER values to stabilize. By day 24, TEER values had increased to 1261 ± 34.67 Ω × cm^2 and had stabilized, with no significant increase from day 24 to day 25 (1302.81 ± 35.162 Ω × cm^2, $P > 0.05$) (Supplementary Figure 2). Although within the range (day 21-29) recommended by Hubatsch et al. (59), day 25 monolayers were checked for senescence, by quantifying mRNA transcript levels of senescence markers p21 and p53 (61). Transcript levels of p21 and p53 did not significantly change in day 25 monolayers compared to day 21 ($P > 0.05$; Supplementary Figure 3).

Once day 25 monolayer were treated with GDC, all 3 GDC concentrations resulted in significantly lower TEER values (Figure 1A, $P < 0.05$) at 2 h compared to monolayers in media alone (0 mM GDC = 1,086.071 ± 01.28; 0.5 mM GDC = 573.34 ± 149.69; 0.8 mM GDC = 403.15 ± 155.29; 1 mM GDC = 233.26 ± 82.20 Ω × cm^2). The calculated fold decreases in TEER relative to the control were as follows: 0.5 mM GDC = 1.89, 0.8 mM GDC = 2.69, 1 mM GDC = 4.65. Once GDC was removed (recovery phase), monolayers treated with 0.5 mM GDC had similar TEER values to values of control monolayers within 1 h ($P > 0.05$). Monolayers treated with 0.8 or 1 mM GDC were still significantly lower than controls at 1 h ($P < 0.0001$). By 24 h in the recovery phase, 0.5 and 0.8 mM GDC monolayers had TEER value increases similar to control monolayers (0 mM GDC = 1,359.05 ± 86.79; 0.5 mM = 1,168.2 ± 85.35; 0.8 mM = 1,133.55 ± 73.76 Ω × cm^2; $P > 0.05$), while 1 mM GDC was still struggling to recover (1 mM = 875.29 ± 145.41 Ω × cm^2, $P < 0.01$).

This recovery is critical to simulate the transient nature of neonatal gut permeability and to enable post-treatment applications, such as digesta exposure or intervention studies that might induce gut barrier restoration. To examine the recovery

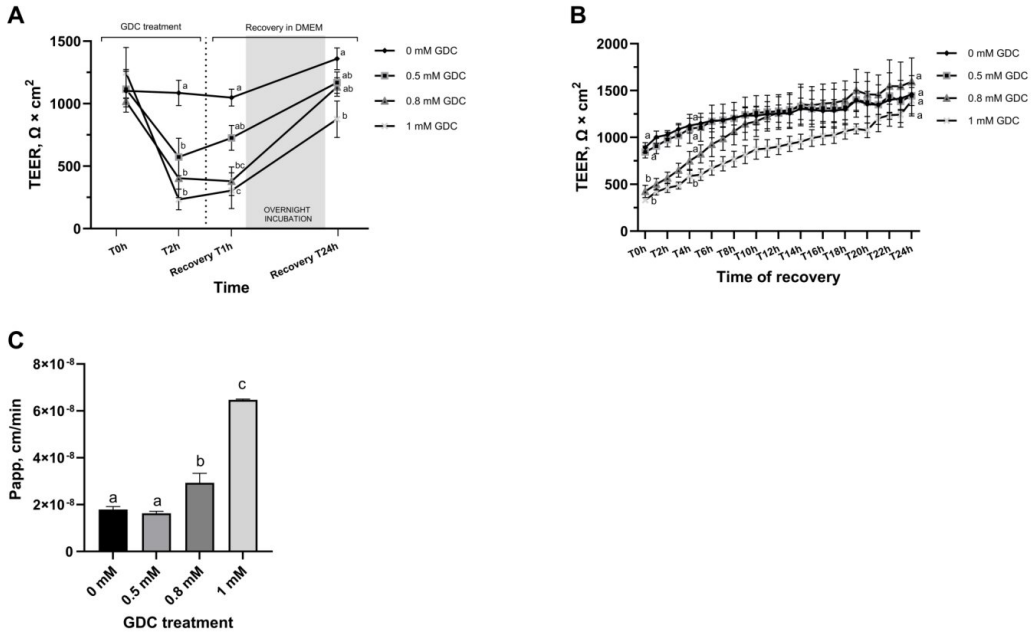


FIGURE 1
(A) Trans-Epithelial Electrical Resistance (TEER) and **(B)** lactulose permeability of GDC-treated Caco-2/HT29-MTX monolayers. TEER value at day 25 = 1,302.81 ± 70.32 Ω × cm^2. Caco-2/HT29-MTX 90:10 monolayers were treated for 2 h (T2h) with 0.5, 0.8 or 1 mM GDC in DMEM D1145. **(A)** GDC treatment with TEER values recorded by Millicell ERS Voltohmmeter. T0 = monolayers washed twice with HBSS and GDC added, T2h = GDC treatment for 2 h, Recovery T1h–T24h = timeline of recovery phase in DMEM D1145 alone. **(B)** Recovery phase (T0–T24h) with TEER values recorded by CellZscope automated TEER monitoring system. **(C)** Lactulose apparent permeability (Papp; cm/min). GDC treated monolayer were washed and treated with lactulose for 4 h. Results are presented as biological triplicates with technical duplicate ± SEM. Statistical difference was assessed **(A, B)** between treatments at a time point by two-way ANOVA or **(C)** with one-way ANOVA with Tukey's multiple comparison. Different letters signify statistical difference ($P < 0.05$).

phase in detail, TEER values were measured every hour for 24 h using a CellZscope real-time cell monitoring system (Figure 1B). At the start of the recovery phase (T0h), TEER values for monolayers treated with 0.8 mM and 1 mM GDC were significantly lower than those of the control monolayers ($P < 0.05$). CellZcope measurements revealed that monolayers treated with 0.5 mM GDC showed no significant difference from 0 mM GDC at the beginning of the recovery phase. TEER values of 0.8 mM GDC treated monolayers reached levels similar to control monolayers by 4 h of recovery (T4h; $P > 0.05$). By the end of the 24-h recovery period (T24h), TEER values for all GDC-treated monolayers had returned to levels comparable to those of the control condition (0 mM GDC, $P > 0.05$).

3.3 GDC-treated monolayers have a higher permeability to lactulose

To evaluate whether decreased TEER values in GDC-treated monolayers corresponded to increased permeability, a lactulose permeability assay was performed on these monolayers (Figure 1C). Caco-2/HT29-MTX monolayers treated with 0.8 mM and 1 mM GDC had a significantly higher lactulose Papp (0.8 mM GDC = $P < 0.05$, 1 mM GDC = $P < 0.001$) compared to 0 mM GDC. The lactulose Papp increased by 0.91-fold for 0.5 mM GDC, 1.64-fold for 0.8 mM GDC and 3.61-fold for 1 mM GDC (Papp 0 mM GDC = 1.79×10^{-8} cm/s ± 1.21×10^{-9}). Mannitol was not included in the permeability assessment, as mannitol is transported paracellularly and transcellularly *in vivo*, while only paracellularly *in vitro* (62).

3.4 GDC treatment does not cause monolayer cytotoxicity

LDH release was measured in the GDC treated monolayers, as LDH leakage indicates cytoplasmic damage. None of the GDC concentrations increased the LDH release, suggesting GDC is not causing cytoplasmic leakage (Figure 2A; $P > 0.05$).

10.3389/fnut.2025.1577369

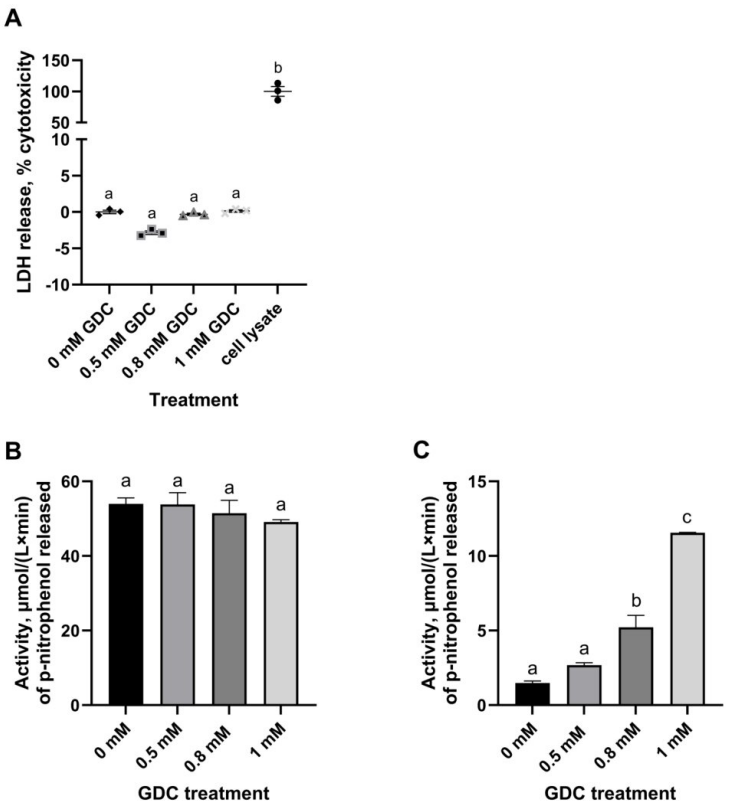


FIGURE 2
Effect of GDC treatment on **(A)** LDH release, **(B)** intracellular and **(C)** extracellular alkaline phosphatase activity in Caco-2/HT29-MTX monolayers. Caco-2/HT29-MTX 90:10 monolayers were grown for 25 days and exposed for 2 h to 0.5, 0.8 or 1 mM GDC. **(A)** % of cytotoxicity measured by the release of LDH in the apical compartment, given by the amount of formazan produced in the enzymatic reaction with the assay mixture. LDH was 0 mM GDC = monolayers in DMEM 1,145 only (set as 0% cytotoxicity); Cell Lysate = positive control, cells lysed with 1% Triton-X (set as 100% cytotoxicity). **(B)** Intracellular (cell lysate) and **(C)** extracellular (apical supernatant) alkaline phosphatase activity was measured using p-nitrophenyl phosphate as substrate. Alkaline phosphatase activity was calculated as µmol/(L x min) of p-nitrophenol released. Results are presented as the average of a biological triplicate and a technical duplicate ± SEM. Statistical difference in the treatments was assessed by one-way ANOVA with Tukey's multiple comparison and is indicated with different letters ($P < 0.05$).

3.5 GDC increases extracellular, but not intracellular, alkaline phosphatase activity

To study the effects of GDC on epithelial function, the intracellular and extracellular alkaline phosphatase activity were measured in GDC treated Caco-2/HT29-MTX monolayers (Figures 2B, C). No significant difference was found in the intracellular alkaline phosphatase activity of the GDC treated monolayers compared to the 0 mM GDC (53.99 ± 1.59 µmol/(L x min); $P > 0.05$). However, the 0.8 and 1 mM GDC-treated monolayers showed a significantly increased extracellular activity ($P < 0.05$ and $P < 0.001$) compared to untreated (Figure 2C). The extracellular alkaline phosphatase activity was: 0 mM GDC = 1.478 ± 0.13, 0.8 mM GDC = 5.219 ± 0.79, 1 mM GDC = 11.55 ± 0.02 µmol/(L x min).

3.6 GDC treatment does not cause monolayer inflammation

To investigate whether or not GDC treatment resulted in an inflammatory response, cytokines IL-8, IL-6 and TNF were tracked in the apical compartment of GDC-treated monolayers. These cytokines were chosen as they activate the key inflammation pathways such as NF-kB and ERK-MAPK (63) and are secreted by Caco-2 monolayers under inflammatory conditions (63, 64). Secreted IL-6 and TNF could not be detected in the 0 mM GDC nor the GDC-treated monolayers. IL-8 was detected but levels did not significantly differ with GDC treatment (0 mM GDC = 5.84 ± 0.59; 0.5 mM GDC = 9.54 ± 4.21; 0.8 mM GDC = 8.33 ± 2.81; 1 mM GDC = 11.32 ± 3.81 ρg/mL).

3.7 GDC reduces OCLN fluorescence intensity and modulates tight junction proteins mRNA expression

To determine the effect of GDC on the gut barrier integrity, OCLN immunofluorescence was performed on the monolayers treated with 0, 0.5, 0.8 and 1 mM GDC (Figures 3A, B). The results revealed a significantly lower fluorescence intensity of OCLN per number of cell nuclei for all GDC treatments (Figure 3B; $P < 0.05$). Specifically, OCLN intensity for 0 mM GDC was 50,758 ± 4,809, for 0.5 mM GDC was 43,214 ± 3,716 (85.28 ± 0.89% of control), for 0.8 mM GDC was 38,447 ± 4,597 (75.79 ± 5.02% of control) and for 1 mM GDC was 29,783 ± 7,740 (57.40 ± 10.26% of control).

To assess if the lower protein levels was due to lower mRNA transcripts, *OCLN* mRNA and associated tight junction biomarkers (*ZO-1*, *CLDN-2/4* and *JAM-1*) were measured in GDC-treated Caco-2/HT29-MTX monolayers (Figure 3C). *OCLN* and *ZO-1* mRNA levels were significantly higher in 1 mM GDC-treated monolayers (*OCLN* = $P < 0.01$; *ZO-1* = $P < 0.05$) compared to 0 mM GDC, whilst treatment of monolayers with 0.5 or 0.8 mM GDC did not alter *OCLN* or *ZO-1* mRNA transcript levels ($P > 0.05$). *CLDN-2*, *CLDN-4* and *JAM-1* expression was increased in 0.8 mM GDC –treated monolayers ($P < 0.05$), compared to 0 mM GDC.

3.8 GDC increases mucus production but not mucins expression

To determine whether GDC treatment affects the mucus layer, GDC-treated monolayers were stained with Alcian blue to quantify acidic mucins. Acidic mucins were selected as the main focus because the neonatal intestinal mucus is enriched in these glycoproteins, particularly sialomucins and sulfomucins, which predominate at birth and play critical roles in early-life gut barrier function and host–microbiota interactions (27).

As shown in Figure 4A, 0.8 mM and 1 mM GDC-treated cells exhibited a significant increase in Alcian blue staining intensity compared to 0 mM ($P < 0.05$). Monolayers treated with 0.5 mM GDC had similar Alcian blue staining 0 mM and 0.8 mM GDC-treated monolayers ($P > 0.05$).

The expression of MUC-1, MUC-2, and MUC-5AC was assessed using RT-qPCR (Figure 4B). The analysis revealed that GDC-treated monolayers had a significantly lower mRNA expression of MUC-1 (0.5 mM GDC = $P < 0.01$, 0.8/ 1 mM = $P < 0.05$) and MUC-2 ($P < 0.05$) compared to 0 mM GDC, with no difference in MUC-5AC.

3.9 GDC does not activate the apoptotic cascade but decreases cAMP levels

To investigate the mechanism of action of this bile salt, Caspase 3 activity assay was performed on undifferentiated Caco-2/HT29-MTX cells, as an indicator of apoptotic pathway activation. No statistical difference was found between GDC treated cells compared to cells in media overnight ($P > 0.05$; Figure 5A).

Whether or not GDC treatment results in modulation of intracellular cAMP levels, cAMP was measured in undifferentiated Caco-2/HT29-MTX cells following treatment with 0, 0.5, 0.8 and 1 mM GDC (Figure 5B). Cells treated with 0.8 and 1 mM GDC resulted in a significantly higher Relative Luminescence Unit (RLU; which equates to lower cAMP levels) compared to control cells without GDC (0 mM GDC = DMEM D1145 + IBMX only; $P < 0.05$). No statistical difference was found between, control and 0.5 mM GDC treated cells ($P > 0.05$). To determine if GDC inhibits PKA activity directly, GDC solutions were mixed with cAMP and prior to PKA activity measurement. There was no significant difference ($P > 0.05$) between media only and GDC solutions, indicating that GDC does not inhibit PKA activity (Supplementary Figure 4).

3.10 GDC (0.8 mM) increases amino acids transport after exposure to digested IMF

Based on permeability, tight junction, mucus data, and timeline to recovery, 0.8 mM GDC was selected as the preferred concentration to create an *in vitro* model of an infant gut barrier. To evaluate whether 0.8 mM GDC-treated monolayers were biocompatible with digested food, IMF was subjected to *in vitro* infant gastrointestinal digestion. This SGID-IMF sample (100.55 ± 3.55 μg protein/cm^2) was applied to 0.8 mM GDC treated monolayers (Figure 6). Preliminary experiments indicated that this IMF digesta was not toxic to intestinal cells (% of viability = 99.56 ± 2.95, MTS assay, Supplementary Figure 5).

As shown in Figure 6A, no significant differences in TEER values were observed between the T0h and T2h in 0 mM GDC and 0.8 mM GDC monolayers following exposure to SGID IMF ($P > 0.05$), indicating that the monolayer was unaffected by digesta addition. As a control, monolayers were exposed to HBSS alone for 2 h, and no significant change in TEER was observed (TEER T2h vs. T0h = 97.95 ± 6.19% for 0 mM GDC; 106 ± 4.98% for 0.8 mM GDC).

To track nutrient absorption post IMF-digesta treatment, total AA concentration in the basolateral chamber was quantified. Interestingly, total AA concentration in the basolateral chamber was significantly higher in GDC treated monolayers compared to control monolayers (80.55 ± 15.45 ρmol/μL compared to 24.09 ± 8.62 ρmol/μL, $P < 0.05$, Figure 6B).

4 Discussion

In our study, we investigated the potential of GDC in converting Caco-2/HT29-MTX monolayers into a model of the infant gut barrier. GDC is a bile salt that has been studied as an epithelial permeation enhancer for oral macromolecule delivery (44, 52). Our main findings are that treatment of Caco-2/HT29-MTX monolayers with 0.8 mM GDC resulted in (a) decreased TEER and increased lactulose paracellular permeability ($P < 0.05$), (b) reduced OCLN at the cell membrane and (c) increased acidic mucins ($P < 0.05$). The monolayer recovered from GDC

10.3389/fnut.2025.1577369

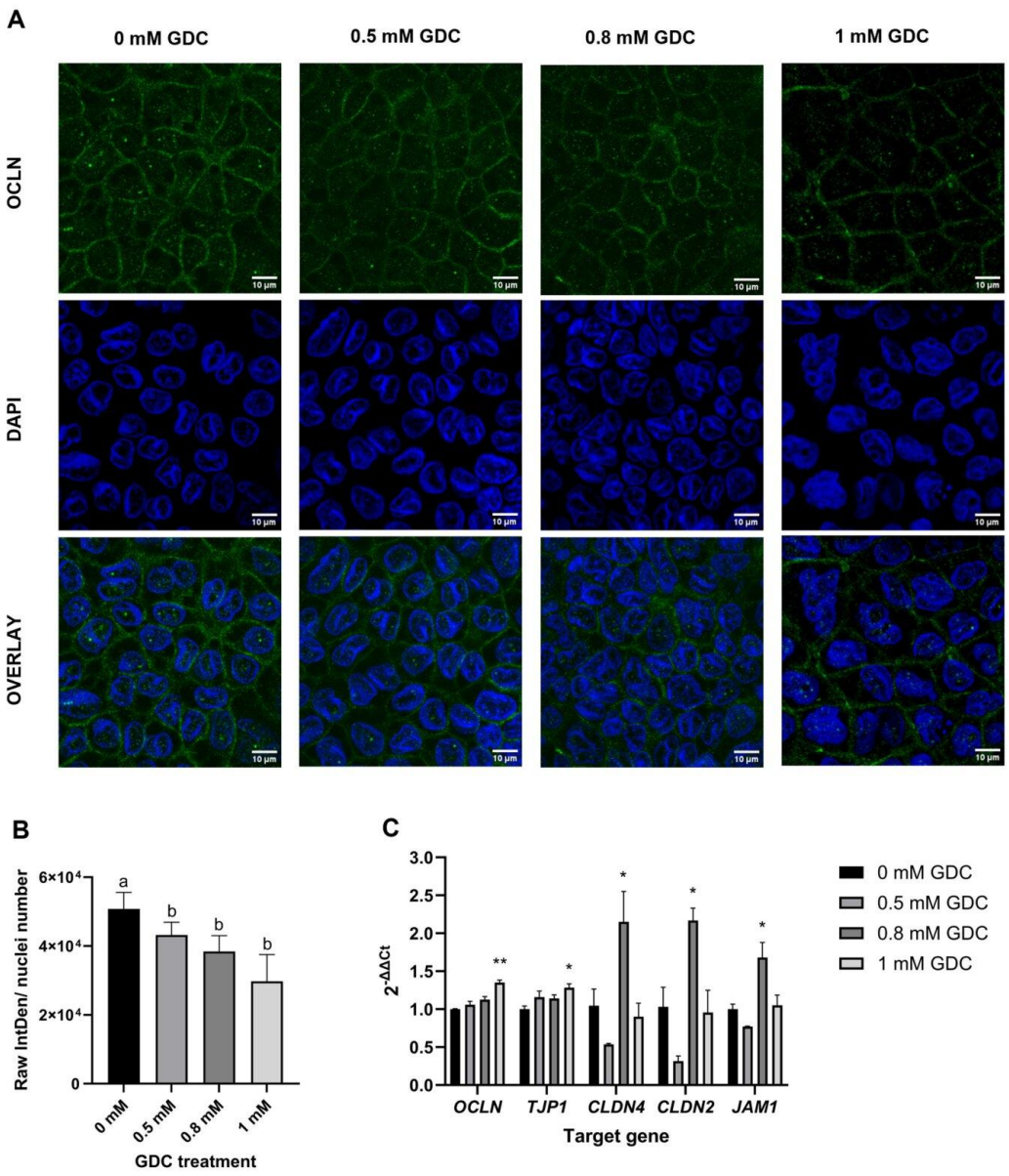


FIGURE 3
Effect of GDC treatment on **(A, B)** occludin (OCLN) localization and **(C)** tight junction protein expression in Caco-2/HT29-MTX monolayers. Caco-2/HT29-MTX 90:10 monolayers were grown for 25 days and treated for 2 h with 0.5, 0.8 and 1 mM GDC. **(A)** Representative confocal microscopy images of monolayers stained with OCLN (Alexa488, green) and nuclei stained with DAPI (blue). Scale bar = 10 µm. OCLN was White arrows indicate OCLN at the cell membrane. **(B)** Fluorescence intensity of OCLN from images using the Otsu thresholding algorithm in Fiji-ImageJ and normalized to the number of nuclei. Results represent the average of three biological replicates and three images for each replicate (mean ± SEM). Statistical differences ($P < 0.05$) between treatments was evaluated using one-way ANOVA and indicated by different letters. 0 mM GDC = monolayers in DMEM 1,145 media only. **(C)** Relative mRNA expression levels of tight junction proteins *OCLN*, zonulin (ZO-1, *TJP1*), claudin-4 (*CLDN4*), claudin-2 (*CLDN2*), and junctional adhesion molecule 1 (*JAM1*) in monolayers treated with GDC. Transcript levels were normalized to the housekeeping gene *RPLP0* mRNA and monolayers in DMEM 1,145 alone (0 mM GDC), employing the $2^{-\Delta\Delta Ct}$ method. Results represent the average of three biological and four technical replicates, presented as mean ± SEM. Statistical significance was evaluated using one-way ANOVA with Dunnett's multiple comparison test (treatment vs. control). Asterisks denote statistical difference between each treatment and 0 mM GDC ($P < 0.05$).

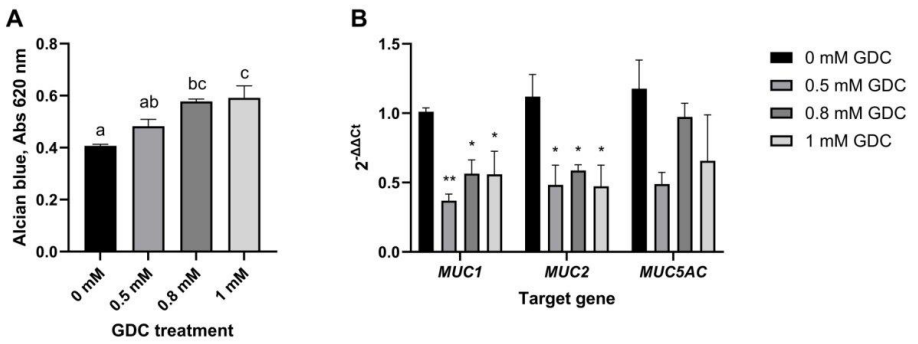


FIGURE 4
(A) Mucus staining **(B)** and mucins mRNA expression in Caco-2/HT29-MTX monolayers treated with GDC. **(A)** 25-day-old Caco-2/HT29-MTX 90:10 monolayers treated with 0.5, 0.8 and 1 mM GDC for 2 h were stained with Alcian Blue, lysed and absorbance at 490 nm recorded. **(B)** mRNA expression of mucin-1 (*MUC1*), mucin-2 (*MUC2*) and mucin-5AC (*MUC5AC*). Transcript levels were determined using RT-PCR and normalized to the housekeeping gene RPLP0 mRNA and monolayers in media alone (0 mM GDC), employing the $2^{-\Delta\Delta Ct}$ method. Results represent the average of three biological and four technical replicates, presented as mean ± SEM. Statistical significance ($P < 0.05$) was evaluated using one-way ANOVA with **(A)** Dunnet's multiple comparison test (treatment vs. control) or **(B)** Tukey's multiple comparison. **(A)** Different letters denote statistical difference between each condition. **(B)** Asterisks denote statistical difference between each treatment and the control within each gene.

treatment within 4 h ($P > 0.05$). This timely recovery is essential for an *in vitro* infant gut model designed to test digested foods, as it allows experiments to be performed in buffer rather than culture media. In addition, it simulates food transit times in the upper gut. It is likely that the mechanism of action of GDC involves the activation of G-protein coupled receptors, leading to a reduction in cAMP ($P < 0.05$), with a knock-on effect that includes an increase in extracellular alkaline phosphatase activity ($P < 0.05$) and modulation of intracellular signaling pathways that modify tight junctions. Importantly, our results indicate that neither cytotoxicity (as assessed by MTS and LDH assays, $P > 0.05$), apoptosis (caspase-3 activity, $P > 0.05$), nor inflammation (IL-8, IL-6, and TNF secretion, $P > 0.05$) were involved. GDC treated monolayers were biocompatible with infant formula digesta and resulted in higher concentrations of bioavailable amino acids ($P < 0.05$)

Our findings revealed a significant but transient reduction in TEER and an increase in lactulose Papp ($P < 0.05$) and mRNA levels of the permeability enhancer marker CLDN-2 upon treatment with 0.8 mM GDC. Brayden and Stuettgen (44) reported a similar TEER reduction of 54 ± 13.1% with 0.5 mM GDC in 21/22-day-old Caco-2 cells, (our study = 53.34 ± 25.77% with 0.5 mM GDC). However, Brayden and Stuettgen (44), reported no recovery after 24 h. The inclusion of a mucus layer provides a protective barrier to Caco-2 monolayers (65–67), which possibly supports recovery once GDC is removed.

In agreement with our lactulose Papp data, Song et al. (52) also observed that treating Caco-2 with 2.15 mM GDC increased salmon calcitonin Papp by 10.66-fold and decreased TEER by 4.57-fold, compared to the control (52). Moreover, the Papp/TEER was 2.33 ± 0.56, whilst for the unconjugated form (sodium deoxycholate) the Papp/TEER was 1.31 ± 0.25, indicating the conjugated form is less harmful to the plasma membrane (68). Indeed Brayden and Stuettgen (44) report no significant changes in Caco-2 membrane fluidity after exposure to 0.5 mM GDC using the Laurdan assay (44). In our study, lactulose Papp across 0.8 mM GDC treated monolayers was ~63.35 ± 22.68% higher than control monolayers. Interestingly *in vivo*, lactulose permeability was reported 55.56% higher in the urine of 3-month-old infants (n of samples = 1,715) compared to 15-month infants (n of samples = 1,582). In addition, increased *CLDN2* mRNA has been reported in the proximal small intestine of 2-week-old mice compared to 12-week mice ($P < 0.05$), in line with significantly increased permeability of orally administered 4 kDa, 10 kDa, 70 kDa dextran ($P < 0.05$) (18). However, despite the higher mRNA expression, CLDN-2 protein was localized intracellularly in villi of infant mice indicating, together with short villi, an immature villi architecture (18).

In our study, confocal microscopy revealed that GDC treatment decreased membrane bound OCLN in a dose-dependent manner ($P < 0.05$). Surprisingly, 0.8 mM GDC significantly increased ($P < 0.05$) mRNA expression of tight junction biomarkers OCLN, Claudin-4, JAM-1 (barrier-forming), and Claudin-2 (permeability-enhancing) (19). This suggests that GDC does not downregulate OCLN transcription but instead promotes post-translational modifications, redistribution, and/or internalization of the protein. Similarly, Zeng et al. (69) and Raimondi et al. (57) reported that, in Caco-2 cells, unconjugated deoxycholic acid (0.1–0.3 mM and 50 μM, respectively), induced OCLN post-translational redistribution, potentially through EGFR–mediated internalization (57).

In vivo studies have shown that there is a significantly higher level of OCLN leakage in feces at birth compared to 3 and 6-month-old infants (median values: birth = 2.36; 3 months = 2.25; 6 months = 2.17; 12 months = 2.17 ng/g), indicating an increased intestinal permeability correlated to OCLN localization (70). *In vivo* data from animal models show contrasting findings. Holmes et al. (20) report no significant changes in ZO-1, OCLN, and JAM-A

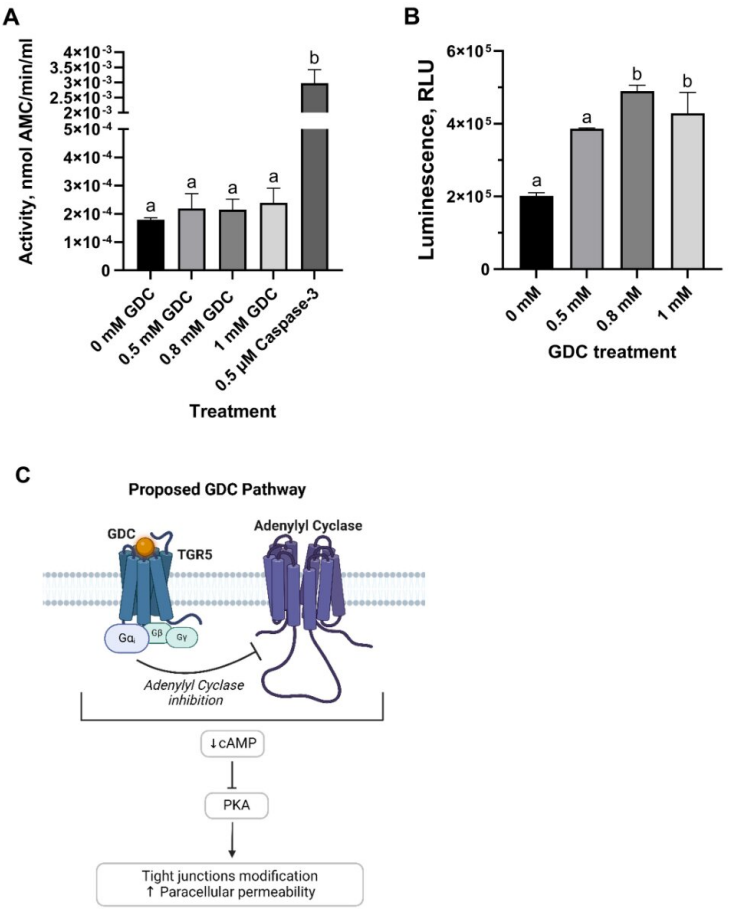


FIGURE 5
(A) Caspase-3 activity and **(B)** intracellular cAMP levels in undifferentiated Caco-2/HT29-MTX cells treated with GDC and **(C)** proposed mechanism of action. Caco-2/HT29-MTX 90:10 cells were seeded at 10^5 cells/well, grown for 24 h and then exposed for 2 h to 0.5, 0.8 or 1 mM GDC. **(A)** Caspase-3 activity, reported as nmol of 7-Amino-4-methylcoumarin—AMC—released per min per mL of cell lysate, was measured using acetyl-Asp-Glu-Val-Asp-7-amido-4-methylcoumarin as the reaction substrate. **(B)** Intracellular cAMP was measured indirectly via protein kinase A activity, where cAMP activates protein kinase A, reducing ATP and thereby decreasing light output in a coupled luciferase reaction. 0 mM GDC = monolayers in DMEM D1145 + IBMX. Results are presented as Relative Light Unit (RLU), which inversely correlates with cAMP levels. 0 mM GDC RLU = 201,707 ± 8,486. The results represent the average of a biological triplicate and a technical duplicate ± SEM. Statistical difference in the treatments was assessed by one-way ANOVA with Tukey's multiple comparison and is indicated with different letters ($P < 0.05$). **(C)** Proposed mechanism of action of GDC. By binding to the G-protein coupled receptor TGR5 (Takeda G protein-coupled Receptor), GDC inhibits adenylate cyclase via the Gαi subunit, leading to reduced cAMP levels and PKA inactivation. Figure 5c was created with BioRender.com.

mRNA expression in mice during neonatal development (1, 14, 28, and 90 days-old) (20). Whilst, Gleeson et al. (18) reported reduced mRNA levels of ZO-1, OCLN, and JAM-A in 2-week-old infant mice compared to 12-week-old adults.

Our treatment with 0.8 and 1 mM GDC significantly increased acidic mucins ($P < 0.05$), as shown by Alcian blue staining. This stain, binds to sialic acid and sulfate groups of acidic mucins (71). In parallel, the GDC treatment downregulated the expression of mucins MUC-1 (0.5 mM, $P < 0.01$; 0.8 and 1 mM, $P < 0.05$) and MUC-2 ($P < 0.05$), while MUC-5AC remained unchanged ($P > 0.05$). These findings indicate that there was a shift toward increased acidic mucus that occurred independently from mucin expression.

Several previous studies have shown that bile salts can stimulate mucin secretion. For example, Klinkspoor et al. (72) and Shekels et al. (73) demonstrated that deoxycholic acid (0.0625 to 0.25 mM and 2.5 mM, respectively) and its taurine-conjugated form (taurodeoxycholic acid—2.5 mM) stimulated mucin secretion in a dose-dependent manner in LS174T and HT29 cells (measured by [^{3}H]-glucosamine labeling) (72, 73).

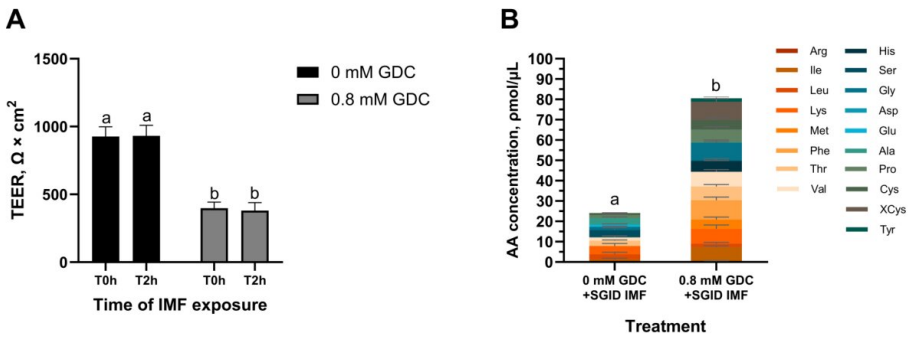


FIGURE 6
(A) TEER values and **(B)** total amino acid content in the basolateral side of Caco-2/HT29-MTX monolayers treated with GDC and digested Infant Milk Formula (IMF). 25-day-old Caco-2/HT29-MTX 90:10 monolayers treated for 2 h with 0.8 mM GDC or DMEM D1145 (0 mM GDC) were washed with HBSS and exposed for 2 h to digested IMF (SGID IMF) diluted 1 in 15 **(A)** TEER values were recorded by Millicell ERS Voltohmmeter after washing (T0h) and after the incubation with the digested IMF (T2h). **(B)** After the 2 h incubation with the IMF digesta, the basolateral samples were subjected to acid hydrolysis and analyzed by UPLC to quantify amino acids. Results represent the average of three biological and two technical replicates ± SEM. Statistical significance ($P < 0.05$) was evaluated using two-way ANOVA with Tukey's multiple comparison **(A)** or Student's *t*-test **(B)**. Different letters indicate significant difference ($P < 0.05$).

This effect is believed to be mediated by intracellular calcium and PKC signaling, pathways known to regulate mucin exocytosis in colonic cell lines such as T84 and HT29-18N2 (74–76). Thus, the increased Alcian Blue signal in our study may reflect GDC-induced exocytosis of preformed mucins rather than transcriptional upregulation.

It has also been reported that sodium deoxycholate, glycocholate and taurodeoxycholate (0.2, 0.5, 2 and 20 mM) decrease the viscosity of human-isolated mucus (77). Given GDC's structural similarity to these bile salts, it is likely that GDC similarly reduces mucus viscosity. This, along with increased acidic mucins, may contribute to the infant-like characteristics of our model. *In vivo* data on colonic mucus in newborn humans, pigs and mice show a predominance of acidic mucins over neutral mucins at birth (27). In mice, MUC-2 protein levels and *Muc-3/2*/5 mRNA expression levels progressively increase from 5 to 15 days and at 6 weeks of age (78). Future work would track mucin expression over the GDC recovery period to investigate its alignment to *in vivo* data.

Bile salts primarily interact with intestinal cells through the surface receptor Takeda G protein-coupled Receptor (TGR5) and the nuclear Farnesoid X Receptor (FXR) (55). TGR5 modulates adenylyl cyclase via the G-protein α subunit stimulatory ($G\alpha_s$) or inhibitory ($G\alpha_i$) (79). In our research, we observed a decrease in the intracellular cAMP for the 0.8 and 1 mM GDC-treated monolayers ($P < 0.05$), indicating adenylyl cyclase inhibition and downstream suppression of PKA, pointing to $G\alpha_i$ involvement. Interestingly, TGR5 activation by deoxycholic acid has been linked to ERK1/2 activation, EGFR phosphorylation, and reduced OCLN immunofluorescence in Caco-2, without the involvement of muscarinic receptors, another secondary receptor for bile salts (57, 58). However, conflicting findings from Zeng et al. (69) report a decrease in ERK1/2 phosphorylation in deoxycholic acid-treated Caco-2 cells (69). Although we cannot rule out that GDC modulation could be via alternative β-arrestin or EGFR pathways, the cAMP reduction we observed favors the hypothesis of $G\alpha_i$ involvement (Figure 5C). Furthermore, although nuclear FXR may play a role in this process, its primary effects are though transcriptional changes (55). Therefore, it is unlikely to be the direct cause of the OCLN redistribution induced by GDC as OCLN mRNA levels were unchanged at 0.8 mM GDC. It is also worth noting that while GDC was selected for its low toxicity and reversible effects, other conjugated bile salts such as taurocholate or glycocholate may offer similar advantages. Future studies could explore whether these alternatives yield comparable or complementary effects on epithelial permeability and mucus modulation.

Interestingly, recent insights suggest that intestinal alkaline phosphatase may regulate tight junction protein expression (21). Hamarneh et al. (24) demonstrated that exogenous alkaline phosphatase increases the mRNA levels of ZO-1, ZO-3, and Claudin-3 in Caco-2 cells (24). In our study, GDC at all tested concentrations significantly increased the activity of secreted alkaline phosphatase ($P < 0.05$), suggesting a potential explanation for tight junction mRNA increases observed in our study. This reinforces the idea that alkaline phosphatase may play a role not only in maintaining gut homeostasis, but also in modulating barrier function in early life (25).

While infant formulas aim to replicate breast milk, the latter offers additional bioactive benefits to the infant barrier. For example, milk proteins and their peptides are known to support gut health and nutrient absorption (5). Caco-2/HT29-MTX monolayers treated with 0.8 mM GDC were sufficiently robust to withstand infant formula digesta (food components, digestive enzymes and bile salts). Although GDC was removed after 2 h, the barrier remained moderately permeable for at least 4 h, providing a physiologically relevant window for nutrient absorption kinetics, as intestinal transit in infants typically occurs

within this timeframe (orocecal transit time in pre-term infants = 3.1 h) (80). No further TEER decline was observed during digesta exposure, confirming the stability of the model for cellular studies. Most importantly, GDC treated monolayers facilitated higher concentration of AA transported in the basolateral compared to control monolayers ($P < 0.05$). Although human data are limited, *in vivo* studies in rats and pigs show that the infant barrier allows higher AA transport (81–83). This further demonstrates GDC-treated Caco-2/HT29-MTX suitability as an infant gut barrier model for nutrition research.

One of the model's strengths is its adaptability to compact experimental timelines. Advanced *in vitro* systems must be time-efficient to offer a practical alternative to animal studies. Following the Hubatsch et al. protocol, monolayers are viable and functional from day 21 to 29; thus, a complete experimental sequence—including transient induction of infant-like permeability, followed by repeated exposure to milk components—can be conducted within a focused 8-day window.

While our model provides an infant-like gut barrier, several limitations must be acknowledged. First, compounds can only be tested for a short duration (e.g., 4 h exposure), which may restrict the ability to detect slower or long-term effects on barrier function or improvement. Furthermore, our model currently captures paracellular and amino acids transport only and has not yet been validated for transporter activity or receptor-mediated uptake. It is also crucial to study the potential effects of GDC on brush border enzymes, as well as mucus viscoelastic properties and neutral mucins. Studying neutral mucins will, however, require method development to use Periodic Acid-Schiff with cell lysates. Complementary Alcian Blue and PAS staining post-recovery would help determine if GDC alters acidic and neutral mucin composition through changes in secretion, regulation, or glycosylation. Future studies should also explore whether the conjugated bile salt GDC activates molecular pathways involving β-arrestin, EGFR, and FXR. Additionally, testing the model with breast milk would track its response to breast milk components allowing comparison with *in vivo* data.

5 Conclusions

This study proposes 0.8 mM GDC as a suitable treatment for Caco-2/HT29-MTX monolayers to create a reversible, infant-like gut barrier model, which is currently appropriate for infant nutrition research focused on paracellular and AA transport.

Data availability statement

The raw data supporting the conclusions of this article will be made available by the authors, without undue reservation.

Ethics statement

Ethical approval was not required for the studies on humans in accordance with the local legislation and institutional requirements because only commercially available established cell lines were used.

Author contributions

FB: Conceptualization, Data curation, Formal analysis, Investigation, Methodology, Validation, Visualization, Writing – original draft, Writing – review & editing. EA: Methodology, Supervision, Validation, Writing – review & editing. BM: Methodology, Resources, Supervision, Validation, Writing – review & editing. CG-M: Formal analysis, Investigation, Methodology, Writing – review & editing. ER: Methodology, Supervision, Validation, Writing – review & editing. AL: Methodology, Supervision, Validation, Writing – review & editing. LG: Conceptualization, Formal analysis, Funding acquisition, Methodology, Project administration, Resources, Supervision, Validation, Writing – review & editing.

Funding

The author(s) declare that financial support was received for the research and/or publication of this article. This research was supported by Teagasc (InfBar MDBY1370). Francesca Bietto is in receipt of a Teagasc Walsh Scholarship 2021007.

Acknowledgments

The authors would like to acknowledge Cathal Dold for providing the mucins primers and the Alcian Blue protocol, and Orla Cooney for proofreading this manuscript. Graphical abstract was created in BioRender: Bietto, F. (2025) (https://BioRender.com/x63i210). Figure 5C was created in BioRender. Bietto, F. (2025). (https://BioRender.com/68ie44l).

Conflict of interest

The authors declare that the research was conducted in the absence of any commercial or financial relationships that could be construed as a potential conflict of interest.

Generative AI statement

The author(s) declare that no Gen AI was used in the creation of this manuscript.

Publisher's note

All claims expressed in this article are solely those of the authors and do not necessarily represent those of their affiliated organizations, or those of the publisher, the editors and the reviewers. Any product that may be evaluated in this article, or claim that may be made by its manufacturer, is not guaranteed or endorsed by the publisher.

Supplementary material

The Supplementary Material for this article can be found online at: https://www.frontiersin.org/articles/10.3389/fnut.2025.1577369/full#supplementary-material

References

1. Catassi C, Bonucci A, Coppa GV, Carlucci A, Giorgi PL. Intestinal permeability changes during the first month: effect of natural versus artificial feeding. *J Pediatr Gastroenterol Nutr.* (1995) 21:383–6. doi: 10.1097/00005176-199511000-00003

2. Kosek MN, Lee GO, Guerrant RL, Haque R, Kang G, Ahmed T, et al. Age and sex normalization of intestinal permeability measures for the improved assessment of enteropathy in infancy and early childhood: results from the MAL-ED study. *J Pediatr Gastroenterol Nutr.* (2017) 65:31–9. doi: 10.1097/MPG.0000000000001610

3. Weaver LT, Laker MF, Nelson R. Intestinal permeability in the newborn. *Arch Dis Child.* (1984) 59:236–41. doi: 10.1136/adc.59.3.236

4. Weström B, Arévalo Sureda E, Pierzynowska K, Pierzynowski SG, Pérez-Cano F-J. The immature gut barrier and its importance in establishing immunity in newborn mammals. *Front Immunol.* (2020) 11:1153. doi: 10.3389/fimmu.2020.01153

5. Su M-Y, Broadhurst M, Liu C-P, Gathercole J, Cheng W-L, Qi X-Y, et al. Comparative analysis of human milk and infant formula derived peptides following *in vitro* digestion. *Food Chem.* (2017) 221:1895–903. doi: 10.1016/j.foodchem.2016.10.041

6. Jensen RG, Hagerty MM, McMahon KE. Lipids of human milk and infant formulas: a review. *Am J Clin Nutr.* (1978) 31:990–1016. doi: 10.1093/ajcn/31.6.990

7. Michalski MC, Briard V, Michel F, Tasson F, Poulain P. Size distribution of fat globules in human colostrum, breast milk, and infant formula. *J Dairy Sci.* (2005) 88:1927–40. doi: 10.3168/jds.S0022-0302(05)72868-X

8. Bode L. Human milk oligosaccharides: every baby needs a sugar mama. *Glycobiology.* (2012) 22:1147–62. doi: 10.1093/glycob/cws074

9. Lea T. Caco-2 Cell Line. In: Verhoeckx K, Cotter P, López-Expósito I, Kleiveland C, Lea T, Mackie A, et al., editors. *The Impact of Food Bioactives on Health: In Vitro and Ex Vivo Models*. Cham: Springer International Publishing (2015). p. 103–11.

10. Hilgendorf C, Spahn-Langguth H, Regårdh CG, Lipka E, Amidon GL, Langguth P. Caco-2 versus Caco-2/HT29-MTX Co-cultured cell lines: permeabilities via diffusion, inside- and outside-directed carrier-mediated transport. *J Pharm Sci.* (2000) 89:63–75. doi: 10.1002/(SICI)1520-6017(200001)89:1<63::AID-JPS7>3.0.CO;2-6

11. Sun H, Chow EC, Liu S, Du Y, Pang KS. The Caco-2 cell monolayer: usefulness and limitations. *Expert Opin Drug Metab Toxicol.* (2008) 4:395–411. doi: 10.1517/17425255.4.4.395

12. Vergauwen H. The IPEC-J2 Cell Line. In: Verhoeckx K, Cotter P, López-Expósito I, Kleiveland C, Lea T, Mackie A, et al., editors. *The Impact of Food Bioactives on Health: In Vitro and Ex Vivo Models*. Cham (CH): Springer (2015). Available online at: http://www.ncbi.nlm.nih.gov/books/NBK500147/ (accessed September 11, 2022)

13. Noel G, In JG, Lemme-Dumit JM, DeVine LR, Cole RN, Guerrerio AL, et al. Human breast milk enhances intestinal mucosal barrier function and innate immunity in a healthy pediatric human enteroid model. *Front Cell Dev Biol.* (2021) 9:685171. doi: 10.3389/fcell.2021.685171

14. Sangild PT, Ney DM, Sigalet DL, Vegge A, Burrin D. Animal models of gastrointestinal and liver diseases. Animal models of infant short bowel syndrome: translational relevance and challenges. *Am J Physiol Gastrointest Liver Physiol.* (2014) 307:G1147–68. doi: 10.1152/ajpgi.00088.2014

15. Fine KD, Santa Ana CA, Porter JL, Fordtran JS. Effect of changing intestinal flow rate on a measurement of intestinal permeability. *Gastroenterology.* (1995) 108:983–9. doi: 10.1016/0016-5085(95)90193-0

16. Johnston SD, Smye M, Watson RGP, McMillan SA, Trimble ER, Love AHG. Lactulose-mannitol intestinal permeability test: a useful screening test for adult coeliac disease. *Ann Clin Biochem.* (2000) 37:512–9. doi: 10.1258/0004563001899500

17. Musa MdA, Kabir M, Hossain MdI, Ahmed E, Siddique A, Rashid H, et al. Measurement of intestinal permeability using lactulose and mannitol with conventional five hours and shortened two hours urine collection by two different methods: HPAE-PAD and LC-MSMS. *PLoS ONE.* (2019) 14:e0220397. doi: 10.1371/journal.pone.0220397

18. Gleeson JP, Fein KC, Chaudhary N, Doerfler R, Newby AN, Whitehead KA. The enhanced intestinal permeability of infant mice enables oral protein and macromolecular absorption without delivery technology. *Int J Pharm.* (2021) 593:120120. doi: 10.1016/j.ijpharm.2020.120120

19. Otani T, Furuse M. Tight junction structure and function revisited. *Trends Cell Biol.* (2020) 30:805–17. doi: 10.1016/j.tcb.2020.08.004

20. Holmes JL, Van Itallie CM, Rasmussen JE, Anderson JM. Claudin profiling in the mouse during postnatal intestinal development and along the gastrointestinal tract reveals complex expression patterns. *Gene Expression Patterns.* (2006) 6:581–8. doi: 10.1016/j.modgep.2005.12.001

21. Lallès J-P. Recent advances in intestinal alkaline phosphatase, inflammation, and nutrition. *Nutr Rev.* (2019) 77:710–24. doi: 10.1093/nutrit/nuz015

22. Kühn F, Adiliaghdam F, Cavallaro PM, Hamarneh SR, Tsurumi A, Hoda RS, et al. Intestinal alkaline phosphatase targets the gut barrier to prevent aging. *JCI Insight.* (2020) 5:e134049. doi: 10.1172/jci.insight.134049

23. Liu W, Hu D, Huo H, Zhang W, Adiliaghdam F, Morrison S, et al. Intestinal alkaline phosphatase regulates tight junction protein levels. *J Am Coll Surg.* (2016) 222:1009–17. doi: 10.1016/j.jamcollsurg.2015.12.006

24. Hamarneh SR, Mohamed MMR, Economopoulos KP, Morrison SA, Phupitakphol T, Tantillo TJ, et al. A novel approach to maintain gut mucosal integrity using an oral enzyme supplement. *Ann Surg.* (2014) 260:706–15. doi: 10.1097/SLA.0000000000000916

25. Lü K-L, Xie S-S, Liu E, Yu X-M, Wang L, Yang Z-Y, et al. Age-wise trends in alkaline phosphatase activity in 167,625 Chinese children aged 0–18 years. *Clin Biochem.* (2020) 79:34–40. doi: 10.1016/j.clinbiochem.2020.03.001

26. Paone P, Cani PD. Mucus barrier, mucins and gut microbiota: the expected slimy partners? *Gut.* (2020) 69:2232–43. doi: 10.1136/gutjnl-2020-322260

27. Deplancke B, Gaskins HR. Microbial modulation of innate defense: goblet cells and the intestinal mucus layer. *Am J Clin Nutr.* (2001) 73:1131S–41S. doi: 10.1093/ajcn/73.6.1131S

28. Filipe MI, Sandey A, Carapeti EA. Goblet cell mucin in human foetal colon, its composition and susceptibility to enzyme degradation: a histochemical study. *Symp Soc Exp Biol.* (1989) 43:249–58.

29. Macierzanka A, Mackie AR, Bajka BH, Rigby NM, Nau F, Dupont D. Transport of particles in intestinal mucus under simulated infant and adult physiological conditions: impact of mucus structure and extracellular DNA. *PLoS ONE.* (2014) 9:e95274. doi: 10.1371/journal.pone.0095274

30. Altobelli E, Angeletti PM, Verrotti A, Petrocelli R. The impact of human milk on necrotizing enterocolitis: a systematic review and meta-analysis. *Nutrients.* (2020) 12:1322. doi: 10.3390/nu12051322

31. Lucas A, Cole TJ. Breast milk and neonatal necrotising enterocolitis. *Lancet.* (1990) 336:1519–23. doi: 10.1016/0140-6736(90)93304-8

32. Fogh J, Wright WC, Loveless JD. Absence of HeLa cell contamination in 169 cell lines derived from human tumors. *J Natl Cancer Inst.* (1977) 58:209–14. doi: 10.1093/jnci/58.2.209

33. Rubas W, Cromwell MEM, Shahrokh Z, Villagran J, Nguyen T-N, Wellton M, et al. Flux measurements across Caco-2 monolayers may predict transport in human large intestinal tissue. *J Pharm Sci.* (1996) 85:165–9. doi: 10.1021/js950267+

34. Watson CJ, Rowland M, Warhurst G. Functional modeling of tight junctions in intestinal cell monolayers using polyethylene glycol oligomers. *Am J Physiol Cell Physiol.* (2001) 281:C388–97. doi: 10.1152/ajpcell.2001.281.2.C388

35. Lesuffleur T, Barbat A, Dussaulx E, Zweibaum A. Growth adaptation to methotrexate of HT-29 human colon carcinoma cells is associated with their ability to differentiate into columnar absorptive and mucus-secreting cells. *Cancer Res.* (1990) 50:6334–43.

36. Araújo F, Sarmento B. Towards the characterization of an in vitro triple co-culture intestine cell model for permeability studies. *Int J Pharm.* (2013) 458:128–34. doi: 10.1016/j.ijpharm.2013.10.003

37. Kondrashina A, Brodkorb A, Giblin L. Sodium butyrate converts Caco-2 monolayers into a leaky but healthy intestinal barrier resembling that of a newborn infant. *Food Funct.* (2021) 12:5066–76. doi: 10.1039/D1FO00519G

38. Grauso M, Lan A, Andriamihaja M, Bouillaud F, Blachier F. Hyperosmolar environment and intestinal epithelial cells: impact on mitochondrial oxygen consumption, proliferation, and barrier function *in vitro*. *Sci Rep.* (2019) 9:11360. doi: 10.1038/s41598-019-47851-9

39. Twarog C, Fattah S, Heade J, Maher S, Fattal E, Brayden DJ. Intestinal permeation enhancers for oral delivery of macromolecules: a comparison between salcaprozate sodium (SNAC) and sodium caprate (C10). *Pharmaceutics.* (2019) 11:78. doi: 10.3390/pharmaceutics11020078

40. Maher S, Mrsny RJ. Intestinal permeation enhancers for oral peptide delivery. *Adv Drug Deliv Rev.* (2016) 106:277–319. doi: 10.1016/j.addr.2016.06.005

41. Brayden DJ, Hill TA, Fairlie DP, Maher S, Mrsny RJ. Systemic delivery of peptides by the oral route: formulation and medicinal chemistry approaches. *Adv Drug Deliv Rev.* (2020) 157:2–36. doi: 10.1016/j.addr.2020.05.007

42. Twarog C, Liu K, O'Brien PJ, Dawson KA, Fattal E, Illel B, et al. head-to-head Caco-2 assay comparison of the mechanisms of action of the intestinal permeation enhancers: SNAC and sodium caprate (C10). *Eur J Pharm Biopharm.* (2020) 152:95–107. doi: 10.1016/j.ejpb.2020.04.023

43. Lindmark T, Schipper N, Lazorová L, De Boer AG, Artursson P. Absorption enhancement in intestinal epithelial Caco-2 monolayers by sodium caprate: assessment of molecular weight dependence and demonstration of transport routes. *J Drug Target.* (1998) 5:215–23. doi: 10.3109/1061186980899587 6

44. Brayden DJ, Stuettgen V. Sodium glycodeoxycholate and sodium deoxycholate as epithelial permeation enhancers: *in vitro* and *ex vivo* intestinal and buccal bioassays. *Eur J Pharm Sci.* (2021) 12:105737. doi: 10.1016/j.ejps.2021.105737

45. Fricker G, Fahr A, Beglinger C, Kissel T, Reiter G, Drewe J. Permeation enhancement of octreotide by specific bile salts in rats and human subjects: *in vitro, in vivo* correlations. *British J Pharmacology.* (1996) 117:217–23. doi: 10.1111/j.1476-5381.1996.tb15177.x

46. Meaney CM, O'Driscoll CM. A comparison of the permeation enhancement potential of simple bile salt and mixed bile salt:fatty acid micellar systems using the CaCo-2 cell culture model. *Int J Pharm.* (2000) 207:21–30. doi: 10.1016/S0378-5173(00)00526-3

47. Mukaizawa F, Taniguchi K, Miyake M, Ogawara K, Odomi M, Higaki K, et al. Novel oral absorption system containing polyamines and bile salts enhances drug transport via both transcellular and paracellular pathways across Caco-2 cell monolayers. *Int J Pharm.* (2009) 367:103–8. doi: 10.1016/j.ijpharm.2008.09.027

48. Mahalingam R, Ravivarapu H, Redkar S, Li X, Jasti BR. Transbuccal delivery of 5-Aza-2′-deoxycytidine: effects of drug concentration, buffer solution, and bile salts on permeation. *AAPS PharmSciTech.* (2007) 8:E28–33. doi: 10.1208/pt0803055

49. Chiang JYL. Bile acids: regulation of synthesis. *J Lipid Res.* (2009) 50:1955–66. doi: 10.1194/jlr.R900010-JLR200

50. Ridlon JM, Kang D-J, Hylemon PB. Bile salt biotransformations by human intestinal bacteria. *J Lipid Res.* (2006) 47:241–59. doi: 10.1194/jlr.R500013-JLR200

51. Hofmann AF, Hagey LR. Bile acids: chemistry, pathochemistry, biology, pathobiology, and therapeutics. *Cell Mol Life Sci.* (2008) 65:2461–83. doi: 10.1007/s00018-008-7568-6

52. Song K-H, Chung S-J, Shim C-K. Enhanced intestinal absorption of salmon calcitonin (sCT) from proliposomes containing bile salts. *J Control Release.* (2005) 106:298–308. doi: 10.1016/j.jconrel.2005.05.016

53. Hoogstraate AJ, Senel S, Cullander C, Verhoef J, Junginger HE, Boddé HE. Effects of bile salts on transport rates and routes of FITC-labelled compounds across porcine buccal epithelium *in vitro*. *J Control Release.* (1996) 40:211–21. doi: 10.1016/0168-3659(95)00187-5

54. Hoogstraate AJ, Verhoef JC, Tuk B, Pijpers A, Van Leengoed LAMG, Verheijden JHM, et al. *In-vivo* buccal delivery of fluorescein isothiocyanate–dextran 4400 with glycodeoxycholate as an absorption enhancer in pigs. *J Pharm Sci.* (1996) 85:457–60. doi: 10.1021/js950129k

55. Schaap FG, Trauner M, Jansen PLM. Bile acid receptors as targets for drug development. *Nat Rev Gastroenterol Hepatol.* (2014) 11:55–67. doi: 10.1038/nrgastro.2013.151

56. Kawamata Y, Fujii R, Hosoya M, Harada M, Yoshida H, Miwa M, et al. A G protein-coupled receptor responsive to bile acids. *J Biol Chem.* (2003) 278:9435–40. doi: 10.1074/jbc.M209706200

57. Raimondi F, Santoro P, Barone MV, Pappacoda S, Barretta ML, Nanayakkara M, et al. Bile acids modulate tight junction structure and barrier function of Caco-2 monolayers via EGFR activation. *Am J Physiol Gastrointest Liver Physiol.* (2008) 294:G906–13. doi: 10.1152/ajpgi.00043.2007

58. Yasuda H, Hirata S, Inoue K, Mashima H, Ohnishi H, Yoshiba M. Involvement of membrane-type bile acid receptor M-BAR/TGR5 in bile acid-induced activation of epidermal growth factor receptor and mitogen-activated protein kinases in gastric carcinoma cells. *Biochem Biophys Res Commun.* (2007) 354:154–9. doi: 10.1016/j.bbrc.2006.12.168

59. Hubatsch I, Ragnarsson EGE, Artursson P. Determination of drug permeability and prediction of drug absorption in Caco-2 monolayers. *Nat Protoc.* (2007) 2:2111–9. doi: 10.1038/nprot.2007.303

60. Brodkorb A, Egger L, Alminger M, Alvito P, Assunção R, Ballance S, et al. INFOGEST static *in vitro* simulation of gastrointestinal food digestion. *Nat Protoc.* (2019) 14:991–1014. doi: 10.1038/s41596-018-0119-1

61. Herbig U, Jobling WA, Chen BPC, Chen DJ, Sedivy JM. Telomere shortening triggers senescence of human cells through a pathway involving ATM, p53, and p21CIP1, but not p16INK4a. *Mol Cell.* (2004) 14:501–13. doi: 10.1016/S1097-2765(04)00256-4

62. Ménard S, Cerf-Bensussan N, Heyman M. Multiple facets of intestinal permeability and epithelial handling of dietary antigens. *Mucosal Immunol.* (2010) 3:247–59. doi: 10.1038/mi.2010.5

63. Iglesias DE, Cremonini E, Fraga CG, Oteiza PI. Ellagic acid protects Caco-2 cell monolayers against inflammation-induced permeabilization. *Free Radic Biol Med.* (2020) 152:776–86. doi: 10.1016/j.freeradbiomed.2020.01.022

64. Jung HC, Eckmann L, Yang SK, Panja A, Fierer J, Morzycka-Wroblewska E, et al. distinct array of proinflammatory cytokines is expressed in human colon epithelial cells in response to bacterial invasion. *J Clin Invest.* (1995) 95:55–65. doi: 10.1172/JCI117676

65. Antoine D, Pellequer Y, Tempesta C, Lorscheidt S, Kettel B, Tamaddon L, et al. Biorelevant media resistant co-culture model mimicking permeability of human intestine. *Int J Pharm.* (2015) 481:27–36. doi: 10.1016/j.ijpharm.2015.01.028

66. Birch D, Diedrichsen RG, Christophersen PC, Mu H, Nielsen HM. Evaluation of drug permeation under fed state conditions using mucus-covered Caco-2 cell epithelium. *Eur J Pharm Sci.* (2018) 118:144–53. doi: 10.1016/j.ejps.2018.02.032

67. Wuyts B, Riethorst D, Brouwers J, Tack J, Annaert P, Augustijns P. Evaluation of fasted state human intestinal fluid as apical solvent system in the Caco-2 absorption model and comparison with FaSSIF. *Eur J Pharm Sci.* (2015) 67:126–35. doi: 10.1016/j.ejps.2014.11.010

68. Carubbi F, Guicciardi ME, Concari M, Bozzoli M, Carulli N. Cytotoxic and protective effects of bile salts *in vitro*. In: Gentilini P, Dianzani MU, editors. *New Trends in Hepatology*. Dordrecht: Springer Netherlands (1996). p. 133–41. doi: 10.1007/978-94-009-0357-9_15

69. Zeng H, Safratowich BD, Cheng W-H, Larson KJ, Briske-Anderson M. Deoxycholic acid modulates cell-junction gene expression and increases intestinal barrier dysfunction. *Molecules.* (2022) 27:723. doi: 10.3390/molecules27030723

70. Sochaczewska D, Zietek M, Dołegowska B, Kordek A, Szczuko M. Implications of indirect biomarkers of intestinal permeability in the stools of newborns and infants with perinatal risk factors for intestinal colonization disorders and infant feeding patterns. *Nutrients.* (2022) 14:2224. doi: 10.3390/nu14112224

71. Hall RL, Miller RJ, Peatfield AC, Richardson PS, Williams I, Lampert I, et al. Colorimetric assay for mucous glycoproteins using Alcian Blue. *Biochem Soc Trans.* (1980) 8:72–72. doi: 10.1042/bst0080072

72. Klinkspoor JH, Mok KS, Van Klinken BJ-W, Tytgat GNJ, Lee SP, Groen AK. Mucin secretion by the human colon cell line LS174T is regulated by bile salts. *Glycobiology.* (1999) 9:13–9. doi: 10.1093/glycob/9.1.13

73. Shekels LL, Lyftogt CT, Ho SB. Bile acid-induced alterations of mucin production in differentiated human colon cancer cell lines. *Int J Biochem Cell Biol.* (1996) 28:193–201. doi: 10.1016/1357-2725(95)00125-5

74. Marcon MA, McCool D, Forstner J, Forstner G. Inhibition of mucin secretion in a colonic adenocarcinoma cell line by DIDS and potassium channel blockers. *Biochim Biophys Acta.* (1990) 1052:17–23. doi: 10.1016/0167-4889(90)90051-E

75. McCool DJ, Marcon MA, Forstner JF, Forstner GG. The T84 human colonic adenocarcinoma cell line produces mucin in culture and releases it in response to various secretagogues. *Biochemical J.* (1990) 267:491–500. doi: 10.1042/bj2670491

76. Lencer WI, Reinhart FD, Neutra MR. Interaction of cholera toxin with cloned human goblet cells in monolayer culture. *Am J Physiol.* (1990) 258:G96–G102. doi: 10.1152/ajpgi.1990.258.1.G96

77. Martin GP, Marriott C, Kellaway IW. Direct effect of bile salts and phospholipids on the physical properties of mucus. *Gut.* (1978) 19:103–7. doi: 10.1136/gut.19.2.103

78. Zhang K, Dupont A, Torow N, Gohde F, Leschner S, Lienenklaus S, et al. Age-dependent enterocyte invasion and microcolony formation by salmonella. *PLoS Pathog.* (2014) 10:e1004385. doi: 10.1371/journal.ppat.1004385

79. Pierce KL, Premont RT, Lefkowitz RJ. Seven-transmembrane receptors. *Nat Rev Mol Cell Biol.* (2002) 3:639–50. doi: 10.1038/nrm908

80. Bodé S, Dreyer M, Greisen G. Gastric emptying and small intestinal transit time in preterm infants: a scintigraphic method. *J Pediatr Gastroenterol Nutr.* (2004) 39:378–82. doi: 10.1002/j.1536-4801.2004.tb00870.x

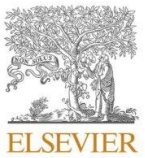
81. Buddington RK, Elnif J, Puchal-Gardiner AA, Sangild PT. Intestinal apical amino acid absorption during development of the pig. *Am J Physiol Regul Integr Comp Physiol.* (2001) 280:R241–7. doi: 10.1152/ajpregu.2001.280.1.R241

82. Toloza EM, Diamond J. Ontogenetic development of nutrient transporters in rat intestine. *Am J Physiol.* (1992) 263:G593–604. doi: 10.1152/ajpgi.1992.263.5.G593

83. Younoszai MK, Smith C, Finch MH. Comparison of *in vitro* jejunal uptake of l-valine and l-lysine in the rat during maturation. *J Pediatr Gastroenterol Nutr.* (1985) 4:992–7. doi: 10.1097/00005176-198512000-00023

84. Ménard O, Bourlieu C, De Oliveira SC, Dellarosa N, Laghi L, Carrière F, et al. A first step towards a consensus static *in vitro* model for simulating full-term infant digestion. *Food Chem.* (2018) 240:338–45. doi: 10.1016/j.foodchem.2017.07.145

Food Research International 235 (2026) 119071



Contents lists available at ScienceDirect

Food Research International

journal homepage: www.elsevier.com/locate/foodres



Comparative effects of digested human milk and infant formulas on peptide transport and gut barrier function in infant- and adult-like Caco-2/HT29-MTX models

Francesca Bietto [a,b], Simona Cirrincione [c], Cristina Gómez-Marín [d], Beatriz Miralles [d], Francesco Romaniello [e], Elena Arranz [d,f], Cristina Lamberti [c], Simona Lucia Bavaro [c], Laura Cavallarin [c], Eva Rath [g], Alice J. Lucey [b], Linda Giblin [a,*]

[a] Teagasc Food Research Centre, Moorepark, Fermoy, Co. Cork, Ireland
[b] School of Food and Nutritional Sciences, University College Cork, Cork, Ireland
[c] Institute of the Science of Food Production (ISPA) – National Research Council, Grugliasco, TO 10095, Italy
[d] Institute of Food Science Research CIAL (CSIC-UAM), Madrid, Spain
[e] National Metrological Institute of Italy (INRIM), Torino 10135, Italy
[f] Sección Departamental de Ciencias de la Alimentación, Universidad Autónoma de Madrid (UAM), Madrid, Spain
[g] Chair of Nutrition and Immunology, School of Life Sciences, Technische Universität München, Freising, Germany

ARTICLE INFO

Keywords:
Human milk
Infant formula
Gut barrier
Peptide transport
Bioactive peptides
Intestinal epithelial cells
Intestinal permeability
In vitro gastrointestinal digestion
Caco-2/HT29-MTX, INFOGEST

ABSTRACT

Early postnatal nutrition is critical for gut barrier maturation, yet infant formulas only partially replicate the functional benefits of human milk. Using infant- and adult-like Caco-2/HT29-MTX models, this *in vitro* study compared the effects of gastrointestinal digested human milk, dairy-, soya-, and amino acid–based infant formulas on gut barrier integrity and peptide transport. Barrier function was assessed by transepithelial electrical resistance and occludin–actin colocalization, while amino acid and peptide transport were profiled by liquid chromatography plus mass spectrometry.

In the infant-like model, human milk uniquely enhanced occludin–actin co-localization ($P < 0.05$) and increased the abundance of basolateral bioactive peptides. Amino acid–based infant formula significantly increased occludin fluorescence intensity in infant-like monolayers but reduced transepithelial electrical resistance (TEER) in adult-like monolayers. For all digested foods, peptide transport and diversity were significantly greater in infant-like than in adult-like monolayers, with human milk promoting the highest basolateral peptide load.

These findings demonstrate distinct functional differences between human milk and infant formulas in their interaction with the gut barrier. They also underscore the importance of using age-appropriate *in vitro* models for accurately evaluating dietary effects during early life, highlighting the need for further research to optimize infant nutrition strategies.

1. Introduction

Human milk is the gold standard of human infant nutrition, offering not only complete nourishment but also bioactive compounds that support the health and development of the infant (Brockway et al., 2024). In the intestinal tract of the infant, human milk plays a critical role in promoting gut barrier integrity (Carr et al., 2021), reducing paracellular permeability (Catassi et al., 1995), and shaping the intestinal microbiome (Bode, 2012; Pannaraj et al., 2017).

The infant gut barrier is characterized by high permeability during early development. In several domestic species (e.g., calves, piglets, lambs), the neonatal small intestine can absorb intact colostral immunoglobulins, predominantly IgG, thereby establishing systemic passive immunity (Weström et al., 2020). In humans, systemic passive immunity is acquired primarily before birth through active FcRn-mediated transplacental transfer of maternal IgG (Atyeo & Alter, 2021). Nevertheless, the human neonatal gut barrier remains highly permeable in early infancy with significantly higher lactulose permeability (Kosek et al.,

* Corresponding author.
E-mail address: Linda.Giblin@teagasc.ie (L. Giblin).

https://doi.org/10.1016/j.foodres.2026.119071
Received 24 November 2025; Received in revised form 19 March 2026; Accepted 2 April 2026
Available online 8 April 2026
0963-9969/© 2026 The Authors. Published by Elsevier Ltd. This is an open access article under the CC BY license (http://creativecommons.org/licenses/by/4.0/).

2017) and a higher lactulose-to-mannitol ratio than adults, indicating predominance of paracellular over transcellular transport pathways (Johnston et al., 2000; Musa et al., 2019; Weaver et al., 1984). These permeability traits are linked to lower expression of tight junction proteins (e.g., Occludin- OCLN, Zonulin-1- ZO1, Tight Junction Protein 1-TJP1) and higher levels of the permeability-enhancing claudin-2 (CLDN2) in early life. Intestinal barrier maturation, as reflected by decreasing permeability, continues for up to 15 months after birth in human infants (Kosek et al., 2017). Human milk promotes this maturation process, as observed by lactulose: mannitol experiments (Catassi et al., 1995). The World Health Organization recommends exclusive breastfeeding in the first 6 months of life (World Health Organization, 2014). However, the choice to breastfeed is deeply personal and can be shaped by a variety of factors (Blum, 1999). Infant formula (IF) can be used as an alternative or supplement for the first 12 months of life (UNICEF. and W. H. O., 2003). Dairy-based IF is the most widely used. Soya-based IF offers a plant-based alternative, whereas highly hydrolysed and amino acid (AA)-based IF are designed for infants with severe protein allergies or gastrointestinal disorders (Martin et al., 2016). Although nutritionally similar to human milk, IFs do not replicate the health benefits of human milk on the gut barrier, particularly in promoting gut maturation, integrity, and reducing the risk of necrotizing enterocolitis (Colaizy et al., 2016; Lucas & Cole, 1990; Quigley et al., 2024).

The Codex Alimentarius (CXS 72–1981), established by FAO/WHO, sets international standards for the composition, safety, and labelling of IF products (Codex Alimentarius Commission, 1981). In the EU, Regulation (EU) 2016/127 governs IF, mandating detailed compositional criteria (European Commission, 2016), including adequate protein or AAs, to meet the requirements for growth and development. During digestion, proteins are broken down into peptides and free AAs (Korhonen & Pihlanto, 2006). While free AAs are absorbed directly via specific transporters (Bröer, 2008), small peptides are taken up either via peptide transporters or by paracellular diffusion (Hevia et al., 2023). Many of these peptides can exert bioactive effects on the gut barrier (Dold et al., 2025; Korhonen & Pihlanto, 2006). Moreover, a recent systematic review also confirms that milk-derived proteins and peptides can be detected in the bloodstream of human infants post-ingestion, supporting their potential for systemic bioactivity (Biondi Ryan et al., 2025).

To study nutrient digestion in the infant gut, the Ménard et al. protocol offers an in vitro static gastrointestinal digestion method to track digestion under infant conditions (Ménard et al., 2018). Recent studies with this protocol have demonstrated comparable overall protein digestibility between human milk and dairy IF, as assessed by free amino acid release, molecular weight distribution, and peptidomic analysis (Komatsu et al., 2024; Sánchez-Hernández et al., 2021). Polarized Caco-2/HT29-MTX monolayers are a well-established in vitro model of the adult gut barrier (Kleiveland, 2015). Absorption of peptides from human milk and IF has been evaluated using Caco-2 monolayers following in vitro digestion of these matrices (Bavaro et al., 2021; Liang et al., 2022). Although few studies have evaluated the effects of human milk–derived peptides on Caco-2/HT29-MTX monolayers' gut barrier properties, peptides released from IF during digestion increased mRNA transcripts of mucins within these monolayers (Dold et al., 2025).

The substantial differences between the infant and adult gut barrier in terms of permeability warrant an age-appropriate transient model to simulate gut maturation and nutrient uptake from human milk and from the various IFs. However, in vitro gut barrier models for this life stage remain scarce. Current models, including cell lines (Sun et al., 2008; Vergauwen, 2015), enteroids (Noel et al., 2021), and animal models (Sangild et al., 2014), are constrained by physiological, ethical, or scalability limitations. In our previous work, we developed a reversible gut barrier model by treating Caco-2/HT29-MTX monolayers with 0.8 mM sodium glycodeoxycholate (GDC). These monolayers mirrored key aspects of the in vivo infant barrier, showing significantly reduced TEER, increased paracellular permeability (a 1.63-fold increase in lactulose transport), and altered OCLN localization, without inflammation or cytotoxicity (Bietto et al., 2025). This phenotype aligns with in vivo observations showing that intestinal permeability in young infants is approximately 55% higher at 3 months than at 15 months of age (Kosek et al., 2017). Reduced OCLN localization is consistent with reports of lower OCLN and ZO1 expression in neonatal intestine compared to adults (Gleeson et al., 2021; Holmes et al., 2006). Moreover, GDC treatment increased acidic mucin production and alkaline phosphatase activity, features consistent with the predominance of acidic mucus in early life (Johansson et al., 2011; Macierzanka et al., 2014) and elevated intestinal alkaline phosphatase reported in neonates (Cummins et al., 1988). Importantly, barrier integrity recovered within 4 h following GDC removal, confirming reversibility and supporting a model of adaptive, non-pathological permeability (Bietto et al., 2025).

The objective of this in vitro study was to compare human milk with dairy IF, soya IF, and AA IF using infant-like models of gastrointestinal digestion and gut barrier function. Specifically, we aimed (i) to evaluate the effects of these foods on structural tight junction remodeling, tracking OCLN localization in infant- and adult-like Caco-2/HT29-MTX monolayers, and (ii) to quantify free AAs and identify individual dietary peptides in the basolateral chambers of these monolayers.

2. Materials and methods

A schematic overview of the experimental workflow and analytical pipeline is provided in Supplementary Fig. 8.

2.1. Materials

Dairy-based, soya-based IF, and AA-based IF were shop-bought. The dairy-based infant formula contained cow's milk proteins as the primary protein source, the soya-based formula contained soy protein isolate, and the amino acid–based formula contained free amino acids as the sole nitrogen source. All products were manufactured within the European Union and complied with the compositional requirements for infant formula as defined by Commission Delegated Regulation (EU) 2016/127 and Codex Alimentarius (CXS 72–1981). Human milk samples were collected from six healthy lactating women approved by the ethics committee of the Hospital Universitario Virgen de las Nieves (Granada, Spain) and registered on ClinicalTrials.gov (accessed 15 April 2019; NCT02811172). Mature milk ($\geq$17 days postpartum) from each donor was pooled to create a composite sample. Rabbit gastric extract 15 (RGE 15; lot no. 1201) was obtained from Lipolyltech. A bicinchoninic acid (BCA) assay kit was purchased from Pierce® (Ireland). XT MES Running Buffer, Precision Plus Protein™ Unstained Standard were sourced from Bio-Rad. AccQ-Tag Ultra Derivatization Kit, Ultra AA Analysis Column, and AA Hydrolysate Standard were purchased from Waters® (MA, USA). Transwell inserts with polyester permeable membranes were obtained from Sarstedt Group (Germany). CellTiter 96® AQueous One Solution Cell Proliferation Assay was supplied by Promega. Rabbit anti-Occludin (Sigma-Aldrich), Alexa Fluor 488 Donkey anti-Rabbit (A-21206), Alexa Fluor 555 Phalloidin (A-34055), DAPI (268298), and ProLong™ Glass Antifade Mountant (P36980) were supplied by Thermo Fisher Scientific (MA, USA). Strata C18-E SPE Solid Phase Extraction and Luna C18 column were purchased from Phenomenex (Torrance, USA). Human intestinal epithelial cell lines Caco-2 (EACC 86010202) and HT29-MTX-E12 (EACC 12040401) were purchased from the European Collection of Cell Culture (UK). All other reagents were purchased from Sigma-Aldrich, unless otherwise stated.

2.2. Simulated static infant gastrointestinal digestion (SGID)

IFs were reconstituted according to the manufacturers' instructions to simulate realistic preparation and feeding conditions for infants. Accordingly, 4.3 g of dairy- and soya-based IF powder and 4.5 g of amino

acid–based IF powder were dissolved in 30 mL of MilliQ water, as specified by the manufacturer for each formulation. Human milk samples were thawed at 4 °C. Crude protein content was determined in duplicate using the Kjeldahl method (FOSS Scrubber 2501 / Kjeltec Sampler 8420 / Kjeltec 8400) on freeze-dried samples. Crude protein was calculated using the standard factor (N × 6.25).

Simulated gastrointestinal digestion (SGID) was performed according to the Ménard et al., 2018 protocol (Ménard et al., 2018). An oral phase was not included. Initially, 5 mL of reconstituted IF or human milk was mixed with 2.94 mL of infant simulated gastric fluid containing 268 U/mL RGE 15 (pepsin activity determined in-house = 596 U/mg). Milli-Q water (5 mL) subjected to the same digestion conditions served as a negative control. This control was included to assess potential contributions from digestive enzymes in the absence of a food matrix. The pH was brought to 5.3 with 1 M HCl. Samples were incubated for 1 h at 37 °C in a shaking incubator (100 rpm). To stop the gastric phase, pH was raised to 7 with 1 M NaOH. For the intestinal phase, 4.88 mL of simulated intestinal fluids containing 16 U/mL pancreatin (lot no. SLCM8903; trypsin activity determined in-house = 8.9 U/mg) and 3.1 mM bovine bile (lot no. SLBV1780; concentration of bile salts = 440 g/mol) were added to the gastric phase. The pH was decreased to 6.6 with 1 M HCl. The samples were incubated again for 1 h at 37 °C in a shaking incubator. Digestion was then stopped by adding the protease inhibitor 4-(2-aminoethyl)benzenesulfonyl fluoride hydrochloride, dissolved in MilliQ water at a final concentration of 1 mM, along with Orlistat, dissolved in ethanol at a final concentration of 0.1 mM. The digesta were aliquoted and stored at −20 °C until use. Samples were collected at 3 time points: G0, collected immediately after mixing the matrix with simulated gastric fluid, gastric enzymes, and adjusting to 5.3, followed by immediate alkalinisation to inactivate gastric enzymes, with no incubation and therefore no proteolysis; G60, collected at the end of the gastric digestion; and I60, collected at the end of the intestinal digestion. G0 serves as food entering the gastric phase.

Each food was digested on 3 separate occasions ($n = 3$).

2.3. SDS-page

Undigested IF and human milk, as well as samples collected at defined phases of digestion (G0, G60, and I60), were analyzed using SDS-PAGE with 12% Bis-tris–polyacrylamide gels (Criterion XT, Bio-Rad, Hercules, California, USA). Protein content was determined using a bicinchoninic acid (BCA) assay kit, following the manufacturer's instructions. Dairy, soya, and human milk samples were diluted at a protein concentration of 0.8 mg/mL in loading buffer and heated at 95 °C for 5 min. The AA IF contains no intact proteins; therefore, dilution factors were adjusted at each digestion stage to ensure that the total material loaded per lane was comparable to that of dairy IF and soya IF. The resulting dilution factors applied to AA IF were: undigested sample = 1:10.25; G0 = 1:12.33; G60 = 1:9, and I60 = 1:3.44. SGID H_2O, containing digestive enzymes but no food matrix, was loaded undiluted.

The loading buffer was 0.05 M Tris-HCL pH 6.8, SDS 1.6% w:v, glycerol 8% w:w, Bromophenol blue 0.002% w:v, β-mercaptoethanol 2% v:v. Precision Plus Protein™ Unstained Standard(15 μL) was loaded as the M_w standard. Electrophoresis was performed at 150 V for 60 min with XT MES running buffer, and gels were stained overnight with InstantBlue™ solution followed by de-staining with Milli-Q water.

2.4. Total nitrogen content by o-phthaldialdehyde (OPA) assay

The degree of protein hydrolysis was measured through the concentration of free NH_2 groups, determined by the o-phthaldialdehyde (OPA) assay (Nielsen et al., 2001). The G0, G60, and I60 samples were defrosted on ice, precipitated with 5% trichloroacetic acid (0.5 mL of sample in 0.83 mL of TCA), and centrifuged for 30 min at 1000 *g*. The supernatants were then diluted 1:1 (dairy, soya IF, and human milk G0 and G60), 1:4 (I60), or 1:9 (AA IF G0, G60) in a 0.1 mol/L borate solution. Dilution factors were adjusted to account for differences in free amino group concentration across digestion stages and formulations, ensuring all measurements fell within the linear detection range of the OPA assay. The OPA reagent was prepared with 0.1 mol/L borate, 10% SDS, 40 g/L OPA in ethanol, and 200 g/L N-Acetyl-L-Methionine Ethyl Ester. Samples (8 μL) were transferred into a UV 96-well plate and incubated for 10 min at 30 °C in the dark with 232 μL OPA solution. Absorbance at 340 nm was measured using a microplate reader (PowerWave XS, BioTek Instruments, Winooski, Vermont, USA). A standard curve of glutamic acid (0–8 mmol/L) was used for quantification. Hydrolysis % was calculated as follows:

Hydrolysis (%) = 100 - [(mmol NH_2 G0 / mmol NH_2 I0) × 100].

2.5. Size exclusion chromatography (SEC)

Digesta samples (I60) were first clarified by centrifugation at 10,000 ×*g* for 10 min at 4 °C. The resulting supernatant was diluted 1:1 and filtered through a 0.22 μm nylon syringe filter. A 20 μL aliquot was injected into two TSKgel columns connected in series (TSKgel G2000SW, 7.5 mm × 30 cm; TSKgel G2000SWXL, 7.8 mm × 30 cm) with a TSKgel SW guard column (7.5 mm × 7.5 cm) upstream. SEC was performed on a Waters HPLC system (Waters 2695 separation module) equipped with a Waters 2487 dual-wavelength absorbance detector set to 214 nm. Separation was achieved by isocratic elution at 0.7 mL/min for 55 min, using a mobile phase of 0.1 M phosphate buffer (pH 6.7) containing 0.1 M Na_2SO_4 and 10% (*v*/v) methanol.

Molecular-size calibration was carried out by applying the same conditions to a series of standards spanning the protein–peptide range: bovine serum albumin (67 kDa), equine carbonic anhydrase (29 kDa), β-lactoglobulin (18.4 kDa), α-lactalbumin (14.4 kDa), cytochrome *c* (12.4 kDa), bacitracin (1.4 kDa), H-Tyr-Leu-OH (0.29 kDa) and phenylalanine (0.17 kDa). Retention times of these standards were plotted against the logarithm of their molecular weights to generate a calibration curve, which was then used to estimate the size distribution of analytes present in the digesta samples.

2.6. Free and total AAs analysis in the digested samples

Free and total AAs in digested samples were quantified using an AccQ-Tag derivatization UPLC method, which is suitable for acid-hydrolysed samples and enables parallel determination of free and total amino acid pools.

Digested samples (I60) were defrosted on ice, and methanol was added for a final concentration of 80% to precipitate proteins (5 mL final volume). Each sample was centrifuged at 1000 *g* for 30 min. The supernatant (220 μL) was subjected to SpeedVac evaporation (SC200, Savant) to eliminate methanol. To quantify free AAs, the pellet was re-suspended in 500 μL 0.1 mM HCl. To quantify total AAs, the pellet was hydrolysed in 6 M HCl for 15 h at 110 °C in a glass vial. Cys (10 and 1 mmol/L) was also hydrolysed to quantify the derivative forms (Cys2). An internal standard of 25 mM (final concentration) Norvaline was added to the samples prior to hydrolysis. All samples were derivatized using the AccQ-Tag Ultra Derivatization Kit following the manufacturer's instructions. Briefly, the samples were neutralized, filtered with a 0.2 μm nylon filter, mixed with 70 μL AccQ•Tag Ultra Borate Buffer and 20 μL AccQ•Tag Ultra reagent, and incubated at 55 °C for 10 min. The derivatized samples were separated using, and an ACQUITY Ultra Performance UPLC® (Waters Corporation, USA) equipped with a tunable ultraviolet/visible (TUV) detector and a flow cell. Separation was performed with AccQ•Tag Ultra AA Analysis Column (Eluent 1 = AccQ•Tag Ultra Eluent A, Eluent 2 = AccQ•Tag Ultra Eluent B; flow rate = 0.7 mL/min; injection volume = 1 μL). The quantification was performed based on a standard three-point curve (AA Hydrolysate Standard). The Empower software (version3.7.0, Waters Corporation) was used to acquire, process, report, and manage chromatographic information.

2.7. Cell culture

Caco-2 and HT29-MTX cell lines were cultured as previously described for intestinal epithelial co-culture models (Hubatsch et al., 2007; Kleiveland, 2015). Caco-2 and HT29-MTX cell lines were cultured in 75-cm^2 tissue culture flasks maintained at 37 °C, 5% CO_2, in a humidified atmosphere. Following thawing, the cells underwent three passages before use. Unless otherwise stated, cells were maintained in 'complete DMEM', consisting of Dulbecco's Modified Eagle Medium (DMEM, D5796) supplemented with 10% heat-inactivated fetal bovine serum (FBS, F7524), 100 U/mL Penicillin-Streptomycin (P4333), and 2.5 μg/mL amphotericin B (A2942). Additionally, for HT29-MTX cells and for co-culture monolayers, 1% MEM Non-essential AA Solution (M7145) was added to complete DMEM. Cells were passaged at 80% confluence every 4–5 days using 0.25% Trypsin-EDTA solution (T4049). After trypsinization, cells were stained with trypan blue and counted with the TC20 cell counter (Bio-Rad, USA). Experiments were performed using Caco-2 cells between passages 21–25 and HT29-MTX cells between passages 64–68.

2.8. MTS assay

Cell viability, following exposure to digested samples, was assessed using the CellTiter 96® AQueous One Solution (MTS) assay, following the manufacturer's instructions and previously reported protocols for Caco-2-based intestinal models (Bavaro et al., 2021).

Digested samples collected at the intestinal phase (I60) were defrosted on ice, diluted in HBSS (1:4, 1:9, 1:14, 1:19), filter-sterilized (0.2 μm syringe filter), and warmed to 37 °C. Caco-2/HT29-MTX were seeded in a 96-well plate (Corning® CellBIND®) at a concentration of 5×10^4 cells/well and incubated for 24 h. Cells were then washed twice with HBSS and incubated for 2 h with diluted digested samples (150 μL). After the incubation period, the digesta was removed. Cells were washed twice with HBSS and incubated for 1 h at 37 °C with the MTS reagent (100 μL), diluted 1:10 in HBSS following the CellTiter 96® AQueous One Solution Cell Proliferation Assay kit instructions. Absorbance was read at 490 nm in a multi-plate reader (BioTek Cytation 5 multimode reader). Cell viability was expressed as a percentage of HBSS-treated control cells. Viability of control cells consistently exceeded 88% of cells maintained in complete DMEM.

2.9. Caco-2/HT29-MTX monolayers exposure to GDC and digesta

A 90:10 ratio (Caco-2:HT29-MTX) was seeded in the apical chamber (500 μL) of 12-well plates containing polyester permeable-membrane inserts (Sarstedt Group), reaching a final density of 6×10^4 cells/well. The basolateral chamber received 1.5 mL of complete DMEM with 1% MEM Non-essential AAs. The culture medium was refreshed every two days. Transepithelial electrical resistance (TEER) was monitored weekly using a Millicell-ERS Voltohmmeter (Merck Millipore, USA), with background TEER values obtained from Transwells without cells. Following our protocol (Bietto et al., 2025), monolayers were washed twice on day 24 and incubated with serum-free DMEM D1145 for 16 h. Only monolayers exhibiting TEER values $>800\ \Omega \times cm^2$ were selected for experiments (Bietto et al., 2025). Monolayers were washed with HBSS and pre-equilibrated in DMEM D1145 (0.4 mL apical, 1.5 mL basolateral) for 30 min at 37 °C. To create the infant-like barrier, monolayers were incubated for 2 h at 37 °C with GDC (0.8 mM). Firstly, GDC (4 mM) was freshly prepared and sterile-filtered in DMEM D1145. A volume of 100 μL was added to the apical compartment with 400 μL DMEM. TEER values were recorded at 0 and 2 h. Control 'adult-like' monolayers were treated with DMEM D1145 during the same timeframe. Following treatment, monolayers were washed twice and incubated with HBSS (0.4 mL apical, 1.5 mL basolateral) for 15 min at 37 °C for acclimatization. Digested IF and human milk samples were thawed on ice, diluted 1:2 in HBSS, sterile-filtered (0.2 μm PES syringe filters), and prewarmed to 37 °C. Subsequently, 100 μL sample was added to the apical chamber, achieving a final ratio of 1:14. TEER values were recorded before and after the 2 h incubation period. Apical and basolateral media were collected after the incubation period (T2-apical, T2-basolateral) and stored at −20 °C for subsequent AA and peptide analysis. Monolayers were fixed for immunofluorescence and confocal microscopy.

2.10. Immunofluorescence and confocal microscopy

Monolayers were washed twice with PBS and fixed for 30 min at room temperature by adding 500 μL of 75% ethanol (prepared in PBS) into the apical chamber. Monolayers were then washed twice with PBS and kept at 4 °C in PBS until use (max 1 week). Monolayers were permeabilized with 75% acetone in PBS for 3 min at room temperature, washed, and incubated for 30 min at room temperature with blocking solution (1% BSA in PBS). The primary antibody (Rabbit anti-Occludin, Sigma Aldrich) was added (1:149 dilution) in blocking solution (150 μL) and incubated overnight at 4 °C. Fixed monolayers were washed twice with PBS. Then, secondary antibody (A-21206, Alexafluor 488 Donkey anti-rabbit, Thermo Fisher Scientific;1:499 dilution) plus actin binder, phalloidin 555 (binds to F-actin, A-34055, Alexa Fluor 555 Phalloidin, Thermo Fisher Scientific; 1:499 dilution), was added to the blocking solution (150 μL). Monolayers were incubated for 1 h in the dark at room temperature, washed three times with PBS, and incubated with DAPI (268,298, Merk; 1:4999 dilution in MilliQ water) for 2 min, in the dark at room temperature to stain cell nuclei. The permeable supports of the Transwell plates were excised with a scalpel and mounted on a microscopy glass slide with 40 μL of mounting media (ProLong™ Glass Antifade Mountant, Thermo Fisher Scientific).

Samples were imaged using STED and FALCON (FLIM) coupled to an inverted DMi8 microscope (Leica Microsystems, Germany) equipped with a white light laser (440–790 nm). The objective used was Plan-Apochsomat 63×/1.4 Oil DIC N2. Pinhole size was set to 85.6 nm. Images were captured with Power HyD S detectors (Leica) at a pixel size of 0.7 μm in the Z dimension and 0.18 μm in the X and Y dimensions. Alexa Fluor 488 acquisition parameters were: 512–542 nm (emission range), 0.4 μs (dwell time), 3.9 (gain), and 56.89% (laser intensity). Alexa Fluor 555 acquisition parameters were: 565–605 (emission range), 0.4 μs (dwell time), 35.5 (gain), and 68.10% (laser intensity). DAPI acquisition parameters were: 450–490 nm (emission range), 0.4 μs (dwell time), 5 (gain), and 14.67% (laser intensity) Line average of 2 was applied to every channel.

Fiji/ImageJ software was used to determine OCLN fluorescence intensity, number of nuclei, colocalization with actin, orthogonal view, and monolayer thickness. The intensity threshold was determined using the Otsu algorithm for intensity quantification. The colocalization between OCLN (Alexa 488) and actin (Alexa 555) was calculated using the JACoP Fiji/ImageJ plugin, with thresholds set to 7000 for Alexa 488 and 8000 for Alexa 555. For each test sample, 3 slides and 3 pictures per slide were analyzed. For figure presentation purposes, brightness and contrast were adjusted uniformly across the entire images to improve the visualization of OCLN localization. These adjustments were applied only to the images used for illustration and were not applied to the raw image files used for quantitative fluorescence intensity or colocalization analyses.

2.11. Free AAs transported in the basolateral side

Free AAs were quantified in the T2-basolateral compartment using an untargeted UHPLC-HRMS method optimized for hydrophilic compounds. This method was selected for its high sensitivity at low amino acid concentrations. Digesta samples were analyzed in parallel for reference. The separation was performed on a Thermo Vanquish Flex UHPLC system using a Thermo Accucore™ Amide-HILIC column (150 × 2.1 mm, 2.6 μm particle size), maintained at 30 °C. Sample (1 μL) was

injected and separated under a flow rate of 400 μL/min using a binary gradient composed of solvent A (H_2O with 10% ammonium formate, 20 mM, pH 2.8) and solvent B (ACN with 10% ammonium formate, 20 mM, pH 2.8). The gradient started at 0% A and ramped to 60% A over 22 min, followed by re-equilibration back to initial conditions for a total run time of 45 min.

UHPLC was coupled to a high-resolution Orbitrap mass spectrometer (Q Exactive Plus, Thermo Fisher Scientific) via a Heated Electrospray Ionization (H-ESI) source. Full MS data were acquired in positive ionization mode with the following parameters: spray voltage 2.80 kV, capillary temperature 150 °C, sheath gas 35 AU, auxiliary gas 10 AU, sweep gas 1 AU, and auxiliary gas heater temperature 150 °C. The S-Lens RF level was set to 50.0. Full MS scans were acquired at a resolution of 70,000, with an AGC target of 3.0e6 and maximum injection time of 100 ms, across an m/z range of 65–250. Data-dependent MS/MS (dd-MS^2) was performed using an isolation window of 2 m/z, resolution 17,500, collision energy of 20 eV, AGC target of 5.0×10^4, and maximum IT of 50 ms, with an intensity threshold of 4.0×10^4.

Quantification of AAs was based on external calibration curves generated at 7 concentration levels ranging from 0.5 to 80 mg/L. Isotopically labelled internal standards were used at 10 mg/L, and the peak areas of each analyte were normalized to its corresponding internal standard.

2.12. Peptide profiling by UHPLC-HRMS/MS

2.12.1. Sample preparation for UHPLC-HRMS/MS

Peptides from digesta, T2-apical and T2-basolateral compartments were purified using solid-phase extraction (SPE) using STRATA C18-E cartridges (55 μm, 70 Å, 1 mL/50 mg). Digesta samples were diluted to match the concentration applied in cell exposure experiments. Briefly, the digesta was diluted 1:2 (*v*/v) with Milli-Q water and filtered using a 0.2 μm PES syringe filter. A further 1:4 (v/v) dilution in Milli-Q water was performed to achieve a 1:14 dilution in line with cell exposure studies. A 483 μL aliquot was then processed using C18 SPE and reconstituted in 120 μL Milli-Q H_2O. For T2-apical samples, 2 technical replicates were pooled (1.0 mL total). A 483 μL aliquot was purified using C18 SPE. For T2-basolateral samples, 1.5 mL from each of 2 technical replicates (3.0 mL total) was pooled. A 2.9 mL aliquot was subjected to C18 SPE.

Prior to loading, SPE cartridges were conditioned with 3 × 1 mL methanol and equilibrated with 3 × 1 mL Milli-Q water. Samples were loaded onto the cartridges by gravity flow, followed by washing with 1 mL of 0.5% (*v*/v) methanol in water. Peptides were eluted with 3 × 1 mL methanol.

Eluates were evaporated to dryness using a nitrogen stream at 45 °C. Dried samples were reconstituted in 120 μL Milli-Q water for digesta and T2-apical samples, and in 12 μL Milli-Q water for T2-basolateral samples. All samples were stored at −20 °C until analysis. A 10 μL injection volume was used for UHPLC–HRMS/MS analysis.

2.12.2. UHPLC-HRMS/MS analysis

Peptide analysis was performed using an Orbitrap Q Exactive Plus mass spectrometer (Thermo Fisher Scientific) coupled to a Vanquish Flex UHPLC binary pump system. Separation was achieved on a Luna C18 reversed-phase column (150 × 1 mm, 3 μm of particle size). The mobile phases consisted of 0.1% (*v*/v) formic acid in Milli-Q water (solvent A) and 0.1% (v/v) formic acid in 30% acetonitrile, 70% methanol (solvent B), delivered at a flow rate of 70.0 μL/min. The elution gradient was programmed to increase solvent B from 3% to 50% over 80 min, with 70% in 5 min, 100% in 1 min, and 5 min, then reconditioned at 3% B for 15 min. The injection volume was 2.0 μL. Column temperature was maintained at 55 °C, and the autosampler was set at 4 °C to preserve sample integrity.

UHPLC was coupled to a high-resolution mass spectrometer via an H-ESI source. Full MS data were acquired in positive ionization mode with the following parameters: spray voltage 3.50 kV, capillary temperature 350 °C, sheath gas 35 AU, auxiliary gas 10 AU, sweep gas 1 AU, and auxiliary gas heater temperature 250 °C. The S-Lens RF level was set to 50.0.

Mass spectra were acquired in data-dependent acquisition mode (Full MS-ddMS^2). Full scan spectra were recorded over an m/z range of 250–1500 with a resolution of 70,000, an AGC (automatic gain control) target of 3×10^6, and a maximum injection time of 200 ms. Up to 6 of the most intense ions in MS1 were selected for fragmentation in the MS/MS mode. The fragmentation spectra resolution was set at 17,500, with a dynamic exclusion of 10 s and an isolation window of 2.0 m/z. The normalized collision energy was set at 28 (eV), the maximum IT at 110 ms, and the AGC target at 1×10^5.

2.12.3. Peptide identification

Raw data were processed using MaxQuant (v2.6.6.0) (Cox & Mann, 2008) with an unspecific digestion mode and a minimum peptide length of 2 AAs, suitable for naturally occurring peptides. The main search mass tolerance was set to 4.5 ppm for precursors and 20 ppm for fragment ions. Variable modifications included oxidation (M), acetylation (protein N-term), phosphorylation (STY), and pyro-glutamate formation (Q/E). No fixed modifications or enzyme constraints were applied. The "second peptide" and "match between runs" features were enabled, with a match time window of 0.7 min. Label-free quantification (LFQ) was enabled with an LFQ minimum ratio count of 2 and stabilization of large ratios. Intensity normalization was based on FastLFQ.

Database searches were performed against custom UniProtKB FASTA files corresponding to *Bos taurus* (dairy, 402 entries), *Glycine* max (soy, 109 entries), or *Homo sapiens* (human milk, 1142 entries) and a manually added contaminants FASTA file (124 entries), retaining only reviewed sequences. Decoy sequences were automatically generated for FDR estimation using the revert mode. Peptide-spectrum match (PSM), peptide, and protein FDR thresholds were each set to 1%. Additional filtering required a minimum Andromeda score of 40 for modified peptides and a minimum delta score of 6. All MS/MS data were searched using Andromeda, with up to 15 candidate matches per spectrum and deisotoping enabled.

2.12.4. Bioinformatics analysis

Raw and annotated peptide data from MaxQuant output files (evidence.txt, peptides.txt) were post-processed using Python (v3.10) (Python Software Foundation, 2021) within a Google Colab (Google Research, n.d.) environment. Data manipulation and filtering were conducted using pandas (v1.5.3) (McKinney, 2010) and numpy (v1.23.5) (Harris et al., 2020) libraries. Peptides were retained only if they had at least one MS/MS count, belonged to a single protein group, and showed non-zero intensity in ≥2 biological replicates per condition. Peptides identified in T2-apical and T2-basolateral compartments were further filtered to ensure their source protein was also detected in the corresponding digesta dataset. Reverse hits and known contaminants were excluded from all analyses.

Shared and unique peptides were identified using set-based comparisons and classified as follows: peptides detected in only one compartment were labelled "compartment-unique," while those in both were "shared." Within each compartment-unique set, we further classified by age group: an "exclusive" label was used for those peptides that were present in only one age group (Infant or Adult), whereas a "shared" label was used when peptides were present in both. Overlaps were visualized via Venn diagrams using matplotlib-venn (Tretyakov, 2012). For count-based statistics, per-peptide PSM counts across Infant and Adult were subjected to equal-variance *t*-tests. For intensity-based analysis, raw intensities were $\log_2$-transformed, then imputed from a left-shifted normal distribution (mean = μ–1.8σ, σ = 0.3·global σ); per-peptide $\log_2$ means and Welch's t-tests were computed on the imputed data. A parallel workflow was applied to modified peptides (grouped by Sequence + Modification). Significantly enriched peptides ($P < 0.05$)

were annotated by source protein and mapped across compartments.

To assess peptide transformation by brush border enzymes, apical-only peptides were analyzed using a classification pipeline. Assignment of brush-border enzymatic cleavage events was performed using a motif-based in silico prediction approach. Apical peptides were matched to longer digesta-derived precursor sequences using a breadth-first search based on established N- and C-terminal cleavage motifs characteristic of known intestinal brush border peptidases.

The cleavage motifs used for prediction were as follows: Dipeptidyl peptidase-4 /8/9: N-terminal dipeptides, X–P/A; Aminopeptidase N: N-terminal single residues, L/I/V/M/A; Aminopeptidase A: N-terminal E/D; Aminopeptidase B: N-terminal R/K; Enteropeptidase: N-terminal D/E/R/K; Carboxypeptidase A: C-terminal F/L/I/W/Y/V/M; Carboxypeptidase B: C-terminal R/K; Dipeptidyl carboxypeptidase: C-terminal dipeptides, G/S/D; Tripeptidyl peptidase II: N-terminal tripeptides.

Bioactivity annotation was conducted via cross-referencing with BIOPEP (Minkiewicz et al., 2019), the Milk Bioactive Peptide Database (MBPD) (Nielsen et al., 2017), and PeptideRanker (Mooney et al., 2012) (score threshold $\geq$0.5). Volcano plots were generated using scikit-learn (v1.2.2) (Pedregosa, 2011), matplotlib (Hunter, 2007), and seaborn (Waskom, 2021) for dimensionality reduction and visual inspection of condition-driven separation.

In parallel, digesta peptides were characterized using sequence-derived physicochemical metrics. Peptide length was calculated as the number of amino acid residues per sequence and summarized as discrete distributions and biologically relevant length categories (2–3, 4–10, 11–20, and > 20 residues). Peptide molecular weight was calculated as the sum of the average residue masses plus 1 water molecule (18.01 Da) and summarized into molecular weight ranges (<500, 500–1000, 1000–2000, and > 2000 Da). Peptide hydrophobicity was calculated using the Kyte–Doolittle scale and expressed as mean hydropathy per residue, with distributions summarized into hydrophilic, neutral, and hydrophobic categories. Amino acid composition was determined as the percentage of total amino acid residues.

The same analytical framework was applied to peptides identified in the T2-basolateral compartment. Within each dietary matrix, peptides were classified as common (detected in both infant- and adult-like models) or model-specific (infant-only or adult-only) based on exact sequence matching. Peptide length, molecular weight, hydropathy (Kyte–Doolittle index), net charge at pH 7, amino acid composition, proline content, and terminal residue frequencies were calculated *in silico*. Descriptive statistics (median and interquartile range) were computed, and the proportion of peptides exceeding three amino acids (>3 AAs) was determined.

All outputs were exported using xlsxwriter (McNamara, 2023), and the entire pipeline was modular, script-based, and reproducible.

2.13. Statistical analysis

All experiments were conducted in triplicate or quadruplicate across three separate days, each with technical duplicates or triplicates. Results are expressed as means ± SEM. Statistical analyses for cellular and functional assays were performed using GraphPad Prism 10.4.2 (GraphPad Software, USA), employing one-way ANOVA with Tukey's = multiple comparison test, except for free amino acid profiles in digesta, which were analyzed using Welch's one-way ANOVA followed by pairwise comparisons with Benjamini–Hochberg false discovery rate (FDR). For individual amino acid comparisons reported in the Supplementary Tables, differences among food matrices were analyzed using two-way ANOVA followed by Tukey's multiple comparisons test, as specified in the Supplementary Materials. Statistical significance was defined as $P < 0.05$.

For peptidomic data, statistical analysis was conducted in Python (v3.10) using Welch's *t*-test via the scipy.stats module (Virtanen, 2020). Peptide-level comparisons were based on $\log_2$-transformed intensity values across conditions, and peptides with $P < 0.05$ were considered significantly differentially enriched.

3. Results

3.1. IFs and human milk exhibit similar protein hydrolysis with differences in molecular size distribution and amino acid profiles

Human milk and 3 commercially available IFs (dairy, soya, and AA-based) were subjected to static gastrointestinal digestion adapted to the infant gut (Ménard et al., 2018). Prior to digestion, crude protein content determined by Kjeldahl was 9.41% for dairy IF, 13.25% for soya IF, 14.16% for AA IF (expressed as protein equivalents from free AAs), and 10.11% for human milk. To mimic the in vivo consumption of these liquid foods, the protein content was not standardised before digestion. However, no significant differences in total protein content were found between dairy IF, soya IF, and human milk, at the end of the intestinal phase (3556 ± 314.4 μg/mL, BCA assay, $P > 0.05$, Supplementary Fig. 1 A).

SDS-PAGE revealed distinct digestion patterns. Dairy IF and human milk showed progressive loss of intact proteins such as caseins and α-lactalbumin, with human milk preserving lactoferrin (Supplementary Fig. 1B). Soya IF displayed a diffuse smear indicative of extensive hydrolysis, and AA IF showed no bands, consistent with its composition of free AAs (Supplementary Fig. 1B).

OPA assay confirmed progressive proteolysis across all samples, with similar degrees of hydrolysis (~82–85%) in dairy IF, soya IF, and human milk. AA IF showed higher initial free NH_2 content due to its formulation, which decreased upon dilution during digestion (Fig. 1A).

Size exclusion chromatography at the I60 timepoint (after gastric and intestinal digestion) revealed that digested AA IF consisted almost entirely of <0.5 kDa molecules (88%). In contrast, dairy IF, soya IF, and human milk revealed that the majority (90%) of compounds were < 5 kDa in size. Human milk uniquely retained a small fraction (>5%) of >50 kDa proteins, suggestive of digestion-resistant proteins (Fig. 1B).

To assess potential contributions from the digestion system itself, the simulated digestion water control (SGID H_2O), containing digestive enzymes but no food matrix, was analyzed in parallel. SDS-PAGE of undiluted SGID H_2O confirmed the presence of residual digestive enzymes (rabbit gastric extract and pancreatin). At the same time, size-exclusion chromatography showed a profile dominated by low-molecular-weight components, with the majority below 0.5 kDa (Supplementary Fig. 2 A and B).

To evaluate the nutritional quality of digested proteins, the concentrations of total hydrolyzed (Fig. 1C) and free (Fig. 1D) AAs were quantified in the bioaccessible fraction of the digesta (I60), defined as the methanol-soluble fraction containing protein digestion products released from the food matrix and present in a solubilized, potentially absorbable form (Grundy et al., 2025). These AAs weregrouped as branched-chain AAs (BCAAs), essential AAs (EAAs), and non-essential AAs (NEAAs).

Among digested dairy IF, soya IF, and human milk, total AA concentrations ranged from 357,060.6 ± 4180.8 μmol/L (human milk) to 430,180.2 ± 10,823.3 μmol/L (soya IF), with dairy IF at 394,794.6 ± 8488.2 μmol/L. Digested soya IF had significantly higher total AA content compared to digested human milk ($P < 0.05$). In digested dairy IF, soya IF, and human milk, NEAAs represented the majority of the total pool. EAAs ($P > 0.05$) and BCAA ($P > 0.05$) were similar across these digested samples.

Glutamic acid was the most abundant AA in dairy IF (51,845.7 ± 1325.9 μmol/L), soya IF (62,339.6 ± 14,38.66 μmol/L; $P < 0.05$), and human milk at the I60 timepoint (50,277.0 ± 699.0 μmol/L) (Fig. 1C and Supplementary Table 1 A). Digested dairy IF had the highest leucine (39,956.1 ± 11,45.6 μmol/L; P < 0.05) and lysine content (29,784.0 ± 573.34 μmol/L; $P < 0.05$). Soya IF had the highest arginine (24,264.6 ± 735.9 μmol/L; $P < 0.05$), glycine (50,334.3 ± 656.4 μmol/L; $P < 0.05$), serine (27,974.4 ± 905.7 μmol/L; $P < 0.05$) and aspartic acid content

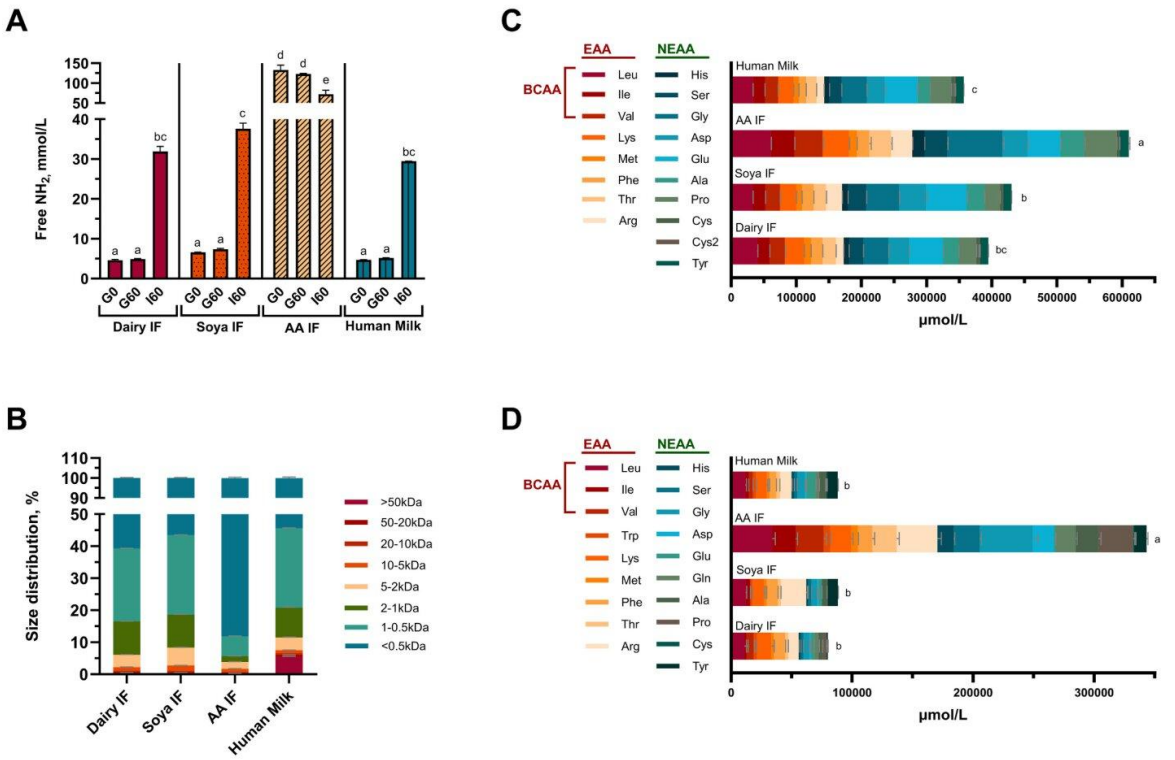


Fig. 1. Infant gastrointestinal digestion of Dairy, Soya and amino acid-based (AA) infant formulas (IF) and Human Milk (A) Degree of protein hydrolysis, assessed by OPA, at G0 (before gastric phase), G60 (after gastric phase) and I60 (after intestinal phase) timepoints. (B) Size exclusion chromatography of the soluble fraction at I60 timepoint. (C) I60 digesta Total amino acids, quantified by UPLC. (D) I60 digesta free amino acids quantified by UPLC. Data represent mean values from three independent digestions performed on separate days. Statistical analysis was performed using one-way ANOVA followed by Tukey's multiple comparisons test (A-C), or (D) Welch's one-way ANOVA followed by pairwise comparisons with Benjamini–Hochberg false discovery rate (FDR) correction. Different letters indicate statistically significant differences ($P < 0.05$). Amino acids are colour-coded as follows: red = branched-chain amino acids (BCAA), red + orange = essential amino acids (EAA), blue/green = non-essential amino acids (NEAA). (For interpretation of the references to colour in this figure legend, the reader is referred to the web version of this article.)

(41,279.4 ± 10,33.28 µmol/L; $P < 0.05$). Digested human milk contained the highest concentration of proline (32,463.9 ± 514.1 µmol/L; $P < 0.05$) (Fig. 1C and Supplementary Table 1 A).

Total free AA values were not significantly different among digested dairy IF (80,016.3 ± 8284.9 µmol/L), soya IF (88,309.6 ± 4960.9 µmol/L), and human milk (88,140.1 ± 5478.3 µmol/L; $P > 0.05$). Free EAAs and BCAA were similar in digested dairy IF, soya IF, and human milk ($P > 0.05$) (Fig. 1D).

Notably, digested soya IF showed significantly higher free arginine compared to dairy IF and human milk (20,914.9 ± 1024.6 µmol/L, $P < 0.05$), while digested human milk had significantly more free glutamic acid (7542.4 ± 588.1 µmol/L) than both dairy IF (2642.8 ± 367.2 µmol/L) and soya IF (2699.9 ± 155.0 µmol/L, $P < 0.05$) (Fig. 1D and Supplementary Table 1C).

Digested AA IF had significantly higher concentrations of AAs across all categories ($P < 0.05$) (Fig. 1 and Supplementary Table 1). Total AAs were 610,221.0 ± 13,721.7 µmol/L, with NEAAs and EAA at 214,226. ± 3090.7 µmol/L and 14,2834.5 ± 1135.39 µmol/L respectively, exceeding all other samples. Free AAs were equally elevated (343,283.8 ± 27,830.0 µmol/L), with glycine, leucine, and arginine ranking as the top three free residues (Supplementary Table 1C).

The total AA content and free AA content of SGID H_2O control were 99,888.9 ± 14,587.4 µmol/L and 25,382.0 ± 8797.2 µmol/L, respectively, indicating minimum AA contribution from digestive enzyme autolysis. In summary, human milk and infant formulas showed similar overall hydrolysis but differed in molecular size distribution and amino acid composition, reflecting matrix-specific digestion patterns. The contribution of amino acids arising from digestive enzyme autoproteolysis is shown in the SGID H_2O control (Supplementary Fig. 2C and D).

3.2. Digested IFs and human milk maintain infant-like barrier integrity

To assess the impact of digested IFs and human milk on intestinal barrier integrity, an infant-like epithelial monolayer was treated with digested samples. For comparison purposes Caco-2/HT29-MTX monolayers were included, representing an adult barrier (Hidalgo et al., 1989).

Initially, MTS assay was employed to determine the appropriate dilution to ensure biocompatibility of the digested samples with Caco-2/HT29-MTX co-cultures (Supplementary Fig. 3). Dilutions ≥1:14 of dairy IF, soya IF, AA IF, and human milk did not significantly affect cell viability compared to the SGID H_2O control ($P > 0.05$). In contrast, dilutions ≤1:9 resulted in a significant decrease in viability ($P < 0.05$). Therefore, 1:14 was selected as the highest non-toxic concentration for subsequent experiments.

To create an infant-like barrier, day 25 Caco-2/HT29-MTX monolayers were treated with 0.8 mM GDC, leading to the expected and

significant reduction in TEER (Bietto et al., 2025) from 1165 ± 11.85 Ω × cm^2 to 412.15 ± 18.98 Ω × cm^2 (experiment baseline TEER) (Fig. 2A). Following 2 h exposure to digesta (T2), infant-like cultures maintained stable TEER values regardless of milk formulation (Fig. 2A; $P > 0.05$).

At baseline (T0), adult-like monolayers had a TEER value of 1010.90 ± 96.96 Ω × cm^2. No significant TEER reduction was observed in adult-like monolayers with the digested dairy IF, soya IF, or human milk samples for 2 h (T2) ($P > 0.05$). Treatment with digested AA IF resulted in a significant drop in TEER in adult-like monolayers (Fig. 2B; $P < 0.05$).

3.3. Digested human milk enhances OCLN–actin co-localization in infant-like monolayers

To investigate whether exposure to digested IFs or human milk promotes gut barrier maturation, tight junction protein OCLN was labelled in Caco-2/HT29-MTX co-cultures under infant- and adult-like conditions after 2 h treatment. OCLN localization was assessed by fluorescence intensity normalized to nuclei count (Fig. 3, Supplementary Fig. 4). Its spatial relationship with the actin cytoskeleton was evaluated through co-localization analysis (Fig. 4).

Infant-like monolayers treated with digested human milk exhibited a distinct pattern of OCLN distribution, characterized by focal accumulation of OCLN at cell junctions, visible as dot-like structures (Fig. 3A, white arrows), which were not present in adult monolayers. In the adult-like model, treatment with dairy IF, AA IF, or human milk digesta resulted in lower OCLN intensity than with soya IF ($P < 0.05$). Digested AA IF significantly increased OCLN fluorescence intensity in infant-like monolayers, compared to digested dairy IF ($P < 0.05$).

When comparing infant- vs. adult-like conditions within each treatment, baseline OCLN fluorescence under HBSS control was significantly lower in infant-like monolayers (120,127 ± 9556) than in adult-like monolayers (201,627 ± 2397; $P < 0.05$, Fig. 3B). Similarly, soya IF treatment induced significantly higher OCLN intensity in adult-like monolayers compared to intensity in the infant-like model ($P < 0.05$).

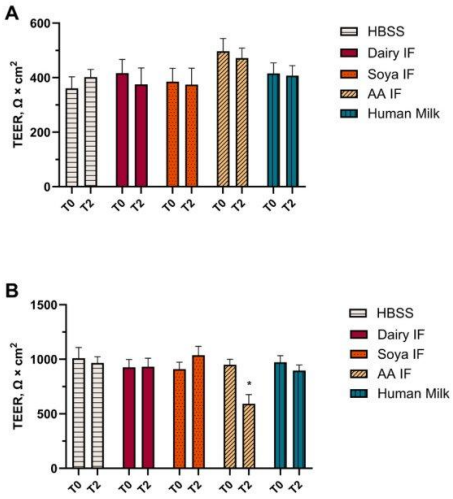


Fig. 2. Transepithelial electrical resistance (TEER) of Caco-2/HT29-MTX monolayers treated with digested infant formulas (IF) or Human Milk. (A) Infant-like and (B) adult-like monolayers (90:10) were exposed for 2 h to digested Dairy IF, Soya IF, amino acid-based (AA) IF, and Human Milk (1:15 in HBSS). TEER at day 25 = 1165 ± 11.85 Ω × cm^2. T0 = Before digesta addiction; T2 = post-treatment. Data are mean ± SEM from six biological replicates (three digestions × two exposures × duplicate wells; $n = 12$). One-way ANOVA with Tukey's test; *$P < 0.05$ vs. HBSS.

To further examine the interaction between OCLN and the actin cytoskeleton, Pearson's and Manders' co-localization coefficients were calculated for OCLN and actin signals (Fig. 4). Pearson's coefficient, which reflects the degree of spatial alignment between OCLN and the actin cytoskeleton, was significantly increased by digested human milk on infant-like monolayers compared to the infant HBSS control (0.32 ± 0.02 vs. 0.37 ± 0.01; $P < 0.05$, Fig. 4A). In contrast, both soya IF and human milk significantly reduced Pearson's coefficient in the adult-like model relative to HBSS ($P < 0.05$).

When comparing across developmental models, HBSS-treated infant monolayers exhibited a significantly lower Pearson's coefficient than adult monolayers (0.27 ± 0.02 vs. 0.40 ± 0.01; $P < 0.05$). Interestingly, both soya IF and human milk significantly increased this coefficient in the infant-like model compared to their adult counterparts ($P < 0.05$), suggesting increased spatial alignment between OCLN and actin under infant conditions.

These findings were supported by Manders' coefficient M1, which reflects the fraction of the OCLN signal that overlaps with actin. M1 was increased in infant-like monolayers treated with soya IF compared to HBSS control ($P < 0.05$, Fig. 4B). In the adult model, M1 was significantly reduced following exposure of monolayers to dairy IF and human milk compared to HBSS control ($P < 0.05$, Fig. 4B). Among all treatments, HBSS-treated infant monolayers displayed significantly lower M1 values than adults (0.33 ± 0.03 vs. 0.65 ± 0.04; $P < 0.05$, Fig. 4B).

M2 (fraction of actin overlapping OCLN) was less biologically informative, as actin is broadly distributed and its overlap with OCLN does not specifically reflect tight junction structure. Nevertheless, M2 was significantly reduced in soya and AA IF groups for infant and dairy and AA IF for adult compared to HBSS (infant coefficient = 0.14 ± 0.03; adult coefficient = 0.25 ± 0.04, $P < 0.05$, Supplementary Fig. 5). No significant difference was found in M2 for adult and infant monolayer with HBSS treatment.

Interestingly, orthogonal views of z-stack images revealed a significant increase in monolayer thickness, reflective of greater cell height, in our infant-like model with HBSS treatment versus the standard Caco-2/HT29-MTX monolayer with HBSS (13.54 ± 0.34 μm vs. 12.12 ± 0.41 μm; $P < 0.05$) (Supplementary Fig. 6).

3.4. AA IF shows the highest basolateral free AAs levels

Fig. 5 depicts the free AA concentration found in the basolateral compartment of Caco-2/ HT29-MTX monolayers after 2 h exposure to digesta (T2-basolateral). Supplementary Tables 2 A and B report the specific concentrations and statistical comparisons for all free AAs measured in the T2-basolateral compartment. Across all conditions, the five most abundant AAs present in the T2-basolateral samples were lysine, aspartic acid, arginine, threonine, and serine. These five AAs accounted for approximately 50–58% of the total free AAs found in the T2-basolateral compartment across all samples.

In the infant model, treatment with AA IF resulted in a mean free AAs concentration of 8.275 ± 0.362 mg/L, which was higher ($P < 0.05$) than that observed for soya IF (6.444 ± 0.335 mg/L), dairy IF (6.634 ± 0.279 mg/L), and human milk (6.915 ± 0.326 mg/L) treatments. In the adult-like model, treatment with AA IF again led to the highest free AAs levels (7.712 ± 0.360 mg/L), exceeding those from soya IF (6.182 ± 0.094 mg/L), dairy IF (5.728 ± 0.015 mg/L), and human milk (6.275 ± 0.308 mg/L) treatments.

Interestingly, the total amount of free AAs found in the T2-basolateral side was significantly higher in the infant-like model than in the adult for dairy IF (6.64 ± 0.09 vs. 5.73 ± 0.01 mg/L; $P < 0.05$), driven largely by increased transport of glycine (0.27 ± 0.02 mg/L) and serine (0.62 ± 0.11 mg/L) in the infant model ($P < 0.05$). Supplementary Fig. 7 shows the total free AA concentrations in the T2-basolateral compartment of the HBSS control condition, which were not significantly different ($P > 0.05$) between infant-like (3.41 ± 0.52 mg/L) and adult-like (3.97 ± 0.17 mg/L) monolayers. Importantly, these

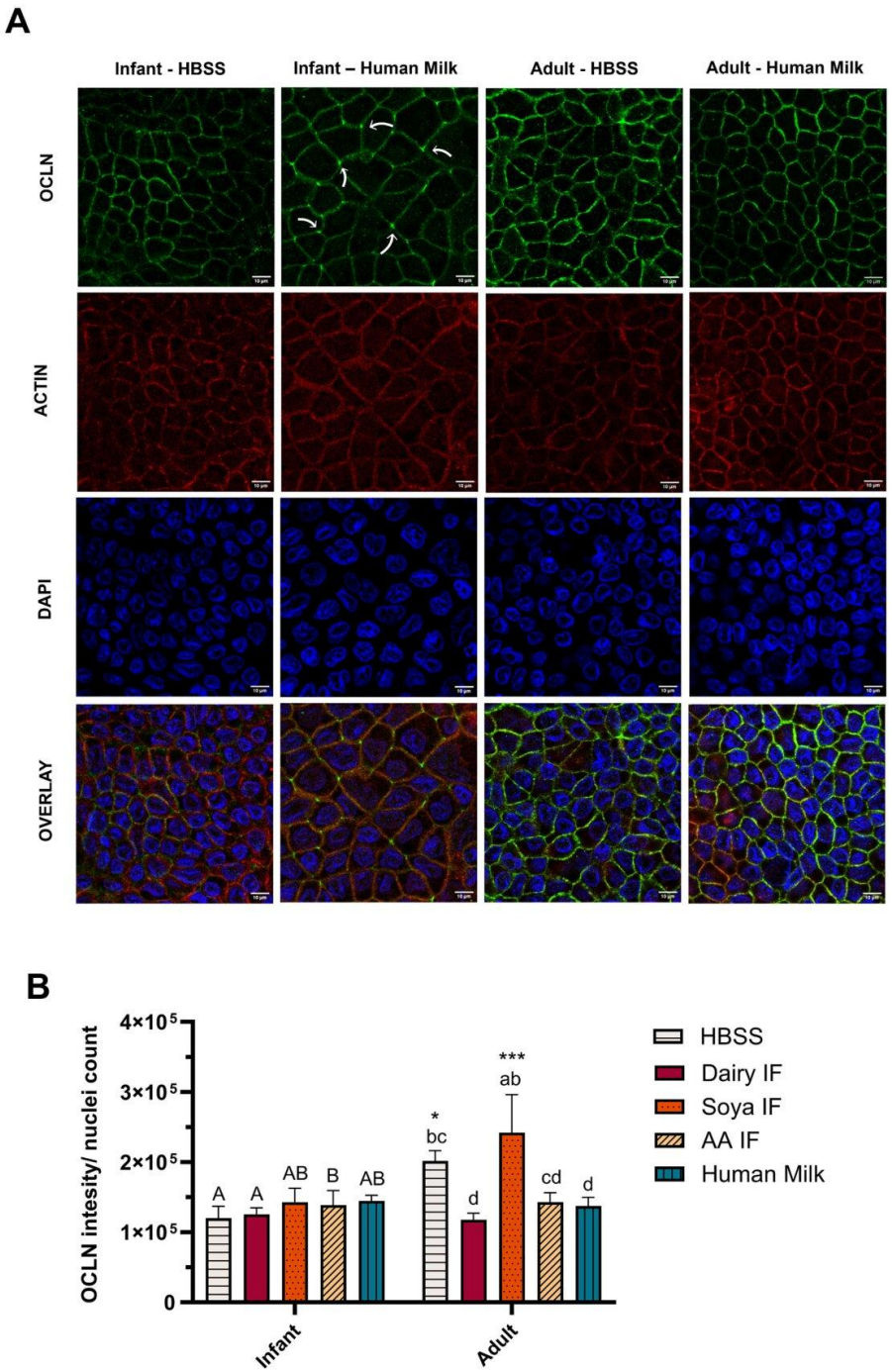


Fig. 3. Occludin (OCLN) localization in infant and adult-like Caco-2/HT29-MTX monolayers treated with digested Human Milk. Monolayers (90:10) were cultured for 25 days and treated for 2 h with HBSS (control) or digested Human Milk. (A) Representative confocal images showing OCLN (green), actin (red), and nuclei (blue); white arrows highlight membrane OCLN with Human Milk. Scale = 10 μm. (B) OCLN fluorescence intensity normalized to nuclei count. Data are mean ± SEM from three biological replicates ($n = 9$). One-way ANOVA with Tukey's test: different letters indicate significant differences within infant (uppercase) or adult (lowercase) models; asterisks indicate significant differences between infant and adult models within the same treatment ($^{*}P < 0.05$; $^{***}P < 0.001$). Fluorescence intensity and co-localization analysis was performed on raw image files. Brightness and contrast were then adjusted equally across the entire image for visualization purposes. (For interpretation of the references to colour in this figure legend, the reader is referred to the web version of this article.)

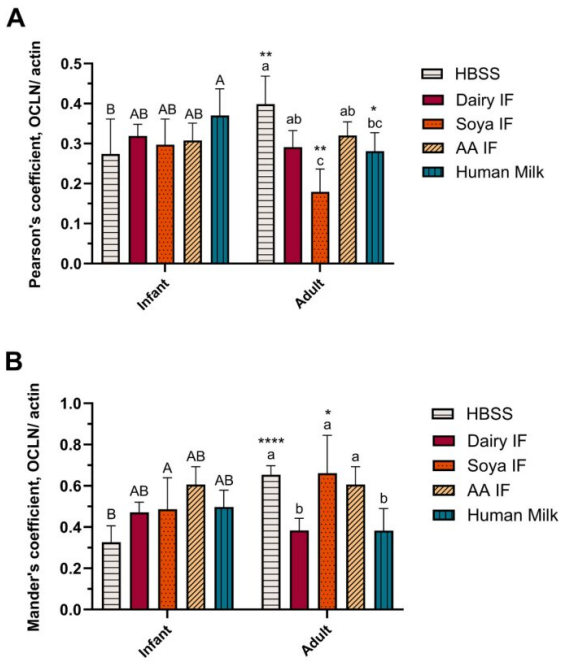


Fig. 4. Colocalization of occludin (OCLN) and actin in infant- and adult-like Caco-2/HT29-MTX monolayers exposed to digested infant formulas (IF) and Human Milk. Adult- and infant-like Caco-2/HT29-MTX (90:10) monolayers (day 25) were treated for 2 h with digested Dairy, Soya, or amino acid-based (AA) IF or Human Milk. Confocal images were analyzed in FIJI (ImageJ). (A) Pearson's coefficient quantifies overall OCLN–actin co-localization. (B) Manders' M1 coefficient shows the fraction of OCLN overlapping with actin. Data are mean ± SEM from three biological replicates (n = 9). One-way ANOVA with Tukey's test: different letters indicate differences between treatments within infant (uppercase) or adult (lowercase) models; asterisks indicate significant differences between infant and adult models ($P < 0.05$).

background levels were ~ 2-fold lower than the T2-basolateral free AA concentrations measured after exposure to digested dairy IF, soya IF, AA IF, and human milk (Fig. 5), indicating that the AAs detected in the transport experiments originated from the formulations rather than the buffer or cell system. Free AA in basolateral T2 samples were quantified by UHPLC–HRMS/MS (Supplementary Fig. 6). Supplementary Tables 2C and 2D also include UHPLC–HRMS/MS data for digesta samples for comparison purposes.

3.5. Infant-like monolayers exhibit higher peptide transport and higher sequence diversity

To identify peptides present post-digestion and post-absorption, UHPLC–HRMS/MS was performed in the digesta (I60), T2-apical and T2-basolateral samples for all foods (dairy IF, soya IF and human milk). Database searches were performed against custom UniProtKB FASTA files corresponding to *Bos taurus* (dairy), *Glycine* max (soya) or *Homo sapiens* (human milk), allowing only data comparisons between infant and adult-like monolayers.

Fig. 6 depicts total unique peptide counts in digesta, infant (A, C, E) and adult (B, D, F) models. Detailed counts of unique and shared peptides across digesta, T2- apical, and T2-basolateral samples for each formulation and model are provided in Supplementary Tables S3.

To define the baseline peptide pool available for epithelial interaction, digesta samples were first characterized for peptide abundance and physicochemical properties (Supplementary Tables S4). A total of 170, 229, and 129 unique peptides were identified in dairy IF, soya IF, and human milk digesta, respectively. Across all formulations, digesta peptides were predominantly short, with oligopeptides (4–10 amino acids) representing 61.17% of dairy IF, 61.14% of soya IF, and 75.19% of human milk peptides. In contrast, peptides longer than 20 amino acids accounted for ≤3.49% of the total in all cases. Consistently, human milk digesta peptides were primarily distributed within the 500–1000 Da range (55.04%), while the 1000–2000 Da range predominated in dairy IF (56.47%) and soya IF (56.33%). Hydrophobicity profiles differed between digesta samples. Dairy IF peptides were predominantly neutral (80.59%), with 17.06% hydrophilic and 2.35% hydrophobic peptides. Soya IF peptides showed a higher proportion of hydrophilic sequences (50.22%) and fewer neutral peptides (48.47%), with hydrophobic peptides remaining rare (1.31%). Human milk peptides displayed an intermediate profile, dominated by neutral peptides (67.44%), with

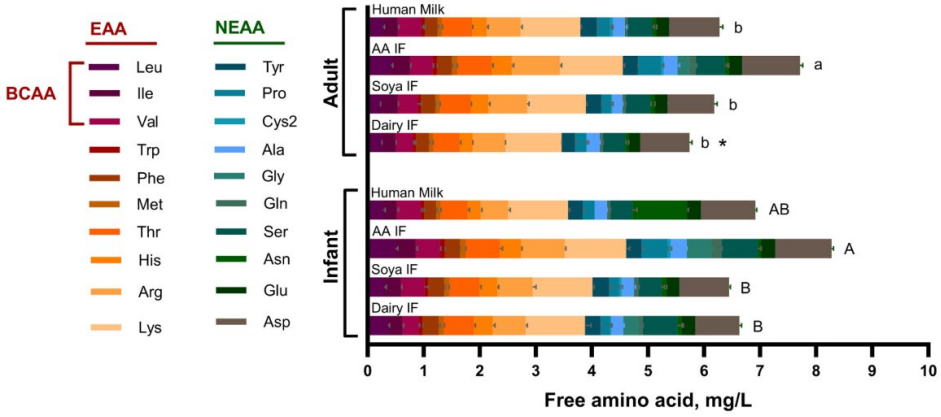


Fig. 5. Free Amino acid concentration in the basolateral compartments of Caco-2/HT29-MTX monolayers treated with digested Infant Formulas (IF) and Human Milk. Free amino acid concentrations (mg/L) in the basolateral compartment of infant-like and adult-like monolayers exposed for 2 h to digested Dairy IF, Soya IF, amino-acid (AA) IF, and Human Milk, measured by UHPLC-HRMS/MS. Data are mean ± SEM from three biological replicates (technical duplicates). One-way ANOVA with Tukey's test: different letters indicate differences between treatments within infant (uppercase) or adult (lowercase) models; asterisks indicate adult vs. infant differences ($P < 0.05$). Amino acids: red = BCAA, red + orange = EAA, blue/green = NEAA. (For interpretation of the references to colour in this figure legend, the reader is referred to the web version of this article.)

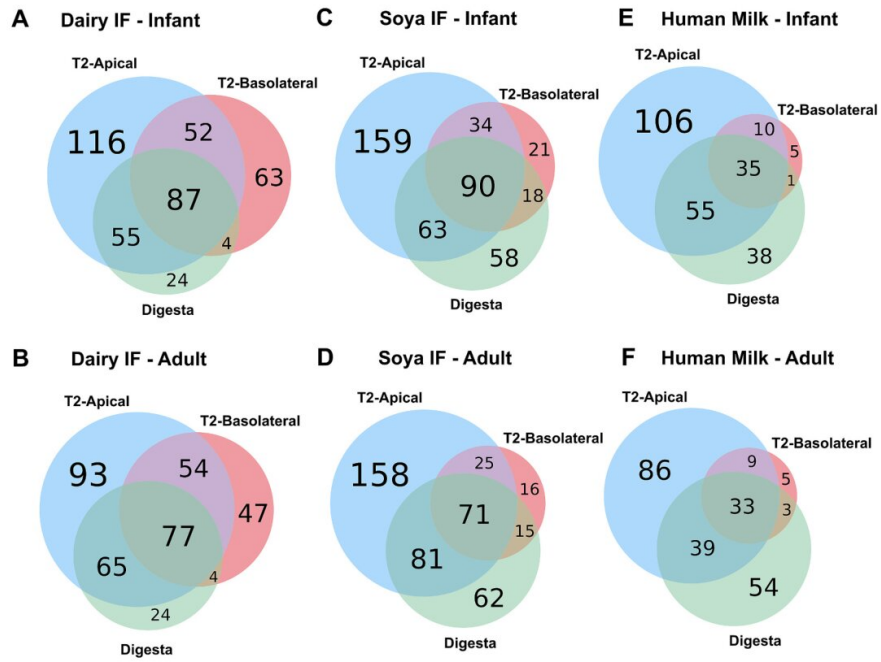


Fig. 6. Venn diagrams of unique peptides detected in infant- and adult-like monolayers treated with digested Dairy IF, Soya IF or Human Milk Infant- and adult-like monolayers were treated for 2 h (T2) with digested Dairy IF, Soya IF, or Human Milk. Peptides identified by UHPLC–HRMS/MS in digesta (green) compartments, in T2-apical (blue) and in T2-basolateral (red. Panels: (A–B) Dairy IF, (C—D) Soya IF, (E–F) Human Milk in infant and adult models. (For interpretation of the references to colour in this figure legend, the reader is referred to the web version of this article.)

28.68% hydrophilic and 3.88% hydrophobic peptides. Amino acid composition of the peptides revealed distinct but biologically consistent differences between digesta samples. Dairy IF and human milk digesta peptides were strongly enriched in proline (26.3% and 25.5%, respectively), whereas soya IF digesta contained a lower proportion of proline (17.0%). In contrast, soya digesta peptides showed a marked enrichment in acidic residues, with glutamic acid and aspartic acid together accounting for approximately 21.09% of total residues, compared with 11.70% in dairy IF and 9.89% in human milk digesta. Branched-chain amino acids (valine, leucine, and isoleucine) were more abundant in dairy IF and human milk digesta (23% and 22.96% respectively) than in soya IF digesta 15.03%), contributing to a higher proportion of neutral peptides. Human milk digesta further exhibited elevated glutamine content (11.6%).

Regarding peptides detected after epithelial exposure, differences in peptide diversity and compartmental overlap were assessed in infant- and adult-like models.

For dairy IF, 206 and 182 unique peptides were identified in the T2-basolateral compartments of infant- and adult-like models, respectively. In the T2-apical compartments, 310 unique peptides were detected in the infant model and 289 in the adult. In the infant model, 139 unique peptides were common to both T2-apical and T2-basolateral samples, 52 of which were absent from the digesta. In the adult monolayer treated with dairy IF digesta, the T2-apical and T2- basolateral samples had 131 peptides in common, of which 54 were not present in the digesta. Additionally, 67 peptides were found in the infant T2-basolateral compartment only (not detected in T2-apical or digesta), compared with 47 in the adult T2-basolateral compartment only.

For soya IF, the infant- and adult-like models yielded 163 and 127 unique peptides in the T2-basolateral compartment and 335 and 366 in the T2-apical compartment, respectively. Of these, 124 (infant) and 96 (adult) were shared across compartments, while 39 and 31 were in the T2-basolateral sample only. Thirty-four peptides (infant) and 25 (adult) were shared between apical and basolateral compartments but were not present in the digesta.

For human milk, the infant- and adult-like models yielded 206 and 167 unique peptides in the T2-apical compartment and 51 and 50 in the T2-basolateral compartment, respectively. Of these, 45 (infant) and 42 (adult) were shared across compartments. Notably, 10 (infant) and 8 (adult) of these shared peptides were absent from the digesta. Six (infant) and 8 (adult) peptides were found in the T2-basolateral side only.

To further characterize basolateral transport, physicochemical properties were analyzed in silico (Supplementary Table S5). In all matrices, the majority of transported peptides (>80% for dairy and 100% for soya and human milk) exceeded 3 AAs. Among peptides common to both models, median length was 7 AAs for dairy IF and 9 AAs for both soya IF and human milk. Among peptides exclusive to a single model, infant-exclusive dairy peptides were the shortest (median 4 AAs), whereas adult-exclusive soya peptides were the longest (median 13 AAs). Soya IF peptides exhibited more negative median charge and lower hydropathy values than dairy IF and human milk peptides. Infant-like monolayers consistently yielded a higher number of unique basolateral peptides across matrices.

Across all foods, the number of peptides identified in the T2-apical samples exceeded those in the original digesta. Moreover, each formula showed a subset of peptides shared between T2-apical and T2-basolateral compartments but absent from the digesta. Together, these findings suggest that brush border enzymes further cleave dietary peptides during the 2 h incubation, generating new fragments capable of transepithelial transport.

Interestingly, the peptides exclusive to the infant-like monolayer with dairy IF treatment had a lower median length (3.5 AAs) than those in the adult-like monolayer (4 AAs) and included a notably higher number of tripeptides (39 vs. 14 in adults). In contrast, peptides

exclusive to the infant-like monolayer with soya IF or human milk treatments were generally longer (soya IF: median infant = 9, adult = 8; human milk: median infant = 8, adult = 4.5), suggesting less hydrolysis.

3.6. Apical peptides reflect active brush border enzyme cleavage

With dairy IF, soya IF, and human milk treatments, a substantial number of unique peptides were detected in the T2-apical compartment that were not present in the digesta, suggesting further processing by epithelial peptidase enzymes. To explore whether the peptides identified in the apical compartment were a result of brush border enzyme activity, peptides present in the T2-apical chamber were assigned to parental digesta peptides with cleavage sites mapped to known intestinal brush border enzymes. Predicted brush border enzyme cleavage events and associated peptide origins are reported in Supplementary Tables S6. Fig. 7 illustrates the total number of times each brush border enzyme was involved in cleaving apical peptides, with higher event counts indicating greater predicted brush border activity. When including both 1-step and multi-step cleavage events, the infant-like model had 51 (dairy IF treatment), 61 (soya IF treatment), and 31 (human milk treatment) cleavage events. The adult-like model had 52 (dairy IF treatment), 59 (soya IF treatment), and 27 (human milk treatment) cleavage events. Tripeptidyl peptidase II, aminopeptidase N, and dipeptidyl peptidase-4 were the most commonly assigned brush border enzymes across all conditions, collectively accounting for the majority of predicted cleavage events.

In terms of peptide counts, the T2-apical sample collected with dairy IF treatment showed 36 single-step and 11 multi-step peptides in the infant-like model, compared to 36 single-step and 10 multi-step in the adult-like model. With soya-IF treatment, the T2-apical sample of infant monolayers had 41 single-step and 12 multi-step peptides, while the T2-apical sample from adult-like monolayers had 38 single-step and 12 multi-step peptides. With human milk treatment, the T2-apical sample of infant-like monolayers yielded 26 single-step and 4 multi-step peptides, compared with 22 and 4 in the T2-apical sample of adult-like model.

3.7. Infant-like monolayers show enhanced basolateral peptide load in response to human milk

To study the total load of peptides transported across the intestinal barrier, both the total peptide intensity (log_2-normalized) and the total number of peptides (including repeated detections of the same sequence) in T2-apical (Fig. 8A, B) and T2-basolateral (Fig. 8C, D) samples were quantified.

In the T2-basolateral compartment, both the total peptide intensity and count were significantly higher in the infant model treated with digested human milk compared to the adult model ($P < 0.05$). Peptide intensity was 30.10 ± 0.24 in infants versus 28.58 ± 0.22 in adults, and peptide count was 68.67 ± 0.67 vs. 60 ± 1, respectively. With dairy and soya IF treatments, no significant differences in peptide intensity or count were detected between infant and adult models on the T2-basolateral side ($P > 0.05$).

In the T2-apical compartment, no significant differences in peptide intensity (reflecting relative abundance) and count were observed between infant and adult monolayers for any of the food conditions ($P >$

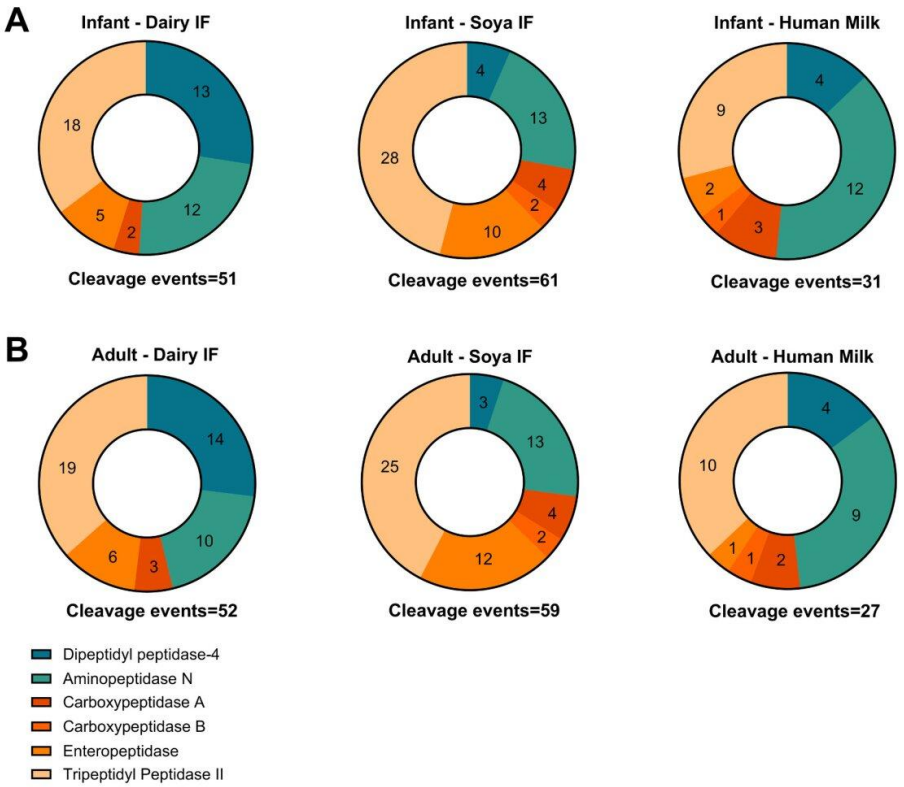


Fig. 7. Cleavage events attributed to specific brush border enzymes. (A) Infant-like and (B) adult-like Caco-2/HT29-MTX monolayers were treated for 2 h (T2) with digested Dairy IF, Soya IF, and Human Milk. Peptides identified in the T2-apical compartment (UHPLC–HRMS/MS) were compared with those in digesta to map new cleavage sites. Cleavage motifs were matched to specific enzymes, with higher event counts indicating greater predicted brush border activity.

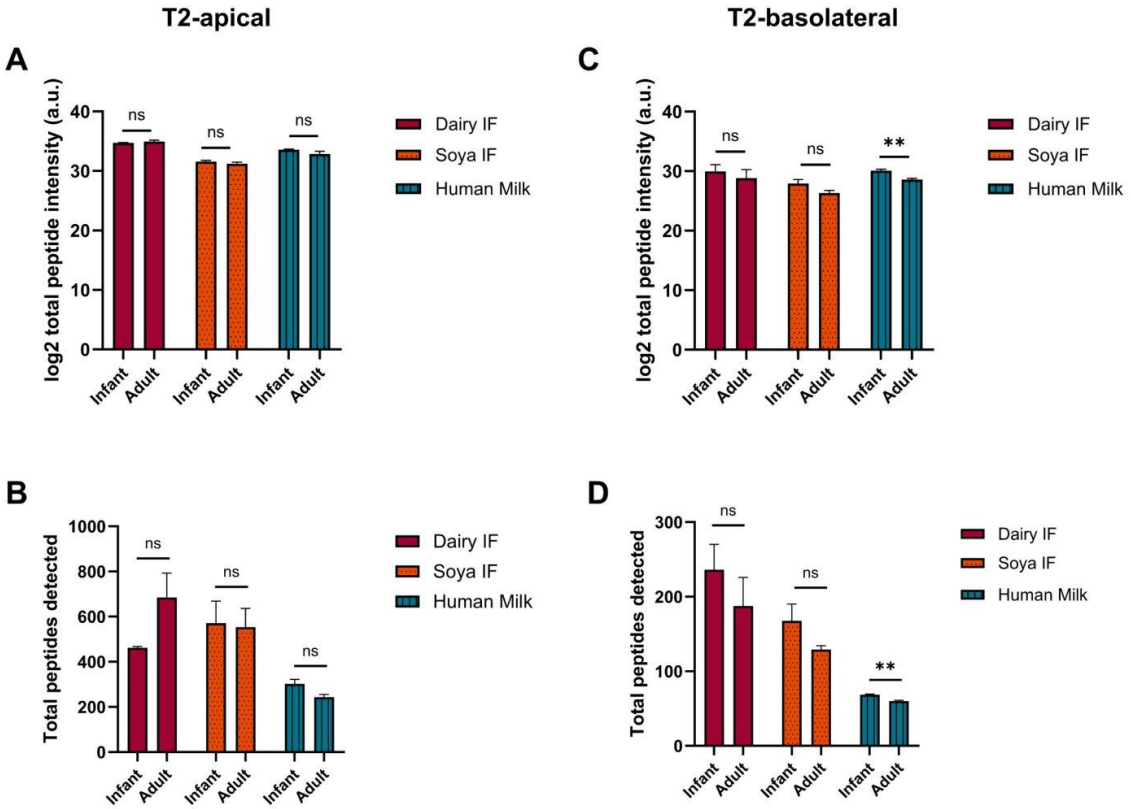


Fig. 8. Peptide transport across infant- and adult-like monolayers after exposure to digested infant formulas (IFs) and Human Milk. Infant-like and adult-like monolayers (day 25, Caco-2/HT29-MTX 90:10) were treated for 2 h (T2) with digested Dairy IF, Soya IF, and Human Milk. UHPLC–HRMS/MS was used to measure: (A, C) log_2-transformed total peptide intensity and (B, D) total peptide count in apical and basolateral compartments at T2. Data are mean ± SEM from three biological replicates. Unpaired *t*-tests compare infant and adult models; asterisks indicate significant differences ($P < 0.05$).

0.05).

3.8. Human milk-derived bioactive peptides are more abundant in infant-like monolayers

To assess whether peptides present in the T2-apical and T2-basolateral compartments exhibited bioactivity, PeptideRanker was employed to predict bioactivity scores based on sequence motifs (Mooney et al., 2012). The results were, matched against the BIOPEP and MBPD databases, which catalogue experimentally validated and predicted bioactive peptides. Fig. 9 displays volcano plots of log_2 intensity differences (infant – adult) for individual peptides, highlighting those with predicted or confirmed bioactivities. All identified bioactive peptides, their predicted functions, and statistical comparisons are reported in Supplementary Tables S7 (dairy IF), S8 (soya IF), S9 (human milk). Peptides with multiple predicted bioactivities were included in the count for each functional category to capture their multifunctional potential.

In the T2-apical compartment, monolayers treated with dairy IF yielded the highest number of bioactive peptides ($n = 86$), primarily linked to ACE inhibition ($n = 45$), antioxidative activity ($n = 21$), DPP-IV inhibition ($n = 12$), immunomodulation ($n = 11$), and AChE inhibition (n = 8). Among these, three peptides with antioxidant, DPP-IV inhibitory, and hypouricemic functions were more abundant in the infant model, while two antiamnestic and ACE-inhibitory peptides were higher in adult-like monoaleyrs. T2-apical samples from monolayers treated with human milk contained 11 bioactive peptides, mostly ACE inhibitors ($n = 6$) and DPP-II inhibitors ($n = 3$), with individual peptides also associated with antioxidant, anticancer, opioid, cholesterol-regulating, and growth-promoting activities (n = 1 each). Two ACE-inhibitory peptides were significantly higher in infant monolayers. T2-apical samples form monolayers treated with soya IF contained only one identified bioactive peptide with both ACE-inhibitory and antioxidant potential.

In the absorbed fraction (T2-basolateral), monolayers treated with dairy IF contained 54 bioactive peptides, with functional classifications including ACE inhibition ($n = 26$), antioxidant ($n = 14$), and DPP-IV inhibition ($n = 12$). One opioid peptide (β-casein ^{75}YPF^{77}) was more abundant in T2-basolateral from infant monolayers, while one ACE-inhibitory peptide (κ-casein ^{77}LPYP^{80}) was higher in adult T2-basolateral. T2-basolateral samples from monolayers treated with soya IF yielded a single antioxidant peptide (β -conglycinin ^{267}SLVNNDDRDS^{276}). T2-basolateral samples from monolayers treated with human milk contained five bioactive peptides: two with ACE-inhibitory activity, one with antioxidant activity, one with both ACE-inhibitory and antioxidant activity, and one with cholesterol-regulating activity. Notably, four of the five peptides were detected at significantly higher intensity in the infant model than in the adult ($P < 0.05$).

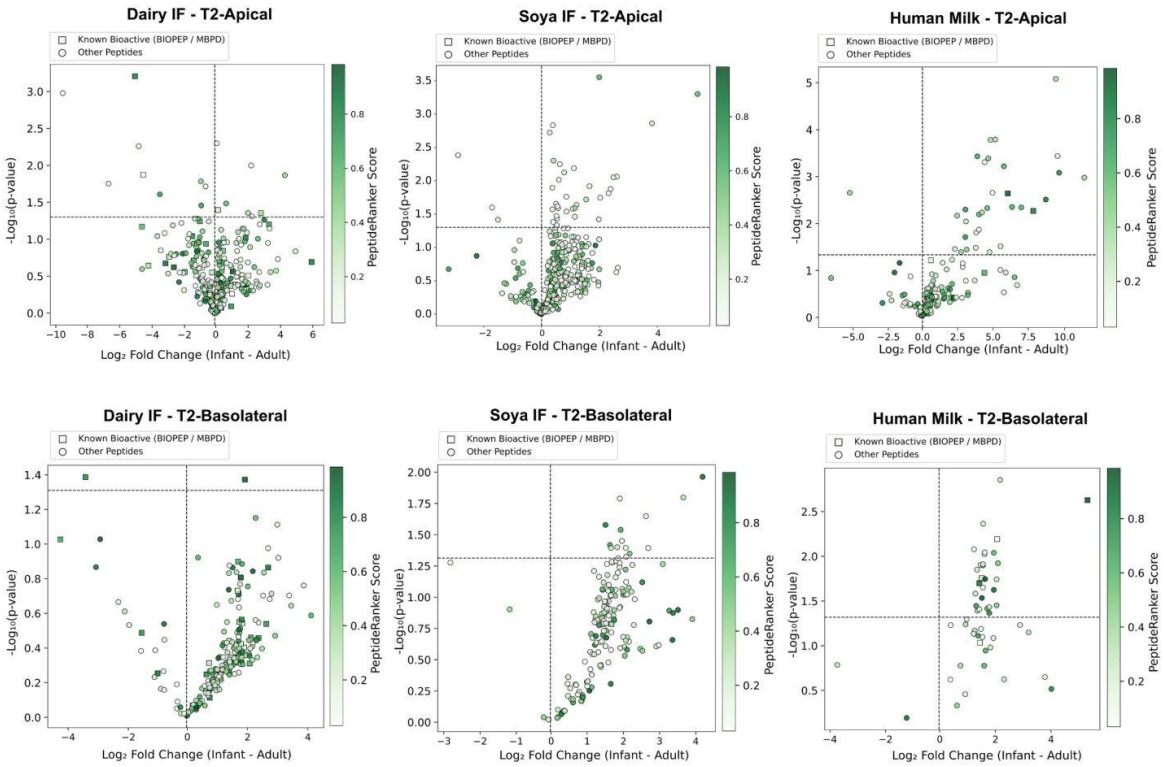


Fig. 9. Volcano plots of peptide abundance differences between infant- and adult-like models after exposure to digested infant formulas (IF) and Human Milk. Infant- and adult-like Caco-2/HT29-MTX monolayers were treated for 2 h (T2) with digested Dairy IF, Soya IF, and Human Milk. Peptides identified by UHPLC–HRMS/MS in the (A) T2-apical and (B) T2-basolateral samples are shown. Each point represents a peptide; X-axis = $\log_2$ fold change (infant − adult), Y-axis = $-\log_{10}$(*P*-value) from unpaired t-tests. Horizontal line indicates $P = 0.05$. The vertical line at $\log_2$ fold change = 0 separates peptides enriched in the infant model (right side, positive values) from those enriched in the adult model (left side, negative values). The upper-right quadrant highlights peptides significantly more abundant in infants, while the upper-left quadrant highlights peptides significantly more abundant in adults. Colour intensity reflects predicted bioactivity (PeptideRanker); darker green = higher bioactivity. Squares = peptides matched to known bioactive sequences (BIOPEP/MBPD), circles = unmatched peptides. (For interpretation of the references to colour in this figure legend, the reader is referred to the web version of this article.)

4. Discussion

In this study, infant- and adult-like Caco-2/HT29-MTX models were treated with gastrointestinal digests of human milk, dairy IF, soya IF or AA IF. The main findings were (i) human milk uniquely enhanced OCLN–actin co-localization and increased basolateral bioactive peptides in the infant-like model, (ii) IFs showed limited effects on both models, with AA–based formula increasing OCLN intensity in infant-like monolayers whilst lowering TEER in adult-like monolayers, and (iii) dietary peptide transport and diversity were consistently higher in infant- than adult-like models, highlighting the value of age-appropriate systems for infant nutrition research.

The primary finding for human milk was that treatment of the infant-like monolayer resulted in significantly increased OCLN/actin co-localization (Fig. 4, $P < 0.05$), indicating tight junction remodeling despite no overall change in OCLN expression or TEER values (Fig. 2; $P > 0.05$). Confocal imaging confirmed brighter OCLN staining at intercellular junctions. Importantly, these effects were unique to the infant-like model and absent in the adult-like condition. OCLN participates in maintaining epithelial barrier function by modulating paracellular permeability and coordinating tight junction assembly through its interactions with cytoplasmic adaptors (e.g., ZO1) and the actin cytoskeleton (Cummins, 2012). Because OCLN is physically anchored to the perijunctional actin ring via scaffold proteins, its spatial organization is inherently linked to actin architecture. Therefore, changes in OCLN–actin co-localization reflect remodeling of tight junction structural organization. Given that actin is broadly distributed throughout the cytoplasm while OCLN is confined to junctional regions, complete pixel overlap is not expected; thus, moderate Pearson's coefficient values are consistent with tight junction biology.

The age-specific difference in OCLN–actin co-localization may reflect differences in intracellular signaling between models. In our previous work, we showed that the GDC-induced infant-like monolayer exhibits reduced intracellular cAMP levels via TGR5–Gαi signaling, associated with altered tight junction organization (Bietto et al., 2025). Because cAMP signaling regulates tight junction organization, reduced baseline cAMP in the infant-like model may contribute to the enhanced OCLN redistribution following exposure to human milk.

These structural changes observed in our infant-like model are interesting in the context of Noel et al. study, who reported that human colostrum induced a granular OCLN pattern in pediatric enteroids, particularly co-localizing with goblet (trefoil factor 3 +) and Paneth (lysozyme +) cells (Noel et al., 2021). Kondrashina et al. (2024) observed no OCLN upregulation ($P > 0.05$) after 4 h exposure to digested human milk and dairy IF (500 μg/cm^2) in Caco-2/HT29-MTX monolayers, although TEER was significantly increased compared with HBSS controls (664 ± 72 Ω·cm^2; $P < 0.05$) (Kondrashina et al., 2024). Kondrashina et al. used an adult-like Caco-2/HT29-MTX model,

whereas our study and that of Noel et al. employed infant-like or pediatric enteroid systems, which may better capture age-specific responses. Although human milk is complex, the peptide and AA profiles post-gastrointestinal digestion may play a role in this OCLN response. SEC revealed large proteins/peptides remaining) at the end of the intestinal phase (MW > 50 kDa-Fig. 1B). SDS-PAGE had a persistent ~80 kDa band likely to be glycosylated lactoferrin, known to be resistant to digestion (Ma et al., 2021; Van Berkel et al., 1995). Lactoferrin has been shown to improve gut barrier function directly, exerting its biological effects in the gut lumen (Conesa et al., 2023). Also, in Caco-2 monolayers, Zhao et al. (2019) demonstrated that treatment with bovine lactoferrin significantly increased both mRNA and protein levels of OCLN and promoted its redistribution to the cell membrane, as shown by immunofluorescence (Zhao et al., 2019). Importantly, there is currently no evidence to support efficient transepithelial transport of intact lactoferrin in term infants (Mastromarino et al., 2014; Scott, 1989). Consistent with in vivo data, no lactoferrin-derived peptides were detected in the basolateral compartment of our Caco-2/HT29-MTX barrier. However, our analytical approach is optimized for low–molecular-weight peptide profiling and does not enable assessment of intact protein uptake.

In addition to lactoferrin, digested human milk contained significantly higher levels of free glutamic acid. In vitro, glutamic acid improves TEER in infant pig IPEC-J2 monolayers (0.5 mmol/L) (Jiao et al., 2015). As both a precursor and product of glutamine, glutamic acid also contributes indirectly to gut barrier maturation, since glutamine upregulates tight junction proteins (OCLN, CLDN1/4, ZO1/2/3) and restores barrier integrity (improved TEER and reduced ^{14}C-mannitol and FITC-dextran flux) in Caco-2 monolayers (Kim & Kim, 2017).

Peptide profiling of human milk revealed greater T2-basolateral transport and diversity in the infant- compared to the adult-like model (51 vs. 50 unique T2-basolateral peptides, UHPLC–HRMS/MS intensity 30.10 ± 0.24 $\log_2$ vs. 28.58 ± 0.22; total counts 68.67 ± 0.67 vs. 60.00 ± 1.00; Figs. 6 and 8; $P < 0.05$). The T2-apical compartment yielded 206 unique milk peptides for the infant and 167 for the adult. Previously, Liang et al. (2022) identified 169 peptides in the apical chamber and 44 peptides in the basolateral chamber after applying a digested human milk extract (10 μg/mL) to Caco-2 monolayers for 12 h. There was overlap with our data, including β-casein ^{138}NLHLPLP^{144} (ACE-inhibitory activity) and additional β-casein fragments such as ^{126}FDPQIPK^{132}, ^{210}PVTQPLAPV^{220}, and ^{96}PEIMEVPKA^{104}. In contrast, Kondrashina et al. (2024) reported only 17 basolateral peptides after 4 h exposure to human milk, of which 6 were common to our study. In terms of peptide abundance in the T2-basolateral compartment, the most abundant peptide for human milk was β-casein ^{126}FDPQIPK^{132} (1.17-fold higher in the infant-like model; $P > 0.05$), followed by β-casein ^{176}VLPIPQ^{181} (1.06-fold higher in the infant-like model; $P < 0.05$), with proven in vitro ACE-inhibitory effects (Kohmura et al., 1989). Notably, T2-basolateral peptides from the infant-like model carried a higher functional load. Five bioactive peptides were identified, four of which were more abundant in the infant-like condition. These included β-casein ^{176}VLPIPQ^{181}, β-casein ^{138}NLHLPLP^{144}, and β-casein ^{169}WSVPQPK^{175}, all exhibiting ACE-inhibitory activity (Hernández-Ledesma et al., 2007; Kohmura et al., 1989), as well as β-casein ^{90}VLPVPQ^{95}, which has been linked to cholesterol-regulating activity (Jiang et al., 2020). Interestingly, ^{169}WSVPQPK^{175} was also found in the gastric digesta of in vivo infants (Nielsen et al., 2018).

For the IF foods, no significant differences were observed in the response of infant-like monolayers to either dairy IF or soya IF, in terms of TEER (Fig. 2), OCLN intensity (Fig. 3), and OCLN/β-actin Pearson's co-localization coefficient (Fig. 4; $P < 0.05$). Consistent findings to our study were also reported by our group previously, where dairy IF digesta did not significantly alter TEER or OCLN levels in Caco-2/HT29-MTX monolayers (Dold et al., 2025). Similarly, Paparo et al. (2021) demonstrated that soya IF digesta did not impair TEER in Caco-2 cells, although it did upregulate OCLN mRNA expression (Paparo et al., 2021).

Notably, AA IF elicited a distinct response in the infant-like model: it significantly increased OCLN fluorescence intensity (Fig. 3B; $P < 0.05$) without a corresponding rise in TEER (Fig. 1A; $P > 0.05$) compared to HBSS. This may suggest that treatment with AA IF causes a selective tightening of the OCLN-regulated leak pathway, while the ion-conductive pore pathway that determines TEER remained unaffected (Al-Sadi et al., 2011). This finding aligns with in vivo data showing that extensively hydrolyzed formulas (no intact proteins) reduce intestinal paracellular permeability in infants (lactulose/mannitol ratio, $P = 0.003$) compared with conventional cow's milk-based formula (Koivusaari et al., 2023). In contrast, Paparo et al. (2021) found no upregulation of OCLN mRNA nor differences in TEER with AA IF in Caco-2 cells.

In the adult-like model, barrier responses to formula digesta diverged from the infant-like phenotype. Dairy IF reduced OCLN fluorescence intensity and Mander's coefficient for OCLN–actin co-localization (Fig. 3B and 4B; $P < 0.05$), Soya IF decreased Pearson's coefficient for OCLN–actin spatial correlation (Fig. 3A; $P < 0.05$), and AA IF significantly lowered TEER (Fig. 2B; $P < 0.05$) without affecting OCLN intensity (Fig. 3; $P > 0.05$). The TEER reduction observed with AA IF may reflect increased amino acid transport activity, as amino acid uptake is coupled to proton and ion fluxes (Bröer, 2008) that transiently influence TEER. This interpretation is supported by the higher basolateral amino acid levels measured in AA IF compared with those in the other samples ($P < 0.05$).

In terms of unique dairy or soya peptides transported to the T2-basolateral compartment, the infant-like monolayers consistently exhibited higher unique peptide counts (Fig. 6). For the dairy IF, we identified 206 unique peptides in the T2-basolateral and 314 in the T2-apical compartments for the infant-like model and 182 and 289 for the adult-like model. Similarly, Bavaro et al. (2021) identified 105 unique peptides in the basolateral and 585 in the apical compartments following 4 h exposure to 200 μg protein/cm^2 of digested heat-treated dairy infant formula (Bavaro et al., 2021). Of these, 132 apical peptides and 25 basolateral peptides matched to our data. In contrast, Kondrashina et al. (2024) identified only 17 peptides in the T2-basolateral side of Caco-2/HT29-MTX monolayers exposed for 4 h to dairy IF (Kondrashina et al., 2024). From their dataset, we identified 11 peptides in common from dairy IF (distributed across both compartments). In a milk protein study, Zenker et al. (2020) treated Caco-2 monolayers with gastrointestinal digested micellar casein and whey (80:20) for 2 h (Zenker et al., 2020). Assessment of milk peptide transport revealed 181 peptides on the basolateral side, including several peptides exhibiting sIgE-binding epitopes. When comparing their dataset with ours, we found four epitope-containing peptides in common—β-casein ^{98}VVPPFLQPE^{106}, ^{96}PVVVPPFLQPEV^{107}, ^{98}VVPPFLQPEV^{107}, and β-lactoglobulin ^{58}YVEELKPTPEGDLE^{71}. These bovine milk peptides were detected in both T2-apical and T2-basolateral compartments but absent in the digesta. With dairy IF treatment the most abundant peptide in the infant model was β-lactoglobulin ^{59}VEELKPTPE^{67} (1.04-fold higher in the infant model; $P > 0.05$), followed by β-casein ^{88}NIPPLTQTPV^{97} (1.08-fold higher; $P > 0.05$), which is also known for its ACE-inhibitory activity (Gobbetti et al., 2000). While dairy IF treatment produced the highest number of total bioactive peptides in the Transwell chambers (54 in T2-basolateral, 86 in T2-apical), these were more evenly distributed between models.

Where the infant-like model was treated with digested soya IF, 163 soya unique peptides were identified in the T2-basolateral and 346 in the T2-apical peptides. For the adult-like model, 127 soya unique peptides were identified in the basolateral and 335 in the apical. Martineau-Côté et al. (2024) identified 17 peptides in the basolateral and 55 in the apical fractions after exposing Caco-2/HT29-MTX monolayers for 2 h to digested soy flour (2240 μg of peptide/mL). When comparing their dataset with ours, we found five peptides in common: β-conglycinin ^{86}EPQQPGEKEEDEDEQPRPI^{104} (detected in both our T2-basolateral and T2-apical compartments), and seed linoleate

9S-lipoxygenase ^{208}NDLGDPDKGENH^{219}, Glycinin G4 ^{309}EQDEDEDEDEDKPRPS^{324} and ^{278}EEEEEEEDEKPQ^{287}, and sucrose-binding protein ^{309}TEVGPDDDEK^{338} (detected in our T2-apical compartment). Notably, these peptides were absent from our soya IF digesta.

The most abundant soya peptides in the Transwell chambers were glycinin ^{263}SVIKPPTDEQ^{272} (1.07-fold higher in the infant-like model; $P > 0.05$) and β-conglycinin ^{578}FVDAQPK^{584} (1.09-fold higher; $P > 0.05$).

Only one known bioactive peptide from soya was identified in the T2-apical compartment (Seed linoleate 13S-lipoxygenase-1 ^{306}TIIPLPV^{312}, ACE inhibitor and antioxidant (Minkiewicz et al., 2019)) and one in the T2-basolateral ^{267}β-conglycinin^{276} SLVNNDDRDS, antioxidant), with no significant difference between the infant and adult models ($P > 0.05$).

From our dataset, Caco-2/HT29-MTX brush border enzymes contributed to substantial protein digestion, as demonstrated by the higher number of peptides identified in the apical chamber after a 2 h incubation with monolayers but which were not present in the digesta (Fig. 7). In the infant model, 46 peptides from dairy IF, 53 from soya IF, and 30 from human milk matched cleavage motifs. The main enzymes implicated were tripeptidyl peptidase II, aminopeptidase N, and dipeptidyl peptidase-4, consistent with brush-border proteolytic activity. Similarly, Lacroix et al. (2017) studied five bioactive milk peptides and found that all underwent partial degradation by Caco-2 peptidases, with only ~70–90% remaining intact in the apical chamber after 2 h (Lacroix et al., 2017). Picariello et al. (2015) further showed that, after digestion of whey protein isolate, the addition of brush border enzymes from porcine jejunum increased the degree of hydrolysis from 53.3% to 70.7%, underscoring the crucial role of brush border enzymes in shaping the final peptide pool (Picariello et al., 2015).

Interestingly, peptides exclusively found in T2-apical of infant-like monolayers post-treatment with dairy-IF were shorter in length. This suggests more extensive cleavage by monolayer brush border enzymes or intracellular processing in response to dairy IF. This enhanced breakdown likely contributed to the higher T2-basolateral free AA levels observed in the infant-like condition compared with the adult model with dairy IF treatment.

The infant-like and adult-like barriers differed in their responses to the foods. Only the infant-like model responded to AA IF with increased OCLN fluorescence, and responded to human milk with enhanced OCLN–actin co-localization. By contrast, the adult model showed a reduction in TEER with AA IF treatment and lower OCLN fluorescence intensity with dairy IF and human milk treatments. Compared to the adult-like model, the infant-like monolayer also exhibited greater dietary peptide transport and diversity, with human milk in particular delivering a higher T2-basolateral load of bioactive peptides. Consistently, AA transport in the T2-basolateral was higher in the infant-like than in the adult-like model for dairy IF. These observations agree with in vivo data showing greater intestinal permeability in neonates, driven by enhanced paracellular transport (Catassi et al., 1995), a key route for peptide absorption (Xu et al., 2019). Thus, the adult Caco-2/HT29-MTX was less representative of the infant epithelium.

Interestingly, basolateral peptides across all dietary matrices exhibited a median length of 7–9 AAs, with the majority exceeding the di−/tri-peptide range that uses PepT1-mediated transport. This indicates that peptide passage across both infant- and adult-like epithelia is unlikely to be driven primarily by PepT1 and is consistent with a predominant contribution of paracellular permeability.

The overlap in basolateral peptide sequences between models suggests a conserved transport-permissive window for mid-length, moderately hydrophilic, and proline-enriched peptides. Notably, a higher number of infant-exclusive peptides were detected across matrices. This may reflect increased paracellular transport, consistent with developmental differences in epithelial maturation. Alternatively, differences in intracellular peptide degradation or transcytotic pathways may contribute to the observed infant-specific peptide profiles.

Limitations of this study include the absence of immune cells, short exposure windows, and a focus only on protein-derived bioactives. Additionally, peptide identification and bioactivity annotation are inherently limited by biases in available databases. Bovine milk proteins are overrepresented in proteomic and bioactive peptide databases compared to soya and human milk proteins. This may lead to an underestimation of peptide diversity or function in soya IF and human milk samples, and to an overrepresentation of bioactive hits in dairy IF. Expanding and diversifying peptide reference databases will be critical for accurate cross-formulation comparisons.

Barrier integrity was assessed using TEER (reflecting small-solute paracellular permeability) and quantitative OCLN–actin colocalization analysis. Moreover, basolateral peptides predominantly exceeded the size range typically transported by PepT1, suggesting a substantial contribution of paracellular permeability. While these approaches provide complementary functional and structural information, direct macromolecular permeability assays (e.g., FITC-dextran flux) and transporter perturbation or competitive inhibition studies would be required.

Future mechanistic studies are needed to determine the pathways underlying the OCLN–actin redistribution observed in response to human milk, including whether cAMP signaling contributes to this effect. Additional studies should assess long-term exposure effects, test lipid and carbohydrate fractions, and incorporate co-cultures with immune or mucus-producing cells. Nonetheless, our model offers a reproducible and efficient platform for early-life nutrition research.

5. Conclusions

In summary, the infant-like model revealed that digested human milk altered the architecture of tight junctions by increasing OCLN–actin co-localization and delivering a more diverse set of absorbed bioactive peptides. For all foods, infant-like monolayers transported more dietary peptides with greater diversity than the adult-like monolayers. For dairy IF, AAs levels in the T2-basolateral were higher in the infant-like than in the adult-like model. These observations align with in vivo data and support our view that in vitro barrier models that mimic the infant, should be used in conjunction with digestion protocols tailored to this life stage. Although both infant- and adult-like models showed similar responses to dairy- and soy-based IFs and human milk, the biomarkers assessed in this study were limited; therefore, future work should expand the biomarker panel. Nonetheless, formula development should prioritize more closely replicating the bioactive and barrier-supportive properties of human milk.

CRediT authorship contribution statement

Francesca Bietto: Writing – review & editing, Writing – original draft, Visualization, Validation, Methodology, Investigation, Formal analysis, Data curation, Conceptualization. **Simona Cirrincione:** Writing – review & editing, Methodology, Investigation, Formal analysis. **Cristina Gómez-Marín:** Writing – review & editing, Methodology, Investigation, Formal analysis. **Beatriz Miralles:** Writing – review & editing, Validation, Supervision, Resources, Methodology. **Francesco Romaniello:** Writing – review & editing, Methodology, Investigation, Formal analysis. **Elena Arranz:** Writing – review & editing, Supervision, Methodology. **Cristina Lamberti:** Writing – review & editing, Validation, Supervision, Resources. **Simona Lucia Bavaro:** Supervision, Resources, Methodology. **Laura Cavallarin:** Writing – review & editing, Supervision, Resources. **Eva Rath:** Writing – review & editing, Supervision, Methodology. **Alice J. Lucey:** Writing – review & editing, Validation, Supervision, Resources, Methodology. **Linda Giblin:** Writing – review & editing, Validation, Supervision, Resources, Project administration, Methodology, Funding acquisition, Conceptualization.

Ethics statement

Human milk was obtained from six healthy lactating women as part of a previously approved clinical study at the Hospital Universitario Virgen de las Nieves (Granada, Spain; Ethics Committee approval, ClinicalTrials.gov NCT02811172). All procedures complied with institutional guidelines and the Declaration of Helsinki. Written informed consent was obtained from all donors, including consent for future research use of their anonymized samples. Donor privacy and confidentiality were fully protected. No new human sample collection was performed for this study.

Declaration of competing interest

The authors declare that they have no known competing financial interests or personal relationships that could have appeared to influence the work reported in this paper.

Acknowledgments

This research was supported by Teagasc (InfBar MDBY1370). Francesca Bietto is in receipt of a Teagasc Walsh Scholarship 2021007. The graphical abstract was created in BioRender (Bietto, F.,2025; https://BioRender.com/yzbm1g7). The methodological flow chart was created in BioRender (Bietto, F., 2026; https://BioRender.com/p17zwmd). The authors would like to acknowledge Orla Cooney for proofreading this manuscript.

Appendix A. Supplementary data

Supplementary data to this article can be found online at https://doi.org/10.1016/j.foodres.2026.119071.

Data availability

Data will be made available on request.

References

Al-Sadi, R., Khatib, K., Guo, S., Ye, D., Youssef, M., & Ma, T. (2011). Occludin regulates macromolecule flux across the intestinal epithelial tight junction barrier. *American Journal of Physiology. Gastrointestinal and Liver Physiology, 300*(6), G1054–G1064. https://doi.org/10.1152/ajpgi.00055.2011

Atyeo, C., & Alter, G. (2021). The multifaceted roles of breast milk antibodies. *Cell, 184*(6), 1486–1499. https://doi.org/10.1016/j.cell.2021.02.031

Bavaro, S. L., Mamone, G., Picariello, G., Callanan, M. J., Chen, Y., Brodkorb, A., & Giblin, L. (2021). Thermal or membrane processing for infant milk formula: Effects on protein digestion and integrity of the intestinal barrier. *Food Chemistry, 347*, Article 129019. https://doi.org/10.1016/j.foodchem.2021.129019

Bietto, F., Arranz, E., Miralles, B., Gómez-Marín, C., Rath, E., Lucey, A. J., & Giblin, L. (2025). Using sodium glycodeoxycholate to develop a temporary infant-like gut barrier model, in vitro. *Frontiers in Nutrition, 12*, Article 1577369. https://doi.org/10.3389/fnut.2025.1577369

Biondi Ryan, M. R., Zukaitis, J., Sutantawong, S., & Dallas, D. C. (2025). Overall evidence for milk-derived proteins and peptides in blood after digestion: A systematic review. *Nutrition Reviews.* , Article nuaf118. https://doi.org/10.1093/nutrit/nuaf118

Blum, L. M. (1999). *At the breast: Ideologies of breastfeeding and motherhood in the contemporary United States*. Beacon Press.

Bode, L. (2012). Human milk oligosaccharides: Every baby needs a sugar mama. *Glycobiology, 22*(9), 1147–1162. https://doi.org/10.1093/glycob/cws074

Brockway, M., Daniel, A. I., Reyes, S. M., Gauglitz, J. M., Granger, M., McDermid, J. M., … Azad, M. B. (2024). Human milk bioactive components and child growth and body composition in the first 2 years: A systematic review. *Advances in Nutrition, 15*(1), Article 100127. https://doi.org/10.1016/j.advnut.2023.09.015

Bröer, S. (2008). Amino acid transport across mammalian intestinal and renal epithelia. *Physiological Reviews, 88*(1), 249–286. https://doi.org/10.1152/physrev.00018.2006

Carr, L. E., Virmani, M. D., Rosa, F., Munblit, D., Matazel, K. S., Elolimy, A. A., & Yeruva, L. (2021). Role of human milk bioactives on infants gut and immune health. *Frontiers in Immunology, 12*. https://doi.org/10.3389/fimmu.2021.604080

Catassi, C., Bonucci, A., Coppa, G. V., Carlucci, A., & Giorgi, P. L. (1995). Intestinal permeability. Changes during the first month: Effect of natural versus artificial feeding. *Journal of Pediatric Gastroenterology and Nutrition, 21*(4), 383–386. https://doi.org/10.1097/00005176-199511000-00003

Codex Alimentarius Commission. (1981). *Codex Alimentarius commission. Standard for infant formula and formulas for special medical purposes intended for infants (CXS 72–1981)*. Rome: FAO/WHO. Revised 2023. https://www.fao.org/fao-who-codexalimentarius/sh-proxy/es/?lnk=1&url=https%253A%252F%252Fworkspace.fao.org%252Fsites%252Fcodex%252FStandards%252FCXS%2B72-1981%252FCXS_072e.pdf.

Colaizy, T. T., Bartick, M. C., Jegier, B. J., Green, B. D., Reinhold, A. G., Schaefer, A. J., … Poulsen, J. (2016). Impact of optimized breastfeeding on the costs of necrotizing enterocolitis in extremely low birthweight infants. *The Journal of Pediatrics, 175*, 100–105.e2. https://doi.org/10.1016/j.jpeds.2016.03.040

Conesa, C., Bellés, A., Grasa, L., & Sánchez, L. (2023). The role of lactoferrin in intestinal health. *Pharmaceutics, 15*(6), 1569. https://doi.org/10.3390/pharmaceutics15061569

Cox, J., & Mann, M. (2008). *MaxQuant* (Version 2.6.6.0) [Computer software]. https://www.maxquant.org/.

Cummins, A. G., Steele, T. W., LaBrooy, J. T., & Shearman, D. J. (1988). Maturation of the rat small intestine at weaning: Changes in epithelial cell kinetics, bacterial flora, and mucosal immune activity. *Gut, 29*(12), 1672–1679. https://doi.org/10.1136/gut.29.12.1672

Cummins, P. M. (2012). Occludin: One protein, many forms. *Molecular and Cellular Biology, 32*(2), 242–250. https://doi.org/10.1128/MCB.06029-11

Dold, C. A., Sahin, A. W., Lawlor, P. G., Hickey, R. M., & Giblin, L. (2025). Employing membrane filtration technology during infant milk formula processing, will improve intestinal barrier function in vitro. *International Dairy Journal, 167*, Article 106283. https://doi.org/10.1016/j.idairyj.2025.106283

European Commission. (2016). Commission delegated regulation (EU) 2016/127 of 25 september 2015 supplementing regulation (EU) no 609/2013 as regards the specific compositional and information requirements for infant formula and follow-on formula and as regards requirements on information relating to infant and young child feeding. *Official Journal of the European Union, L25*, 1–29.

Gleeson, J. P., Fein, K. C., Chaudhary, N., Doerfler, R., Newby, A. N., & Whitehead, K. A. (2021). The enhanced intestinal permeability of infant mice enables oral protein and macromolecular absorption without delivery technology. *International Journal of Pharmaceutics, 593*, Article 120120. https://doi.org/10.1016/j.ijpharm.2020.120120

Gobbetti, M., Ferranti, P., Smacchi, E., Goffredi, F., & Addeo, F. (2000). Production of angiotensin-I-converting-enzyme-inhibitory peptides in fermented milks started by lactobacillus delbrueckii subsp. bulgaricus SS1 and lactococcus lactis subsp. cremoris FT4. *Applied and Environmental Microbiology, 66*(9), 3898–3904. https://doi.org/10.1128/AEM.66.9.3898-3904.2000

Google Research (2026). Google Colaboratory [Computer software]. Retrieved https://colab.research.google.com/.

Grundy, M. M.-L., Deglaire, A., Le Feunteun, S., Reboul, E., Moughan, P. J., Wilde, P. J., … Marze, S. (2025). Bioaccessibility and associated concepts: Terminology in the context of in vitro food digestion studies. *Food Chemistry, 485*, Article 144424. https://doi.org/10.1016/j.foodchem.2025.144424

Harris, C. R., Millman, K. J., Van Der Walt, S. J., Gommers, R., Virtanen, P., Cournapeau, D., … Oliphant, T. E. (2020). Array programming with NumPy. *Nature, 585*(7825), 357–362. https://doi.org/10.1038/s41586-020-2649-2

Hernández-Ledesma, B., Quirós, A., Amigo, L., & Recio, I. (2007). Identification of bioactive peptides after digestion of human milk and infant formula with pepsin and pancreatin. *International Dairy Journal, 17*(1), 42–49. https://doi.org/10.1016/j.idairyj.2005.12.012

Hevia, A., Ruas-Madiedo, P., Faria, M. A., Petit, V., Alves, B., Alvito, P., … Miralles, B. (2023). A shared perspective on in vitro and in vivo models to assay intestinal transepithelial transport of food compounds. *Journal of Agricultural and Food Chemistry, 71*(49), 19265–19276. https://doi.org/10.1021/acs.jafc.3c05479

Hidalgo, I. J., Raub, T. J., & Borchardt, R. T. (1989). Characterization of the human colon carcinoma cell line (caco-2) as a model system for intestinal epithelial permeability. *Gastroenterology, 96*(2), 736–749. https://doi.org/10.1016/S0016-5085(89)80072-1

Holmes, J. L., Van Itallie, C. M., Rasmussen, J. E., & Anderson, J. M. (2006). Claudin profiling in the mouse during postnatal intestinal development and along the gastrointestinal tract reveals complex expression patterns. *Gene Expression Patterns, 6*(6), 581–588. https://doi.org/10.1016/j.modgep.2005.12.001

Hubatsch, I., Ragnarsson, E. G. E., & Artursson, P. (2007). Determination of drug permeability and prediction of drug absorption in caco-2 monolayers. *Nature Protocols, 2*(9), 2111–2119. https://doi.org/10.1038/nprot.2007.303

Hunter, J. D. (2007). Matplotlib [computer software]. https://matplotlib.org/.

Jiang, X., Pan, D., Zhang, T., Liu, C., Zhang, J., Su, M., … Guo, Y. (2020). Novel milk casein–derived peptides decrease cholesterol micellar solubility and cholesterol intestinal absorption in caco-2 cells. *Journal of Dairy Science, 103*(5), 3924–3936. https://doi.org/10.3168/jds.2019-17586

Jiao, N., Wu, Z., Ji, Y., Wang, B., Dai, Z., & Wu, G. (2015). L-glutamate enhances barrier and antioxidative functions in intestinal porcine epithelial cells. *The Journal of Nutrition, 145*(10), 2258–2264. https://doi.org/10.3945/jn.115.217661

Johansson, M. E. V., Ambort, D., Pelaseyed, T., Schütte, A., Gustafsson, J. K., Ermund, A., … Hansson, G. C. (2011). Composition and functional role of the mucus layers in the intestine. *Cellular and Molecular Life Sciences, 68*(22), 3635. https://doi.org/10.1007/s00018-011-0822-3

Johnston, S. D., Smye, M., Watson, R. G. P., McMillan, S. A., Trimble, E. R., & Love, A. H. G. (2000). Lactulose-mannitol intestinal permeability test: A useful screening test for adult coeliac disease. *Annals of Clinical Biochemistry: International Journal of Laboratory Medicine, 37*(4), 512–519. https://doi.org/10.1177/000456320003700413

Kim, M.-H., & Kim, H. (2017). The roles of glutamine in the intestine and its implication in intestinal diseases. *International Journal of Molecular Sciences, 18*(5), 1051. https://doi.org/10.3390/ijms18051051

Kleiveland, C. R. (2015). Co-cultivation of caco-2 and HT-29MTX. *The Impact of Food Bioactives on Health*, 135–140.

Kohmura, M., Nio, N., Kubo, K., Minoshima, Y., Munekata, E., & Ariyoshi, Y. (1989). Inhibition of angiotensin-converting enzyme by synthetic peptides of human β-casein. *Agricultural and Biological Chemistry, 53*(8), 2107–2114. https://doi.org/10.1080/00021369.1989.10869621

Koivusaari, K., Niinistö, S., Nevalainen, J., Honkanen, J., Ruohtula, T., Koreasalo, M., … Virtanen, S. M. (2023). Infant feeding, gut permeability, and gut inflammation markers. *Journal of Pediatric Gastroenterology and Nutrition, 76*(6), 822–829. https://doi.org/10.1097/MPG.0000000000003756

Komatsu, Y., Wada, Y., Shibasaki, T., Kitamura, Y., Ehara, T., Nakamura, H., & Miyaji, K. (2024). Comparison of protein digestibility of human milk and infant formula using the INFOGEST method under infant digestion conditions. *British Journal of Nutrition, 132*(3), 351–358. https://doi.org/10.1017/S0007114524001260

Kondrashina, A., Mamone, G., Giblin, L., & Lane, J. A. (2024). Infant milk formula enriched in dairy cream brings its digestibility closer to human milk and supports intestinal health in pre-clinical studies. *Nutrients, 16*(18), 3065. https://doi.org/10.3390/nu16183065

Korhonen, H., & Pihlanto, A. (2006). Bioactive peptides: Production and functionality. *International Dairy Journal, 16*(9), 945–960. https://doi.org/10.1016/j.idairyj.2005.10.012

Kosek, M. N., Lee, G. O., Guerrant, R. L., Haque, R., Kang, G., Ahmed, T., … Network, the M.-E. (2017). Age and sex normalization of intestinal permeability measures for the improved assessment of enteropathy in infancy and early childhood: Results from the MAL-ED study. *Journal of Pediatric Gastroenterology and Nutrition, 65*(1), 31–39. https://doi.org/10.1097/MPG.0000000000001610

Lacroix, I. M. E., Chen, X.-M., Kitts, D. D., & Li-Chan, E. C. Y. (2017). Investigation into the bioavailability of milk protein-derived peptides with dipeptidyl-peptidase IV inhibitory activity using caco-2 cell monolayers. *Food & Function, 8*(2), 701–709. https://doi.org/10.1039/C6FO01411A

Liang, N., Kim, B. J., & Dallas, D. C. (2022). Bioavailability of peptides derived from the in vitro digestion of human milk assessed by caco-2 cell monolayers. *Journal of Agricultural and Food Chemistry, 70*(23), 7077–7084. https://doi.org/10.1021/acs.jafc.2c01246

Lucas, A., & Cole, T. J. (1990). Breast milk and neonatal necrotising enterocolitis. *The Lancet, 336*(8730–8731), 1519–1523. https://doi.org/10.1016/0140-6736(90)93304-8

Ma, Y., Hou, Y., Xie, K., Zhang, L., & Zhou, P. (2021). Digestive differences in immunoglobulin g and lactoferrin among human, bovine, and caprine milk following in vitro digestion. *International Dairy Journal, 120*, Article 105081. https://doi.org/10.1016/j.idairyj.2021.105081

Macierzanka, A., Mackie, A. R., Bajka, B. H., Rigby, N. M., Nau, F., & Dupont, D. (2014). Transport of particles in intestinal mucus under simulated infant and adult physiological conditions: Impact of mucus structure and extracellular DNA. *PLoS One, 9*(4), Article e95274. https://doi.org/10.1371/journal.pone.0095274

Martin, C., Ling, P.-R., & Blackburn, G. (2016). Review of infant feeding: Key features of breast milk and infant formula. *Nutrients, 8*(5), 279. https://doi.org/10.3390/nu8050279

Martineau-Côté, D., Achouri, A., Pitre, M., Karboune, S., & L'Hocine, L. (2024). Bioaccessibility and Antioxidant Activity of Faba Bean Peptides in Comparison to those of Pea and Soy after In Vitro Gastrointestinal Digestion and Transepithelial Transport across Caco-2 and HT29-MTX-E12 Cells. *J. Agric. Food Chem., 72*(32), 17953–17963. https://doi.org/10.1021/acs.jafc.4c02948

Mastromarino, P., Capobianco, D., Campagna, G., Laforgia, N., Drimaco, P., Dileone, A., & Baldassarre, M. E. (2014). Correlation between lactoferrin and beneficial microbiota in breast milk and infant's feces. *BioMetals, 27*(5), 1077–1086. https://doi.org/10.1007/s10534-014-9762-3

McKinney, W. (2010). Pandas (version 1.5.3) [computer software]. https://pandas.pydata.org/.

McNamara, J. (2023). XlsxWriter: A python module for creating excel XLSX files. [computer software]. https://github.com/jmcnamara/XlsxWriter.

Ménard, O., Bourlieu, C., De Oliveira, S. C., Dellarosa, N., Laghi, L., Carrière, F., … Deglaire, A. (2018). A first step towards a consensus static in vitro model for simulating full-term infant digestion. *Food Chemistry, 240*, 338–345. https://doi.org/10.1016/j.foodchem.2017.07.145

Minkiewicz, P., Iwaniak, A., & Darewicz, M. (2019). BIOPEP-UWM database of bioactive peptides: Current opportunities. *International Journal of Molecular Sciences, 20*(23), 5978. https://doi.org/10.3390/ijms20235978

Mooney, C., Haslam, N. J., Pollastri, G., & Shields, D. C. (2012). Towards the improved discovery and design of functional peptides: Common features of diverse classes permit generalized prediction of bioactivity. *PLoS One, 7*(10), Article e45012. https://doi.org/10.1371/journal.pone.0045012

Musa, M. A., Kabir, M., Hossain, M. I., Ahmed, E., Siddique, A., Rashid, H., … Haque, R. (2019). Measurement of intestinal permeability using lactulose and mannitol with conventional five hours and shortened two hours urine collection by two different methods: HPAE-PAD and LC-MSMS. *PLoS One, 14*(8), Article e0220397. https://doi.org/10.1371/journal.pone.0220397

Nielsen, P. M., Petersen, D., & Dambmann, C. (2001). Improved method for determining food protein degree of hydrolysis. *Journal of Food Science, 66*(5), 642–646. https://doi.org/10.1111/j.1365-2621.2001.tb04614.x

Nielsen, S. D., Beverly, R. L., Qu, Y., & Dallas, D. C. (2017). Milk bioactive peptide database: A comprehensive database of milk protein-derived bioactive peptides and novel visualization. *Food Chemistry, 232*, 673–682. https://doi.org/10.1016/j.foodchem.2017.04.056

Nielsen, S. D., Beverly, R. L., Underwood, M. A., & Dallas, D. C. (2018). Release of functional peptides from mother's milk and fortifier proteins in the premature infant stomach. *PLoS One, 13*(11), Article e0208204. https://doi.org/10.1371/journal.pone.0208204

Noel, G., In, J. G., Lemme-Dumit, J. M., DeVine, L. R., Cole, R. N., Guerrerio, A. L., … Pasetti, M. F. (2021). Human breast milk enhances intestinal mucosal barrier function and innate immunity in a healthy pediatric human enteroid model. *Frontiers in Cell and Developmental Biology, 9*, Article 685171. https://doi.org/10.3389/fcell.2021.685171

Pannaraj, P. S., Li, F., Cerini, C., Bender, J. M., Yang, S., Rollie, A., … Aldrovandi, G. M. (2017). Association between breast milk bacterial communities and establishment and development of the infant gut microbiome. *JAMA Pediatrics, 171*(7), 647. https://doi.org/10.1001/jamapediatrics.2017.0378

Paparo, L., Picariello, G., Bruno, C., Pisapia, L., Canale, V., Sarracino, A., … Berni Canani, R. (2021). Tolerogenic effect elicited by protein fraction derived from different formulas for dietary treatment of cows milk allergy in human cells. *Frontiers in Immunology, 11*, Article 604075. https://doi.org/10.3389/fimmu.2020.604075

Pedregosa, F. (2011). Scikit-learn (version 1.2.2) [computer software]. https://scikit-learn.org/.

Picariello, G., Miralles, B., Mamone, G., Sánchez-Rivera, L., Recio, I., Addeo, F., & Ferranti, P. (2015). Role of intestinal brush border peptidases in the simulated digestion of milk proteins. *Molecular Nutrition & Food Research, 59*(5), 948–956. https://doi.org/10.1002/mnfr.201400856

Python Software Foundation (2021). *Python Language Reference, Version 3.10* (Version 3.10) [Computer software].

Quigley, M., Embleton, N. D., Meader, N., & McGuire, W. (2024). Donor human milk for preventing necrotising enterocolitis in very preterm or very low-birthweight infants. *Cochrane Database of Systematic Reviews, 2024*(9). https://doi.org/10.1002/14651858.CD002971.pub6

Sánchez-Hernández, S., Théron, L., Jiménez-Barrios, P., Olalla-Herrera, M., Recio, I., & Miralles, B. (2021). Protein profile and simulated digestive behavior of breast milk from overweight and normal weight mothers. *Foods, 10*(4), 887. https://doi.org/10.3390/foods10040887

Sangild, P. T., Ney, D. M., Sigalet, D. L., Vegge, A., & Burrin, D. (2014). Animal models of gastrointestinal and liver diseases. Animal models of infant short bowel syndrome: Translational relevance and challenges. *American Journal of Physiology. Gastrointestinal and Liver Physiology, 307*(12), G1147–G1168. https://doi.org/10.1152/ajpgi.00088.2014

Scott, P. H. (1989). Enzyme immunoassay of lactoferrin in newborn term infants: Reference values and influence of diet. *Annals of Clinical Biochemistry: International Journal of Laboratory Medicine, 26*(5), 407–411. https://doi.org/10.1177/000456328902600505

Sun, H., Chow, E. C., Liu, S., Du, Y., & Pang, K. S. (2008). The caco-2 cell monolayer: Usefulness and limitations. *Expert Opinion on Drug Metabolism & Toxicology, 4*(4), 395–411. https://doi.org/10.1517/17425255.4.4.395

Tretyakov, K. (2012). Matplotlib-venn: A python library for plotting venn diagrams. [computer software]. https://github.com/konstantint/matplotlib-venn.

UNICEF, & W. H. O. (2003). *Global strategy for infant and young child feeding*. World Health Organization.

Van Berkel, P. H. C., Geerts, M. E. J., Van Veen, H. A., Kooiman, P. M., Pieper, F. R., De Boer, H. A., & Nuijens, J. H. (1995). Glycosylated and unglycosylated human lactoferrins both bind iron and show identical affinities towards human lysozyme and bacterial lipopolysaccharide, but differ in their susceptibilities towards tryptic proteolysis. *Biochemical Journal, 312*(1), 107–114. https://doi.org/10.1042/bj3120107

Vergauwen, H. (2015). The IPEC-J2 cell line. In K. Verhoeckx, P. Cotter, I. López-Expósito, C. Kleiveland, T. Lea, A. Mackie, … H. Wichers (Eds.), *The impact of food bioactives on health: In vitro and ex vivo models*. Springer. http://www.ncbi.nlm.nih.gov/books/NBK500147/.

Virtanen, P. (2020). SciPy (version 1.10.1) [computer software]. https://scipy.org/.

Waskom, M. (2021). Seaborn [computer software]. https://seaborn.pydata.org/.

Weaver, L. T., Laker, M. F., & Nelson, R. (1984). Intestinal permeability in the newborn. *Archives of Disease in Childhood, 59*(3), 236–241. https://doi.org/10.1136/adc.59.3.236

Weström, B., Arévalo Sureda, E., Pierzynowska, K., Pierzynowski, S. G., & Pérez-Cano, F.-J. (2020). The immature gut barrier and its importance in establishing immunity in newborn mammals. *Frontiers in Immunology, 11*. https://www.frontiersin.org/articles/10.3389/fimmu.2020.01153.

World Health Organization. (2014). *Global nutrition targets 2025: Breastfeeding policy brief*. World Health Organization. https://www.who.int/publications/i/item/WHO-NMH-NHD-14.7.

Xu, Q., Hong, H., Wu, J., & Yan, X. (2019). Bioavailability of bioactive peptides derived from food proteins across the intestinal epithelial membrane: A review. *Trends in Food Science & Technology, 86*, 399–411. https://doi.org/10.1016/j.tifs.2019.02.050

Zenker, H. E., Wichers, H. J., Tomassen, M. M. M., Boeren, S., De Jong, N. W., & Hettinga, K. A. (2020). Peptide release after simulated infant in vitro digestion of dry heated cows milk protein and transport of potentially immunoreactive peptides across the caco-2 cell monolayer. *Nutrients, 12*(8), 2483. https://doi.org/10.3390/nu12082483

Zhao, X., Xu, X.-X., Liu, Y., Xi, E.-Z., An, J.-J., Tabys, D., & Liu, N. (2019). The in vitro protective role of bovine lactoferrin on intestinal epithelial barrier. *Molecules, 24*(1), 148. https://doi.org/10.3390/molecules24010148

Appendix B

Full Peptide Data from Chapter 4

Appendix Table 1 Summary matrix reporting the unique peptides in each compartment (digesta, apical, basolateral), their overlaps, and unique distributions across infant- and adult-like models for Dairy IF.

Sequence	FASTA Header	Apical	Basolateral	Digesta	Exclusive Infant	Exclusive Adult
LYPA	sp|Q28019|LTBP2_BOVIN Latent-transforming growth factor beta-binding protein 2 OS=Bos taurus OX=9913 GN=LTBP2 PE=1 SV=2	No	No	Yes	No	No
QPNLPLP	sp|P02817|AMELX_BOVIN Amelogenin, X isoform OS=Bos taurus OX=9913 GN=AMELX PE=1 SV=2	No	No	Yes	No	No
NPWDQ	sp|P02663|CASA2_BOVIN Alpha-S2-casein OS=Bos taurus OX=9913 GN=CSN1S2 PE=1 SV=2	No	No	Yes	No	No
VVPPFLQPEVM	sp|P02666|CASB_BOVIN Beta-casein OS=Bos taurus OX=9913 GN=CSN2 PE=1 SV=2	No	No	Yes	No	No
TVVYRDINSQQ	sp|A7MBJ4|PTPRF_BOVIN Receptor-type tyrosine-protein phosphatase F OS=Bos taurus OX=9913 GN=PTPRF PE=2 SV=1	No	No	Yes	No	No
QKEPMIGV	sp|P02662|CASA1_BOVIN Alpha-S1-casein OS=Bos taurus OX=9913 GN=CSN1S1 PE=1 SV=2	No	No	Yes	No	No
KITVDDK	sp|P02663|CASA2_BOVIN Alpha-S2-casein OS=Bos taurus OX=9913 GN=CSN1S2 PE=1 SV=2	No	No	Yes	No	No
VAPGGT	sp|Q28173|RAGE_BOVIN Advanced glycosylation end product-specific receptor OS=Bos taurus OX=9913 GN=AGER PE=1 SV=1	No	No	Yes	No	No
EPMIG	sp|P02662|CASA1_BOVIN Alpha-S1-casein OS=Bos taurus OX=9913 GN=CSN1S1 PE=1 SV=2	No	No	Yes	No	No
PKVP	sp|P81282|CSPG2_BOVIN Versican core protein OS=Bos taurus OX=9913 GN=VCAN PE=1 SV=2	No	No	Yes	No	No
VVVPPFLQPE	sp|P02666|CASB_BOVIN Beta-casein OS=Bos taurus OX=9913 GN=CSN2 PE=1 SV=2	No	No	Yes	No	No
GIETVGGVMTKLIPR	sp|Q0VCX2|BIP_BOVIN Endoplasmic reticulum chaperone BiP OS=Bos taurus OX=9913 GN=HSPA5 PE=2 SV=1	No	No	Yes	No	No
EPMIGV	sp|P02662|CASA1_BOVIN Alpha-S1-casein OS=Bos taurus OX=9913 GN=CSN1S1 PE=1 SV=2	No	No	Yes	No	No

HGSPELAEPI	sp|P26201|CD36_BOVIN Platelet glycoprotein 4 OS=Bos taurus OX=9913 GN=CD36 PE=1 SV=5	No	No	Yes	No	No
LIPLQPS	sp|P18892|BT1A1_BOVIN Butyrophilin subfamily 1 member A1 OS=Bos taurus OX=9913 GN=BTN1A1 PE=1 SV=2	No	No	Yes	No	No
PQSQNPK	sp|P80195|GLCM1_BOVIN Glycosylation-dependent cell adhesion molecule 1 OS=Bos taurus OX=9913 GN=GLYCAM1 PE=1 SV=2	No	No	Yes	No	No
TPIVGQPSIPGGPV	sp|P12763|FETUA_BOVIN Alpha-2-HS-glycoprotein OS=Bos taurus OX=9913 GN=AHSG PE=1 SV=2	No	No	Yes	No	No
IFDVQNPDEV	sp|P26201|CD36_BOVIN Platelet glycoprotein 4 OS=Bos taurus OX=9913 GN=CD36 PE=1 SV=5	No	No	Yes	No	No
DLTGIPPAPRGVPQ	sp|Q0VCX2|BIP_BOVIN Endoplasmic reticulum chaperone BiP OS=Bos taurus OX=9913 GN=HSPA5 PE=2 SV=1	No	No	Yes	No	No
NANEEE	sp|P02663|CASA2_BOVIN Alpha-S2-casein OS=Bos taurus OX=9913 GN=CSN1S2 PE=1 SV=2	No	No	Yes	No	No
PGL	sp|Q58DL5|BCAR3_BOVIN Breast cancer anti-estrogen resistance protein 3 homolog OS=Bos taurus OX=9913 GN=BCAR3 PE=2 SV=2	Yes	No	No	apical	No
GLD	sp|P02754|LACB_BOVIN Beta-lactoglobulin OS=Bos taurus OX=9913 GN=LGB PE=1 SV=3	Yes	No	No	apical	No
NLQ	sp|P80195|GLCM1_BOVIN Glycosylation-dependent cell adhesion molecule 1 OS=Bos taurus OX=9913 GN=GLYCAM1 PE=1 SV=2	Yes	No	No	apical	No
PSYG	sp|P02668|CASK_BOVIN Kappa-casein OS=Bos taurus OX=9913 GN=CSN3 PE=1 SV=1	Yes	No	No	apical	No
TSGYDT	sp|P00711|LALBA_BOVIN Alpha-lactalbumin OS=Bos taurus OX=9913 GN=LALBA PE=1 SV=2	Yes	No	No	apical	No
PHA	sp|Q5E9N9|APEX2_BOVIN DNA-(apurinic or apyrimidinic site) endonuclease 2 OS=Bos taurus OX=9913 GN=APEX2 PE=2 SV=1	Yes	No	No	apical	No
QVT	sp|P02668|CASK_BOVIN Kappa-casein OS=Bos taurus OX=9913 GN=CSN3 PE=1 SV=1	Yes	No	No	apical	No
SGPLRP	sp|P18892|BT1A1_BOVIN Butyrophilin subfamily 1 member A1 OS=Bos taurus OX=9913 GN=BTN1A1 PE=1 SV=2	Yes	No	No	apical	No
TDVEN	sp|P02666|CASB_BOVIN Beta-casein OS=Bos taurus OX=9913 GN=CSN2 PE=1 SV=2	Yes	No	No	apical	No
TKL	sp|P02663|CASA2_BOVIN Alpha-S2-casein OS=Bos taurus OX=9913 GN=CSN1S2 PE=1 SV=2	Yes	No	No	apical	No
LPQNIPPLTQT	sp|P02666|CASB_BOVIN Beta-casein OS=Bos taurus OX=9913 GN=CSN2 PE=1 SV=2	Yes	No	No	apical	No

VLNP	sp|P02663|CASA2_BOVIN Alpha-S2-casein OS=Bos taurus OX=9913 GN=CSN1S2 PE=1 SV=2	Yes	No	No	apical	No
IGVNQ	sp|P02662|CASA1_BOVIN Alpha-S1-casein OS=Bos taurus OX=9913 GN=CSN1S1 PE=1 SV=2	Yes	No	No	apical	No
PEW	sp|P00711|LALBA_BOVIN Alpha-lactalbumin OS=Bos taurus OX=9913 GN=LALBA PE=1 SV=2	Yes	No	No	apical	No
YPVEPF	sp|P02666|CASB_BOVIN Beta-casein OS=Bos taurus OX=9913 GN=CSN2 PE=1 SV=2	Yes	No	No	apical	No
SVGWYPEPQ	sp|P18892|BT1A1_BOVIN Butyrophilin subfamily 1 member A1 OS=Bos taurus OX=9913 GN=BTN1A1 PE=1 SV=2	Yes	No	No	apical	No
SEDL	sp|Q58DL5|BCAR3_BOVIN Breast cancer anti-estrogen resistance protein 3 homolog OS=Bos taurus OX=9913 GN=BCAR3 PE=2 SV=2	Yes	No	No	apical	No
VPN	sp|P02662|CASA1_BOVIN Alpha-S1-casein OS=Bos taurus OX=9913 GN=CSN1S1 PE=1 SV=2	Yes	No	No	apical	No
DSATPV	sp|Q5E9N9|APEX2_BOVIN DNA-(apurinic or apyrimidinic site) endonuclease 2 OS=Bos taurus OX=9913 GN=APEX2 PE=2 SV=1	Yes	No	No	apical	No
QGPIV	sp|P02663|CASA2_BOVIN Alpha-S2-casein OS=Bos taurus OX=9913 GN=CSN1S2 PE=1 SV=2	Yes	No	No	apical	No
QVTST	sp|P02668|CASK_BOVIN Kappa-casein OS=Bos taurus OX=9913 GN=CSN3 PE=1 SV=1	Yes	No	No	apical	No
LPLPL	sp|P02666|CASB_BOVIN Beta-casein OS=Bos taurus OX=9913 GN=CSN2 PE=1 SV=2	Yes	No	No	apical	No
YVEELKPTPEGDL	sp|P02754|LACB_BOVIN Beta-lactoglobulin OS=Bos taurus OX=9913 GN=LGB PE=1 SV=3	Yes	No	No	apical	No
QEQPL	sp|Q58DL5|BCAR3_BOVIN Breast cancer anti-estrogen resistance protein 3 homolog OS=Bos taurus OX=9913 GN=BCAR3 PE=2 SV=2	Yes	No	No	apical	No
LTDVE	sp|P02666|CASB_BOVIN Beta-casein OS=Bos taurus OX=9913 GN=CSN2 PE=1 SV=2	Yes	No	No	apical	No
APFPE	sp|P02662|CASA1_BOVIN Alpha-S1-casein OS=Bos taurus OX=9913 GN=CSN1S1 PE=1 SV=2	Yes	No	No	apical	No
LVLDT	sp|P02754|LACB_BOVIN Beta-lactoglobulin OS=Bos taurus OX=9913 GN=LGB PE=1 SV=3	Yes	No	No	apical	No
TEDE	sp|P02666|CASB_BOVIN Beta-casein OS=Bos taurus OX=9913 GN=CSN2 PE=1 SV=2	Yes	No	No	apical	No
PPLTQTPVVVPPFLQPEVM	sp|P02666|CASB_BOVIN Beta-casein OS=Bos taurus OX=9913 GN=CSN2 PE=1 SV=2	Yes	No	No	apical	No

WRL	sp|P18892|BT1A1_BOVIN Butyrophilin subfamily 1 member A1 OS=Bos taurus OX=9913 GN=BTN1A1 PE=1 SV=2	Yes	No	No	apical	No
NLC	sp|P02663|CASA2_BOVIN Alpha-S2-casein OS=Bos taurus OX=9913 GN=CSN1S2 PE=1 SV=2	Yes	No	No	apical	No
LKT	sp|P02663|CASA2_BOVIN Alpha-S2-casein OS=Bos taurus OX=9913 GN=CSN1S2 PE=1 SV=2	Yes	No	No	apical	No
PVEP	sp|P02666|CASB_BOVIN Beta-casein OS=Bos taurus OX=9913 GN=CSN2 PE=1 SV=2	Yes	No	No	apical	No
PLGT	sp|P02662|CASA1_BOVIN Alpha-S1-casein OS=Bos taurus OX=9913 GN=CSN1S1 PE=1 SV=2	Yes	No	No	apical	No
LNKPEDET	sp|P80195|GLCM1_BOVIN Glycosylation-dependent cell adhesion molecule 1 OS=Bos taurus OX=9913 GN=GLYCAM1 PE=1 SV=2	Yes	No	No	apical	No
QLP	sp|P18892|BT1A1_BOVIN Butyrophilin subfamily 1 member A1 OS=Bos taurus OX=9913 GN=BTN1A1 PE=1 SV=2	Yes	No	No	apical	No
ASGEPT	sp|P02668|CASK_BOVIN Kappa-casein OS=Bos taurus OX=9913 GN=CSN3 PE=1 SV=1	Yes	No	No	apical	No
YKK	sp|P02754|LACB_BOVIN Beta-lactoglobulin OS=Bos taurus OX=9913 GN=LGB PE=1 SV=3	Yes	No	No	apical	No
VVP	sp|P02666|CASB_BOVIN Beta-casein OS=Bos taurus OX=9913 GN=CSN2 PE=1 SV=2	Yes	No	No	apical	No
VYVEELKPTP	sp|P02754|LACB_BOVIN Beta-lactoglobulin OS=Bos taurus OX=9913 GN=LGB PE=1 SV=3	Yes	No	No	No	No
QGPIVLNPWDQ	sp|P02663|CASA2_BOVIN Alpha-S2-casein OS=Bos taurus OX=9913 GN=CSN1S2 PE=1 SV=2	Yes	No	No	No	No
EMPFP	sp|P02666|CASB_BOVIN Beta-casein OS=Bos taurus OX=9913 GN=CSN2 PE=1 SV=2	Yes	No	No	No	No
PNSLPQ	sp|P02666|CASB_BOVIN Beta-casein OS=Bos taurus OX=9913 GN=CSN2 PE=1 SV=2	Yes	No	No	No	No
YPVEP	sp|P02666|CASB_BOVIN Beta-casein OS=Bos taurus OX=9913 GN=CSN2 PE=1 SV=2	Yes	No	No	No	No
SLPQNIPPLT	sp|P02666|CASB_BOVIN Beta-casein OS=Bos taurus OX=9913 GN=CSN2 PE=1 SV=2	Yes	No	No	No	No
HQPHQPLPPTVMFPPQ	sp|P02666|CASB_BOVIN Beta-casein OS=Bos taurus OX=9913 GN=CSN2 PE=1 SV=2	Yes	No	No	No	No
EELKPT	sp|P02754|LACB_BOVIN Beta-lactoglobulin OS=Bos taurus OX=9913 GN=LGB PE=1 SV=3	Yes	No	No	No	No
QTPVVVPPFLQPE	sp|P02666|CASB_BOVIN Beta-casein OS=Bos taurus OX=9913 GN=CSN2 PE=1 SV=2	Yes	No	No	No	No

VPQLEIVPN	sp|P02662|CASA1_BOVIN Alpha-S1-casein OS=Bos taurus OX=9913 GN=CSN1S1 PE=1 SV=2	Yes	No	No	No	No
TVMFPPQ	sp|P02666|CASB_BOVIN Beta-casein OS=Bos taurus OX=9913 GN=CSN2 PE=1 SV=2	Yes	No	No	No	No
LPPTVMFPPQSV	sp|P02666|CASB_BOVIN Beta-casein OS=Bos taurus OX=9913 GN=CSN2 PE=1 SV=2	Yes	No	No	No	No
TPEVDDE	sp|P02754|LACB_BOVIN Beta-lactoglobulin OS=Bos taurus OX=9913 GN=LGB PE=1 SV=3	Yes	No	No	No	No
SLVYPFP	sp|P02666|CASB_BOVIN Beta-casein OS=Bos taurus OX=9913 GN=CSN2 PE=1 SV=2	Yes	No	No	No	No
KNQDKTEIPT	sp|P02668|CASK_BOVIN Kappa-casein OS=Bos taurus OX=9913 GN=CSN3 PE=1 SV=1	Yes	No	No	No	No
ALPQ	sp|P02663|CASA2_BOVIN Alpha-S2-casein OS=Bos taurus OX=9913 GN=CSN1S2 PE=1 SV=2	Yes	No	No	No	No
NIPPLTQTP	sp|P02666|CASB_BOVIN Beta-casein OS=Bos taurus OX=9913 GN=CSN2 PE=1 SV=2	Yes	No	No	No	No
YPFPGPI	sp|P02666|CASB_BOVIN Beta-casein OS=Bos taurus OX=9913 GN=CSN2 PE=1 SV=2	Yes	No	No	No	No
QPLPPTVMFPPQ	sp|P02666|CASB_BOVIN Beta-casein OS=Bos taurus OX=9913 GN=CSN2 PE=1 SV=2	Yes	No	No	No	No
YPFP	sp|P02666|CASB_BOVIN Beta-casein OS=Bos taurus OX=9913 GN=CSN2 PE=1 SV=2	Yes	No	No	No	No
PQNIPPLTQTPVVVPPFLQPE	sp|P02666|CASB_BOVIN Beta-casein OS=Bos taurus OX=9913 GN=CSN2 PE=1 SV=2	Yes	No	No	No	No
AMEDI	sp|P02662|CASA1_BOVIN Alpha-S1-casein OS=Bos taurus OX=9913 GN=CSN1S1 PE=1 SV=2	Yes	No	No	No	No
AASDIS	sp|P02754|LACB_BOVIN Beta-lactoglobulin OS=Bos taurus OX=9913 GN=LGB PE=1 SV=3	Yes	No	No	No	No
PQNIPPLTQTPV	sp|P02666|CASB_BOVIN Beta-casein OS=Bos taurus OX=9913 GN=CSN2 PE=1 SV=2	Yes	No	No	No	No
FPGPI	sp|P02666|CASB_BOVIN Beta-casein OS=Bos taurus OX=9913 GN=CSN2 PE=1 SV=2	Yes	No	No	No	No
IPPLTQTPVVVPPFLQPE	sp|P02666|CASB_BOVIN Beta-casein OS=Bos taurus OX=9913 GN=CSN2 PE=1 SV=2	Yes	No	No	No	No
ILNKPEDE	sp|P80195|GLCM1_BOVIN Glycosylation-dependent cell adhesion molecule 1 OS=Bos taurus OX=9913 GN=GLYCAM1 PE=1 SV=2	Yes	No	No	No	No
QLEEQ	sp|P02754|LACB_BOVIN Beta-lactoglobulin OS=Bos taurus OX=9913 GN=LGB PE=1 SV=3	Yes	No	No	No	No

PLPPTVMFPPQ	sp|P02666|CASB_BOVIN Beta-casein OS=Bos taurus OX=9913 GN=CSN2 PE=1 SV=2	Yes	No	No	No	No
EDVPSE	sp|P02662|CASA1_BOVIN Alpha-S1-casein OS=Bos taurus OX=9913 GN=CSN1S1 PE=1 SV=2	Yes	No	No	No	No
PFPGPIPN	sp|P02666|CASB_BOVIN Beta-casein OS=Bos taurus OX=9913 GN=CSN2 PE=1 SV=2	Yes	No	No	No	No
HQPHQPLPPTVMFPPQS	sp|P02666|CASB_BOVIN Beta-casein OS=Bos taurus OX=9913 GN=CSN2 PE=1 SV=2	Yes	No	No	No	No
KSPIFGPEEV	sp|P81265|PIGR_BOVIN Polymeric immunoglobulin receptor OS=Bos taurus OX=9913 GN=PIGR PE=2 SV=1	Yes	No	No	No	No
KFLDDDLTDDI	sp|P00711|LALBA_BOVIN Alpha-lactalbumin OS=Bos taurus OX=9913 GN=LALBA PE=1 SV=2	Yes	No	No	No	No
SLPQNIPPLTQTP	sp|P02666|CASB_BOVIN Beta-casein OS=Bos taurus OX=9913 GN=CSN2 PE=1 SV=2	Yes	No	No	No	No
PPLTQTPVVVPPFLQPE	sp|P02666|CASB_BOVIN Beta-casein OS=Bos taurus OX=9913 GN=CSN2 PE=1 SV=2	Yes	No	No	No	No
PLPPTVMFPP	sp|P02666|CASB_BOVIN Beta-casein OS=Bos taurus OX=9913 GN=CSN2 PE=1 SV=2	Yes	No	No	No	No
LNVPGEIVES	sp|P02666|CASB_BOVIN Beta-casein OS=Bos taurus OX=9913 GN=CSN2 PE=1 SV=2	Yes	No	No	No	No
VDDK	sp|P02663|CASA2_BOVIN Alpha-S2-casein OS=Bos taurus OX=9913 GN=CSN1S2 PE=1 SV=2	Yes	No	No	No	No
SFNPT	sp|P02754|LACB_BOVIN Beta-lactoglobulin OS=Bos taurus OX=9913 GN=LGB PE=1 SV=3	Yes	No	No	No	No
PSFSDIPNPI	sp|P02662|CASA1_BOVIN Alpha-S1-casein OS=Bos taurus OX=9913 GN=CSN1S1 PE=1 SV=2	Yes	No	No	No	No
MHQPHQPLPPTVMFPPQS	sp|P02666|CASB_BOVIN Beta-casein OS=Bos taurus OX=9913 GN=CSN2 PE=1 SV=2	Yes	No	No	No	No
PVVVPPFLQP	sp|P02666|CASB_BOVIN Beta-casein OS=Bos taurus OX=9913 GN=CSN2 PE=1 SV=2	Yes	No	No	No	No
EELNVPGEIVE	sp|P02666|CASB_BOVIN Beta-casein OS=Bos taurus OX=9913 GN=CSN2 PE=1 SV=2	Yes	No	No	No	No
PPLTQTPVVVPP	sp|P02666|CASB_BOVIN Beta-casein OS=Bos taurus OX=9913 GN=CSN2 PE=1 SV=2	Yes	No	No	No	No
HQPHQPLPPTVMFPPQSV	sp|P02666|CASB_BOVIN Beta-casein OS=Bos taurus OX=9913 GN=CSN2 PE=1 SV=2	Yes	No	No	No	No
VYPFPGPIP	sp|P02666|CASB_BOVIN Beta-casein OS=Bos taurus OX=9913 GN=CSN2 PE=1 SV=2	Yes	No	No	No	No

NIPPLTQTPVVVPPF	sp|P02666|CASB_BOVIN Beta-casein OS=Bos taurus OX=9913 GN=CSN2 PE=1 SV=2	Yes	No	No	No	No
HIQKEDVPSE	sp|P02662|CASA1_BOVIN Alpha-S1-casein OS=Bos taurus OX=9913 GN=CSN1S1 PE=1 SV=2	Yes	No	No	No	No
IPPLTQTPVVVPP	sp|P02666|CASB_BOVIN Beta-casein OS=Bos taurus OX=9913 GN=CSN2 PE=1 SV=2	Yes	No	No	No	No
YQGPI	sp|P02663|CASA2_BOVIN Alpha-S2-casein OS=Bos taurus OX=9913 GN=CSN1S2 PE=1 SV=2	Yes	No	No	No	No
PPLTQTPVVVPPFLQPEV	sp|P02666|CASB_BOVIN Beta-casein OS=Bos taurus OX=9913 GN=CSN2 PE=1 SV=2	Yes	No	No	No	No
IPPLTQTPVVVPPFLQPEV	sp|P02666|CASB_BOVIN Beta-casein OS=Bos taurus OX=9913 GN=CSN2 PE=1 SV=2	Yes	No	No	No	No
HKEMPFPK	sp|P02666|CASB_BOVIN Beta-casein OS=Bos taurus OX=9913 GN=CSN2 PE=1 SV=2	Yes	No	No	No	No
FPPQ	sp|P02666|CASB_BOVIN Beta-casein OS=Bos taurus OX=9913 GN=CSN2 PE=1 SV=2	Yes	No	No	No	No
VEELKPTPEGDL	sp|P02754|LACB_BOVIN Beta-lactoglobulin OS=Bos taurus OX=9913 GN=LGB PE=1 SV=3	Yes	No	No	No	No
GPV	sp|P02666|CASB_BOVIN Beta-casein OS=Bos taurus OX=9913 GN=CSN2 PE=1 SV=2	Yes	No	No	No	No
WDQ	sp|P02663|CASA2_BOVIN Alpha-S2-casein OS=Bos taurus OX=9913 GN=CSN1S2 PE=1 SV=2	Yes	No	No	No	No
QGLPQ	sp|P02662|CASA1_BOVIN Alpha-S1-casein OS=Bos taurus OX=9913 GN=CSN1S1 PE=1 SV=2	Yes	No	No	No	No
EVDDEALE	sp|P02754|LACB_BOVIN Beta-lactoglobulin OS=Bos taurus OX=9913 GN=LGB PE=1 SV=3	Yes	No	No	No	No
SLVYPFPGP	sp|P02666|CASB_BOVIN Beta-casein OS=Bos taurus OX=9913 GN=CSN2 PE=1 SV=2	Yes	No	No	No	No
TDAPSFSDIPNPIG	sp|P02662|CASA1_BOVIN Alpha-S1-casein OS=Bos taurus OX=9913 GN=CSN1S1 PE=1 SV=2	Yes	No	No	No	No
MHQPHQPLPPTVMFPP	sp|P02666|CASB_BOVIN Beta-casein OS=Bos taurus OX=9913 GN=CSN2 PE=1 SV=2	Yes	No	No	No	No
LPH	sp|Q58DL5|BCAR3_BOVIN Breast cancer anti-estrogen resistance protein 3 homolog OS=Bos taurus OX=9913 GN=BCAR3 PE=2 SV=2	Yes	No	No	No	No
VRTPEVDDEALE	sp|P02754|LACB_BOVIN Beta-lactoglobulin OS=Bos taurus OX=9913 GN=LGB PE=1 SV=3	Yes	No	No	No	No

EELNVPGEIV	sp|P02666|CASB_BOVIN Beta-casein OS=Bos taurus OX=9913 GN=CSN2 PE=1 SV=2	Yes	No	No	No	No
GGVSLPEW	sp|P00711|LALBA_BOVIN Alpha-lactalbumin OS=Bos taurus OX=9913 GN=LALBA PE=1 SV=2	Yes	No	No	No	No
HQPHQPLPPTVMFPP	sp|P02666|CASB_BOVIN Beta-casein OS=Bos taurus OX=9913 GN=CSN2 PE=1 SV=2	Yes	No	No	No	No
AVDVTLDPDT	sp|P18892|BT1A1_BOVIN Butyrophilin subfamily 1 member A1 OS=Bos taurus OX=9913 GN=BTN1A1 PE=1 SV=2	Yes	No	No	No	No
YYVPL	sp|P02662|CASA1_BOVIN Alpha-S1-casein OS=Bos taurus OX=9913 GN=CSN1S1 PE=1 SV=2	Yes	No	No	No	No
GPFPI	sp|P02666|CASB_BOVIN Beta-casein OS=Bos taurus OX=9913 GN=CSN2 PE=1 SV=2	Yes	No	No	No	No
YTDAPSFSDIPNPI	sp|P02662|CASA1_BOVIN Alpha-S1-casein OS=Bos taurus OX=9913 GN=CSN1S1 PE=1 SV=2	Yes	No	No	No	No
NLENT	sp|P80195|GLCM1_BOVIN Glycosylation-dependent cell adhesion molecule 1 OS=Bos taurus OX=9913 GN=GLYCAM1 PE=1 SV=2	Yes	No	No	No	No
VLP	sp|P02666|CASB_BOVIN Beta-casein OS=Bos taurus OX=9913 GN=CSN2 PE=1 SV=2	Yes	No	No	No	No
TPEVDDEALEKFD	sp|P02754|LACB_BOVIN Beta-lactoglobulin OS=Bos taurus OX=9913 GN=LGB PE=1 SV=3	Yes	No	No	No	No
LYQEPV	sp|P02666|CASB_BOVIN Beta-casein OS=Bos taurus OX=9913 GN=CSN2 PE=1 SV=2	Yes	No	No	No	No
QYTDAPSFSDIPNP	sp|P02662|CASA1_BOVIN Alpha-S1-casein OS=Bos taurus OX=9913 GN=CSN1S1 PE=1 SV=2	Yes	No	No	No	No
TVMFPPQS	sp|P02666|CASB_BOVIN Beta-casein OS=Bos taurus OX=9913 GN=CSN2 PE=1 SV=2	Yes	No	No	No	No
FPL	sp|Q58DL5|BCAR3_BOVIN Breast cancer anti-estrogen resistance protein 3 homolog OS=Bos taurus OX=9913 GN=BCAR3 PE=2 SV=2	Yes	No	No	No	No
LVYPFPGPIP	sp|P02666|CASB_BOVIN Beta-casein OS=Bos taurus OX=9913 GN=CSN2 PE=1 SV=2	Yes	No	No	No	No
QFLPYP	sp|P02668|CASK_BOVIN Kappa-casein OS=Bos taurus OX=9913 GN=CSN3 PE=1 SV=1	Yes	No	No	No	No
LVG	sp|P00711|LALBA_BOVIN Alpha-lactalbumin OS=Bos taurus OX=9913 GN=LALBA PE=1 SV=2	Yes	No	No	No	No
YVEELKPTP	sp|P02754|LACB_BOVIN Beta-lactoglobulin OS=Bos taurus OX=9913 GN=LGB PE=1 SV=3	Yes	No	No	No	No

INNQFLPYP	sp|P02668|CASK_BOVIN Kappa-casein OS=Bos taurus OX=9913 GN=CSN3 PE=1 SV=1	Yes	No	No	No	No
VVPPFLQP	sp|P02666|CASB_BOVIN Beta-casein OS=Bos taurus OX=9913 GN=CSN2 PE=1 SV=2	Yes	No	No	No	No
RNAVPITPT	sp|P02663|CASA2_BOVIN Alpha-S2-casein OS=Bos taurus OX=9913 GN=CSN1S2 PE=1 SV=2	Yes	No	No	No	No
QSLVYPFPGPIPN	sp|P02666|CASB_BOVIN Beta-casein OS=Bos taurus OX=9913 GN=CSN2 PE=1 SV=2	Yes	No	No	No	No
VYVEELKPTPEGDLE	sp|P02754|LACB_BOVIN Beta-lactoglobulin OS=Bos taurus OX=9913 GN=LGB PE=1 SV=3	Yes	No	No	No	No
WA	sp|P18892|BT1A1_BOVIN Butyrophilin subfamily 1 member A1 OS=Bos taurus OX=9913 GN=BTN1A1 PE=1 SV=2	Yes	No	No	No	No
QKLPEKPE	sp|P18892|BT1A1_BOVIN Butyrophilin subfamily 1 member A1 OS=Bos taurus OX=9913 GN=BTN1A1 PE=1 SV=2	Yes	No	No	No	No
LGE	sp|P81265|PIGR_BOVIN Polymeric immunoglobulin receptor OS=Bos taurus OX=9913 GN=PIGR PE=2 SV=1	Yes	No	No	No	No
PGPIPN	sp|P02666|CASB_BOVIN Beta-casein OS=Bos taurus OX=9913 GN=CSN2 PE=1 SV=2	Yes	No	No	No	No
YQKFPQ	sp|P02663|CASA2_BOVIN Alpha-S2-casein OS=Bos taurus OX=9913 GN=CSN1S2 PE=1 SV=2	Yes	No	No	No	No
SLPE	sp|P00711|LALBA_BOVIN Alpha-lactalbumin OS=Bos taurus OX=9913 GN=LALBA PE=1 SV=2	Yes	No	No	No	No
GYGGVSLPE	sp|P00711|LALBA_BOVIN Alpha-lactalbumin OS=Bos taurus OX=9913 GN=LALBA PE=1 SV=2	Yes	No	No	No	No
QKFPQ	sp|P02663|CASA2_BOVIN Alpha-S2-casein OS=Bos taurus OX=9913 GN=CSN1S2 PE=1 SV=2	Yes	No	No	No	No
LNT	sp|Q5E9N9|APEX2_BOVIN DNA-(apurinic or apyrimidinic site) endonuclease 2 OS=Bos taurus OX=9913 GN=APEX2 PE=2 SV=1	Yes	No	No	No	No
SLPQNIPPLTQTPVVVPP	sp|P02666|CASB_BOVIN Beta-casein OS=Bos taurus OX=9913 GN=CSN2 PE=1 SV=2	Yes	No	No	No	No
ASGEPTSTPT	sp|P02668|CASK_BOVIN Kappa-casein OS=Bos taurus OX=9913 GN=CSN3 PE=1 SV=1	Yes	No	No	No	No
PPLTQTPV	sp|P02666|CASB_BOVIN Beta-casein OS=Bos taurus OX=9913 GN=CSN2 PE=1 SV=2	Yes	No	No	No	No
MHQPHQPLPPTVMFPPQSV	sp|P02666|CASB_BOVIN Beta-casein OS=Bos taurus OX=9913 GN=CSN2 PE=1 SV=2	Yes	No	No	No	No
FLQPEV	sp|P02666|CASB_BOVIN Beta-casein OS=Bos taurus OX=9913 GN=CSN2 PE=1 SV=2	Yes	No	No	No	No

QPLPPTVMFPPQSV	sp|P02666|CASB_BOVIN Beta-casein OS=Bos taurus OX=9913 GN=CSN2 PE=1 SV=2	Yes	No	No	No	No
SLVYPFPGPIP	sp|P02666|CASB_BOVIN Beta-casein OS=Bos taurus OX=9913 GN=CSN2 PE=1 SV=2	Yes	No	No	No	No
NIPPLTQTPVVVPPFLQP	sp|P02666|CASB_BOVIN Beta-casein OS=Bos taurus OX=9913 GN=CSN2 PE=1 SV=2	Yes	No	No	No	No
VYPFPGP	sp|P02666|CASB_BOVIN Beta-casein OS=Bos taurus OX=9913 GN=CSN2 PE=1 SV=2	Yes	No	No	No	No
YVP	sp|P02662|CASA1_BOVIN Alpha-S1-casein OS=Bos taurus OX=9913 GN=CSN1S1 PE=1 SV=2	Yes	No	No	No	No
LTQTPVVVPPFLQPE	sp|P02666|CASB_BOVIN Beta-casein OS=Bos taurus OX=9913 GN=CSN2 PE=1 SV=2	Yes	No	No	No	No
PVVVPPF	sp|P02666|CASB_BOVIN Beta-casein OS=Bos taurus OX=9913 GN=CSN2 PE=1 SV=2	Yes	No	No	No	No
TTMP	sp|P02662|CASA1_BOVIN Alpha-S1-casein OS=Bos taurus OX=9913 GN=CSN1S1 PE=1 SV=2	Yes	No	No	No	No
TLTDVEN	sp|P02666|CASB_BOVIN Beta-casein OS=Bos taurus OX=9913 GN=CSN2 PE=1 SV=2	Yes	No	No	No	No
RTPEVDDE	sp|P02754|LACB_BOVIN Beta-lactoglobulin OS=Bos taurus OX=9913 GN=LGB PE=1 SV=3	Yes	No	No	No	No
TVDDK	sp|P02663|CASA2_BOVIN Alpha-S2-casein OS=Bos taurus OX=9913 GN=CSN1S2 PE=1 SV=2	Yes	No	No	No	No
PFPK	sp|P02666|CASB_BOVIN Beta-casein OS=Bos taurus OX=9913 GN=CSN2 PE=1 SV=2	Yes	No	No	No	No
VEQ	sp|P02662|CASA1_BOVIN Alpha-S1-casein OS=Bos taurus OX=9913 GN=CSN1S1 PE=1 SV=2	Yes	No	No	No	No
RLSFNPT	sp|P02754|LACB_BOVIN Beta-lactoglobulin OS=Bos taurus OX=9913 GN=LGB PE=1 SV=3	Yes	No	No	No	No
VIESPPEIN	sp|P02668|CASK_BOVIN Kappa-casein OS=Bos taurus OX=9913 GN=CSN3 PE=1 SV=1	Yes	No	No	No	No
PPLT	sp|P02666|CASB_BOVIN Beta-casein OS=Bos taurus OX=9913 GN=CSN2 PE=1 SV=2	Yes	No	No	No	No
HQPLPPTVMFPPQ	sp|P02666|CASB_BOVIN Beta-casein OS=Bos taurus OX=9913 GN=CSN2 PE=1 SV=2	Yes	No	No	No	No
YFYPE	sp|P02662|CASA1_BOVIN Alpha-S1-casein OS=Bos taurus OX=9913 GN=CSN1S1 PE=1 SV=2	Yes	No	No	No	No
APFDVIGPQEPI	sp|P18892|BT1A1_BOVIN Butyrophilin subfamily 1 member A1 OS=Bos taurus OX=9913 GN=BTN1A1 PE=1 SV=2	Yes	No	No	No	No

MFPPQSV	sp|P02666|CASB_BOVIN Beta-casein OS=Bos taurus OX=9913 GN=CSN2 PE=1 SV=2	Yes	No	No	No	No
VEELKPTPEGD	sp|P02754|LACB_BOVIN Beta-lactoglobulin OS=Bos taurus OX=9913 GN=LGB PE=1 SV=3	Yes	No	No	No	No
GAW	sp|P02662|CASA1_BOVIN Alpha-S1-casein OS=Bos taurus OX=9913 GN=CSN1S1 PE=1 SV=2	Yes	No	No	No	No
VSTLVPL	sp|P81265|PIGR_BOVIN Polymeric immunoglobulin receptor OS=Bos taurus OX=9913 GN=PIGR PE=2 SV=1	Yes	No	No	No	No
LENT	sp|P80195|GLCM1_BOVIN Glycosylation-dependent cell adhesion molecule 1 OS=Bos taurus OX=9913 GN=GLYCAM1 PE=1 SV=2	Yes	No	No	No	No
QPLPPTVMFPP	sp|P02666|CASB_BOVIN Beta-casein OS=Bos taurus OX=9913 GN=CSN2 PE=1 SV=2	Yes	No	No	No	No
WMHQPHQPLPPT	sp|P02666|CASB_BOVIN Beta-casein OS=Bos taurus OX=9913 GN=CSN2 PE=1 SV=2	Yes	No	No	No	No
VLE	sp|P81265|PIGR_BOVIN Polymeric immunoglobulin receptor OS=Bos taurus OX=9913 GN=PIGR PE=2 SV=1	Yes	No	No	No	No
SLPQ	sp|P02666|CASB_BOVIN Beta-casein OS=Bos taurus OX=9913 GN=CSN2 PE=1 SV=2	Yes	No	No	No	apical
TEDELQDKIHP	sp|P02666|CASB_BOVIN Beta-casein OS=Bos taurus OX=9913 GN=CSN2 PE=1 SV=2	Yes	No	No	No	apical
VAD	sp|P18892|BT1A1_BOVIN Butyrophilin subfamily 1 member A1 OS=Bos taurus OX=9913 GN=BTN1A1 PE=1 SV=2	Yes	No	No	No	apical
QPHQPLPPT	sp|P02666|CASB_BOVIN Beta-casein OS=Bos taurus OX=9913 GN=CSN2 PE=1 SV=2	Yes	No	No	No	apical
LNVPGEIVE	sp|P02666|CASB_BOVIN Beta-casein OS=Bos taurus OX=9913 GN=CSN2 PE=1 SV=2	Yes	No	No	No	apical
ALC	sp|P00711|LALBA_BOVIN Alpha-lactalbumin OS=Bos taurus OX=9913 GN=LALBA PE=1 SV=2	Yes	No	No	No	apical
NVPGEIVE	sp|P02666|CASB_BOVIN Beta-casein OS=Bos taurus OX=9913 GN=CSN2 PE=1 SV=2	Yes	No	No	No	apical
TPEVDDEA	sp|P02754|LACB_BOVIN Beta-lactoglobulin OS=Bos taurus OX=9913 GN=LGB PE=1 SV=3	Yes	No	No	No	apical
AVPYP	sp|P02666|CASB_BOVIN Beta-casein OS=Bos taurus OX=9913 GN=CSN2 PE=1 SV=2	Yes	No	No	No	apical
HQPHQPLPP	sp|P02666|CASB_BOVIN Beta-casein OS=Bos taurus OX=9913 GN=CSN2 PE=1 SV=2	Yes	No	No	No	apical
PQNIPPLTQTPVVVPPFLQPEV	sp|P02666|CASB_BOVIN Beta-casein OS=Bos taurus OX=9913 GN=CSN2 PE=1 SV=2	Yes	No	No	No	apical

PLV	sp|Q58DL5|BCAR3_BOVIN Breast cancer anti-estrogen resistance protein 3 homolog OS=Bos taurus OX=9913 GN=BCAR3 PE=2 SV=2	Yes	No	No	No	apical
YVPL	sp|P02662|CASA1_BOVIN Alpha-S1-casein OS=Bos taurus OX=9913 GN=CSN1S1 PE=1 SV=2	Yes	No	No	No	apical
VEELKP	sp|P02754|LACB_BOVIN Beta-lactoglobulin OS=Bos taurus OX=9913 GN=LGB PE=1 SV=3	Yes	No	No	No	apical
DAAGGPGAPADPGRPTG	sp|P81265|PIGR_BOVIN Polymeric immunoglobulin receptor OS=Bos taurus OX=9913 GN=PIGR PE=2 SV=1	Yes	No	No	No	apical
VAGT	sp|P02754|LACB_BOVIN Beta-lactoglobulin OS=Bos taurus OX=9913 GN=LGB PE=1 SV=3	Yes	No	No	No	apical
VNH	sp|Q58DL5|BCAR3_BOVIN Breast cancer anti-estrogen resistance protein 3 homolog OS=Bos taurus OX=9913 GN=BCAR3 PE=2 SV=2	No	Yes	No	basolateral	No
WKG	sp|Q58DL5|BCAR3_BOVIN Breast cancer anti-estrogen resistance protein 3 homolog OS=Bos taurus OX=9913 GN=BCAR3 PE=2 SV=2	No	Yes	No	basolateral	No
LAE	sp|P81282|CSPG2_BOVIN Versican core protein OS=Bos taurus OX=9913 GN=VCAN PE=1 SV=2	No	Yes	No	basolateral	No
FYP	sp|P02662|CASA1_BOVIN Alpha-S1-casein OS=Bos taurus OX=9913 GN=CSN1S1 PE=1 SV=2	No	Yes	No	basolateral	No
MLP	sp|P81282|CSPG2_BOVIN Versican core protein OS=Bos taurus OX=9913 GN=VCAN PE=1 SV=2	No	Yes	No	basolateral	No
SNG	sp|Q28106|CNTN1_BOVIN Contactin-1 OS=Bos taurus OX=9913 GN=CNTN1 PE=2 SV=1	No	Yes	No	basolateral	No
VFT	sp|P02663|CASA2_BOVIN Alpha-S2-casein OS=Bos taurus OX=9913 GN=CSN1S2 PE=1 SV=2	No	Yes	No	basolateral	No
GPL	sp|P81282|CSPG2_BOVIN Versican core protein OS=Bos taurus OX=9913 GN=VCAN PE=1 SV=2	No	Yes	No	basolateral	No
WLA	sp|P00711|LALBA_BOVIN Alpha-lactalbumin OS=Bos taurus OX=9913 GN=LALBA PE=1 SV=2	No	Yes	No	basolateral	No
PWP	sp|P81282|CSPG2_BOVIN Versican core protein OS=Bos taurus OX=9913 GN=VCAN PE=1 SV=2	No	Yes	No	basolateral	No
YGGV	sp|P00711|LALBA_BOVIN Alpha-lactalbumin OS=Bos taurus OX=9913 GN=LALBA PE=1 SV=2	No	Yes	No	basolateral	No
QPLPPT	sp|P02666|CASB_BOVIN Beta-casein OS=Bos taurus OX=9913 GN=CSN2 PE=1 SV=2	No	Yes	No	basolateral	No

ALV	sp|P81265|PIGR_BOVIN Polymeric immunoglobulin receptor OS=Bos taurus OX=9913 GN=PIGR PE=2 SV=1	No	Yes	No	basolateral	No
FWG	sp|P81282|CSPG2_BOVIN Versican core protein OS=Bos taurus OX=9913 GN=VCAN PE=1 SV=2	No	Yes	No	basolateral	No
GYGGV	sp|P00711|LALBA_BOVIN Alpha-lactalbumin OS=Bos taurus OX=9913 GN=LALBA PE=1 SV=2	No	Yes	No	basolateral	No
YPF	sp|P02666|CASB_BOVIN Beta-casein OS=Bos taurus OX=9913 GN=CSN2 PE=1 SV=2	No	Yes	No	basolateral	No
PLVTLMEREAV	sp|Q58DL5|BCAR3_BOVIN Breast cancer anti-estrogen resistance protein 3 homolog OS=Bos taurus OX=9913 GN=BCAR3 PE=2 SV=2	No	Yes	No	basolateral	No
TGP	sp|P81282|CSPG2_BOVIN Versican core protein OS=Bos taurus OX=9913 GN=VCAN PE=1 SV=2	No	Yes	No	basolateral	No
QHH	sp|P81282|CSPG2_BOVIN Versican core protein OS=Bos taurus OX=9913 GN=VCAN PE=1 SV=2	No	Yes	No	basolateral	No
SPLV	sp|Q58DL5|BCAR3_BOVIN Breast cancer anti-estrogen resistance protein 3 homolog OS=Bos taurus OX=9913 GN=BCAR3 PE=2 SV=2	No	Yes	No	basolateral	No
DLTGIPPAPR	sp|Q0VCX2|BIP_BOVIN Endoplasmic reticulum chaperone BiP OS=Bos taurus OX=9913 GN=HSPA5 PE=2 SV=1	No	Yes	No	basolateral	No
QLL	sp|P02662|CASA1_BOVIN Alpha-S1-casein OS=Bos taurus OX=9913 GN=CSN1S1 PE=1 SV=2	No	Yes	No	basolateral	No
QLV	sp|Q0VCX2|BIP_BOVIN Endoplasmic reticulum chaperone BiP OS=Bos taurus OX=9913 GN=HSPA5 PE=2 SV=1	No	Yes	No	No	No
LFH	sp|P00711|LALBA_BOVIN Alpha-lactalbumin OS=Bos taurus OX=9913 GN=LALBA PE=1 SV=2	No	Yes	No	No	No
VESWVEITP	sp|P81282|CSPG2_BOVIN Versican core protein OS=Bos taurus OX=9913 GN=VCAN PE=1 SV=2	No	Yes	No	No	No
WRP	sp|P81282|CSPG2_BOVIN Versican core protein OS=Bos taurus OX=9913 GN=VCAN PE=1 SV=2	No	Yes	No	No	No
VHF	sp|Q5E9N9|APEX2_BOVIN DNA-(apurinic or apyrimidinic site) endonuclease 2 OS=Bos taurus OX=9913 GN=APEX2 PE=2 SV=1	No	Yes	No	No	No
LAV	sp|P02663|CASA2_BOVIN Alpha-S2-casein OS=Bos taurus OX=9913 GN=CSN1S2 PE=1 SV=2	No	Yes	No	No	No
NVPGEIV	sp|P02666|CASB_BOVIN Beta-casein OS=Bos taurus OX=9913 GN=CSN2 PE=1 SV=2	No	Yes	No	No	No
NVPGEIVESL	sp|P02666|CASB_BOVIN Beta-casein OS=Bos taurus OX=9913 GN=CSN2 PE=1 SV=2	No	Yes	No	No	No

SRD	sp|P81265|PIGR_BOVIN Polymeric immunoglobulin receptor OS=Bos taurus OX=9913 GN=PIGR PE=2 SV=1	No	Yes	No	No	No
FYPE	sp|P02662|CASA1_BOVIN Alpha-S1-casein OS=Bos taurus OX=9913 GN=CSN1S1 PE=1 SV=2	No	Yes	No	No	No
LYP	sp|P81282|CSPG2_BOVIN Versican core protein OS=Bos taurus OX=9913 GN=VCAN PE=1 SV=2	No	Yes	No	No	No
WKK	sp|Q28106|CNTN1_BOVIN Contactin-1 OS=Bos taurus OX=9913 GN=CNTN1 PE=2 SV=1	No	Yes	No	No	No
VPC	sp|P81282|CSPG2_BOVIN Versican core protein OS=Bos taurus OX=9913 GN=VCAN PE=1 SV=2	No	Yes	No	No	No
NVPGEIVES	sp|P02666|CASB_BOVIN Beta-casein OS=Bos taurus OX=9913 GN=CSN2 PE=1 SV=2	No	Yes	No	No	No
YQGPIV	sp|P02663|CASA2_BOVIN Alpha-S2-casein OS=Bos taurus OX=9913 GN=CSN1S2 PE=1 SV=2	No	Yes	No	No	No
YSR	sp|Q58DL5|BCAR3_BOVIN Breast cancer anti-estrogen resistance protein 3 homolog OS=Bos taurus OX=9913 GN=BCAR3 PE=2 SV=2	No	Yes	No	No	No
GCS	sp|P81265|PIGR_BOVIN Polymeric immunoglobulin receptor OS=Bos taurus OX=9913 GN=PIGR PE=2 SV=1	No	Yes	No	No	No
VYLP	sp|P81282|CSPG2_BOVIN Versican core protein OS=Bos taurus OX=9913 GN=VCAN PE=1 SV=2	No	Yes	No	No	No
WPK	sp|P81282|CSPG2_BOVIN Versican core protein OS=Bos taurus OX=9913 GN=VCAN PE=1 SV=2	No	Yes	No	No	No
VAPFPEVFG	sp|P02662|CASA1_BOVIN Alpha-S1-casein OS=Bos taurus OX=9913 GN=CSN1S1 PE=1 SV=2	No	Yes	No	No	No
VLH	sp|Q58DL5|BCAR3_BOVIN Breast cancer anti-estrogen resistance protein 3 homolog OS=Bos taurus OX=9913 GN=BCAR3 PE=2 SV=2	No	Yes	No	No	No
RNF	sp|Q28106|CNTN1_BOVIN Contactin-1 OS=Bos taurus OX=9913 GN=CNTN1 PE=2 SV=1	No	Yes	No	No	No
YTT	sp|P81282|CSPG2_BOVIN Versican core protein OS=Bos taurus OX=9913 GN=VCAN PE=1 SV=2	No	Yes	No	No	No
LGPV	sp|P02666|CASB_BOVIN Beta-casein OS=Bos taurus OX=9913 GN=CSN2 PE=1 SV=2	No	Yes	No	No	No
LGV	sp|P81282|CSPG2_BOVIN Versican core protein OS=Bos taurus OX=9913 GN=VCAN PE=1 SV=2	No	Yes	No	No	No
AVPITPT	sp|P02663|CASA2_BOVIN Alpha-S2-casein OS=Bos taurus OX=9913 GN=CSN1S2 PE=1 SV=2	No	Yes	No	No	No

FPQ	sp|P02663|CASA2_BOVIN Alpha-S2-casein OS=Bos taurus OX=9913 GN=CSN1S2 PE=1 SV=2	No	Yes	No	No	No
WLK	sp|Q28106|CNTN1_BOVIN Contactin-1 OS=Bos taurus OX=9913 GN=CNTN1 PE=2 SV=1	No	Yes	No	No	No
VW	sp|Q28106|CNTN1_BOVIN Contactin-1 OS=Bos taurus OX=9913 GN=CNTN1 PE=2 SV=1	No	Yes	No	No	No
YQH	sp|P02663|CASA2_BOVIN Alpha-S2-casein OS=Bos taurus OX=9913 GN=CSN1S2 PE=1 SV=2	No	Yes	No	No	No
VLGPV	sp|P02666|CASB_BOVIN Beta-casein OS=Bos taurus OX=9913 GN=CSN2 PE=1 SV=2	No	Yes	No	No	No
HCK	sp|P81282|CSPG2_BOVIN Versican core protein OS=Bos taurus OX=9913 GN=VCAN PE=1 SV=2	No	Yes	No	No	No
VQK	sp|Q0VCX2|BIP_BOVIN Endoplasmic reticulum chaperone BiP OS=Bos taurus OX=9913 GN=HSPA5 PE=2 SV=1	No	Yes	No	No	No
GLPQEV	sp|P02662|CASA1_BOVIN Alpha-S1-casein OS=Bos taurus OX=9913 GN=CSN1S1 PE=1 SV=2	No	Yes	No	No	No
LPLP	sp|P02666|CASB_BOVIN Beta-casein OS=Bos taurus OX=9913 GN=CSN2 PE=1 SV=2	No	Yes	No	No	No
TRL	sp|Q58DL5|BCAR3_BOVIN Breast cancer anti-estrogen resistance protein 3 homolog OS=Bos taurus OX=9913 GN=BCAR3 PE=2 SV=2	No	Yes	No	No	No
PYPQ	sp|P02666|CASB_BOVIN Beta-casein OS=Bos taurus OX=9913 GN=CSN2 PE=1 SV=2	No	Yes	No	No	No
MGA	sp|P81265|PIGR_BOVIN Polymeric immunoglobulin receptor OS=Bos taurus OX=9913 GN=PIGR PE=2 SV=1	No	Yes	No	No	No
TTR	sp|P81282|CSPG2_BOVIN Versican core protein OS=Bos taurus OX=9913 GN=VCAN PE=1 SV=2	No	Yes	No	No	basolateral
LPYP	sp|P02668|CASK_BOVIN Kappa-casein OS=Bos taurus OX=9913 GN=CSN3 PE=1 SV=1	No	Yes	No	No	basolateral
LFP	sp|P81282|CSPG2_BOVIN Versican core protein OS=Bos taurus OX=9913 GN=VCAN PE=1 SV=2	No	Yes	No	No	basolateral
NYH	sp|P81282|CSPG2_BOVIN Versican core protein OS=Bos taurus OX=9913 GN=VCAN PE=1 SV=2	No	Yes	No	No	basolateral
RGPFPI	sp|P02666|CASB_BOVIN Beta-casein OS=Bos taurus OX=9913 GN=CSN2 PE=1 SV=2	No	Yes	No	No	basolateral
QFLP	sp|P02668|CASK_BOVIN Kappa-casein OS=Bos taurus OX=9913 GN=CSN3 PE=1 SV=1	No	Yes	No	No	basolateral

YRP	sp|Q28106|CNTN1_BOVIN Contactin-1 OS=Bos taurus OX=9913 GN=CNTN1 PE=2 SV=1	No	Yes	No	No	basolateral
PNK	sp|P81282|CSPG2_BOVIN Versican core protein OS=Bos taurus OX=9913 GN=VCAN PE=1 SV=2	No	Yes	No	No	basolateral
VVPPFLQPE	sp|P02666|CASB_BOVIN Beta-casein OS=Bos taurus OX=9913 GN=CSN2 PE=1 SV=2	Yes	Yes	No	No	No
LYQGPI	sp|P02663|CASA2_BOVIN Alpha-S2-casein OS=Bos taurus OX=9913 GN=CSN1S2 PE=1 SV=2	Yes	Yes	No	No	No
ITVDDK	sp|P02663|CASA2_BOVIN Alpha-S2-casein OS=Bos taurus OX=9913 GN=CSN1S2 PE=1 SV=2	Yes	Yes	No	No	No
TVDMESTEV	sp|P02663|CASA2_BOVIN Alpha-S2-casein OS=Bos taurus OX=9913 GN=CSN1S2 PE=1 SV=2	Yes	Yes	No	No	No
VPPFLQPE	sp|P02666|CASB_BOVIN Beta-casein OS=Bos taurus OX=9913 GN=CSN2 PE=1 SV=2	Yes	Yes	No	No	No
AVPYPQ	sp|P02666|CASB_BOVIN Beta-casein OS=Bos taurus OX=9913 GN=CSN2 PE=1 SV=2	Yes	Yes	No	No	No
FLDDDLTDDIM	sp|P00711|LALBA_BOVIN Alpha-lactalbumin OS=Bos taurus OX=9913 GN=LALBA PE=1 SV=2	Yes	Yes	No	No	No
QKF	sp|P02663|CASA2_BOVIN Alpha-S2-casein OS=Bos taurus OX=9913 GN=CSN1S2 PE=1 SV=2	Yes	Yes	No	apical/basolateral	No
TDAPSFSDIPNP	sp|P02662|CASA1_BOVIN Alpha-S1-casein OS=Bos taurus OX=9913 GN=CSN1S1 PE=1 SV=2	Yes	Yes	No	No	No
TQTPVVVPPFLQPEV	sp|P02666|CASB_BOVIN Beta-casein OS=Bos taurus OX=9913 GN=CSN2 PE=1 SV=2	Yes	Yes	No	No	No
PFPEV	sp|P02662|CASA1_BOVIN Alpha-S1-casein OS=Bos taurus OX=9913 GN=CSN1S1 PE=1 SV=2	Yes	Yes	No	No	No
NMAINPS	sp|P02663|CASA2_BOVIN Alpha-S2-casein OS=Bos taurus OX=9913 GN=CSN1S2 PE=1 SV=2	Yes	Yes	No	No	No
LYQEPVLGPV	sp|P02666|CASB_BOVIN Beta-casein OS=Bos taurus OX=9913 GN=CSN2 PE=1 SV=2	Yes	Yes	No	No	No
NNQFLPYP	sp|P02668|CASK_BOVIN Kappa-casein OS=Bos taurus OX=9913 GN=CSN3 PE=1 SV=1	Yes	Yes	No	No	No
PLPPTVMFPPQS	sp|P02666|CASB_BOVIN Beta-casein OS=Bos taurus OX=9913 GN=CSN2 PE=1 SV=2	Yes	Yes	No	No	No
TPEVDDEALE	sp|P02754|LACB_BOVIN Beta-lactoglobulin OS=Bos taurus OX=9913 GN=LGB PE=1 SV=3	Yes	Yes	No	No	No
VAPFPE	sp|P02662|CASA1_BOVIN Alpha-S1-casein OS=Bos taurus OX=9913 GN=CSN1S1 PE=1 SV=2	Yes	Yes	No	No	No

NIPPLTQTPVVVPPFLQPEV	sp|P02666|CASB_BOVIN Beta-casein OS=Bos taurus OX=9913 GN=CSN2 PE=1 SV=2	Yes	Yes	No	No	No
MHQPHQPLPPTVMFPPQ	sp|P02666|CASB_BOVIN Beta-casein OS=Bos taurus OX=9913 GN=CSN2 PE=1 SV=2	Yes	Yes	No	No	No
ESPPEIN	sp|P02668|CASK_BOVIN Kappa-casein OS=Bos taurus OX=9913 GN=CSN3 PE=1 SV=1	Yes	Yes	No	No	No
LPPT	sp|P02666|CASB_BOVIN Beta-casein OS=Bos taurus OX=9913 GN=CSN2 PE=1 SV=2	Yes	Yes	No	No	No
SPPEINT	sp|P02668|CASK_BOVIN Kappa-casein OS=Bos taurus OX=9913 GN=CSN3 PE=1 SV=1	Yes	Yes	No	No	No
EELKPTPE	sp|P02754|LACB_BOVIN Beta-lactoglobulin OS=Bos taurus OX=9913 GN=LGB PE=1 SV=3	Yes	Yes	No	No	No
ILNKPEDET	sp|P80195|GLCM1_BOVIN Glycosylation-dependent cell adhesion molecule 1 OS=Bos taurus OX=9913 GN=GLYCAM1 PE=1 SV=2	Yes	Yes	No	No	No
TPEVDDEALEK	sp|P02754|LACB_BOVIN Beta-lactoglobulin OS=Bos taurus OX=9913 GN=LGB PE=1 SV=3	Yes	Yes	No	No	No
QLDAYPS	sp|P02662|CASA1_BOVIN Alpha-S1-casein OS=Bos taurus OX=9913 GN=CSN1S1 PE=1 SV=2	Yes	Yes	No	No	No
NIPPLTQTPV	sp|P02666|CASB_BOVIN Beta-casein OS=Bos taurus OX=9913 GN=CSN2 PE=1 SV=2	Yes	Yes	No	No	No
AYFYPE	sp|P02662|CASA1_BOVIN Alpha-S1-casein OS=Bos taurus OX=9913 GN=CSN1S1 PE=1 SV=2	Yes	Yes	No	No	No
FVAPFPEV	sp|P02662|CASA1_BOVIN Alpha-S1-casein OS=Bos taurus OX=9913 GN=CSN1S1 PE=1 SV=2	Yes	Yes	No	No	No
VIESPPEINT	sp|P02668|CASK_BOVIN Kappa-casein OS=Bos taurus OX=9913 GN=CSN3 PE=1 SV=1	Yes	Yes	No	No	No
KVPQLEIVPN	sp|P02662|CASA1_BOVIN Alpha-S1-casein OS=Bos taurus OX=9913 GN=CSN1S1 PE=1 SV=2	Yes	Yes	No	No	No
VLDTD	sp|P02754|LACB_BOVIN Beta-lactoglobulin OS=Bos taurus OX=9913 GN=LGB PE=1 SV=3	Yes	Yes	No	No	No
VEELKPTPEGDLE	sp|P02754|LACB_BOVIN Beta-lactoglobulin OS=Bos taurus OX=9913 GN=LGB PE=1 SV=3	Yes	Yes	No	No	No
VYPFPGPIPN	sp|P02666|CASB_BOVIN Beta-casein OS=Bos taurus OX=9913 GN=CSN2 PE=1 SV=2	Yes	Yes	No	No	No
QPEV	sp|P02666|CASB_BOVIN Beta-casein OS=Bos taurus OX=9913 GN=CSN2 PE=1 SV=2	Yes	Yes	No	No	No
DIGSESTEDQ	sp|P02662|CASA1_BOVIN Alpha-S1-casein OS=Bos taurus OX=9913 GN=CSN1S1 PE=1 SV=2	Yes	Yes	No	No	No

YVEELKPTPE	sp|P02754|LACB_BOVIN Beta-lactoglobulin OS=Bos taurus OX=9913 GN=LGB PE=1 SV=3	Yes	Yes	No	No	No
HQPLPPT	sp|P02666|CASB_BOVIN Beta-casein OS=Bos taurus OX=9913 GN=CSN2 PE=1 SV=2	Yes	Yes	No	No	No
YQQKPV	sp|P02668|CASK_BOVIN Kappa-casein OS=Bos taurus OX=9913 GN=CSN3 PE=1 SV=1	Yes	Yes	No	No	No
HLPLP	sp|P02666|CASB_BOVIN Beta-casein OS=Bos taurus OX=9913 GN=CSN2 PE=1 SV=2	Yes	Yes	No	No	No
PFPGPI	sp|P02666|CASB_BOVIN Beta-casein OS=Bos taurus OX=9913 GN=CSN2 PE=1 SV=2	Yes	Yes	No	No	No
PPFLQPEV	sp|P02666|CASB_BOVIN Beta-casein OS=Bos taurus OX=9913 GN=CSN2 PE=1 SV=2	Yes	Yes	No	No	No
SDIPNPI	sp|P02662|CASA1_BOVIN Alpha-S1-casein OS=Bos taurus OX=9913 GN=CSN1S1 PE=1 SV=2	Yes	Yes	No	No	No
TQTPVVVPPFLQPE	sp|P02666|CASB_BOVIN Beta-casein OS=Bos taurus OX=9913 GN=CSN2 PE=1 SV=2	Yes	Yes	No	No	No
GGVSLPE	sp|P00711|LALBA_BOVIN Alpha-lactalbumin OS=Bos taurus OX=9913 GN=LALBA PE=1 SV=2	Yes	Yes	No	No	No
GGVSLPEWV	sp|P00711|LALBA_BOVIN Alpha-lactalbumin OS=Bos taurus OX=9913 GN=LALBA PE=1 SV=2	Yes	Yes	No	No	No
MFPPQ	sp|P02666|CASB_BOVIN Beta-casein OS=Bos taurus OX=9913 GN=CSN2 PE=1 SV=2	Yes	Yes	No	No	No
LSFNPT	sp|P02754|LACB_BOVIN Beta-lactoglobulin OS=Bos taurus OX=9913 GN=LGB PE=1 SV=3	Yes	Yes	No	No	No
SLPQNIPPL	sp|P02666|CASB_BOVIN Beta-casein OS=Bos taurus OX=9913 GN=CSN2 PE=1 SV=2	Yes	Yes	No	No	No
FLDDDLTDDI	sp|P00711|LALBA_BOVIN Alpha-lactalbumin OS=Bos taurus OX=9913 GN=LALBA PE=1 SV=2	Yes	Yes	No	No	No
PPFLQPE	sp|P02666|CASB_BOVIN Beta-casein OS=Bos taurus OX=9913 GN=CSN2 PE=1 SV=2	Yes	Yes	No	No	No
PQEV	sp|P02662|CASA1_BOVIN Alpha-S1-casein OS=Bos taurus OX=9913 GN=CSN1S1 PE=1 SV=2	Yes	Yes	No	No	No
SLVYPFPGPIPN	sp|P02666|CASB_BOVIN Beta-casein OS=Bos taurus OX=9913 GN=CSN2 PE=1 SV=2	Yes	Yes	No	No	No
EVDDEALEKFD	sp|P02754|LACB_BOVIN Beta-lactoglobulin OS=Bos taurus OX=9913 GN=LGB PE=1 SV=3	Yes	Yes	No	No	No
NPW	sp|P02663|CASA2_BOVIN Alpha-S2-casein OS=Bos taurus OX=9913 GN=CSN1S2 PE=1 SV=2	Yes	Yes	No	No	No

MFPPQS	sp|P02666|CASB_BOVIN Beta-casein OS=Bos taurus OX=9913 GN=CSN2 PE=1 SV=2	Yes	Yes	No	No	No
IPPLTQTPV	sp|P02666|CASB_BOVIN Beta-casein OS=Bos taurus OX=9913 GN=CSN2 PE=1 SV=2	Yes	Yes	No	No	No
VPYPQ	sp|P02666|CASB_BOVIN Beta-casein OS=Bos taurus OX=9913 GN=CSN2 PE=1 SV=2	Yes	Yes	No	No	No
LPPTVMFPPQS	sp|P02666|CASB_BOVIN Beta-casein OS=Bos taurus OX=9913 GN=CSN2 PE=1 SV=2	Yes	Yes	No	No	No
PVVVPPFLQPE	sp|P02666|CASB_BOVIN Beta-casein OS=Bos taurus OX=9913 GN=CSN2 PE=1 SV=2	Yes	Yes	No	No	No
VEELKPTPE	sp|P02754|LACB_BOVIN Beta-lactoglobulin OS=Bos taurus OX=9913 GN=LGB PE=1 SV=3	Yes	Yes	No	No	No
ELKPTPE	sp|P02754|LACB_BOVIN Beta-lactoglobulin OS=Bos taurus OX=9913 GN=LGB PE=1 SV=3	Yes	Yes	No	No	No
VYPFPGPI	sp|P02666|CASB_BOVIN Beta-casein OS=Bos taurus OX=9913 GN=CSN2 PE=1 SV=2	Yes	Yes	No	No	No
YVEELKPT	sp|P02754|LACB_BOVIN Beta-lactoglobulin OS=Bos taurus OX=9913 GN=LGB PE=1 SV=3	Yes	Yes	No	No	No
LPQNIPPLTQTPV	sp|P02666|CASB_BOVIN Beta-casein OS=Bos taurus OX=9913 GN=CSN2 PE=1 SV=2	Yes	Yes	No	No	No
EMPFPK	sp|P02666|CASB_BOVIN Beta-casein OS=Bos taurus OX=9913 GN=CSN2 PE=1 SV=2	Yes	Yes	No	No	No
EIVPN	sp|P02662|CASA1_BOVIN Alpha-S1-casein OS=Bos taurus OX=9913 GN=CSN1S1 PE=1 SV=2	Yes	Yes	No	No	No
MHQPHQPLPPT	sp|P02666|CASB_BOVIN Beta-casein OS=Bos taurus OX=9913 GN=CSN2 PE=1 SV=2	Yes	Yes	No	No	No
NIPPLTQTPVVVPP	sp|P02666|CASB_BOVIN Beta-casein OS=Bos taurus OX=9913 GN=CSN2 PE=1 SV=2	Yes	Yes	No	No	No
VAPFPEV	sp|P02662|CASA1_BOVIN Alpha-S1-casein OS=Bos taurus OX=9913 GN=CSN1S1 PE=1 SV=2	Yes	Yes	No	No	No
TPVVVPPFLQPEV	sp|P02666|CASB_BOVIN Beta-casein OS=Bos taurus OX=9913 GN=CSN2 PE=1 SV=2	Yes	Yes	No	No	No
DAQSAPL	sp|P02754|LACB_BOVIN Beta-lactoglobulin OS=Bos taurus OX=9913 GN=LGB PE=1 SV=3	Yes	Yes	No	No	No
APSFSDIPNPI	sp|P02662|CASA1_BOVIN Alpha-S1-casein OS=Bos taurus OX=9913 GN=CSN1S1 PE=1 SV=2	Yes	Yes	No	No	No
YYVP	sp|P02662|CASA1_BOVIN Alpha-S1-casein OS=Bos taurus OX=9913 GN=CSN1S1 PE=1 SV=2	Yes	Yes	No	No	No

DAAGGPGAPADPGRPT	sp|P81265|PIGR_BOVIN Polymeric immunoglobulin receptor OS=Bos taurus OX=9913 GN=PIGR PE=2 SV=1	Yes	Yes	No	No	No
VLPVPQ	sp|P02666|CASB_BOVIN Beta-casein OS=Bos taurus OX=9913 GN=CSN2 PE=1 SV=2	Yes	Yes	No	No	No
FVAPFPE	sp|P02662|CASA1_BOVIN Alpha-S1-casein OS=Bos taurus OX=9913 GN=CSN1S1 PE=1 SV=2	Yes	Yes	No	No	No
DAPSFSDIPNPI	sp|P02662|CASA1_BOVIN Alpha-S1-casein OS=Bos taurus OX=9913 GN=CSN1S1 PE=1 SV=2	Yes	Yes	No	No	No
SLVYPFPGPI	sp|P02666|CASB_BOVIN Beta-casein OS=Bos taurus OX=9913 GN=CSN2 PE=1 SV=2	Yes	Yes	No	No	No
SLPQNIPPLTQTPVVVPPFLQPEV	sp|P02666|CASB_BOVIN Beta-casein OS=Bos taurus OX=9913 GN=CSN2 PE=1 SV=2	Yes	Yes	No	No	No
AMEDIK	sp|P02662|CASA1_BOVIN Alpha-S1-casein OS=Bos taurus OX=9913 GN=CSN1S1 PE=1 SV=2	Yes	Yes	No	No	No
LVYPFPGPI	sp|P02666|CASB_BOVIN Beta-casein OS=Bos taurus OX=9913 GN=CSN2 PE=1 SV=2	Yes	Yes	No	No	No
HQGLPQ	sp|P02662|CASA1_BOVIN Alpha-S1-casein OS=Bos taurus OX=9913 GN=CSN1S1 PE=1 SV=2	Yes	Yes	No	No	No
LPVPQ	sp|P02666|CASB_BOVIN Beta-casein OS=Bos taurus OX=9913 GN=CSN2 PE=1 SV=2	Yes	Yes	No	No	No
NPWD	sp|P02663|CASA2_BOVIN Alpha-S2-casein OS=Bos taurus OX=9913 GN=CSN1S2 PE=1 SV=2	Yes	Yes	No	No	No
SFSDIPNPI	sp|P02662|CASA1_BOVIN Alpha-S1-casein OS=Bos taurus OX=9913 GN=CSN1S1 PE=1 SV=2	Yes	Yes	No	No	No
VPPFLQPEV	sp|P02666|CASB_BOVIN Beta-casein OS=Bos taurus OX=9913 GN=CSN2 PE=1 SV=2	Yes	Yes	No	No	No
LDDDLTDDI	sp|P00711|LALBA_BOVIN Alpha-lactalbumin OS=Bos taurus OX=9913 GN=LALBA PE=1 SV=2	Yes	Yes	No	No	No
EVDDEALEK	sp|P02754|LACB_BOVIN Beta-lactoglobulin OS=Bos taurus OX=9913 GN=LGB PE=1 SV=3	Yes	Yes	No	No	No
MAIPPK	sp|P02668|CASK_BOVIN Kappa-casein OS=Bos taurus OX=9913 GN=CSN3 PE=1 SV=1	Yes	Yes	No	No	No
QTPVVVPPFLQPEV	sp|P02666|CASB_BOVIN Beta-casein OS=Bos taurus OX=9913 GN=CSN2 PE=1 SV=2	Yes	Yes	No	No	No
VFG	sp|P02662|CASA1_BOVIN Alpha-S1-casein OS=Bos taurus OX=9913 GN=CSN1S1 PE=1 SV=2	Yes	Yes	No	No	No
QNIPPLTQTPV	sp|P02666|CASB_BOVIN Beta-casein OS=Bos taurus OX=9913 GN=CSN2 PE=1 SV=2	Yes	Yes	No	No	No

PVVVPPFLQPEV	sp|P02666|CASB_BOVIN Beta-casein OS=Bos taurus OX=9913 GN=CSN2 PE=1 SV=2	Yes	Yes	No	No	No
NIPPLTQTPVVVPPFLQPE	sp|P02666|CASB_BOVIN Beta-casein OS=Bos taurus OX=9913 GN=CSN2 PE=1 SV=2	Yes	Yes	No	No	No
NQDKTEIPT	sp|P02668|CASK_BOVIN Kappa-casein OS=Bos taurus OX=9913 GN=CSN3 PE=1 SV=1	Yes	Yes	No	No	No
VYP	sp|P02666|CASB_BOVIN Beta-casein OS=Bos taurus OX=9913 GN=CSN2 PE=1 SV=2	Yes	Yes	No	No	No
QLEIVPN	sp|P02662|CASA1_BOVIN Alpha-S1-casein OS=Bos taurus OX=9913 GN=CSN1S1 PE=1 SV=2	Yes	Yes	No	No	No
YQEPVLGPV	sp|P02666|CASB_BOVIN Beta-casein OS=Bos taurus OX=9913 GN=CSN2 PE=1 SV=2	Yes	Yes	No	No	No
DDDLTDDIM	sp|P00711|LALBA_BOVIN Alpha-lactalbumin OS=Bos taurus OX=9913 GN=LALBA PE=1 SV=2	Yes	Yes	No	No	No
FVAPFPEVFG	sp|P02662|CASA1_BOVIN Alpha-S1-casein OS=Bos taurus OX=9913 GN=CSN1S1 PE=1 SV=2	Yes	Yes	No	No	No
QPLPPTVMFPPQS	sp|P02666|CASB_BOVIN Beta-casein OS=Bos taurus OX=9913 GN=CSN2 PE=1 SV=2	Yes	Yes	No	No	No
QYTDAPSFSDIPNPI	sp|P02662|CASA1_BOVIN Alpha-S1-casein OS=Bos taurus OX=9913 GN=CSN1S1 PE=1 SV=2	Yes	Yes	No	No	No
LVYPFPGPIPN	sp|P02666|CASB_BOVIN Beta-casein OS=Bos taurus OX=9913 GN=CSN2 PE=1 SV=2	Yes	Yes	No	No	No
LDDDLTDDIM	sp|P00711|LALBA_BOVIN Alpha-lactalbumin OS=Bos taurus OX=9913 GN=LALBA PE=1 SV=2	Yes	Yes	No	No	No
VVPPFLQPEV	sp|P02666|CASB_BOVIN Beta-casein OS=Bos taurus OX=9913 GN=CSN2 PE=1 SV=2	Yes	Yes	No	No	No
NLHLPLP	sp|P02666|CASB_BOVIN Beta-casein OS=Bos taurus OX=9913 GN=CSN2 PE=1 SV=2	Yes	Yes	No	No	No
QEPVLGPV	sp|P02666|CASB_BOVIN Beta-casein OS=Bos taurus OX=9913 GN=CSN2 PE=1 SV=2	Yes	Yes	No	No	No
NIPPLTQT	sp|P02666|CASB_BOVIN Beta-casein OS=Bos taurus OX=9913 GN=CSN2 PE=1 SV=2	Yes	Yes	No	No	No
TPVVVPPFLQPE	sp|P02666|CASB_BOVIN Beta-casein OS=Bos taurus OX=9913 GN=CSN2 PE=1 SV=2	Yes	Yes	No	No	No
YKVPQ	sp|P02662|CASA1_BOVIN Alpha-S1-casein OS=Bos taurus OX=9913 GN=CSN1S1 PE=1 SV=2	Yes	Yes	No	No	No
HQPHQPLPPT	sp|P02666|CASB_BOVIN Beta-casein OS=Bos taurus OX=9913 GN=CSN2 PE=1 SV=2	Yes	Yes	No	No	No

VEELKPT	sp|P02754|LACB_BOVIN Beta-lactoglobulin OS=Bos taurus OX=9913 GN=LGB PE=1 SV=3	Yes	Yes	No	No	No
YPFPGPIPN	sp|P02666|CASB_BOVIN Beta-casein OS=Bos taurus OX=9913 GN=CSN2 PE=1 SV=2	Yes	Yes	No	No	No
TDAPSFSDIPNPI	sp|P02662|CASA1_BOVIN Alpha-S1-casein OS=Bos taurus OX=9913 GN=CSN1S1 PE=1 SV=2	Yes	Yes	No	No	No
VRTPEVDDE	sp|P02754|LACB_BOVIN Beta-lactoglobulin OS=Bos taurus OX=9913 GN=LGB PE=1 SV=3	Yes	Yes	No	No	No
VYVEELKPTPE	sp|P02754|LACB_BOVIN Beta-lactoglobulin OS=Bos taurus OX=9913 GN=LGB PE=1 SV=3	Yes	Yes	No	No	No
DKTEIPT	sp|P02668|CASK_BOVIN Kappa-casein OS=Bos taurus OX=9913 GN=CSN3 PE=1 SV=1	Yes	Yes	No	No	No
ILNKPEDETHLEAQPT	sp|P80195|GLCM1_BOVIN Glycosylation-dependent cell adhesion molecule 1 OS=Bos taurus OX=9913 GN=GLYCAM1 PE=1 SV=2	Yes	Yes	No	No	No
VYVEELKPT	sp|P02754|LACB_BOVIN Beta-lactoglobulin OS=Bos taurus OX=9913 GN=LGB PE=1 SV=3	Yes	Yes	No	No	No
VLDT	sp|P02754|LACB_BOVIN Beta-lactoglobulin OS=Bos taurus OX=9913 GN=LGB PE=1 SV=3	Yes	Yes	No	No	No
APFPEV	sp|P02662|CASA1_BOVIN Alpha-S1-casein OS=Bos taurus OX=9913 GN=CSN1S1 PE=1 SV=2	Yes	Yes	No	No	No
IQKEDVPSE	sp|P02662|CASA1_BOVIN Alpha-S1-casein OS=Bos taurus OX=9913 GN=CSN1S1 PE=1 SV=2	Yes	Yes	No	No	No
NAVPITPT	sp|P02663|CASA2_BOVIN Alpha-S2-casein OS=Bos taurus OX=9913 GN=CSN1S2 PE=1 SV=2	Yes	Yes	No	No	No
SLPQNIPPLTQTPVVVPPFLQPE	sp|P02666|CASB_BOVIN Beta-casein OS=Bos taurus OX=9913 GN=CSN2 PE=1 SV=2	Yes	Yes	No	No	No
PVPQ	sp|P02666|CASB_BOVIN Beta-casein OS=Bos taurus OX=9913 GN=CSN2 PE=1 SV=2	Yes	Yes	No	No	No
SLPQNIPPLTQTPV	sp|P02666|CASB_BOVIN Beta-casein OS=Bos taurus OX=9913 GN=CSN2 PE=1 SV=2	Yes	Yes	No	No	No
AQSAPL	sp|P02754|LACB_BOVIN Beta-lactoglobulin OS=Bos taurus OX=9913 GN=LGB PE=1 SV=3	Yes	Yes	No	No	No
GVSLPE	sp|P00711|LALBA_BOVIN Alpha-lactalbumin OS=Bos taurus OX=9913 GN=LALBA PE=1 SV=2	Yes	Yes	No	No	No
LPPTVMFPPQ	sp|P02666|CASB_BOVIN Beta-casein OS=Bos taurus OX=9913 GN=CSN2 PE=1 SV=2	Yes	Yes	No	No	No
HLEAQPT	sp|P80195|GLCM1_BOVIN Glycosylation-dependent cell adhesion molecule 1 OS=Bos taurus OX=9913 GN=GLYCAM1 PE=1 SV=2	Yes	Yes	No	No	No

TKIPA	sp|P02754|LACB_BOVIN Beta-lactoglobulin OS=Bos taurus OX=9913 GN=LGB PE=1 SV=3	Yes	Yes	No	No	No
FSDIPNPI	sp|P02662|CASA1_BOVIN Alpha-S1-casein OS=Bos taurus OX=9913 GN=CSN1S1 PE=1 SV=2	Yes	Yes	No	No	No
LEIVPN	sp|P02662|CASA1_BOVIN Alpha-S1-casein OS=Bos taurus OX=9913 GN=CSN1S1 PE=1 SV=2	Yes	Yes	No	No	No
SLPQNIPPLTQT	sp|P02666|CASB_BOVIN Beta-casein OS=Bos taurus OX=9913 GN=CSN2 PE=1 SV=2	Yes	Yes	No	No	No
YVEELKPTPEGDLE	sp|P02754|LACB_BOVIN Beta-lactoglobulin OS=Bos taurus OX=9913 GN=LGB PE=1 SV=3	Yes	Yes	No	No	No
ALPM	sp|P02754|LACB_BOVIN Beta-lactoglobulin OS=Bos taurus OX=9913 GN=LGB PE=1 SV=3	Yes	Yes	No	No	No
FLDDDLTDD	sp|P00711|LALBA_BOVIN Alpha-lactalbumin OS=Bos taurus OX=9913 GN=LALBA PE=1 SV=2	Yes	Yes	No	No	No
ESPPEINT	sp|P02668|CASK_BOVIN Kappa-casein OS=Bos taurus OX=9913 GN=CSN3 PE=1 SV=1	Yes	Yes	No	No	No
IDLQVLEPE	sp|P81265|PIGR_BOVIN Polymeric immunoglobulin receptor OS=Bos taurus OX=9913 GN=PIGR PE=2 SV=1	Yes	Yes	No	No	No
LHLPLP	sp|P02666|CASB_BOVIN Beta-casein OS=Bos taurus OX=9913 GN=CSN2 PE=1 SV=2	Yes	Yes	No	No	No
PVLGPV	sp|P02666|CASB_BOVIN Beta-casein OS=Bos taurus OX=9913 GN=CSN2 PE=1 SV=2	Yes	Yes	No	No	No
VVVPPFLQPEV	sp|P02666|CASB_BOVIN Beta-casein OS=Bos taurus OX=9913 GN=CSN2 PE=1 SV=2	Yes	Yes	No	No	No
HLPLPL	sp|P02666|CASB_BOVIN Beta-casein OS=Bos taurus OX=9913 GN=CSN2 PE=1 SV=2	Yes	Yes	No	No	No
LPM	sp|P02754|LACB_BOVIN Beta-lactoglobulin OS=Bos taurus OX=9913 GN=LGB PE=1 SV=3	Yes	Yes	No	No	No
VEELKPTP	sp|P02754|LACB_BOVIN Beta-lactoglobulin OS=Bos taurus OX=9913 GN=LGB PE=1 SV=3	Yes	Yes	No	No	No
PLPPT	sp|P02666|CASB_BOVIN Beta-casein OS=Bos taurus OX=9913 GN=CSN2 PE=1 SV=2	Yes	Yes	No	No	No
PVVVPP	sp|P02666|CASB_BOVIN Beta-casein OS=Bos taurus OX=9913 GN=CSN2 PE=1 SV=2	Yes	Yes	No	No	No
VLPVP	sp|P02666|CASB_BOVIN Beta-casein OS=Bos taurus OX=9913 GN=CSN2 PE=1 SV=2	Yes	Yes	No	No	No
MAASDI	sp|P02754|LACB_BOVIN Beta-lactoglobulin OS=Bos taurus OX=9913 GN=LGB PE=1 SV=3	Yes	Yes	No	No	No

LPM	sp|P02754|LACB_BOVIN Beta-lactoglobulin OS=Bos taurus OX=9913 GN=LGB PE=1 SV=3	Yes	Yes	No	No	apical/basolateral

Appendix Table 2 Summary matrix reporting the unique peptides in each compartment (digesta, apical, basolateral), their overlaps, and unique distributions across infant- and adult-like models for Soya IF.

Sequence	FASTA Header	Apical	Basolateral	Digesta	Exclusive Infant	Exclusive Adult
LPTEV	sp|P09439|LOX2_SOYBN Seed linoleate 9S-lipoxygenase-2 OS=Glycine max OX=3847 GN=LOX1.2 PE=2 SV=1	No	No	Yes	No	No
AIGINAENNQRNFLA	sp|P0DO16|GLCA1_SOYBN Beta-conglycinin alpha subunit 1 OS=Glycine max OX=3847 GN=CG-3 PE=1 SV=1;sp|P0DO15|GLCA2_SOYBN Beta-conglycinin alpha subunit 2 OS=Glycine max OX=3847 GN=CG-2 PE=1 SV=1	No	No	Yes	No	No
AGSQDNVIS	sp|P0DO16|GLCA1_SOYBN Beta-conglycinin alpha subunit 1 OS=Glycine max OX=3847 GN=CG-3 PE=1 SV=1;sp|P0DO15|GLCA2_SOYBN Beta-conglycinin alpha subunit 2 OS=Glycine max OX=3847 GN=CG-2 PE=1 SV=1	No	No	Yes	No	No
PIPFPRPQP	sp|P0DO16|GLCA1_SOYBN Beta-conglycinin alpha subunit 1 OS=Glycine max OX=3847 GN=CG-3 PE=1 SV=1;sp|P0DO15|GLCA2_SOYBN Beta-conglycinin alpha subunit 2 OS=Glycine max OX=3847 GN=CG-2 PE=1 SV=1	No	No	Yes	No	No
YQQEQGGHQ	sp|P04776|GLYG1_SOYBN Glycinin G1 OS=Glycine max OX=3847 GN=GY1 PE=1 SV=2	No	No	Yes	No	No
EPQQPGEKEEDEDEQPRPIPFPRP	sp|P0DO16|GLCA1_SOYBN Beta-conglycinin alpha subunit 1 OS=Glycine max OX=3847 GN=CG-3 PE=1 SV=1;sp|P0DO15|GLCA2_SOYBN Beta-conglycinin alpha subunit 2 OS=Glycine max OX=3847 GN=CG-2 PE=1 SV=1	No	No	Yes	No	No
LFEITPEK	sp|P11827|GLCAP_SOYBN Beta-conglycinin alpha subunit OS=Glycine max OX=3847 GN=CG-1 PE=1 SV=2	No	No	Yes	No	No
YIVNRDEND	sp|Q04672|SBP_SOYBN Sucrose-binding protein OS=Glycine max OX=3847 GN=SBP PE=1 SV=1	No	No	Yes	No	No
FPRPPH	sp|P0DO16|GLCA1_SOYBN Beta-conglycinin alpha subunit 1 OS=Glycine max OX=3847 GN=CG-3 PE=1 SV=1;sp|P0DO15|GLCA2_SOYBN Beta-conglycinin alpha subunit 2 OS=Glycine max OX=3847 GN=CG-2 PE=1 SV=1	No	No	Yes	No	No
DMNEGALLLPHFNS	sp|P0DO16|GLCA1_SOYBN Beta-conglycinin alpha subunit 1 OS=Glycine max OX=3847 GN=CG-3 PE=1 SV=1;sp|P0DO15|GLCA2_SOYBN Beta-conglycinin alpha subunit 2 OS=Glycine max OX=3847 GN=CG-2 PE=1 SV=1	No	No	Yes	No	No
EPQQPGEKEEDEDEQPRPIP	sp|P0DO16|GLCA1_SOYBN Beta-conglycinin alpha subunit 1 OS=Glycine max OX=3847 GN=CG-3 PE=1	No	No	Yes	No	No

	SV=1;sp|P0DO15|GLCA2_SOYBN Beta-conglycinin alpha subunit 2 OS=Glycine max OX=3847 GN=CG-2 PE=1 SV=1					
VINEGDANIE	sp|P0DO16|GLCA1_SOYBN Beta-conglycinin alpha subunit 1 OS=Glycine max OX=3847 GN=CG-3 PE=1 SV=1;sp|P0DO15|GLCA2_SOYBN Beta-conglycinin alpha subunit 2 OS=Glycine max OX=3847 GN=CG-2 PE=1 SV=1	No	No	Yes	No	No
FVDAQPQ	sp|P11827|GLCAP_SOYBN Beta-conglycinin alpha subunit OS=Glycine max OX=3847 GN=CG-1 PE=1 SV=2	No	No	Yes	No	No
FPRPQPR	sp|P0DO16|GLCA1_SOYBN Beta-conglycinin alpha subunit 1 OS=Glycine max OX=3847 GN=CG-3 PE=1 SV=1;sp|P0DO15|GLCA2_SOYBN Beta-conglycinin alpha subunit 2 OS=Glycine max OX=3847 GN=CG-2 PE=1 SV=1	No	No	Yes	No	No
EEDEDEQPRPIPFPRPQ	sp|P0DO16|GLCA1_SOYBN Beta-conglycinin alpha subunit 1 OS=Glycine max OX=3847 GN=CG-3 PE=1 SV=1;sp|P0DO15|GLCA2_SOYBN Beta-conglycinin alpha subunit 2 OS=Glycine max OX=3847 GN=CG-2 PE=1 SV=1	No	No	Yes	No	No
EITPEKNPQLRDLDV	sp|P11827|GLCAP_SOYBN Beta-conglycinin alpha subunit OS=Glycine max OX=3847 GN=CG-1 PE=1 SV=2	No	No	Yes	No	No
SIVDMNEGALLLPH	sp|P0DO16|GLCA1_SOYBN Beta-conglycinin alpha subunit 1 OS=Glycine max OX=3847 GN=CG-3 PE=1 SV=1;sp|P0DO15|GLCA2_SOYBN Beta-conglycinin alpha subunit 2 OS=Glycine max OX=3847 GN=CG-2 PE=1 SV=1	No	No	Yes	No	No
RVPSGTT	sp|P0DO16|GLCA1_SOYBN Beta-conglycinin alpha subunit 1 OS=Glycine max OX=3847 GN=CG-3 PE=1 SV=1;sp|P0DO15|GLCA2_SOYBN Beta-conglycinin alpha subunit 2 OS=Glycine max OX=3847 GN=CG-2 PE=1 SV=1	No	No	Yes	No	No
FFEITPEKNPQ	sp|P0DO16|GLCA1_SOYBN Beta-conglycinin alpha subunit 1 OS=Glycine max OX=3847 GN=CG-3 PE=1 SV=1;sp|P0DO15|GLCA2_SOYBN Beta-conglycinin alpha subunit 2 OS=Glycine max OX=3847 GN=CG-2 PE=1 SV=1	No	No	Yes	No	No
LRQNIGQNSSPDI	sp|P04405|GLYG2_SOYBN Glycinin G2 OS=Glycine max OX=3847 GN=GY2 PE=1 SV=2	No	No	Yes	No	No
FFEITPE	sp|P0DO16|GLCA1_SOYBN Beta-conglycinin alpha subunit 1 OS=Glycine max OX=3847 GN=CG-3 PE=1 SV=1;sp|P0DO15|GLCA2_SOYBN Beta-conglycinin alpha subunit 2 OS=Glycine max OX=3847 GN=CG-2 PE=1 SV=1	No	No	Yes	No	No
EDEQPRPIPFPRPQPR	sp|P0DO16|GLCA1_SOYBN Beta-conglycinin alpha subunit 1 OS=Glycine max OX=3847 GN=CG-3 PE=1	No	No	Yes	No	No

	SV=1;sp|P0DO15|GLCA2_SOYBN Beta-conglycinin alpha subunit 2 OS=Glycine max OX=3847 GN=CG-2 PE=1 SV=1					
DMNEGALLLP	sp|P0DO16|GLCA1_SOYBN Beta-conglycinin alpha subunit 1 OS=Glycine max OX=3847 GN=CG-3 PE=1 SV=1;sp|P0DO15|GLCA2_SOYBN Beta-conglycinin alpha subunit 2 OS=Glycine max OX=3847 GN=CG-2 PE=1 SV=1	No	No	Yes	No	No
LVTDADNVIPK	sp|P26987|SAM22_SOYBN Stress-induced protein SAM22 OS=Glycine max OX=3847 GN=PR-10 PE=1 SV=1	No	No	Yes	No	No
DEDEQPRPIPFPRPQP	sp|P0DO16|GLCA1_SOYBN Beta-conglycinin alpha subunit 1 OS=Glycine max OX=3847 GN=CG-3 PE=1 SV=1;sp|P0DO15|GLCA2_SOYBN Beta-conglycinin alpha subunit 2 OS=Glycine max OX=3847 GN=CG-2 PE=1 SV=1	No	No	Yes	No	No
RLQSGDA	sp|P0DO16|GLCA1_SOYBN Beta-conglycinin alpha subunit 1 OS=Glycine max OX=3847 GN=CG-3 PE=1 SV=1;sp|P0DO15|GLCA2_SOYBN Beta-conglycinin alpha subunit 2 OS=Glycine max OX=3847 GN=CG-2 PE=1 SV=1	No	No	Yes	No	No
NEGALLLPH	sp|P0DO16|GLCA1_SOYBN Beta-conglycinin alpha subunit 1 OS=Glycine max OX=3847 GN=CG-3 PE=1 SV=1;sp|P0DO15|GLCA2_SOYBN Beta-conglycinin alpha subunit 2 OS=Glycine max OX=3847 GN=CG-2 PE=1 SV=1	No	No	Yes	No	No
FMPE	sp|P09186|LOX3_SOYBN Seed linoleate 9S-lipoxygenase-3 OS=Glycine max OX=3847 GN=LOX1.3 PE=1 SV=1	No	No	Yes	No	No
PIPFPRPQPR	sp|P0DO16|GLCA1_SOYBN Beta-conglycinin alpha subunit 1 OS=Glycine max OX=3847 GN=CG-3 PE=1 SV=1;sp|P0DO15|GLCA2_SOYBN Beta-conglycinin alpha subunit 2 OS=Glycine max OX=3847 GN=CG-2 PE=1 SV=1	No	No	Yes	No	No
RLVIEDYP	sp|P09186|LOX3_SOYBN Seed linoleate 9S-lipoxygenase-3 OS=Glycine max OX=3847 GN=LOX1.3 PE=1 SV=1	No	No	Yes	No	No
DAQPK	sp|P0DO16|GLCA1_SOYBN Beta-conglycinin alpha subunit 1 OS=Glycine max OX=3847 GN=CG-3 PE=1 SV=1;sp|P0DO15|GLCA2_SOYBN Beta-conglycinin alpha subunit 2 OS=Glycine max OX=3847 GN=CG-2 PE=1 SV=1	No	No	Yes	No	No
EPQQPGEKEEDEDEQPRPIPFPRPQ	sp|P0DO16|GLCA1_SOYBN Beta-conglycinin alpha subunit 1 OS=Glycine max OX=3847 GN=CG-3 PE=1 SV=1;sp|P0DO15|GLCA2_SOYBN Beta-conglycinin alpha subunit 2 OS=Glycine max OX=3847 GN=CG-2 PE=1 SV=1	No	No	Yes	No	No
FAFG	sp|P11827|GLCAP_SOYBN Beta-conglycinin alpha subunit OS=Glycine max OX=3847 GN=CG-1 PE=1 SV=2	No	No	Yes	No	No

EQQQEEQPL	sp|P0DO16|GLCA1_SOYBN Beta-conglycinin alpha subunit 1 OS=Glycine max OX=3847 GN=CG-3 PE=1 SV=1;sp|P0DO15|GLCA2_SOYBN Beta-conglycinin alpha subunit 2 OS=Glycine max OX=3847 GN=CG-2 PE=1 SV=1	No	No	Yes	No	No
PFPRPP	sp|P0DO16|GLCA1_SOYBN Beta-conglycinin alpha subunit 1 OS=Glycine max OX=3847 GN=CG-3 PE=1 SV=1;sp|P0DO15|GLCA2_SOYBN Beta-conglycinin alpha subunit 2 OS=Glycine max OX=3847 GN=CG-2 PE=1 SV=1	No	No	Yes	No	No
EEDEDEQPRPIPFPRPQP	sp|P0DO16|GLCA1_SOYBN Beta-conglycinin alpha subunit 1 OS=Glycine max OX=3847 GN=CG-3 PE=1 SV=1;sp|P0DO15|GLCA2_SOYBN Beta-conglycinin alpha subunit 2 OS=Glycine max OX=3847 GN=CG-2 PE=1 SV=1	No	No	Yes	No	No
EDEQPRPIPFPRPQP	sp|P0DO16|GLCA1_SOYBN Beta-conglycinin alpha subunit 1 OS=Glycine max OX=3847 GN=CG-3 PE=1 SV=1;sp|P0DO15|GLCA2_SOYBN Beta-conglycinin alpha subunit 2 OS=Glycine max OX=3847 GN=CG-2 PE=1 SV=1	No	No	Yes	No	No
VINEGDANIEL	sp|P0DO16|GLCA1_SOYBN Beta-conglycinin alpha subunit 1 OS=Glycine max OX=3847 GN=CG-3 PE=1 SV=1;sp|P0DO15|GLCA2_SOYBN Beta-conglycinin alpha subunit 2 OS=Glycine max OX=3847 GN=CG-2 PE=1 SV=1	No	No	Yes	No	No
DEDEQPRPIPFPRPQPR	sp|P0DO16|GLCA1_SOYBN Beta-conglycinin alpha subunit 1 OS=Glycine max OX=3847 GN=CG-3 PE=1 SV=1;sp|P0DO15|GLCA2_SOYBN Beta-conglycinin alpha subunit 2 OS=Glycine max OX=3847 GN=CG-2 PE=1 SV=1	No	No	Yes	No	No
AIGINAENNQRN	sp|P0DO16|GLCA1_SOYBN Beta-conglycinin alpha subunit 1 OS=Glycine max OX=3847 GN=CG-3 PE=1 SV=1;sp|P0DO15|GLCA2_SOYBN Beta-conglycinin alpha subunit 2 OS=Glycine max OX=3847 GN=CG-2 PE=1 SV=1	No	No	Yes	No	No
LVINEGDANIEL	sp|P0DO16|GLCA1_SOYBN Beta-conglycinin alpha subunit 1 OS=Glycine max OX=3847 GN=CG-3 PE=1 SV=1;sp|P0DO15|GLCA2_SOYBN Beta-conglycinin alpha subunit 2 OS=Glycine max OX=3847 GN=CG-2 PE=1 SV=1	No	No	Yes	No	No
DEDEQPRPIPFPRPQ	sp|P0DO16|GLCA1_SOYBN Beta-conglycinin alpha subunit 1 OS=Glycine max OX=3847 GN=CG-3 PE=1 SV=1;sp|P0DO15|GLCA2_SOYBN Beta-conglycinin alpha subunit 2 OS=Glycine max OX=3847 GN=CG-2 PE=1 SV=1	No	No	Yes	No	No
EPQQPGEKEEDEDEQPRPIPFPR	sp|P0DO16|GLCA1_SOYBN Beta-conglycinin alpha subunit 1 OS=Glycine max OX=3847 GN=CG-3 PE=1	No	No	Yes	No	No

	SV=1;sp|P0DO15|GLCA2_SOYBN Beta-conglycinin alpha subunit 2 OS=Glycine max OX=3847 GN=CG-2 PE=1 SV=1					
LPNHADAD	sp|P0DO16|GLCA1_SOYBN Beta-conglycinin alpha subunit 1 OS=Glycine max OX=3847 GN=CG-3 PE=1 SV=1;sp|P0DO15|GLCA2_SOYBN Beta-conglycinin alpha subunit 2 OS=Glycine max OX=3847 GN=CG-2 PE=1 SV=1	No	No	Yes	No	No
YFVDAQPQ	sp|P11827|GLCAP_SOYBN Beta-conglycinin alpha subunit OS=Glycine max OX=3847 GN=CG-1 PE=1 SV=2	No	No	Yes	No	No
FFEITPEK	sp|P0DO16|GLCA1_SOYBN Beta-conglycinin alpha subunit 1 OS=Glycine max OX=3847 GN=CG-3 PE=1 SV=1;sp|P0DO15|GLCA2_SOYBN Beta-conglycinin alpha subunit 2 OS=Glycine max OX=3847 GN=CG-2 PE=1 SV=1	No	No	Yes	No	No
KTNDTPMIG	sp|P04776|GLYG1_SOYBN Glycinin G1 OS=Glycine max OX=3847 GN=GY1 PE=1 SV=2	No	No	Yes	No	No
RQNIGQNSSPDI	sp|P04405|GLYG2_SOYBN Glycinin G2 OS=Glycine max OX=3847 GN=GY2 PE=1 SV=2	No	No	Yes	No	No
PFPRPQPR	sp|P0DO16|GLCA1_SOYBN Beta-conglycinin alpha subunit 1 OS=Glycine max OX=3847 GN=CG-3 PE=1 SV=1;sp|P0DO15|GLCA2_SOYBN Beta-conglycinin alpha subunit 2 OS=Glycine max OX=3847 GN=CG-2 PE=1 SV=1	No	No	Yes	No	No
SPYPR	sp|P02858|GLYG4_SOYBN Glycinin G4 OS=Glycine max OX=3847 GN=GY4 PE=1 SV=2	No	No	Yes	No	No
EEDEDEQPRPIPFPRPQPR	sp|P0DO16|GLCA1_SOYBN Beta-conglycinin alpha subunit 1 OS=Glycine max OX=3847 GN=CG-3 PE=1 SV=1;sp|P0DO15|GLCA2_SOYBN Beta-conglycinin alpha subunit 2 OS=Glycine max OX=3847 GN=CG-2 PE=1 SV=1	No	No	Yes	No	No
TLVNNDDRDS	sp|P11827|GLCAP_SOYBN Beta-conglycinin alpha subunit OS=Glycine max OX=3847 GN=CG-1 PE=1 SV=2	No	No	Yes	No	No
KQEEDEDEEQ	sp|P0DO16|GLCA1_SOYBN Beta-conglycinin alpha subunit 1 OS=Glycine max OX=3847 GN=CG-3 PE=1 SV=1;sp|P0DO15|GLCA2_SOYBN Beta-conglycinin alpha subunit 2 OS=Glycine max OX=3847 GN=CG-2 PE=1 SV=1	No	No	Yes	No	No
HLPSYSPYPR	sp|P02858|GLYG4_SOYBN Glycinin G4 OS=Glycine max OX=3847 GN=GY4 PE=1 SV=2	Yes	No	No	No	apical
YIQQGNGIFG	sp|P04405|GLYG2_SOYBN Glycinin G2 OS=Glycine max OX=3847 GN=GY2 PE=1 SV=2	Yes	No	No	No	apical
LRQNIGQN	sp|P04405|GLYG2_SOYBN Glycinin G2 OS=Glycine max OX=3847 GN=GY2 PE=1 SV=2	Yes	No	No	No	apical

SGGIKLPT	sp|P09186|LOX3_SOYBN Seed linoleate 9S-lipoxygenase-3 OS=Glycine max OX=3847 GN=LOX1.3 PE=1 SV=1	Yes	No	No	No	apical
ISTIIP	sp|P08170|LOX1_SOYBN Seed linoleate 13S-lipoxygenase-1 OS=Glycine max OX=3847 GN=LOX1.1 PE=1 SV=2	Yes	No	No	No	apical
SEGGLIQT	sp|P02858|GLYG4_SOYBN Glycinin G4 OS=Glycine max OX=3847 GN=GY4 PE=1 SV=2	Yes	No	No	No	apical
PFPRPRQP	sp|P11827|GLCAP_SOYBN Beta-conglycinin alpha subunit OS=Glycine max OX=3847 GN=CG-1 PE=1 SV=2	Yes	No	No	No	apical
NWGPL	sp|P02858|GLYG4_SOYBN Glycinin G4 OS=Glycine max OX=3847 GN=GY4 PE=1 SV=2	Yes	No	No	No	apical
QVFLP	sp|P09186|LOX3_SOYBN Seed linoleate 9S-lipoxygenase-3 OS=Glycine max OX=3847 GN=LOX1.3 PE=1 SV=1	Yes	No	No	No	apical
NELDKGIGT	sp|P01070|ITRA_SOYBN Trypsin inhibitor A OS=Glycine max OX=3847 GN=KTI3 PE=1 SV=2	Yes	No	No	No	apical
RSNDVYLP	sp|P09186|LOX3_SOYBN Seed linoleate 9S-lipoxygenase-3 OS=Glycine max OX=3847 GN=LOX1.3 PE=1 SV=1	Yes	No	No	No	apical
EDEQIPSHPP	sp|P02858|GLYG4_SOYBN Glycinin G4 OS=Glycine max OX=3847 GN=GY4 PE=1 SV=2	Yes	No	No	No	apical
KNDGTLRPL	sp|P09186|LOX3_SOYBN Seed linoleate 9S-lipoxygenase-3 OS=Glycine max OX=3847 GN=LOX1.3 PE=1 SV=1	Yes	No	No	No	apical
LSLPHPAG	sp|P09439|LOX2_SOYBN Seed linoleate 9S-lipoxygenase-2 OS=Glycine max OX=3847 GN=LOX1.2 PE=2 SV=1	Yes	No	No	No	apical
KFLVPPQE	sp|P04776|GLYG1_SOYBN Glycinin G1 OS=Glycine max OX=3847 GN=GY1 PE=1 SV=2	Yes	No	No	No	apical
LQSPDDER	sp|P02858|GLYG4_SOYBN Glycinin G4 OS=Glycine max OX=3847 GN=GY4 PE=1 SV=2	Yes	No	No	apical	No
SFLVPPQE	sp|P04405|GLYG2_SOYBN Glycinin G2 OS=Glycine max OX=3847 GN=GY2 PE=1 SV=2	Yes	No	No	apical	No
EDDDDEEEQPQ	sp|P04405|GLYG2_SOYBN Glycinin G2 OS=Glycine max OX=3847 GN=GY2 PE=1 SV=2	Yes	No	No	apical	No
FPRPR	sp|P11827|GLCAP_SOYBN Beta-conglycinin alpha subunit OS=Glycine max OX=3847 GN=CG-1 PE=1 SV=2	Yes	No	No	apical	No
NDLGDPDKGENH	sp|P09186|LOX3_SOYBN Seed linoleate 9S-lipoxygenase-3 OS=Glycine max OX=3847 GN=LOX1.3 PE=1 SV=1	Yes	No	No	apical	No
VPPGHP	sp|Q04672|SBP_SOYBN Sucrose-binding protein OS=Glycine max OX=3847 GN=SBP PE=1 SV=1	Yes	No	No	apical	No
IESEGGLIE	sp|P04776|GLYG1_SOYBN Glycinin G1 OS=Glycine max OX=3847 GN=GY1 PE=1 SV=2	Yes	No	No	apical	No

ISSDLKPGM	sp|Q04672|SBP_SOYBN Sucrose-binding protein OS=Glycine max OX=3847 GN=SBP PE=1 SV=1	Yes	No	No	apical	No
DVLVIPLGV	sp|P04347|GLYG5_SOYBN Glycinin G5 OS=Glycine max OX=3847 GN=GY5 PE=1 SV=1	Yes	No	No	apical	No
HQQEEEEEGGSV	sp|P02858|GLYG4_SOYBN Glycinin G4 OS=Glycine max OX=3847 GN=GY4 PE=1 SV=2	Yes	No	No	apical	No
TLLHPN	sp|P09439|LOX2_SOYBN Seed linoleate 9S-lipoxygenase-2 OS=Glycine max OX=3847 GN=LOX1.2 PE=2 SV=1	Yes	No	No	apical	No
AIKDPSAPH	sp|P09439|LOX2_SOYBN Seed linoleate 9S-lipoxygenase-2 OS=Glycine max OX=3847 GN=LOX1.2 PE=2 SV=1	Yes	No	No	apical	No
EQDEDEDEDEDKPRPS	sp|P02858|GLYG4_SOYBN Glycinin G4 OS=Glycine max OX=3847 GN=GY4 PE=1 SV=2	Yes	No	No	apical	No
EEEEEEEDEKPQ	sp|P04776|GLYG1_SOYBN Glycinin G1 OS=Glycine max OX=3847 GN=GY1 PE=1 SV=2	Yes	No	No	apical	No
DLGNPDHGEN	sp|P09439|LOX2_SOYBN Seed linoleate 9S-lipoxygenase-2 OS=Glycine max OX=3847 GN=LOX1.2 PE=2 SV=1	Yes	No	No	apical	No
EDIPNHGS	sp|P09186|LOX3_SOYBN Seed linoleate 9S-lipoxygenase-3 OS=Glycine max OX=3847 GN=LOX1.3 PE=1 SV=1	Yes	No	No	apical	No
GSSTHPYP	sp|P09439|LOX2_SOYBN Seed linoleate 9S-lipoxygenase-2 OS=Glycine max OX=3847 GN=LOX1.2 PE=2 SV=1	Yes	No	No	apical	No
QEEEEEGGSV	sp|P02858|GLYG4_SOYBN Glycinin G4 OS=Glycine max OX=3847 GN=GY4 PE=1 SV=2	Yes	No	No	apical	No
IQQGNGIFG	sp|P04405|GLYG2_SOYBN Glycinin G2 OS=Glycine max OX=3847 GN=GY2 PE=1 SV=2	Yes	No	No	apical	No
TEVGPDDDEK	sp|Q04672|SBP_SOYBN Sucrose-binding protein OS=Glycine max OX=3847 GN=SBP PE=1 SV=1	Yes	No	No	apical	No
TYLPSETPAPL	sp|P09186|LOX3_SOYBN Seed linoleate 9S-lipoxygenase-3 OS=Glycine max OX=3847 GN=LOX1.3 PE=1 SV=1	Yes	No	No	apical	No
QTSSPDIYNPQ	sp|P04776|GLYG1_SOYBN Glycinin G1 OS=Glycine max OX=3847 GN=GY1 PE=1 SV=2	Yes	No	No	apical	No
KPQQEEDDDDEEEQPQ	sp|P04405|GLYG2_SOYBN Glycinin G2 OS=Glycine max OX=3847 GN=GY2 PE=1 SV=2	Yes	No	No	apical	No
EGGIKLPR	sp|P08170|LOX1_SOYBN Seed linoleate 13S-lipoxygenase-1 OS=Glycine max OX=3847 GN=LOX1.1 PE=1 SV=2	Yes	No	No	No	No
GLQEFPPK	sp|P09439|LOX2_SOYBN Seed linoleate 9S-lipoxygenase-2 OS=Glycine max OX=3847 GN=LOX1.2 PE=2 SV=1	Yes	No	No	No	No
YLAGNPDIEHPE	sp|P04347|GLYG5_SOYBN Glycinin G5 OS=Glycine max OX=3847 GN=GY5 PE=1 SV=1	Yes	No	No	No	No

STPGKFEE	sp|Q04672|SBP_SOYBN Sucrose-binding protein OS=Glycine max OX=3847 GN=SBP PE=1 SV=1	Yes	No	No	No	No
NGLHLPSYSPYPR	sp|P02858|GLYG4_SOYBN Glycinin G4 OS=Glycine max OX=3847 GN=GY4 PE=1 SV=2	Yes	No	No	No	No
YLPSETPAPL	sp|P09186|LOX3_SOYBN Seed linoleate 9S-lipoxygenase-3 OS=Glycine max OX=3847 GN=LOX1.3 PE=1 SV=1	Yes	No	No	No	No
DEDEDEDEDDEDEQIPSHPPR	sp|P02858|GLYG4_SOYBN Glycinin G4 OS=Glycine max OX=3847 GN=GY4 PE=1 SV=2	Yes	No	No	No	No
STIMPL	sp|P09439|LOX2_SOYBN Seed linoleate 9S-lipoxygenase-2 OS=Glycine max OX=3847 GN=LOX1.2 PE=2 SV=1	Yes	No	No	No	No
DLNFTPNE	sp|P09439|LOX2_SOYBN Seed linoleate 9S-lipoxygenase-2 OS=Glycine max OX=3847 GN=LOX1.2 PE=2 SV=1	Yes	No	No	No	No
EHPRPHQPH	sp|P11827|GLCAP_SOYBN Beta-conglycinin alpha subunit OS=Glycine max OX=3847 GN=CG-1 PE=1 SV=2	Yes	No	No	No	No
IESEGGLIETWNPN	sp|P04776|GLYG1_SOYBN Glycinin G1 OS=Glycine max OX=3847 GN=GY1 PE=1 SV=2	Yes	No	No	No	No
AFDLNFTPR	sp|P09186|LOX3_SOYBN Seed linoleate 9S-lipoxygenase-3 OS=Glycine max OX=3847 GN=LOX1.3 PE=1 SV=1	Yes	No	No	No	No
QQHGEKEEDEGEQPRP	sp|P11827|GLCAP_SOYBN Beta-conglycinin alpha subunit OS=Glycine max OX=3847 GN=CG-1 PE=1 SV=2	Yes	No	No	No	No
RQNIGQNSSPDIYNPQ	sp|P04405|GLYG2_SOYBN Glycinin G2 OS=Glycine max OX=3847 GN=GY2 PE=1 SV=2	Yes	No	No	No	No
EEDEGEQPRP	sp|P11827|GLCAP_SOYBN Beta-conglycinin alpha subunit OS=Glycine max OX=3847 GN=CG-1 PE=1 SV=2	Yes	No	No	No	No
SLPHPQ	sp|P09186|LOX3_SOYBN Seed linoleate 9S-lipoxygenase-3 OS=Glycine max OX=3847 GN=LOX1.3 PE=1 SV=1	Yes	No	No	No	No
IAEGHP	sp|P01070|ITRA_SOYBN Trypsin inhibitor A OS=Glycine max OX=3847 GN=KTI3 PE=1 SV=2	Yes	No	No	No	No
EQDQDQDEDEDEDEDQPR	sp|P02858|GLYG4_SOYBN Glycinin G4 OS=Glycine max OX=3847 GN=GY4 PE=1 SV=2	Yes	No	No	No	No
QDEDEDEDEDDEDEQIPSHPP	sp|P02858|GLYG4_SOYBN Glycinin G4 OS=Glycine max OX=3847 GN=GY4 PE=1 SV=2	Yes	No	No	No	No
IIPLPV	sp|P08170|LOX1_SOYBN Seed linoleate 13S-lipoxygenase-1 OS=Glycine max OX=3847 GN=LOX1.1 PE=1 SV=2	Yes	No	No	No	No
HLSVVHP	sp|P09186|LOX3_SOYBN Seed linoleate 9S-lipoxygenase-3 OS=Glycine max OX=3847 GN=LOX1.3 PE=1 SV=1	Yes	No	No	No	No
RHNIGQTSSPDIYNPQ	sp|P04776|GLYG1_SOYBN Glycinin G1 OS=Glycine max OX=3847 GN=GY1 PE=1 SV=2	Yes	No	No	No	No

IFEEDKD	sp|Q04672|SBP_SOYBN Sucrose-binding protein OS=Glycine max OX=3847 GN=SBP PE=1 SV=1	Yes	No	No	No	No
EEEEEGGSV	sp|P02858|GLYG4_SOYBN Glycinin G4 OS=Glycine max OX=3847 GN=GY4 PE=1 SV=2	Yes	No	No	No	No
EEDEGEQPRPFP	sp|P11827|GLCAP_SOYBN Beta-conglycinin alpha subunit OS=Glycine max OX=3847 GN=CG-1 PE=1 SV=2	Yes	No	No	No	No
NIGQNSSPD	sp|P04405|GLYG2_SOYBN Glycinin G2 OS=Glycine max OX=3847 GN=GY2 PE=1 SV=2	Yes	No	No	No	No
HNIGQTSSPDIFNPQ	sp|P11828|GLYG3_SOYBN Glycinin G3 OS=Glycine max OX=3847 GN=GY3 PE=1 SV=1	Yes	No	No	No	No
ALVTDADNVIPK	sp|P26987|SAM22_SOYBN Stress-induced protein SAM22 OS=Glycine max OX=3847 GN=PR-10 PE=1 SV=1	Yes	No	No	No	No
IFEEDKDFE	sp|Q04672|SBP_SOYBN Sucrose-binding protein OS=Glycine max OX=3847 GN=SBP PE=1 SV=1	Yes	No	No	No	No
MLGGL	sp|P09186|LOX3_SOYBN Seed linoleate 9S-lipoxygenase-3 OS=Glycine max OX=3847 GN=LOX1.3 PE=1 SV=1	Yes	No	No	No	No
NDGGVIEQ	sp|P09186|LOX3_SOYBN Seed linoleate 9S-lipoxygenase-3 OS=Glycine max OX=3847 GN=LOX1.3 PE=1 SV=1	Yes	No	No	No	No
NLQGENEGEDKG	sp|P04776|GLYG1_SOYBN Glycinin G1 OS=Glycine max OX=3847 GN=GY1 PE=1 SV=2	Yes	No	No	No	No
ANQTYLPSETPAPL	sp|P09186|LOX3_SOYBN Seed linoleate 9S-lipoxygenase-3 OS=Glycine max OX=3847 GN=LOX1.3 PE=1 SV=1	Yes	No	No	No	No
TLEPGDMIHIPAGTPL	sp|Q04672|SBP_SOYBN Sucrose-binding protein OS=Glycine max OX=3847 GN=SBP PE=1 SV=1	Yes	No	No	No	No
AALQTPK	sp|Q04672|SBP_SOYBN Sucrose-binding protein OS=Glycine max OX=3847 GN=SBP PE=1 SV=1	Yes	No	No	No	No
VLVIPPGVP	sp|P02858|GLYG4_SOYBN Glycinin G4 OS=Glycine max OX=3847 GN=GY4 PE=1 SV=2	Yes	No	No	No	No
IGQTSSPDIYNPQ	sp|P04776|GLYG1_SOYBN Glycinin G1 OS=Glycine max OX=3847 GN=GY1 PE=1 SV=2	Yes	No	No	No	No
DIEYPE	sp|P02858|GLYG4_SOYBN Glycinin G4 OS=Glycine max OX=3847 GN=GY4 PE=1 SV=2	Yes	No	No	No	No
EWSVVEDLPEGPA	sp|P01070|ITRA_SOYBN Trypsin inhibitor A OS=Glycine max OX=3847 GN=KTI3 PE=1 SV=2	Yes	No	No	No	No
DFVLDNEGNPLE	sp|P01070|ITRA_SOYBN Trypsin inhibitor A OS=Glycine max OX=3847 GN=KTI3 PE=1 SV=2	Yes	No	No	No	No
DHTSQIT	sp|P09186|LOX3_SOYBN Seed linoleate 9S-lipoxygenase-3 OS=Glycine max OX=3847 GN=LOX1.3 PE=1 SV=1	Yes	No	No	No	No

KYQGNSGPL	sp|P04347|GLYG5_SOYBN Glycinin G5 OS=Glycine max OX=3847 GN=GY5 PE=1 SV=1	Yes	No	No	No	No
AGKDNIVS	sp|Q04672|SBP_SOYBN Sucrose-binding protein OS=Glycine max OX=3847 GN=SBP PE=1 SV=1	Yes	No	No	No	No
ANQTYLPSETPAP	sp|P09186|LOX3_SOYBN Seed linoleate 9S-lipoxygenase-3 OS=Glycine max OX=3847 GN=LOX1.3 PE=1 SV=1	Yes	No	No	No	No
DEGEQPRPFPFP	sp|P11827|GLCAP_SOYBN Beta-conglycinin alpha subunit OS=Glycine max OX=3847 GN=CG-1 PE=1 SV=2	Yes	No	No	No	No
DLHEGGIKLPT	sp|P09439|LOX2_SOYBN Seed linoleate 9S-lipoxygenase-2 OS=Glycine max OX=3847 GN=LOX1.2 PE=2 SV=1	Yes	No	No	No	No
NQTYLPSETPAPL	sp|P09186|LOX3_SOYBN Seed linoleate 9S-lipoxygenase-3 OS=Glycine max OX=3847 GN=LOX1.3 PE=1 SV=1	Yes	No	No	No	No
GGLSVIKPPTDEQQQRPQ	sp|P04776|GLYG1_SOYBN Glycinin G1 OS=Glycine max OX=3847 GN=GY1 PE=1 SV=2	Yes	No	No	No	No
GLSVIKPPT	sp|P04776|GLYG1_SOYBN Glycinin G1 OS=Glycine max OX=3847 GN=GY1 PE=1 SV=2	Yes	No	No	No	No
FDSFDEVHG	sp|P09186|LOX3_SOYBN Seed linoleate 9S-lipoxygenase-3 OS=Glycine max OX=3847 GN=LOX1.3 PE=1 SV=1	Yes	No	No	No	No
QNIGQNSSPD	sp|P04405|GLYG2_SOYBN Glycinin G2 OS=Glycine max OX=3847 GN=GY2 PE=1 SV=2	Yes	No	No	No	No
LRQNIGQ	sp|P04405|GLYG2_SOYBN Glycinin G2 OS=Glycine max OX=3847 GN=GY2 PE=1 SV=2	Yes	No	No	No	No
DFVLDNEGNP	sp|P01070|ITRA_SOYBN Trypsin inhibitor A OS=Glycine max OX=3847 GN=KTI3 PE=1 SV=2	Yes	No	No	No	No
PHPQ	sp|P09186|LOX3_SOYBN Seed linoleate 9S-lipoxygenase-3 OS=Glycine max OX=3847 GN=LOX1.3 PE=1 SV=1	Yes	No	No	No	No
LTEVGPDDDEK	sp|Q04672|SBP_SOYBN Sucrose-binding protein OS=Glycine max OX=3847 GN=SBP PE=1 SV=1	Yes	No	No	No	No
PFPRPR	sp|P11827|GLCAP_SOYBN Beta-conglycinin alpha subunit OS=Glycine max OX=3847 GN=CG-1 PE=1 SV=2	Yes	No	No	No	No
AGNPDIEHPE	sp|P04347|GLYG5_SOYBN Glycinin G5 OS=Glycine max OX=3847 GN=GY5 PE=1 SV=1	Yes	No	No	No	No
NLRGDGTGE	sp|P09186|LOX3_SOYBN Seed linoleate 9S-lipoxygenase-3 OS=Glycine max OX=3847 GN=LOX1.3 PE=1 SV=1	Yes	No	No	No	No
NLQGENEGEDKGA	sp|P04776|GLYG1_SOYBN Glycinin G1 OS=Glycine max OX=3847 GN=GY1 PE=1 SV=2	Yes	No	No	No	No
QQEEEEEGGSV	sp|P02858|GLYG4_SOYBN Glycinin G4 OS=Glycine max OX=3847 GN=GY4 PE=1 SV=2	Yes	No	No	No	No

GVAIKDPSAPH	sp|P09439|LOX2_SOYBN Seed linoleate 9S-lipoxygenase-2 OS=Glycine max OX=3847 GN=LOX1.2 PE=2 SV=1	Yes	No	No	No	No
LQGENEEEDSGA	sp|P04405|GLYG2_SOYBN Glycinin G2 OS=Glycine max OX=3847 GN=GY2 PE=1 SV=2	Yes	No	No	No	No
KFLVPPQ	sp|P04776|GLYG1_SOYBN Glycinin G1 OS=Glycine max OX=3847 GN=GY1 PE=1 SV=2	Yes	No	No	No	No
GNPDIEYPE	sp|P02858|GLYG4_SOYBN Glycinin G4 OS=Glycine max OX=3847 GN=GY4 PE=1 SV=2	Yes	No	No	No	No
LEDIPNHGSIH	sp|P09186|LOX3_SOYBN Seed linoleate 9S-lipoxygenase-3 OS=Glycine max OX=3847 GN=LOX1.3 PE=1 SV=1	Yes	No	No	No	No
NTNEDIAE	sp|P02858|GLYG4_SOYBN Glycinin G4 OS=Glycine max OX=3847 GN=GY4 PE=1 SV=2	Yes	No	No	No	No
FLEGIIT	sp|P09186|LOX3_SOYBN Seed linoleate 9S-lipoxygenase-3 OS=Glycine max OX=3847 GN=LOX1.3 PE=1 SV=1	Yes	No	No	No	No
SGGIKLPTDI	sp|P09186|LOX3_SOYBN Seed linoleate 9S-lipoxygenase-3 OS=Glycine max OX=3847 GN=LOX1.3 PE=1 SV=1	Yes	No	No	No	No
SLSQIVQPA	sp|P08170|LOX1_SOYBN Seed linoleate 13S-lipoxygenase-1 OS=Glycine max OX=3847 GN=LOX1.1 PE=1 SV=2	Yes	No	No	No	No
SATKPL	sp|P09439|LOX2_SOYBN Seed linoleate 9S-lipoxygenase-2 OS=Glycine max OX=3847 GN=LOX1.2 PE=2 SV=1	Yes	No	No	No	No
TNDTPM	sp|P04776|GLYG1_SOYBN Glycinin G1 OS=Glycine max OX=3847 GN=GY1 PE=1 SV=2	Yes	No	No	No	No
EQAGEQGFE	sp|P02858|GLYG4_SOYBN Glycinin G4 OS=Glycine max OX=3847 GN=GY4 PE=1 SV=2	Yes	No	No	No	No
LAGNPDIEYPET	sp|P02858|GLYG4_SOYBN Glycinin G4 OS=Glycine max OX=3847 GN=GY4 PE=1 SV=2	Yes	No	No	No	No
GLHLPSYSPYP	sp|P02858|GLYG4_SOYBN Glycinin G4 OS=Glycine max OX=3847 GN=GY4 PE=1 SV=2	Yes	No	No	No	No
HFNEGDVLVIPPGVP	sp|P02858|GLYG4_SOYBN Glycinin G4 OS=Glycine max OX=3847 GN=GY4 PE=1 SV=2	Yes	No	No	No	No
NGLHLPSYSP	sp|P02858|GLYG4_SOYBN Glycinin G4 OS=Glycine max OX=3847 GN=GY4 PE=1 SV=2	Yes	No	No	No	No
EDEGEQPRPFPFPRP	sp|P11827|GLCAP_SOYBN Beta-conglycinin alpha subunit OS=Glycine max OX=3847 GN=CG-1 PE=1 SV=2	Yes	No	No	No	No
YQGNSGPL	sp|P04347|GLYG5_SOYBN Glycinin G5 OS=Glycine max OX=3847 GN=GY5 PE=1 SV=1	Yes	No	No	No	No
SEGGLIETWNPNNKP	sp|P04776|GLYG1_SOYBN Glycinin G1 OS=Glycine max OX=3847 GN=GY1 PE=1 SV=2	Yes	No	No	No	No

IHIPAGTPL	sp|Q04672|SBP_SOYBN Sucrose-binding protein OS=Glycine max OX=3847 GN=SBP PE=1 SV=1	Yes	No	No	No	No
LAGNPDIEHPET	sp|P04347|GLYG5_SOYBN Glycinin G5 OS=Glycine max OX=3847 GN=GY5 PE=1 SV=1	Yes	No	No	No	No
FLKNDGTLRP	sp|P09186|LOX3_SOYBN Seed linoleate 9S-lipoxygenase-3 OS=Glycine max OX=3847 GN=LOX1.3 PE=1 SV=1	Yes	No	No	No	No
NLQSGDA	sp|P11827|GLCAP_SOYBN Beta-conglycinin alpha subunit OS=Glycine max OX=3847 GN=CG-1 PE=1 SV=2	Yes	No	No	No	No
IGQNSSPDIYNPQ	sp|P04405|GLYG2_SOYBN Glycinin G2 OS=Glycine max OX=3847 GN=GY2 PE=1 SV=2	Yes	No	No	No	No
DVLVIPPGVP	sp|P02858|GLYG4_SOYBN Glycinin G4 OS=Glycine max OX=3847 GN=GY4 PE=1 SV=2	Yes	No	No	No	No
SPYP	sp|P02858|GLYG4_SOYBN Glycinin G4 OS=Glycine max OX=3847 GN=GY4 PE=1 SV=2	Yes	No	No	No	No
QTPK	sp|Q04672|SBP_SOYBN Sucrose-binding protein OS=Glycine max OX=3847 GN=SBP PE=1 SV=1	Yes	No	No	No	No
NTNEDIAEK	sp|P02858|GLYG4_SOYBN Glycinin G4 OS=Glycine max OX=3847 GN=GY4 PE=1 SV=2	Yes	No	No	No	No
GGLSVIKPPTDE	sp|P04776|GLYG1_SOYBN Glycinin G1 OS=Glycine max OX=3847 GN=GY1 PE=1 SV=2	Yes	No	No	No	No
HLSVVHPI	sp|P09186|LOX3_SOYBN Seed linoleate 9S-lipoxygenase-3 OS=Glycine max OX=3847 GN=LOX1.3 PE=1 SV=1	Yes	No	No	No	No
TFLEGIIT	sp|P09186|LOX3_SOYBN Seed linoleate 9S-lipoxygenase-3 OS=Glycine max OX=3847 GN=LOX1.3 PE=1 SV=1	Yes	No	No	No	No
LQGENEEEDSGAI	sp|P04405|GLYG2_SOYBN Glycinin G2 OS=Glycine max OX=3847 GN=GY2 PE=1 SV=2	Yes	No	No	No	No
TIIPLPV	sp|P08170|LOX1_SOYBN Seed linoleate 13S-lipoxygenase-1 OS=Glycine max OX=3847 GN=LOX1.1 PE=1 SV=2	Yes	No	No	No	No
GVAIKDPSTPH	sp|P08170|LOX1_SOYBN Seed linoleate 13S-lipoxygenase-1 OS=Glycine max OX=3847 GN=LOX1.1 PE=1 SV=2	Yes	No	No	No	No
NEEEDSGAIV	sp|P04405|GLYG2_SOYBN Glycinin G2 OS=Glycine max OX=3847 GN=GY2 PE=1 SV=2	Yes	No	No	No	No
GLHLPSYSP	sp|P02858|GLYG4_SOYBN Glycinin G4 OS=Glycine max OX=3847 GN=GY4 PE=1 SV=2	Yes	No	No	No	No
NLQGENEEEDSGA	sp|P04405|GLYG2_SOYBN Glycinin G2 OS=Glycine max OX=3847 GN=GY2 PE=1 SV=2	Yes	No	No	No	No
EDLPEGPA	sp|P01070|ITRA_SOYBN Trypsin inhibitor A OS=Glycine max OX=3847 GN=KTI3 PE=1 SV=2	Yes	No	No	No	No

FVLEL	sp|P13708|SUS_SOYBN Sucrose synthase OS=Glycine max OX=3847 GN=SS PE=1 SV=2	Yes	No	No	No	No
EGGLIETWNPNNKP	sp|P04776|GLYG1_SOYBN Glycinin G1 OS=Glycine max OX=3847 GN=GY1 PE=1 SV=2	Yes	No	No	No	No
LGGNDTFPYP	sp|P09186|LOX3_SOYBN Seed linoleate 9S-lipoxygenase-3 OS=Glycine max OX=3847 GN=LOX1.3 PE=1 SV=1	Yes	No	No	No	No
QLDQNPR	sp|P04347|GLYG5_SOYBN Glycinin G5 OS=Glycine max OX=3847 GN=GY5 PE=1 SV=1	Yes	No	No	No	No
AQQLPK	sp|P13917|7SB1_SOYBN Basic 7S globulin OS=Glycine max OX=3847 GN=BG PE=1 SV=2	Yes	No	No	No	No
IGENKDAMDG	sp|P01070|ITRA_SOYBN Trypsin inhibitor A OS=Glycine max OX=3847 GN=KTI3 PE=1 SV=2	Yes	No	No	No	No
VFDGELQEGGVLIVPQ	sp|P04405|GLYG2_SOYBN Glycinin G2 OS=Glycine max OX=3847 GN=GY2 PE=1 SV=2	Yes	No	No	No	No
NIQFEWDESMGIPGA	sp|P09439|LOX2_SOYBN Seed linoleate 9S-lipoxygenase-2 OS=Glycine max OX=3847 GN=LOX1.2 PE=2 SV=1	Yes	No	No	No	No
SEELEEK	sp|P19594|2SS_SOYBN 2S seed storage albumin protein OS=Glycine max OX=3847 PE=1 SV=2	Yes	No	No	No	No
LDQNPR	sp|P04347|GLYG5_SOYBN Glycinin G5 OS=Glycine max OX=3847 GN=GY5 PE=1 SV=1	Yes	No	No	No	No
DMNEGALFLPH	sp|P11827|GLCAP_SOYBN Beta-conglycinin alpha subunit OS=Glycine max OX=3847 GN=CG-1 PE=1 SV=2	Yes	No	No	No	No
QGNSGPL	sp|P04347|GLYG5_SOYBN Glycinin G5 OS=Glycine max OX=3847 GN=GY5 PE=1 SV=1	Yes	No	No	No	No
LREDGTLKPV	sp|P08170|LOX1_SOYBN Seed linoleate 13S-lipoxygenase-1 OS=Glycine max OX=3847 GN=LOX1.1 PE=1 SV=2	Yes	No	No	No	No
DEGEQPRPFPFPRP	sp|P11827|GLCAP_SOYBN Beta-conglycinin alpha subunit OS=Glycine max OX=3847 GN=CG-1 PE=1 SV=2	Yes	No	No	No	No
TLEPGDMIHIPA	sp|Q04672|SBP_SOYBN Sucrose-binding protein OS=Glycine max OX=3847 GN=SBP PE=1 SV=1	Yes	No	No	No	No
NIHFEWDGSMGIPGA	sp|P08170|LOX1_SOYBN Seed linoleate 13S-lipoxygenase-1 OS=Glycine max OX=3847 GN=LOX1.1 PE=1 SV=2	Yes	No	No	No	No
PFPFP	sp|P11827|GLCAP_SOYBN Beta-conglycinin alpha subunit OS=Glycine max OX=3847 GN=CG-1 PE=1 SV=2	Yes	No	No	No	No
LSGAVS	sp|P09439|LOX2_SOYBN Seed linoleate 9S-lipoxygenase-2 OS=Glycine max OX=3847 GN=LOX1.2 PE=2 SV=1	Yes	No	No	No	No
QAALQTPK	sp|Q04672|SBP_SOYBN Sucrose-binding protein OS=Glycine max OX=3847 GN=SBP PE=1 SV=1	Yes	No	No	No	No

VTDADNVIPK	sp|P26987|SAM22_SOYBN Stress-induced protein SAM22 OS=Glycine max OX=3847 GN=PR-10 PE=1 SV=1	Yes	No	No	No	No
KEEDEGEQPRPFPFPRP	sp|P11827|GLCAP_SOYBN Beta-conglycinin alpha subunit OS=Glycine max OX=3847 GN=CG-1 PE=1 SV=2	Yes	No	No	No	No
GGLSVISPPTEEQ	sp|P11828|GLYG3_SOYBN Glycinin G3 OS=Glycine max OX=3847 GN=GY3 PE=1 SV=1	Yes	No	No	No	No
RQNIGQ	sp|P04405|GLYG2_SOYBN Glycinin G2 OS=Glycine max OX=3847 GN=GY2 PE=1 SV=2	Yes	No	No	No	No
QQEEENEGSNILS	sp|P04405|GLYG2_SOYBN Glycinin G2 OS=Glycine max OX=3847 GN=GY2 PE=1 SV=2	Yes	No	No	No	No
KFPPPK	sp|P09186|LOX3_SOYBN Seed linoleate 9S-lipoxygenase-3 OS=Glycine max OX=3847 GN=LOX1.3 PE=1 SV=1	Yes	No	No	No	No
EHPRPH	sp|P11827|GLCAP_SOYBN Beta-conglycinin alpha subunit OS=Glycine max OX=3847 GN=CG-1 PE=1 SV=2	Yes	No	No	No	No
DEDEDEDEDDEDEQIPSHPP	sp|P02858|GLYG4_SOYBN Glycinin G4 OS=Glycine max OX=3847 GN=GY4 PE=1 SV=2	Yes	No	No	No	No
SFNTNEDTAE	sp|P04347|GLYG5_SOYBN Glycinin G5 OS=Glycine max OX=3847 GN=GY5 PE=1 SV=1	Yes	No	No	No	No
LVIPPGVP	sp|P02858|GLYG4_SOYBN Glycinin G4 OS=Glycine max OX=3847 GN=GY4 PE=1 SV=2	Yes	No	No	No	No
REQDEDEDEDEDKPRPSRPSQG	sp|P02858|GLYG4_SOYBN Glycinin G4 OS=Glycine max OX=3847 GN=GY4 PE=1 SV=2	Yes	No	No	No	No
KFPPPHV	sp|P09439|LOX2_SOYBN Seed linoleate 9S-lipoxygenase-2 OS=Glycine max OX=3847 GN=LOX1.2 PE=2 SV=1	Yes	No	No	No	No
SVISPPTEE	sp|P11828|GLYG3_SOYBN Glycinin G3 OS=Glycine max OX=3847 GN=GY3 PE=1 SV=1	Yes	No	No	No	No
LQYQPQ	sp|P11828|GLYG3_SOYBN Glycinin G3 OS=Glycine max OX=3847 GN=GY3 PE=1 SV=1	Yes	No	No	No	No
QQHGEKEEDEGEQPRPFPFPRP	sp|P11827|GLCAP_SOYBN Beta-conglycinin alpha subunit OS=Glycine max OX=3847 GN=CG-1 PE=1 SV=2	Yes	No	No	No	No
LKNDGTLRPL	sp|P09186|LOX3_SOYBN Seed linoleate 9S-lipoxygenase-3 OS=Glycine max OX=3847 GN=LOX1.3 PE=1 SV=1	Yes	No	No	No	No
GGNDTFPYP	sp|P09186|LOX3_SOYBN Seed linoleate 9S-lipoxygenase-3 OS=Glycine max OX=3847 GN=LOX1.3 PE=1 SV=1	Yes	No	No	No	No
KREQDEDEDEDEDKPRPSRPS	sp|P02858|GLYG4_SOYBN Glycinin G4 OS=Glycine max OX=3847 GN=GY4 PE=1 SV=2	Yes	No	No	No	No
QQRPQ	sp|P04776|GLYG1_SOYBN Glycinin G1 OS=Glycine max OX=3847 GN=GY1 PE=1 SV=2	Yes	No	No	No	No

DVISTIIPLPV	sp|P08170|LOX1_SOYBN Seed linoleate 13S-lipoxygenase-1 OS=Glycine max OX=3847 GN=LOX1.1 PE=1 SV=2	Yes	No	No	No	No
GDHTSQIT	sp|P09186|LOX3_SOYBN Seed linoleate 9S-lipoxygenase-3 OS=Glycine max OX=3847 GN=LOX1.3 PE=1 SV=1	Yes	No	No	No	No
EGGIKLPTEV	sp|P09439|LOX2_SOYBN Seed linoleate 9S-lipoxygenase-2 OS=Glycine max OX=3847 GN=LOX1.2 PE=2 SV=1	Yes	No	No	No	No
SIDHDDGT	sp|P01070|ITRA_SOYBN Trypsin inhibitor A OS=Glycine max OX=3847 GN=KTI3 PE=1 SV=2	Yes	No	No	No	No
TNDTPMIGT	sp|P04776|GLYG1_SOYBN Glycinin G1 OS=Glycine max OX=3847 GN=GY1 PE=1 SV=2	Yes	No	No	No	No
VLDNEGNPL	sp|P01070|ITRA_SOYBN Trypsin inhibitor A OS=Glycine max OX=3847 GN=KTI3 PE=1 SV=2	Yes	No	No	No	No
GQTSSPDIYNPQ	sp|P04776|GLYG1_SOYBN Glycinin G1 OS=Glycine max OX=3847 GN=GY1 PE=1 SV=2	Yes	No	No	No	No
AIKDPSTPH	sp|P08170|LOX1_SOYBN Seed linoleate 13S-lipoxygenase-1 OS=Glycine max OX=3847 GN=LOX1.1 PE=1 SV=2	Yes	No	No	No	No
GSHLPSYLPYPQ	sp|P04347|GLYG5_SOYBN Glycinin G5 OS=Glycine max OX=3847 GN=GY5 PE=1 SV=1	Yes	No	No	No	No
GEKEEDEGEQPRPFPFPRP	sp|P11827|GLCAP_SOYBN Beta-conglycinin alpha subunit OS=Glycine max OX=3847 GN=CG-1 PE=1 SV=2	Yes	No	No	No	No
WQEQQDEDEDEDEDDEDEQIP SHPP	sp|P02858|GLYG4_SOYBN Glycinin G4 OS=Glycine max OX=3847 GN=GY4 PE=1 SV=2	Yes	No	No	No	No
SLVNDGGVIEQ	sp|P09186|LOX3_SOYBN Seed linoleate 9S-lipoxygenase-3 OS=Glycine max OX=3847 GN=LOX1.3 PE=1 SV=1	Yes	No	No	No	No
NDLGDPDKGEN	sp|P09186|LOX3_SOYBN Seed linoleate 9S-lipoxygenase-3 OS=Glycine max OX=3847 GN=LOX1.3 PE=1 SV=1	Yes	No	No	No	No
GNPDIEHPE	sp|P04347|GLYG5_SOYBN Glycinin G5 OS=Glycine max OX=3847 GN=GY5 PE=1 SV=1	Yes	No	No	No	No
EHLEPN	sp|P09186|LOX3_SOYBN Seed linoleate 9S-lipoxygenase-3 OS=Glycine max OX=3847 GN=LOX1.3 PE=1 SV=1	Yes	No	No	No	No
LKNDGTLRP	sp|P09186|LOX3_SOYBN Seed linoleate 9S-lipoxygenase-3 OS=Glycine max OX=3847 GN=LOX1.3 PE=1 SV=1	Yes	No	No	No	No
VVNPDNDEN	sp|P11827|GLCAP_SOYBN Beta-conglycinin alpha subunit OS=Glycine max OX=3847 GN=CG-1 PE=1 SV=2	Yes	No	No	No	No
NDTPM	sp|P04776|GLYG1_SOYBN Glycinin G1 OS=Glycine max OX=3847 GN=GY1 PE=1 SV=2	Yes	No	No	No	No
TLLLPH	sp|P11827|GLCAP_SOYBN Beta-conglycinin alpha subunit OS=Glycine max OX=3847 GN=CG-1 PE=1 SV=2	Yes	No	No	No	No

NEGDVLVIPPGVP	sp|P02858|GLYG4_SOYBN Glycinin G4 OS=Glycine max OX=3847 GN=GY4 PE=1 SV=2	Yes	No	No	No	No
GRGPTVTDPN	sp|P08170|LOX1_SOYBN Seed linoleate 13S-lipoxygenase-1 OS=Glycine max OX=3847 GN=LOX1.1 PE=1 SV=2	Yes	No	No	No	No
MLHIPV	sp|Q04672|SBP_SOYBN Sucrose-binding protein OS=Glycine max OX=3847 GN=SBP PE=1 SV=1	Yes	No	No	No	No
KREQDEDEDEDEDKPRPSRPSQG	sp|P02858|GLYG4_SOYBN Glycinin G4 OS=Glycine max OX=3847 GN=GY4 PE=1 SV=2	Yes	No	No	No	No
QDEDEDEDEDDEDEQIPSHPPR	sp|P02858|GLYG4_SOYBN Glycinin G4 OS=Glycine max OX=3847 GN=GY4 PE=1 SV=2	Yes	No	No	No	No
GNDTFPYP	sp|P09186|LOX3_SOYBN Seed linoleate 9S-lipoxygenase-3 OS=Glycine max OX=3847 GN=LOX1.3 PE=1 SV=1	Yes	No	No	No	No
LDQTPR	sp|P02858|GLYG4_SOYBN Glycinin G4 OS=Glycine max OX=3847 GN=GY4 PE=1 SV=2	Yes	No	No	No	No
DGELQEGGVLIVPQ	sp|P04405|GLYG2_SOYBN Glycinin G2 OS=Glycine max OX=3847 GN=GY2 PE=1 SV=2	Yes	No	No	No	No
YEGNWGPL	sp|P02858|GLYG4_SOYBN Glycinin G4 OS=Glycine max OX=3847 GN=GY4 PE=1 SV=2	Yes	No	No	No	No
IVNRDEND	sp|Q04672|SBP_SOYBN Sucrose-binding protein OS=Glycine max OX=3847 GN=SBP PE=1 SV=1	Yes	No	No	No	No
TVDEAIQN	sp|P09186|LOX3_SOYBN Seed linoleate 9S-lipoxygenase-3 OS=Glycine max OX=3847 GN=LOX1.3 PE=1 SV=1	Yes	No	No	No	No
NFNNQLDQTP	sp|P02858|GLYG4_SOYBN Glycinin G4 OS=Glycine max OX=3847 GN=GY4 PE=1 SV=2	Yes	No	No	No	No
IVVQG	sp|P04347|GLYG5_SOYBN Glycinin G5 OS=Glycine max OX=3847 GN=GY5 PE=1 SV=1	Yes	No	No	No	No
LQTPK	sp|Q04672|SBP_SOYBN Sucrose-binding protein OS=Glycine max OX=3847 GN=SBP PE=1 SV=1	Yes	No	No	No	No
GLSVIKPPTDEQQQRPQ	sp|P04776|GLYG1_SOYBN Glycinin G1 OS=Glycine max OX=3847 GN=GY1 PE=1 SV=2	Yes	No	No	No	No
LSAE	sp|P04776|GLYG1_SOYBN Glycinin G1 OS=Glycine max OX=3847 GN=GY1 PE=1 SV=2	Yes	No	No	No	No
GLSVISPPTEEQ	sp|P11828|GLYG3_SOYBN Glycinin G3 OS=Glycine max OX=3847 GN=GY3 PE=1 SV=1	Yes	No	No	No	No
GLSVIKPPTDE	sp|P04776|GLYG1_SOYBN Glycinin G1 OS=Glycine max OX=3847 GN=GY1 PE=1 SV=2	Yes	No	No	No	No
DQNSEKPGEV	sp|P09439|LOX2_SOYBN Seed linoleate 9S-lipoxygenase-2 OS=Glycine max OX=3847 GN=LOX1.2 PE=2 SV=1	Yes	No	No	No	No

TLEDVPNQGT	sp|P09439|LOX2_SOYBN Seed linoleate 9S-lipoxygenase-2 OS=Glycine max OX=3847 GN=LOX1.2 PE=2 SV=1	Yes	No	No	No	No
STIIPLPV	sp|P08170|LOX1_SOYBN Seed linoleate 13S-lipoxygenase-1 OS=Glycine max OX=3847 GN=LOX1.1 PE=1 SV=2	Yes	No	No	No	No
LVVLPV	sp|P13917|7SB1_SOYBN Basic 7S globulin OS=Glycine max OX=3847 GN=BG PE=1 SV=2	Yes	No	No	No	No
IKPPTDEQQQRPQ	sp|P04776|GLYG1_SOYBN Glycinin G1 OS=Glycine max OX=3847 GN=GY1 PE=1 SV=2	Yes	No	No	No	No
DFVLDNEGNPLENGGT	sp|P01070|ITRA_SOYBN Trypsin inhibitor A OS=Glycine max OX=3847 GN=KTI3 PE=1 SV=2	Yes	No	No	No	No
EEDEGEQPRPFPFP	sp|P11827|GLCAP_SOYBN Beta-conglycinin alpha subunit OS=Glycine max OX=3847 GN=CG-1 PE=1 SV=2	Yes	No	No	No	No
NNNPFSFLVPPQES	sp|P04405|GLYG2_SOYBN Glycinin G2 OS=Glycine max OX=3847 GN=GY2 PE=1 SV=2	Yes	No	No	No	No
ESEGGLIETWNPNNKP	sp|P04776|GLYG1_SOYBN Glycinin G1 OS=Glycine max OX=3847 GN=GY1 PE=1 SV=2	Yes	No	No	No	No
VINEGEAN	sp|P11827|GLCAP_SOYBN Beta-conglycinin alpha subunit OS=Glycine max OX=3847 GN=CG-1 PE=1 SV=2	Yes	No	No	No	No
GLHLPS	sp|P02858|GLYG4_SOYBN Glycinin G4 OS=Glycine max OX=3847 GN=GY4 PE=1 SV=2	Yes	No	No	No	No
STIIPL	sp|P08170|LOX1_SOYBN Seed linoleate 13S-lipoxygenase-1 OS=Glycine max OX=3847 GN=LOX1.1 PE=1 SV=2	Yes	No	No	No	No
GQNSSPDIYNPQ	sp|P04405|GLYG2_SOYBN Glycinin G2 OS=Glycine max OX=3847 GN=GY2 PE=1 SV=2	Yes	No	No	No	No
DMNEGALFLPHFNS	sp|P11827|GLCAP_SOYBN Beta-conglycinin alpha subunit OS=Glycine max OX=3847 GN=CG-1 PE=1 SV=2	Yes	No	No	No	No
NLQGENEGEDK	sp|P04776|GLYG1_SOYBN Glycinin G1 OS=Glycine max OX=3847 GN=GY1 PE=1 SV=2	Yes	No	No	No	No
RISSDLKPG	sp|Q04672|SBP_SOYBN Sucrose-binding protein OS=Glycine max OX=3847 GN=SBP PE=1 SV=1	Yes	No	No	No	No
AGNPDIEYPE	sp|P02858|GLYG4_SOYBN Glycinin G4 OS=Glycine max OX=3847 GN=GY4 PE=1 SV=2	Yes	No	No	No	No
TNDTPMIG	sp|P04776|GLYG1_SOYBN Glycinin G1 OS=Glycine max OX=3847 GN=GY1 PE=1 SV=2	Yes	No	No	No	No
KPPTDEQQQRPQ	sp|P04776|GLYG1_SOYBN Glycinin G1 OS=Glycine max OX=3847 GN=GY1 PE=1 SV=2	Yes	No	No	No	No
DLDV	sp|P11827|GLCAP_SOYBN Beta-conglycinin alpha subunit OS=Glycine max OX=3847 GN=CG-1 PE=1 SV=2	Yes	No	No	No	No

NALEPDHRVESEGGLIET	sp|P04347|GLYG5_SOYBN Glycinin G5 OS=Glycine max OX=3847 GN=GY5 PE=1 SV=1	Yes	No	No	No	No
ANHTYVPSETPAPL	sp|P08170|LOX1_SOYBN Seed linoleate 13S-lipoxygenase-1 OS=Glycine max OX=3847 GN=LOX1.1 PE=1 SV=2	Yes	No	No	No	No
NSGPL	sp|P04347|GLYG5_SOYBN Glycinin G5 OS=Glycine max OX=3847 GN=GY5 PE=1 SV=1	Yes	No	No	No	No
SFNTNEDTAEK	sp|P04347|GLYG5_SOYBN Glycinin G5 OS=Glycine max OX=3847 GN=GY5 PE=1 SV=1	Yes	No	No	No	No
VIKPPT	sp|P04776|GLYG1_SOYBN Glycinin G1 OS=Glycine max OX=3847 GN=GY1 PE=1 SV=2	Yes	No	No	No	No
EPQQPGEKEEDEDEQPRPI	sp|P0DO16|GLCA1_SOYBN Beta-conglycinin alpha subunit 1 OS=Glycine max OX=3847 GN=CG-3 PE=1 SV=1;sp|P0DO15|GLCA2_SOYBN Beta-conglycinin alpha subunit 2 OS=Glycine max OX=3847 GN=CG-2 PE=1 SV=1	No	Yes	No	No	basolateral
SVVDM	sp|P11827|GLCAP_SOYBN Beta-conglycinin alpha subunit OS=Glycine max OX=3847 GN=CG-1 PE=1 SV=2	No	Yes	No	basolateral	No
GNWGPL	sp|P02858|GLYG4_SOYBN Glycinin G4 OS=Glycine max OX=3847 GN=GY4 PE=1 SV=2	No	Yes	No	basolateral	No
PFPRPPH	sp|P0DO16|GLCA1_SOYBN Beta-conglycinin alpha subunit 1 OS=Glycine max OX=3847 GN=CG-3 PE=1 SV=1;sp|P0DO15|GLCA2_SOYBN Beta-conglycinin alpha subunit 2 OS=Glycine max OX=3847 GN=CG-2 PE=1 SV=1	No	Yes	No	basolateral	No
SIVDM	sp|P0DO16|GLCA1_SOYBN Beta-conglycinin alpha subunit 1 OS=Glycine max OX=3847 GN=CG-3 PE=1 SV=1;sp|P0DO15|GLCA2_SOYBN Beta-conglycinin alpha subunit 2 OS=Glycine max OX=3847 GN=CG-2 PE=1 SV=1	No	Yes	No	basolateral	No
QQPGEKEEDEDEQPRPIPFPRPQPR	sp|P0DO16|GLCA1_SOYBN Beta-conglycinin alpha subunit 1 OS=Glycine max OX=3847 GN=CG-3 PE=1 SV=1;sp|P0DO15|GLCA2_SOYBN Beta-conglycinin alpha subunit 2 OS=Glycine max OX=3847 GN=CG-2 PE=1 SV=1	No	Yes	No	basolateral	No
DIFNPQ	sp|P11828|GLYG3_SOYBN Glycinin G3 OS=Glycine max OX=3847 GN=GY3 PE=1 SV=1	No	Yes	No	basolateral	No
QFPFPRPP	sp|P0DO16|GLCA1_SOYBN Beta-conglycinin alpha subunit 1 OS=Glycine max OX=3847 GN=CG-3 PE=1 SV=1;sp|P0DO15|GLCA2_SOYBN Beta-conglycinin alpha subunit 2 OS=Glycine max OX=3847 GN=CG-2 PE=1 SV=1	No	Yes	No	basolateral	No
QQPGEKEEDEDEQPRPIPFPRPQP	sp|P0DO16|GLCA1_SOYBN Beta-conglycinin alpha subunit 1 OS=Glycine max OX=3847 GN=CG-3 PE=1	No	Yes	No	basolateral	No

	SV=1;sp|P0DO15|GLCA2_SOYBN Beta-conglycinin alpha subunit 2 OS=Glycine max OX=3847 GN=CG-2 PE=1 SV=1					
FPFPRPPH	sp|P0DO16|GLCA1_SOYBN Beta-conglycinin alpha subunit 1 OS=Glycine max OX=3847 GN=CG-3 PE=1 SV=1;sp|P0DO15|GLCA2_SOYBN Beta-conglycinin alpha subunit 2 OS=Glycine max OX=3847 GN=CG-2 PE=1 SV=1	No	Yes	No	basolateral	No
SVGGIIG	sp|P09186|LOX3_SOYBN Seed linoleate 9S-lipoxygenase-3 OS=Glycine max OX=3847 GN=LOX1.3 PE=1 SV=1	No	Yes	No	basolateral	No
QFPFPRPPH	sp|P0DO16|GLCA1_SOYBN Beta-conglycinin alpha subunit 1 OS=Glycine max OX=3847 GN=CG-3 PE=1 SV=1;sp|P0DO15|GLCA2_SOYBN Beta-conglycinin alpha subunit 2 OS=Glycine max OX=3847 GN=CG-2 PE=1 SV=1	No	Yes	No	basolateral	No
QEWP	sp|P0DO16|GLCA1_SOYBN Beta-conglycinin alpha subunit 1 OS=Glycine max OX=3847 GN=CG-3 PE=1 SV=1;sp|P0DO15|GLCA2_SOYBN Beta-conglycinin alpha subunit 2 OS=Glycine max OX=3847 GN=CG-2 PE=1 SV=1	No	Yes	No	No	No
EDEQPRPI	sp|P0DO16|GLCA1_SOYBN Beta-conglycinin alpha subunit 1 OS=Glycine max OX=3847 GN=CG-3 PE=1 SV=1;sp|P0DO15|GLCA2_SOYBN Beta-conglycinin alpha subunit 2 OS=Glycine max OX=3847 GN=CG-2 PE=1 SV=1	No	Yes	No	No	No
LLPNHADAD	sp|P0DO16|GLCA1_SOYBN Beta-conglycinin alpha subunit 1 OS=Glycine max OX=3847 GN=CG-3 PE=1 SV=1;sp|P0DO15|GLCA2_SOYBN Beta-conglycinin alpha subunit 2 OS=Glycine max OX=3847 GN=CG-2 PE=1 SV=1	No	Yes	No	No	No
FPFPRPP	sp|P0DO16|GLCA1_SOYBN Beta-conglycinin alpha subunit 1 OS=Glycine max OX=3847 GN=CG-3 PE=1 SV=1;sp|P0DO15|GLCA2_SOYBN Beta-conglycinin alpha subunit 2 OS=Glycine max OX=3847 GN=CG-2 PE=1 SV=1	No	Yes	No	No	No
PFPRPQP	sp|P0DO16|GLCA1_SOYBN Beta-conglycinin alpha subunit 1 OS=Glycine max OX=3847 GN=CG-3 PE=1 SV=1;sp|P0DO15|GLCA2_SOYBN Beta-conglycinin alpha subunit 2 OS=Glycine max OX=3847 GN=CG-2 PE=1 SV=1	No	Yes	No	No	No
SLVNNDDRDS	sp|P0DO16|GLCA1_SOYBN Beta-conglycinin alpha subunit 1 OS=Glycine max OX=3847 GN=CG-3 PE=1 SV=1;sp|P0DO15|GLCA2_SOYBN Beta-conglycinin alpha subunit 2 OS=Glycine max OX=3847 GN=CG-2 PE=1 SV=1	No	Yes	No	No	No
ISIDHDDGT	sp|P01070|ITRA_SOYBN Trypsin inhibitor A OS=Glycine max OX=3847 GN=KTI3 PE=1 SV=2	No	Yes	No	No	No

VVNPDNNEN	sp|P0DO16|GLCA1_SOYBN Beta-conglycinin alpha subunit 1 OS=Glycine max OX=3847 GN=CG-3 PE=1 SV=1;sp|P0DO15|GLCA2_SOYBN Beta-conglycinin alpha subunit 2 OS=Glycine max OX=3847 GN=CG-2 PE=1 SV=1	No	Yes	No	No	No
DLHEGGIK	sp|P09439|LOX2_SOYBN Seed linoleate 9S-lipoxygenase-2 OS=Glycine max OX=3847 GN=LOX1.2 PE=2 SV=1	No	Yes	No	No	No
VVPPGHP	sp|Q04672|SBP_SOYBN Sucrose-binding protein OS=Glycine max OX=3847 GN=SBP PE=1 SV=1	No	Yes	No	No	No
QLDQTPR	sp|P02858|GLYG4_SOYBN Glycinin G4 OS=Glycine max OX=3847 GN=GY4 PE=1 SV=2	No	Yes	No	No	No
ELVEV	sp|P09186|LOX3_SOYBN Seed linoleate 9S-lipoxygenase-3 OS=Glycine max OX=3847 GN=LOX1.3 PE=1 SV=1	No	Yes	No	No	No
YSPYPR	sp|P02858|GLYG4_SOYBN Glycinin G4 OS=Glycine max OX=3847 GN=GY4 PE=1 SV=2	No	Yes	No	No	No
LFGSN	sp|P0DO16|GLCA1_SOYBN Beta-conglycinin alpha subunit 1 OS=Glycine max OX=3847 GN=CG-3 PE=1 SV=1;sp|P0DO15|GLCA2_SOYBN Beta-conglycinin alpha subunit 2 OS=Glycine max OX=3847 GN=CG-2 PE=1 SV=1	No	Yes	No	No	No
REEQEWP	sp|P0DO16|GLCA1_SOYBN Beta-conglycinin alpha subunit 1 OS=Glycine max OX=3847 GN=CG-3 PE=1 SV=1;sp|P0DO15|GLCA2_SOYBN Beta-conglycinin alpha subunit 2 OS=Glycine max OX=3847 GN=CG-2 PE=1 SV=1	No	Yes	No	No	No
TNPTKPI	sp|Q8RVH5|7SBG2_SOYBN Basic 7S globulin 2 OS=Glycine max OX=3847 PE=1 SV=1	No	Yes	No	No	No
QLQGV	sp|P19594|2SS_SOYBN 2S seed storage albumin protein OS=Glycine max OX=3847 PE=1 SV=2	No	Yes	No	No	No
PFPRPQ	sp|P0DO16|GLCA1_SOYBN Beta-conglycinin alpha subunit 1 OS=Glycine max OX=3847 GN=CG-3 PE=1 SV=1;sp|P0DO15|GLCA2_SOYBN Beta-conglycinin alpha subunit 2 OS=Glycine max OX=3847 GN=CG-2 PE=1 SV=1	No	Yes	No	No	No
IPPGVP	sp|P02858|GLYG4_SOYBN Glycinin G4 OS=Glycine max OX=3847 GN=GY4 PE=1 SV=2	No	Yes	No	No	No
YVVNPDNNEN	sp|P0DO16|GLCA1_SOYBN Beta-conglycinin alpha subunit 1 OS=Glycine max OX=3847 GN=CG-3 PE=1 SV=1;sp|P0DO15|GLCA2_SOYBN Beta-conglycinin alpha subunit 2 OS=Glycine max OX=3847 GN=CG-2 PE=1 SV=1	No	Yes	No	No	No
DMNEGALLLPH	sp|P0DO16|GLCA1_SOYBN Beta-conglycinin alpha subunit 1 OS=Glycine max OX=3847 GN=CG-3 PE=1	No	Yes	No	No	No

	SV=1;sp|P0DO15|GLCA2_SOYBN Beta-conglycinin alpha subunit 2 OS=Glycine max OX=3847 GN=CG-2 PE=1 SV=1					
YFVDAQPK	sp|P0DO16|GLCA1_SOYBN Beta-conglycinin alpha subunit 1 OS=Glycine max OX=3847 GN=CG-3 PE=1 SV=1;sp|P0DO15|GLCA2_SOYBN Beta-conglycinin alpha subunit 2 OS=Glycine max OX=3847 GN=CG-2 PE=1 SV=1	No	Yes	No	No	No
DITAFG	sp|P01070|ITRA_SOYBN Trypsin inhibitor A OS=Glycine max OX=3847 GN=KTI3 PE=1 SV=2	No	Yes	No	No	No
NLQGENEGEDKGAI	sp|P04776|GLYG1_SOYBN Glycinin G1 OS=Glycine max OX=3847 GN=GY1 PE=1 SV=2	No	Yes	No	No	No
FVDAQPK	sp|P0DO16|GLCA1_SOYBN Beta-conglycinin alpha subunit 1 OS=Glycine max OX=3847 GN=CG-3 PE=1 SV=1;sp|P0DO15|GLCA2_SOYBN Beta-conglycinin alpha subunit 2 OS=Glycine max OX=3847 GN=CG-2 PE=1 SV=1	No	Yes	No	No	No
QQPGEKEEDEDEQPRPI	sp|P0DO16|GLCA1_SOYBN Beta-conglycinin alpha subunit 1 OS=Glycine max OX=3847 GN=CG-3 PE=1 SV=1;sp|P0DO15|GLCA2_SOYBN Beta-conglycinin alpha subunit 2 OS=Glycine max OX=3847 GN=CG-2 PE=1 SV=1	No	Yes	No	No	No
YSPYP	sp|P02858|GLYG4_SOYBN Glycinin G4 OS=Glycine max OX=3847 GN=GY4 PE=1 SV=2	No	Yes	No	No	No
EEQEWPR	sp|P0DO16|GLCA1_SOYBN Beta-conglycinin alpha subunit 1 OS=Glycine max OX=3847 GN=CG-3 PE=1 SV=1;sp|P0DO15|GLCA2_SOYBN Beta-conglycinin alpha subunit 2 OS=Glycine max OX=3847 GN=CG-2 PE=1 SV=1	No	Yes	No	No	No
GLSVIKPPTDEQ	sp|P04776|GLYG1_SOYBN Glycinin G1 OS=Glycine max OX=3847 GN=GY1 PE=1 SV=2	Yes	Yes	No	No	No
EQDEDEDEDEDKPRPSRPS	sp|P02858|GLYG4_SOYBN Glycinin G4 OS=Glycine max OX=3847 GN=GY4 PE=1 SV=2	Yes	Yes	No	No	No
IESEGGLIET	sp|P04776|GLYG1_SOYBN Glycinin G1 OS=Glycine max OX=3847 GN=GY1 PE=1 SV=2	Yes	Yes	No	No	No
NNQLDQTP	sp|P02858|GLYG4_SOYBN Glycinin G4 OS=Glycine max OX=3847 GN=GY4 PE=1 SV=2	Yes	Yes	No	No	No
PPGVP	sp|P02858|GLYG4_SOYBN Glycinin G4 OS=Glycine max OX=3847 GN=GY4 PE=1 SV=2	Yes	Yes	No	No	No
SLLDT	sp|P02858|GLYG4_SOYBN Glycinin G4 OS=Glycine max OX=3847 GN=GY4 PE=1 SV=2	Yes	Yes	No	No	No
NGLHLPSYSPYP	sp|P02858|GLYG4_SOYBN Glycinin G4 OS=Glycine max OX=3847 GN=GY4 PE=1 SV=2	Yes	Yes	No	No	No

VTPTKPI	sp|P13917|7SB1_SOYBN Basic 7S globulin OS=Glycine max OX=3847 GN=BG PE=1 SV=2	Yes	Yes	No	No	No
ISSDLKPG	sp|Q04672|SBP_SOYBN Sucrose-binding protein OS=Glycine max OX=3847 GN=SBP PE=1 SV=1	Yes	Yes	No	No	No
LSVIKPPTDEQ	sp|P04776|GLYG1_SOYBN Glycinin G1 OS=Glycine max OX=3847 GN=GY1 PE=1 SV=2	Yes	Yes	No	No	No
ISPLPV	sp|P09186|LOX3_SOYBN Seed linoleate 9S-lipoxygenase-3 OS=Glycine max OX=3847 GN=LOX1.3 PE=1 SV=1	Yes	Yes	No	No	No
TLEDIPNHGSIH	sp|P09186|LOX3_SOYBN Seed linoleate 9S-lipoxygenase-3 OS=Glycine max OX=3847 GN=LOX1.3 PE=1 SV=1	Yes	Yes	No	No	No
EEDEGEQPRPFPFPRP	sp|P11827|GLCAP_SOYBN Beta-conglycinin alpha subunit OS=Glycine max OX=3847 GN=CG-1 PE=1 SV=2	Yes	Yes	No	No	No
HFDSEV	sp|Q04672|SBP_SOYBN Sucrose-binding protein OS=Glycine max OX=3847 GN=SBP PE=1 SV=1	Yes	Yes	No	No	No
TLEPGDM	sp|Q04672|SBP_SOYBN Sucrose-binding protein OS=Glycine max OX=3847 GN=SBP PE=1 SV=1	Yes	Yes	No	No	No
SSPDIFNPQ	sp|P11828|GLYG3_SOYBN Glycinin G3 OS=Glycine max OX=3847 GN=GY3 PE=1 SV=1	Yes	Yes	No	No	No
NLVVLPV	sp|P13917|7SB1_SOYBN Basic 7S globulin OS=Glycine max OX=3847 GN=BG PE=1 SV=2	Yes	Yes	No	No	No
GNPDIEHPET	sp|P04347|GLYG5_SOYBN Glycinin G5 OS=Glycine max OX=3847 GN=GY5 PE=1 SV=1	Yes	Yes	No	No	No
NPDIEYPET	sp|P02858|GLYG4_SOYBN Glycinin G4 OS=Glycine max OX=3847 GN=GY4 PE=1 SV=2	Yes	Yes	No	No	No
GNSGPL	sp|P04347|GLYG5_SOYBN Glycinin G5 OS=Glycine max OX=3847 GN=GY5 PE=1 SV=1	Yes	Yes	No	No	No
SGGIKLPTDIIS	sp|P09186|LOX3_SOYBN Seed linoleate 9S-lipoxygenase-3 OS=Glycine max OX=3847 GN=LOX1.3 PE=1 SV=1	Yes	Yes	No	No	No
EQDEDEDEDEDKPRPSRPSQG	sp|P02858|GLYG4_SOYBN Glycinin G4 OS=Glycine max OX=3847 GN=GY4 PE=1 SV=2	Yes	Yes	No	No	No
SVIKPPT	sp|P04776|GLYG1_SOYBN Glycinin G1 OS=Glycine max OX=3847 GN=GY1 PE=1 SV=2	Yes	Yes	No	No	No
AGNPDIEYPET	sp|P02858|GLYG4_SOYBN Glycinin G4 OS=Glycine max OX=3847 GN=GY4 PE=1 SV=2	Yes	Yes	No	No	No
NNQLDQNPR	sp|P04347|GLYG5_SOYBN Glycinin G5 OS=Glycine max OX=3847 GN=GY5 PE=1 SV=1	Yes	Yes	No	No	No
SFLVPPK	sp|P11828|GLYG3_SOYBN Glycinin G3 OS=Glycine max OX=3847 GN=GY3 PE=1 SV=1	Yes	Yes	No	No	No

GNPDIEYPET	sp|P02858|GLYG4_SOYBN Glycinin G4 OS=Glycine max OX=3847 GN=GY4 PE=1 SV=2	Yes	Yes	No	No	No
NQLDQNPR	sp|P04347|GLYG5_SOYBN Glycinin G5 OS=Glycine max OX=3847 GN=GY5 PE=1 SV=1	Yes	Yes	No	No	No
VIPPGVP	sp|P02858|GLYG4_SOYBN Glycinin G4 OS=Glycine max OX=3847 GN=GY4 PE=1 SV=2	Yes	Yes	No	No	No
DIEHPET	sp|P04347|GLYG5_SOYBN Glycinin G5 OS=Glycine max OX=3847 GN=GY5 PE=1 SV=1	Yes	Yes	No	No	No
EEPQQPQ	sp|P04776|GLYG1_SOYBN Glycinin G1 OS=Glycine max OX=3847 GN=GY1 PE=1 SV=2	Yes	Yes	No	No	No
LTEVGPDDDEKS	sp|Q04672|SBP_SOYBN Sucrose-binding protein OS=Glycine max OX=3847 GN=SBP PE=1 SV=1	Yes	Yes	No	No	No
LLDT	sp|P02858|GLYG4_SOYBN Glycinin G4 OS=Glycine max OX=3847 GN=GY4 PE=1 SV=2	Yes	Yes	No	No	No
ALQTPK	sp|Q04672|SBP_SOYBN Sucrose-binding protein OS=Glycine max OX=3847 GN=SBP PE=1 SV=1	Yes	Yes	No	No	No
KTNDTPMIGT	sp|P04776|GLYG1_SOYBN Glycinin G1 OS=Glycine max OX=3847 GN=GY1 PE=1 SV=2	Yes	Yes	No	No	No
NNQLDQNP	sp|P04347|GLYG5_SOYBN Glycinin G5 OS=Glycine max OX=3847 GN=GY5 PE=1 SV=1	Yes	Yes	No	No	No
VIKPPTDEQQQRPQ	sp|P04776|GLYG1_SOYBN Glycinin G1 OS=Glycine max OX=3847 GN=GY1 PE=1 SV=2	Yes	Yes	No	No	No
HLPSYSP	sp|P02858|GLYG4_SOYBN Glycinin G4 OS=Glycine max OX=3847 GN=GY4 PE=1 SV=2	Yes	Yes	No	No	No
ELSLPHPA	sp|P09439|LOX2_SOYBN Seed linoleate 9S-lipoxygenase-2 OS=Glycine max OX=3847 GN=LOX1.2 PE=2 SV=1	Yes	Yes	No	No	No
YLAGNPDIEYPET	sp|P02858|GLYG4_SOYBN Glycinin G4 OS=Glycine max OX=3847 GN=GY4 PE=1 SV=2	Yes	Yes	No	No	No
ELSLPHPAG	sp|P09439|LOX2_SOYBN Seed linoleate 9S-lipoxygenase-2 OS=Glycine max OX=3847 GN=LOX1.2 PE=2 SV=1	Yes	Yes	No	No	No
VFDGELQEGGV	sp|P04405|GLYG2_SOYBN Glycinin G2 OS=Glycine max OX=3847 GN=GY2 PE=1 SV=2	Yes	Yes	No	No	No
ALIQV	sp|P04776|GLYG1_SOYBN Glycinin G1 OS=Glycine max OX=3847 GN=GY1 PE=1 SV=2	Yes	Yes	No	No	No
GLEEFPPK	sp|P08170|LOX1_SOYBN Seed linoleate 13S-lipoxygenase-1 OS=Glycine max OX=3847 GN=LOX1.1 PE=1 SV=2	Yes	Yes	No	No	No
SVVEDLPEGPA	sp|P01070|ITRA_SOYBN Trypsin inhibitor A OS=Glycine max OX=3847 GN=KTI3 PE=1 SV=2	Yes	Yes	No	No	No

NIGQNSSPDIYNPQ	sp|P04405|GLYG2_SOYBN Glycinin G2 OS=Glycine max OX=3847 GN=GY2 PE=1 SV=2	Yes	Yes	No	No	No
IAEGHPL	sp|P01070|ITRA_SOYBN Trypsin inhibitor A OS=Glycine max OX=3847 GN=KTI3 PE=1 SV=2	Yes	Yes	No	No	No
TFEEPQQPQ	sp|P04776|GLYG1_SOYBN Glycinin G1 OS=Glycine max OX=3847 GN=GY1 PE=1 SV=2	Yes	Yes	No	No	No
GNGIFG	sp|P04405|GLYG2_SOYBN Glycinin G2 OS=Glycine max OX=3847 GN=GY2 PE=1 SV=2	Yes	Yes	No	No	No
NIGQNSSPDI	sp|P04405|GLYG2_SOYBN Glycinin G2 OS=Glycine max OX=3847 GN=GY2 PE=1 SV=2	Yes	Yes	No	No	No
LFEITPE	sp|P11827|GLCAP_SOYBN Beta-conglycinin alpha subunit OS=Glycine max OX=3847 GN=CG-1 PE=1 SV=2	Yes	Yes	No	No	No
VVEDLPEGPA	sp|P01070|ITRA_SOYBN Trypsin inhibitor A OS=Glycine max OX=3847 GN=KTI3 PE=1 SV=2	Yes	Yes	No	No	No
NLQGENEGEDKGAIV	sp|P04776|GLYG1_SOYBN Glycinin G1 OS=Glycine max OX=3847 GN=GY1 PE=1 SV=2	Yes	Yes	No	No	No
SFNTNEDIAE	sp|P02858|GLYG4_SOYBN Glycinin G4 OS=Glycine max OX=3847 GN=GY4 PE=1 SV=2	Yes	Yes	No	No	No
VISPPTEEQ	sp|P11828|GLYG3_SOYBN Glycinin G3 OS=Glycine max OX=3847 GN=GY3 PE=1 SV=1	Yes	Yes	No	No	No
NEGEDKGAIV	sp|P04776|GLYG1_SOYBN Glycinin G1 OS=Glycine max OX=3847 GN=GY1 PE=1 SV=2	Yes	Yes	No	No	No
IESEGGLIETWNPNNKP	sp|P04776|GLYG1_SOYBN Glycinin G1 OS=Glycine max OX=3847 GN=GY1 PE=1 SV=2	Yes	Yes	No	No	No
NIGQTSSPDIFNPQ	sp|P11828|GLYG3_SOYBN Glycinin G3 OS=Glycine max OX=3847 GN=GY3 PE=1 SV=1	Yes	Yes	No	No	No
YLAGNPDIEHPET	sp|P04347|GLYG5_SOYBN Glycinin G5 OS=Glycine max OX=3847 GN=GY5 PE=1 SV=1	Yes	Yes	No	No	No
EGGVLIVPQ	sp|P04405|GLYG2_SOYBN Glycinin G2 OS=Glycine max OX=3847 GN=GY2 PE=1 SV=2	Yes	Yes	No	No	No
NGLHLPS	sp|P02858|GLYG4_SOYBN Glycinin G4 OS=Glycine max OX=3847 GN=GY4 PE=1 SV=2	Yes	Yes	No	No	No
HIPAGTPL	sp|Q04672|SBP_SOYBN Sucrose-binding protein OS=Glycine max OX=3847 GN=SBP PE=1 SV=1	Yes	Yes	No	No	No
SVIKPPTDE	sp|P04776|GLYG1_SOYBN Glycinin G1 OS=Glycine max OX=3847 GN=GY1 PE=1 SV=2	Yes	Yes	No	No	No
PDIEHPET	sp|P04347|GLYG5_SOYBN Glycinin G5 OS=Glycine max OX=3847 GN=GY5 PE=1 SV=1	Yes	Yes	No	No	No

KFLVPPQES	sp|P04776|GLYG1_SOYBN Glycinin G1 OS=Glycine max OX=3847 GN=GY1 PE=1 SV=2	Yes	Yes	No	No	No
VIKPPTDEQ	sp|P04776|GLYG1_SOYBN Glycinin G1 OS=Glycine max OX=3847 GN=GY1 PE=1 SV=2	Yes	Yes	No	No	No
EFDSFDEVHG	sp|P09186|LOX3_SOYBN Seed linoleate 9S-lipoxygenase-3 OS=Glycine max OX=3847 GN=LOX1.3 PE=1 SV=1	Yes	Yes	No	No	No
NGSHLPSYLPYPQ	sp|P04347|GLYG5_SOYBN Glycinin G5 OS=Glycine max OX=3847 GN=GY5 PE=1 SV=1	Yes	Yes	No	No	No
VIKPPTDE	sp|P04776|GLYG1_SOYBN Glycinin G1 OS=Glycine max OX=3847 GN=GY1 PE=1 SV=2	Yes	Yes	No	No	No
SFLVPPQES	sp|P04405|GLYG2_SOYBN Glycinin G2 OS=Glycine max OX=3847 GN=GY2 PE=1 SV=2	Yes	Yes	No	No	No
FVVPPGHP	sp|Q04672|SBP_SOYBN Sucrose-binding protein OS=Glycine max OX=3847 GN=SBP PE=1 SV=1	Yes	Yes	No	No	No
AGNPDIEHPET	sp|P04347|GLYG5_SOYBN Glycinin G5 OS=Glycine max OX=3847 GN=GY5 PE=1 SV=1	Yes	Yes	No	No	No
NSSPDI	sp|P04405|GLYG2_SOYBN Glycinin G2 OS=Glycine max OX=3847 GN=GY2 PE=1 SV=2	Yes	Yes	No	No	No
IKPPTDEQ	sp|P04776|GLYG1_SOYBN Glycinin G1 OS=Glycine max OX=3847 GN=GY1 PE=1 SV=2	Yes	Yes	No	No	No
DLNFTPN	sp|P09439|LOX2_SOYBN Seed linoleate 9S-lipoxygenase-2 OS=Glycine max OX=3847 GN=LOX1.2 PE=2 SV=1	Yes	Yes	No	No	No
NEPWWPK	sp|P09186|LOX3_SOYBN Seed linoleate 9S-lipoxygenase-3 OS=Glycine max OX=3847 GN=LOX1.3 PE=1 SV=1	Yes	Yes	No	No	No
LVINEGEANIE	sp|P11827|GLCAP_SOYBN Beta-conglycinin alpha subunit OS=Glycine max OX=3847 GN=CG-1 PE=1 SV=2	Yes	Yes	No	No	No
TLEDIPNHG	sp|P09186|LOX3_SOYBN Seed linoleate 9S-lipoxygenase-3 OS=Glycine max OX=3847 GN=LOX1.3 PE=1 SV=1	Yes	Yes	No	No	No
DLHEGGIKLPTEV	sp|P09439|LOX2_SOYBN Seed linoleate 9S-lipoxygenase-2 OS=Glycine max OX=3847 GN=LOX1.2 PE=2 SV=1	Yes	Yes	No	No	No
YVVNPDNDEN	sp|P11827|GLCAP_SOYBN Beta-conglycinin alpha subunit OS=Glycine max OX=3847 GN=CG-1 PE=1 SV=2	Yes	Yes	No	No	No
LFEITPEKNPQ	sp|P11827|GLCAP_SOYBN Beta-conglycinin alpha subunit OS=Glycine max OX=3847 GN=CG-1 PE=1 SV=2	Yes	Yes	No	No	No
DEDEQIPSHPP	sp|P02858|GLYG4_SOYBN Glycinin G4 OS=Glycine max OX=3847 GN=GY4 PE=1 SV=2	Yes	Yes	No	No	No
GGLSVIKPPTDEQ	sp|P04776|GLYG1_SOYBN Glycinin G1 OS=Glycine max OX=3847 GN=GY1 PE=1 SV=2	Yes	Yes	No	No	No

SSDLKPG	sp|Q04672|SBP_SOYBN Sucrose-binding protein OS=Glycine max OX=3847 GN=SBP PE=1 SV=1	Yes	Yes	No	No	No
TSSPDIFNPQ	sp|P11828|GLYG3_SOYBN Glycinin G3 OS=Glycine max OX=3847 GN=GY3 PE=1 SV=1	Yes	Yes	No	No	No
PDIEYPET	sp|P02858|GLYG4_SOYBN Glycinin G4 OS=Glycine max OX=3847 GN=GY4 PE=1 SV=2	Yes	Yes	No	No	No
SLPHPAG	sp|P09439|LOX2_SOYBN Seed linoleate 9S-lipoxygenase-2 OS=Glycine max OX=3847 GN=LOX1.2 PE=2 SV=1	Yes	Yes	No	No	No
DLNFTPR	sp|P09186|LOX3_SOYBN Seed linoleate 9S-lipoxygenase-3 OS=Glycine max OX=3847 GN=LOX1.3 PE=1 SV=1	Yes	Yes	No	No	No
KYEGNWGPL	sp|P02858|GLYG4_SOYBN Glycinin G4 OS=Glycine max OX=3847 GN=GY4 PE=1 SV=2	Yes	Yes	No	No	No
VESEGGLIET	sp|P04347|GLYG5_SOYBN Glycinin G5 OS=Glycine max OX=3847 GN=GY5 PE=1 SV=1	Yes	Yes	No	No	No
DLPEGPA	sp|P01070|ITRA_SOYBN Trypsin inhibitor A OS=Glycine max OX=3847 GN=KTI3 PE=1 SV=2	Yes	Yes	No	No	No
DIEYPET	sp|P02858|GLYG4_SOYBN Glycinin G4 OS=Glycine max OX=3847 GN=GY4 PE=1 SV=2	Yes	Yes	No	No	No
HNIGQTSSPDIYNPQ	sp|P04776|GLYG1_SOYBN Glycinin G1 OS=Glycine max OX=3847 GN=GY1 PE=1 SV=2	Yes	Yes	No	No	No
SQVFLPADEGVES	sp|P09186|LOX3_SOYBN Seed linoleate 9S-lipoxygenase-3 OS=Glycine max OX=3847 GN=LOX1.3 PE=1 SV=1	Yes	Yes	No	No	No
TLLLPS	sp|P09186|LOX3_SOYBN Seed linoleate 9S-lipoxygenase-3 OS=Glycine max OX=3847 GN=LOX1.3 PE=1 SV=1	Yes	Yes	No	No	No
FEEPQQPQ	sp|P04776|GLYG1_SOYBN Glycinin G1 OS=Glycine max OX=3847 GN=GY1 PE=1 SV=2	Yes	Yes	No	No	No
TSSPDIYNPQ	sp|P04776|GLYG1_SOYBN Glycinin G1 OS=Glycine max OX=3847 GN=GY1 PE=1 SV=2	Yes	Yes	No	No	No
NDGTLRPL	sp|P09186|LOX3_SOYBN Seed linoleate 9S-lipoxygenase-3 OS=Glycine max OX=3847 GN=LOX1.3 PE=1 SV=1	Yes	Yes	No	No	No
NFNNQLDQNPR	sp|P04347|GLYG5_SOYBN Glycinin G5 OS=Glycine max OX=3847 GN=GY5 PE=1 SV=1	Yes	Yes	No	No	No
QNIGQNSSPDI	sp|P04405|GLYG2_SOYBN Glycinin G2 OS=Glycine max OX=3847 GN=GY2 PE=1 SV=2	Yes	Yes	No	No	No
NSSPDIYNPQ	sp|P04405|GLYG2_SOYBN Glycinin G2 OS=Glycine max OX=3847 GN=GY2 PE=1 SV=2	Yes	Yes	No	No	No
REDGTLKPV	sp|P08170|LOX1_SOYBN Seed linoleate 13S-lipoxygenase-1 OS=Glycine max OX=3847 GN=LOX1.1 PE=1 SV=2	Yes	Yes	No	No	No

KTNDTPM	sp|P04776|GLYG1_SOYBN Glycinin G1 OS=Glycine max OX=3847 GN=GY1 PE=1 SV=2	Yes	Yes	No	No	No
LRSPDDE	sp|P04347|GLYG5_SOYBN Glycinin G5 OS=Glycine max OX=3847 GN=GY5 PE=1 SV=1	Yes	Yes	No	No	No
SVVHPI	sp|P09186|LOX3_SOYBN Seed linoleate 9S-lipoxygenase-3 OS=Glycine max OX=3847 GN=LOX1.3 PE=1 SV=1	Yes	Yes	No	No	No
SVISPPTEEQ	sp|P11828|GLYG3_SOYBN Glycinin G3 OS=Glycine max OX=3847 GN=GY3 PE=1 SV=1	Yes	Yes	No	No	No
NIGQTSSPDIYNPQ	sp|P04776|GLYG1_SOYBN Glycinin G1 OS=Glycine max OX=3847 GN=GY1 PE=1 SV=2	Yes	Yes	No	No	No
NDLGNPDHGEN	sp|P09439|LOX2_SOYBN Seed linoleate 9S-lipoxygenase-2 OS=Glycine max OX=3847 GN=LOX1.2 PE=2 SV=1	Yes	Yes	No	No	No
VINEGEANIE	sp|P11827|GLCAP_SOYBN Beta-conglycinin alpha subunit OS=Glycine max OX=3847 GN=CG-1 PE=1 SV=2	Yes	Yes	No	No	No
VEDLPEGPA	sp|P01070|ITRA_SOYBN Trypsin inhibitor A OS=Glycine max OX=3847 GN=KTI3 PE=1 SV=2	Yes	Yes	No	No	No
NPDIEHPET	sp|P04347|GLYG5_SOYBN Glycinin G5 OS=Glycine max OX=3847 GN=GY5 PE=1 SV=1	Yes	Yes	No	No	No
HLPSYSPYP	sp|P02858|GLYG4_SOYBN Glycinin G4 OS=Glycine max OX=3847 GN=GY4 PE=1 SV=2	Yes	Yes	No	No	No
SVIKPPTDEQ	sp|P04776|GLYG1_SOYBN Glycinin G1 OS=Glycine max OX=3847 GN=GY1 PE=1 SV=2	Yes	Yes	No	No	No
DFVLDNEGNPL	sp|P01070|ITRA_SOYBN Trypsin inhibitor A OS=Glycine max OX=3847 GN=KTI3 PE=1 SV=2	Yes	Yes	No	No	No
FIAEGHP	sp|P01070|ITRA_SOYBN Trypsin inhibitor A OS=Glycine max OX=3847 GN=KTI3 PE=1 SV=2	Yes	Yes	No	No	No
SVPGVS	sp|P09439|LOX2_SOYBN Seed linoleate 9S-lipoxygenase-2 OS=Glycine max OX=3847 GN=LOX1.2 PE=2 SV=1	Yes	Yes	No	No	No
NNQLDQTPR	sp|P02858|GLYG4_SOYBN Glycinin G4 OS=Glycine max OX=3847 GN=GY4 PE=1 SV=2	Yes	Yes	No	No	No
SVIKPPTDEQQQRPQ	sp|P04776|GLYG1_SOYBN Glycinin G1 OS=Glycine max OX=3847 GN=GY1 PE=1 SV=2	Yes	Yes	No	No	No
QNIGQNSSPDIYNPQ	sp|P04405|GLYG2_SOYBN Glycinin G2 OS=Glycine max OX=3847 GN=GY2 PE=1 SV=2	Yes	Yes	No	No	No
EGNWGPL	sp|P02858|GLYG4_SOYBN Glycinin G4 OS=Glycine max OX=3847 GN=GY4 PE=1 SV=2	Yes	Yes	No	No	No
SVVEDLPEGPAV	sp|P01070|ITRA_SOYBN Trypsin inhibitor A OS=Glycine max OX=3847 GN=KTI3 PE=1 SV=2	Yes	Yes	No	No	No

IFEEDKDFET	sp|Q04672|SBP_SOYBN Sucrose-binding protein OS=Glycine max OX=3847 GN=SBP PE=1 SV=1	Yes	Yes	No	No	No
NGIYSPH	sp|P02858|GLYG4_SOYBN Glycinin G4 OS=Glycine max OX=3847 GN=GY4 PE=1 SV=2	Yes	Yes	No	No	No
VESEGGLIQT	sp|P02858|GLYG4_SOYBN Glycinin G4 OS=Glycine max OX=3847 GN=GY4 PE=1 SV=2	Yes	Yes	No	No	No
NDGTLRP	sp|P09186|LOX3_SOYBN Seed linoleate 9S-lipoxygenase-3 OS=Glycine max OX=3847 GN=LOX1.3 PE=1 SV=1	Yes	Yes	No	No	No
IAEGHPL	sp|P01070|ITRA_SOYBN Trypsin inhibitor A OS=Glycine max OX=3847 GN=KTI3 PE=1 SV=2	Yes	Yes	No	apical/basolateral	No

Appendix Table 3 Summary matrix reporting the unique peptides in each compartment (digesta, apical, basolateral), their overlaps, and unique distributions across infant- and adult-like models for Human Milk.

Sequence	FASTA Header	Apical	Basolateral	Digesta	Exclusive Infant	Exclusive Adult
VVPYPQ	sp|P05814|CASB_HUMAN Beta-casein OS=Homo sapiens OX=9606 GN=CSN2 PE=1 SV=4	No	No	Yes	No	No
LVDSEGWVKAQYEGRLS	sp|P01833|PIGR_HUMAN Polymeric immunoglobulin receptor OS=Homo sapiens OX=9606 GN=PIGR PE=1 SV=4	No	No	Yes	No	No
KDEY	sp|Q9Y4H2|IRS2_HUMAN Insulin receptor substrate 2 OS=Homo sapiens OX=9606 GN=IRS2 PE=1 SV=2	No	No	Yes	No	No
LNQEL	sp|P05814|CASB_HUMAN Beta-casein OS=Homo sapiens OX=9606 GN=CSN2 PE=1 SV=4	No	No	Yes	No	No
KQIGLYPV	sp|P01833|PIGR_HUMAN Polymeric immunoglobulin receptor OS=Homo sapiens OX=9606 GN=PIGR PE=1 SV=4	No	No	Yes	No	No
KLAP	sp|P04114|APOB_HUMAN Apolipoprotein B-100 OS=Homo sapiens OX=9606 GN=APOB PE=1 SV=3	No	No	Yes	No	No
TLMP	sp|P49815|TSC2_HUMAN Tuberin OS=Homo sapiens OX=9606 GN=TSC2 PE=1 SV=2	No	No	Yes	No	No
VKPS	sp|P98164|LRP2_HUMAN Low-density lipoprotein receptor-related protein 2 OS=Homo sapiens OX=9606 GN=LRP2 PE=1 SV=3	No	No	Yes	No	No
PKSF	sp|P11388|TOP2A_HUMAN DNA topoisomerase 2-alpha OS=Homo sapiens OX=9606 GN=TOP2A PE=1 SV=3	No	No	Yes	No	No
VLTD	sp|Q96RW7|HMCN1_HUMAN Hemicentin-1 OS=Homo sapiens OX=9606 GN=HMCN1 PE=1 SV=2	No	No	Yes	No	No
SEEDMVGRPLP	sp|P47989|XDH_HUMAN Xanthine dehydrogenase/oxidase OS=Homo sapiens OX=9606 GN=XDH PE=1 SV=4	No	No	Yes	No	No
YPPQ	sp|Q09472|EP300_HUMAN Histone acetyltransferase p300 OS=Homo sapiens OX=9606 GN=EP300 PE=1 SV=2	No	No	Yes	No	No
KPEEFTPLDPT	sp|P47989|XDH_HUMAN Xanthine dehydrogenase/oxidase OS=Homo sapiens OX=9606 GN=XDH PE=1 SV=4	No	No	Yes	No	No
LPQNILPL	sp|P05814|CASB_HUMAN Beta-casein OS=Homo sapiens OX=9606 GN=CSN2 PE=1 SV=4	No	No	Yes	No	No
FDPQIP	sp|P05814|CASB_HUMAN Beta-casein OS=Homo sapiens OX=9606 GN=CSN2 PE=1 SV=4	No	No	Yes	No	No
MQQVPQPIPQT	sp|P05814|CASB_HUMAN Beta-casein OS=Homo sapiens OX=9606 GN=CSN2 PE=1 SV=4	No	No	Yes	No	No

VLVGEPTTSPI	sp|Q9UKN1|MUC12_HUMAN Mucin-12 OS=Homo sapiens OX=9606 GN=MUC12 PE=1 SV=2	No	No	Yes	No	No
LPILNQPS	sp|Q99541|PLIN2_HUMAN Perilipin-2 OS=Homo sapiens OX=9606 GN=PLIN2 PE=1 SV=2	No	No	Yes	No	No
QDYE	sp|Q01814|AT2B2_HUMAN Plasma membrane calcium-transporting ATPase 2 OS=Homo sapiens OX=9606 GN=ATP2B2 PE=1 SV=2	No	No	Yes	No	No
LALPPQP	sp|P05814|CASB_HUMAN Beta-casein OS=Homo sapiens OX=9606 GN=CSN2 PE=1 SV=4	No	No	Yes	No	No
VVPYP	sp|P05814|CASB_HUMAN Beta-casein OS=Homo sapiens OX=9606 GN=CSN2 PE=1 SV=4	No	No	Yes	No	No
WLW	sp|Q9Y6R7|FCGBP_HUMAN IgGFc-binding protein OS=Homo sapiens OX=9606 GN=FCGBP PE=1 SV=3	No	No	Yes	No	No
TTGLV	sp|Q14689|DIP2A_HUMAN Disco-interacting protein 2 homolog A OS=Homo sapiens OX=9606 GN=DIP2A PE=1 SV=2	No	No	Yes	No	No
ISADDVPGSNIT	sp|P47989|XDH_HUMAN Xanthine dehydrogenase/oxidase OS=Homo sapiens OX=9606 GN=XDH PE=1 SV=4	No	No	Yes	No	No
YFPK	sp|Q5JRA6|TGO1_HUMAN Transport and Golgi organization protein 1 homolog OS=Homo sapiens OX=9606 GN=MIA3 PE=1 SV=1	No	No	Yes	No	No
QKDN	sp|O15146|MUSK_HUMAN Muscle, skeletal receptor tyrosine-protein kinase OS=Homo sapiens OX=9606 GN=MUSK PE=1 SV=1	No	No	Yes	No	No
QPAVVLPVPQ	sp|P05814|CASB_HUMAN Beta-casein OS=Homo sapiens OX=9606 GN=CSN2 PE=1 SV=4	No	No	Yes	No	No
IYPSFQPQP	sp|P05814|CASB_HUMAN Beta-casein OS=Homo sapiens OX=9606 GN=CSN2 PE=1 SV=4	No	No	Yes	No	No
IYPVTQP	sp|P05814|CASB_HUMAN Beta-casein OS=Homo sapiens OX=9606 GN=CSN2 PE=1 SV=4	No	No	Yes	No	No
FQEVPK	sp|P47989|XDH_HUMAN Xanthine dehydrogenase/oxidase OS=Homo sapiens OX=9606 GN=XDH PE=1 SV=4	No	No	Yes	No	No
WLNPDPS	sp|P10451|OSTP_HUMAN Osteopontin OS=Homo sapiens OX=9606 GN=SPP1 PE=1 SV=1	No	No	Yes	No	No
FVNEESTIPR	sp|P01833|PIGR_HUMAN Polymeric immunoglobulin receptor OS=Homo sapiens OX=9606 GN=PIGR PE=1 SV=4	No	No	Yes	No	No
RPNLHPS	sp|P07498|CASK_HUMAN Kappa-casein OS=Homo sapiens OX=9606 GN=CSN3 PE=1 SV=3	No	No	Yes	No	No
VPFPP	sp|P47710|CASA1_HUMAN Alpha-S1-casein OS=Homo sapiens OX=9606 GN=CSN1S1 PE=1 SV=1	No	No	Yes	No	No

VVLPVP	sp|P05814|CASB_HUMAN Beta-casein OS=Homo sapiens OX=9606 GN=CSN2 PE=1 SV=4	No	No	Yes	No	No
INNPYVPR	sp|P07498|CASK_HUMAN Kappa-casein OS=Homo sapiens OX=9606 GN=CSN3 PE=1 SV=3	No	No	Yes	No	No
KPEEFTPLDPTQEPIFPPE	sp|P47989|XDH_HUMAN Xanthine dehydrogenase/oxidase OS=Homo sapiens OX=9606 GN=XDH PE=1 SV=4	No	No	Yes	No	No
NKYPDA	sp|P10451|OSTP_HUMAN Osteopontin OS=Homo sapiens OX=9606 GN=SPP1 PE=1 SV=1	No	No	Yes	No	No
KVLPIPQ	sp|P05814|CASB_HUMAN Beta-casein OS=Homo sapiens OX=9606 GN=CSN2 PE=1 SV=4	Yes	No	No	apical	No
YVPFPPFSDI	sp|P47710|CASA1_HUMAN Alpha-S1-casein OS=Homo sapiens OX=9606 GN=CSN1S1 PE=1 SV=1	Yes	No	No	apical	No
LTDLENLHLPLP	sp|P05814|CASB_HUMAN Beta-casein OS=Homo sapiens OX=9606 GN=CSN2 PE=1 SV=4	Yes	No	No	apical	No
QVPQPIPQ	sp|P05814|CASB_HUMAN Beta-casein OS=Homo sapiens OX=9606 GN=CSN2 PE=1 SV=4	Yes	No	No	apical	No
QDKIYPSFQPQP	sp|P05814|CASB_HUMAN Beta-casein OS=Homo sapiens OX=9606 GN=CSN2 PE=1 SV=4	Yes	No	No	apical	No
VKHEDQQQGEDEHQDK	sp|P05814|CASB_HUMAN Beta-casein OS=Homo sapiens OX=9606 GN=CSN2 PE=1 SV=4	Yes	No	No	apical	No
NIWVPQG	sp|P19835|CEL_HUMAN Bile salt-activated lipase OS=Homo sapiens OX=9606 GN=CEL PE=1 SV=3	Yes	No	No	apical	No
SILAQFAGEDPV	sp|O95714|HERC2_HUMAN E3 ubiquitin-protein ligase HERC2 OS=Homo sapiens OX=9606 GN=HERC2 PE=1 SV=2	Yes	No	No	apical	No
PPKP	sp|Q9Y4H2|IRS2_HUMAN Insulin receptor substrate 2 OS=Homo sapiens OX=9606 GN=IRS2 PE=1 SV=2	Yes	No	No	apical	No
PELM	sp|O95714|HERC2_HUMAN E3 ubiquitin-protein ligase HERC2 OS=Homo sapiens OX=9606 GN=HERC2 PE=1 SV=2	Yes	No	No	apical	No
PQKP	sp|Q07157|ZO1_HUMAN Tight junction protein 1 OS=Homo sapiens OX=9606 GN=TJP1 PE=1 SV=3	Yes	No	No	apical	No
LPPK	sp|Q99102|MUC4_HUMAN Mucin-4 OS=Homo sapiens OX=9606 GN=MUC4 PE=1 SV=5	Yes	No	No	apical	No
VAVS	sp|Q8NDA2|HMCN2_HUMAN Hemicentin-2 OS=Homo sapiens OX=9606 GN=HMCN2 PE=1 SV=4	Yes	No	No	apical	No
VIDGDFIPADPI	sp|P19835|CEL_HUMAN Bile salt-activated lipase OS=Homo sapiens OX=9606 GN=CEL PE=1 SV=3	Yes	No	No	apical	No
WSVP	sp|P05814|CASB_HUMAN Beta-casein OS=Homo sapiens OX=9606 GN=CSN2 PE=1 SV=4	Yes	No	No	apical	No

PAVVLPVPQPEI	sp|P05814|CASB_HUMAN Beta-casein OS=Homo sapiens OX=9606 GN=CSN2 PE=1 SV=4	Yes	No	No	apical	No
QIGLYPV	sp|P01833|PIGR_HUMAN Polymeric immunoglobulin receptor OS=Homo sapiens OX=9606 GN=PIGR PE=1 SV=4	Yes	No	No	apical	No
TIPFFDPQIPK	sp|P05814|CASB_HUMAN Beta-casein OS=Homo sapiens OX=9606 GN=CSN2 PE=1 SV=4	Yes	No	No	apical	No
DLNAPSDWD	sp|P10451|OSTP_HUMAN Osteopontin OS=Homo sapiens OX=9606 GN=SPP1 PE=1 SV=1	Yes	No	No	apical	No
PIINYPQ	sp|O75165|DJC13_HUMAN DnaJ homolog subfamily C member 13 OS=Homo sapiens OX=9606 GN=DNAJC13 PE=1 SV=5	Yes	No	No	apical	No
MEVPK	sp|P05814|CASB_HUMAN Beta-casein OS=Homo sapiens OX=9606 GN=CSN2 PE=1 SV=4	Yes	No	No	apical	No
VVRPH	sp|P07498|CASK_HUMAN Kappa-casein OS=Homo sapiens OX=9606 GN=CSN3 PE=1 SV=3	Yes	No	No	apical	No
QPAVVLPVPQPE	sp|P05814|CASB_HUMAN Beta-casein OS=Homo sapiens OX=9606 GN=CSN2 PE=1 SV=4	Yes	No	No	apical	No
VKHEDQQQGEDEHQDKIYPS	sp|P05814|CASB_HUMAN Beta-casein OS=Homo sapiens OX=9606 GN=CSN2 PE=1 SV=4	Yes	No	No	apical	No
LDPL	sp|Q8NDA2|HMCN2_HUMAN Hemicentin-2 OS=Homo sapiens OX=9606 GN=HMCN2 PE=1 SV=4	Yes	No	No	apical	No
HLPL	sp|P05814|CASB_HUMAN Beta-casein OS=Homo sapiens OX=9606 GN=CSN2 PE=1 SV=4	Yes	No	No	apical	No
NLHLPLPL	sp|P05814|CASB_HUMAN Beta-casein OS=Homo sapiens OX=9606 GN=CSN2 PE=1 SV=4	Yes	No	No	apical/ basolateral	No
QDKIYPSFQPQPL	sp|P05814|CASB_HUMAN Beta-casein OS=Homo sapiens OX=9606 GN=CSN2 PE=1 SV=4	Yes	No	No	apical	No
PLMQQVPQPIPQ	sp|P05814|CASB_HUMAN Beta-casein OS=Homo sapiens OX=9606 GN=CSN2 PE=1 SV=4	Yes	No	No	apical	No
VPYP	sp|P05814|CASB_HUMAN Beta-casein OS=Homo sapiens OX=9606 GN=CSN2 PE=1 SV=4	Yes	No	No	apical	No
DLENLHLPLPL	sp|P05814|CASB_HUMAN Beta-casein OS=Homo sapiens OX=9606 GN=CSN2 PE=1 SV=4	Yes	No	No	apical	No
RRPDIQYPDATDEDITS	sp|P10451|OSTP_HUMAN Osteopontin OS=Homo sapiens OX=9606 GN=SPP1 PE=1 SV=1	Yes	No	No	apical	No
VAGE	sp|Q8NDA2|HMCN2_HUMAN Hemicentin-2 OS=Homo sapiens OX=9606 GN=HMCN2 PE=1 SV=4	Yes	No	No	apical	No
DDISEIQSLASDHSG	sp|Q07157|ZO1_HUMAN Tight junction protein 1 OS=Homo sapiens OX=9606 GN=TJP1 PE=1 SV=3	Yes	No	No	apical	No

LPVPQPEI	sp|P05814|CASB_HUMAN Beta-casein OS=Homo sapiens OX=9606 GN=CSN2 PE=1 SV=4	Yes	No	No	apical	No
PVIPQPE	sp|O43623|SNAI2_HUMAN Zinc finger protein SNAI2 OS=Homo sapiens OX=9606 GN=SNAI2 PE=1 SV=1	Yes	No	No	apical	No
KSPTIPF	sp|P05814|CASB_HUMAN Beta-casein OS=Homo sapiens OX=9606 GN=CSN2 PE=1 SV=4	Yes	No	No	apical	No
LPQNILP	sp|P05814|CASB_HUMAN Beta-casein OS=Homo sapiens OX=9606 GN=CSN2 PE=1 SV=4	Yes	No	No	apical	No
HQIYPVTQPLAPV	sp|P05814|CASB_HUMAN Beta-casein OS=Homo sapiens OX=9606 GN=CSN2 PE=1 SV=4	Yes	No	No	apical	No
ALENPQPHPGWQG	sp|P19835|CEL_HUMAN Bile salt-activated lipase OS=Homo sapiens OX=9606 GN=CEL PE=1 SV=3	Yes	No	No	apical	No
VQLP	sp|O95714|HERC2_HUMAN E3 ubiquitin-protein ligase HERC2 OS=Homo sapiens OX=9606 GN=HERC2 PE=1 SV=2	Yes	No	No	apical	No
HQIYPVTQPL	sp|P05814|CASB_HUMAN Beta-casein OS=Homo sapiens OX=9606 GN=CSN2 PE=1 SV=4	Yes	No	No	apical	No
VGLE	sp|Q9NYQ8|FAT2_HUMAN Protocadherin Fat 2 OS=Homo sapiens OX=9606 GN=FAT2 PE=1 SV=2	Yes	No	No	No	apical
PFVEPIP	sp|P05814|CASB_HUMAN Beta-casein OS=Homo sapiens OX=9606 GN=CSN2 PE=1 SV=4	Yes	No	No	No	apical
WWG	sp|Q7Z7M0|MEGF8_HUMAN Multiple epidermal growth factor-like domains protein 8 OS=Homo sapiens OX=9606 GN=MEGF8 PE=1 SV=2	Yes	No	No	No	apical
FPPFS	sp|P47710|CASA1_HUMAN Alpha-S1-casein OS=Homo sapiens OX=9606 GN=CSN1S1 PE=1 SV=1	Yes	No	No	No	apical
LLPLP	sp|Q8NDA2|HMCN2_HUMAN Hemicentin-2 OS=Homo sapiens OX=9606 GN=HMCN2 PE=1 SV=4	Yes	No	No	No	apical
LQPL	sp|P05814|CASB_HUMAN Beta-casein OS=Homo sapiens OX=9606 GN=CSN2 PE=1 SV=4	Yes	No	No	No	apical
NEESTIPR	sp|P01833|PIGR_HUMAN Polymeric immunoglobulin receptor OS=Homo sapiens OX=9606 GN=PIGR PE=1 SV=4	Yes	No	No	No	No
AVPV	sp|P05814|CASB_HUMAN Beta-casein OS=Homo sapiens OX=9606 GN=CSN2 PE=1 SV=4	Yes	No	No	No	No
PSFQPQPL	sp|P05814|CASB_HUMAN Beta-casein OS=Homo sapiens OX=9606 GN=CSN2 PE=1 SV=4	Yes	No	No	No	No
QNPSESSEPIP	sp|P47710|CASA1_HUMAN Alpha-S1-casein OS=Homo sapiens OX=9606 GN=CSN1S1 PE=1 SV=1	Yes	No	No	No	No

YLPN	sp|P07498|CASK_HUMAN Kappa-casein OS=Homo sapiens OX=9606 GN=CSN3 PE=1 SV=3	Yes	No	No	No	No
ENLHLPLP	sp|P05814|CASB_HUMAN Beta-casein OS=Homo sapiens OX=9606 GN=CSN2 PE=1 SV=4	Yes	No	No	No	No
TTSW	sp|Q99102|MUC4_HUMAN Mucin-4 OS=Homo sapiens OX=9606 GN=MUC4 PE=1 SV=5	Yes	No	No	No	No
ALENPQPHPGWQGT	sp|P19835|CEL_HUMAN Bile salt-activated lipase OS=Homo sapiens OX=9606 GN=CEL PE=1 SV=3	Yes	No	No	No	No
LALPPQPL	sp|P05814|CASB_HUMAN Beta-casein OS=Homo sapiens OX=9606 GN=CSN2 PE=1 SV=4	Yes	No	No	No	No
YPVTQPL	sp|P05814|CASB_HUMAN Beta-casein OS=Homo sapiens OX=9606 GN=CSN2 PE=1 SV=4	Yes	No	No	No	No
VLPVPQP	sp|P05814|CASB_HUMAN Beta-casein OS=Homo sapiens OX=9606 GN=CSN2 PE=1 SV=4	Yes	No	No	No	No
NSYP	sp|P07498|CASK_HUMAN Kappa-casein OS=Homo sapiens OX=9606 GN=CSN3 PE=1 SV=3	Yes	No	No	No	No
FRRPDIQYPDATDEDIT	sp|P10451|OSTP_HUMAN Osteopontin OS=Homo sapiens OX=9606 GN=SPP1 PE=1 SV=1	Yes	No	No	No	No
VSLG	sp|O43623|SNAI2_HUMAN Zinc finger protein SNAI2 OS=Homo sapiens OX=9606 GN=SNAI2 PE=1 SV=1	Yes	No	No	No	No
VTVG	sp|Q9NYQ8|FAT2_HUMAN Protocadherin Fat 2 OS=Homo sapiens OX=9606 GN=FAT2 PE=1 SV=2	Yes	No	No	No	No
PFPPFS	sp|P47710|CASA1_HUMAN Alpha-S1-casein OS=Homo sapiens OX=9606 GN=CSN1S1 PE=1 SV=1	Yes	No	No	No	No
PADPI	sp|P19835|CEL_HUMAN Bile salt-activated lipase OS=Homo sapiens OX=9606 GN=CEL PE=1 SV=3	Yes	No	No	No	No
RPDIQYPDATDEDIT	sp|P10451|OSTP_HUMAN Osteopontin OS=Homo sapiens OX=9606 GN=SPP1 PE=1 SV=1	Yes	No	No	No	No
SNPL	sp|Q9NYQ8|FAT2_HUMAN Protocadherin Fat 2 OS=Homo sapiens OX=9606 GN=FAT2 PE=1 SV=2	Yes	No	No	No	No
IYPSFQP	sp|P05814|CASB_HUMAN Beta-casein OS=Homo sapiens OX=9606 GN=CSN2 PE=1 SV=4	Yes	No	No	No	No
VQCD	sp|O95714|HERC2_HUMAN E3 ubiquitin-protein ligase HERC2 OS=Homo sapiens OX=9606 GN=HERC2 PE=1 SV=2	Yes	No	No	No	No
LTDDL	sp|Q9H9A6|LRC40_HUMAN Leucine-rich repeat-containing protein 40 OS=Homo sapiens OX=9606 GN=LRRC40 PE=1 SV=1	Yes	No	No	No	No
QNPSESSEPIPL	sp|P47710|CASA1_HUMAN Alpha-S1-casein OS=Homo sapiens OX=9606 GN=CSN1S1 PE=1 SV=1	Yes	No	No	No	No

LQNPSESSEPI	sp|P47710|CASA1_HUMAN Alpha-S1-casein OS=Homo sapiens OX=9606 GN=CSN1S1 PE=1 SV=1	Yes	No	No	No	No
DKIYPSFQPQPL	sp|P05814|CASB_HUMAN Beta-casein OS=Homo sapiens OX=9606 GN=CSN2 PE=1 SV=4	Yes	No	No	No	No
VDPK	sp|P10451|OSTP_HUMAN Osteopontin OS=Homo sapiens OX=9606 GN=SPP1 PE=1 SV=1	Yes	No	No	No	No
PSFQPQP	sp|P05814|CASB_HUMAN Beta-casein OS=Homo sapiens OX=9606 GN=CSN2 PE=1 SV=4	Yes	No	No	No	No
TLALPPQPL	sp|P05814|CASB_HUMAN Beta-casein OS=Homo sapiens OX=9606 GN=CSN2 PE=1 SV=4	Yes	No	No	No	No
VPVIDGDFIPADPI	sp|P19835|CEL_HUMAN Bile salt-activated lipase OS=Homo sapiens OX=9606 GN=CEL PE=1 SV=3	Yes	No	No	No	No
IDGDFIPADPI	sp|P19835|CEL_HUMAN Bile salt-activated lipase OS=Homo sapiens OX=9606 GN=CEL PE=1 SV=3	Yes	No	No	No	No
QLVP	sp|Q8NDA2|HMCN2_HUMAN Hemicentin-2 OS=Homo sapiens OX=9606 GN=HMCN2 PE=1 SV=4	Yes	No	No	No	No
VWD	sp|Q8NDA2|HMCN2_HUMAN Hemicentin-2 OS=Homo sapiens OX=9606 GN=HMCN2 PE=1 SV=4	Yes	No	No	No	No
KSPIFGPEEV	sp|P01833|PIGR_HUMAN Polymeric immunoglobulin receptor OS=Homo sapiens OX=9606 GN=PIGR PE=1 SV=4	Yes	No	No	No	No
DSPL	sp|Q99102|MUC4_HUMAN Mucin-4 OS=Homo sapiens OX=9606 GN=MUC4 PE=1 SV=5	Yes	No	No	No	No
FLPQ	sp|P05814|CASB_HUMAN Beta-casein OS=Homo sapiens OX=9606 GN=CSN2 PE=1 SV=4	Yes	No	No	No	No
TLALPPQP	sp|P05814|CASB_HUMAN Beta-casein OS=Homo sapiens OX=9606 GN=CSN2 PE=1 SV=4	Yes	No	No	No	No
LLDT	sp|O60658|PDE8A_HUMAN High affinity cAMP-specific and IBMX-insensitive 3,5-cyclic phosphodiesterase 8A OS=Homo sapiens OX=9606 GN=PDE8A PE=1 SV=2	Yes	No	No	No	No
FDPQ	sp|P05814|CASB_HUMAN Beta-casein OS=Homo sapiens OX=9606 GN=CSN2 PE=1 SV=4	Yes	No	No	No	No
LVTP	sp|Q9NYQ8|FAT2_HUMAN Protocadherin Fat 2 OS=Homo sapiens OX=9606 GN=FAT2 PE=1 SV=2	Yes	No	No	No	No
NENSHVQVP	sp|P47710|CASA1_HUMAN Alpha-S1-casein OS=Homo sapiens OX=9606 GN=CSN1S1 PE=1 SV=1	Yes	No	No	No	No
AQPAVVLPVPQPE	sp|P05814|CASB_HUMAN Beta-casein OS=Homo sapiens OX=9606 GN=CSN2 PE=1 SV=4	Yes	No	No	No	No

SNPT	sp|P47710|CASA1_HUMAN Alpha-S1-casein OS=Homo sapiens OX=9606 GN=CSN1S1 PE=1 SV=1	Yes	No	No	No	No
TLDN	sp|O95714|HERC2_HUMAN E3 ubiquitin-protein ligase HERC2 OS=Homo sapiens OX=9606 GN=HERC2 PE=1 SV=2	Yes	No	No	No	No
WSVPQP	sp|P05814|CASB_HUMAN Beta-casein OS=Homo sapiens OX=9606 GN=CSN2 PE=1 SV=4	Yes	No	No	No	No
YLPNSHPPT	sp|P07498|CASK_HUMAN Kappa-casein OS=Homo sapiens OX=9606 GN=CSN3 PE=1 SV=3	Yes	No	No	No	No
QPQPL	sp|P05814|CASB_HUMAN Beta-casein OS=Homo sapiens OX=9606 GN=CSN2 PE=1 SV=4	Yes	No	No	No	No
LPNSHPPT	sp|P07498|CASK_HUMAN Kappa-casein OS=Homo sapiens OX=9606 GN=CSN3 PE=1 SV=3	Yes	No	No	No	No
YVPFPPFS	sp|P47710|CASA1_HUMAN Alpha-S1-casein OS=Homo sapiens OX=9606 GN=CSN1S1 PE=1 SV=1	Yes	No	No	No	No
YAQP	sp|Q07157|ZO1_HUMAN Tight junction protein 1 OS=Homo sapiens OX=9606 GN=TJP1 PE=1 SV=3	Yes	No	No	No	No
YPTP	sp|Q8NDA2|HMCN2_HUMAN Hemicentin-2 OS=Homo sapiens OX=9606 GN=HMCN2 PE=1 SV=4	Yes	No	No	No	No
LGTV	sp|Q9NYQ8|FAT2_HUMAN Protocadherin Fat 2 OS=Homo sapiens OX=9606 GN=FAT2 PE=1 SV=2	Yes	No	No	No	No
LSTGDANLPGN	sp|P19835|CEL_HUMAN Bile salt-activated lipase OS=Homo sapiens OX=9606 GN=CEL PE=1 SV=3	Yes	No	No	No	No
PVIDGDFIPADPI	sp|P19835|CEL_HUMAN Bile salt-activated lipase OS=Homo sapiens OX=9606 GN=CEL PE=1 SV=3	Yes	No	No	No	No
TGDPNMGDSAVPT	sp|P19835|CEL_HUMAN Bile salt-activated lipase OS=Homo sapiens OX=9606 GN=CEL PE=1 SV=3	Yes	No	No	No	No
DLENLHLPLP	sp|P05814|CASB_HUMAN Beta-casein OS=Homo sapiens OX=9606 GN=CSN2 PE=1 SV=4	Yes	No	No	No	No
MQQVPQPIP	sp|P05814|CASB_HUMAN Beta-casein OS=Homo sapiens OX=9606 GN=CSN2 PE=1 SV=4	Yes	No	No	No	No
TESWAQDPSQEN	sp|P19835|CEL_HUMAN Bile salt-activated lipase OS=Homo sapiens OX=9606 GN=CEL PE=1 SV=3	Yes	No	No	No	No
TMC	sp|O75165|DJC13_HUMAN DnaJ homolog subfamily C member 13 OS=Homo sapiens OX=9606 GN=DNAJC13 PE=1 SV=5	Yes	No	No	No	No
PPFSDISNPT	sp|P47710|CASA1_HUMAN Alpha-S1-casein OS=Homo sapiens OX=9606 GN=CSN1S1 PE=1 SV=1	Yes	No	No	No	No
YPFVEPI	sp|P05814|CASB_HUMAN Beta-casein OS=Homo sapiens OX=9606 GN=CSN2 PE=1 SV=4	Yes	No	No	No	No

SQLG	sp|Q07954|LRP1_HUMAN Prolow-density lipoprotein receptor-related protein 1 OS=Homo sapiens OX=9606 GN=LRP1 PE=1 SV=2	Yes	No	No	No	No
IIEGEPN	sp|P01833|PIGR_HUMAN Polymeric immunoglobulin receptor OS=Homo sapiens OX=9606 GN=PIGR PE=1 SV=4	Yes	No	No	No	No
QLTP	sp|Q9NYQ8|FAT2_HUMAN Protocadherin Fat 2 OS=Homo sapiens OX=9606 GN=FAT2 PE=1 SV=2	Yes	No	No	No	No
NPVP	sp|Q8NDA2|HMCN2_HUMAN Hemicentin-2 OS=Homo sapiens OX=9606 GN=HMCN2 PE=1 SV=4	Yes	No	No	No	No
PQQVVPYPQ	sp|P05814|CASB_HUMAN Beta-casein OS=Homo sapiens OX=9606 GN=CSN2 PE=1 SV=4	Yes	No	No	No	No
VKHEDQQQGEDEH	sp|P05814|CASB_HUMAN Beta-casein OS=Homo sapiens OX=9606 GN=CSN2 PE=1 SV=4	Yes	No	No	No	No
VLDA	sp|Q07954|LRP1_HUMAN Prolow-density lipoprotein receptor-related protein 1 OS=Homo sapiens OX=9606 GN=LRP1 PE=1 SV=2	Yes	No	No	No	No
ALENPQPHPG	sp|P19835|CEL_HUMAN Bile salt-activated lipase OS=Homo sapiens OX=9606 GN=CEL PE=1 SV=3	Yes	No	No	No	No
QLSN	sp|Q9H9A6|LRC40_HUMAN Leucine-rich repeat-containing protein 40 OS=Homo sapiens OX=9606 GN=LRRC40 PE=1 SV=1	Yes	No	No	No	No
GEDEHQDKIYPSFQPQPL	sp|P05814|CASB_HUMAN Beta-casein OS=Homo sapiens OX=9606 GN=CSN2 PE=1 SV=4	Yes	No	No	No	No
LLNQE	sp|P05814|CASB_HUMAN Beta-casein OS=Homo sapiens OX=9606 GN=CSN2 PE=1 SV=4	Yes	No	No	No	No
VTSP	sp|Q99102|MUC4_HUMAN Mucin-4 OS=Homo sapiens OX=9606 GN=MUC4 PE=1 SV=5	Yes	No	No	No	No
PAVVLPVPQP	sp|P05814|CASB_HUMAN Beta-casein OS=Homo sapiens OX=9606 GN=CSN2 PE=1 SV=4	Yes	No	No	No	No
NMF	sp|Q07954|LRP1_HUMAN Prolow-density lipoprotein receptor-related protein 1 OS=Homo sapiens OX=9606 GN=LRP1 PE=1 SV=2	Yes	No	No	No	No
YWK	sp|O60658|PDE8A_HUMAN High affinity cAMP-specific and IBMX-insensitive 3,5-cyclic phosphodiesterase 8A OS=Homo sapiens OX=9606 GN=PDE8A PE=1 SV=2	Yes	No	No	No	No
DIQYPDATDEDITS	sp|P10451|OSTP_HUMAN Osteopontin OS=Homo sapiens OX=9606 GN=SPP1 PE=1 SV=1	Yes	No	No	No	No
VRPH	sp|P07498|CASK_HUMAN Kappa-casein OS=Homo sapiens OX=9606 GN=CSN3 PE=1 SV=3	Yes	No	No	No	No

VEDG	sp|Q9NYQ8|FAT2_HUMAN Protocadherin Fat 2 OS=Homo sapiens OX=9606 GN=FAT2 PE=1 SV=2	Yes	No	No	No	No
NPTHQIYPV	sp|P05814|CASB_HUMAN Beta-casein OS=Homo sapiens OX=9606 GN=CSN2 PE=1 SV=4	Yes	No	No	No	No
AVVLPVPQPE	sp|P05814|CASB_HUMAN Beta-casein OS=Homo sapiens OX=9606 GN=CSN2 PE=1 SV=4	Yes	No	No	No	No
ENLHLPLPL	sp|P05814|CASB_HUMAN Beta-casein OS=Homo sapiens OX=9606 GN=CSN2 PE=1 SV=4	Yes	No	No	No	No
GFLP	sp|P05814|CASB_HUMAN Beta-casein OS=Homo sapiens OX=9606 GN=CSN2 PE=1 SV=4	Yes	No	No	No	No
FRRPDIQYPDATDEDITS	sp|P10451|OSTP_HUMAN Osteopontin OS=Homo sapiens OX=9606 GN=SPP1 PE=1 SV=1	Yes	No	No	No	No
KQETLPS	sp|P10451|OSTP_HUMAN Osteopontin OS=Homo sapiens OX=9606 GN=SPP1 PE=1 SV=1	Yes	No	No	No	No
YVPFPPFSDISNPT	sp|P47710|CASA1_HUMAN Alpha-S1-casein OS=Homo sapiens OX=9606 GN=CSN1S1 PE=1 SV=1	Yes	No	No	No	No
YPSFQPQPL	sp|P05814|CASB_HUMAN Beta-casein OS=Homo sapiens OX=9606 GN=CSN2 PE=1 SV=4	Yes	No	No	No	No
MQQVPQP	sp|P05814|CASB_HUMAN Beta-casein OS=Homo sapiens OX=9606 GN=CSN2 PE=1 SV=4	Yes	No	No	No	No
NPLS	sp|Q9NYQ8|FAT2_HUMAN Protocadherin Fat 2 OS=Homo sapiens OX=9606 GN=FAT2 PE=1 SV=2	Yes	No	No	No	No
SDGQLQEGSPI	sp|P01833|PIGR_HUMAN Polymeric immunoglobulin receptor OS=Homo sapiens OX=9606 GN=PIGR PE=1 SV=4	Yes	No	No	No	No
STGDANLPGN	sp|P19835|CEL_HUMAN Bile salt-activated lipase OS=Homo sapiens OX=9606 GN=CEL PE=1 SV=3	Yes	No	No	No	No
VPFPPFS	sp|P47710|CASA1_HUMAN Alpha-S1-casein OS=Homo sapiens OX=9606 GN=CSN1S1 PE=1 SV=1	Yes	No	No	No	No
PDIQYPDATDEDITS	sp|P10451|OSTP_HUMAN Osteopontin OS=Homo sapiens OX=9606 GN=SPP1 PE=1 SV=1	Yes	No	No	No	No
YVPFPPFSD	sp|P47710|CASA1_HUMAN Alpha-S1-casein OS=Homo sapiens OX=9606 GN=CSN1S1 PE=1 SV=1	Yes	No	No	No	No
VLPVPQPE	sp|P05814|CASB_HUMAN Beta-casein OS=Homo sapiens OX=9606 GN=CSN2 PE=1 SV=4	Yes	No	No	No	No
QYVPFPP	sp|P47710|CASA1_HUMAN Alpha-S1-casein OS=Homo sapiens OX=9606 GN=CSN1S1 PE=1 SV=1	Yes	No	No	No	No
NLDV	sp|P08922|ROS1_HUMAN Proto-oncogene tyrosine-protein kinase ROS OS=Homo sapiens OX=9606 GN=ROS1 PE=1 SV=3	Yes	No	No	No	No

VVLPVPQPEIMEV	sp|P05814|CASB_HUMAN Beta-casein OS=Homo sapiens OX=9606 GN=CSN2 PE=1 SV=4	Yes	No	No	No	No
VGSLDGL	sp|Q9Y4H2|IRS2_HUMAN Insulin receptor substrate 2 OS=Homo sapiens OX=9606 GN=IRS2 PE=1 SV=2	Yes	No	No	No	No
VVLPVPQPEIM	sp|P05814|CASB_HUMAN Beta-casein OS=Homo sapiens OX=9606 GN=CSN2 PE=1 SV=4	Yes	No	No	No	No
RRPDIQYPDATDEDIT	sp|P10451|OSTP_HUMAN Osteopontin OS=Homo sapiens OX=9606 GN=SPP1 PE=1 SV=1	Yes	No	No	No	No
PNPL	sp|Q99102|MUC4_HUMAN Mucin-4 OS=Homo sapiens OX=9606 GN=MUC4 PE=1 SV=5	Yes	No	No	No	No
YPSFQPQ	sp|P05814|CASB_HUMAN Beta-casein OS=Homo sapiens OX=9606 GN=CSN2 PE=1 SV=4	Yes	No	No	No	No
QNLLAPQ	sp|P10451|OSTP_HUMAN Osteopontin OS=Homo sapiens OX=9606 GN=SPP1 PE=1 SV=1	Yes	No	No	No	No
PQPIPQ	sp|P05814|CASB_HUMAN Beta-casein OS=Homo sapiens OX=9606 GN=CSN2 PE=1 SV=4	Yes	No	No	No	No
VLPVP	sp|P05814|CASB_HUMAN Beta-casein OS=Homo sapiens OX=9606 GN=CSN2 PE=1 SV=4	Yes	No	No	No	No
RPDIQYPDATDEDITS	sp|P10451|OSTP_HUMAN Osteopontin OS=Homo sapiens OX=9606 GN=SPP1 PE=1 SV=1	Yes	No	No	No	No
LNIWVPQ	sp|P19835|CEL_HUMAN Bile salt-activated lipase OS=Homo sapiens OX=9606 GN=CEL PE=1 SV=3	Yes	No	No	No	No
VPFPPFSD	sp|P47710|CASA1_HUMAN Alpha-S1-casein OS=Homo sapiens OX=9606 GN=CSN1S1 PE=1 SV=1	Yes	No	No	No	No
FQLS	sp|Q8NDA2|HMCN2_HUMAN Hemicentin-2 OS=Homo sapiens OX=9606 GN=HMCN2 PE=1 SV=4	Yes	No	No	No	No
FAGE	sp|O95714|HERC2_HUMAN E3 ubiquitin-protein ligase HERC2 OS=Homo sapiens OX=9606 GN=HERC2 PE=1 SV=2	Yes	No	No	No	No
VTDV	sp|Q99102|MUC4_HUMAN Mucin-4 OS=Homo sapiens OX=9606 GN=MUC4 PE=1 SV=5	Yes	No	No	No	No
NWT	sp|P08922|ROS1_HUMAN Proto-oncogene tyrosine-protein kinase ROS OS=Homo sapiens OX=9606 GN=ROS1 PE=1 SV=3	Yes	No	No	No	No
PAVVLPVPQ	sp|P05814|CASB_HUMAN Beta-casein OS=Homo sapiens OX=9606 GN=CSN2 PE=1 SV=4	Yes	No	No	No	No
RHC	sp|Q99102|MUC4_HUMAN Mucin-4 OS=Homo sapiens OX=9606 GN=MUC4 PE=1 SV=5	Yes	No	No	No	No
IYPFVEPI	sp|P05814|CASB_HUMAN Beta-casein OS=Homo sapiens OX=9606 GN=CSN2 PE=1 SV=4	Yes	No	No	No	No

DGDFIPADPI	sp|P19835|CEL_HUMAN Bile salt-activated lipase OS=Homo sapiens OX=9606 GN=CEL PE=1 SV=3	Yes	No	No	No	No
PQIPK	sp|P05814|CASB_HUMAN Beta-casein OS=Homo sapiens OX=9606 GN=CSN2 PE=1 SV=4	Yes	No	No	No	No
GFLPQ	sp|P05814|CASB_HUMAN Beta-casein OS=Homo sapiens OX=9606 GN=CSN2 PE=1 SV=4	Yes	No	No	No	No
SLSSSEESITE	sp|P05814|CASB_HUMAN Beta-casein OS=Homo sapiens OX=9606 GN=CSN2 PE=1 SV=4	No	Yes	No	No	No
RETIESLSSSEESITE	sp|P05814|CASB_HUMAN Beta-casein OS=Homo sapiens OX=9606 GN=CSN2 PE=1 SV=4	No	Yes	No	No	No
LTDLE	sp|P05814|CASB_HUMAN Beta-casein OS=Homo sapiens OX=9606 GN=CSN2 PE=1 SV=4	No	Yes	No	No	No
DLNAPSDWDSR	sp|P10451|OSTP_HUMAN Osteopontin OS=Homo sapiens OX=9606 GN=SPP1 PE=1 SV=1	No	Yes	No	No	No
WSVPQPK	sp|P05814|CASB_HUMAN Beta-casein OS=Homo sapiens OX=9606 GN=CSN2 PE=1 SV=4	No	Yes	No	No	No
VVLPVPQPEIMEVPK	sp|P05814|CASB_HUMAN Beta-casein OS=Homo sapiens OX=9606 GN=CSN2 PE=1 SV=4	Yes	Yes	No	No	No
QYLPNSHPPT	sp|P07498|CASK_HUMAN Kappa-casein OS=Homo sapiens OX=9606 GN=CSN3 PE=1 SV=3	Yes	Yes	No	No	No
APVHNPI	sp|P05814|CASB_HUMAN Beta-casein OS=Homo sapiens OX=9606 GN=CSN2 PE=1 SV=4	Yes	Yes	No	No	No
MQQVPQPIPQ	sp|P05814|CASB_HUMAN Beta-casein OS=Homo sapiens OX=9606 GN=CSN2 PE=1 SV=4	Yes	Yes	No	No	No
VLPIPQ	sp|P05814|CASB_HUMAN Beta-casein OS=Homo sapiens OX=9606 GN=CSN2 PE=1 SV=4	Yes	Yes	No	No	No
MQQVPQPI	sp|P05814|CASB_HUMAN Beta-casein OS=Homo sapiens OX=9606 GN=CSN2 PE=1 SV=4	Yes	Yes	No	No	No
NLHLPLP	sp|P05814|CASB_HUMAN Beta-casein OS=Homo sapiens OX=9606 GN=CSN2 PE=1 SV=4	Yes	Yes	No	No	No
DLNAPSDWDS	sp|P10451|OSTP_HUMAN Osteopontin OS=Homo sapiens OX=9606 GN=SPP1 PE=1 SV=1	Yes	Yes	No	No	No
LPVPQPE	sp|P05814|CASB_HUMAN Beta-casein OS=Homo sapiens OX=9606 GN=CSN2 PE=1 SV=4	Yes	Yes	No	No	No
QYVPFPPFSDISNPT	sp|P47710|CASA1_HUMAN Alpha-S1-casein OS=Homo sapiens OX=9606 GN=CSN1S1 PE=1 SV=1	Yes	Yes	No	No	No
NNPYVPR	sp|P07498|CASK_HUMAN Kappa-casein OS=Homo sapiens OX=9606 GN=CSN3 PE=1 SV=3	Yes	Yes	No	No	No

VVLPVPQPEI	sp|P05814|CASB_HUMAN Beta-casein OS=Homo sapiens OX=9606 GN=CSN2 PE=1 SV=4	Yes	Yes	No	No	No
PVPQPE	sp|P05814|CASB_HUMAN Beta-casein OS=Homo sapiens OX=9606 GN=CSN2 PE=1 SV=4	Yes	Yes	No	No	No
VLPVPQPEI	sp|P05814|CASB_HUMAN Beta-casein OS=Homo sapiens OX=9606 GN=CSN2 PE=1 SV=4	Yes	Yes	No	No	No
VLPVPQ	sp|P05814|CASB_HUMAN Beta-casein OS=Homo sapiens OX=9606 GN=CSN2 PE=1 SV=4	Yes	Yes	No	No	No
FDPQIPK	sp|P05814|CASB_HUMAN Beta-casein OS=Homo sapiens OX=9606 GN=CSN2 PE=1 SV=4	Yes	Yes	No	No	No
VNEESTIPR	sp|P01833|PIGR_HUMAN Polymeric immunoglobulin receptor OS=Homo sapiens OX=9606 GN=PIGR PE=1 SV=4	Yes	Yes	No	No	No
VPFPPFSDISNPT	sp|P47710|CASA1_HUMAN Alpha-S1-casein OS=Homo sapiens OX=9606 GN=CSN1S1 PE=1 SV=1	Yes	Yes	No	No	No
LKSPTIP	sp|P05814|CASB_HUMAN Beta-casein OS=Homo sapiens OX=9606 GN=CSN2 PE=1 SV=4	Yes	Yes	No	No	No
QYVPFPPFSDI	sp|P47710|CASA1_HUMAN Alpha-S1-casein OS=Homo sapiens OX=9606 GN=CSN1S1 PE=1 SV=1	Yes	Yes	No	No	No
PVTQPL	sp|P05814|CASB_HUMAN Beta-casein OS=Homo sapiens OX=9606 GN=CSN2 PE=1 SV=4	Yes	Yes	No	No	No
QDKIYPS	sp|P05814|CASB_HUMAN Beta-casein OS=Homo sapiens OX=9606 GN=CSN2 PE=1 SV=4	Yes	Yes	No	No	No
QQVPQPIPQ	sp|P05814|CASB_HUMAN Beta-casein OS=Homo sapiens OX=9606 GN=CSN2 PE=1 SV=4	Yes	Yes	No	No	No
PSFQPQPLIY	sp|P05814|CASB_HUMAN Beta-casein OS=Homo sapiens OX=9606 GN=CSN2 PE=1 SV=4	Yes	Yes	No	No	No
FPPFSDISNPT	sp|P47710|CASA1_HUMAN Alpha-S1-casein OS=Homo sapiens OX=9606 GN=CSN1S1 PE=1 SV=1	Yes	Yes	No	No	No
PEIMEVPK	sp|P05814|CASB_HUMAN Beta-casein OS=Homo sapiens OX=9606 GN=CSN2 PE=1 SV=4	Yes	Yes	No	No	No
VLKPEPE	sp|P01833|PIGR_HUMAN Polymeric immunoglobulin receptor OS=Homo sapiens OX=9606 GN=PIGR PE=1 SV=4	Yes	Yes	No	No	No
QVVPYPQ	sp|P05814|CASB_HUMAN Beta-casein OS=Homo sapiens OX=9606 GN=CSN2 PE=1 SV=4	Yes	Yes	No	No	No
TQPLAPV	sp|P05814|CASB_HUMAN Beta-casein OS=Homo sapiens OX=9606 GN=CSN2 PE=1 SV=4	Yes	Yes	No	No	No
VVLPVPQ	sp|P05814|CASB_HUMAN Beta-casein OS=Homo sapiens OX=9606 GN=CSN2 PE=1 SV=4	Yes	Yes	No	No	No

PLMQQVPQPI	sp|P05814|CASB_HUMAN Beta-casein OS=Homo sapiens OX=9606 GN=CSN2 PE=1 SV=4	Yes	Yes	No	No	No
LPPQPL	sp|P05814|CASB_HUMAN Beta-casein OS=Homo sapiens OX=9606 GN=CSN2 PE=1 SV=4	Yes	Yes	No	No	No
PFPPFSDISNPT	sp|P47710|CASA1_HUMAN Alpha-S1-casein OS=Homo sapiens OX=9606 GN=CSN1S1 PE=1 SV=1	Yes	Yes	No	No	No
LQNPSESSEPIP	sp|P47710|CASA1_HUMAN Alpha-S1-casein OS=Homo sapiens OX=9606 GN=CSN1S1 PE=1 SV=1	Yes	Yes	No	No	No
FQPQPL	sp|P05814|CASB_HUMAN Beta-casein OS=Homo sapiens OX=9606 GN=CSN2 PE=1 SV=4	Yes	Yes	No	No	No
LQNPSESSEPIPL	sp|P47710|CASA1_HUMAN Alpha-S1-casein OS=Homo sapiens OX=9606 GN=CSN1S1 PE=1 SV=1	Yes	Yes	No	No	No
PAVVLPVPQPE	sp|P05814|CASB_HUMAN Beta-casein OS=Homo sapiens OX=9606 GN=CSN2 PE=1 SV=4	Yes	Yes	No	No	No
DPQIPK	sp|P05814|CASB_HUMAN Beta-casein OS=Homo sapiens OX=9606 GN=CSN2 PE=1 SV=4	Yes	Yes	No	No	No
QYVPFPPFS	sp|P47710|CASA1_HUMAN Alpha-S1-casein OS=Homo sapiens OX=9606 GN=CSN1S1 PE=1 SV=1	Yes	Yes	No	No	No
VVLPVPQP	sp|P05814|CASB_HUMAN Beta-casein OS=Homo sapiens OX=9606 GN=CSN2 PE=1 SV=4	Yes	Yes	No	No	No
VVLPVPQPE	sp|P05814|CASB_HUMAN Beta-casein OS=Homo sapiens OX=9606 GN=CSN2 PE=1 SV=4	Yes	Yes	No	No	No
QYVPFPPFSD	sp|P47710|CASA1_HUMAN Alpha-S1-casein OS=Homo sapiens OX=9606 GN=CSN1S1 PE=1 SV=1	Yes	Yes	No	No	No
ALPPQPL	sp|P05814|CASB_HUMAN Beta-casein OS=Homo sapiens OX=9606 GN=CSN2 PE=1 SV=4	Yes	Yes	No	No	No
PVTQPLAPV	sp|P05814|CASB_HUMAN Beta-casein OS=Homo sapiens OX=9606 GN=CSN2 PE=1 SV=4	Yes	Yes	No	No	No
DIQYPDATDEDIT	sp|P10451|OSTP_HUMAN Osteopontin OS=Homo sapiens OX=9606 GN=SPP1 PE=1 SV=1	Yes	Yes	No	No	No
VPQPIPQ	sp|P05814|CASB_HUMAN Beta-casein OS=Homo sapiens OX=9606 GN=CSN2 PE=1 SV=4	Yes	Yes	No	No	No
QQVPQPI	sp|P05814|CASB_HUMAN Beta-casein OS=Homo sapiens OX=9606 GN=CSN2 PE=1 SV=4	Yes	Yes	No	No	No

Appendix Table 4 Bioactive peptides comparisons in the apical and basoalteral compartments between infant- and adult-like models exposed to digested Dairy IF. Columns include the peptide sequence, source protein, average peptide detection count (Infant_count, Adult_count), and corresponding Welch's t-test p-value. Peptide abundance (mean log_2 intensity) and its statistical comparison are also shown (Intensity Adult, Intensity Infant, Intensity_p_value). A color code highlights peptides significantly more abundant in the infant model (green) or adult model (red) based on intensity p-value ($P < 0.05$). Additional columns indicate whether the peptide was also found in the basolateral compartment and functional annotations from the BIOPEP and MBPD databases.

Apical									
Sequence	**Protein**	**Infant_ count**	**Adult_ count**	**p_value**	**Intensity Adult**	**Intensity Infant**	**Intensity_ p_value**	**Shared with basolateral**	**BIOPEP &MBPD_Activity**
AVPYP	Beta-casein	0.000	0.667	0.116	23.130	18.626	0.068	No	ACE inhibitor
LNVPGEIVE	Beta-casein	0.000	1.000	0.000	21.976	17.556	0.013	No	ACE inhibitor
PFPGPIPN	Beta-casein	3.000	4.667	0.067	24.458	24.509	0.863	No	ACE inhibitor
PGL	Breast cancer anti-estrogen resistance protein 3 homolog	1.333	0.000	0.016	18.759	20.554	0.413	No	ACE inhibitor
VLP	Beta-casein	2.667	2.333	0.519	23.528	23.964	0.244	No	ACE inhibitor
YVP	Alpha-S1-casein	1.000	1.333	0.374	23.100	22.917	0.282	No	ACE inhibitor
WA	Butyrophilin subfamily 1 member A1	1.667	1.000	0.116	17.793	18.895	0.273	No	ACE inhibitor , activating ubiquitin-mediated proteolysis , dipeptidyl peptidase IV inhibitor
GPV	Beta-casein	2.000	2.333	0.643	21.933	22.426	0.143	No	ACE inhibitor , dipeptidyl peptidase IV inhibitor
YPFPGPI	Beta-casein	3.000	3.333	0.374	25.658	25.363	0.404	No	AChE inhibitor , immunomodulating , opioid agonist , anticancer , BChE inhibitor , ACE inhibitor , antioxidative
NLQ	Glycosylation-dependent cell adhesion molecule 1	1.000	0.000	0.000	18.951	18.382	0.382	No	anti inflammatory
VYPFPGPIP	Beta-casein	1.000	1.333	0.374	26.175	25.117	0.142	No	antiamnestic
HKEMPFPK	Beta-casein	0.667	0.667	1.000	21.167	21.182	0.995	No	antibacterial , antithrombotic
PGPIPN	Beta-casein	1.333	1.000	0.374	21.936	22.478	0.201	No	ACE-inhibitory, Anticancer, Immunomodulatory

PHA	DNA-(apurinic or apyrimidinic site) endonuclease 2	1.000	0.000	0.000	18.605	18.655	0.911	No	antioxidative
HQPHQPLPPTV MFPPQ	Beta-casein	5.333	11.000	0.235	25.587	24.198	0.090	No	ACE-inhibitory, Immunomodulatory
VIESPPEIN	Kappa-casein	1.000	1.000		19.909	21.986	0.310	No	binding
GPFPI	Beta-casein	0.667	1.667	0.101	23.914	21.382	0.240	No	cathepsin B inhibitor
APFPE	Alpha-S1-casein	0.667	0.000	0.116	17.781	21.118	0.063	No	dipeptidyl peptidase IV inhibitor
LPLPL	Beta-casein	0.667	0.000	0.116	17.890	19.783	0.095	No	dipeptidyl peptidase IV inhibitor
WRL	Butyrophilin subfamily 1 member A1	1.000	0.000	0.000	18.671	18.909	0.798	No	dipeptidyl peptidase IV inhibitor
PEW	Alpha-lactalbumin	0.667	0.000	0.116	18.795	19.252	0.603	No	hypouricemic , antioxidative
GAW	Alpha-S1-casein	0.667	0.667	1.000	20.789	21.177	0.844	No	ACE-inhibitory
YPFP	Beta-casein	1.000	1.667	0.116	21.865	21.190	0.186	No	Anticancer, Opioid
YPVEPF	Beta-casein	0.667	0.000	0.116	19.054	18.854	0.680	No	Antimicrobial, Antioxidant, DPP-IV Inhibitory, Increase mucin secretion, Opioid
HLPLP	Beta-casein	0.667	1.000	0.643	22.743	23.746	0.811	Yes	ACE inhibitor
LHLPLP	Beta-casein	1.000	1.000		25.750	26.163	0.410	Yes	ACE inhibitor
NIPPLTQTPV	Beta-casein	1.333	3.000	0.189	30.476	29.676	0.362	Yes	ACE inhibitor
NLHLPLP	Beta-casein	1.000	1.667	0.116	24.326	24.391	0.928	Yes	ACE inhibitor
VYP	Beta-casein	1.000	1.000	1.000	21.357	23.465	0.466	Yes	ACE inhibitor
AYFYPE	Alpha-S1-casein	1.000	1.000		21.158	21.668	0.534	Yes	ACE inhibitor , antioxidative
IPPLTQTPV	Beta-casein	1.000	1.333	0.374	27.485	26.990	0.395	Yes	ACE inhibitor , dipeptidyl peptidase IV inhibitor
YPFPGPIPN	Beta-casein	1.000	0.667	0.374	23.233	25.168	0.406	Yes	ACE inhibitor , dipeptidyl peptidase IV inhibitor
HLPLPL	Beta-casein	0.000	1.000	0.000	23.411	18.481	0.001	Yes	antiamnestic
EMPFPK	Beta-casein	2.000	3.000	0.158	26.030	25.875	0.822	Yes	ACE-inhibitory, Antimicrobial, Bradykinin-Potentiating, Increase mucin secretion
FVAPFPEVFG	Alpha-S1-casein	1.000	1.000		24.924	25.219	0.527	Yes	anticancer

LPM	Beta-lactoglobulin	0.000	0.667	0.116	21.167	18.124	0.211	Yes	antioxidative
VVPPFLQPE	Beta-casein	1.000	1.000		29.400	29.533	0.785	Yes	antioxidative
MAIPPK	Kappa-casein	4.333	28.000	0.002	27.682	25.834	0.276	Yes	antithrombotic , ACE inhibitor
VRTPEVDDE	Beta-lactoglobulin	2.000	2.333	0.374	23.220	22.972	0.410	Yes	binding
PFPGPI	Beta-casein	1.000	0.667	0.374	21.420	22.652	0.410	Yes	cathepsin B inhibitor
TPEVDDEALEK	Beta-lactoglobulin	1.000	5.667	0.083	23.069	22.278	0.241	Yes	Antimicrobial, DPP-IV Inhibitory
VPYPQ	Beta-casein	0.667	0.000	0.116	18.204	21.037	0.044	Yes	dipeptidyl peptidase IV inhibitor , antioxidative
LDDDLTDDIM	Alpha-lactalbumin	3.000	2.667	0.374	23.252	23.562	0.693	Yes	hypouricemic
TQTPVVVPPFLQPE	Beta-casein	2.000	2.000		25.832	26.023	0.040	Yes	hypouricemic, Antioxidant
VYPFPGPI	Beta-casein	2.000	2.333	0.374	29.708	29.563	0.771	Yes	hypouricemic , antiamnestic , ACE inhibitor, Prolyl endopeptidase-inhibitory
ALPM	Beta-lactoglobulin	0.667	0.000	0.116	18.766	24.737	0.203	Yes	xanthine oxidase inhibitor , ACE-inhibitory
Basolateral									
Sequence	**Protein**	**Infant_ count**	**Adult_ count**	**p_value**	**Intensity Adult**	**Intensity Infant**	**Intensity_ p_value**	**Shared with basolateral**	**BIOPEP &MBPD_Activity**
HLPLP	Beta-casein	1.000	0.667	0.374	19.154	21.800	0.295	Yes	ACE Inhibitor
LHLPLP	Beta-casein	0.000	1.333	0.016	20.549	16.357	0.096	Yes	ACE Inhibitor
NIPPLTQTPV	Beta-casein	1.000	1.000		23.765	25.568	0.424	Yes	ACE Inhibitor
NLHLPLP	Beta-casein	0.667	0.000	0.116	16.793	18.354	0.491	Yes	ACE Inhibitor
VYP	Beta-casein	1.333	0.667	0.422	18.073	18.583	0.826	Yes	ACE Inhibitor
FVAPFPEVFG	Alpha-S1-casein	0.667	0.667	1.000	17.823	19.472	0.401	Yes	Anticancer, ACE-Inhibitory
LPLP	Beta-casein	1.000	0.667	0.374	18.855	19.513	0.577	No	Hypotensive , ACE Inhibitor
ALPM	Beta-lactoglobulin	1.000	1.000		23.071	24.483	0.553	Yes	Xanthine Oxidase Inhibitor
HQPHQPLPPT	Beta-casein	2.000	2.000	1.000	17.956	20.056	0.500	Yes	ACE-Inhibitory
LVYPFPGPI	Beta-casein	1.000	1.000		19.299	21.012	0.434	Yes	ACE-Inhibitory

EMPFPK	Beta-casein	1.667	2.000	0.643	23.117	23.404	0.891	Yes	ACE-Inhibitory, Antimicrobial, Bradykinin-Potentiating, Increase Mucin Secretion
AYFYPE	Alpha-S1-casein	0.667	0.667	1.000	17.453	17.657	0.871	Yes	ACE Inhibitor , Antioxidative
VYPFPGPIPN	Beta-casein	1.000	1.000		22.224	24.361	0.353	Yes	ACE-Inhibitory, Antioxidant
YPFPGPIPN	Beta-casein	1.000	0.667	0.374	18.980	20.808	0.279	Yes	ACE Inhibitor , Dipeptidyl Peptidase IV Inhibitor
PVVVPPFLQPE	Beta-casein	1.000	1.000		21.287	23.018	0.475	Yes	Antimicrobial
TPEVDDEALEK	Beta-lactoglobulin	1.000	1.000	1.000	18.195	18.845	0.698	Yes	Dipeptidyl Peptidase IV Inhibitor
PYPQ	Beta-casein	1.000	1.000		20.493	22.142	0.493	No	Antioxidative
TQTPVVVPPFLQPE	Beta-casein	1.000	0.667	0.374	18.448	19.447	0.582	Yes	Hypouricemic, Antioxidant
NVPGEIVESL	Beta-casein	1.667	1.667	1.000	19.322	21.169	0.292	No	Antioxidant
VPYPQ	Beta-casein	1.000	0.667	0.374	16.794	18.544	0.287	Yes	Dipeptidyl Peptidase IV Inhibitor , Antioxidative
PFPGPI	Beta-casein	0.667	0.000	0.116	16.852	18.584	0.198	Yes	Cathepsin B Inhibitor
VAPFPE	Alpha-S1-casein	2.333	2.000	0.815	20.000	20.796	0.692	Yes	Cholesterol Regulation
VLPVPQ	Beta-casein	2.000	1.667	0.374	23.234	25.036	0.384	Yes	Cholesterol Regulation
LPVPQ	Beta-casein	1.000	0.667	0.374	17.915	19.330	0.370	Yes	Dpp-Iv Inhibitory
SLPQNIPPL	Beta-casein	1.000	1.000		19.837	21.573	0.417	Yes	Dpp-Iv Inhibitory
WLA	Alpha-lactalbumin	1.000	0.000	0.158	15.799	16.782	0.556	No	Immunomodulatory
VYPFPGPI	Beta-casein	1.000	1.000		21.563	23.414	0.432	Yes	Hypouricemic , Antiamnestic , ACE Inhibitor, Prolyl Endopeptidase-Inhibitory
GPL	Versican core protein	0.667	0.000	0.116	15.749	18.459	0.139	No	ACE Inhibitor
LGV	Versican core protein	1.000	0.667	0.374	19.262	21.172	0.404	No	ACE Inhibitor
LYP	Versican core protein	1.667	1.000	0.374	16.665	18.372	0.129	No	ACE Inhibitor
TGP	Versican core protein	0.667	0.000	0.116	16.499	18.176	0.385	No	ACE Inhibitor
YRP	Contactin-1	0.000	0.667	0.116	17.836	16.346	0.332	No	ACE Inhibitor
WRP	Versican core protein	1.333	1.333	1.000	18.220	19.691	0.497	No	ACE Inhibitor , Dipeptidyl Peptidase IV Inhibitor

IPPLTQTPV	Beta-casein	1.000	1.000		21.904	23.180	0.521	Yes	ACE Inhibitor , Dipeptidyl Peptidase IV Inhibitor
HLPLPL	Beta-casein	1.000	1.000	1.000	20.173	20.940	0.785	Yes	Antiamnestic
FWG	Versican core protein	0.667	0.000	0.116	15.723	17.524	0.159	No	Antioxidative
QHH	Versican core protein	0.667	0.000	0.116	16.241	17.933	0.190	No	Antioxidative
LPM	Beta-lactoglobulin	0.000	1.000	0.158	17.756	16.792	0.569	Yes	Antioxidative
VVPPFLQPE	Beta-casein	1.000	1.000		22.444	24.188	0.454	Yes	Antioxidative
MAIPPK	Kappa-casein	10.333	2.000	0.375	19.767	21.241	0.477	Yes	Antithrombotic , ACE Inhibitor
VRTPEVDDE	Beta-lactoglobulin	1.000	1.000		18.622	19.285	0.717	Yes	Binding
VW	Contactin-1	1.333	0.667	0.230	16.649	19.039	0.356	No	Dipeptidyl Peptidase IV Inhibitor , Hypouricemic , Alpha-Glucosidase Inhibitor , ACE Inhibitor , Antioxidative
LPYP	Kappa-casein	0.000	0.667	0.116	18.807	15.449	0.042	No	HMG-Coa Reductase Inhibitor , ACE Inhibitor
LDDDLTDDIM	Alpha-lactalbumin	0.667	0.667	1.000	17.551	18.298	0.496	Yes	Hypouricemic
YPF	Beta-casein	0.667	0.000	0.116	15.508	17.446	0.043	No	Opioid

Appendix Table 5 Bioactive peptides comparisons in the apical and basoalteral compartments between infant- and adult-like models exposed to digested Soya IF. Columns include the peptide sequence, source protein, average peptide detection count (Infant_count, Adult_count), and corresponding Welch's t-test p-value. Peptide abundance (mean log_2 intensity) and its statistical comparison are also shown (Intensity Adult, Intensity Infant, Intensity_p_value). A color code highlights peptides significantly more abundant in the infant model (green) or adult model (red) based on intensity p-value ($P < 0.05$). Additional columns indicate whether the peptide was also found in the basolateral compartment and functional annotations from the BIOPEP and MBPD databases

Apical									
Sequence	**Protein**	**Infant_ count**	**Adult_ count**	**p_value**	**Intensity Adult**	**Intensity Infant**	**Intensity_ p_value**	**Shared with basolateral**	**BIOPEP &MBPD_Activity**
TIIPLPV	Seed linoleate 13S-lipoxygenase-1	2.000	1.667	0.374	21.179	21.671	0.549	No	ACE inhibitor , Antioxidative
Basolateral									
Sequence	**Protein**	**Infant_ count**	**Adult_ count**	**p_value**	**Intensity Adult**	**Intensity Infant**	**Intensity_ p_value**	**Shared with basolateral**	**BIOPEP &MBPD_Activity**
SLVNNDDRDS	Beta-conglycinin alpha subunit 1	1.333	1.000	0.374	19.070	20.757	0.168	No	Antioxidative

Appendix Table 6 Bioactive peptides comparisons in the apical and basoalteral compartments between infant- and adult-like models exposed to digested Human Milk.

Columns include the peptide sequence, source protein, average peptide detection count (Infant_count, Adult_count), and corresponding Welch's t-test p-value. Peptide abundance (mean $\log_2$ intensity) and its statistical comparison are also shown (Intensity Adult, Intensity Infant, Intensity_p_value). A color code highlights peptides significantly more abundant in the infant model (green) or adult model (red) based on intensity p-value ($P < 0.05$). Additional columns indicate whether the peptide was also found in the basolateral compartment and functional annotations from the BIOPEP and MBPD databases

Apical									
Sequence	**Protein**	**Infant_ count**	**Adult_ count**	**p_value**	**Intensity Adult**	**Intensity Infant**	**Intensity_ p_value**	**Shared with basolateral**	**BIOPEP &MBPD_Activity**
ENLHLPLP	Beta-casein	1.000	1.000	1.000	23.172	23.643	0.527	No	ACE Inhibitor
LPQNILP	Beta-casein	1.333	0.000	0.116	16.369	20.756	0.121	No	ACE Inhibitor
NLHLPLP	Beta-casein	2.000	0.000	0.000	17.899	25.745	0.006	Yes	ACE Inhibitor
VLPIPQ	Beta-casein	2.000	1.667	0.374	29.371	29.970	0.066	Yes	ACE Inhibitor
YPFVEPI	Beta-casein	2.000	1.000	0.158	20.461	22.497	0.410	No	Dipeptidyl Peptidase III Inhibitor, Anticancer, Increase Cellular Growth, Opioid
QVVPYPQ	Beta-casein	3.000	2.333	0.374	27.680	27.640	0.925	Yes	Antioxidative
VLPVPQ	Beta-casein	2.000	1.667	0.374	25.577	25.820	0.530	Yes	Cholesterol Regulation
PPKP	Insulin receptor substrate 2	1.333	0.000	0.016	17.175	23.213	0.002	No	ACE Inhibitor
QLVP	Hemicentin-2	1.000	1.000	1.000	21.460	21.926	0.504	No	ACE Inhibitor
Basolateral									
Sequence	**Protein**	**Infant_ count**	**Adult_ count**	**p_value**	**Intensity Adult**	**Intensity Infant**	**Intensity_ p_value**	**Shared with basolateral**	**BIOPEP &MBPD_Activity**
VLPIPQ	Beta-casein	2.000	2.000	1.000	25.798	27.338	0.018	Yes	ACE Inhibitor
NLHLPLP	Beta-casein	1.000	0.000	0.000	17.145	22.485	0.002	Yes	ACE Inhibitor
WSVPQPK	Beta-casein	2.000	1.000	0.000	22.608	24.059	0.021	No	ACE Inhibitor , Antioxidative

QVVPYPQ	Beta-casein	1.000	1.000	1.000	23.504	24.977	0.096	Yes	Antioxidative
VLPVPQ	Beta-casein	1.000	1.000	1.000	21.139	23.229	0.007	Yes	Cholesterol Regulation

Appendix C

Additional Research Outputs and Activities

Webinars and Invited Talks

Francesca Bietto. *"Developing Infant-like Gut Barrier Models to Study Human Milk and Infant Formula."*

INFOGEST Viva Webinar, 5 November 2025. Recording available here.

Departmental and Institutional Seminars

- Francesca Bietto. *Developing an In Vitro Model of the Infant Gut Barrier.* Department of Food and Nutritional Sciences, University College Cork, 12 September 2023.
- Francesca Bietto. *Pioneering In Vitro Models of the Immature Gut Barrier for Advancing Infant Formula.* Moorepark Food Biosciences Department Seminar, 22 October 2024.

Short-Term Scientific Missions

1. **Spanish National Research Council (CSIC) – Institute of Food Science Research (CIAL)**, Madrid, Spain
   Hosting supervisor: Dr. Beatriz Miralles
   8 October – 22 December 2023 (3 months)
2. **National Research Council of Italy (CNR-ISPA)** – Torino, Italy
   Hosting supervisors: Dr. Simona Bavaro and Dr. Simona Cirrincione
   1 November – 23 December 2024

Other Collaborations

- **INRAE, France**: Dr. Myriam Grundy visited Moorepark (Sept 2023) for three weeks of tissue culture training under the author's supervision; the collaboration remains ongoing.
- **Murine study with Ramya Balasubramanian (Teagasc)**: The author participated in a mouse trial investigating immune responses to dietary interventions, assisting in animal culling, dissection, and splenocyte isolation. This study, led by Dr. Balasubramanian as part of her Ph.D., is in preparation for publication, on which the author will be listed as a co-author.

Public Engagement

- Moorepark Open Day 2023 (4 July 2023): Human digestive system and food digestion demonstrations (~10,000 visitors).
- Native Scientist Workshops (UCC, 28 April 2023 & 22 March 2024): Italian-speaking children (ages 4–11); activity: *Microorganisms in Food.*
- National Ploughing Championships 2024 (Ratheniska, Co. Laois, 19 September 2024): Human digestive system and digestion demonstrations (~78,000 visitors).

Education Engagement

- VistaMilk Career Days, Moorepark (23 March 2023): Talk and Q&A with secondary school students (16–17 years old).
- Primary School Demonstration, Castlelyons School (28 May 2022).
- Munster Math and Science Fair (17 October 2022).

- Reviewer, *Climate Detective Project* – European Space Agency.
- Transition-Year Student Training: Supervised seven transition-year students (2023–2025) from local secondary schools as part of Teagasc's outreach programme, providing short laboratory training in safety, aseptic technique, and basic cell culture.

Reviewer Activity

- Francesca Bietto, *Journal of Functional Foods*
- Francesca Bietto, *Food and Chemical Toxicology*

UCC Modules

- PG6001 - STEPS Scientific Trng for Enhanced PG Studies
- PG6015 - Intro Research Integrity, Ethics, Open Science
- PG7016 - Systematic Reviews for the Health Sciences

Training Courses

- Manual Handling in the Workplace – The Learning Rooms, completed 20 February 2025
- Risk Management Overview – Interaction Training, completed 24 January 2025
- Introduction to GDPR in the Workplace – The Learning Rooms, completed 24 January 2025
- Office Ergonomics – ViaUp, completed 25 October 2024
- Human Intestinal On-Demand Training Course – Suite 500, Station Street, Vancouver, Canada, completed 26 April 2024

- Data Protection Training 2022 – Teagasc, completed 28 September 2022
- Using Liquid Nitrogen Safely Within Universities – Gas Safety Training (UK), completed 2 August 2022
- Using Gas Cylinders Safely Within Universities – Gas Safety Training (UK), completed 2 August 2022
- Diversity and Inclusion Awareness – Teagasc / TCPDF Certified, completed 28 July 2025

Organizational and Leadership Activities

- Member of the Social Committee, organizing two Christmas parties, several potlucks, one joint BBQ with Grassland Department, and weekly lunchtime Zumba classes (1 year).
- Walsh Scholar Representative for the Food Centre:
    - Reinstated the role post-COVID to improve Ph.D. representation.
    - Co-led a petition and case study advocating for increased Ph.D. stipends.
    - Designed and launched a Buddy System for new student onboarding (proposal, posters, and student matching).
- Assisted in organizing the *7th Food Digestion Conference* (2022, Cork, Ireland).